Genesis of Hydrothermal High Field Strength Element Mineral Deposits: Evidence from Laser Ablation – Inductively Coupled Plasma Mass Spectrometry

Joel Edward Gagnon

Department of Earth & Planetary Sciences
McGill University, Montreal

February 2006

A thesis submitted to McGill University
In partial fulfillment of the requirements of the degree of
Doctor of Philosophy (Geology)

Your file Votre référence
ISBN: 978-0-494-25149-2
Our file Notre référence
ISBN: 978-0-494-25149-2

Abstract

High field strength elements (HFSE) are geologically and economically important. These elements were once thought to be immobile during metasomatic processes, however, a growing body of empirical evidence indicates that HFSE can be mobilized under certain conditions. Despite this evidence, little is known about the factors controlling solubility, transport and deposition of HFSE by aqueous fluids, apart from some theoretical estimates and rare experimental studies. Therefore, the study of natural systems (e.g., HFSE ore deposits) provides an excellent opportunity to evaluate HFSE mobility by aqueous fluids. Five localities where evidence of hydrothermal transport of HFSE has been previously documented were included in this study: Gallinas Mountains, New Mexico; South Platte, Colorado; Rock Canyon Creek, British Columbia; St. Lawrence, Newfoundland; and Strange Lake, Quebec/Labrador. Minerals and, in the case of South Platte, fluid inclusions from these localities were analyzed using petrography and laser ablation inductively-coupled plasma mass spectrometry (LA-ICPMS) to evaluate the source of the HFSE and the hydrothermal fluids responsible for HFSE transport, and factors controlling HFSE and gangue mineral (e.g., fluorite, quartz) precipitation. Analysis of some of the important gangue minerals, which are also the primary host of fluid inclusions in many of these deposits (e.g., fluorite), is difficult using 266 nm Nd:YAG-based LA-ICPMS. Furthermore, complex mineral intergrowths and the desire to quantify the chemical composition of unknown minerals required the development of analytical and data reduction protocols for LA-ICPMS. Methods for conducting traversed opening of fluid inclusions, removing the host mineral contribution to fluid inclusion signals by calculating count rate ratios, and quantifying the composition of minerals without using an internal standard are presented. In general, hydrothermal enrichment of HFSE in these deposits appears to have resulted from interaction of an HFSE- and F-bearing magmatic fluid with another, Ca-bearing fluid or with Ca-bearing wall rocks or preexisting minerals. In most cases, HFSE appear to be derived locally, within the associated igneous intrusion.

Sommaire

Les éléments élevés de force de champ (HFSE) sont géologiquement et économiquement importants. Ces éléments étaient une fois que la pensée pour être immobile pendant des processus métasomatiques, cependant, un corps croissant d'évidence empirique indique que HFSE peut être mobilisé dans certaines conditions. En dépit de cette évidence, peu est connu au sujet des facteurs commandant la solubilité, le transport et le dépôt de HFSE par les fluides aqueux, indépendamment de quelques évaluations théoriques et études expérimentales rares. Par conséquent, l'étude des systèmes normaux (par exemple, gisements de minerai de HFSE) fournit une excellente occasion d'évaluer la mobilité de HFSE par les fluides aqueux. Cinq localités où l'évidence du transport hydrothermique de HFSE a été précédemment documentée ont été incluses dans cette étude: Gallinas Mountains, New Mexico; South Platte, Colorado; Rock Canyon Creek, British Columbia; St. Lawrence, Newfoundland; et Strange Lake, Quebec/Labrador. Des minerais et, dans le cas de South Platte, les inclusions liquides de ces localités ont été analysés en utilisant la pétrographie et la spectrométrie de masse inductif-couplée par ablation de plasma de laser (LA-ICPMS) pour évaluer la source du HFSE et des fluides hydrothermiques responsables du transport de HFSE, et des facteurs commandant la précipitation de minerai de HFSE et de gangue (par exemple, fluorite, quartz). L'analyse de certains des minerais importants de gangue, qui sont également le centre serveur primaire des inclusions liquides dans plusieurs de ces dépôts (par exemple, fluorite), est difficile en utilisant la LA-ICPMS de 266 nm Nd:YAG-based. En outre, les intergrowths minéraux complexes et le désir de mesurer la composition chimique des minerais inconnus ont exigé le développement des protocoles analytique et de données de réduction pour la LA-ICPMS. Les méthodes pour conduire ont traversé l'ouverture des inclusions liquides, enlevant la contribution minérale de centre serveur aux signaux liquides d'inclusion par des rapports calculateurs de taux de compte, et mesurant la composition des minerais sans employer une norme interne sont présentés. En général, l'enrichissement hydrothermique de HFSE dans ces dépôts semble avoir résulté de l'interaction d'un fluide de HFSE- et de F-roulement magmatique avec des autres, du fluide de Ca-roulement ou avec des roches au mur de Ca-roulement ou des minerais la préexistence. Dans la plupart des cas, HFSE semblent être dérivés localement, dans l'intrusion ignée associée.

Dedication

This thesis is dedicated to:

My maternal grandfather, Joseph Edouard Napoleon LePage, for quite unwittingly introducing me to geology during summer vacations near Parry Sound, Ontario,

My maternal grandmother, Marguerite Emily LePage, for instilling in me an appreciation of the lasting value of education,

My father, Eugene Louis Gagnon, for first challenging me to pursue a university education in lieu of other pursuits, and

My wonderful wife, Rhonda Lynn Marguerite Boucher, and beautiful children, Marguerite, Jacob and Jacqueline, whose unfailing support, sacrifice, and encouragement have made this thesis possible.

Acknowledgements

I extend my deepest appreciation and gratitude to my thesis supervisors, Dr. Iain M. Samson, Dr. Anthony E. 'Willy' Williams-Jones, and Dr. Brian J. Fryer. I thank them for taking a chance and supporting me in my attempts to pursue this project after being away from university for 10 years. Without their early support and encouragement, this project would never have happened. I have also been truly fortunate to have worked with three outstanding scientists and teachers whose enthusiasm for their craft has contributed greatly to my success. I thank them for their generous financial support and, in particular, for the opportunity given to me by Dr. Fryer to manage the ICPMS laboratory at the Great Lakes Institute for Environmental Research at the University of Windsor. Not only did this position give me the financial means necessary to pursue this project, it provided unlimited access (and Brian's trust) to use and experiment with LA-ICPMS instrumentation. This experience has been extraordinarily rewarding and invaluable. The kindness, support and enthusiasm shown by these three individuals have enabled me to be successful in this endeavor and I consider them true benefactors.

I thank the faculty, staff and students in the Department of Earth and Planetary Sciences at McGill University for their warm reception upon my arrival there. I also thank the Department of Earth and Planetary Sciences and McGill University for allowing me to conduct my research activities largely outside of the department. Without such accommodation, this project would have been impossible. In particular, I thank fellow McGill University Ph.D. students Kate Ault, Annick Chouinard, and Sandy Archibald for 'adopting' me into their extended 'family' and educating me on the academic and some non-academic aspects of McGill University and Montreal in general. I extend a special thank you to Ms. Claudette Fortier for her wonderful accommodations during my weekly commute to Montreal from Windsor. I have never before experienced such hospitality as I did when I visited Montreal. Merci beaucoup.

Special thanks go to my office 'roommate' at the Great Lakes Institute, Jean Claude 'JC' Barrette and to Ms. Mary Lou Scratch for their daily help and support. I also thank the Technical Services Center staff at the University of Windsor, particularly Mr. Andy Jenner and Mr. Steve Budinsky, for transferring concepts for LA-ICPMS equipment into hard parts.

Table of Contents

Preface

Chapter 1 – Introduction

Table of Contents (continued)

Chapter 2 – Compositional Heterogeneity in Fluorite and the Genesis of Fluorite Deposits – Insights from LA-ICP-MS

Chapter 3 – LA-ICP-MS Analysis of Fluid Inclusions

Table of Contents (continued)

Chapter 3 (continued)

Chapter 4 – The composition and origin of hydrothermal fluids in an NYF-type granitic pegmatite, South Platte District, Colorado: Evidence from LA-ICP-MS analysis of fluorite- and quartz-hosted fluid inclusions

Table of Contents (continued)

Chapter 4 (continued)

Chapter 5 – Quantitative analysis of silicates by LA-ICPMS with and without an internal standard

Table of Contents (continued)

Chapter 5 (continued)

Chapter 6 – Extreme hydrothermal HFSE mobility and enrichment in the Strange Lake peralkaline complex, northeastern Canada

Table of Contents (continued)

Chapter 6 (continued)

Chapter 7 – Conclusions

List of Figures

Chapter 2 – Compositional Heterogeneity in Fluorite and the Genesis of Fluorite Deposits – Insights from LA-ICP-MS

Chapter 3 – LA-ICP-MS Analysis of Fluid Inclusions

Chapter 4 – The composition and origin of hydrothermal fluids in an NYF-type granitic pegmatite, South Platte District, Colorado: Evidence from LA-ICP-MS analysis of fluorite- and quartz-hosted fluid inclusions

List of Figures (continued)

Chapter 4 (continued)

Chapter 5 – Quantitative analysis of silicates by LA-ICPMS with and without an internal standard

Chapter 6 – Extreme hydrothermal HFSE mobility and enrichment in the Strange Lake peralkaline complex, northeastern Canada

List of Tables

Chapter 2 – Compositional Heterogeneity in Fluorite and the Genesis of Fluorite Deposits – Insights from LA-ICP-MS

Chapter 4 – The composition and origin of hydrothermal fluids in an NYF-type granitic pegmatite, South Platte District, Colorado: Evidence from LA-ICP-MS analysis of fluorite- and quartz-hosted fluid inclusions

Chapter 5 – Quantitative analysis of silicates by LA-ICPMS with and without an internal standard

List of Tables (continued)

Chapter 5 (continued)

Chapter 6 – Extreme hydrothermal HFSE mobility and enrichment in the Strange Lake peralkaline complex, northeastern Canada

List of Appendices

Appendix

A. Appendix to Chapter 2 – Compositional Heterogeneity in Fluorite and the Genesis of Fluorite Deposits – Insights from LA-ICP-MS Analysis

B. Appendix to Chapter 3 – LA-ICP-MS Analysis of Fluid Inclusions – Example of a Quantitative Fluid Inclusion Calculation

C. Appendix to Chapter 4 – The composition and origin of hydrothermal fluids in an NYF-type granitic pegmatite, South Platte District, Colorado: Evidence from LA-ICP-MS analysis of fluorite- and quartz-hosted fluid inclusions

D. Appendix to Chapter 5 – Quantitative analysis of silicates by LA-ICPMS with and without an internal standard

E. Appendix to Chapter 6 – Extreme hydrothermal HFSE mobility and enrichment in the Strange Lake peralkaline complex, northeastern Canada

Preface

Thesis Format

This thesis comprises five manuscripts, three of which (Chapters 2 through 4) are published in scientific journals. Chapter 2 presents the results of an investigation into the composition of fluorite from four localities (South Platte, Colorado; St. Lawrence, Newfoundland; Gallinas Mountains, New Mexico; and Rock Canyon Creek, British Columbia) and was published as an article entitled "Compositional heterogeneity in fluorite and the genesis of fluorite deposits: insights from LA-ICP-MS analysis" in *The Canadian Mineralogist* (Vol. 41, pp. 365 to 382, 2003). Chapter 3 is a summary of methods and techniques for the LA-ICP-MS analysis of fluid inclusions and includes new approaches to fluid inclusion opening and data reduction. This manuscript was published as a chapter entitled "LA-ICP-MS Analysis of Fluid Inclusions" in a *Mineralogical Association of Canada* short course volume (Vol. 32, pp. 291 to 318, 2003). Chapter 4 presents the results of an investigation of the composition of fluid inclusions from the South Platte district, Colorado using LA-ICP-MS, and was published as an article entitled "The composition and origin of hydrothermal fluids in an NYF-type granitic pegmatite, South Platte District, Colorado: evidence from LA-ICP-MS analysis of fluorite- and quartz-hosted fluid inclusions" in *The Canadian Mineralogist* (Vol. 42, pp. 1331 to 1355, 2004).

The remaining two chapters (Chapters 5 and 6) will be submitted for publication in scientific journals. Chapter 5, entitled "Quantitative analysis of silicates by LA-ICPMS with and without an internal standard" presents a method for conducting quantitative LA-ICP-MS analysis of silicates without using an internal standard and demonstrates the accuracy and precision of the method using standard reference materials and a compositionally complex silicate mineral (arfvedsonite) from a hydrothermal HFSE deposit (Strange Lake, Quebec/Labrador). The manuscript will be submitted for publication in the *Journal of Analytical Atomic Spectrometry*. The final manuscript (Chapter 6),

entitled "Extreme hydrothermal HFSE mobility and enrichment in the Strange Lake peralkaline complex, northeastern Canada" presents the results of an investigation of the petrography, mineral chemistry (using the methods presented in Chapter 5) and alteration reactions associated with a major, hydrothermal HFSE deposit. The manuscript will be submitted for publication in *Contributions to Mineralogy and Petrology*.

The data presented in the individual chapters consists of summaries of all data collected during each of the various investigations comprising this thesis. Summation of the data was required for brevity in order to publish the manuscripts in scientific journals. The raw data that were used to prepare the data summaries presented in the individual chapters are provided as Appendices A through E in this thesis.

Contributions

The first author of the five manuscripts comprising this thesis (Joel E. Gagnon) was responsible for sample selection and preparation, petrographic analysis and description, LA-ICP-MS experiment design, data collection and sample analysis, development of analytical equipment and methods (e.g., laser aperture, traversed opening of fluid inclusions), data reduction protocols (e.g., removal of host mineral contributions to fluid inclusion signal, oxide scaling) and interpretations of the data. The coauthors of the manuscripts (Dr. Iain M. Samson, Dr. Anthony E. Williams-Jones, and Dr. Brian J. Fryer) provided input into experiment design, guidance during the investigations, and editorial review of drafts of the manuscripts. Mr. C.J. Collins performed the LA-ICP-MS analysis of fluorite from the Lawn Barite vein, St. Lawrence, Newfoundland, which is presented in Chapter 2. Dr. A.E. Williams-Jones performed the modeling of water/rock reactions using HCh software that is presented in Chapter 4. Mr. R. L. Levasseur, Ms. I. Drouin-Brisebois and Ms. M. Price performed some of the fluid inclusion microthermometry included in Chapter 4.

Chapter 1

Introduction

High field strength elements (HFSE), which include Sc, Ti, V, Zr, Nb, Hf, Ta and the rare earth elements (REE), have important economic and geologic applications. The unique, physical and electromagnetic properties of HFSE have resulted in their industrial use in magnets, alloys, pigments, coatings, phosphors and catalysts. They are geologically important because HFSE historically have been considered to be immobile during metasomatism (e.g., metamorphism, hydrothermal alteration), which has resulted in their use in classifying rocks (e.g., Pearce and Cann, 1973; Floyd and Winchester, 1975; 1978; Pearce and Norry, 1979), modeling geologic processes (e.g., Munker et al., 2004), and quantifying mass or volume changes during deformation and alteration (e.g., O'Hara and Blackburn, 1989; MacLean, 1990; Fujimoto et al., 2001).

A growing body of evidence, however, indicates that HFSE have been mobilized under certain hydrothermal conditions (e.g., MacLean, 1988; Salvi and Williams-Jones, 1996; Williams-Jones et al., 2000; Salvi et al., 2004). Despite their economic and geologic significance and the number of empirical studies indicating that HFSE can be mobilized, very little is known about the conditions and factors controlling transport and deposition of these elements by hydrothermal fluids. Some theoretical estimates of the ligands likely capable of causing HFSE mobility in hydrothermal systems (e.g., F, Cl) have been calculated (e.g., Wood, 1990; Haas et al., 1995, Wood, 2003; Samson and Wood, 2005). Experimental investigations specifically designed to quantify HFSE solubility and complexation in hydrothermal fluids, however, are rare (e.g., Migdisov and Williams-Jones, 2002). The paucity of experimental data makes the study of natural systems in which these elements have been mobilized by hydrothermal processes (e.g., HFSE ore deposits) particularly relevant to our understanding of HFSE solubility, transport and precipitation by aqueous fluids.

Evidence of HFSE mobility and enrichment by hydrothermal processes is particularly convincing in some alkaline igneous systems (e.g., Truman et al., 1988; Sørensen, 1992; Salvi and Williams-Jones, 1996; Salvi et al., 2000; Salvi and Williams-Jones, 2005). Where empirical evidence has been observed, HFSE mobility is thought to have resulted from aqueous fluids with unusual compositions (e.g., high F). This is based on mineralogical evidence, such as the association of HFSE enrichment with F-bearing minerals (e.g., Salvi and Williams-Jones, 1992; Salvi et al., 2000; Williams-Jones et al., 2000; Samson et al., 2001). This enrichment is often associated spatially with hydrothermal alteration (e.g., fenitization, albitization, Ca-metasomatism, or hematization), however, some (e.g., Kovalenko et al., 1995; Miller, 1996) question whether there is a genetic link between the alteration and HFSE mineralization. Establishing the extent of secondary, hydrothermal enrichment and its association with mineralogical alteration is often complicated by anomalously high, primary magmatic concentrations of HFSE in many of the alkaline intrusions that host these deposits (e.g., Strange Lake). This has led some investigators (e.g., Miller, 1996) to conclude that all HFSE enrichment is magmatic and that *significant* remobilization of HFSE by hydrothermal processes did not occur in these intrusions.

Despite an apparent association, the genetic link between HFSE enrichment by hydrothermal processes and mineralogical alteration within these intrusions remains equivocal. Understanding the relationship between mineralogical alteration and HFSE enrichment is critical to understanding the mobility of these elements in hydrothermal systems, and has important implications for the exploration and development of these deposits. Detailed petrographic and quantitative elemental analysis of minerals and fluid inclusions from these deposits is required to determine whether, and to what extent, HFSE have been transported by aqueous fluids, the potential sources of HFSE, complexing ligands responsible for HFSE transport in aqueous fluids, and factors controlling formation of hydrothermal HFSE mineralization. Laser ablation inductively-coupled plasma mass spectrometry (LA-ICP-MS) is an extremely

powerful microanalytical technique that can be used to obtain quantitative, chemical data on minerals and fluid inclusions from HFSE deposits. Application of LA-ICP-MS techniques to the study of hydrothermal HFSE mineralization can provide insights into the formation of these deposits. Method development to address some of the limitations of LA-ICP-MS, principally non-representative sampling of minerals and fluid inclusions, is required, however, in order to obtain accurate and precise data from these deposits.

The manuscripts presented in this thesis include a combination of LA-ICP-MS method development and application to minerals and fluid inclusions from HFSE mineral deposits. The mineral deposits and specific LA-ICP-MS methods that were included in this thesis are presented below.

Hydrothermal HFSE Mineral Deposits

Five occurrences of hydrothermal HFSE mineralization were investigated. These deposits were selected because the role of hydrothermal processes in their formation has been indicated by previous studies.

Strange Lake, Quebec/Labrador

The Mesoproterozoic Strange Lake peralkaline complex, which is located along the Quebec/Labrador border, approximately 150 km west of Nain, Labrador, and 250 km northeast of Schefferville, Quebec, hosts one of the largest occurrences of Zr-REE-Y-Nb-Be mineralization in the world. The pluton and associated HFSE mineralization have been described by Zajac et al. (1984a; b), Currie (1985), Miller (1985; 1986; 1988; 1990; 1996), Pillet (1985), Pillet et al. (1989; 1992), Hill and Miller (1990), Salvi and Williams-Jones (1990; 1991; 1992; 1995; 1996; 1997; 2005), Birkett and Miller (1991), Birkett et al. (1992), Nassif and Martin (1991), Nassif (1993), Boily and Williams-Jones (1994), and Miller et al. (1997).

Although the entire intrusion contains anomalously high concentrations of HFSE (Zajac et al., 1984; Miller, 1986; Salvi and Williams-Jones, 1996), the most

enriched rocks occur in the north-central part of the pluton, within relatively small zones that exhibit mineralogical and chemical evidence of secondary, hydrothermal alteration (Salvi and Williams-Jones, 1990; 1995; 1996). The most significant individual occurrence of HFSE mineralization (the main lens, Miller, 1986) is a layered, approximately dome-shaped body that averages 6 to 10 meters in thickness, has an approximate area and volume of 0.75 km^2 and 0.175 km^3, respectively (Miller, 1996), and has been partly eroded. Miller (1986) concluded that the main lens formed from an incompatible element-enriched silicate melt that was emplaced into the upper portions of the subsolvus granite. Miller (1986) noted the presence of chemical zoning within the granite that is independent of the apparently primary magmatic layering, but did not interpret its origin. Salvi and Williams-Jones (1990; 1992; 1996) attributed this zoning to hydrothermal processes, and showed that most of the subsolvus granite underwent at least two episodes of hydrothermal alteration. Whole-rock mass-balance calculations conducted by Salvi and Williams-Jones (1996), however, indicate that hydrothermal processes resulted in HFSE enrichment that was typically greater than 20 wt % more than in unaltered rocks, and occurred on a scale that was large enough to create a potential ore deposit comprising approximately 30 million tonnes grading 3.25 % ZrO_2, 0.66 % Y_2O_3, 0.56 % Nb_2O_5, 0.12 % BeO and 1.30 % REE (Iron Ore Company of Canada, unpublished data).

The primary mineralogical change associated with HFSE mineralization in the Strange Lake pluton has been reported to be the replacement of magmatic HFSE silicates by hydrothermal phases, e.g., elpidite by gittinsite, through a Na-Ca exchange reaction (Salvi and Williams-Jones, 1995). This replacement was accompanied by hematization of the host granite and pegmatite (Miller, 1996; Salvi and Williams-Jones, 1996). Although hydrothermal processes played a role in HFSE mobility and enrichment in the Strange Lake pluton, the processes causing extreme HFSE enrichment in excess of replacement of elpidite by gittinsite, and the genetic link, if any, to alteration (hematization), are poorly understood. The evidence of hydrothermal HFSE mobility and enrichment (e.g.,

Salvi and Williams-Jones, 1996) make the Strange Lake pluton an ideal candidate for evaluating HFSE transport by aqueous fluids.

Gallinas Mountains, New Mexico

Rare element mineralization in the Gallinas Mountains district of east-central New Mexico has been described by Perhac and Heinrich (1964), Schreiner (1993), and Williams-Jones et al. (2000). Fluorite-REE mineralization is associated with Oligocene felsic intrusive bodies and occurs within breccia pipes and fault-hosted breccias hosted by these intrusive rocks and the country rocks. Fluorite, the predominant mineral in the breccia matrix, occurs with REE minerals (mainly bastnäsite), quartz, barite, calcite, pyrite and hematite. In the Pinatosa deposit, a 100-meter wide breccia pipe hosted by quartz syenite, three generations of fluorite (P1, P2 and P3) have been identified (Williams-Jones et al., 2000). The earliest, P1, is rimmed and replaced by P2, P3 fluorite replaces and forms the matrix to P1 and P2 fluorite and other minerals.

Williams-Jones et al. (2000) proposed that the fluorite-REE mineralization formed as a result of the progressive mixing of magmatic fluids with formation waters on the basis of data obtained from fluorite-hosted fluid inclusions. No information was available, however, on the differences in the compositions of the three generations of fluorite or what implications the composition of the fluorite might have on hydrothermal fluid source(s) or evolution.

South Platte, Colorado

The South Platte district rare-element mineralization in central Colorado has been described by Simmons and Heinrich (1980), Simmons et al. (1987) and Levasseur (1997). The mineralization occurs within concentrically-zoned, REE-F-Y-Nb-U-enriched granitic pegmatites hosted by the Proterozoic, anorogenic Pikes Peak granitic batholith (Hedge, 1970; Simmons and Heinrich, 1970; 1980; Simmons et al., 1987). Some of the zoned pegmatites contain secondary hydrothermal replacement minerals that include fluorite (Simmons and Heinrich, 1970; 1980; Brewster, 1986). Six varieties of fluorite have been identified -

primary (magmatic) green, and secondary (hydrothermal) purple, colorless, white, brown and gray (Simmons and Heinrich, 1980). The deposits occur entirely within, and are genetically linked to, the host granitic batholith. Levasseur (1997) and Levasseur and Samson (1996) interpreted the REE in the hydrothermal fluorite to have been leached from the primary green fluorite by magmatic solutions.

Although some preliminary fluid inclusion microthermometric analyses have been conducted (e.g., Levasseur, 1997), very little is known about the composition and source(s) of the fluids responsible for the formation of the fluorite-REE mineralization. Furthermore, although spatially associated with pegmatites, the relationship between the secondary hydrothermal mineralization and pegmatite formation, if any, is unclear.

St. Lawrence, Newfoundland

The St. Lawrence fluorspar deposits in southeastern Newfoundland have been described by Van Alstine (1948), Strong et al. (1984) and Collins and Strong (1988). The deposits comprise fluorite veins that mostly occur within the Lower Carboniferous St. Lawrence granitic pluton (e.g., Iron Springs vein) and related porphyry dikes (e.g., Grebe's Nest vein), but which also extend into the country rocks (e.g., Lawn Barite vein) (Strong et al., 1984; Collins and Strong, 1988). The veins are genetically linked to the granitic pluton and formed as open-space fillings in tension fractures caused by cooling of the granite (Van Alstine, 1948). Fluorite is the predominant vein mineral and has well-developed colored growth-zones (Strong et al., 1984). Quartz, calcite, minor chalcopyrite, sphalerite, galena, and rare barite also occur within the veins. Strong et al. (1984) and Collins and Strong (1988) presented genetic models in which fluorite deposition occurred as a result of cooling or boiling of fluid, or mixing of formation water with magmatic fluid.

The St. Lawrence fluorite veins differ from the other deposits included in this thesis because fluorite generally was the only REE-bearing mineral to precipitate from the hydrothermal fluid. Therefore, the veins present a unique

opportunity to examine the compositional evolution of a REE-bearing orthomagmatic fluid, as indicated by the compositional evolution of fluorite, without the complication of coprecipitating, HFSE-bearing mineral phases complicating elemental partitioning.

Rock Canyon Creek, British Columbia

The Rock Canyon Creek rare element mineralization in southeastern British Columbia has been described by Pell and Hora (1987), Samson et al. (2000), and Samson et al. (2001). Fluorite-REE mineralization occurs mainly as an elongate, approximately strata-parallel zone hosted by predominantly Ordovician- and Devonian-aged limestone and dolomite. Mineralization comprises early, fine-grained, patchy, disseminated, purple-colored fluorite and later vein and breccia-matrix, yellow- and purple-colored fluorite (Samson et al., 2001). REE minerals (mostly synchysite and parisite) are associated with the early, disseminated fluorite. Barite, quartz, carbonate, pyrochlore and Nb-bearing rutile occur with the fluorite and REE minerals (Samson et al., 2001).

Although a magmatic association has not been documented in the field, the geochemical, mineralogic and isotopic character of the deposit indicates fluid derivation from alkalic magma (Pell and Hora, 1987; Samson et al., 2001). Precipitation of the disseminated fluorite-REE mineralization is thought to have resulted from interaction of F- and REE-bearing hydrothermal fluids with carbonate wall rocks (Samson et al., 2001).

LA-ICPMS Analysis

Introduction

Conceptual models have been developed to explain the formation of many hydrothermal HFSE mineral deposits. These models are, however, largely based on qualitative to semi-quantitative empirical data, and the factors controlling the formation of many of these deposits (e.g., fluid source and composition, causes of mineral precipitation) remain poorly understood. To better understand the genesis of hydrothermal HFSE mineral deposits, it is necessary to accurately and precisely determine the physicochemical conditions under which HFSE minerals are formed. To accomplish this, the temporal and spatial variations in the composition, temperature and pressure of the fluid systems (i.e., fluid architecture) responsible for the formation of hydrothermal HFSE mineral deposits need to be determined.

Laser ablation ICP-MS has emerged as one of the leading microanalytical techniques for obtaining quantitative analyses of minerals and fluid inclusions. The first use of lasers for sampling earth and other solid materials dates from the 1980s and early 1990s (e.g., Gray 1985, Arrowsmith 1987, Moenke-Blankenburg et al. 1990, Jackson et al. 1992, Longerich et al. 1993). The products of the interaction of laser radiation with samples are numerous and include heating, melting, vaporization, atomization, excitation and ionization (Fabre et al. 2002). The result is that ablation can occur in a controlled or explosive manner depending on the characteristics of the material being ablated and the wavelength of the laser radiation. Consequently, numerous analytical challenges result from the complexity of the interaction of laser energy with samples (e.g., elemental fractionation, explosive opening of fluid inclusions) (Fryer et al., 1995; Günther et al., 1998).

Despite improvements in LA-ICP-MS systems, significant analytical challenges remain in conducting routine, representative analysis of minerals and fluid inclusions. Some of these challenges affect all LA-ICP-MS systems (e.g., removal of host mineral contributions to fluid inclusion signals, conducting

analyses without having to use an internal standard), while others (e.g., explosive opening of fluid inclusions) tend to affect LA-ICP-MS systems that incorporate longer wavelength lasers (e.g., 266 nm Nd:YAG) to a greater degree than shorter wavelength lasers (e.g., 193 nm ArF Excimer). Development of LA-ICPMS methods specifically designed to address these limitations is required in order to obtain accurate and precise analytical data on a routine basis and to ensure that valid conclusions are made regarding the factors controlling the formation of hydrothermal HFSE mineral deposits or any other system studied.

Analysis of Poorly-absorbing Materials

Two approaches have been employed in laser ablation systems in order to provide for more controlled ablation of poorly-absorbing minerals (e.g., quartz, fluorite, and calcite): 1) shortening of the wavelength of the laser energy (i.e., from the infrared to the ultraviolet) (Jackson, 2001; Günther, 2001), and 2) beam homogenization (Guillong et al., 2002; Günther et al., 1998). The ability to ablate transparent minerals has improved dramatically, however, difficulties remain for representative sampling of some minerals (e.g., fluorite) using 266 nm Nd:YAG LA-ICP-MS systems. Consequently, obtaining representative analyses of fluid inclusions in fluorite can be problematic using this type of system.

The poor absorption of the laser energy from 266 nm Nd:YAG systems results, in part, from the Gaussian energy distribution within the laser beam. Beam homogenization of 193 nm ArF Excimer laser systems has been shown to create a homogeneous energy distribution across the entire ablation pit, which results in controlled and more uniform ablation (Günther et al., 1998). Similar improvements in ablation properties, without loss of beam coherence or significant amounts of energy, can be obtained using a non-homogenized Nd:YAG laser beam and installing beam constrictors (i.e., irises) in the beam path. The beam constrictors trim the outer, lower energy portion of the Gaussian energy distribution which results in more uniform ablation and reduced elemental fractionation (Crowe et al. 2003). Using a trimmed, non-homogenized Nd:YAG beam preserves the high energy core of the beam, allows for sizing of the beam

to match the desired diameter for mineral or fluid inclusion analysis and, for relatively small diameter constrictors centered on the core of the beam, approximates a beam with uniform energy distribution.

The improved ablation characteristics of fluorite using a 266 nm Nd:YAG laser system equipped with an iris enables more controlled ablation of fluorite. Representative sampling of fluorite is important because the trace element composition of fluorite from hydrothermal mineral deposits has been used to identify fluid sources (e.g., magmatic versus formation waters), evaluate depositional mechanisms, develop conceptual genetic models, and make inferences about the ore potential of individual deposits and the regions in which they occur (e.g., Möller et al., 1976; Richardson and Holland, 1979; Eppinger and Closs, 1990; Hill et al., 2000). Most of these interpretations, however, are based on the bulk composition of fluorite crystals, which commonly show fine-scale color banding (e.g., Strong et al., 1984), suggesting the possibility that the trace-element distribution varies on a fine scale.

Fluid Inclusion Analysis

A number of studies of fluid inclusions have been performed using LA-ICP-MS (e.g., Shepherd & Chenery 1995, Moissette et al. 1996, Ghazi et al. 1996, Audetat et al. 1998, Samson et al. 1998, Shepherd et al. 1998, Günther et al. 1998, Heinrich et al. 1999, Ulrich et al. 1999, Audetat et al. 2000, Muller et al. 2001, Gagnon et al. 2002, Landtwing et al. 2002, Heinrich et al. 2002, Audetat & Pettke 2003). The earlier investigations generally comprised reconnaissance studies and presented analytical results in terms of element ratios rather than concentrations. Later investigations (e.g., Audetat et al. 1998, Günther et al. 1998, Heinrich et al. 1999, Ulrich et al. 1999, Audetat et al. 2000, Gagnon et al. 2002, Landtwing et al. 2002, Audetat & Pettke 2003) used measurements of total salinity, obtained through microthermometric analysis, to determine the concentration of Na, which was subsequently used as an internal standard against which all other elemental concentrations within the fluid inclusion were calculated.

Improvements in the ability to conduct controlled ablation using a 266 nm Nd:YAG-based system equipped with an iris also contributes to more representative sampling of fluid inclusions within transparent minerals. Despite the ability to conduct controlled opening of fluid inclusions, it is impossible to perform LA-ICP-MS analysis of fluid inclusions without including some of the host mineral. Even minerals that are generally considered to be compositionally simple (e.g., quartz), may contain concentrations of trace elements sufficient to affect the accuracy of fluid inclusion compositions (Samson et al. 2003). Fluid overpressures created within a fluid inclusion at the point of opening may cause a burst of sample comprising a mixture of host mineral and fluid inclusion material that is disproportionate to the mixture of host mineral and fluid inclusion that would be introduced to the ICP-MS under controlled ablation, thus contributing to the host mineral effect on the fluid inclusion signal. This sudden introduction of material to the ICP-MS will affect the concentrations calculated from the fluid inclusion spectra unless the data are corrected prior to final calculation of the fluid inclusion composition. Subtraction of the host mineral background counts from the fluid inclusion signal is not always adequate to correct for a significant host mineral contribution and an alternate method is required to remove these contributions. Therefore, data reduction protocols are necessary that remove the contribution of the host mineral to the fluid inclusion signal in order to obtain quantitative fluid inclusion analyses.

Standardless Analysis

Quantitative analysis of silicates by LA-ICPMS typically has been limited to the determination of minor and trace element concentrations using an internal standard estimated from stoichiometry (e.g., element proportion in an 'ideal' mineral formula) or obtained using another analytical method (e.g., electron microprobe). Alternative methods of standardization, such as simultaneous addition of desolvated liquid standards (Leach et al., 1999; Halicz and Günther, 2004), also have been used. These quantification techniques require that the concentration of at least one element in unknown samples be analyzed

independently, and add a degree of complexity to LA-ICPMS analyses, potentially contribute to problematic molecular ion interferences (e.g., oxides, hydrides), or may preclude quantitative analysis of some elements (e.g., Cu, Halicz and Günther, 2004). Precise and accurate methods for determining major, minor and trace element concentrations in silicates are required that are simple, do not necessarily rely on internal standards, and do not contribute to problematic interferences. This would allow LA-ICPMS analysis of chemically complex, unknown materials.

Purpose and Organization

The composition of the fluid(s) responsible for HFSE deposits and the conditions controlling their formation are poorly understood. The purpose of this investigation is, therefore, to improve our understanding of the formation of these geologically and economically important deposits through the detailed petrographic and LA-ICPMS analysis of minerals and fluid inclusions from a number of hydrothermal HFSE deposits. Unfortunately, the gangue minerals that are associated with many occurrences of HFSE mineralization, and that are often the primary host to the fluid inclusions of interest, do not absorb 266 nm Nd:YAG laser radiation well (e.g., quartz) and/or have complex compositions that potentially interfere with the quantitative analysis of the fluid inclusions (e.g., fluorite). The result of these deleterious host mineral properties and influences is non-representative sampling of minerals and fluid inclusions. Therefore, a major portion of this study involved the development of laser ablation sampling and data reduction protocols that are intended to overcome these limitations. Accurate inferences regarding the genesis of hydrothermal HFSE deposits can only result from accurate and precise LA-ICPMS analysis of fluid inclusions and minerals from these deposits.

This thesis is divided into seven chapters. Chapter 1 presents a review of the relevant literature and outlines the objectives and organization of the thesis. Chapter 2 presents the results of an investigation of the composition of fluorite

from four localities (Gallinas Mountains, New Mexico; Rock Canyon Creek, British Columbia; South Platte, Colorado, and St. Lawrence, Newfoundland). The study includes the development of a beam constriction device (i.e., iris) that was used to trim off the outer, lower-energy edge of the laser beam. This resulted in much more controlled ablation of fluorite, which is critical to obtaining representative sampling of fluid inclusions (Chapter 4). The data obtained on the spatial and paragenetic variability in the composition of fluorite from these four localities are used to make inferences about the geologic affinity of the fluorite, source(s) and compositional evolution of the hydrothermal fluid, and the general usefulness of fluorite as a guide to exploration.

A review of the 'state of the science' regarding LA-ICPMS analysis of fluid inclusions is presented in Chapter 3. The chapter includes an overview of LA-ICPMS and alternative methods and instrumentation for fluid inclusion analysis, project design, approaches to standardization, inclusion opening techniques, data reduction and analysis, and method limitations. Included in this chapter is a novel technique for quantitatively removing the contribution to the fluid inclusion signal from a compositionally complex host mineral (i.e., fluorite). Application of the technique to the quantitative analysis of fluid inclusions in fluorite is presented in a subsequent chapter (Chapter 4).

The South Platte district, Colorado is a major pegmatite district and host to numerous (> 50) individual occurrences of fluorite-REE mineralization within zoned pegmatites. Chapter 4 presents the results of a LA-ICPMS investigation of fluid inclusions hosted within quartz and fluorite from one of the best examples of fluorite-REE mineralization in the district (the Oregon No. 3 pegmatite). The technique developed in Chapter 3 is applied to the analysis of fluorite-hosted fluid inclusions and differences and trends in the fluid inclusion compositions are used to make inferences regarding the possible sources and relationships of the hydrothermal fluids, causes of compositional variation in the hydrothermal fluids, and the timing and causes of fluorite-REE mineralization.

A major limitation of LA-ICPMS analysis is the need to obtain the concentration of at least one element in the material being ablated that can be used as an internal standard to correct for differences in the rate of ablation between the unknown sample and the external calibration standard. Historically, the internal standard has been estimated using another analytical technique (e.g., electron microprobe or microthermometry, Chapter 4), or using the element proportion based on an 'ideal' mineral formula (i.e., mineral stoichiometry, Chapter 2). Unfortunately, mineral compositions can change significantly over very small scales (e.g., growth zones, cf. Chapter 2; or zones of alteration along fractures, cf. Chapter 6) or analysis of an unknown mineral phase or solid inclusion may be desired (Chapter 6). These situations make estimating an internal standard element concentration using mineral stoichiometry impossible or use of an alternative analytical method infeasible or undesirable. A method for obtaining quantitative analyses of minerals using LA-ICPMS without using an internal standard is developed in Chapter 5. The applicability of this method is demonstrating by analyzing synthetic silicate glass standard reference materials and a natural, compositionally-complex silicate mineral (arfvedsonite). This method expands the application of LA-ICPMS analysis to the determination of quantitative element concentrations in unknown, silicate materials.

Chapter 6 presents the results of a detailed petrographic and LA-ICPMS investigation of minerals from the Strange Lake peralkaline complex. This intrusion is host to one of the largest HFSE deposits in the world in which the involvement of hydrothermal processes in concentrating HFSE was documented previously (e.g., Salvi and Williams-Jones, 1996). The relationship between HFSE enrichment and hematization is poorly understood, and the mineralogical changes accompanying HFSE enrichment in excess of that resulting from the pseudomorphous replacement of a magmatic (elpidite) by a hydrothermal (gittinsite) zirconosilicate mineral have not been documented. This chapter presents detailed petrographic evidence and the results of LA-ICPMS analysis of minerals and alteration products which clearly document the relationship between hematization and HFSE enrichment. The compositions of minerals and

alteration zones within minerals were determined using the method developed in Chapter 5. The chemical changes between unaltered and altered minerals are used to characterize, in a semi-quantitative manner, which element concentrations increased and which decreased as a result of the hydrothermal alteration. These results are compared with the whole rock data presented by Salvi and Williams-Jones (1996).

Chapter 7 presents a summation of the conclusions of the thesis and contributions to knowledge, and provides recommendations for additional investigation.

Bibliography

Arrowsmith, P. (1987): Laser ablation of solids for elemental analysis by inductively coupled plasma mass spectrometry. *Analytical Chemistry,* **59**, 1437-1444.

Audetat, A., Günther, D. and Heinrich, C.A. (1998): Formation of Magmatic-Hydrothermal Ore Deposits: Insights with LA-ICP-MS Analysis of Fluid Inclusions. *Science,* **279**, 2091-2094.

Audetat, A., Günther, D. and Heinrich, C.A. (2000): Causes for large-scale metal zonation around mineralization plutons: Fluid inclusion LA-ICP-MS evidence from the Mole Granite, Australia. *Economic Geology,* **95**, 1563-1581.

Audetat, A. and Pettke, T. (2003): The magmatic-hydrothermal evolution of two barren granites: A melt and fluid inclusion study of the Rito del Medio and Canada Pinabete plutons in northern New Mexico (USA). *Geochimica et Cosmochimica Acta,* **67**, 97-121.

Birkett, T.C. and Miller, R.R. (1991): The role of hyrothermal processes in the granite-hosted Zr, Y, REE deposit at Strange Lake, Quebec/Labrador; evidence from fluid inclusions; discussion. *Geochimica et Cosmochimica Acta*, **55**. 3433-3449.

Birkett, T. C., Miller, R.R., Roberts, A.C., and Mariano, A.N. (1992): Zirconium-bearing minerals of the Strange Lake Intrusive Complex, Quebec-Labrador. *Canadian Mineralogist*, **30**, 191-205.

Boily, M. and Williams-Jones, A.E. (1994): The role of magmatic and hydrothermal processes in the chemical evolution of the Strange Lake plutonic complex, Quebec-Labrador. *Contributions to Mineralogy and Petrology*, **118**, 33-47.

Brewster, R.H. (1986): The distribution and chemistry of rare-earth minerals in the South Platte pegmatite district, Colorado, and their genetic implications. M.S. thesis, Univ. of New Orleans, New Orleans, Louisiana, 139 p.

Collins, C.J., and Strong, D.F. (1988): A fluid inclusion and trace element study of fluorite veins associated with the peralkaline St. Lawrence Granite, Newfoundland. *Canadian Institute of Mining and Metallurgy*, Special Volume **39**, 291-302.

Crowe, S.A., Fryer, B.J., Samson, I.M. and Gagnon, J.E. (2003): Precise Isotope Ratio Determination of Common Pb Using Quadrupole LA-ICP-MS with Optimized Laser Sampling Conditions and a Robust Mixed-Gas Plasma. *Journal of Analytical Atomic Spectrometry*, **18**, 1331-1338.

Currie, K.L. (1985): An unusual peralkaline granite near Lac Brisson, Quebec-Labrador. *Geological Survey of Canada Paper* **85-1A**, 73-80.

Eppinger, R.G., and Closs, L.G. (1990): Variations of trace elements and rare earth elements in fluorite: a possible tool for exploration. *Economic Geology*, **85**, 1896-1907.

Fabre, C., Boiron, M.-C., Dubessy, J., Cathelineau, M. and Banks, D.A., (2002): Paleofluid chemistry of a single fluid event: bulk and in-situ multi-technique analysis (LIBS, Raman Spectroscopy) of an Alpine fluid (Mont-Blanc). *Chemical Geology,* **182**, 249-264.

Floyd, P.A. and Winchester, J.A. (1975): Magma type and tectonic setting discrimination using immobile elements. *Earth and Planetary Science Letters*, **27**, 211-218.

Floyd, P.A. and Winchester, J.A. (1978): Identification and discrimination of altered and metamorphosed volcanic rocks using immobile elements. *Chemical Geology*, **21**, 291-306.

Fryer, B.J., Jackson, S.E. and Longerich, H.P. (1995): The design, operation and role of the laser-ablation microprobe coupled with an inductively coupled plasma – mass spectrometer (LAM-ICP-MS) in the earth sciences. *The Canadian Mineralogist*, **33**, 303-312.

Fujimoto, K., Tanaka, H., Higuchi, T., Tomida, N., Ohtani, T., and Ito, H. (2001): Alteration and mass transfer inferred from the Hirabayashi GSJ drill penetrating the Nojima Fault, Japan. *The Island Arc*, **10**, 401-410.

Gagnon, J.E., Samson, I.M., Fryer, B.J. and Williams-Jones, A.E. (2002): Hydrothermal fluids in NYF pegmatites, South Platte, Colorado – preliminary insights from LA-ICP-MS analysis of quartz- and fluorite-hosted fluid inclusions. 8th Biennial Pan-American Conference on Research on Fluid Inclusions, Program with Abstracts, 25-27.

Ghazi, A.M., McCandless, T.E., Vanko, D.A. and Ruiz, J. (1996): New quantitative approach in trace elemental analysis of single fluid inclusions: Applications of laser-ablation inductively coupled plasma-mass spectrometry (LA-ICP-MS). *Journal of Analytical Atomic Spectrometry,* **11**, 667-674.

Gray, A.L. (1985): Solid sample introduction by laser ablation for inductively coupled plasma source mass spectrometry. *Analyst,* **110**, 551-556.

Guillong, M., Horn, I. and Günther, D. (2002): Capabilities of a homogenized 266 nm Nd:YAG laser ablation system for LA-ICP-MS. *Journal of Analytical Atomic Spectrometry,* **17**, 8-14.

Günther, D. (2001): Quantitative Fluid Inclusion Analysis Using a 193 nm Excimer Laser-Ablations System Coupled to ICP-MS. *In* Laser-Ablation-ICPMS in the Earth Sciences Principles and Applications (P. Sylvester, ed.), *Mineralogical Association of Canada, Short Course* **29**, 47-61.

Günther, D., Audétat, A., Frischknecht, R. and Heinrich, C.A. (1998): Quantitative analysis of major, minor and trace elements in fluid inclusions using laser ablation-inductively coupled plasma-mass spectrometry (LA-ICP-MS). *Journal of Analytical Atomic Spectrometry,* **13**, 263-270.

Haas, J.R., Shock, E.L., and Sassani, D.C. (1995): Rare earth elements in hydrothermal systems: Estimates of standard partial molal thermodynamic properties of aqueous complexes of the rare earth elements at high pressures and temperatures. *Geochimica et Cosmochimica Acta*, **59**, 4329-4250.

Halicz, L. and Günther, D. (2004): Quantitative analysis of silicates using LA-ICP-MS with liquid calibration. *Journal of Analytical Atomic Spectrometry*, **19**, 1539-1545.

Hedge, C.E. (1970): Whole rock Rb-Sr age of the Pikes Peak Batholith, Colorado. U.S. Geological Survey, Professional Paper 700B, 86-89.

Heinrich, C.A., Günther, D., Audétat, A., Ulrich, T. and Frischknecht, R. (1999): Metal fractionation between magmatic brine and vapor, determined by microanalysis of fluid inclusions. *Geology*, **27**, 755-758.

Heinrich, C.A., Pettke, T., Halter, W., Aigner, M., Audétat, A., Günther, D., Hattendorf, B., Bleiner, D., Guillong, M. and Horn, I. (2002): Quantitative Multi-element Analysis of Minerals, Fluid and Melt Inclusions by Laser Ablation Inductively-Couple-Plasma Mass-Spectrometry. 8th Biennial Pan-American Conference on Research on Fluid Inclusions, Program with Abstracts, 38.

Hill, G.T., Campbell, A.R., and Kyle, P.R. (2000): Geochemistry of southwestern New Mexico fluorite occurrences: implications for precious metals exploration in fluorite-bearing systems. *J. of Geochem. Exp.* **68**, 1-20.

Hill, J.D. and Miller, R.R. (1990): A review of Middle Proterozoic epigenic felsic magmatism in Labrador. *In* Mid-Proterozoic Laurentia – Baltica (C.F. Gower, T. Rivers and B. Ryan, eds.), *Geological Association of Canada Special Paper* **38**, 417-431.

Jackson, S.E. (2001): The Application of Nd:YAG Lasers in LA-ICP-MS. *In* Laser-Ablation-ICPMS in the Earth Sciences Principles and Applications (P. Sylvester, ed.), *Mineralogical Association of Canada, Short Course* **29**, 29-45.

Jackson, S.E., Longerich, H.P., Dunning, G.R. and Fryer, B.J. (1992): The application of laser ablation microprobe-inductively coupled plasma-mass spectrometry (LAM-ICP-MS) to in situ trace element determinations in minerals. *Canadian Mineralogist,* **30**, 1049-1064.

Kovalenko, V.I., Tsaryeva, G.M., Goreglyad, A.V., Yarmoluk, V.V., and Troitsky, V.A. (1995): The peralkaline-granite related Khaldzan-Buregtey Rare metal (Zr, Nb, REE) deposit, Western Mongolia. *Economic Geology*, **90**, 530-547.

Landtwing, M.R., Redmond, P.B., Einaudi, M.T., Heinrich, C.A., Halter, W.E. and Pettke, T. (2002): Veining, Timing of Sulphide Deposition and Fluid Evolution at the Bingham Cu-Au-Mo-Ag Porphyry Deposit – Fluid Inclusion LA-ICP-MS Results. 8th Biennial Pan-American Conference on Research on Fluid Inclusions, Program with Abstracts, 49-50.

Leach, J.J., Allen, L.A., Aeschliman, D.B., and Houk, R.S. (1999): Calibration of Laser Ablation Inductively Coupled Plasma Mass Spectrometry Using Standard Additions with Dried Solution Aerosols. *Analytical Chemistry*, **71**, 440-445.

Levasseur, R.L. (1997): *Fluid Inclusion Studies of Rare Element Pegmatites, South Platte District, Colorado.* M.Sc. thesis, Univ. of Windsor, Windsor, Ontario.

Levasseur, R.L., and Samson, I.M. (1996): Fluid inclusion characteristics of REE-Y-Nb pegmatites, South Platte district, Colorado (abs.): Programs with Abstracts, v. 21, Geological Association of Canada – Mineralogical Association of Canada Annual Meeting, Winnipeg, A56.

Longerich, H.P., Jackson, S.E., Fryer, B.J. and Strong, D.F. (1993): The laser ablation microprobe-inductively coupled plasma-mass spectrometer. *Geoscience Canada,* **20**, 21-27.

MacLean, W.H. (1988): Rare earth mobility at constant inter-REE ratios in the alteration zone at the Phelps Dodge Massive Sulfide Deposit, Mattagami, Quebec. *Mineralium Deposita*, **23**, 231-238.

MacLean, W.H. (1990): Mass change calculations in altered rock series. *Mineralium Deposita*, **25**, 44-49.

Migdisov, A.A. and Williams-Jones, A.E. (2002): A spectrophotometric study of neodymium(III) complexation in chloride solutions. *Geochimica et Cosmichimica Acta*, **66**, 4311-4323.

Miller, R.R. (1985): Geology of the Strange Lake alkalic complex and the associated Zr-Y-Nb-Be-REE mineralization. *In* Granite-Related Mineral Deposits: Geology, Petrogenesis and Tectonic Setting (R.P. Taylor and D.F. Strong, eds.), *Canadian Institute for Mining and Metallurgy, Extended Abstract,* 193-196.

Miller, R.R. (1986): Geology of the Strange Lake Alkalic Complex and the associated Zr-Y-Nb-Be-REE mineralization. *Newfoundland Department of Mines, Mineral Development Division,* Report **86-1**, 11-19.

Miller, R.R. (1988): Yttrium (Y) and other rare metals (Be, Nb, REE, Ta, Zr) in Labrador. *Newfoundland Department of Mines, Mineral Development Division,* Report **88-1**, 229-245.

Miller, R.R. (1990): The Strange Lake pegmatite-aplite hosted rare-metal deposit, Labrador, *Newfoundland Department of Mines and Energy, Geological Survey Branch*, Report **90-1**, 171-182.

Miller, R.R. (1996): Structural and textural evolution of the Strange Lake peralkaline rare-element (NYF) granitic pegmatite, Quebec-Labrador, *The Canadian Mineralogist*, **34**, 349-371.

Miller, R.R., Heaman, L.M., and Birkett, T.C. (1997): U-Pb zircon age of the Strange Lake peralkaline complex: implications for Mesoproterzoic peralkaline magmatism in north-central Labrador. *Precambrian Research*, **81**, 67-92.

Möller, P., Parekh, P.P., and Schneider, H. J. (1976): The Application of Tb/Ca-Tb/La Abundance Ratios to Problems of Fluorospar Genesis. *Mineralium Deposita,* **11**, 111-116.

Moenke-Blankenburg, L., Gäckle, M., Günther, D. and Kammel, J. (1990): Processes of laser ablation and vapour transport to the ICP. *In* Plasma Source Mass Spectrometry, Proc. Third Surrey Conf. on Plasma Source Mass Spectrometry (K.E. Jarvis, A.L. Gray, I. Jarvis and J. Williams, eds.). The Royal Society of Chemistry, Cambridge, U.K., 1-17.

Moissette, A., Shepherd, T.J. and Chenery, S.R. (1996): Calibration Strategies for the Elemental Analysis of Individual Aqueous Fluid Inclusions by Laser Ablation-Inductively Coupled Plasma-Mass Spectrometry. *Journal of Analytical Atomic Spectrometry,* **11**, 177-185.

Munker, C., Wömer, G., Yogodzinski, G., and Churikova, T. (2004): Behavior of high field strength elements in subduction zones: constraints from Kamchatka-Aleutian arc lavas. *Earth and Planetary Science Letters*, **224**, 275-293.

Nassif, G.J. (1993): *The Strange Lake Peralkaline Complex, Quebec-Labrador: the Hypersolvus-Subsolvus Granite Transition and Feldspar Mineralogy.* M.Sc. thesis, McGill University, Montreal, Quebec.

Nassif, G.J., and Martin, R.F. (1991): The hypersolvus granite-subsolvus granite transition at Strange Lake, Quebec-Labrador. *GAC-MAC-CSPG Annual Meeting Toronto,* **A89** (abstract).

O'Hara, K. and Blackburn, W.H. (1989): Volume-loss model for trace-element enrichments in mylonites. *Geology*, **17**, 524-527.

Pearce, J.A. and Cann, J.R. (1973): Tectonic setting of basic volcanic rocks determined using trace element analysis. *Earth and Planetary Science Letters*, **19**, 290-300.

Pearce, J.A. and Norry, M.J. (1979): Petrogenetic implications of Ti, Zr, Y, and Nb variations in volcanic rocks. *Contributions to Mineralogy and Petrology*, **69**, 33-47.

Pell, J., and Hora, Z.D. (1987): Geology of the Rock Canyon Creek fluorite/rare earth element showing, southern Rocky Mountains. British Columbia Ministry of Energy, Mines and Petroleum Resources, Geological Fieldwork 1986, Paper 1987-1, 255-261.

Perhac, R.M., and Heinrich, E.W. (1964): Fluorite-bastnaesite deposits of the Gallinas Mountains, New Mexico and bastnaesite paragenesis. *Economic Geology,* **59**, 226-239.

Pillet, D. (1985): Le granite peralcaline du Lac Brisson, Territoire du Nouveau-Quebec: resultats preliminaries. Ministere de l'Energie et des Resources, Quebec, **MB 85-37**, SNRC 024A/08.

Pillet, D., Bonhomme, M.G., Duthou, J.L., and Chenevoy, M. (1989): Chronologie Rb/Sr et K/Ar du granite peralcalin du lac Brisson, Labrador central, Nouveau-Quebec. *Canadian Journal of Earth Science*, **26**, 328-332.

Pillet, D., Chenevoy, M., and Belanger, M. (1992): Petrologie du granite peralcalin du Lac Brisson, Labrador central, Nouveau-Quebec. I. Mode de mise en place et evolution chimique. *Canadian Journal of Earth Science*, **29**, 353-372.

Richardson C.K. and Holland, H.D., (1979): Fluorite deposition in hydrothermal systems. *Geochimica et Cosmochimica Acta*, **43**, 1327-1335.

Salvi, S., and Williams-Jones, A.E. (1990): The role of hydrothermal processes in the granite-hosted Zr, Y, REE deposit at Strange Lake, Quebec/Labrador: evidence from fluid inclusions. *Geochimica et Cosmochimica Acta*, **54**, 2403-2418.

Salvi S. and Williams-Jones, A.E. (1991): The role of hyrothermal processes in the granite-hosted Zr, Y, REE deposit at Strange Lake, Quebec/Labrador; evidence from fluid inclusions; reply. *Geochimica et Cosmochimica Acta*, **55**. 3433-3449.

Salvi, S., and Williams-Jones, A.E. (1992): Reduced orthomagmatic C-O-H-N-NaCl fluids in the Strange Lake rare-metal granitic complex, Quebec/Labrador, Canada. *European Journal of Mineralogy,* **4**, 1155-1174.

Salvi, S. and Williams-Jones, A.E. (1995): Zirconosilicate phase relations in the Strange Lake (Lac Brisson) pluton, Quebec-Labrador, Canada. *American Mineralogist*, **80**, 1031-1040.

Salvi, S. and Williams-Jones (1996): The role of hydrothermal processes in concentrating high-field strength elements in the Strange Lake peralkaline complex, northeastern Canada. *Geochimica et Cosmochimica Acta*, **60**, 1917-1932.

Salvi, S. and Williams-Jones, A.E. (1997): Fischer-Tropsch synthesis of hydrocarbons during sub-solidus alteration of the Strange Lake peralkaline granite, Quebec/Labrador, Canada. *Geochimica et Cosmochimica Acta*, **61**, 83-99.

Salvi, S., and Williams-Jones, A.E., (in press): Alkaline granite-syenite hosted deposits: in Linnen, R.L., and Samson, I.M., eds., *Rare-Element Geochemistry and Mineral Deposits*, Geological Association of Canada Short Course Notes, **17**, 315-341.

Salvi, S., Fontan, F., Monchoux, P., Williams-Jones, A.E., and Moine, B. (2000): Hydrothermal Mobilization of High Field Strength Elements in Alkaline Igneous Systems: Evidence from the Tamazeght Complex (Morocco). *Economic Geology*, **95**, 559-576.

Samson, I.M., and Wood, S.A., (in press): The rare-earth elements: Behaviour in hydrothermal fluids and concentration in hydrothermal mineral deposits, exclusive of alkaline settings: in Linnen, R.L., and Samson, I.M., eds., *Rare-Element Geochemistry and Mineral Deposits*, Geological Association of Canada Short Course Notes, **17**, 269-297.

Samson, I.M., Chen, Z., Fryer, B.J. and Walker, R.T. (1998): High sensitivity in situ analysis of cation/anion compositions of individual fluid inclusions by LAM-ICP-MS using a cold plasma ionization source. Abstracts with Programs **30**, Geol. Soc. Amer. Annual Meeting, Toronto, A-81.

Samson, I.M., Al-Aasm, I.S., and Zhu, L. (2000): Dolomitization and Mineralization in the Rock Canyon Creek fluorite-REE deposit, B.C.. Program and Abstracts, GeoCanada 2000, Calgary.

Samson, I.M., Kerr, I.D. and Graf, C. (2001): The Rock Canyon Creek fluorite-REE deposit, British Columbia. *In* Industrial Minerals in Canada. *Canadian Institute of Mining and Metallurgy, Special Volume* **53**, 1-10.

Samson, I.M., Fryer, B.J., and Gagnon, J.E. (2003): The trace element chemistry of hydrothermal quartz: a tool for paragenetic studies. GAC-MAC-SEG Joint Meeting, Vancouver.

Schreiner, R.A. (1993): Mineral investigation of the rare-earth-element-bearing deposits, Red Cloud mining district, Gallinas Mountains, Lincoln County, New Mexico: U.S. Bureau of Mines, Open File Report 99-93, 189 p.

Shepherd, T.J. and Chenery, S.R. (1995): Laser ablation ICP-MS elemental analysis of individual fluid inclusions: An evaluation study. *Geochimica et Cosmochimica Acta,* **59**, 3997-4007.

Shepherd, T.J., Ayora, C., Cendon, D.I., Chenery, S.R. and Moissette, A. (1998): Quantitative solute analysis of single fluid inclusions in halite by LA-ICP-MS and cryo-SEM-EDS: complementary microbeam techniques. *European Journal of Mineralogy,* **10**, 1097-1108.

Simmons, W.B., and Heinrich, E.W. (1970): Rare-earth-fluorine pegmatites of the South Platte district, Jefferson County, Colorado. Geological Association of Canada-Mineralogical Association of Canada, Joint Annual Meeting, Abstracts of Papers, 48-49.

Simmons, W.B., and Heinrich, E.W. (1980): Rare-earth pegmatites of the South Platte district, Colorado, Colorado Geological Survey, Department of Natural Resources, Resource Series **11**, 131 p.

Simmons, W.B., Lee, M.T., and Brewster, R.H. (1987): Geochemistry and evolution of the South Platte granite-pegmatite system, Jefferson County, Colorado. *Geochimica et Cosmochimica Acta*, **51**, 455-471.

Sørensen, H. (1992): Agpaitic nepheline syenites: a potential source of rare elements. *Applied Geochemistry*, **7**, 417-427.

Strong, D.F., Fryer, B.J., and Kerrich, R., 1984. Genesis of the St. Lawrence Fluorospar Deposits as Indicated by Fluid Inclusion, Rare Earth Element, and Isotopic Data. *Economic Geology,* **79**, 1142-1158.

Ulrich, T., Günther, D. and Heinrich, C.A. (1999): Gold concentrations of magmatic brines and the metal budget of porphyry copper deposits. *Nature,* **399**, 676-679.

Van Alstine, R.R. (1948): Geology and Mineral Deposits of the St. Lawrence Area, Burin Peninsula, Newfoundland: Geological Survey of Newfoundland, Bulletin 23, 64 p.

Williams-Jones, A.E. and Samson, I.M. (1990): Theoretical estimation of halite solubility in the system NaCl-$CaCl_2$-H_2O: Applications to fluid inclusions. *Canadian Mineralogist*, **28**, 299-304.

Williams-Jones, A.E., Samson, I.M., and Olivo, G.R. (2000): The Genesis of Hydrothermal Fluorite-REE Deposits in the Gallinas Mountains, New Mexico. *Economic Geology*, **95**, 327-342.

Wood, S.A. (1990): The aqueous geochemistry of the rare-earth elements and yttrium 2. Theoretical predictions of speciation in hydrothermal solutions to 350 °C at saturation water vapor pressure. *Chemical Geology*, **88**, 99-125.

Wood, S.A. (2003): The geochemistry of rare earth elements and yttrium in geothermal waters. *In* Simmons, S.F. and Graham, E., eds., Volcanic, Geothermal and Ore-Forming Fluids: Rulers and Witnesses of Processes within the Earth. *Society of Economic Geologists*, Special Publication **10**, 133-158.

Zajac, I.S., Miller, R.R., Birkett, T.C., and Nantel, S. (1984a): The Strange Lake deposit, Quebec-Labrador. *Canadian Institute for Mining and Metallurgy Bulletin*, **77**, 60 (abstract).

Zajac, I.S., Miller, R.R., Birkett, T.C., and Nantel, S. (1984b): Le gite de Zr, Y, Nb, et Be du complexe alcalin de Strange Lake, Quebec-Labrador. *Ministere de l'Energie et des Resources, Quebec*, **DV 84-18**, 127-142.

Chapter 2

Compositional Heterogeneity in Fluorite and the Genesis of Fluorite Deposits - Insights from LA-ICP-MS Analysis

Preface

Chapter 2 presents the results of an investigation of the composition of fluorite from four hydrothermal fluorite-REE mineral deposits: Gallinas Mountains, New Mexico; Rock Canyon Creek, British Columbia; South Platte, Colorado, and St. Lawrence, Newfoundland. The bulk composition of fluorite has been used widely to make inferences about the genesis of these types of deposits and as a guide to exploration. The obvious zoning and multiple stages of fluorite genesis in many of these deposits, however, indicate that the composition of fluorite likely varies on a small scale, potentially making use of bulk compositional data to make inferences regarding fluorite deposit genesis and affinity invalid. This chapter presents the results of a LA-ICPMS investigation of the microscale variation in the composition of fluorite from these four localities and attempts to use variations in the fluorite composition to make inferences regarding hydrothermal fluid source, composition and evolution.

Fluorite is a relatively poor absorber of laser radiation at 266 nm wavelength and the Gaussian energy distribution of Nd:YAG lasers results in inconsistent ablation across the ablation site. This leads to spalling, poor count rates and non-representative sampling of fluorite. Unlike Excimer lasers, beam homogenization for our Surelite I 266 nm Nd:YAG laser is not an option due to loss of coherence. In order to conduct representative laser sampling of fluorite, a pinhole device was developed that trims the relatively low energy portion of the outer edge of the laser beam. This improves the quality of the ablation and sensitivity. The ultimate goal of this study was to improve the ablation characteristics for sampling fluorite in order that representative sampling of fluid inclusions would be possible (Chapter 4).

Compositional Heterogeneity in Fluorite and the Genesis of Fluorite Deposits - Insights from LA-ICP-MS Analysis

Joel E. Gagnon[1], Iain M. Samson[2], Brian J. Fryer[2] and Anthony E. Williams-Jones[1]

[1] *Department of Earth and Planetary Sciences, McGill University, Montreal, Quebec, H3A 2A7*
[2] *Department of Earth Sciences, University of Windsor, Windsor, Ontario, N9B 3P4*

Abstract

Fluorite from four fluorite-REE mineral deposits has been analyzed using LA-ICP-MS to determine the viability of this method for fluorite and to assess spatial and paragenetic compositional heterogeneity in the fluorite. Two of the deposits studied have alkalic affinities (Gallinas Mountains, New Mexico and Rock Canyon Creek, British Columbia) and two are associated with granites (South Platte, Colorado and St. Lawrence, Newfoundland). This study shows that LA-ICP-MS is a valid technique for the analysis of fluorite and that the nature of, and controls on, the trace element content of fluorite are more complex than previously indicated from bulk analyses. Significant, small-scale (less than 2 mm) variation occurs in the trace element composition of fluorite within individual deposits. Patterns of trace element enrichment and depletion differ between, but are generally consistent within, individual deposits. Fluorite associated with alkalic magmatism is characterized by a flat to LREE-enriched chondrite-normalized REE pattern that lacks a negative Eu anomaly and has a positive Y anomaly. Fluorite associated with granitic magmatism is characterized by a flat to LREE-depleted chondrite-normalized REE pattern that has a negative Eu anomaly and a positive Y anomaly. With the exception of the Eu and Y anomalies, the chondrite-normalized REE patterns of the fluorite are similar to the associated intrusive rocks. Compositional heterogeneity of fluorite indicates that its use as a guide in classifying mineralization or in mineral exploration should be limited to instances where small-scale analyses (LA-ICP-MS) are available.

Introduction

The trace element composition of fluorite from hydrothermal mineral deposits has been used to identify fluid sources (e.g., magmatic versus formation waters), evaluate depositional mechanisms, develop conceptual genetic models, and make inferences about the ore potential of individual deposits and the regions in which they occur (e.g., Möller et al., 1976; Richardson and Holland, 1979; Eppinger and Closs, 1990; Hill et al., 2000). Most of these interpretations are based on the bulk composition of fluorite crystals, however, such crystals commonly show fine-scale colour banding (e.g., Strong et al., 1984), suggesting the possibility that the trace-element distribution varies on a fine scale.

The trace element composition of minerals, including fluorite, can now be quantitatively determined on small spatial scales ($\lesssim$ 10 μm) and to low elemental concentrations ($\lesssim$ μg/g) using laser ablation - inductively coupled plasma - mass spectrometry (LA-ICP-MS)(Jackson et al., 1992; Fryer et al., 1995). In order to assess the nature and magnitude of fine-scale variations in the trace-element chemistry of fluorite, the composition of fluorite from four mineral deposits was investigated using LA-ICP-MS analysis: Gallinas Mountains, New Mexico; Rock Canyon Creek, British Columbia; South Platte, Colorado, and St. Lawrence, Newfoundland. These deposits were selected because they represent a spectrum of fluorite-bearing mineral deposits associated with granitic and alkalic magmatism, and all contain multiple generations of fluorite. In this paper, we show that there can be significant variation in the trace-element chemistry of fluorite within deposits at a variety of scales, and that this variation has the potential to provide useful insights into mineralizing processes.

Geology of the Selected Mineral Deposits

Gallinas Mountains, New Mexico

Rare element mineralization in the Gallinas Mountains district of east-central New Mexico has been described by Perhac and Heinrich (1964), Schreiner (1993), and Williams-Jones et al. (2000). Fluorite-rare earth element

(REE) mineralization is associated with Oligocene felsic intrusive bodies and occurs within breccia pipes and fault-hosted breccias hosted by these intrusive rocks and the country rocks. Fluorite, the predominant mineral in the breccia matrix, occurs with REE minerals (mainly bastnäsite), quartz, barite, calcite, pyrite and hematite. In the Pinatosa deposit, a 100-meter wide breccia pipe hosted by quartz syenite, three generations of fluorite (P1, P2 and P3) have been identified (Williams-Jones et al., 2000). The earliest, P1, is rimmed and replaced by P2, P3 fluorite replaces and forms the matrix to P1 and P2 fluorite and other minerals. Williams-Jones et al. (2000) proposed that the mineralization formed as a result of the progressive mixing of magmatic fluids with formation waters.

Rock Canyon Creek, British Columbia

The Rock Canyon Creek rare element mineralization in southeastern British Columbia has been described by Pell and Hora (1987), Samson et al. (2000) and Samson et al. (2001). Fluorite-REE mineralization occurs mainly as an elongate, approximately strata-parallel zone hosted by predominantly Ordovician- and Devonian-aged limestone and dolomite. Mineralization comprises early, fine-grained, patchy disseminated fluorite and later vein and breccia-matrix fluorite (Samson et al., 2001). REE minerals (mostly synchysite and parisite) are associated with the early, disseminated fluorite. Barite, quartz, carbonate, pyrochlore and Nb-bearing rutile occur with the fluorite and REE minerals (Samson et al., 2001). Although a magmatic association has not been documented in the field, the geochemical, mineralogic and isotopic character of the deposit indicates fluid derivation from alkalic magma (Pell and Hora, 1987; Samson et al., 2001). Precipitation of the disseminated fluorite-REE mineralization is thought to have resulted from interaction of F- and REE-bearing hydrothermal fluids with carbonate wall rocks (Samson et al., 2001). Samples of early purple disseminated fluorite and later yellow and purple, zoned breccia-matrix and vein fluorite were included in this study.

South Platte, Colorado

The South Platte district rare-element mineralization in central Colorado has been described by Simmons and Heinrich (1980), Simmons et al. (1987) and Levasseur (1997). The mineralization occurs within concentrically-zoned, REE-F-Y-Nb-U-enriched granitic pegmatites hosted by the Proterozoic, anorogenic Pikes Peak granitic batholith (Hedge, 1970; Simmons and Heinrich, 1970; 1980; Simmons et al., 1987). Some of the zoned pegmatites contain secondary hydrothermal replacement minerals that include fluorite (Simmons and Heinrich, 1970; 1980; Brewster, 1986). Six varieties of fluorite have been identified - primary (magmatic) green, and secondary (hydrothermal) purple, colorless, white, brown and gray (Simmons and Heinrich, 1980). The deposits occur entirely within, and are genetically linked to, the host granitic batholith. Levasseur (1997) and Levasseur and Samson (1996) interpreted the REE in the hydrothermal fluorite to have been leached from the primary green fluorite by magmatic solutions. Samples of green, purple, colorless and white fluorite included in this study were obtained from the White Cloud and Oregon 3 pegmatites.

St. Lawrence, Newfoundland

The St. Lawrence fluorspar deposits in southeastern Newfoundland have been described by Van Alstine (1948), Strong et al. (1984) and Collins and Strong (1988). The deposits comprise fluorite veins that mostly occur within the Lower Carboniferous St. Lawrence granitic pluton and related porphyry dikes, but which also extend into the country rocks. The veins are genetically linked to the granitic pluton and formed as open-space fillings in tension fractures caused by cooling of the granite (Van Alstine, 1948). Fluorite is the predominant vein mineral and has well-developed coloured growth-zones (Strong et al., 1984). Quartz, calcite, minor chalcopyrite, sphalerite, galena, and rare barite also occur within the veins. Strong et al. (1984) and Collins and Strong (1988) presented genetic models in which fluorite deposition occurred as a result of cooling or boiling of fluid, or mixing of formation water with magmatic fluid. Samples of

fluorite included in this study were obtained from the Iron Springs, Grebe's Nest and Lawn Barite veins. The Iron Springs vein is located within the St. Lawrence granite and the Grebe's Nest and Lawn Barite veins are located within a granitic dike and the country rocks to the St. Lawrence granite, respectively (Strong et al., 1984; Collins and Strong, 1988). A summary of the locales and the types of fluorite studied is provided in Table 2-1.

Table 2-1 – Summary of Fluorite Varieties

Deposit	Magmatic Fluorite	Hydrothermal Fluorite
Alkalic-associated		
Gallinas Mountains	- -	P1 → P2 → P3*
Rock Canyon Creek	- -	Disseminated → Vein/Breccia* Replacement
Granite-associated		
South Platte	Green	Purple/White → Colorless*
St. Lawrence	- -	Grebe's Nest, Iron Springs, Lawn Barite

* Arranged in order of paragenesis.

LA-ICP-MS Analysis

Analysis of fluorite samples from Gallinas Mountains, Rock Canyon Creek, South Platte and the majority of the fluorite samples from St. Lawrence was conducted at the LA-ICP-MS facility in the Great Lakes Institute for Environmental Research at the University of Windsor. Some of the St. Lawrence fluorite samples were analyzed at the LA-ICP-MS facility in the Department of Earth Sciences at Memorial University of Newfoundland. Both facilities are equipped with solid-state, 266 nm Nd-doped yttrium aluminum garnet (Nd-YAG) pulsed lasers. Analyses were performed on doubly-polished wafers bonded to glass slides and all samples were cleaned prior to analysis by washing with distilled, deionized water and ethanol. Sample ablation was conducted within an argon-filled sampling cell mounted to the stage of a conventional polarizing microscope. The ablated material was transported from the ablation cell to the ICP-MS via argon carrier gas. Laser sampling locations on individual fluorite

grains were selected to minimize the possibility of encountering solid or liquid inclusions. Sampling locations included single spots for samples that exhibited a relatively high degree of visual heterogeneity, such as multiple generations of fluorite (Gallinas Mountains) or growth bands (St. Lawrence, Rock Canyon Creek), and traverses for samples that appeared relatively homogeneous (South Platte and St. Lawrence). Photomicrographs of typical laser ablation pits and traverses in fluorite from St. Lawrence are provided in Figure 2-1.

Fluorite analyses conducted at the University of Windsor were performed using a ThermoElemental PlasmaQuad-3 ICP-MS and those at Memorial University were performed using a Sciex ICP-MS. The fluorite samples were analyzed for most or all of the REE as well as a number of other elements. Calibration of the ICP-MS was accomplished using NIST glass standards 610 and 612. The conversion of the ICP-MS output data (counts/second) to concentration units (µg/g) was accomplished using the LAMTRACE program developed by S. E. Jackson (van Achterbergh et al., 2001). The stoichiometric proportion of Ca in ideal fluorite was used as an internal standard for the calculation of the trace element abundances. This choice is reasonable considering that in most cases fluorite comprises over 99% CaF_2 (Deer et al., 1992). Elements that readily substitute for Ca (Ce, Sr, and Y) were sought and generally found to occur at total concentrations of less than approximately 0.4 wt. % in our samples. A summary of the equipment specifications and general instrument operating conditions used during analysis of fluorite is provided in Table 2-2. An example of time-resolved spectra obtained from green fluorite from South Platte is provided in Figure 2-2, showing that several elements were detected at significant and relatively uniform count rates within fluorite indicating the presence of these elements within the fluorite structure and not as small solid or liquid inclusions within fluorite.

Figure 2-1. **A.** Photomicrograph of a thin section of Grebe's Nest vein fluorite from St. Lawrence, Newfoundland showing well-developed parallel growth bands, laser ablation pits (P) and traverses (T). **B.** Photomicrograph of typical laser traverses in Grebe's Nest vein fluorite. The photomicrographs illustrate how the ablation characteristics of fluorite can be modified by adjusting laser energy. The traverse on the right shows poor ablation characteristics obtained at low power (5 mJ). The traverse on the right shows good ablation characteristics obtained at higher power (20 mJ).

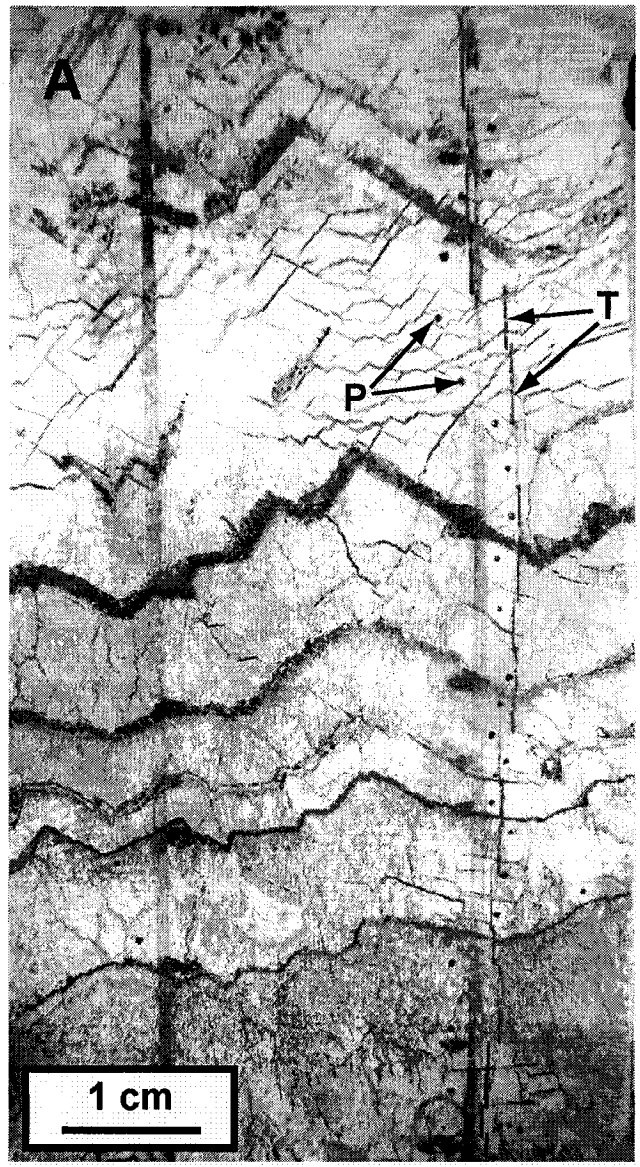
A
T
P
1 cm

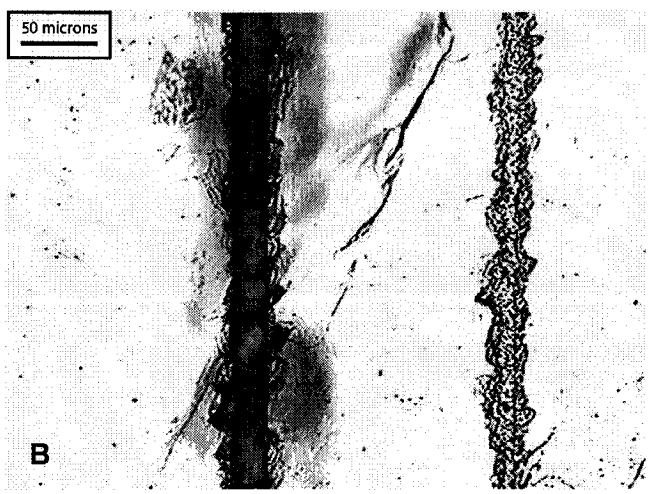
50 microns
B

Results and Discussion

The results of the LA-ICP-MS analyses are summarized in Tables 2-3 through 2-6. Reported in the tables are the types of fluorite analyzed, the average abundance of elements present (reported as µg/g) in concentrations above the detection limits of the analytical method, and the number of analyses performed (n). Included in Table 2-3 is the average composition of the quartz syenite associated with the Gallinas Mountains fluorite-REE mineralization calculated from data presented by Schreiner (1993). Included in Table 2-5 is the average composition of the Pike's Peak granite associated with the fluorite-REE mineralization calculated from data presented by Smith et al. (1999). Included in Table 2-6 is the average composition of the St. Lawrence granite associated with the fluorite-REE mineralization calculated from previously unpublished data collected by B. J. Fryer.

Table 2-2 – Summary of Instrument Conditions

Laser Sampling System	
Manufacturer	Continuum
Model	Surelite I
Wavelength	266 nm
Energy	20 mJ
Mode	Q-Switched
Repetition Rate	20 Hz
Pulsewidth	4 to 6 ns
Laser Spot Diameter	10 to 15 microns
ICP-MS	
Manufacturer	ThermoElemental
Model	PQ3
Mode	Peak-jumping
Dwell Time/Isotope	10 ms
Average Sensitivity (solution mode)	200,000,000 counts/second/ppm
Scan Time	150 to 400 ms/scan

Figure 2-2. An example of time-resolved ICP-MS spectra obtained from green fluorite from South Platte. In addition to the elements presented in the figure, Si, K, Cu, Zn and Nb were also analyzed but were found to be below the lower limit of detection.

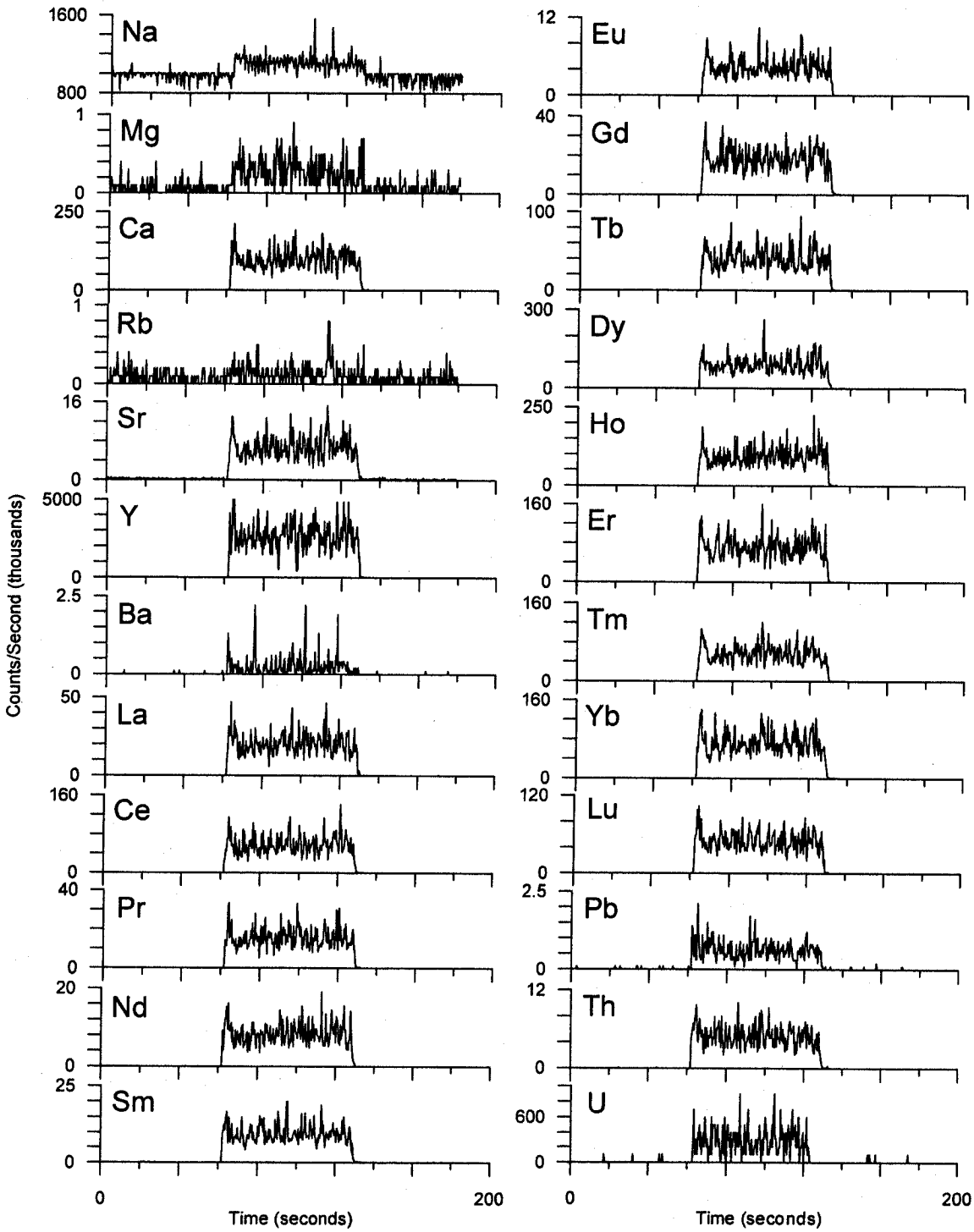
Counts/Second (thousands)
Na
1600
800
Mg
1
0
Ca
250
0
Rb
1
0
Sr
16
0
Y
5000
0
Ba
2.5
0
La
50
0
Ce
160
0
Pr
40
0
Nd
20
0
Sm
25
0
Eu
12
0
Gd
40
0
Tb
100
0
Dy
300
0
Ho
250
0
Er
160
0
Tm
160
0
Yb
160
0
Lu
120
0
Pb
2.5
0
Th
12
0
U
600
0
0
200
Time (seconds)
0
200
Time (seconds)

Table 2-3 – Summary of Fluorite Analyses – Gallinas Mountains, New Mexico

Element (ug/g)	Average Fluorite Composition			Average Syenite Composition* (n = 9)
	P1 (n = 11)	P2 (n = 12)	P3 (n = 11)	
Na	1,380	5,270	2,740	60,700
Mg	10	80	680	500
Si	1,070	12,220	10,200	307,500
K	100	170	170	24,700
Mn	20	220	1,060	0.09
Cu	6.0	6.0	669	9.7
Zn	1.7	4.1	194	29.8
Rb	0.4	0.5	0.7	NA
Sr	243	698	2,930	194
Y	179	676	2,620	58.9
Nb	0.1	1.6	32.2	142
Ba	5.4	1,480	10,400	1,190
La	73	5,510	55,100	137
Ce	68	4,720	45,300	214
Pr	5.9	478	4,760	< DL
Nd	26	1,350	13,500	58.6
Sm	4.4	140	1,070	9.8
Eu	1.2	32.6	264	2.1
Tb	0.8	14.7	95.7	0.7
Dy	4.8	65.8	613	3.0
Ho	1.3	14.1	75.5	1.0
Er	4.2	41.1	209	< DL
Tm	0.6	6.3	50.5	< DL
Yb	3.4	38	193	5.2
Lu	0.4	4.2	16.4	0.7
Pb	141	605	9,110	63.4
Th	0.2	17.2	768	62.3
U	0.3	39.0	344	9.8

Table 2-3 Footnotes:

< DL Concentration below analytical method detection limit.

* Source: Schreiner,1993.

Table 2-4 – Summary of Fluorite Analyses – Rock Canyon Creek, British Columbia

Element *(ug/g)*	Average Fluorite Composition	
	Disseminated *(n = 19)*	Vein/Breccia *(n = 44)*
Na	420	390
Mg	4,280	680
Si	1,520	1,150
K	20	20
Cu	4.6	4.2
Zn	5.6	11.2
Rb	0.1	0.2
Sr	627	648
Y	211	469
Nb	18.1	0.8
Ba	2,650	29.4
La	25,400	51.7
Ce	19,200	116
Pr	1,620	17.7
Nd	3,660	83
Sm	117	31.7
Eu	27.5	16.1
Tb	7.8	13.6
Dy	22.5	111
Ho	4.5	23.9
Er	12.5	65.8
Tm	2.3	10.4
Yb	17.0	64.1
Lu	2.4	8.7
Pb	6.4	11.8
Th	673	1,880
U	0.2	0.7

Table 2-4 Footnotes:

< DL Concentration below analytical method detection limit.

Table 2-5 – Summary of Fluorite Analyses – South Platte, Colorado

Element (ug/g)	Average Fluorite Composition				Average Granite Composition* (n = 4)
	Green (n = 7)	White (n = 6)	Purple (n = 9)	Colorless (n = 7)	
Na	1,640	4,110	1,940	1,870	24,100
Mg	20	250	220	30	1,400
Si	1,910	410	890	360	336,100
K	10	220	210	20	45,900
Cu	0.7	1.8	9.5	1.2	- -
Zn	0.3	3.6	2.9	1	90
Rb	0.2	0.6	0.3	0.3	214
Sr	169	45.2	149	208	85.5
Y	8,320	2,330	993	9,770	81.7
Nb	0.1	13.5	10.2	0.1	21.5
Ba	3.9	4.7	4.8	3.2	659.3
La	141	719	104	220	166.5
Ce	232	851	116	370	312.3
Pr	42.9	157	22.5	66	- -
Nd	253	499	103	398	133.6
Sm	139	202	42.0	218	23.4
Eu	16.6	5.5	3.9	22.8	1.8
Tb	90.5	32.0	21.7	123	2.6
Dy	693	194	53.8	1,010	- -
Ho	206	54.9	48.8	247	- -
Er	675	203	165	796	- -
Tm	97.4	22.2	8.5	144	- -
Yb	820	370	208	998	9.0
Lu	114	49.6	28.4	139	1.4
Pb	1.9	11.3	4.2	4.7	- -
Th	43.3	258	122	99.1	- -
U	0.7	12.8	1.2	0.8	3.3

Table 2-5 Footnotes:

< DL Concentration below analytical method detection limit.

- - Sample was not analyzed for this element.

* Source: Smith et al., 1999.

Table 2-6 – Summary of Fluorite Analyses – St. Lawrence, Newfoundland

Element (ug/g)	Average Fluorite Composition			Average Granite Composition (n = 2)
	Grebe's Nest (n = 48)	Iron Springs (n = 12)	Lawn Barite (n = 13)	
Mg	20	10	- -	1,030
Si	1,000	840	- -	361,300
Cu	4.6	1,030	- -	< DL
Zn	153	1,950	- -	29
Rb	0.6	1.7	- -	218
Sr	56.1	67.2	184	41.4
Y	2,060	3,570	1,120	68.3
Nb	0.1	0.8	- -	55.5
Ba	13.6	6.3	150	40.7
La	21.6	9.7	25.6	45.6
Ce	30.9	15.9	60.9	95.8
Pr	2.7	2.8	9.4	12.0
Nd	44.0	13.2	48.6	45.2
Sm	13.7	7.7	23.0	11.3
Eu	2.0	0.5	3.2	0.2
Tb	1.4	5.0	7.9	1.9
Dy	26.5	36.6	60.0	12.3
Ho	2.0	9.3	12.9	2.6
Er	16.1	24.4	35.8	7.6
Tm	0.6	3.5	4.4	1.2
Yb	11.0	19.1	23.4	7.4
Lu	0.5	2.4	2.2	1.1
Pb	24.0	731	2,360	39
Th	0.1	0.1	0.4	19.1
U	0.1	16.6	< DL	7

Table 2-6 Footnotes:

< DL Concentration below analytical method detection limit.

- - Sample was not analyzed for this element.

Spatial and Paragenetic Changes in Fluorite Compositions

Petrographic analysis of the Gallinas Mountains fluorite-REE mineralization by Williams-Jones et al. (2000) determined that the sequence of fluorite precipitation was P1, then P2 and, finally, P3. These authors postulated that, early in the evolution of the hydrothermal system, the quartz syenite, or a related magma at depth, was the dominant fluid source. Figure 2-3a presents the average compositions of P1, P2 and P3 fluorite relative to the average composition of the quartz syenite, based on published data for the syenite from Schreiner (1993). The average compositions of the three generations of fluorite are different from each other and from the quartz syenite. Crystals of P1 fluorite have similar Sr and heavy REE (HREE), five to one thousand times lower Na, Mg, Si, K, Cu, Zn, Nb, Ba, light REE (LREE), Th and U, and two to three times higher Y and Pb concentrations than the quartz syenite. Crystals of P2 fluorite have five to over one hundred times lower Na, Mg, Si, K, Cu, Zn, Nb and Th and four to forty times higher Sr, Y, REE, Pb and U concentrations than the quartz syenite. Crystals of P2 and P3 fluorite have similar or higher concentrations of all of the elements analyzed relative to P1 and P2 fluorite, respectively. Although the relative enrichments and depletions of individual elements vary between the different types of fluorite, the shapes of the enrichment/depletion patterns generally are similar and parallel to one another.

The Gallinas Mountains quartz syenite has a relatively flat chondrite-normalized REE pattern that is slightly LREE-enriched and has a slight, positive Y anomaly (Fig. 2-3b). Yttrium, which is similar in charge and ionic radius to Ho, has been included between Dy and Ho in the chondrite-normalized REE diagrams. P1 fluorite has a similar chondrite-normalized REE pattern and REE concentrations (particularly the HREE) to the quartz syenite, with a distinct, positive Y anomaly. REE concentrations within P1 fluorite and the quartz syenite

Figure 2-3. **A.** Element enrichment/depletion factors for Gallinas Mountains P1, P2 and P3 fluorite relative to quartz syenite. These factors are calculated by dividing the average element concentration in the fluorite by the average element concentration in quartz syenite (Schriener, 1993) and represent the degree of enrichment or depletion of elements in the P1, P2 and P3 fluorite types relative to the quartz syenite. **B.** Chondrite-normalized REE patterns for Gallinas Mountains quartz syenite and fluorite. P1 fluorite has similar REE concentrations and chondrite-normalized REE pattern to the associated syenite. P2 and P3 fluorite have significantly higher REE concentrations and are more LREE-enriched than P1 fluorite. P1 fluorite has a well-developed, positive Y anomaly, in P2 fluorite, the anomaly is less well-developed, and in P3 fluorite there is no anomaly.

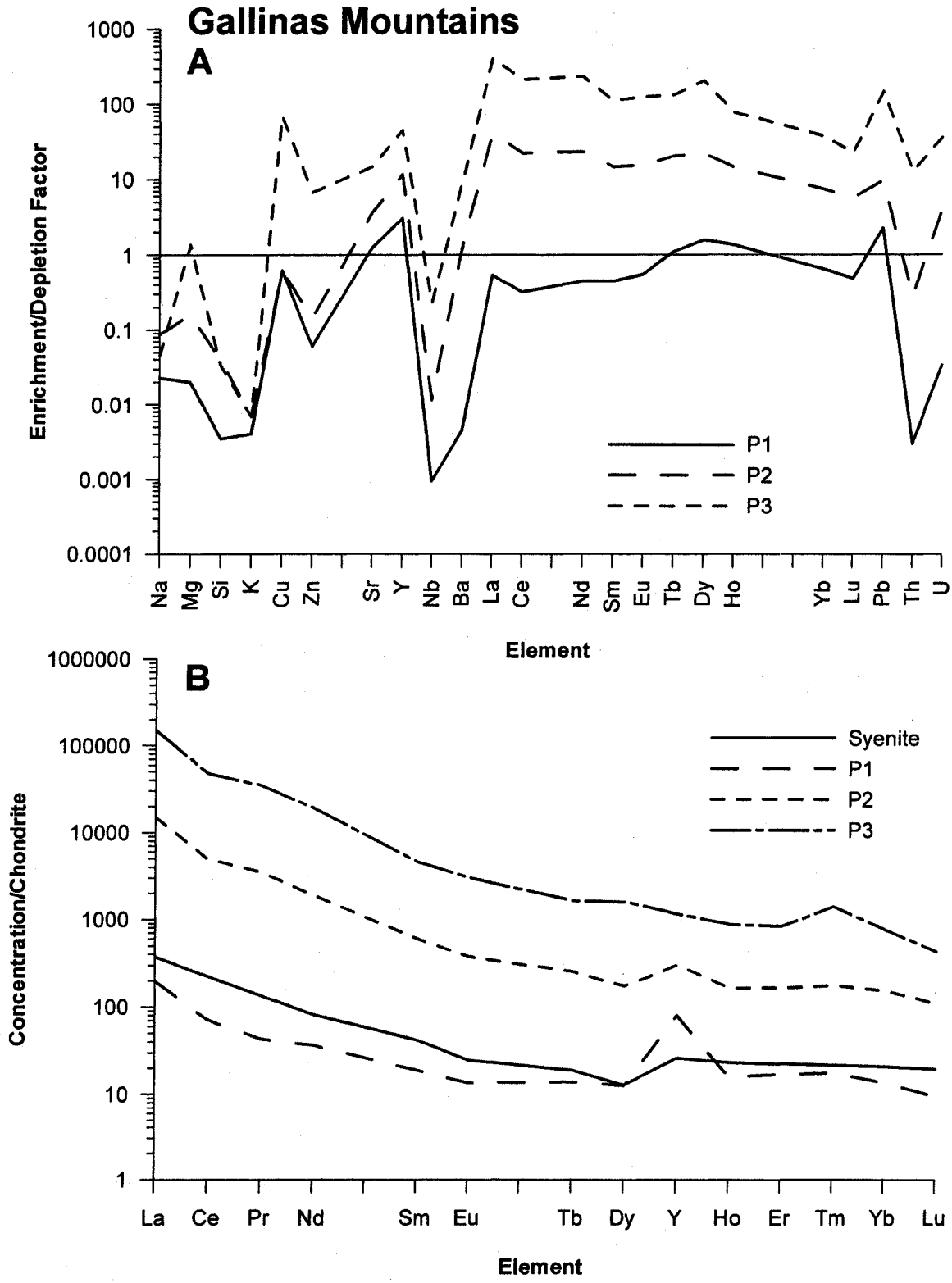
Gallinas Mountains
A
Enrichment/Depletion Factor
1000
100
10
1
0.1
0.01
0.001
0.0001
P1
P2
P3
Na Mg Si K Cu Zn Sr Y Nb Ba La Ce Nd Sm Eu Tb Dy Ho Yb Lu Pb Th U
Element
B
Concentration/Chondrite
1000000
100000
10000
1000
100
10
1
Syenite
P1
P2
P3
La Ce Pr Nd Sm Eu Tb Dy Y Ho Er Tm Yb Lu
Element

vary between approximately ten to one hundred times chondrite. The concentrations of all REE, but particularly the LREE, are higher in P2 fluorite than in P1, and higher still in P3 fluorite. The pronounced positive Y anomaly displayed by P1 fluorite is less pronounced in P2 and absent in P3 fluorite. REE concentrations are 10 to 100 times higher in P2 fluorite than in P1 fluorite (approximately 100 to 1,000 times chondrite) and are 10 to 1,000 times higher for P3 fluorite relative to P1 fluorite (approximately 10^2 to 10^5 times chondrite). Unlike the quartz syenite, the chondrite-normalized REE patterns for P1, P2 and P3 fluorite all have slight negative Ce anomalies.

Study of the Rock Canyon Creek fluorite-REE mineralization by Samson et al. (2001) determined that disseminated fluorite precipitated prior to breccia and vein fluorite. Figure 2-4a presents the average compositions of breccia and vein fluorite relative to disseminated fluorite and illustrates that the two generations of fluorite have very different average compositions. Relative to disseminated fluorite, breccia and vein fluorite have similar Na, Si, K, Cu, Rb, and Sr, approximately two to seven times higher Zn, Y, HREE, Pb, Th, and U, and approximately five to five hundred times lower Mg, Nb, Ba, and LREE concentrations.

Disseminated fluorite from Rock Canyon Creek has chondrite-normalized REE patterns that are LREE enriched and are approximately ten to one hundred times chondrite (Fig. 2-4b). The chondrite-normalized REE pattern for disseminated fluorite has a slight negative Ce anomaly and positive Y anomaly. Breccia and vein fluorite at Rock Canyon Creek have a flat chondrite-normalized REE pattern that is slightly LREE-depleted, with a slight negative Y anomaly. REE concentrations within breccia and vein fluorite vary between approximately 100 and 300 times chondrite.

Figure 2-4. **A.** Element enrichment/depletion factors for Rock Canyon Creek breccia and vein fluorite relative to disseminated fluorite. These factors are calculated by dividing the average element concentration in the breccia and vein fluorite by the average element concentration in the disseminated fluorite. **B.** Chondrite-normalized REE patterns for Rock Canyon Creek fluorite. Disseminated fluorite has a slightly LREE-enriched pattern with a positive Y anomaly and breccia/vein fluorite has a flat REE pattern with a slight negative Y anomaly.

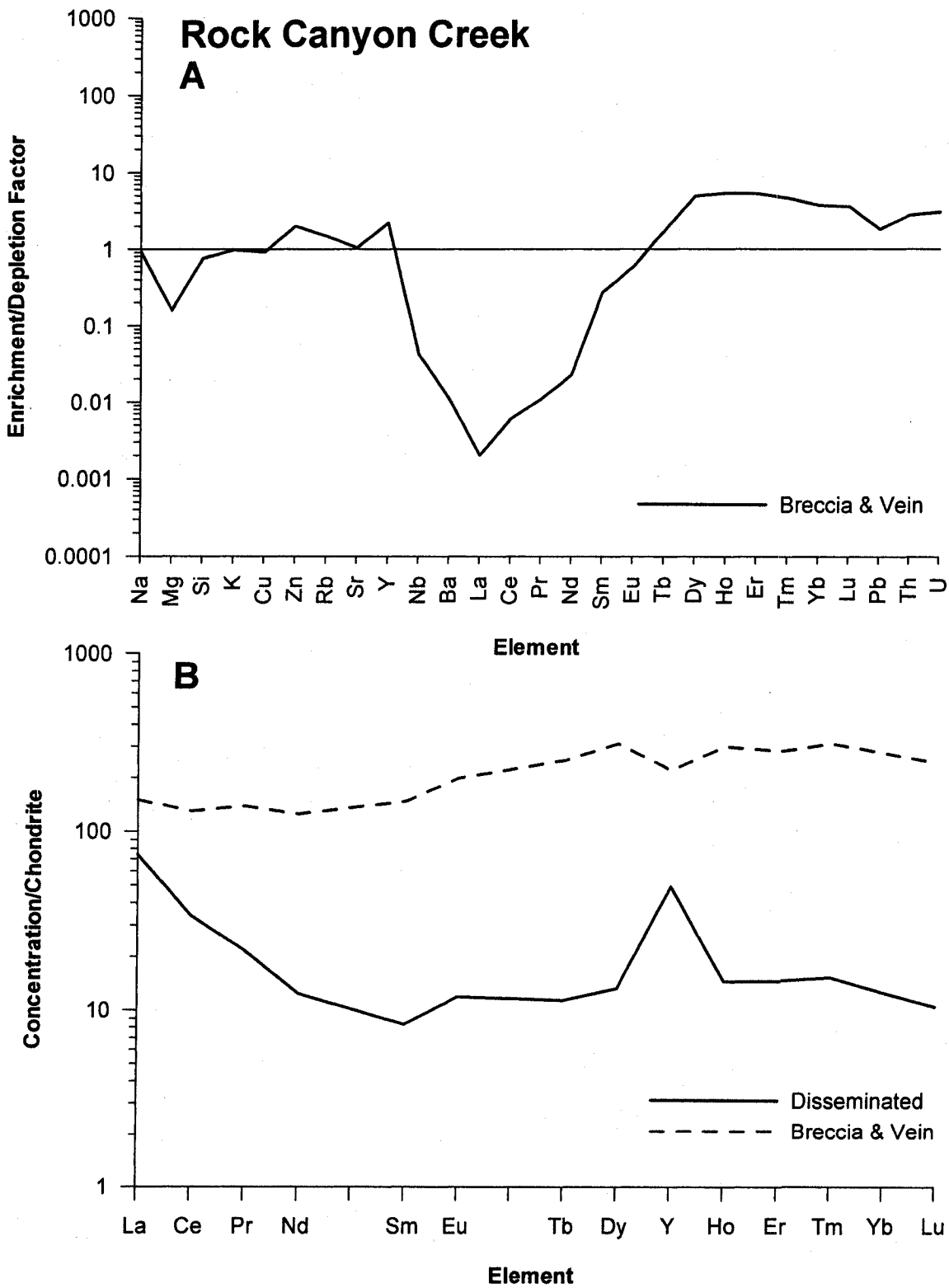
Rock Canyon Creek
A
Enrichment/Depletion Factor
1000
100
10
1
0.1
0.01
0.001
0.0001
Na Mg Si K Cu Zn Rb Sr Y Nb Ba La Ce Pr Nd Sm Eu Tb Dy Ho Er Tm Yb Lu Pb Th U
Element
Breccia & Vein
B
Concentration/Chondrite
1000
100
10
1
La Ce Pr Nd Sm Eu Tb Dy Y Ho Er Tm Yb Lu
Element
Disseminated
Breccia & Vein

Figure 2-5. **A.** Element enrichment/depletion factors for South Platte District pegmatite-hosted, magmatic, green and hydrothermal, colorless, purple and white fluorite relative to the Pikes Peak granite (Smith et al., 1999). All fluorite types show generally similar patterns of elemental enrichment and depletion relative to the associated granite. **B.** Chondrite-normalized REE patterns for South Platte district fluorite and granite. The granite has a LREE-enriched pattern with a negative Eu anomaly. REE patterns and concentrations in colorless, hydrothermal fluorite are identical to those of green, magmatic fluorite. Purple and white hydrothermal fluorite generally has similar REE patterns but significantly lower REE concentrations than green fluorite. All varieties of fluorite have negative Eu anomalies. Green and colorless fluorite have a slight negative Y anomaly, whereas purple and white fluorite have a variable, but typically positive Y anomaly.

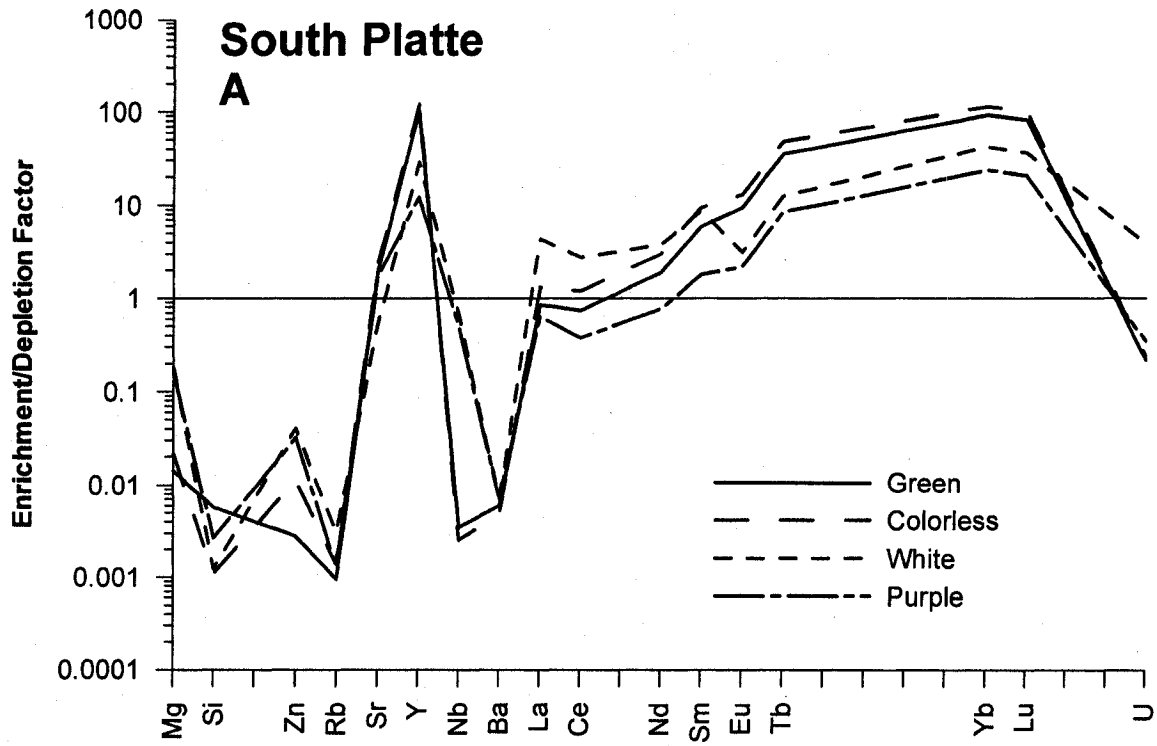
South Platte
A
Enrichment/Depletion Factor
1000
100
10
1
0.1
0.01
0.001
0.0001
Mg
Si
Zn
Rb
Sr
Y
Nb
Ba
La
Ce
Nd
Sm
Eu
Tb
Yb
Lu
U
Green
Colorless
White
Purple

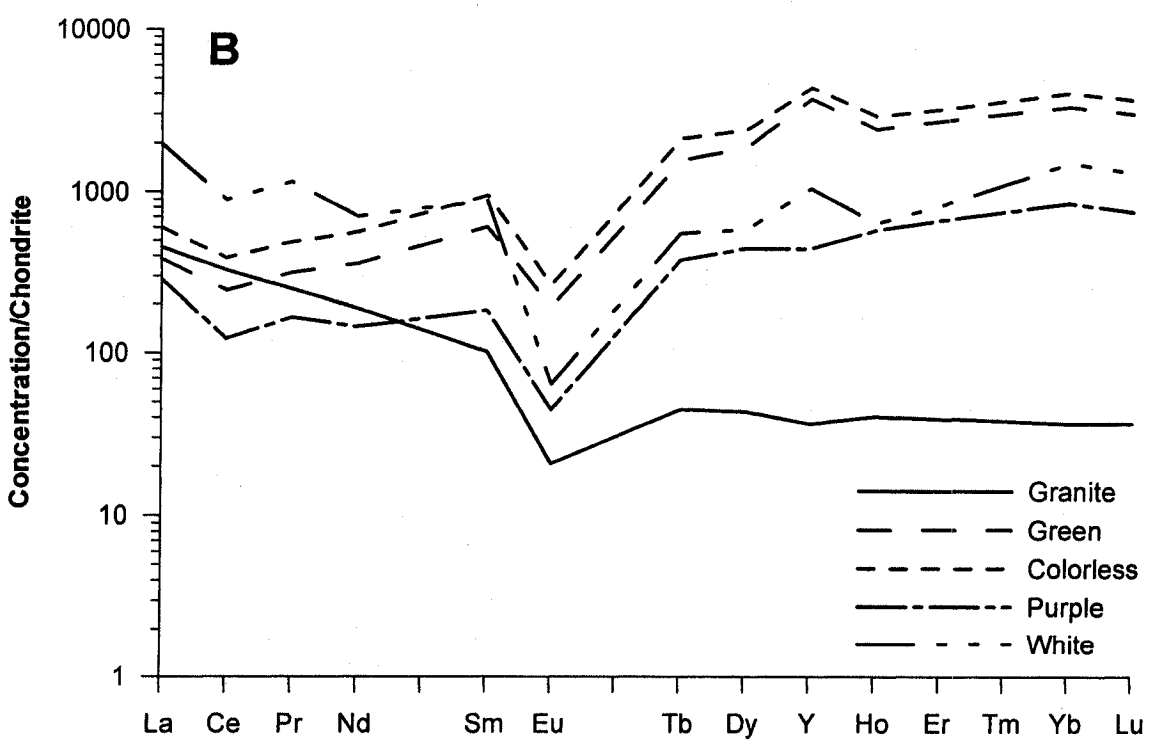
B
Concentration/Chondrite
10000
1000
100
10
1
La
Ce
Pr
Nd
Sm
Eu
Tb
Dy
Y
Ho
Er
Tm
Yb
Lu
Granite
Green
Colorless
Purple
White

Petrographic analysis of the South Platte district pegmatites by Levasseur and Samson (1996) and Levasseur (1997) showed that colorless, purple, and white hydrothermal varieties of fluorite replace primary green magmatic fluorite. Figure 2-5a presents the average composition of green, colorless, white and purple fluorite relative to the average composition of the associated Pike's Peak granite, based on published data for the granite from Smith et al. (1999). Because the fluorite-REE mineralization is contained within pegmatites hosted by the granite, the granite is the most likely source for the fluids from which the hydrothermal fluorite precipitated. The average composition of the magmatic and hydrothermal fluorite are significantly different from, but exhibit similar patterns of enrichment and depletion relative to, the host granite. Relative to the average composition of the granite, crystals of primary magmatic and hydrothermal fluorite have similar Sr, La, Ce and U, approximately 10 to 1000 times lower Mg, Si, Zn, Rb, Nb and Ba, and approximately five to 100 times higher Y, Nd, Sm, Eu, Tb, Yb and Lu concentrations. The average composition of green fluorite is very similar to that of colorless fluorite, whereas purple and white fluorite display greater compositional variability, compared to green and colorless fluorite.

Relative to magmatic and hydrothermal fluorite, South Platte district granite has generally lower REE abundances and a LREE-enriched chondrite-normalized pattern that lacks a negative Ce anomaly, and has negative Eu and Y anomalies (Fig. 2-5b). Green and colorless fluorite have relatively flat, HREE-enriched chondrite-normalized REE patterns, with negative Ce and Eu anomalies, positive Y anomalies, and REE concentrations between 500 and 4000 times chondrite. The similarity between the composition of green and colorless fluorite suggests that the colorless fluorite may be altered, relict green fluorite within hydrothermal fluorite. In general, purple and white hydrothermal fluorite exhibit chondrite-normalized REE patterns that are similar to those of green and colorless fluorite but have REE concentrations that are up to 100 times lower, with purple fluorite having the lowest REE concentrations (Fig. 2-5b). White fluorite exhibits a positive Y anomaly, rather than the slight negative Y anomaly exhibited by purple fluorite. With the exception of a few elements (e.g.,

Y), chondrite-normalized REE patterns suggest that replacement of green fluorite by purple and white fluorite simply resulted in lower REE concentrations in the replacement fluorite, without significant inter-element fractionation. The similarities in chondrite-normalized REE patterns suggest that the composition of the primary fluorite was the predominant control on the compositions of later, hydrothermal fluorite.

Strong et al. (1984) concluded that the St. Lawrence fluorite veins were formed from hydrothermal fluids that were exsolved from the St. Lawrence granite. The veins occur both in the granite (Iron Springs and Grebe's Nest veins) and in the host rocks to the granite (Lawn Barite vein). The occurrence of the fluorite veins within and outside of the granite enables examination of potential large-scale spatial variations in fluorite composition. Figure 2-6a presents the average composition of fluorite from the Iron Springs, Grebe's Nest and Lawn Barite veins relative to the average composition of the associated St. Lawrence granite. Relative to the granite, fluorite from Iron Springs, Grebe's Nest and Lawn Barite veins generally exhibit similar patterns of elemental enrichment and depletion; crystals of vein fluorite have similar Sr and REE, approximately 10 to 1000 times lower Mg, Si, Rb, Nb, Ba and Th, and approximately 10 to 100 times higher Zn, Y, and Eu concentrations. Notable exceptions are Ba, Pb and U. Relative to the granite, Ba is enriched in Lawn Barite fluorite and depleted in Iron Springs and Grebe's Nest fluorite, Pb is enriched in Iron Springs and Grebe's Nest fluorite and depleted in Lawn Barite fluorite, and U is enriched in Iron Springs fluorite and depleted in Lawn Barite fluorite. Although the granite has been interpreted to be the source of the hydrothermal fluids and REE (Strong et al., 1984), veins outside of the granite (e.g., Lawn Barite) have higher average REE concentrations than veins within the granite (e.g. Iron Springs). The former are also more LREE-enriched than the latter.

Figure 2-6. **A.** Element enrichment/depletion factors, relative to the St. Lawrence granite, for St. Lawrence Grebe's Nest and Lawn Barite vein fluorite, which occur external to the granite, and Iron Springs vein fluorite, which is hosted by the granite. All fluorite types show generally similar patterns of elemental enrichment and depletion relative to the granite. **B.** Chondrite-normalized REE patterns for St. Lawrence fluorite. Granite-hosted (Iron Springs vein) fluorite has relatively LREE-depleted patterns relative to country rock-hosted (Grebe's Nest and Lawn Barite veins) fluorite and the granite. The St. Lawrence granite and all varieties of fluorite have well-developed negative Eu and the fluorite has positive Y anomalies.

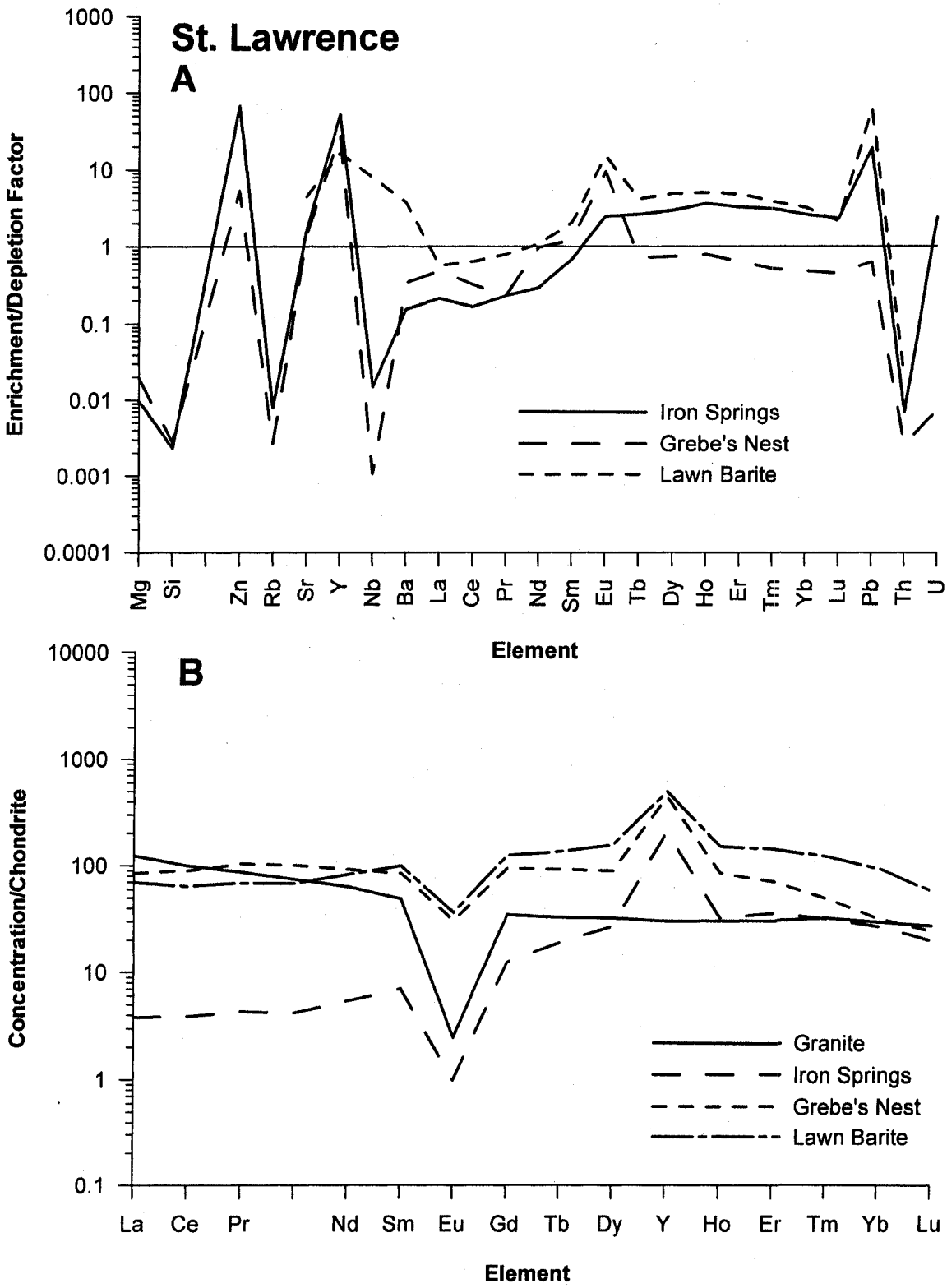
St. Lawrence
A
Enrichment/Depletion Factor
1000
100
10
1
0.1
0.01
0.001
0.0001
Iron Springs
Grebe's Nest
Lawn Barite
Mg Si Zn Rb Sr Y Nb Ba La Ce Pr Nd Sm Eu Tb Dy Ho Er Tm Yb Lu Pb Th U
Element
B
Concentration/Chondrite
10000
1000
100
10
1
0.1
Granite
Iron Springs
Grebe's Nest
Lawn Barite
La Ce Pr Nd Sm Eu Gd Tb Dy Y Ho Er Tm Yb Lu
Element

The St. Lawrence granite has REE concentrations between two and one hundred times chondrite, with a chondrite-normalized REE pattern that is relatively flat and slightly LREE-enriched (Fig. 2-6b). Fluorite from the Grebe's Nest and Lawn Barite veins has REE concentrations between 10 and 1000 times chondrite and relatively flat chondrite-normalized REE patterns. Relative to fluorite from the Lawn Barite and Grebe's Nest veins, fluorite from Lawn Barite veins has lower LREE concentrations and similar HREE concentrations. The chondrite-normalized REE patterns for the granite and fluorite all have negative Eu anomalies, however, only the fluorite has positive Y anomalies.

Fluorite Composition as an Indicator of Geologic Affinity

Fluorite from Gallinas Mountains and Rock Canyon Creek, which are associated with alkalic magmatism, are characterized by relatively flat to LREE-enriched chondrite-normalized REE patterns that lack Eu anomalies and may or may not show slight negative Ce anomalies, or slight positive Y anomalies. In the case of Gallinas Mountains, the earliest generation of fluorite (P1) has REE abundances and a chondrite-normalized REE pattern similar to the associated quartz syenite. In contrast, fluorite from South Platte and St. Lawrence, which are associated with granitic magmatism, are characterized by relatively flat to HREE-enriched chondrite-normalized REE patterns that have distinct negative Eu anomalies and positive Y anomalies. In the case of St. Lawrence, the fluorite has REE abundances and chondrite-normalized REE patterns that are similar to the associated granite, although the granite lacks a positive Y anomaly. At South Platte, the fluorite has HREE-enriched chondrite-normalized REE patterns that differ markedly from the LREE-enriched pattern of the associated granite. Although the absolute concentration of individual elements may vary, the patterns of elemental enrichment and depletion shown by all types of fluorite relative to the associated intrusive rocks are consistent within an individual deposit; regardless of whether the fluorite is primary magmatic or secondary and hydrothermal (e.g. South Platte).

Elemental discriminant diagrams have been used in a variety of studies to interpret fluorite compositions, characterize and differentiate fluorite occurrences, and make inferences about the depositional environment and ore potential of individual fluorite deposits and mining districts (e.g., Schneider et al., 1975; Möller et al., 1976; Eppinger and Closs, 1990; Hill et al., 2000). Möller et al. (1976) used Tb/Ca and Tb/La values to discriminate fluorite occurrences according to their sedimentary, hydrothermal or pegmatitic affinities. Furthermore, they interpreted trends in Tb/Ca and Tb/La as resulting from progressive incorporation of REE into fluorite during hydrothermal precipitation, which they refer to as the crystallochemical trend, or from differences in the relative strength of fluorocomplexes, which they refer to as the remobilization trend. Below, we examine the composition of the fluorite analyzed in this study in terms of Tb/Ca and Tb/La values and the fields and trends defined by Möller et al. (1976). Use of a constant, stoichiometric abundance of Ca in ideal fluorite (presented as Ca*) as an internal standard for LA-ICP-MS analyses suggests that the use of the Tb/Ca* ratio may be inappropriate. However, varying the Ca* concentration by as much as 10 % (~ 5 % from the stoichiometric value), which is unreasonably large considering that the elements that readily substitute for Ca were generally found to occur at total concentrations less than approximately 0.5 wt. % in our samples, shows virtually no effect on the discriminant diagram. This indicates that variation in the Ca concentration of fluorite is not a relevant variable in discriminating the different occurrences of fluorite discussed here and plotting Tb versus Tb/La would yield comparable results.

Most of the fluorite from Gallinas Mountains plots within the pegmatite field, and each type (P1, P2 and P3) occurs within a relatively well-defined population (Fig. 2-7a). The change in Tb/Ca* and Tb/La values defined by P1, P2 and P3 fluorite defines a progressive compositional evolution from relatively high Tb/La and low Tb/Ca* (P1 fluorite) to relatively low Tb/La and high Tb/Ca* (P3 fluorite). This evolutionary trend is approximately orthogonal to the crystallochemical trend and is in the opposite direction to the remobilization trend of Möller et al. (1976).

Figure 2-7. Log Tb/Ca* and log Tb/La values in Gallinas Mountains (A), Rock Canyon Creek (B), South Platte (C), and St. Lawrence (D) fluorite. Fluorite from Gallinas Mountains and Rock Canyon Creek plot within the hydrothermal and pegmatitic fields of Möller et al. (1976). The compositional trends shown by Gallinas Mountains P1 to P2 to P3 (1, 2 and 3) and Rock Canyon Creek disseminated and vein/breccia fluorite (D and B) are indicated by arrows. The compositional trend for Gallinas Mountains fluorite differs from the remobilization (RRF) and crystallochemical (CCF) trends of Möller et al. (1976). Fluorite from South Platte and St. Lawrence plot within the hydrothermal and pegmatitic fields of Möller et al. (1976). The compositional trend for South Platte green and colorless (G and C) fluorite to purple (P) and white (W) fluorite is indicated by the arrow. St. Lawrence Iron Springs (I), Grebe's Nest (G), and Lawn Barite (L) veins are indicated by the circled fields. The compositional trend for South Platte fluorite also differs from the remobilization (RRF) and crystallochemical (CCF) trends of Möller et al. (1976).

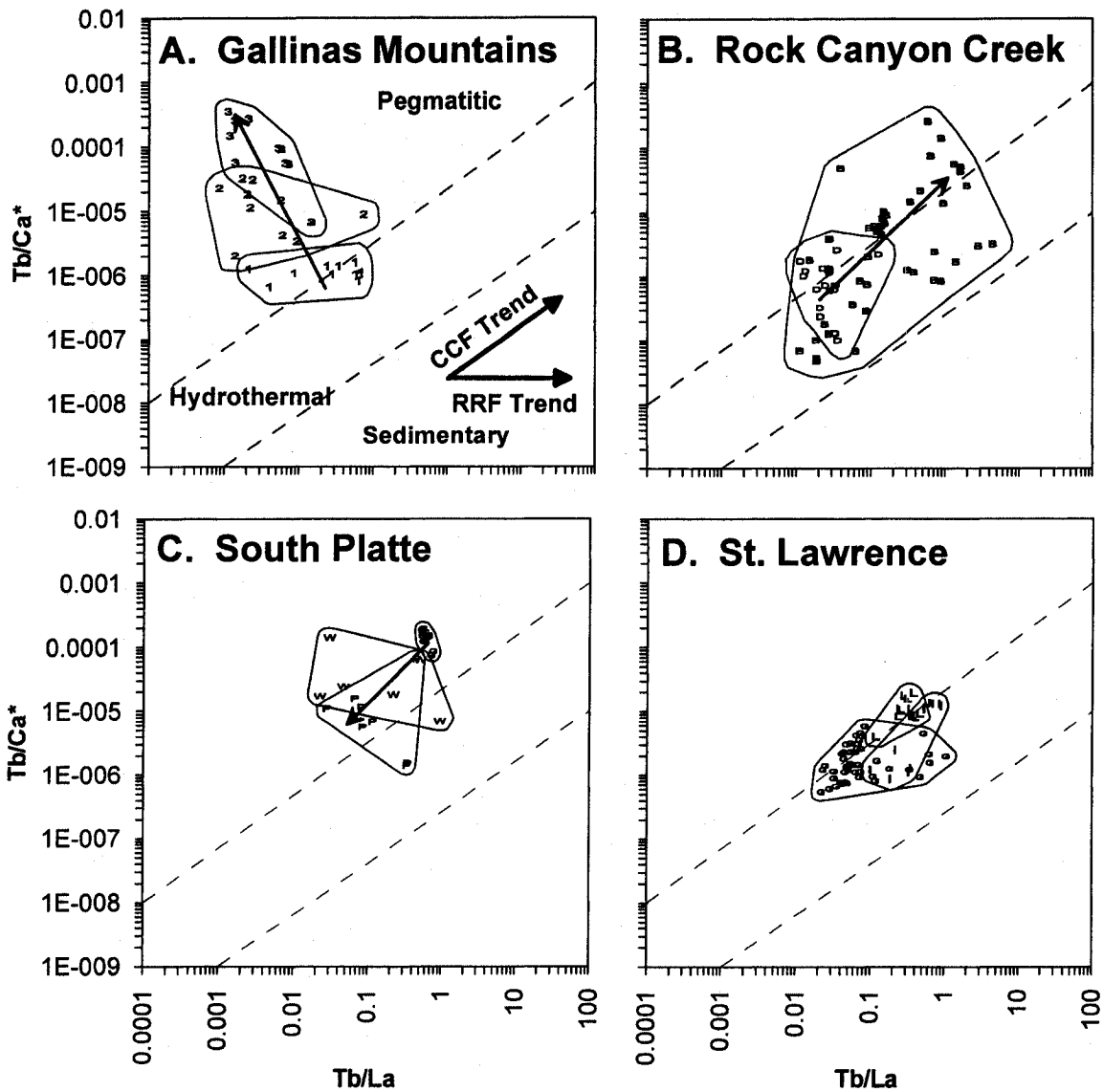
A. Gallinas Mountains
Pegmatitic
CCF Trend
RRF Trend
Hydrothermal
Sedimentary
B. Rock Canyon Creek
C. South Platte
D. St. Lawrence
Tb/Ca*
Tb/La
0.01
0.001
0.0001
1E-005
1E-006
1E-007
1E-008
1E-009
0.0001
0.001
0.01
0.1
1
10
100

Fluorite from Rock Canyon Creek straddles the boundary between the pegmatite and hydrothermal fields (Fig. 2-7a). Disseminated fluorite plots in a relatively tight cluster, however, the vein and breccia fluorite exhibits much greater compositional variation, and overlaps the field defined by the paragenetically earlier, disseminated fluorite. Some of the disseminated and vein/breccia fluorite define a compositional trend that parallels the boundary between the pegmatitic and hydrothermal fields and the crystallochemical trend of Möller et al. (1976). However, some of the late (vein and breccia) fluorite plots at lower Tb/La and Tb/Ca* ratios than the early (disseminated) fluorite suggesting that the composition of some vein and breccia fluorite could be interpreted to define a compositional trend opposite to the crystallochemical trend proposed by Möller et al. (1976).

South Platte fluorite plots primarily within the pegmatite field, which is consistent with its occurrence within granite-hosted pegmatites (Fig. 2-7b). Purple and white fluorite, which replace the green fluorite, have lower Tb/Ca* and Tb/La values than green and colorless fluorite. The range of magmatic and hydrothermal fluorite compositions defines a trend similar in slope, but opposite in direction, to the crystallochemical trend of Möller et al. (1976).

Fluorite from the St. Lawrence Grebe's Nest and Lawn Barite veins plots in a relatively tight cluster within the pegmatite field, whereas fluorite from the Iron Springs vein plots in the hydrothermal field (Fig. 2-7b). The data array for fluorite from the Iron Springs vein crudely parallels the crystallochemical trend. In contrast, most of the fluorite from the Grebe's Nest and Lawn Barite veins plot in relatively tight clusters, and systematic trends in composition are not apparent.

Samples of green magmatic and colorless hydrothermal fluorite from South Platte plot entirely within the pegmatite field, as defined by Möller et al. (1976). The majority of South Platte purple and white, approximately half of Rock Canyon Creek, and all of Gallinas Mountains P2 and P3 hydrothermal fluorite plot within the pegmatitic field, rather than the hydrothermal field. At St. Lawrence, the granite-hosted Iron Springs vein fluorite plots within the

hydrothermal field rather than the pegmatitic field. Therefore, Tb/Ca* and Tb/La values are not a reliable indicator of the geologic affinity of hydrothermal fluorite.

The trends in Tb/Ca* and Tb/La values obtained in this study are more complex than can be explained by the crystallochemical and remobilization trends proposed by Möller et al. (1976). Trends in the composition of fluorite are opposite to (e.g., South Platte) or inconsistent with (e.g., Gallinas Mountains, and St. Lawrence) the remobilization or crystallochemical trends. The controls on trends defined by Tb/Ca* and Tb/La values remain poorly understood.

Fluorite Composition as an Indicator of Source of the Hydrothermal Fluid

Both magmatic and formation waters have been identified from, or proposed to have been involved in, REE-bearing hydrothermal systems (e.g., Strong et al.,1984; Norman et al., 1985; Banks et al., 1994; Salvi and Williams-Jones, 1992; Palmer and Williams-Jones, 1996; Williams-Jones et al., 2000; Samson et al., 2000). If the composition of fluorite within these deposits is unique to a particular type of ore-forming system (e.g., granitic versus alkalic), then compositional data on fluorite from deposits of known affinity could potentially be used to make inferences about the genesis of REE-bearing deposits where the source of the hydrothermal fluid is poorly constrained. In the case of South Platte, Gallinas Mountains and St. Lawrence, the composition of green, P1 and Iron Springs vein fluorite, respectively, is considered most likely to represent crystallization from a magma or fluids of predominantly magmatic derivation on the basis of geologic, textural and paragenetic relationships and the fluid inclusion and isotopic data presented by Simmons and Heinrich (1970; 1980), Strong et al. (1984), Collins and Strong (1988), Levasseur (1997) and Williams-Jones et al. (2000). This fluorite is characterized by relatively flat chondrite-normalized REE patterns that vary from slightly LREE-depleted (South Platte green fluorite and St. Lawrence Iron Springs vein fluorite) to slightly LREE-enriched, with weakly to well-developed negative Eu anomalies, and weakly to well-developed positive Y anomalies. Of these samples of "magmatic" fluorite, those associated with granitic magmatism are characterized by flat to LREE-

depleted chondrite-normalized REE patterns that generally have distinct negative Eu and positive Y anomalies. The chondrite-normalized REE patterns of the associated granitic rocks have distinct negative Eu anomalies but differ from the associated fluorite in being LREE enriched and lacking positive Y anomalies. The samples of "magmatic" fluorite closely associated with alkalic magmatism (Gallinas Mountains) are characterized by LREE-enriched chondrite-normalized REE patterns that lack negative Eu and have slight positive Y anomalies. The chondrite-normalized REE patterns of the associated alkalic rocks are very similar to the associated fluorite.

For the hydrothermal fluorite in general, distinct compositional differences exist between early- and late-formed fluorite. For example, early, P1 fluorite from Gallinas Mountains has relatively flat chondrite-normalized REE patterns with well developed positive Y anomalies and late, P3 fluorite has LREE-enriched chondrite-normalized REE patterns without positive Y anomalies. In contrast, the opposite evolutionary trend is observed between early, disseminated and late, breccia and vein fluorite at Rock Canyon Creek. The cause of the differences in the fluorite compositional trends is not known and more comprehensive and systematic analyses of fluorite are required. In addition, other factors need to be evaluated for the deposits in question, including the effect of element partitioning into coprecipitated phases, information on melt/fluid partitioning (e.g., REE), aqueous complexation at high temperatures, and fluid composition (e.g., microthermometric and LA-ICP-MS analysis of fluid inclusions).

Fluorite Composition as an Indicator of Evolution of the Hydrothermal Fluid

Multiple generations of fluorite occur in the Gallinas Mountains, Rock Canyon Creek, South Platte, and St. Lawrence deposits (Simmons and Heinrich, 1980; Strong et al., 1984; Williams-Jones et al., 2000; Samson et al., 2001). The composition of fluorite within these deposits varies with paragenetic position (Gallinas Mountains, Rock Canyon Creek, and South Platte) or with spatial location (St. Lawrence). Also, significant compositional variation occurs within optically homogeneous fluorite. Compared to magmatic fluorite, post-magmatic,

hydrothermal fluorite within the South Platte pegmatites is generally characterized by higher concentrations of Mg, K, Cu, Zn, Pb, Th and U, and similar or lower concentrations of Si, Rb, Y, and Ba (Table 2-5). The variation in Na, Sr, Nb, REE, Th, U concentrations is less systematic, and chondrite-normalized REE patterns are similar between primary magmatic and hydrothermal, replacement fluorite. It is likely that, in some systems, the coprecipitation of REE-rich minerals will locally affect fluid chemistry, and therefore the composition of coprecipitated fluorite (cf., Hill et al., 2000). In the South Platte district pegmatites, REE-bearing minerals (e.g. bastnäsite and synchysite) were interpreted to be coprecipitated with the hydrothermal fluorite (Simmons and Heinrich, 1970; 1980). However, fluorite compositions indicate that REE fractionation was minimal during replacement of the magmatic fluorite, suggesting that coprecipitation of REE minerals did not play a major role in changing the composition of the hydrothermal fluids. Furthermore, as noted above, the evolution in composition from early- to late-formed fluorite is opposite to the crystallochemical trend of Möller et al. (1976).

Evolutionary trends in fluorite composition within the South Platte district pegmatites (decreasing Sr, Ba, Y and REE) are opposite to trends observed in the Gallinas Mountains, Rock Canyon Creek and St. Lawrence fluorite (increasing Sr, Ba, Y and REE), where formation waters (e.g., Strong et al., 1984; Williams-Jones et al., 2000) or wall rock interaction (e.g., Samson et al., 2001) have been interpreted to play a significant role in the formation of the deposits. In addition to elemental enrichment, compositional evolution of Gallinas Mountains, Rock Canyon Creek and St. Lawrence fluorite is accompanied by significant REE fractionation (see following discussion). These different trends suggest that compositional evolution of the South Platte fluorite occurred within a relatively closed system and resulted from factors other than changes in the composition of the hydrothermal fluid (e.g., a reduction in temperature). The compositional variations observed in fluorite at South Platte supports the model proposed by Levasseur (1997) and Levasseur and Samson (1996) in which the composition of late-stage fluorite was controlled by the

primary fluorite and not by introduction of fluids derived externally to the granite (i.e., formation waters).

The difference in composition between early- and late-formed hydrothermal fluorite at Gallinas Mountains is generally characterized by higher concentrations of all elements except Cu and Zn for P2 relative to P1 fluorite, and Na, Si and K for P3 relative to P2 fluorite. The LREE show particularly significant enrichment from P1 to P2 to P3. Similar enrichment trends, representing spatial variations, occur within the St. Lawrence fluorite veins and are characterized by relatively higher concentrations of most elements within veins hosted by the country rocks (Grebe's Nest and Lawn Barite veins) compared with veins hosted by the St. Lawrence granite (Iron Springs vein) (Table 2-6). Notable exceptions are Cu, Zn, and Y, which occur in higher concentrations in Iron Springs vein fluorite. Early, hydrothermal fluorite from Gallinas Mountains (P1) was coprecipitated with REE minerals (particularly bastnäsite) or replaced bastnäsite (P2 and P3) (Williams-Jones et al., 2000). Coprecipitation of REE minerals with P1 fluorite could have sequestered the LREE preferentially resulting in relatively low REE concentrations in the coprecipitated fluorite. Subsequent replacement of the early REE minerals likely influenced the composition of P2 and P3 fluorite. In contrast, fluorite is the only mineral within the St. Lawrence fluorite veins that contains significant concentrations of REE. Therefore, coprecipitation or replacement of other REE minerals cannot have caused the REE compositional trends observed within the St. Lawrence veins, and other factors must be considered.

The difference in composition between early- to late-formed hydrothermal fluorite at Rock Canyon Creek is characterized by higher concentrations of Zn, Y, HREE, Pb, Th and U and lower concentrations of Mg, Nb, Ba and LREE (Table 2-4). With respect to the LREE, the trend in compositional evolution of fluorite at Rock Canyon Creek is opposite to that observed at Gallinas Mountains. The cause of the different compositional trend at Rock Canyon Creek is presently not understood.

The fluorite with the highest concentrations of trace elements in the Gallinas Mountains (P3 fluorite) is interpreted to have formed during collapse of the magmatic hydrothermal fluid system, when the influx of formation waters increased (Williams-Jones et al., 2000). Similarly, fluorite with the most significant elemental enrichment in the St. Lawrence deposits (Grebe's Nest and Lawn Barite veins) occurs within veins external to the granite, where the potential influence of country rock or formation waters would be expected to be more significant than in veins hosted by the granite (i.e., Iron Springs vein). Strong et al. (1984) and Collins and Strong (1988) determined that the mixing of magmatic and formation waters was a significant factor in the formation of the St. Lawrence fluorite veins. Therefore, elemental enrichments in the fluorite from these deposits could potentially result from contributions from earlier-formed minerals (Gallinas Mountains), formation waters (Gallinas Mountains and St. Lawrence), or be the result of physicochemical conditions promoting the concentration of REE within fluorite (complexation effects). The latter may reflect changes in fluid composition associated with the introduction of formation waters into the hydrothermal system. Similar, host rock or fluid mixing controls on fluorite composition have been suggested for other fluorite deposits (e.g., Hill et al., 2000).

Fluorite Composition as an Exploration Guide

The LA-ICP-MS results presented indicate that the composition of fluorite, even within an individual deposit, can be highly variable. The range in composition observed within a deposit (e.g., Gallinas Mountains) is as great as, or greater than, the compositional variation observed between some of the deposits studied. Presently, it is not known whether or not the compositional ranges and trends observed in fluorite represent those that might occur in fluorite deposits with other geologic affinities. Furthermore, numerous compositional trends can occur within an individual deposit (e.g., St. Lawrence), which may or may not be consistent with compositional trends expected from crystallochemical fractionation or aqueous complexation of REE (cf., Möller et al., 1976).

Therefore, the use of fluorite composition as an indicator of the ore potential of a deposit or region should be approached with care. Complementary data (e.g., isotopic or fluid inclusion data) would improve the validity of the predictions regarding the ore potential of an individual fluorite deposit or geographic region (e.g., Strong et al., 1984; Hill et al., 2000).

Recommendations for Further Work

The use of fluorite chemistry to test genetic models for the deposits considered in this paper, and other deposits, will benefit from a better understanding of the variables controlling fluorite formation and composition. To improve our understanding of the evolution of these ore-forming hydrothermal systems, it is necessary that the following be better understood.

- Mineral parageneses need to be determined and quantitative mineral analyses conducted in order to assess the potential influence that coprecipitation and replacement of minerals other than fluorite have on the compositional evolution of fluorite within these hydrothermal systems.
- It is possible that much of the compositional variation exhibited by fluorite could be controlled by only a few intensive variables (i.e., temperature). To better understand the potential effect of intensive variables on the composition of fluorite, additional data (i.e., microthermometry) on the hydrothermal system responsible for these deposits are required.
- The composition of the hydrothermal solutions needs to be determined. Combined microthermometric, LA-ICP-MS, and other types of analyses will enable quantitative determination of the compositions of fluid inclusions within fluorite and other minerals. Determination of the compositions of the host minerals and fluid inclusions will enable calculation of the distribution coefficients between the hydrothermal solution and minerals in order to assess the role that intensive variables play in controlling fluorite composition (cf., Banks et al., 1994).

Conclusions

Based on the results of this study, the following conclusions can be made:

- LA-ICP-MS is an effective method for determining elemental concentrations in fluorite. The ability of LA-ICP-MS to sample small volumes with high sensitivity has enabled the identification of compositional heterogeneities and trends in fluorite not previously documented; indicating that bulk analysis of fluorite is inadequate to fully characterize the compositional heterogeneity of fluorite.
- Differences in composition were observed between early- and late-formed fluorite (Gallinas Mountains, Rock Canyon Creek and South Platte) and between fluorite hosted within granite and country rock (St. Lawrence). The composition of hydrothermal fluorite at South Platte was controlled by the primary magmatic fluorite and replacement occurred within a relatively closed hydrothermal system. Fluorite from Gallinas Mountains, Rock Canyon Creek and St. Lawrence exhibit compositional trends that may be representative of progressive mixing of hydrothermal fluids or interaction of hydrothermal fluid with wall rocks.
- Fluorite from granite-associated deposits (South Platte and St. Lawrence) is characterized by relatively flat chondrite-normalized REE patterns with well-developed negative Eu anomalies. Fluorite from alkalic-associated deposits (Gallinas Mountains and Rock Canyon Creek) is characterized by relatively flat to strongly LREE-enriched chondrite-normalized REE patterns that lack negative Eu anomalies. The chondrite-normalized REE patterns for the associated magmatic rocks are similar to the REE patterns for the magmatic or earliest-formed hydrothermal fluorite within these deposits.
- The variability in fluorite composition observed within these deposits indicates that significantly different conclusions could be drawn on the affinity of the fluorite, and possibly the ore potential of the mineral deposit or region, depending on which fluorite crystal, or part thereof, that is

sampled. Furthermore, distinctive compositional ranges that might be indicative of a particular geologic setting, and which could be used as an exploration tool, were not identified, and Tb/Ca and Tb/La ratios in fluorite do not appear to be reliable indicators of the affinity of fluorite (e.g., hydrothermal fluorite can be classified as pegmatitic). Therefore, care must be exercised when using fluorite compositions to make inferences about ore potential or affinity.

Acknowledgements

The authors thank C. J. Collins for performing the LA-ICP-MS analyses of the Lawn Barite vein fluorite. Dr. T. Pettke and Dr. A. R. Campbell are thanked for their reviews which resulted in significant improvements to this manuscript. Dr. P. J. Sylvester and Dr. R. F. Martin are thanked for their editorial handling of the manuscript. This study was supported by NSERC grants to I.M.S., B.J.F. and A.E.W-J and by a McGill University graduate student fellowship and a Geological Society of America student research grant to J.E.G.

References

Banks, D.A., Yardley, B.W.D., Campbell, A.R., and Jarvis, K.E. (1994): REE composition of an aqueous magmatic fluid; a fluid inclusion study from the Capitan Pluton, New Mexico, U.S.A. *Chemical Geology*, **113**, 259-272.

Brewster, R.H. (1986): *The distribution and chemistry of rare-earth minerals in the South Platte pegmatite district, Colorado, and their genetic implications.* M.S. thesis, Univ. of New Orleans, New Orleans, Louisiana.

Collins, C.J., and Strong, D.F. (1988): A fluid inclusion and trace element study of fluorite veins associated with the peralkaline St. Lawrence Granite, Newfoundland. Canadian Institute of Mining and Metallurgy, Special Volume 39, pp. 291-302.

Deer, W.A., Howie, R.A., and Zussman, J. (1992): *An Introduction to the Rock-Forming Minerals*, 2nd Edition, Longman Group UK Limited, 696 p.

Eppinger, R.G., and Closs, L.G. (1990): Variations of trace elements and rare earth elements in fluorite: a possible tool for exploration. *Economic Geology*, **85**, 1896-1907.

Fryer, B.J., Jackson, S.E., and Longerich, H.P. (1995): The design, operation and role of the laser-ablation microprobe coupled with an inductively coupled plasma-mass spectrometer (LAM-ICP-MS) in the earth sciences. *Can. Mineral.* **33**, 303-312.

Hedge, C.E. (1970): Whole rock Rb-Sr age of the Pikes Peak Batholith, Colorado. U.S. Geological Survey, Professional Paper 700B, 86-89.

Hill, G.T., Campbell, A.R., and Kyle, P.R. (2000): Geochemistry of southwestern New Mexico fluorite occurrences: implications for precious metals exploration in fluorite-bearing systems. *J. of Geochem. Exp.* **68**, 1-20.

Jackson, S.E., Longerich, H.P., Dunning, G.R., and Fryer, B.J. (1992): The application of laser ablation microprobe-inductively coupled plasma-mass spectrometry (LAM-ICP-MS) to in situ trace element determinations in minerals. *Can. Mineral.* **30**, 1049-1064.

Levasseur, R.L. (1997): *Fluid Inclusion Studies of Rare Element Pegmatites, South Platte District, Colorado.* M.Sc. thesis, Univ. of Windsor, Windsor, Ontario.

Levasseur, R.L., and Samson, I.M. (1996): Fluid inclusion characteristics of REE-Y-Nb pegmatites, South Platte district, Colorado (abs.): Programs with Abstracts, v. 21, Geological Association of Canada – Mineralogical Association of Canada Annual Meeting, Winnipeg, A56.

Möller, P., Parekh, P.P., and Schneider, H. J. (1976): The Application of Tb/Ca-Tb/La Abundance Ratios to Problems of Fluorospar Genesis. *Min. Dep.* **11**, 111-116.

Norman, D.I., Ting, W., Putnam, B. R. III, and Smith, R.W. (1985): Mineralization of the Hansonburg Mississippi-Valley-type Deposit, New Mexico: Insight from Composition of Gases in Fluid Inclusions. *Can. Mineral.* **23**, 353-368.

Palmer, D.A.S., and Williams-Jones, A.E. (1996): Genesis of the carbonatite-hosted fluorite deposit at Amba Dongar, India; evidence from fluid inclusions, stable isotopes, and whole rock-mineral geochemistry. *Econ. Geol.* **91**, 934-950.

Pell, J., and Hora, Z.D. (1987): Geology of the Rock Canyon Creek fluorite/rare earth element showing, southern Rocky Mountains. British Columbia Ministry of Energy, Mines and Petroleum Resources, Geological Fieldwork 1986, Paper 1987-1, 255-261.

Perhac, R.M., and Heinrich, E.W. (1964): Fluorite-bastnaesite deposits of the Gallinas Mountains, New Mexico and bastnaesite paragenesis. *Econ. Geol.* **59**, 226-239.

Richardson, C.K., and Holland, H.D. (1979): The solubility of fluorite in hydrothermal solutions; an experimental study. *Geochimica et Cosmochimica Acta*, **43**, 1313-1326.

Salvi, S., and Williams-Jones, A.E. (1992): Reduced orthomagmatic C-O-H-NaCl fluids in the Strange Lake rare-metal granitic complex, Quebec/Labrador, Canada. *Eur. J. of Mineral.* **4**, 1155-1174.

Samson, I.M., Al-Aasm, I.S., and Zhu, L. (2000): Dolomitization and Mineralization in the Rock Canyon Creek fluorite-REE deposit, B.C.. Program and Abstracts, GeoCanada 2000, Calgary.

Samson, I.M., Kerr, I.D., and Graf, C. (2001): The Rock Canyon Creek fluorite-REE deposit, British Columbia. In CIM Special Volume: Industrial Minerals in Canada, 1-10.

Schneider, H. J., Möller, P., and Parekh, P.P. (1975): Rare Earth Element distribution in fluorites and carbonate sediments of the East-Alpine Mid-Triassic sequences in the Nordliche Kalkalpen. *Min. Dep.* **10**, 330-344.

Schreiner, R.A. (1993): Mineral investigation of the rare-earth-element-bearing deposits, Red Cloud mining district, Gallinas Mountains, Lincoln County, New Mexico: U.S. Bureau of Mines, Open File Report 99-93, 189 p.

Simmons, W.B., and Heinrich, E.W. (1970): Rare-earth-fluorine pegmatites of the South Platte district, Jefferson County, Colorado. Geological Association of Canada-Mineralogical Association of Canada, Joint Annual Meeting, Abstracts of Papers, p. 48-49.

Simmons, W.B., and Heinrich, E.W. (1980): Rare-earth pegmatites of the South Platte district, Colorado, Colorado Geological Survey, Department of Natural Resources, Resource Series 11, 131 p.

Simmons, W.B., Lee, M.T., and Brewster, R.H. (1987): Geochemistry and evolution of the South Platte granite-pegmatite system, Jefferson County, Colorado. *Geochimica et Cosmochimica Acta*, **51**, 455-471.

Smith, D.R., Noblett, J., Wobus, R.A., Unruh, D., Douglass, J., Beane, R., Davis, C., Goldman, S., Kay, G., Gustavson, B., Saltoun, B., and Stewart, J. (1999): Petrology and geochemistry of late-stage intrusions of the A-type, mid-Proterozoic Pikes Peak batholith (Central Colorado, USA): implications for petrogenetic models. *Precambrian Research*, **98**, 271-305.

Strong, D.F., Fryer, B.J., and Kerrich, R., 1984. Genesis of the St. Lawrence Fluorospar Deposits as Indicated by Fluid Inclusion, Rare Earth Element, and Isotopic Data. *Econ. Geol.* **79**, 1142-1158.

van Achterbergh, E., Ryan, C.G., Jackson, S.E., and Griffin, W.L. (2001): Data Reduction Software for LA-ICP-MS. *In* Laser-Ablation-ICPMS in the Earth Sciences, Mineralogical Association of Canada, Short Course Series, **29**, 239-243.

Van Alstine, R.R. (1948): Geology and Mineral Deposits of the St. Lawrence Area, Burin Peninsula, Newfoundland: Geological Survey of Newfoundland, Bulletin 23, 64 p.

Williams-Jones, A.E., Samson, I.M., and Olivo, G.R. (2000): The Genesis of Hydrothermal Fluorite-REE Deposits in the Gallinas Mountains, New Mexico. Economic Geology, v. 95, p. 327-342.

Chapter 3

LA-ICP-MS Analysis of Fluid Inclusions

Preface

Chapter 3 is primarily a literature review of the LA-ICP-MS analysis of fluid inclusions that was prepared for a *Mineralogical Association of Canada* short course. The chapter presents a summary of the instrumentation, methods, and techniques for the analysis of fluid inclusions.

Two original techniques presented in Chapter 3 are a method for removing the host mineral contribution to the fluid inclusion signal and traversed fluid inclusion opening. In addition to conducting controlled opening of fluid inclusions, removal of any host mineral influence is necessary to obtain accurate and precise analyses of fluid inclusions. The data reduction method involves calculating the ratio of the count rates for all elements analyzed in the fluid inclusion versus the count rate obtained for an element present in significant (i.e., weight %) concentrations in the host mineral. The applicability of the method is demonstrated by the determination of the composition of a fluid inclusion hosted by fluorite. The goal of the hardware modification presented in Chapter 2 (i.e., beam constriction), and the combined traversed fluid inclusion opening and data reduction protocols presented in Chapter 3 are the representative and quantitative analysis of fluid inclusions in minerals with complex compositions that poorly absorb laser energy at 266 nm wavelength. These techniques are applied to the analysis of quartz- and fluorite-hosted fluid inclusions from a fluorite-REE mineral deposit in a subsequent chapter (Chapter 4).

LA-ICP-MS Analysis of Fluid Inclusions

J. E. Gagnon[1, 2], I.M. Samson[1], and B.J. Fryer[1]

[1] *Department of Earth Sciences, University of Windsor*
Windsor, Ontario, Canada, N9B 3P4
[2] *Department of Earth and Planetary Sciences, McGill University*
Montreal, Quebec, Canada, H3A 2A7

Introduction

The methods available for the quantitative chemical analysis of individual fluid inclusions increased in the 1990s with the application of new micro-analytical techniques to fluid inclusions, notably laser ablation inductively-coupled plasma mass spectrometry (LA-ICP-MS), laser ablation inductively-coupled plasma optical emission spectroscopy (LA-ICP-OES), laser-induced breakdown spectroscopy (LIBS), proton-induced x-ray emission (PIXE), proton-induced gamma-ray emission (PIGE), and synchrotron x-ray fluorescence (cf. Anderson & Mayanovic 2003), that are capable of measuring fluid compositions in fluid volumes less than 1000 μm^3. Of these methods, LA-ICP-MS has emerged as a frontrunner in the quantitative elemental analysis of individual fluid inclusions, largely due to relatively low capital costs, ease of use, ability to obtain data from depths significantly below the surface of samples, and adaptability to a wide range of analytical problems. The strengths of LA-ICP-MS analysis are minimal sample preparation and disturbance, the ability to obtain quantitative elemental analysis of individual fluid inclusions, high spatial resolution (down to 2 μm), high sensitivity (detection limits of less than 1 μg/g), moderate to high precision (5 to 30 %), and the ability to provide rapid, multi-element analysis over wide mass (normally 6 to 240 amu) and dynamic (up to 11 orders of magnitude) ranges (Montaser et al. 1998, Ridley & Lichte 1998, Shepherd & Rankin 1998, Heinrich et al. 2002). Despite these attributes, significant challenges remain in the routine application of LA-ICP-MS to the analysis of fluid inclusions that include internal standardization, correction of host mineral contribution to fluid inclusion signal, data reduction, and elimination of spectral interferences. Although LA-ICP-MS

analysis is capable of determining the concentrations of the majority of elements in the periodic table within a variety of matrices, it generally cannot provide data on extremely electronegative elements (e.g., F), or molecular species (e.g., SO_4, CO_2), for which bulk methods (Gleeson 2003, Salvi & Williams-Jones) or other spectroscopic methods (Burruss 2003, Anderson & Mayanovic 2003) are necessary.

The objective of this chapter is to provide an overview of the LA-ICP-MS method, review common LA-ICP-MS instrumentation, and discuss project design, data collection and data evaluation strategies for the analysis of individual fluid inclusions. The chapter is also designed to enable the reader to determine the applicability of LA-ICP-MS analysis to the problem at hand and how LA-ICP-MS can be applied to address specific geologic problems of interest to the reader.

Background

What is Laser Ablation?

The discovery of laser action dates from the late 1950s, however, the application of lasers as a means of ablating and sampling earth and other solid materials did not rise to prominence until the 1980s and early 1990s (e.g., Gray 1985, Arrowsmith 1987, Moenke-Blankenburg et al. 1990, Jackson et al. 1992, Longerich et al. 1993). Laser ablation is a micro-sampling technique where a high-energy, small-diameter, typically monochromatic, pulsed laser beam (typically 5 to greater than 1000 mJ, and 5 to 200 μm) is used to ablate small volumes of sample material. Focusing of the laser beam onto the sample typically is achieved using a specially constructed or modified petrographic (polarizing light) microscope. The results of absorption of the laser radiation by the sample are numerous and include heating, melting, vaporization, atomization, excitation and ionization (Fabre et al. 2002a), which can occur in a controlled or explosive manner depending on the characteristics of the material being ablated and the wavelength of laser radiation. Consequently, numerous analytical challenges result from the complexity of the interaction of laser energy with the

sample, one of the most notable being elemental fractionation (e.g., Fryer et al. 1995, Guillong & Günther 2002). The ablated material typically comprises a mixture of fine particles, ions, and gases that are transported from the point of ablation (usually a sampling cell) to the ICP-MS using a single (typically Ar or He) or mixture of carrier gases. Several different wavelengths of laser energy, ranging from the infrared (e.g., 1064 nm) to the far ultraviolet (e.g., 193 nm), have been used for laser ablation applications. Currently the two most commonly used are ultraviolet solid state (e.g., 266 nm and 213 nm neodymium-doped, yttrium-aluminum garnet (Nd:YAG)) and gas (e.g., 193 nm ArF Excimer) lasers. For ArF Excimer lasers, the 193 nm wavelength is the fundamental wavelength, whereas the 266 and 213 nm wavelengths of Nd:YAG lasers are achieved through the use of frequency quadrupling and quintupling crystals, respectively, of the 1064 nm fundamental wavelength. Ideally, the wavelength of laser energy used for ablation should be selected based on the absorption characteristics of the specific material to be sampled; however, UV laser light is typically selected because it is efficiently absorbed by a wide range of materials. Recent studies (e.g., St-Onge et al. 2002) have demonstrated the simultaneous use of multiple wavelengths of laser energy to achieve enhanced laser ablation sampling efficiency.

What is LIBS?

The use of lasers for creating a plasma for spectral analysis dates from the 1960s (e.g., Brech & Cross 1962). Unlike LA-ICP-MS, where a laser beam is used to ablate a sample that is subsequently transported to an ICP-MS for analysis, LIBS utilizes the optical emission spectrum emitted from the plasma generated by the laser beam at the point of sampling. Spectral analysis of the emitted radiation is conducted using a spectrograph (e.g., Fabre et al. 2002b). The application of LIBS analysis to the spectral analysis of solids, liquids and gases has been extensive (e.g., Cremers & Radziemski 1983, Cremers et al. 1984, Fabre et al. 2002a, St-Onge et al. 2002). However, application of LIBS specifically to the analysis of fluid inclusions has been limited to only a few

studies that have generally provided data on major element ratios only (e.g., Derome et al. 2002, Fabre et al. 2002b). Presently, LIBS has higher limits of detection and approximately two orders of magnitude less dynamic range relative to LA-ICP-MS, which limit the ability of LIBS to conduct multielement analysis over wide concentration ranges (i.e., from trace to major elements). However, the number of studies and analytical capabilities are likely to increase as the use of LIBS instrumentation designed specifically for fluid inclusion analysis becomes commercially available. Recent descriptions and reviews of LIBS have been presented by Radziemski (2002) and Tognoni et al. (2002) and this technique will not be considered further in this chapter.

What is ICP-MS?

The use of ICP-MS as a method for elemental analysis dates from the 1960s; however, significant expansion of the use of ICP-MS did not occur until the late 1980s, largely as a result of the development of relatively low-cost commercial instrumentation. In general, ICP-MS can be used to determine the concentration of any element that can be converted to a positive ion in the presence of a gas plasma (typically Ar). An ICP mass spectrometer typically consists of four principal elements – an ion source (the plasma), an ion focusing system (e.g., electronic lenses), a mass analyzer (typically a quadrupole for LA-ICP-MS analysis), and an ion detector. For most types of ICP-MS analysis, a wet sample, introduced in the form of an aerosol, is desolvated, vaporized, atomized, and ionized by a plasma created by passing a high current through Ar gas. The Ar plasma has gas and electron temperatures ranging from 4,500 to 10,000 K (Montaser et al. 1998). These temperatures are adequate to ionize a significant proportion of most elements with the exception of the more electronegative elements (e.g., S, Cl) where a lesser proportion of the elements are ionized.

A standard resolution quadrupole mass analyzer uses electrical fields to discriminate elements based on their mass/charge (m/z) ratio (see also Salvi & Williams-Jones 2003). Therefore, a typical quadrupole ICP-MS cannot

differentiate between elements and molecules that have similar m/z ratios. One of the fundamental challenges in ICP-MS analysis is avoiding spectral interferences, i.e. those components of the signal that are not contributed by the element (ion) of interest at a particular m/z ratio. Examples of common spectral interferences include molecular and isobaric interferences. Molecular interferences result from positively-charged molecules that have similar m/z ratios as individual elements (e.g., $Cu^{63}Ar^{40}$ and Rh^{103}). Most molecular interferences are created in the ICP and result from the presence of atmospheric gases, water, or plasma and sampling gases (e.g., H, He, C, N, O, S, Cl, and Ar) and their impurities (Ne, Kr, Xe, and Hg) that form hydride/hydroxide, carbide, nitride/nitrate, oxide/hydroxide and argide interferences that correspond with the m/z ratio of the analytes of interest. The combination of gas species with matrix elements (e.g., $Ar^{40}Cl^{35}$) can result in molecular interferences that coincide with other elements of interest (e.g., As^{75}). Molecular interferences can often be reduced or eliminated through a combination of using ultra-high purity gases, instrument tuning, sample desolvation or through the use of a collision/reaction cell (e.g., Hattendorf & Günther 2000, Mason 2001). Isobaric spectral interferences result from isotopes of different elements that have the same masses (e.g., Ar^{40} and Ca^{40}). Isobaric interferences can generally be avoided by selecting alternate isotopes of the desired element or can be corrected using natural abundances of the isotopes and subtracting the contribution to the analysis resulting from the isobaric interference.

The ion detector consists of either an ion counting (i.e., pulse) or an analogue detector, or a combination of the two in the form of a dual mode detector. Use of a dual mode detector extends the dynamic range of the ICP-MS instrument and enables the detection of major, minor and trace elements within a single analysis. For laser ablation sampling, the strengths of ICP-MS are relatively low detection limits (typically µg/g), good precision (generally 2 to 5 % relative standard deviation), detection of most elements, and wide dynamic range (up to 11 orders of magnitude) (Fryer et al. 1995, Montaser et al. 1998).

A quadrupole ICP-MS is generally preferred for multi-element chemical analysis because of its ability to rapidly analyze a large number of isotopes over wide ranges of mass and concentration. Other types of mass spectrometers have been used for laser ablation analyses (e.g., single or multiple collector sector field, time of flight). However, the use of these instruments is limited to specific applications such as isotopic analysis (e.g., Jackson et al. 2001) and materials engineering (e.g., Varel et al. 1998) where higher precision or molecular/structural information is required. Furthermore, inductively-coupled plasma time of flight mass spectrometers (ICP-TOF-MS) currently lack the sensitivity and dynamic range required for fluid inclusion analysis (Bleiner et al. 2000).

Two other phenomena affecting ICP-MS analysis are memory effects and elevated backgrounds. Ions introduced to the ICP-MS during analysis may be retained within the ICP-MS for a period of time after cessation of sample introduction, resulting in memory effects. Elevated backgrounds result from a number of factors including long-term memory effects (e.g., ion optics and detector contamination), photons entering the mass analyzer, electronic instrument noise and sample matrix effects. The result of memory effects and background are similar in that they elevate the limits of detection or prevent the detection of subtle, low level or short term compositional variations within transient signals and are particularly detrimental to the analysis of fluid inclusions.

What is ICP-OES?

ICP-OES is similar to ICP-MS in that an Ar plasma is used to ionize an aerosolized sample but differs from ICP-MS in the manner that the sample is analyzed. In ICP-OES, spectral analysis consists of the precise measurement of the wavelength of the radiation emitted by the analyte as a result of ionization in the Ar plasma. This is accomplished using a spectrograph comprising a complex system of mirrors, gratings, slits, apertures, collimators, prisms, lenses and detectors. Thompson et al. (1981) were the first to attempt integration of an ICP-

OES with laser ablation. The subsequent development of higher-powered ultraviolet lasers has lead to the continued application of LA-ICP-OES to the analysis of earth materials, including fluid inclusions (e.g., Pettke et al. 2000). However, ICP-OES is less desirable than ICP-MS for the analysis of fluid inclusions due to the poorer sensitivity, inability of the method to determine isotopic ratios and detection limits that are 10 to 100 times higher than ICP-MS (Wilkinson et al. 1994, Shepherd & Chenery 1995, Moissette et al. 1996, Pettke et al. 2000). LA-ICP-OES will not be considered further in this chapter.

Fluid Inclusion Analysis by LA-ICP-MS

Conceptually, the analysis of fluid inclusions using LA-ICP-MS is simple. The fluid inclusion is sampled by the laser beam within an Ar- or He-filled sampling cell. The laser beam is focused onto the sample using a microscope lens, the laser beam 'bores' into the sample, and the ablated material is transported from the sampling cell to the ICP-MS using an Ar and/or He carrier gas. The ICP-MS conducts the analysis and the data output is processed using either the software provided with the ICP-MS, third-party software, such as GLITTER or LAMTRACE (van Achterbergh et al. 2001), or using other means (e.g., commercial spectral analysis and spreadsheet software).

The apparent ease of conceptual analysis notwithstanding, practical application of LA-ICP-MS to the analysis of fluid inclusions is complicated by many factors. These include, but are not limited to, the requirement for an internal standard against which the concentrations of all other elements within the fluid inclusion can be determined, the availability of matrix-matched standards, potentially poor ablation characteristics due to low absorbance of the laser energy by the fluid inclusion host mineral (e.g., quartz), differential ablation of fluid inclusion contents (e.g., trapped or daughter solids relative to liquid), excessively large laser beam spot diameter relative to fluid inclusion size, extremely small fluid inclusion sample volumes (i.e., mass of analyte), uncontrolled opening of the fluid inclusion, mixing of host mineral and fluid inclusion constituents, short-term transient signals, and elemental fractionation at

the point of sampling and within the ICP-MS. Add to these factors the spectral interferences within the ICP-MS and analysis and interpretation of fluid inclusions by LA-ICP-MS can become exceedingly complicated. Altogether, these factors potentially result in non-representative sampling of fluid inclusions or imprecision in the calculation of quantitative fluid inclusion compositions.

A number of studies of fluid inclusions have been performed using LA-ICP-MS (e.g., Shepherd & Chenery 1995, Moissette et al. 1996, Ghazi et al. 1996, Audetat et al. 1998, Samson et al. 1998, Shepherd et al. 1998, Günther et al. 1998, Heinrich et al. 1999, Ulrich et al. 1999, Audetat et al. 2000, Muller et al. 2001, Gagnon et al. 2002, Landtwing et al. 2002, Heinrich et al. 2002, Audetat & Pettke 2003). The earlier investigations generally comprised reconnaissance studies and presented analytical results in terms of element ratios rather than concentrations. Later investigations (e.g., Audetat et al. 1998, Günther et al. 1998, Heinrich et al. 1999, Ulrich et al. 1999, Audetat et al. 2000, Gagnon et al. 2002, Landtwing et al. 2002, Audetat & Pettke 2003) used measurements of total salinity, obtained through microthermometric analysis, to determine the concentration of Na, which was subsequently used as an internal standard against which all other elemental concentrations within the fluid inclusion were calculated. This approach provided the internal standard that is required to calculate elemental concentrations but such calibration strategies suffer from the limitations inherent in estimates of salinity obtained using microthermometry; i.e., the estimate of the Na concentration may not be accurate due to the presence of other dissolved elements (e.g., Ca, K, Mg, and Fe) and may need to be corrected in order to obtain a quantitative analysis.

The effect of different sample matrices on ICP-MS analysis is well documented (e.g., Horlick & Montaser 1998). The analysis of highly saline, Cl-bearing, aqueous fluid inclusions in minerals such as quartz, which is essentially free of H_2O and Cl relative to the fluid inclusions, poses one of the most dramatic changes in sample matrices that could be encountered during a single analysis using ICP-MS. For example, Cl-related molecular interferences create some of the most problematic matrix effects for the analysis of As and V using ICP-MS

(Horlick & Montaser 1998). Although matrix effects during fluid inclusion analysis have been studied (e.g., Günther et al. 1997), extensive evaluation and quantification of possible matrix effects (e.g., molecular interferences, effects on instrumental mass bias, etc.) for a wide variety of fluid inclusion compositions has not been conducted. Furthermore, a time dependency on the isotopic composition of LA-ICP-MS analysis resulting from elemental fractionation has been demonstrated for solid materials (e.g., Fryer et al. 1995, Guillong & Günther 2002, Jackson & Günther 2003) but has not been evaluated for fluid inclusions. Presumably, both effects may have the potential to influence the quantitative analysis of fluid inclusions, particularly those that are dramatically different in composition from the calibration standard or vary significantly in depth relative to the sample surface.

Strategies have been developed for the quantitative determination of fluid inclusion compositions that use the ratio of the relative sensitivity (i.e., integrated counts/second (icps) per µg/g) of Na in a standard material (e.g., NIST 610 and 612 glasses) to fluid inclusions (e.g., Günther et al. 1998, Heinrich et al. 2002). Although the use of an estimate of Na from the fluid inclusion (corrected for the presence of other cations) is a requirement for the quantitative analysis of fluid inclusions, using the ratio of the Na sensitivity for NIST silicate glass relative to that in the fluid inclusion may compensate for, but does not identify, quantify, or quantitatively correct for matrix effects potentially resulting from the introduction of saline, aqueous fluids to the ICP-MS. Whether of not the relative ICP-MS instrument response for Na can be applied to all other elements for all potential fluid inclusion compositions remains unknown. To fully understand and quantify potential fluid inclusion matrix effects, a study of a wide range of known fluid inclusion compositions needs to be undertaken. Without such an evaluation, one of the greatest uncertainties to the application of LA-ICP-MS for the routine quantitative determination of individual elemental concentrations in fluid inclusions of widely varying composition is the lack of rapid, proven calibration methods that (1) effectively simulate, as close as is reasonably possible, the

range of host mineral and fluid compositions and the volumes typical of natural fluid inclusions, and (2) are relatively rapid and inexpensive to prepare.

The potential user must recognize that LA-ICP-MS combines two complicated processes (and all associated limitations) into a single method. Many of the causes of some of the phenomena associated with LA-ICP-MS (e.g., interaction of photons with matter, elemental fractionation) are only starting to be understood (e.g., Guillong & Günther 2002, Jackson & Günther 2003). Therefore, it is imperative that the potential user tenor expectation against what is reasonably achievable. Obviously, perseverance and innovation can, and have already, overcome some of the earlier limitations of the method.

Equipment

Introduction

Infrared Nd:YAG lasers, operated at the fundamental frequency of 1064 nm, were used to construct the initial laser ablation systems used for earth science applications (e.g., Jackson et al. 1992). However, many minerals, including common fluid inclusion host minerals (e.g., quartz, apatite, calcite, and fluorite), are not strong absorbers of electromagnetic radiation in the infrared region. This resulted in uncontrolled ablation of some host minerals and explosive rupturing of fluid inclusions, effectively preventing quantitative analysis of the inclusions. To obtain improved ablation characteristics for a wider variety of minerals, Nd:YAG laser ablation equipment was modified to provide frequency-quadrupled (266 nm) radiation through the use of two doubling, harmonic-generating crystals, and subsequently to provide frequency-quintupled (213 nm) radiation, by the addition of a 5^{th}-harmonic generating crystal. These wavelengths provide better ablation characteristics for a wider range of materials. Other types of lasers, most notably ArF gas Excimer lasers operated at 193 nm, were also adapted for the analysis of earth materials including fluid inclusions (e.g., Günther 2001). These three laser configurations comprise the majority of the purpose-built and commercial laser systems presently being used for the

analysis of fluid inclusions (e.g., Günther et al. 1998, Gagnon et al. 2002, Landtwing et al. 2002). Other highly specialized systems which use lasers of different wavelengths (e.g., 156 nm Excimer) or combinations of fundamental and frequency-multiplied wavelengths (e.g., 1064 and 266 nm, St-Onge et al. 2002) are either currently in the development stages or have been constructed or used for very specific applications and will not be addressed in any detail in this chapter.

Much of the authors' practical understanding of LA-ICP-MS analysis of fluid inclusions has come from the use of the instrumentation housed within the Great Lakes Institute at the University of Windsor. The purpose-built facility comprises a Continuum® Surelite® I-20 Q-switched, 266 nm Nd:YAG pulsed laser and ThermoElemental® X-7 quadrupole ICP-MS. Our understanding of other research and commercial laser ablation systems has been gained through interaction with researchers, the published literature, and manufacturers' specifications for commercial systems.

Lasers Systems

Detailed discussions of 266 and 213 nm Nd:YAG, and 193 nm ArF Excimer laser ablation systems used in earth science applications, are presented in Jackson (2001) and Günther (2001), respectively, and only a brief summary of these systems is presented here. Neodymium:YAG and ArF Excimer laser ablation systems commonly comprise a laser head (source of laser energy), an electronics control box and various devices for manipulating (e.g., separating, trimming, dumping, expanding, constricting, homogenizing, polarizing) and measuring the laser beam. In addition, Nd:YAG systems include harmonic-generating crystals (2^{nd}, 3^{rd}, 4^{th}, and 5^{th}) that are required to shorten the wavelength of the laser energy from the fundamental infrared wavelength (1064 nm) to the ultraviolet range (266 nm). Since ArF Excimer lasers have a fundamental wavelength in the ultraviolet region (193 nm), the use of harmonic-generating crystals is unnecessary. A consequence of using harmonic-generating crystals and a wavelength separator in Nd:YAG systems is a

considerable loss of laser power. For example, the specification output power of a frequency-quadrupled Nd:YAG laser drops from approximately 400 mJ at 1064 nm to 50 mJ at 266 nm as a result of the combination of frequency quadrupling and wavelength separation.

Beam homogenization during fluid inclusion analysis has been used with both Nd:YAG (Guillong et al. 2002) and ArF Excimer (Günther et al. 1998) lasers to compensate for the Gaussian and non-uniform energy distributions within Nd:YAG and ArF Excimer laser beams, respectively. Beam homogenization has been shown to create a homogeneous energy distribution across the entire ablation pit, which results in controlled and more uniform ablation and reduced elemental fractionation. Similar improvements in ablation properties can be obtained using a non-homogenized Nd:YAG laser beam and installing beam constrictors (i.e., 'pinholes') in the beam path. The beam constrictors trim the outer, lower energy portion of the Gaussian energy distribution which results in more uniform ablation and reduced elemental fractionation (Crowe et al. 2003). Using a trimmed, non-homogenized Nd:YAG beam preserves the high energy core of the beam, allows for sizing of the beam to match the desired diameter for fluid inclusion analysis and, for relatively small diameter constrictors centered on the core of the beam, approximates a beam with uniform energy distribution. All of this is achieved without the loss of power associated with beam homogenization, which is a definite benefit to Nd:YAG systems that are already at a disadvantage to ArF Excimer systems in terms of energy and power output.

Advantages of the Nd:YAG systems relative to ArF Excimer systems are lower initial capital and operating costs, robustness of the technology (widespread industrial application of solid state Nd:YAG lasers has led to significant improvements in laser energy, stability and longevity), and tunability of the laser line through the use of harmonic-generating crystals. The ArF Excimer lasers are at a distinct advantage when working with poorly-absorbing minerals (e.g., quartz) due to the shorter wavelength and higher energy and power output of this type of laser, which is more than adequate to compensate for any power losses resulting from beam homogenization. In all cases, having an abundance

of laser power that can be attenuated through the use of optical elements (e.g., beam splitters and dumps) is preferable to not having enough power.

Several commercial Nd:YAG and Excimer laser systems constructed specifically for the analysis of earth materials have entered the market since the late 1990s. Generally, the advantage of purpose-built over commercial systems is the ability to readily modify the system to perform application-specific analyses (e.g., adding beam attenuators and restrictors to limit laser energy and select laser spot size). An advantage that commercial systems commonly have over purpose-built systems is the level of integration between the hardware and instrument control software which contributes to the relatively more 'user-friendly' nature of commercial systems. However, it is important to consider that many of the apparent limitations of any of these systems can commonly be overcome through the construction of equipment- and application-specific hardware and instrument modifications.

Microscope and Sampling Cell

Laser ablation systems typically use some sort of purpose-built or modified petrographic microscope equipped with specially-constructed, ultraviolet-tolerant mirrors, beam splitters and objective lenses to redirect and focus the laser beam onto the sample. A schematic diagram of a purpose-built Nd:YAG system is illustrated in Figure 3-1. Apart from having all optical components within the microscope that interact with the laser beam made of materials that can tolerate the energy of the laser beam, the construction of the objective lenses is critical in obtaining good imaging and focusing of the laser energy for fluid inclusion analysis. Presently, there are two common types of laser-focusing objective lenses, namely refracting and reflecting (Schwarzschild). In general, refracting lenses tend to provide better laser energy focusing and visible imaging, which is critical to observing fluid inclusion behavior during analysis. The poorer focusing of the laser beam by reflecting lenses results from reflectance and focusing losses of laser energy within the lenses due to the use of multiple mirrors in the lens construction that are not 100% reflective in the

Figure 3-1. Photograph (**A**) and schematic diagram (**B**) of laser ablation system at the University of Windsor.

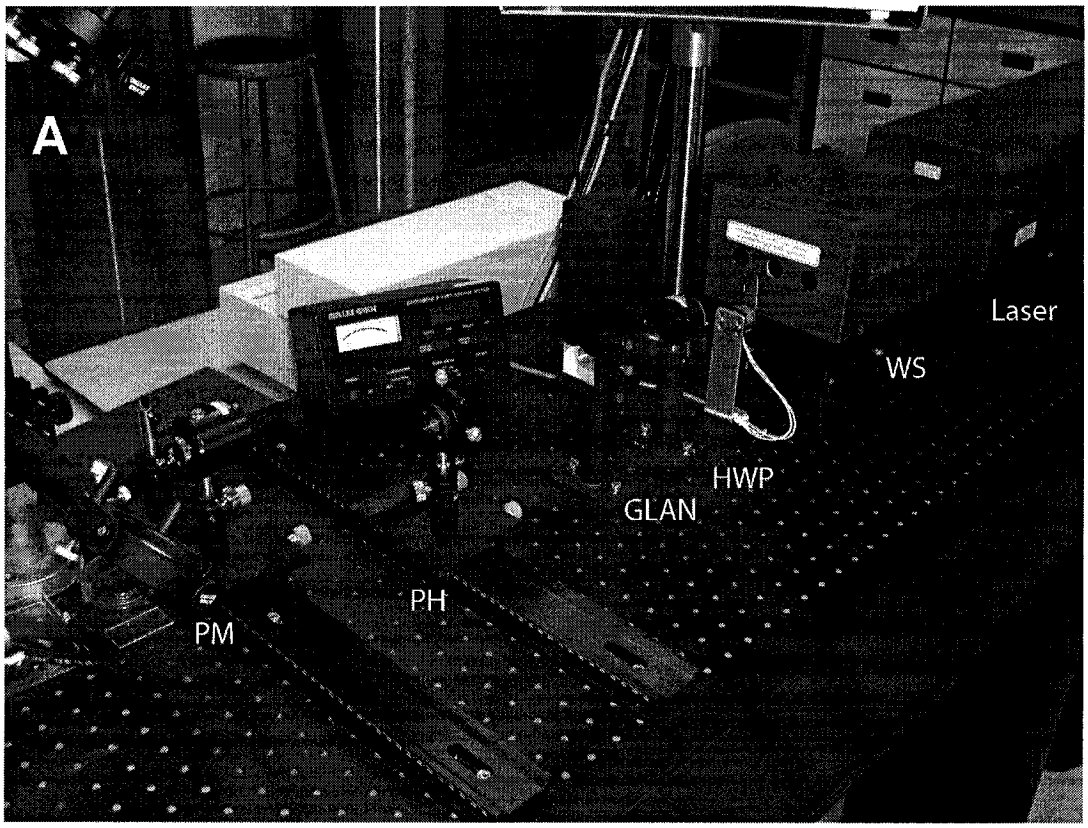
A
Laser
WS
HWP
GLAN
PH
PM

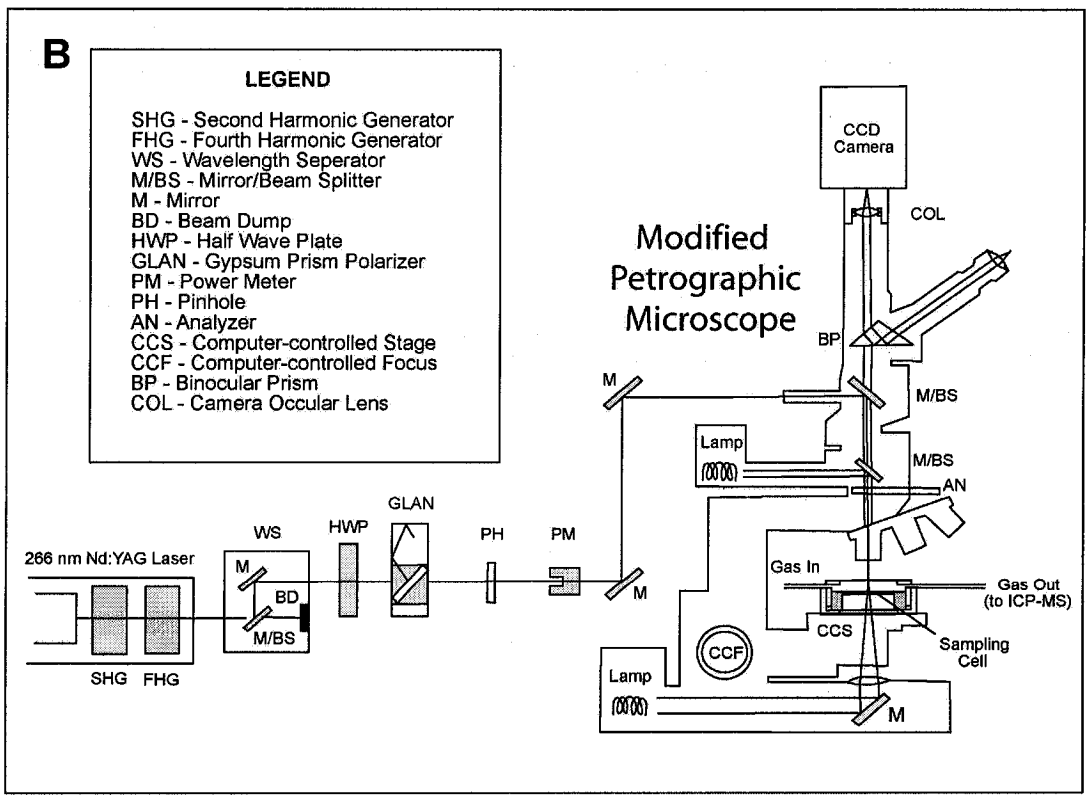
B
LEGEND
SHG - Second Harmonic Generator
FHG - Fourth Harmonic Generator
WS - Wavelength Seperator
M/BS - Mirror/Beam Splitter
M - Mirror
BD - Beam Dump
HWP - Half Wave Plate
GLAN - Gypsum Prism Polarizer
PM - Power Meter
PH - Pinhole
AN - Analyzer
CCS - Computer-controlled Stage
CCF - Computer-controlled Focus
BP - Binocular Prism
COL - Camera Occular Lens
Modified Petrographic Microscope
CCD Camera
COL
BP
M
M/BS
Lamp
M/BS
AN
Gas In
Gas Out (to ICP-MS)
CCS
Sampling Cell
CCF
Lamp
M
266 nm Nd:YAG Laser
SHG
FHG
WS
M
BD
M/BS
HWP
GLAN
PH
PM
M

ultraviolet region. An advantage of reflecting over refracting lenses is the longer working distance of the former at similar magnifications. Therefore, to take advantage of the better imaging and energy focusing of refracting lenses, the design of the sampling cell should minimize the working distance by using, for example, thin optical windows and large lens recesses.

The design of the laser ablation sampling cell is an exercise in managing compromises. There are two broad categories of sampling cells, large-volume, multi-purpose cells and small-volume, purpose-specific cells (Fig. 3-2). The earliest sampling cells used for laser ablation purposes were not designed specifically for fluid inclusion analysis and had relatively large sample volumes in order to accommodate a number of different sample sizes, types and shapes. Although providing flexibility, the large sample volumes result in extended mixing of ablated material with the carrier gas within the cell, which has the effect of prolonging the duration and lessening the amplitude of the fluid inclusion signal. This can have the effect of completely obscuring the fluid inclusion signal, particularly when analyzing small fluid inclusions within poorly-absorbing materials with complex compositions (e.g., fluorite, synthetic glasses). Laser ablation sampling cells designed specifically for fluid inclusion sampling tend to have relatively small volumes to minimize mixing, and are configured to optimize the flow of the carrier gas over the area where the laser ablation sampling occurs to enhance sample transport efficiency (e.g., Günther 2001). Unlike larger sampling cells, smaller cells provide less flexibility in accommodating samples, but provide a better fluid inclusion signal response relative to the host mineral background signal.

Figure 3-2. Examples of sampling cell configurations used for laser ablation sampling. Sampling cell on the left (**A**) provides a large sampling volume to accommodate a number of sample configurations. Through the use of spacers under the sample holder, this cell can accommodate samples up to several millimeters thick. The cell on the right (**B**) is designed specifically to minimize sampling volume and to channel the flow of carrier gas across the sampling site to improve signal to background for small volume samples such as fluid inclusions. Although significantly smaller in volume than the cell on the left, the cell on the right maintains the tunability of the sampling volume through the use of sleeved sample holders that are held in place by set screws that are accessible from the exterior of the sampling cell.

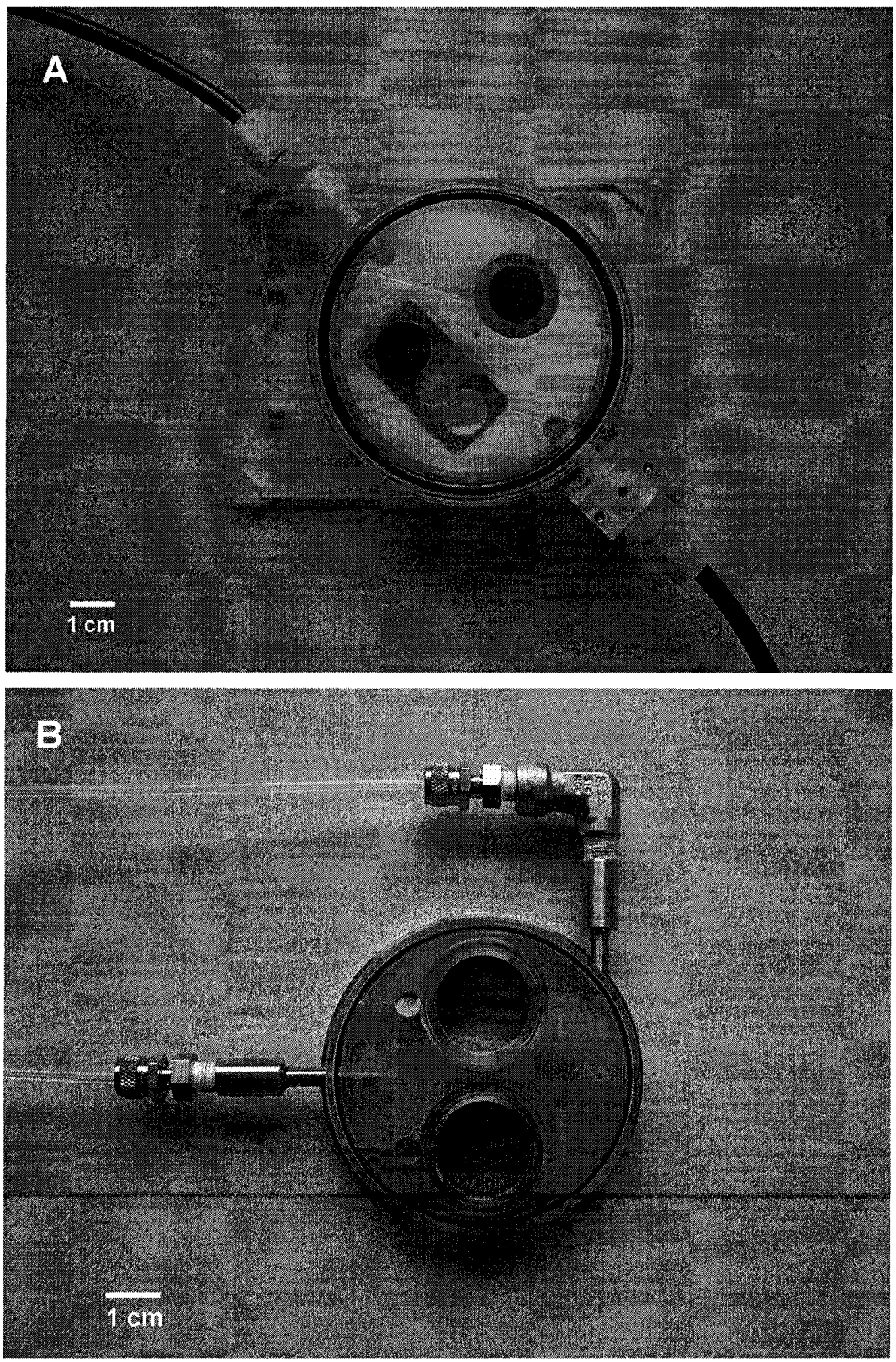
A
1 cm
B
1 cm

Although the fluid inclusion signal to host mineral background signal ratio can be improved dramatically through the use of smaller cell volumes, the point at which the amplitude of the fluid inclusion signal is maximized approximately corresponds with the point were the duration of the fluid inclusion signal is shortest, potentially resulting in insufficient signal duration to obtain a reliable analysis, particularly for fluid inclusions of small volume. Since many other factors affect the fluid inclusion signal relative to host mineral background (e.g., carrier gas type and flow rate, dynamics of gas flow within the cell and transfer tubing, 'wet' or 'dry' ICP-MS plasma conditions), there is no optimal sample cell volume for all possible equipment configurations and fluid inclusion sizes. Constructing a sample cell where the volume can be 'tuned' through adjustment (e.g., insertion of spacers to eliminate 'dead space') is advisable if a variety of fluid inclusion sizes are to be analyzed. This allows an additional means of extending the duration of fluid inclusion signals where relatively high precision is required or maximizing fluid inclusion signal to host background where the detection of trace elements is desired.

Carrier Gas

One of the most significant factors affecting sensitivity is the type of gas used within the ablation cell (Eggins et al. 1998, Günther & Heinrich 1999). Argon was first used as a carrier gas for LA-ICP-MS and is still in use for application-specific analyses. Helium has largely replaced Ar because it has been shown to result in increased sample transport efficiency resulting in an approximately 2- to 5-times increase in analytical sensitivity (Eggins et al. 1998, Günther & Heinrich 1999, Jackson 2001, Günther 2001). Other gases (e.g., H, N) can also be used to enhance sensitivity and experimentation within our lab has shown an increase in sensitivity of approximately 2 to 3 times, particularly for light elements, when H or N is added to the sample prior to introduction to the ICP-MS (Crowe et al. 2003). However, use of additional gases to enhance sensitivity may result in the formation of additional molecular interferences (e.g.,

nitrides and hydrides). If the resulting interferences do not correspond with the analytes of interest, the improved sensitivity can dramatically affect the sensitivity and enable quantification of elemental concentrations that would otherwise be below the limit of detection.

ICP-MS

A high-sensitivity, high-resolution quadrupole ICP mass spectrometer is generally the instrument of choice for laser ablation analysis of fluid inclusions. Due to the short duration of fluid inclusion signals relative to typical ICP-MS solution analysis, it is desirable to select an ICP-MS that has very high sensitivity (at least 10^8 icps per µg/g) and low backgrounds. It is also desirable to have element-specific, tunable mass resolution. This is particularly relevant for fluid inclusion analysis because Na is monoisotopic, typically present at weight percent concentrations in fluid inclusions, and is used as the internal standard for the calculation of fluid inclusion compositions. Therefore, it is often necessary to dampen the Na sensitivity relative to the other elements of interest using a tunable mass resolution setting to prevent saturation of the detector. If ICP-MS detector saturation occurs during analysis of a fluid inclusion, quantitative determination of the fluid inclusion composition will be impossible.

In addition to sensitivity and resolution, a quadrupole ICP-MS is typically selected because of relatively low cost, and the ability to conduct rapid multi-element analysis over wide mass (normally 6 to 240 amu) and dynamic (up to 11 orders of magnitude) ranges (Montaser et al. 1998, Ridley & Lichte 1998, Shepherd & Rankin 1998). The quadrupole ICP-MS trades resolution of individual masses for rapid scanning of a wide mass range. The result is relatively poor resolution of molecular interferences from elemental spectra. However, the rapid scanning of many masses over a wide mass range is ideal for the relatively short-term, transient signals generally produced during laser ablation sampling, and for fluid inclusions in particular. If higher resolution is required, such as is necessary for isotopic determinations, then a multiple collector sector field ICP-MS is required (e.g., Jackson et al. 2001).

In addition to technical specifications and instrumental ability, the choice of mass spectrometer is often based on a number of intangible factors, most of which are gained through experience with prior instrument ownership (e.g., instrument dependability, tactile instrument 'feel', intuitive obviousness of instrument control software). Longerich (2001) presents an insightful discussion of factors to consider when purchasing an ICP-MS.

Conclusions on Instrumentation

The foregoing discussion presents some of the complexities and opportunities presented by various instrument configurations. The fundamental message is to build, buy or use the system that suits the majority of the applications that are foreseen and to provide for some flexibility to accommodate applications that may be unforeseen. In general, there is a trade-off between commercial systems which exchange convenience, ease of use and automation for the adaptability of purpose-built systems.

Technique and Methodology

Project Design

As with any other analytical method, preliminary work and good project design are critical in obtaining precise, quantitative data using LA-ICP-MS. When considering the time required for LA-ICP-MS equipment start-up, stabilization, calibration, and sampling cell flushing, it is imperative that the selected fluid inclusions be located quickly to minimize analytical cost and time and to maximize data collection efficiency. Furthermore, it is critical to understand the capabilities of the specific LA-ICP-MS equipment to be used for the analysis (e.g., spot size, sensitivity, ablation characteristics) in order that the appropriate sample preparation and fluid inclusion size range are considered during inclusion selection and sample preparation. When the appropriate preliminary work is conducted, a large amount of data can be obtained in a

relatively short period of time (typically in excess of 10 fluid inclusion analyses per hour).

When preparing to conduct laser ablation analyses, several preliminary steps are required. Obviously, it is imperative that ***all*** other desired data be obtained from the fluid inclusions (e.g., microthermometry, Raman spectroscopy) prior to conducting laser ablation analysis because the method is destructive. This also applies to fluid inclusions that are proximal to the inclusions to be analyzed because the mechanical agitation and localized heating of the sample associated with laser ablation may cause stretching, leakage or decrepitation, rendering subsequent microthermometric analyses inaccurate. Furthermore, a proportion (typically 10 to 20 %) of the inclusions being ablated will not yield analyses due to uncontrolled ablation. This may result from the inclusions being too close to the sample surface; cryptic host mineral trace element zonation, mineral cleavage, solid inclusions and imperfections causing differential absorption of the laser energy; or decrepitation as a result of conductive heating from the laser sampling. Therefore, it is important to factor in the possible loss of some inclusions during selection to ensure that a representative sample set is ultimately obtained. In relatively problematic host minerals (e.g., minerals with good cleavages), it may be beneficial to delay sampling the most desirable inclusions until some experimentation has been conducted to determine if laser system optimization (e.g., laser spot size, energy, repetition rate) or refinement in the inclusion opening technique is required to minimize the loss of data due to catastrophic fluid inclusion opening.

Presently, the lower size limit for obtaining quantitative fluid inclusion analyses is approximately 5 μm. It is possible to obtain signals from smaller inclusions; however, the exceedingly short duration of the signal obtained from fluid inclusions in this size range makes reliable quantification difficult. If a very restricted element list is used, at a minimum, the major element abundance ratios of small, high salinity fluid inclusions can be determined. Ongoing improvements in quadrupole ICP-MS instrumentation (e.g., higher sensitivity, lower backgrounds, faster scanning, and shorter quadrupole settling times) will further

lower the size limit at which fluid inclusion compositions can be quantitatively determined. Presently, approximately 5 μm should be considered as the lower limit and fluid inclusions should be selected accordingly.

If possible, visit or send representative samples to the LA-ICP-MS facility where the fluid inclusion analyses will be performed in order to confirm that the sample quality (e.g., thickness, polish) and configuration (e.g., size, mounting medium) are appropriate. Alternatively, consult the LA-ICP-MS facility prior to preparing the samples for analysis because different system configurations and imaging abilities may result in significant variability in the capabilities of different laser ablation facilities to handle particular sample configurations. It may be necessary to obtain specially-sized mounting media (e.g., glass sections) from the laboratory facility where the analyses will be conducted in order to accommodate the sampling cell configuration. Furthermore, the relatively high magnifications typically used to conduct microthermometric analysis on smaller fluid inclusions often are not achievable within laser ablation systems due to the need for specialized, long working distance lenses. It is necessary to understand, and accommodate for, the limitations in sampling and imaging abilities early in the sample selection and preparation process in order to ensure that it will be possible to conduct LA-ICP-MS analyses on the selected fluid inclusions.

Having high resolution photomicrographs of the fluid inclusions, at a number of magnifications, is particularly beneficial during analysis. The photomicrographs provide a 'roadmap' that can be used to readily locate and analyze the selected fluid inclusions. Digitizing the individual fluid inclusion locations and using a computer-controlled sampling stage on the laser sampling system can also significantly increase efficiency in locating the fluid inclusions. Detailed high resolution photomicrographs are also useful for annotating information pertaining to the timing and behavior of fluid inclusion opening that can subsequently be used during interpretation of the ICP-MS spectral data.

It may be beneficial to conduct preliminary analyses at the LA-ICP-MS facility to be used for the project. An initial phase of exploratory LA-ICP-MS

analyses would confirm that adequate sample preparation has been completed, allow evaluation of the ablation characteristics of the host mineral, and enable identification of the elements that may be present at concentrations that can be reasonably quantified. Although microthermometry will provide insights into the major elements that may be present within the fluid inclusions, preliminary LA-ICP-MS analyses will give the analyst an opportunity to determine the most appropriate element list, look at signal duration, conduct data reduction to ascertain which elements can be reliably quantified, and determine whether the estimate of Na obtained from microthermometry will require correction due to the presence of other dissolved cations. Based on the results of the preliminary analyses, it is may be necessary to revise the analytical approach (e.g., sample preparation, opening technique, analyte list) to accommodate the host mineral ablation characteristics or relatively short fluid inclusion signal duration.

Fluid Inclusion Analysis

There are a large number of variables to consider when conducting LA-ICP-MS analysis of fluid inclusions, two of the most significant being laser ablation equipment type and configuration, and fluid inclusion host mineral ablation characteristics and composition. Therefore, the approach to be used during analysis of the fluid inclusions may largely be determined during performance of the preliminary analyses described in the previous section. A number of fluid inclusion sampling strategies have been developed to accommodate the various types of laser ablation systems in use, overcome the catastrophic ablation exhibited by some fluid inclusion host minerals, and to provide more precise fluid inclusion analysis. These approaches include direct opening, stepwise opening (Günther et al. 1998), and traversed opening of fluid inclusions.

The earliest attempts at analysis involved sampling by 'drilling' directly into the fluid inclusion using a laser beam of approximately the same diameter as the inclusion. However, the abrupt thermal and mechanical shock to the sample often resulted in catastrophic opening of the inclusion. The uncontrolled,

explosive opening of the inclusion may result in non-representative sampling of the fluid inclusion due to the loss of the inclusion contents through deposition on the sample surface or to the loss of fluid inclusion daughter or trapped phases, or could result in exceedingly short fluid inclusion signal durations preventing reliable spectral integration. Although increases in laser power and shortening of the laser wavelength improved coupling of the laser beam with the host mineral and resulted in more controlled ablation, other opening techniques were devised to improve sampling precision (e.g., stepwise opening) or to overcome complications associated with the ablation characteristics of the host mineral (e.g., traversed opening). However, direct opening of the fluid inclusions works well for minerals lacking cleavage (e.g., quartz) and for fluid inclusions that are significantly below the surface of the mineral. Figure 3-3 illustrates some examples of laser ablation holes directly drilled into fluid inclusions in quartz.

To overcome some of the difficulties associated with direct opening of fluid inclusions and to improve analytical precision, Günther et al. (1998) developed a stepwise method of sampling inclusions. This method involves first opening the fluid inclusion with a relatively small diameter laser beam (approximately 4 to 10 μm), followed by overdrilling of the inclusion with a laser beam of slightly larger diameter than the fluid inclusion. This technique serves to prolong the fluid inclusion signal duration, which improves precision, relieves the overpressure created within the fluid inclusion as a result of heating by the laser beam prior to opening, and limits the amount of host mineral that is sampled with the inclusion, which assists in subsequent reduction of the data. However, this opening technique tends to be applicable only to larger inclusions (greater than approximately 30 μm) and may result in elevated detection limits relative to direct opening of the inclusions (Günther et al. 1998).

Another sampling method designed to address the same issues as stepwise opening is traversed opening. This method involves focusing a laser beam that is approximately the same size as the inclusion on the host mineral at

Figure 3-3. Photomicrograph of laser ablation holes in sample of quartz from South Platte, Colorado. This image illustrates the spatial resolution that is achievable with laser ablation sampling and some of the disruption of the sample that may occur proximal to the sampling location.

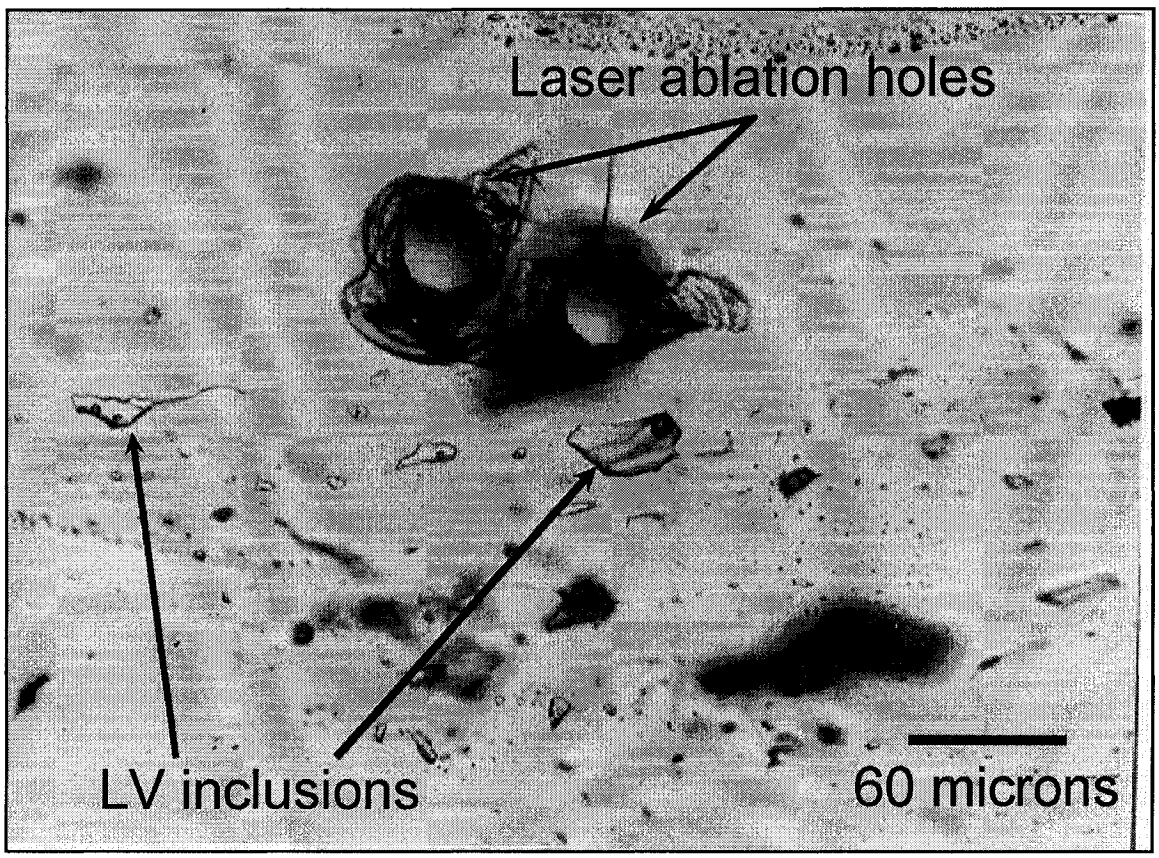
Laser ablation holes
LV inclusions
60 microns

a location away from the fluid inclusion, traversing across the sample surface until the laser beam is over top of the inclusion, and then allowing the laser beam to drill into the inclusion. This overcomes the sudden thermal and mechanical shock to the fluid inclusion observed in direct opening, allows for the establishment of a plasma at the point of sampling prior to opening of the inclusion, and has the added benefit of enabling determination of the host mineral composition from the pre-inclusion signal. This is particularly beneficial in host minerals with relatively poor ablation characteristics (e.g., minerals with relatively poor absorption, good cleavages) and complex compositions (e.g., fluorite) where the host mineral composition may be needed to separate the fluid inclusion composition from the total signal (e.g., Gagnon et al. 2002).

The most appropriate opening technique will depend on the nature of ***each*** fluid inclusion analyzed, as the combination of host mineral type and fluid inclusion depth is potentially unique for each inclusion. Another benefit of the stepwise and traversed opening methods is that the point at which the fluid inclusion is sampled can be accurately determined through direct observation, which is beneficial during subsequent data reduction, particularly for fluid inclusions with complex signals such as those obtained during stepwise opening or traversed opening of inclusions within a compositionally complex host mineral. The opening method that is used is largely determined as a result of trial and error during preliminary analyses.

Calibration Methods

Introduction

Calculation of quantitative elemental concentrations within fluid inclusions requires that (1) a calibration standard be used to generate a single-point calibration line to convert the raw data (i.e., icps) into concentration units (typically µg/g) for the standards, and subsequently the unknowns, and (2) the concentration of at least one element within the inclusion is independently known

and can be used as an internal standard against which all other elemental abundances can be calculated.

Calibration Standards

Several calibration standards have been used for the quantitative LA-ICP-MS analysis of fluid inclusions and minerals. These include synthetic glasses (e.g., NIST and USGS), synthetic fluid inclusions, desolvated standard solutions, microcapillaries, microwells, and fluid inclusion analogs (e.g., Shepherd & Chenery 1995, Moissette et al. 1996, Günther et al. 1998, Günther & Heinrich 1999, Pickhardt et al. 2000). Many of these standards have been evaluated to varying degrees for ease of implementation, accuracy and precision for LA-ICP-MS analysis of fluid inclusions, but most only on a limited basis.

Typically, the fundamental requirements of calibration standards for ICP-MS analysis are that they exhibit similar concentration ranges as the samples to be analyzed and that the standards comprise the same matrix or are contained within a matrix that has the same effect on analytical conditions as the unknown samples (i.e., they are matrix-matched). Intuitively, the ideal calibration standard for LA-ICP-MS analysis of fluid inclusions would consist of aliquots of fluid, similar in volume and composition to the fluid inclusions to be analyzed, set in a matrix similar in composition and ablation characteristics to the host mineral containing the fluid inclusions to be analyzed. Rarely are all these conditions met. LA-ICP-MS analysis of a limited range of synthetic fluid inclusion compositions with quartz suggests that matrix effects during fluid inclusion analysis are limited (Günther et al. 1997, 1998). However, the effect on analytical precision and accuracy of matrix-matching of standards during the analysis of fluid inclusions of a wide range of composition or within compositionally complex host minerals (i.e., fluorite) has not yet been fully evaluated.

NIST and USGS Synthetic Glasses: NIST glasses have become the most widely used standard material for analyses conducted using LA-ICP-MS,

including fluid inclusions, due to their availability, range of compositions, ruggedness, and high degree of certification. Together, NIST and USGS glasses cover a relatively wide range of compositions applicable to many fluid inclusion host minerals and fluid inclusions. Although NIST and USGS glasses do not meet the requirements of matrix-matched standards for fluid inclusion analysis, Günther et al. (1997, 1998) demonstrated that for a limited range of synthetic fluid inclusion compositions hosted by quartz, the use of NIST glass standards results in acceptable analytical precision and accuracy.

Synthetic Fluid Inclusions: Fluid inclusions can be synthesized at relatively low temperatures (less than 100°C) and atmospheric pressures within halide and sulfate minerals (e.g., Pironon 1990) or at relatively high temperatures and pressures in quartz or other silicate minerals and glasses (e.g., Bodnar & Sterner 1987). Fluid inclusions for use as LA-ICP-MS standards can be readily synthesized in halite and sylvite using a low temperature hotplate and other common laboratory hardware (Fig. 3-4). The benefits of synthetic fluid inclusions are that they provide true matrix-matched standards with a wide range of possible compositions. Limitations with this method are that some of the synthesized host minerals (e.g., halite) interfere with some of the more relevant fluid inclusion analytes (e.g., Na) and extremely pure reagents (e.g., NaCl) must be used because the presence of impurities will affect the compositions of the trapped inclusions. Preparation of synthetic fluid inclusions at higher temperatures in quartz requires specialized equipment and procedures and reaction of the reagents with the enclosing capsule may result in contamination of the experimental charge.

Desolvated Solution Standards: A calibration solution can be continuously aspirated during ICP-MS analysis; however, the addition of significant amounts of water contributes to the formation of interferences (e.g., oxides, hydrides, hydroxides) and elevated backgrounds. To overcome the detrimental effects associated with direct standard solution aspiration, a desolvating ultrasonic or

Figure 3-4. Photomicrographs of primary liquid-vapor inclusions synthesized in halite (**A**) and sylvite (**B**). The consistent phase ratios and alignment of fluid inclusions parallel to crystal faces confirms the primary nature of the fluid inclusions. Such fluid inclusions can be synthesized using simple laboratory equipment (hotplate, beaker, ultrapure reagents) and low temperatures (100 °C). Adjusting cooling rate through the use of either a programmable hotplate or insulating blankets can substantially affect fluid inclusion density and size.

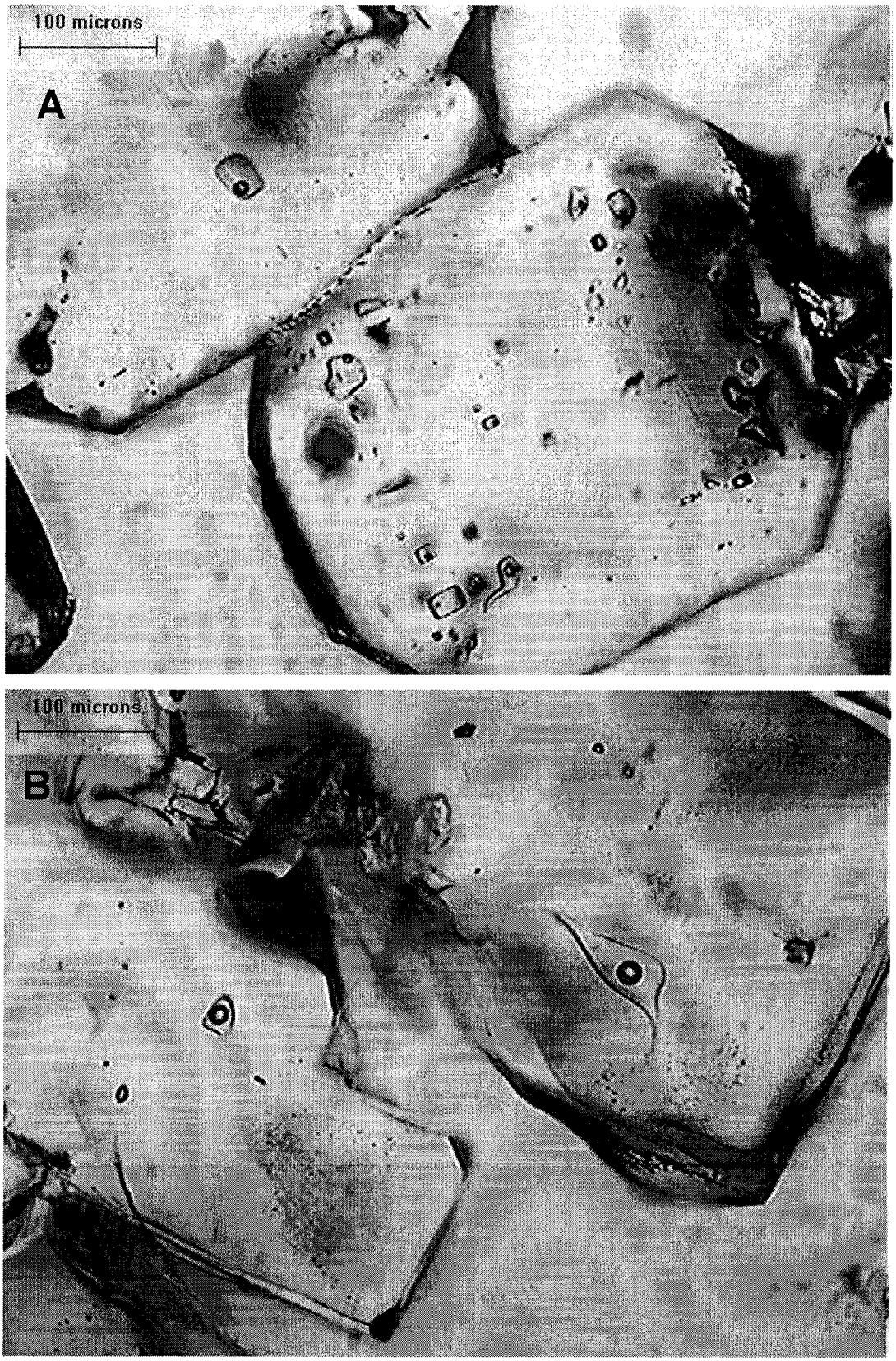
100 microns
A
100 microns
B

microconcentric nebulizer can be used to remove water from standard solutions (e.g., Pickhardt et al. 2000). The desolvated standard solution is then introduced to the plasma as an aerosol during LA-ICP-MS analysis. Although the application of this technique is questionable for use in quantifying fluid inclusion compositions, the introduction of a desolvated standard can provide a means of measuring instrumental drift throughout an experimental run. A secondary benefit of using a desolvating nebulizer is that other gases (e.g., H, N), which increase the ionization efficiency of the ICP-MS plasma resulting in significant increases in instrumental sensitivity, can be metered into the ICP-MS. Even though desolvation can substantially increase sensitivity, it is not completely effective at eliminating water-related interferences. Although oxides are substantially reduced, backgrounds for some elements are elevated when desolvated standards are added relative to when they are not; indicating that oxides are not eliminated entirely (e.g., $Ar^{40}O^{16}$ on Fe^{56}).

Microcapillaries: Small bore (e.g., 50 to 100 μm inside diameter), high-purity, fused silica microcapillaries can be used to prepare standards for LA-ICP-MS analysis of fluid inclusions. Standard solutions can be drawn into the capillaries by applying a vacuum and, once filled, the capillaries can be fused closed with a heated metal instrument (e.g., a soldering iron). The advantages of microcapillaries are that they are easily prepared, can be filled with a wide range of solution compositions, and comprise a material very similar in composition and ablation characteristics to quartz. The major disadvantage to microcapillaries is that they are significantly larger in volume than many fluid inclusions and the relatively large mass of water being added to the plasma could potentially cause a change in plasma conditions during analysis that are greater in magnitude than that caused during typical fluid inclusion analysis.

Microwells: Microwells can be prepared by placing standard calibration solutions in small holes drilled within a plastic or glass substrate (e.g., Shepherd & Chenery 1995, Moissette et al. 1996). A laser can be used to drill holes in a

glass slide that are similar in volume to the fluid inclusions to be analyzed. However, it is very difficult to get fluid into the small microwells drilled with a laser due to liquid surface tension, and larger wells drilled mechanically contain a volume of liquid that is too large to accurately simulate conditions typical of fluid inclusions.

Fluid Inclusion Analogues: Standard calibration solutions encapsulated as microdroplets within epoxy resins have been used as standards for LA-ICP-MS analysis of fluid inclusions (Shepherd & Chenery 1995). In order to synthesize fluid inclusion analogues, it is necessary to obtain an epoxy resin that is clear, hydrophobic, and does not contain trace elements. Epoxy resins used for biological mounts or for marine applications, which are extremely hydrophobic, can be used. An obvious benefit of fluid inclusion analogues is the apparent relative ease of preparation and the ability to encapsulate a standard solution of virtually any composition. However, the extremely hydrophobic behavior of these resins tends to occlude the standard solutions making it very difficult to trap the microdroplets as fluid inclusions. Furthermore, even the most hydrophobic of resins will absorb water over time thus modifying the composition of the trapped microdroplets (Shepherd & Chenery 1995).

Internal Standards

Typically, the concentration of a major cation (e.g., Na), obtained by microthermometric analysis is used as the internal standard and all other elemental concentrations are calculated relative to this cation. This method is most accurate for fluids that contain only Na or contain, in addition to Na, a combination of dissolved cations for which phase relationships are well understood (e.g., NaCl-$CaCl_2$-H_2O). Potential errors may arise from the assumption that Na is the only or dominant cation in solution. Using hydrate equilibria (Crawford 1981, Bodnar 2003) or combinations of melting measurements (Vanko et al. 1988, Williams-Jones & Samson 1990) may provide insights into the other cations that may be present in a fluid inclusion and the

estimate of Na concentration can be adjusted accordingly. Alternatively, an estimate of chlorinity obtained using Raman spectroscopic analysis (Mernagh & Wilde 1989, Dubessy et al. 2002) could be used; however, this method has not been applied to the quantitative LA-ICP-MS analysis of fluid inclusions.

It is imperative that all elements that may be present in concentrations significant enough to have a marked effect on the apparent Na concentration (e.g., Ca, Fe, K, Mg and Mn) be analyzed so that the Na concentration obtained from microthermometry can be adjusted accordingly during subsequent calculation (e.g., Heinrich et al. 2002). This is important when using Na for the calculation of other elemental concentrations because any inaccuracy in the determination of the Na concentration is factored into the other elemental concentrations during subsequent calculations. The Na concentration estimated from microthermometry should be revised to accommodate for the presence of other dissolved cations using the results of the LA-ICP-MS analyses prior to calculation of the abundance of the remaining elements.

Data Reduction and Analysis

Introduction

The method by which the raw data obtained during analysis of fluid inclusions using LA-ICP-MS are converted to quantitative concentrations is somewhat dependent on the method employed during analysis of the inclusions. If direct opening of inclusions within compositionally simple host minerals (e.g., quartz) is performed, then the time-resolved analysis software provided with the ICP-MS instrumentation or available through third parties is often capable of interpreting the relatively simple signals. If stepwise opening of inclusions is performed or if the inclusions are hosted within compositionally complex host minerals (e.g., fluorite), then an alternative means is required to analyze the data due to the lack of commercially-available software capable of analyzing the relatively complex host/fluid inclusion signals.

A method for obtaining quantitative fluid inclusion concentrations from raw ICP-MS data is presented below. A detailed example calculation of the quantitative composition of a fluid inclusion within fluorite using a combination of commercially-available spectral analysis and spreadsheet software is presented in Appendix B. The method presented here differs from that used by other researchers for analyzing melt and fluid inclusions (e.g., Halter et al. 2002, Heinrich et al. 2002) in that correction factors are calculated for each element in the fluid inclusion rather than a single relative sensitivity factor (RSF), calculated for Na, being applied to all elements. Although this makes the data reduction routine somewhat more complicated than that proposed in Halter et al. (2002) and Heinrich et al. (2002), the assumption that all elements show the same relative sensitivity to Na in NIST glass versus the fluid inclusion does not seem justified for all potential fluid inclusion compositions considering the potential matrix and instrumental mass bias effects that could occur during analysis of fluid inclusions. Additionally, the data reduction method described below includes a routine for ratioing the elements in the fluid inclusion to an element in the host mineral for the purpose of removing host mineral contributions to the fluid inclusion signal when simple background subtraction does not remove the host mineral contribution.

Quantification

The first step in the data reduction process is to extract the raw data obtained during LA-ICP-MS analysis of the fluid inclusions from the ICP-MS. The raw data (i.e., icps) are typically included in the ICP-MS software in a form that can be readily copied or exported into a commercial spreadsheet program (e.g., Microsoft Excel®).

Once the data have been exported and the format edited for compatibility, the spectra obtained for each fluid inclusion and calibration standard can be viewed and the peak areas determined using a spectral analysis software program (e.g., Peakfit®); the output is expressed as total icps for the entire time interval represented by each fluid inclusion. If the peak areas for the fluid

inclusion signal are determined relative to the background host mineral signal, and no host mineral contribution is present in the fluid inclusion signal, then further background correction is not necessary. Otherwise, subtraction of the instrumental and host mineral backgrounds should be conducted prior to determination of the fluid inclusion peak areas. For the complex fluid inclusion signals obtained using a stepwise opening procedure, each of the peaks comprising the spectrum is integrated and the icps obtained from each peak summed to obtain the total number of icps for the entire fluid inclusion analysis.

The slope of the calibration line (i.e., the correction factor) for each isotope of interest contained within the calibration standard that was used during the LA-ICP-MS analysis needs to be calculated. The correction factor $\left(CF_{Std}^{X}\right)$ is calculated from the concentration of an element (X) in the standard ratioed against the concentration of Na in the standard $\left(\frac{W_{Std}^{X}}{W_{Std}^{Na}}\right)$ and the total icps that were obtained for the element in the standard ratioed against the total icps that were obtained for Na in the standard $\left(\frac{C_{Std}^{X}}{C_{Std}^{Na}}\right)$ using a reorganization of the equation for a straight line with a Y axis intercept of zero. Figure 3-5 illustrates graphically how the slopes of the calibration curves are calculated from the total counts.

$$CF_{Std}^{X} = \left[\frac{\left(\frac{W_{Std}^{X}}{W_{Std}^{Na}}\right)}{\left(\frac{C_{Std}^{X}}{C_{Std}^{Na}}\right)}\right] \qquad (1)$$

Where:

CF_{Std}^{X} = the slope of the calibration line for an element (X) in the standard

W_{Std}^{X} = concentration of X in the standard

W_{Std}^{Na} = concentration of Na in the standard

C_{Std}^{X} = total icps obtained for X in the standard

C_{Std}^{Na} = total icps obtained for Na in the standard

Once the correction factors have been calculated for each element in the standard, the concentration of an element (X) in the sample is then calculated using the following equation.

$$W_{Samp}^{X} = \left(\frac{C_{Samp}^{X}}{C_{Samp}^{Na}} \right) \bullet CF_{Std}^{X} \bullet W_{Samp}^{Na} \qquad (2)$$

Where:

W_{Samp}^{X} = concentration of X in the fluid inclusion

C_{Samp}^{X} = total icps obtained for X in the sample

C_{Samp}^{Na} = total icps obtained for Na in the sample

CF_{Std}^{X} = correction factor for X in the standard

W_{Samp}^{Na} = concentration of Na in the sample obtained from microthermometry (corrected for the presence of other cations)

This method provides a relatively straight-forward means of calculating fluid inclusion compositions using Na as the internal standard. If another element is selected as the internal standard, all of the elements in the standards and samples will need to be ratioed against that element. Once a spreadsheet has

Figure 3-5. Graphical representation of a calibration line calculated from the total counts (C) obtained for an element (X) and Na in the standard versus the concentration (W) of an element (X) and Na in the standard. The slope of the line (m) is used as a correction factor in the subsequent calculation of the concentrations of elements in the sample.

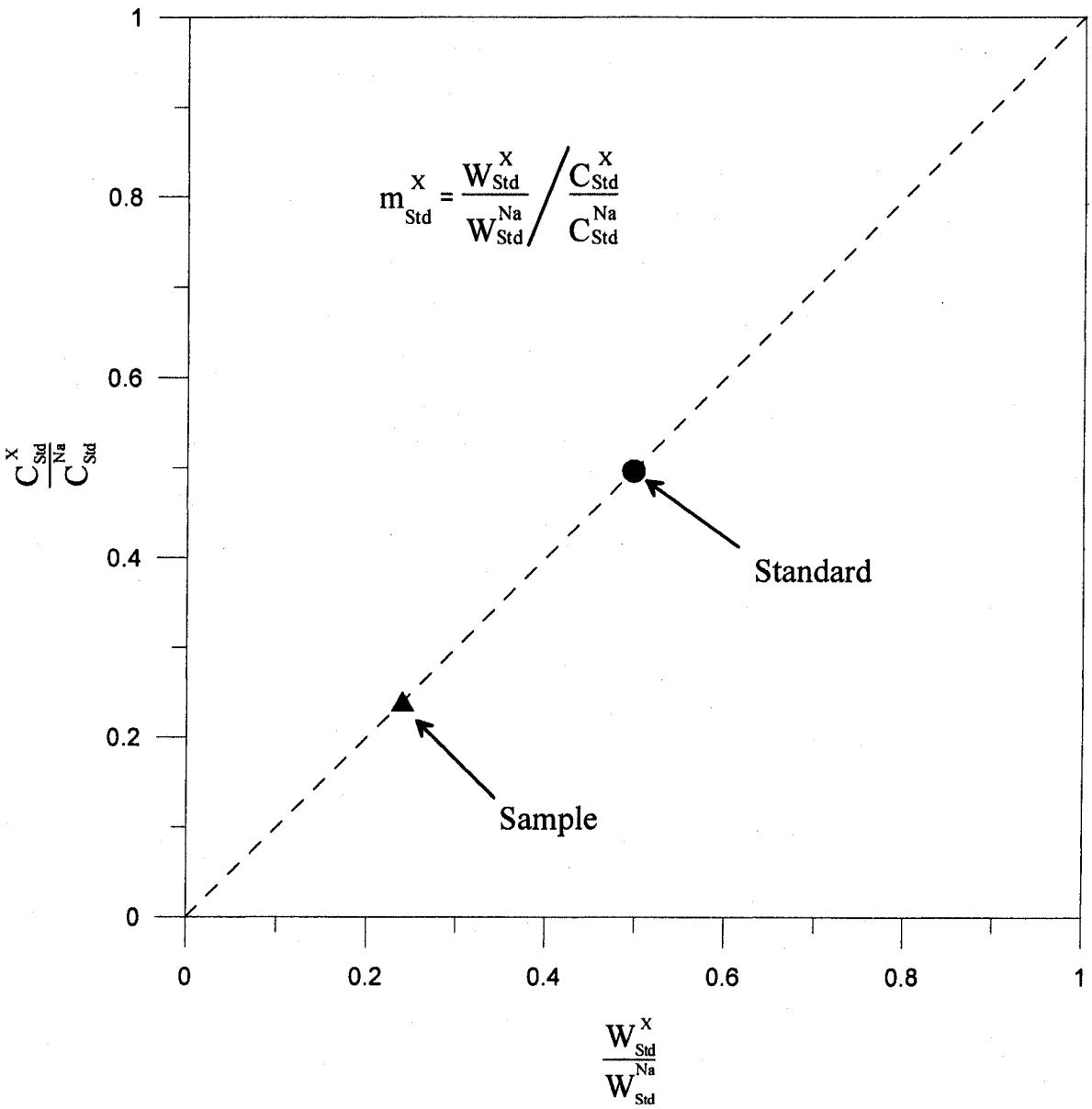
$m^{X}_{Std} = \frac{W^{X}_{Std}}{W^{Na}_{Std}} \Big/ \frac{C^{X}_{Std}}{C^{Na}_{Std}}$
Standard
Sample
$\frac{C^{X}_{Std}}{C^{Na}_{Std}}$
$\frac{W^{X}_{Std}}{W^{Na}_{Std}}$
0
0.2
0.4
0.6
0.8
1

been developed that includes the described operations, calculation of fluid inclusion compositions can be done relatively quickly; the most time being spent integrating the individual spectra to obtain the total integrated standard and sample icps.

Data Correction for Host Mineral Contribution

It is impossible to conduct laser ablation sampling of fluid inclusions without some of the host mineral being included in the sample that is introduced to the ICP-MS. Even minerals that are generally considered to be compositionally simple (e.g., quartz), may contain concentrations of trace elements sufficient to affect the quantitative calculation of fluid inclusion compositions (Samson et al. 2003). Fluid overpressures created within a fluid inclusion at the point of opening may cause a burst of sample comprising a mixture of host mineral and fluid inclusion material that is disproportionate to the mixture of host mineral and fluid inclusion that would be introduced to the ICP-MS under controlled ablation, thus contributing to the host mineral effect on the fluid inclusion signal. This sudden introduction of material to the ICP-MS will affect the concentrations calculated from the fluid inclusion spectra unless the data are corrected prior to final calculation of the fluid inclusion composition. Correction for potential host mineral constituents in the fluid inclusion signal is particularly relevant for compositionally complex host minerals, which may contain the same elements as the fluid inclusions, but at different relative concentrations (fluorite, apatite). Although data correction is an option, it is preferable to conduct laser sampling in a manner that limits the amount of host mineral that is included in the sample.

Prior to performing the calculations described above, the duration of the peak obtained for each element should be compared to the duration of the peak obtained from Na. If the elements detected during the analysis are contained homogeneously within the fluid inclusions (i.e., are not sequestered within isolated, daughter or trapped phases), then the duration of the signals obtained for the other elements should be approximately the same as that for Na.

Shortening of the fluid inclusion signal obtained for some elements relative to Na may occur for elements present at trace concentrations as a result of the decay of the signal to concentrations that are below the limit of detection of the analysis. If the elements detected during the analysis are only present or are present at significantly higher concentrations early in the signal and concentrations decline rapidly relative to the duration of the Na signal, then it is likely that some of the host mineral has contributed to the early part of the signal. Another means of determining whether a host mineral contribution has occurred is to compare the peaks for the fluid inclusions relative to the host mineral background. For example, it is impossible for a fluid inclusion hosted by fluorite to have a higher dissolved Ca concentration than the host fluorite. Therefore, the spectrum for Ca should show a negative peak during the period of time that sampling of the fluid inclusion is conducted. Unfortunately, the negative peak is generally not apparent because of the time lag resulting from mixing in the sampling cell and tubing and transport prior to introduction to the ICP-MS or due to relative abundance of an analyte in the host masking the fluid inclusion signal (e.g., Ca in fluorite). However, a strong, early, positive Ca peak trailing off prior to the Na peak is clearly indicative of a contribution from the host fluorite to the fluid inclusion signal and data correction for host mineral contribution is required prior to calculation of the fluid inclusion composition.

Subtraction of the host mineral background counts from the fluid inclusion signal is not always adequate to correct for a significant host mineral contribution and an alternate method is required to remove these contributions. First, it is necessary to conduct a correction for all elements that have non-zero backgrounds during measurement of the pre-ablation signal (i.e., gas blank). The average count rates detected during measurement of the gas blank are subtracted from the count rates obtained during host mineral and fluid inclusion data collection. Failure to subtract the gas blank prior to data correction may result in masking of spectral peaks, particularly for elements that have high instrumental or gas backgrounds (e.g., Na). Following correction of the data for the gas background, the count rates are divided for each time increment for the

element of interest by the counts rates obtained for an element known to be a significant constituent in the host mineral (e.g., Ca for fluorite). Once ratioed against a host mineral constituent, the resulting spectrum (e.g., K/Ca) can be integrated using peak integration software and the resulting total icps used in the calculation procedures described above. An example of the effect that the host mineral constituent ratioing procedure has on the resulting fluid inclusion spectra is illustrated in Figure 3-6. Simple subtraction of the instrumental and host mineral background count rates is inadequate to correct for the host mineral contribution in the early data obtained for this fluid inclusion. The spectra generated from the unfiltered data suggest that this fluid inclusion contained Na, K, Ca, Sr, Y, Ba, Ce, Sm Th and U. However, the spectra generated from the corrected data clearly show that Y and possibly Sm were only apparently present in the fluid inclusion signal because of the host mineral contribution. A worked example of the quantification of a fluid inclusion composition, including the data correction procedure, is presented in Appendix B. Although this procedure is effective at reducing or eliminating the early-time effect on fluid inclusion compositions caused by host mineral contributions, the effect on analytical precision has not been fully evaluated at this time.

Method Precision and Accuracy

Introduction

In addition to the complexities of laser ablation sampling and ICP-MS analysis, LA-ICP-MS analysis of fluid inclusions is further complicated by the relatively short term, transient nature of the fluid inclusion signals. When designing an experiment, it is important to understand the precision of the method that is reasonably achievable, what factors will limit method precision, and to maximize analytical precision using prudent experiment design. The accuracy of a single inclusion analysis performed using LA-ICP-MS analysis will never be known because the composition of the fluid inclusion is not known prior to analysis.

Figure 3-6a. Raw time-resolved spectra obtained from an approximately 12 μm diameter, primary liquid-vapor inclusion in purple fluorite from South Platte, Colorado. The raw time-resolved spectra show well developed peaks for Na, K, Sr, Y, Ce, Th and U and weak peaks for Ca, Ba, and Sm suggesting that detectable concentrations of these elements occur within the fluid inclusions. However, the occurrence of a positive Ca peak indicates a host mineral contribution to the fluid inclusion signal necessitating data filtering in order to obtain a quantitative fluid inclusion composition.

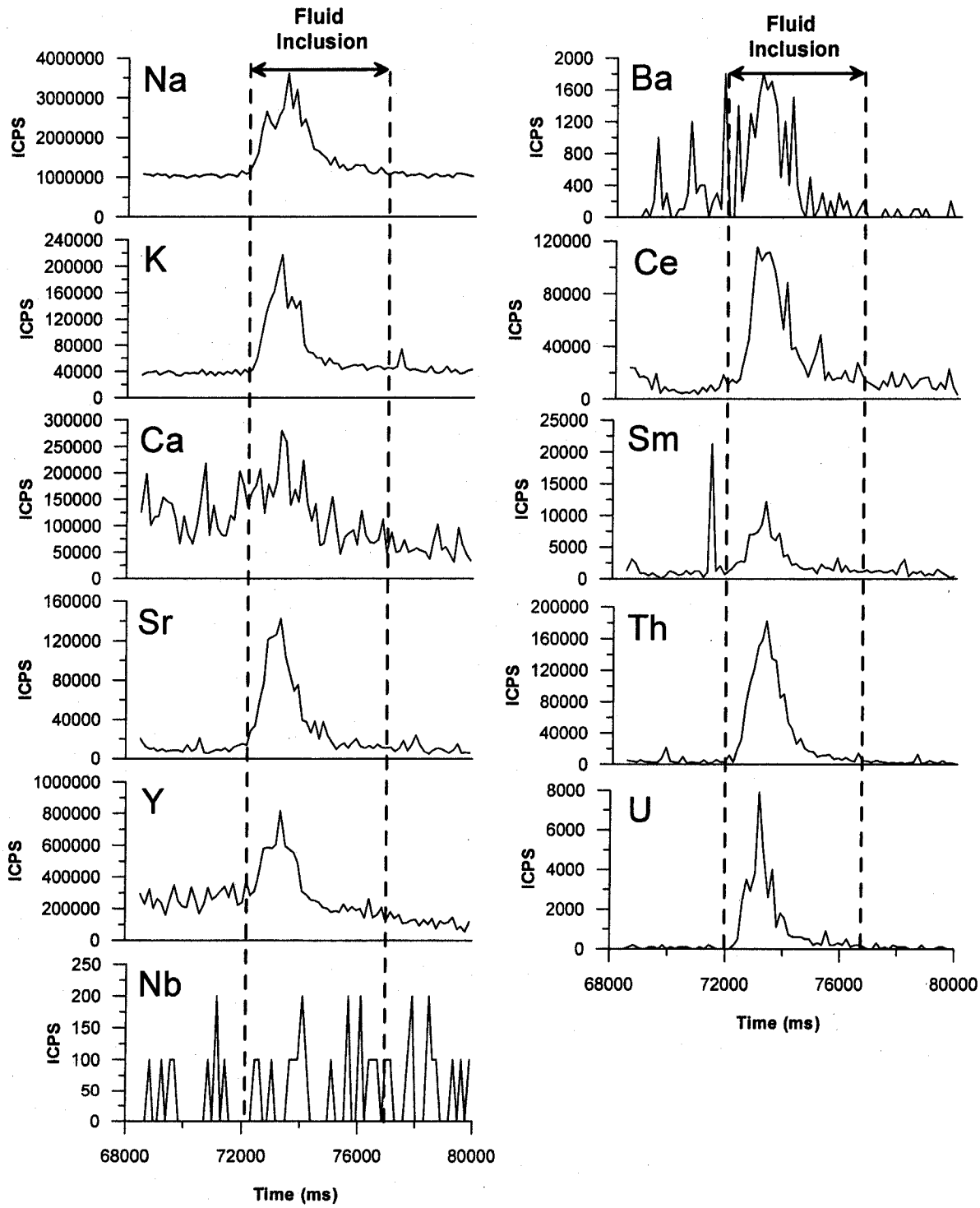
Fluid Inclusion
Na
K
Ca
Sr
Y
Nb
Ba
Ce
Sm
Th
U
ICPS
Time (ms)
68000
72000
76000
80000

Figure 3-6b. The time-resolved spectra presented in Figure 3-6a after filtering by subtraction of gas background and ratioing to Ca abundance. Strong peaks remain for Na, K, Sr, Ce, Th and U confirming the presence of these elements within the fluid inclusion. The peak for Y present in the unfiltered spectra is absent from the filtered spectra indicating that the Y peak was present as a result of host mineral contribution and Y is below the limit of detection in the fluid inclusion. The filtered spectra suggest that Ba and possibly Sm are present within the inclusion but the concentrations are close to the analytical limit of detection.

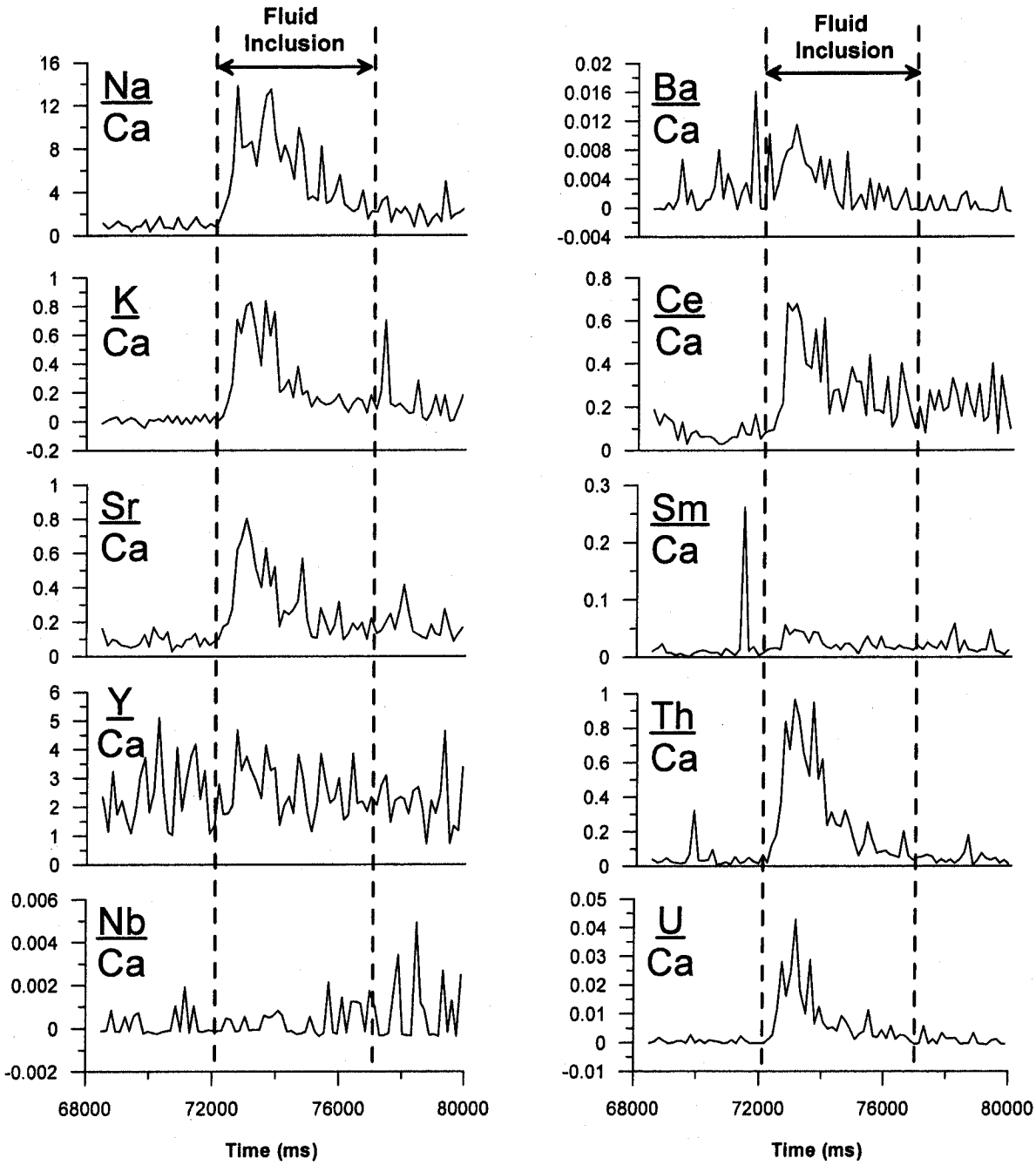
Fluid Inclusion
Na/Ca
K/Ca
Sr/Ca
Y/Ca
Nb/Ca
Ba/Ca
Ce/Ca
Sm/Ca
Th/Ca
U/Ca
68000
72000
76000
80000
Time (ms)

Instrument Limitations

Quadrupole ICP-MS instruments analyze the selected isotopes in a sequential manner. A relatively short period of time, referred to as the 'dwell' time, is spent acquiring data for each of the selected masses (e.g., 10 ms). An additional amount of 'settling' time (e.g., 0.1 to 15 ms) is required per mass for the instrument to move to the next mass and stabilize prior to acquiring data. Assuming a dwell time of 10 ms/isotope, an average settling time of 2 ms, and an analyte list of 15 isotopes, a quadrupole ICP-MS could require up to 180 ms (i.e., 15 x 10 ms dwell time plus 15 x 2 ms settling time) to complete one scan of the selected masses. Considering that relatively small fluid inclusion signals may only be 1 to 3 seconds in duration, the instrument may only be able to collect between 5 and 17 scans of the selected masses during the fluid inclusion analysis. In addition, a portion of the fluid inclusion signal is affected by sampling system 'uptake' and 'washout', where mixing occurs with the host mineral. Therefore, it is possible that only 2 to 14 of the mass scans acquired during the analysis may be representative of the fluid inclusion composition. Arguably, two mass scans of a transient signal do not represent a statistically valid sampling event.

To counteract the limitations posed by instrument scan rates, the shortest possible list of isotopes should be selected when attempting to conduct quantitative fluid inclusion analyses. The number of isotopes that can be determined for an individual fluid inclusion is a function of the size of the inclusion. A review of published and unpublished LA-ICP-MS data for fluid inclusions suggests that a reasonable expectation is that approximately 1 isotope can be determined for each μm of fluid inclusion diameter (e.g., from approximately 10 isotopes for a 10 μm to 40 isotopes for a 40 μm inclusion). Obviously, this estimate is dependant on a number of factors, instrument- and procedure-related (e.g., type of ICP-MS used, fluid inclusion size, opening technique, signal duration), but is a reasonable range based on the systems currently in use. Preliminary, 'non-quantitative' analyses, using a greater number

of isotopes, can be conducted to determine which elements are present and which isotopes should be included in the subsequent quantitative analysis.

Although quadrupole ICP-MS instrument software typically reports the data in the form of icps, the data is collected using significantly shorter dwell times than one second (e.g., 10 ms). Consequently, an apparently significant count rate of 10,000 icps only represents 100 counts measured by the detector. Considering the limited number of scans that are possible during the analysis of an inclusion, maximizing precision requires maximizing sensitivity while extending fluid inclusion sampling duration. This underscores a significant compromise that has to be made during LA-ICP-MS analysis of fluid inclusions; the maximum fluid inclusion to background signal occurs when the entire contents of the inclusion are sampled in the shortest period of time; however, this prevents obtaining an adequate number of scans to obtain a statistically relevant data set for multielement analyses. Therefore, any strategy to increase sensitivity (i.e., mixed gases, plasma screens, improved ICP-MS instrumentation, etc.) while prolonging signal duration should be considered when attempting to conduct quantitative fluid inclusion analyses. Notwithstanding the apparent limitations posed by the ICP-MS scan and count rates, external reproducibility as low as 5 % RSD is obtainable (Heinrich et al. 2002).

Limits of Detection

Determining the limit of detection of LA-ICP-MS analysis of fluid inclusions is problematic. In subjective terms, any time a fluid inclusion spectrum indicates an element is present above the background, the element is detectable. In terms of statistical significance, if the count rates observed during sampling of the fluid inclusion exceed the mean value plus three standard deviations of the background counts, the fluid inclusion signal is considered statistically relevant and, therefore, the element is considered detectable. However, newer ICP-MS instrumentation (e.g., ThermoElemental® X-7®), which may have instrument backgrounds of 0 icps with a variance of 0 icps, complicates the determination of the statistical relevance of fluid inclusion signals with respect to instrumental

background. As a result, the determination of limits of detection is often a function of the instrumentation used during analysis and the backgrounds inherent in the instrumentation.

Conclusions

The development of LA-ICP-MS and its application to fluid inclusions marked a dramatic leap forward in our abilities to understand fluid-related geologic processes. For the first time, quantitative elemental analyses of individual fluid inclusions can be conducted without the limitations posed by the semi-quantitative or non-unique nature of other microanalytical (e.g., microthermometry) or bulk (e.g., crush/leach) techniques. LA-ICP-MS, however, is not capable of addressing all of the analytical questions of interest to the fluid inclusionist (e.g., the presence of molecular species) and a full understanding of fluid inclusion composition is only achieved through the application of multiple analytical techniques.

It is now possible to more precisely fingerprint individual fluid compositions, and, when combined with careful petrographic and other analyses, provide new opportunities to understand the temporal and spatial chemical architecture of fluid systems. This will provide better assessment of the evolution of fluid-mineral systems, and, for example, allow better testing of geological process models (e.g. fluid mixing), provide more complete chemical data for input into thermodynamic models (cf. Wood & Samson 1998), and provide more complete data against which to test the output from such models (e.g. Reed 1998).

The application of LA-ICP-MS to the analysis of fluid inclusions, however, is still relatively new, and significant challenges remain in the routine application of LA-ICP-MS. Through a combination of equipment and software development and improvements in analytical abilities and methodology, continued increases in method capability, precision and ease of use will occur. Of particular interest will be the continued development of precise isotopic determinations that, along with

quantitative elemental concentrations, will provide even greater insights into geologic fluid systems.

Acknowledgements

The authors thank Dr. Thomas Pettke and Dr. Theresa Jeffries for their detailed and insightful reviews of an earlier version of this manuscript. The authors also acknowledge the many collaborators, past and present, who have contributed, directly and indirectly, to the development and operation of LA-ICP-MS at the University of Windsor, particularly Dr. Henry Longerich, and Dr. Simon Jackson. This work was supported by NSERC and CFI equipment and Discovery grants to IMS and BJF and by a McGill University graduate student fellowship to JEG.

References

Anderson, A. & Mayanovic, R. (2003): Electron, Nuclear and X-ray Probe Microanalysis of Fluid Inclusions. *In* Fluid Inclusions: Analysis and Interpretation (I. Samson, A. Anderson, & D. Marshall, eds.) *Mineralogical Association of Canada, Short Course* **32**, 321-349.

Arrowsmith, P. (1987): Laser ablation of solids for elemental analysis by inductively coupled plasma mass spectrometry. *Analytical Chemistry* **59**, 1437-1444.

Audetat, A., Günther, D. & Heinrich, C.A. (1998): Formation of a Magmatic-Hydrothermal Ore Deposits: Insights with LA-ICP-MS Analysis of Fluid Inclusions. *Science* **279**, 2091-2094.

Audetat, A., Günther, D. & Heinrich, C.A. (2000): Causes for large-scale metal zonation around mineralization plutons: Fluid inclusion LA-ICP-MS evidence from the Mole Granite, Australia. *Economic Geology* **95**, 1563-1581.

Audetat, A. & Pettke, T. (2003): The magmatic-hydrothermal evolution of two barren granites: A melt and fluid inclusion study of the Rito del Medio and Canada Pinabete plutons in northern New Mexico (USA). *Geochimica et Cosmochimica Acta* **67**, 97-121.

Bleiner, D., Hametner, K. & Günther, D. (2000): Optimization of a laser ablation-inductively couple plasma 'time of flight' mass spectrometry system for short transient signal acquisition. *Fresenius Journal of Analytical Chemistry* **368**, 37-44.

Bodnar, R.J. (2003): Interpretation of Data from Aqueous-Electrolyte Fluid Inclusions. *In* Fluid Inclusions: Analysis and Interpretation (I. Samson, A. Anderson, & D. Marshall, eds.) *Mineralogical Association of Canada, Short Course* **32**, 81-100.

Bodnar, R.J. & Sterner, S.M. (1987): Synthetic fluid inclusions. In *Hydrothermal Experimental Techniques*, G.C. Ulmer & H.L. Barnes, eds., Wiley-Interscience, New York. 423-457.

Brech, F & Cross, L. (1962): Optical microemission stimulated by a ruby laser. *Applied Spectroscopy,* **16**, 59.

Burruss, R.C. (2003): Raman Spectroscopy of Fluid Inclusions. *In* Fluid Inclusions: Analysis and Interpretation (I. Samson, A. Anderson, & D. Marshall, eds.) *Mineralogical Association of Canada, Short Course* **32**, 277-287.

Crawford M. L. (1981): *In* Fluid inclusions: applications to petrology (L. S. Hollister & M. L. Crawford, eds.), *Mineralogical Association of Canada, Short Course* **6**, 75-100.

Cremers, D.A. & Radziemski, L.J. (1983): Detection of chlorine and fluorine in air by laser-induced breakdown spectrometry. *Analytical Chemistry* **55**, 1252-1256.

Cremers, D.A., Radziemski, L.J. & Loree, T.R. (1984): Spectrochemical analysis of liquids using the laser spark. *Applied Spectroscopy* **38**, 721-729.

Crowe, S.A., Fryer, B.J., Samson, I.M. & Gagnon, J.E. (2003): Precise Isotope Ratio Determination of Common Pb Using Quadrupole LA-ICP-MS with Optimized Laser Sampling Conditions and a Robust Mixed-Gas Plasma. Submitted to *Journal of Analytical Atomic Spectrometry.*

Derome, D., Cuney, M., Cathelineau, M., Fabre, C. & Lhomme, T., (2002): Reconstitution of the composition of individual fluid inclusion using microthermometry, Raman microspectroscopy and Laser Induced Breakdown Spectroscopy. Application to the Shea Creek uranium deposit (Saskatchewan, Canada). Abstracts volume, GAC-MAC Joint Annual Meeting **27**, 27.

Dubessy J., Lhomme, T., Boiron, M.-C. & Rull, F. (2002): Determination of chlorinity in aqueous fluids using Raman spectroscopy of the stretching band of water at room temperature: application to fluid inclusions. *Applied Spectroscopy* **56**, 99-106.

Eggins, S.M., Kinsley, L.P.J & Shelley, J.M.G. (1998): Deposition and element fractionation processes occurring during atmospheric pressure sampling for analysis by ICP-MS. *Applied Surface Science* **129**, 278-286.

Fabre, C., Boiron, M.-C., Dubessy, J., Cathelineau, M. & Banks, D.A., (2002a): Paleofluid chemistry of a single fluid event: bulk and in-situ multi-technique analysis (LIBS, Raman Spectroscopy) of an Alpine fluid (Mont-Blanc). *Chemical Geology* **182**, 249-264.

Fabre, C., Boiron, M.-C., Dubessy, J., Chabiron, A., Charoy, B., & Crespo, T.M. (2002b): Advances in lithium analysis in solids by means of laser-induced breakdown spectroscopy: An exploratory study. *Geochimica et Cosmochimica Acta* **66**, 1401-1407.

Fryer, B.J., Jackson, S.E. & Longerich, H.P. (1995): The design, operation and role of the laser-ablation microprobe coupled with an inductively coupled plasma-mass spectrometer (LAM-ICP-MS) in the earth sciences. *Canadian Mineralogist* **33**, 303-312.

Gagnon, J.E., Samson, I.M., Fryer, B.J. & Williams-Jones, A.E. (2002): Hydrothermal fluids in NYF pegmatites, South Platte, Colorado – preliminary insights from LA-ICP-MS analysis of quartz- and fluorite-hosted fluid inclusions. 8th Biennial Pan-American Conference on Research on Fluid Inclusions, Program with Abstracts, 25-27.

Ghazi, A.M., McCandless, T.E., Vanko, D.A. & Ruiz, J. (1996): New quantitative approach in trace elemental analysis of single fluid inclusions: Applications of laser-ablation inductively coupled plasma-mass spectrometry (LA-ICP-MS). *Journal of Analytical Atomic Spectrometry* **11**, 667-674.

Gleeson, S. (2003): Bulk Analysis of Electrolytes in Fluid Inclusions. *In* Fluid Inclusions: Analysis and Interpretation (I. Samson, A. Anderson, & D. Marshall, eds.) *Mineralogical Association of Canada, Short Course* **32**, 231-244.

Gray, A.L. (1985): Solid sample introduction by laser ablation for inductively coupled plasma source mass spectrometry. *Analyst* **110**, 551-556.

Guillong, M. & Günther, D. (2002): Effect of particle size distribution on ICP-induced elemental fractionation in laser ablation-inductively coupled plasma-mass spectrometry. *Journal of Analytical Atomic Spectrometry* **17**, 831-837.

Guillong, M., Horn, I. & Günther, D. (2002): Capabilities of a homogenized 266 nm Nd:YAG laser ablation system for LA-ICP-MS. *Journal of Analytical Atomic Spectrometry,* **17**, 8-14.

Günther, D. (2001): Quantitative Fluid Inclusion Analysis Using a 193 nm Excimer Laser-Ablations System Coupled to ICP-MS. *In* Laser-Ablation-ICPMS in the Earth Sciences Principles and Applications (P. Sylvester, ed.), *Mineralogical Association of Canada, Short Course* **29**, 47-61.

Günther, D., Frischknecht, R., Müschenborn, H.-J. & Heinrich, C.A. (1997): Direct liquid ablation: a new calibration strategy for laser ablation-ICP-MS microanalysis of solids and liquids. *Fresenius Journal of Analytical Chemistry* **359**, 390-393.

Günther, D., Audetat, A., Frischknecht, R. & Heinrich, C.A. (1998): Quantitative analysis of major, minor and trace elements in fluid inclusions using laser ablation-inductively coupled plasma-mass spectrometry (LA-ICP-MS). *Journal of Analytical Atomic Spectrometry* **13**, 263-270.

Günther, D. & Heinrich, C.A. (1999): Enhanced sensitivity in LA-ICP-MS using helium-argon mixtures as aerosol carrier. *Journal of Analytical Atomic Spectrometry* **14**, 1363-1368.

Halter, W. E., Pettke, T., Heinrich, C.A. & Rothen-Rutishauser, B. (2002): Major to trace element analysis of melt inclusions by laser-ablation ICP-MS: methods of quantification. *Chemical Geology* **183**, 63-86.

Hattendorf, B. & Günther, D. (2000): Characteristics and capabilities of an ICP-MS with a dynamic reaction cell for dry aerosols and laser ablation. *Journal of Analytical Atomic Spectrometry* **15**, 1125-1131.

Heinrich, C.A., Günther, D., Audetat, A., Ulrich, T. & Frischknecht, R. (1999): Metal fractionation between magmatic brine and vapor, determined by microanalysis of fluid inclusions. *Geology* **27**, 755-758.

Heinrich, C.A., Pettke, T., Halter, W., Aigner, M., Audétat, A., Günther, D., Hattendorf, B., Bleiner, D., Guillong, M. & Horn, I. (2002): Quantitative Multi-element Analysis of Minerals, Fluid and Melt Inclusions by Laser Ablation Inductively-Couple-Plasma Mass-Spectrometry. 8th Biennial Pan-American Conference on Research on Fluid Inclusions, Program with Abstracts, 38.

Horlick, G. & Montaser, A. (1998): Analytical Characteristics of ICPMS. In *Inductively Coupled Plasma Mass Spectrometry* (A. Montaser, ed.) Wiley-VCH, Toronto, 503-613.

Jackson, S.E., Longerich, H.P., Dunning, G.R. & Fryer, B.J. (1992): The application of laser ablation microprobe-inductively coupled plasma-mass spectrometry (LAM-ICP-MS) to in situ trace element determinations in minerals. *Canadian Mineralogist* **30**, 1049-1064.

Jackson, S.E. (2001): The Application of Nd:YAG Lasers in LA-ICP-MS. *In* Laser-Ablation-ICPMS in the Earth Sciences Principles and Applications (P. Sylvester, ed.), *Mineralogical Association of Canada, Short Course* **29**, 29-45.

Jackson, S.E., Pearson, N.J. & Griffin, W.L. (2001): In situ isotope ratio determination using laser-ablation-magnetic sector-ICP-MS. *In* Laser-Ablation-ICPMS in the Earth Sciences Principles and Applications (P. Sylvester, ed.), *Mineralogical Association of Canada, Short Course* **29**, 105-119.

Jackson, S.E. & Günther, D (2003): The nature and sources of laser induced isotopic fractionation in laser ablation-multicollector-inductively coupled plasma-mass spectrometry. *Journal of Analytical Atomic Spectrometry* **18**, 205-212.

Landtwing, M.R., Redmond, P.B., Einaudi, M.T., Heinrich, C.A., Halter, W.E. & Pettke, T. (2002): Veining, Timing of Sulphide Deposition and Fluid Evolution at the Bingham Cu-Au-Mo-Ag Porphyry Deposit – Fluid Inclusion LA-ICP-MS Results. 8th Biennial Pan-American Conference on Research on Fluid Inclusions, Program with Abstracts, 49-50.

Longerich, H.P. (2001): Some Thoughts on Buying a New ICPMS. *In* Laser-Ablation-ICPMS in the Earth Sciences Principles and Applications (P. Sylvester, ed.), *Mineralogical Association of Canada, Short Course* **29**, 225-235.

Longerich, H.P., Jackson, S.E., Fryer, B.J. & Strong, D.F. (1993): The laser ablation microprobe-inductively coupled plasma-mass spectrometer. *Geoscience Canada* **20**, 21-27.

Mason, P. (2001): Expanding the capabilities of laser-ablation ICP-MS with collision and reaction cells. *In* Laser-Ablation-ICPMS in the Earth Sciences Principles and Applications (P. Sylvester, ed.), *Mineralogical Association of Canada, Short Course* **29**, 63-81.

Mernagh T. P. & Wilde A. R. (1989): The use of the laser Raman microprobe for the determination of salinity in fluid inclusions. *Geochimica et Cosmochimica Acta* **53**, 765-771.

Moenke-Blankenburg, L., Gäckle, M., Günther, D. & Kammel, J. (1990): Processes of laser ablation and vapour transport to the ICP. *In* Plasma Source Mass Spectrometry, Proc. Third Surrey Conf. on Plasma Source Mass Spectrometry (K.E. Jarvis, A.L. Gray, I. Jarvis & J. Williams, eds.). The Royal Society of Chemistry, Cambridge, U.K., 1-17.

Moissette, A., Shepherd, T.J. & Chenery, S.R. (1996): Calibration Strategies for the Elemental Analysis of Individual Aqueous Fluid Inclusions by Laser Ablation-Inductively Coupled Plasma-Mass Spectrometry. *Journal of Analytical Atomic Spectrometry* **11**, 177-185.

Montaser, A., McLean, J.A., Liu, H. & Mermet, J.-M. (1998): An introduction to ICP spectrometries for elemental analysis. *In Inductively Coupled Plasma Mass Spectrometry* (A. Montaser, ed.) Wiley-VCH, Toronto, 1-31.

Müller, B., Frischknecht, R., Seward, T.M., Heinrich, C.A. & Gallegos, W.C. (2001): A fluid inclusion reconnaissance study of the Huanuni tin deposit (Bolivia), using LA-ICP-MS micro-analysis. *Mineralium Deposita* **36**, 680-688.

Pettke, T., Heinrich, C.A., Ciocan, A.C. & Günther, D. (2000): Quadrupole mass spectrometry and optical emission spectrometry: detection capabilities and representative sampling of short transient signals from laser-ablation. *Journal of Analytical Atomic Spectrometry* **15**, 1149-1155.

Pickhardt, C., Becker, J.S. & Dietze, H.-J. (2000): A new strategy of solution calibration in laser ablation inductively coupled plasma mass spectrometry for multielement trace analysis of geological samples. *Fresenius Journal of Analytical Chemistry* **368**, 173-181.

Pironon, J. (1990): Synthesis of hydrocarbon fluid inclusions at low temperature. *American Mineralogist* **75**, 226-229.

Radziemski, L.J. (2002): From LASER to LIBS, the path of technology development. *Spectrochimica Acta* **57**, 1109-1113.

Reed, M.H. (1998): Calculation of simultaneous chemical equilibria in aqueous-mineral-gas systems and its application to modeling hydrothermal processes. *In* Techniques in Hydrothermal Ore Deposit Geology (J.P. Richards & P. Larson, eds.), *Reviews in Economic Geology* 10, Ch. 5, Society of Economic Geologists, 109-124.

Ridley, W.I. & Lichte, F.E. (1998): Major, Trace, and Ultratrace Element Analysis by Laser Ablation ICP-MS. *In* Applications of Microanalytical Techniques to Understanding Mineralizing Processes (M.A. McKibbem, W,C. Shanks, III & Ridley, W.I., eds.) *Reviews in Economic Geology* 7, Ch. 11, 199-215.

St-Onge, L., Detalle, V. & Sabsabi, M. (2002): Enhanced laser-induced breakdown spectroscopy using the combination of fourth-harmonic and fundamental Nd:YAG laser pulses. *Spectrochimica Acta* **57**, 121-135.

Salvi, S. & Williams-Jones, A.E. (2003): Bulk analysis of volatiles in fluid inclusions. *In* Fluid Inclusions: Analysis and Interpretation (I. Samson, A. Anderson, & D. Marshall, Eds.) *Mineralogical Association of Canada, Short Course* **32**, 245-276.

Samson, I.M., Chen, Z., Fryer, B.J. & Walker, R.T. (1998): High sensitivity in situ analysis of cation/anion compositions of individual fluid inclusions by LAM-ICP-MS using a cold plasma ionization source. Abstracts with Programs **30**, Geol. Soc. Amer. Annual Meeting, Toronto, A-81.

Samson, I.M., Fryer, B.J., & Gagnon, J.E. (2003): The trace element chemistry of hydrothermal quartz: a tool for paragenetic studies. GAC-MAC-SEG Joint Meeting, Vancouver.

Shepherd, T.J. & Chenery, S.R. (1995): Laser ablation ICP-MS elemental analysis of individual fluid inclusions: An evaluation study. *Geochimica et Cosmochimica Acta* **59**, 3997-4007.

Shepherd. T.J. & Rankin, A.H. (1998): Fluid Inclusion Techniques of Analysis. . *In* Techniques in Hydrothermal Ore Deposit Geology (J.P. Richards & P. Larson, eds.), *Reviews in Economic Geology* 10, Ch. 6, Society of Economic Geologists, 125-149.

Shepherd, T.J., Ayora, C., Cendon, D.I., Chenery, S.R. & Moissette, A. (1998): Quantitative solute analysis of single fluid inclusions in halite by LA-ICP-MS and cryo-SEM-EDS: complementary microbeam techniques. *European Journal of Mineralogy* **10**, 1097-1108.

Thompson, M., Goulter, J.E. & Steuwer, D. (1981): Laser Ablation for the Introduction of Solid Samples into an Inductively Coupled Plasma for Atomic Emission Spectrometry. *Analyst* **106**, 32-39.

Tognoni, E., Palleschi, V., Corsi, M. & Christoforetti, G. (2002): Quantitative micro-analysis by laser-induced breakdown spectroscopy: a review of the experimental approaches. *Spectrochimica Acta* **57**, 1115-1130.

Ulrich, T., Günther, D. & Heinrich, C.A. (1999): Gold concentrations of magmatic brines and the metal budget of porphyry copper deposits. *Nature* **399**, 676-679.

van Achterbergh, E., Ryan, C., Jackson, S. & Griffin, W. (2001): Data Reduction Software for LA-ICP-MS. *In* Laser-Ablation-ICPMS in the Earth Sciences Principles and Applications (P. Sylvester, ed.), *Mineralogical Association of Canada, Short Course* **29**, 239-243.

Vanko D. A., Bodnar R. J. & Sterner S. M. (1988): Fluid Inclusions: VIII. Vapor-saturated halite solubility in part of the system NaCl-$CaCl_2$-H_2O, with application to fluid inclusions from oceanic hydrothermal systems. *Geochimica et Cosmochimica Acta* **52**, 2451-2456.

Varel, H., Wähmer, M., Rosenfeld, A., Ashkenasi, D. & Campbell, E.E.B. (1998): Femtosecond laser ablation of sapphire: time-of-flight analysis of ablation plume. *Applied Surface Science* **127-129**, 128-133.

Wilkinson, J.J., Rankin, A.H., Mulshaw, S.C., Nolan, J. & Ramsey, M.H. (1994): Laser ablation-ICP-AES for the determination of metals in fluid inclusions: An application to the study of magmatic ore fluids. *Geochimica et Cosmochimica Acta* **58**, 1133-1146.

Williams-Jones A. E. & Samson I. M. (1990): Theoretical calculations of halite solubility in the system NaCl-$CaCl_2$-H_2O: applications to fluid inclusions. *Canadian Mineralogist* **28**, 299-304.

Wood, S.A. & Samson, I.M. (1998): Solubility of ore minerals and complexation of ore metals in hydrothermal solutions. *In* Techniques in Hydrothermal Ore Deposit Geology (J.P. Richards & P. Larson, eds.), *Reviews in Economic Geology* 10, Ch. 2, Society of Economic Geologists, p. 33-80.

Chapter 4

The composition and origin of hydrothermal fluids in an NYF-type granitic pegmatite, South Platte District, Colorado: Evidence from LA-ICP-MS analysis of fluorite- and quartz-hosted fluid inclusions

Preface

The methods developed for the quantitative analysis of fluid inclusions in compositionally complex, poorly-absorbing host minerals (i.e., beam constriction, traversed opening, ratioed count rates) presented in earlier chapters are applied to the analysis of quartz- and fluorite-hosted fluid inclusions from the South Platte district, Colorado in Chapter 4. The investigation presents some of the first quantitative data obtained from single fluid inclusions from hydrothermal fluorite-REE mineralization and provides new insights into the composition and source of the hydrothermal fluids and the factors influencing fluid composition and fluorite-REE mineral deposition.

The composition and origin of hydrothermal fluids in an NYF-type granitic pegmatite, South Platte District, Colorado: Evidence from LA-ICP-MS analysis of fluorite- and quartz-hosted fluid inclusions

Joel E. Gagnon[1], Iain M. Samson[2], Brian J. Fryer[2]
and Anthony E. Williams-Jones[1]

[1]*Department of Earth and Planetary Sciences, McGill University, Montreal, Quebec H3A 2A7, Canada*
[2]*Department of Earth Sciences, University of Windsor, Windsor, Ontario N9B 3P4, Canada*

Abstract

Hydrothermal fluorite-REE mineralization in zoned, niobium-yttrium-fluorine (NYF)-type pegmatites hosted by the Proterozoic Pikes Peak granite in north-central Colorado comprises secondary albite, fluorite and REE minerals (predominantly samarskite and fergusonite) that replace primary pegmatitic core-zone quartz, core-margin zone fluorite and wall-zone quartz and perthite. Primary fluid inclusions in hydrothermal, purple, white and colorless fluorite and secondary and pseudosecondary inclusions in pegmatitic core-zone quartz were analyzed using microthermometry and laser ablation ICP-MS (LA-ICP-MS). LA-ICP-MS analysis of fluid inclusions in fluorite is problematic due to compositional complexity, poor energy absorbance, and cleavage in fluorite. However, representative and quantitative analysis was accomplished using a combination of a constricted laser beam, a traversed opening technique, and by correcting for host contribution to the fluid inclusion signal.

Microthermometric and LA-ICP-MS analyses indicate that four assemblages of compositionally-distinct fluid inclusions occur in pegmatite core-zone quartz (fluids F1 through F3) and hydrothermal purple, white and colourless fluorite (fluids F2 and F4). Fluids F1, F2, and F3 are represented by secondary and pseudosecondary L-V and L-V-H inclusions in quartz and primary(?) L-V-H inclusions in white fluorite. These inclusions have homogenization temperatures of 93 to 149 °C and comprise moderate to high salinity (22 to 29 equiv. wt. % NaCl) fluids that can be characterized as Na + K + Sr + Ba ± Ca solutions. These three fluids (F1, F2, and F3) could not be distinguished from one another

using microthermometry, however, they have distinct chemical characteristics that are apparent from the LA-ICP-MS data; F2 contains detectable concentrations of Ca and F1 and F3 do not. Fluid F4 is represented by primary L-V inclusions in purple, white and clear fluorite. These inclusions have homogenization temperatures of 81 to 114 °C and comprise a low salinity (9 to 13 equiv. wt. % NaCl) fluid that can be characterized as a Na + K + Sr + Ba solution. Only F4 appears to have been directly involved in the formation of the fluorite-REE mineralization and these inclusions, particularly those hosted by purple fluorite, contain the highest REE, Y, Th and U concentrations. Some compositional variation shown by F2, however, can be explained by either wall-zone albitization, which accompanies hydrothermal fluorite-REE mineralization, or by fluorite dissolution. Fluid-rock reaction modeling indicates that all four fluids appear to have been derived from within the pegmatite, during its later stages of crystallization. Fluorite-REE mineralization appears to have occurred at relatively constant T and pH, largely as a result of mixing of Ca liberated from the pegmatite wall-zone during albitization with an F-bearing hydrothermal fluid.

Introduction

Hydrothermal processes responsible for fluorite-rare earth element (REE) mineralization have been documented from a number of localities (e.g., Salvi & Williams-Jones 1992, Williams-Jones et al. 2000, Samson et al. 2001, Bühn et al. 2003) including mineralization hosted by niobium-yttrium-fluorine (NYF)-type granitic pegmatites in the South Platte district, Colorado (e.g., Simmons & Heinrich 1980, Levasseur & Samson 1996, Levasseur 1997, Gagnon et al. 2002). Detailed mapping and description of the mineralogy of the South Platte pegmatites and fluorite-REE mineralization have been conducted, however, only limited microthermometric data are available on the fluids responsible for the mineralization (e.g., Simmons & Heinrich 1980, Levasseur 1997). Furthermore, very little quantitative information is available on the composition of the fluids responsible for the formation of hydrothermal REE mineral deposits in general.

Laser ablation - inductively coupled plasma - mass spectrometry (LA-ICP-MS) has been used in a number of studies to quantitatively determine elemental concentrations within individual fluid inclusions (e.g., Audétat et al. 1998, 2000, Shepherd et al. 1998, Günther et al. 1998, Heinrich et al. 1999, Ulrich et al. 1999, Müller et al. 2001, Landtwing et al. 2002). These investigators have concentrated on relatively large fluid inclusions (greater than 30 μm in diameter) hosted by quartz, a mineral that is compositionally simple and lacks cleavage. In many geologic settings, including the South Platte district fluorite-REE mineralization, the fluid inclusions of interest are small (1 to 15 μm) and are hosted by compositionally complex minerals that may have well-developed cleavages (e.g., fluorite). Collectively, these fluid inclusion and host-mineral attributes make analysis by LA-ICP-MS more problematic and analytical procedures and data reduction strategies applicable to larger fluid inclusions in compositionally simple host minerals are not necessarily valid.

In this study, we discuss a procedure adapted to laser sampling of fluid inclusions hosted by primary magmatic pegmatitic quartz and secondary hydrothermal fluorite from the Oregon No. 3 pegmatite in the South Platte district, Colorado. Using this method, relatively small fluorite- and quartz-hosted fluid inclusions have been analyzed and the potential effect of host-mineral composition on fluid-inclusion composition quantitatively removed. The LA-ICP-MS analyses of fluid inclusions have been used to constrain: 1) the character and potential source(s) of the fluid(s) responsible for the fluorite-REE mineralization, and 2) the timing of this mineralization relative to formation of the associated pegmatites.

Fluorite-REE Mineralization, South Platte, Colorado

The Oregon No. 3 Pegmatite

The fluorite-REE mineralization in the South Platte District occurs within complex, concentrically zoned, REE-F-Y-Nb-U-enriched granitic pegmatites hosted by the Proterozoic, anorogenic Pikes Peak granitic batholith in north-central Colorado (Hedge 1970, Simmons & Heinrich 1970, 1980, Simmons et al.

1987) (Fig. 4-1). Over 50 pegmatites occur within the reversely zoned northern portion of the batholith, which is referred to as the Buffalo Park Intrusive Center. With the exception of one, all of the pegmatites are hosted within the outer, granitic portion of the batholith rather than the quartz monzonite core. Generally, the pegmatites are characterized by high concentrations of fluorine, REE and ferric iron (as hematite) (Simmons & Heinrich 1980).

Some of the zoned pegmatites contain secondary, hydrothermal fluorite and REE minerals (Simmons & Heinrich 1970, 1980, Brewster 1986). The Oregon No. 3 pegmatite is approximately 200 m long by up to 90 m wide and is crudely elliptical. This pegmatite is moderate in size and relatively simple compared with other pegmatites in the district, as it comprises only three primary zones: a quartz-microcline-biotite wall-zone, a fluorite core-margin zone and a quartz core zone, and one secondary zone, a core-margin hydrothermal replacement zone (Fig. 4-2). Primary, magmatic, core-margin fluorite and secondary, hydrothermal, replacement mineralization hosted by the Oregon No. 3 pegmatite are some of the best examples of this mineralization in the district. The volumetrically largest unit of the pegmatite is the wall-zone, which consists of intergrown quartz and microcline-perthite with accessory biotite. The core-margin zone, which is up to 25 cm thick, comprises massive, coarse-grained green fluorite and typically occurs as discontinuous, scattered pods and irregular bodies along the outer edge of the quartz core. Primary fluorite occurs rarely as crudely formed, idiomorphic crystals (Simmons & Heinrich 1980). The core zone of the Oregon No. 3 pegmatite consists almost entirely of white and clear quartz. Vugs, ranging from less than 25 mm to meters in diameter, occur within the core and contain large, well-formed crystals of smoky quartz. In some cases, these crystals are in excess of 30 cm wide and up to 150 cm long (Simmons & Heinrich 1980). On the basis of surface exposure, the wall, core-margin and core zones are estimated to comprise approximately 63, 2 and 35% of the pegmatite, respectively (Simmons & Heinrich 1980).

Figure 4-1. Geology of the Proterozoic Pikes Peak batholith, north-central Colorado (modified from Simmons & Heinrich 1980). Over 50 pegmatites occur in the South Platte District, which is situated in the granitic, Buffalo Park Intrusive Center.

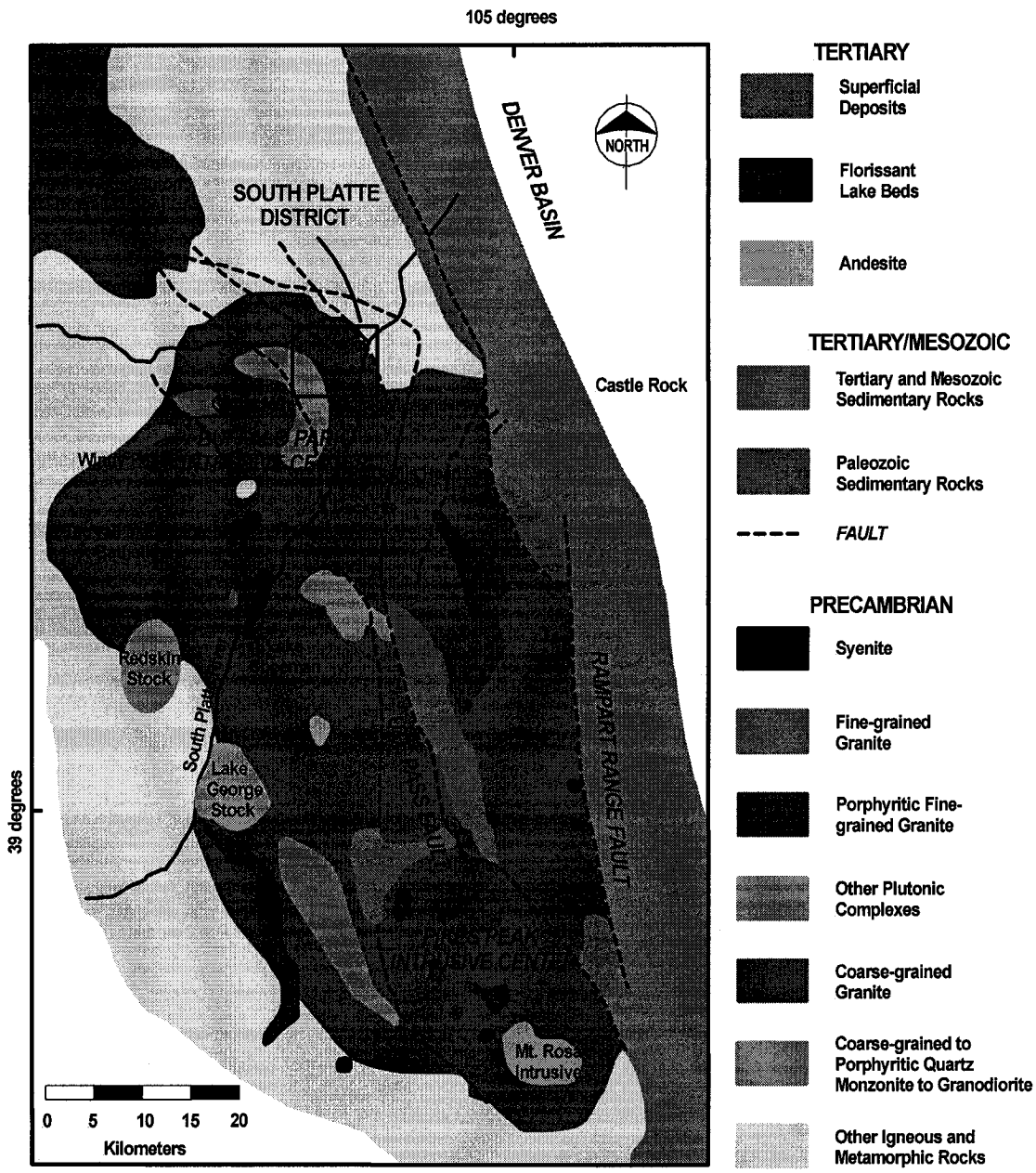
105 degrees
39 degrees
DENVER BASIN
NORTH
SOUTH PLATTE DISTRICT
Castle Rock
Redskin Stock
Lake George Stock
RAMPART RANGE FAULT
Mt. Rosa Intrusive
0 5 10 15 20
Kilometers
TERTIARY
Superficial Deposits
Florissant Lake Beds
Andesite
TERTIARY/MESOZOIC
Tertiary and Mesozoic Sedimentary Rocks
Paleozoic Sedimentary Rocks
FAULT
PRECAMBRIAN
Syenite
Fine-grained Granite
Porphyritic Fine-grained Granite
Other Plutonic Complexes
Coarse-grained Granite
Coarse-grained to Porphyritic Quartz Monzonite to Granodiorite
Other Igneous and Metamorphic Rocks

Hydrothermal Fluorite-REE Mineralization

Secondary, hydrothermal mineralization occurs at the border between the core zone and wall-zone, principally in the wall-zone or core-margin fluorite, and comprises, in decreasing order of abundance, albite, quartz, fluorite, hematite, REE minerals (predominantly samarskite and fergusonite) and white mica (Simmons & Heinrich 1980). Hydrothermal mineralization is concentrated near the upper part of the pegmatite. The latest fluorite preferentially replaces primary green fluorite in the primary core-margin zone. Albite, along with fluorite and REE minerals, typically replaces wall-zone perthite, and comprises either cross-cutting bladed aggregates of albite or, more predominantly, patchy, granular replacements (Simmons & Heinrich 1980).

Three types of hydrothermal fluorite replace minerals of the core-margin zone within the Oregon No. 3 pegmatite. These are, in decreasing relative abundance, purple, white and colourless fluorite, and these three occur as stockwork and patchy replacements, from 1 mm to several cm wide, within green fluorite and wall-zone feldspar. Purple fluorite commonly contains inclusions of REE minerals (samarskite, fergusonite, monazite, xenotime, gadolinite, allanite, yttrofluorite and bastnäsite), hematite and quartz (Simmons & Heinrich 1980) and, in some instances, is opaque due to the high proportion of mineral inclusions. Patchy white fluorite replaces green fluorite and, in some instances, occurs peripherally to purple fluorite veins and patches. Purple, white and colourless fluorite also occur as vug fillings (Simmons & Heinrich 1980). Paragenetically, purple fluorite is earliest and is mantled by later white or zoned white and purple fluorite. Purple and white fluorite commonly grade into one another or are intergrown as patchy replacements of green fluorite. Colourless fluorite postdates purple and white fluorite as it occurs interstitially to euhedral crystals of purple fluorite, lining vugs between purple and white fluorite euhedra, and as veinlets cross-cutting purple and white fluorite (Levasseur 1997).

REE minerals (principally samarskite and fergusonite) commonly occur as coarser-grained aggregates, associated primarily with purple and less commonly with white fluorite, within albitized K-feldspar (Simmons & Heinrich 1980,

Levasseur 1997). These textural relationships indicate that albitization of K-feldspar and deposition of relatively coarse-grained REE minerals accompanied the deposition of purple fluorite.

Fluid-Inclusion Petrography

Three samples from the Oregon No. 3 pegmatite were chosen for detailed analysis of the fluid inclusions. The first sample, RL-94-55b, was collected from the north-central edge of the core, from a hydrothermally altered portion of the core-margin zone. The sample comprises green, purple, white and colourless fluorite, REE minerals, quartz and hematite. Patches of relict, primary, green fluorite and K-feldspar occur in a matrix of predominantly purple and white fluorite. The purple and white fluorite grade into one another and patches of dark purple fluorite occur within white fluorite and as stockwork replacements within green fluorite. The second sample, RL-94-60, which comprises coarse, primary clear quartz with minor hematite stains, was collected from the approximate center of the quartz core. The third sample, RL-94-63, was collected at the southern edge of the core, from a hydrothermally altered portion of the core-margin zone. The sample comprises primarily quartz and pink K-feldspar that have been partially replaced by dark purple and white fluorite. The locations of the three samples are shown in Figure 4-2.

Fluid-inclusion petrography was performed on chips taken from doubly-polished wafers prepared from core-zone quartz (RL-94-60) and hydrothermal purple (RL-94-63), white (RL-94-55b and RL-94-63), and colourless (RL-94-55b) fluorite. The samples were evaluated using standard petrographic techniques, and fluid-inclusion assemblages were classified according to the types and proportions of phases present in the fluid inclusions at room temperature. Two principal types of fluid inclusion were identified: 1) aqueous, liquid-vapour (L-V) inclusions, hosted by core-zone quartz (Fig. 4-3a) and hydrothermal purple, white and colourless fluorite (Fig. 4-3b), and 4-2) aqueous liquid-vapour-halite (L-V-H) inclusions, hosted by core-zone quartz (Fig. 4-3c) and hydrothermal white fluorite. The two types of fluid inclusion identified in this study comprise a subset

of the fluid inclusions previously documented within the South Platte district pegmatites by Simmons & Heinrich (1980) and Levasseur (1997).

Aqueous L-V inclusions in purple, white and colourless fluorite are typically equant, and generally range in diameter from 5 to 30 μm. The majority of the inclusions are, however, relatively small (less than 20 μm) (Fig. 4-3b). The inclusions typically occur either isolated from other inclusions or in clusters of 5 to 15 inclusions arranged in three-dimensional, non-planar arrays. In some instances, clusters of inclusions are concentrated in zones that parallel crystal faces or color zoning within the fluorite, indicating that the inclusions were trapped along primary growth-zones. The inclusions are dominated by liquid (estimated to be approximately 70% by volume), and the relative proportions of the phases within inclusions of a given assemblage are consistent. The occurrence, distribution and consistent phase-ratios of this fluid-inclusion assemblage indicate a primary origin for these inclusions.

Aqueous L-V inclusions in quartz mostly range in size from 5 to 40 μm, are elongate with aspect ratios of 2:1 to 3:1, and generally occur in clusters of greater than 10 inclusions arranged in planar arrays (Fig. 4-3a). The orientations of the long axes of the inclusions comprising an individual cluster are similar and parallel to the plane defined by the fluid inclusions. The L-V inclusions are dominated by liquid (estimated to be approximately 70 to 80% by volume), and the relative proportions of the phases are consistent within an individual plane of inclusions. The distribution along planes within the quartz indicates a secondary origin for these inclusions (along healed fractures), although given the large size of these crystals, a pseudosecondary origin cannot be ruled out.

Figure 4-2. Plan of the Oregon No. 3 pegmatite (modified from Simmons & Heinrich 1980). This pegmatite is relatively simple compared with other zoned pegmatites in the district and comprises only three primary zones: a quartz core, a fluorite-albite-REE mineral core-margin zone, and a quartz-perthite-biotite wall-zone. Secondary, hydrothermal fluorite-REE mineralization occurs predominantly in the core-margin zone and immediately adjacent wall-zone.

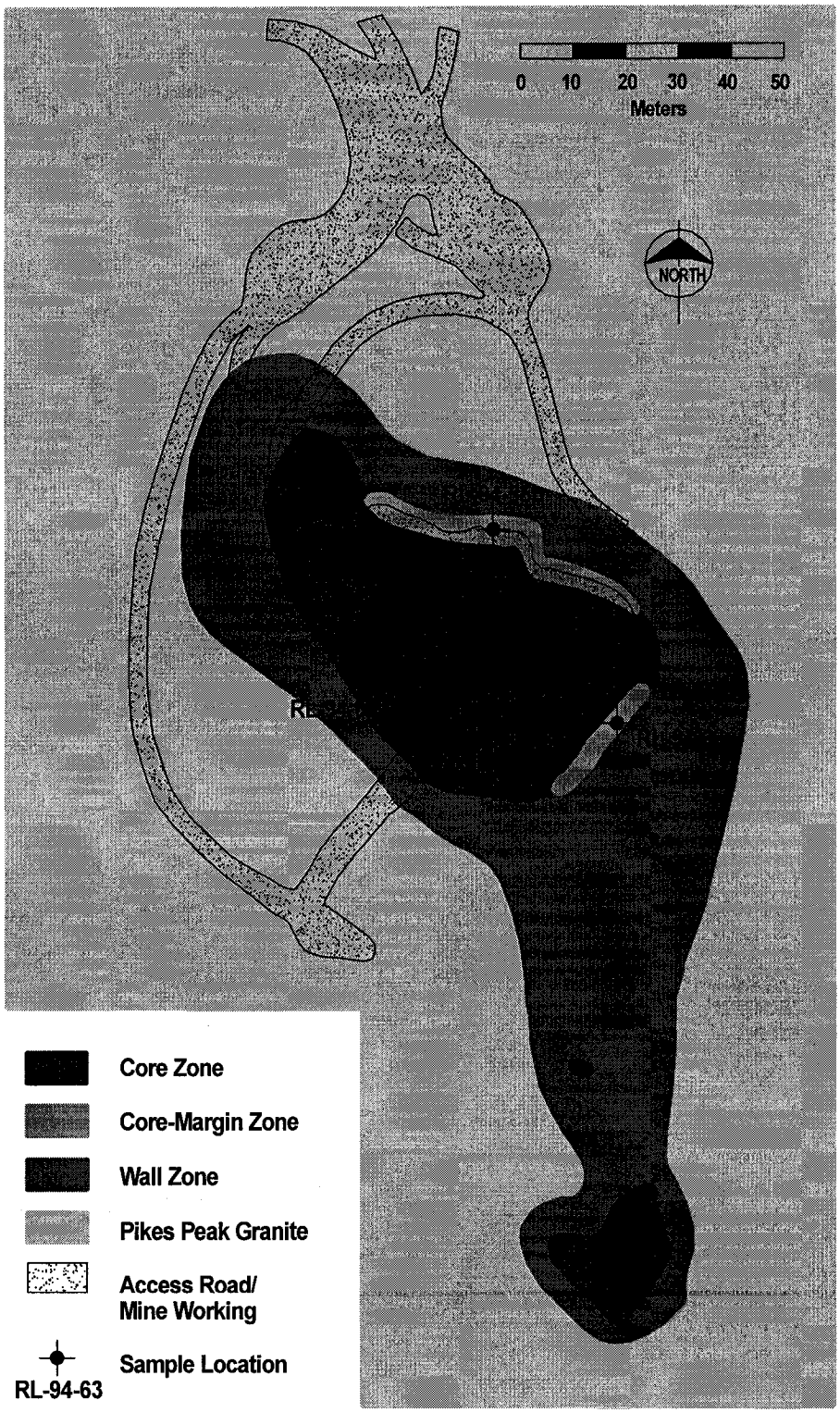
0 10 20 30 40 50
Meters
NORTH
Core Zone
Core-Margin Zone
Wall Zone
Pikes Peak Granite
Access Road/
Mine Working
Sample Location
RL-94-63

Figure 4-3. Photomicrographs of quartz-hosted, secondary, L-V inclusions (Fig. 4-3a), purple fluorite-hosted primary L-V inclusions (Fig. 4-3b) and quartz-hosted secondary L-V-H inclusions (Fig. 4-3c). Quartz-bearing, secondary, L-V and L-V-H inclusions can be further subdivided into Ca-bearing and Ca-"free" (i.e. below detection) varieties based on the results of LA-ICP-MS analysis, despite having similar microthermometric behavior, suggesting a single fluid inclusion assemblage.

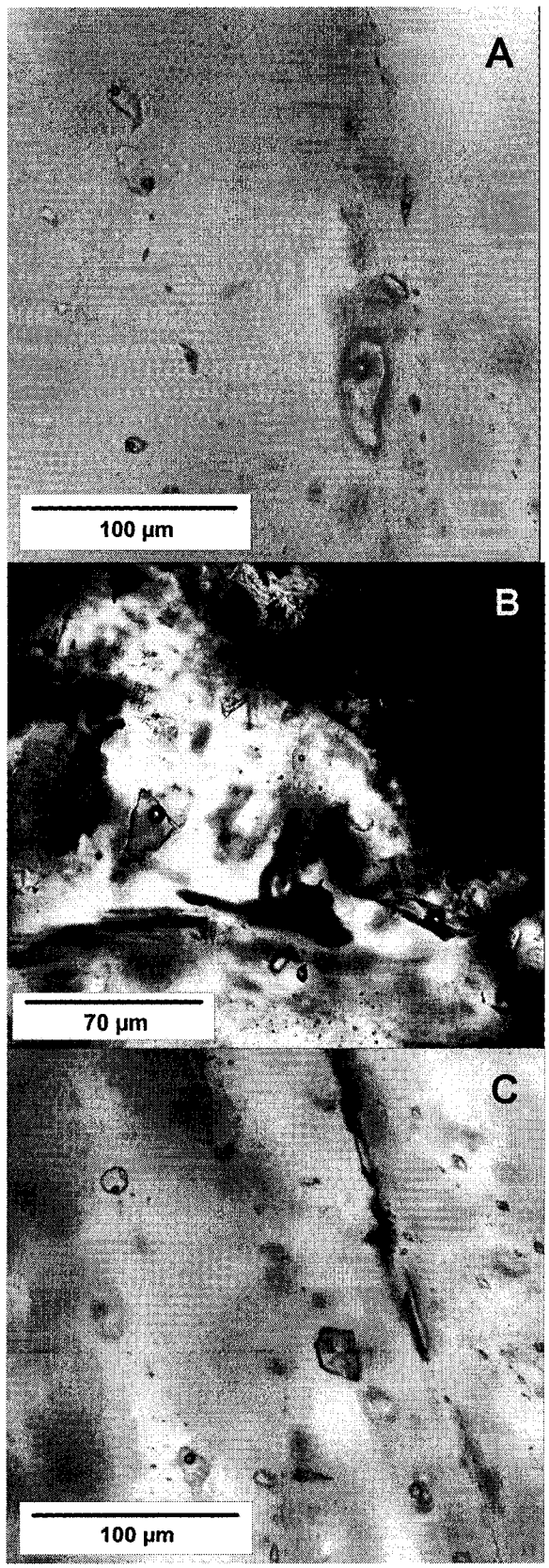
A
100 µm
B
70 µm
C
100 µm

Figure 4-4. Photograph (Fig. 4-4a) and schematic diagram (Fig. 4-4b) of LA-ICP-MS facility at the Great Lakes Institute for Environmental Research, University of Windsor.

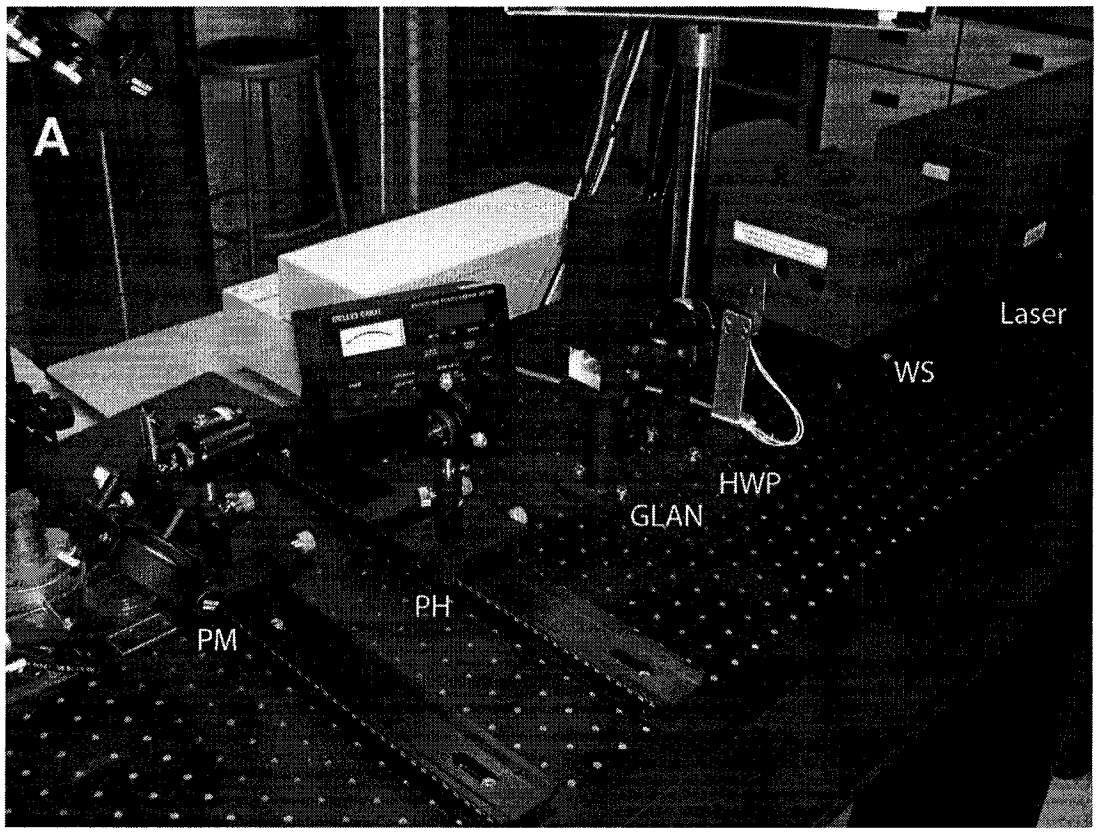

B

LEGEND

SHG - Second Harmonic Generator
FHG - Fourth Harmonic Generator
WS - Wavelength Seperator
M/BS - Mirror/Beam Splitter
M - Mirror
BD - Beam Dump
HWP - Half Wave Plate
GLAN - Gypsum Prism Polarizer
PM - Power Meter
PH - Pinhole
AN - Analyzer
CCS - Computer-controlled Stage
CCF - Computer-controlled Focus
BP - Binocular Prism
COL - Camera Occular Lens

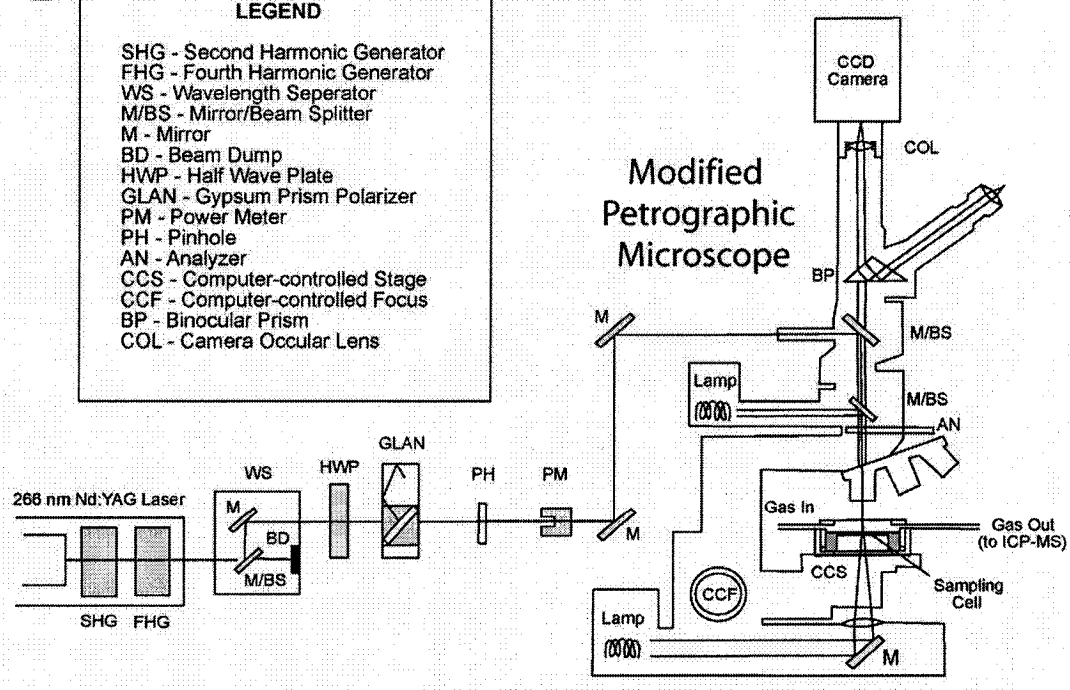

Aqueous L-V-H inclusions are typically equant, generally range in size from 10 to 30 μm, and are abundant in quartz (Fig. 4-3c) and rare in white fluorite. These inclusions are dominated by liquid (estimated to be approximately 70% by volume), with the vapor and solid phases occupying approximately 20 and 10% by volume, respectively. Phase proportions are generally consistent within an assemblage. The solid is interpreted to be a halite daughter crystal as it is cubic, isotropic, reacts to form hydrohalite, and consistently occupies the same percentage of the volume of an inclusion in a given assemblage. In quartz, L-V-H inclusions typically occur in clusters of greater than five inclusions arranged in planar arrays, suggesting that these fluid inclusions are secondary or pseudosecondary in origin. In white fluorite, L-V-H inclusions typically occur in clusters of less than five inclusions that do not appear to be arranged in planar arrays. The three-dimensional arrangement is consistent with a primary origin for these inclusions; the lack of any obvious color growth zoning in the white fluorite, however, prevents any conclusive statement being made regarding their origin. A summary of the fluid-inclusion assemblages analyzed as part of the study is provided in Table 4-1.

Table 4-1. Summary of fluid inclusions analyzed – Oregon No. 3 pegmatite, South Platte, Colorado

Fluorite-hosted				
Variety	**Zone**	**Sample**	**Type**	**Origin**
Purple	Core-margin	RL-94-63	Aqueous LV	Primary
White	Core-margin	RL-94-63	Aqueous LV	Primary
		RL-94-55b	Aqueous LVH	Primary?
Colourless	Core-margin	RL-94-55b	Aqueous LV	Primary
Quartz-hosted				
Variety	**Zone**	**Sample**	**Type**	**Origin**
Clear	Core	RL-94-60	Aqueous LV	Secondary
			Aqueous LVH	Secondary

Fluid-Inclusion Microthermometry

Microthermometric measurements were conducted using a Linkam THMSG 600 heating-freezing stage. To reduce the risk of stretching or decrepitating the fluid inclusions, heating experiments were conducted on fluorite-hosted fluid inclusions prior to conducting cooling experiments. The salinity of the L-V inclusions was determined from the final temperature of melting of ice or hydrohalite. The salinity of the L-V-H inclusions was determined from the final temperature of dissolution of halite. The results of the microthermometric analyses are summarized in Table 4-2.

Table 4-2. Summary of microthermometric data – Oregon No. 3 pegmatite, South Platte, Colorado

Fluorite-hosted						
Type	**Data**	T_e	T_m(hH)	T_m(ice)	T_h(L-V)	T_m(NaCl)
LV	Range	-46.4 to -34.5	-43.4 to -24.7	-9.1 to -5.6	80.7 to 114.5	- -
	Average	-40.8	-27.7	-7.2	96.3	- -
LVH	Range	-57.7 to -22.4	- -	-34.2 to -7.4	104.3 to 108.5	137
	Average	-38.4	- -	-17.8	106.4	137
Quartz-hosted						
Type	**Data**	T_e	T_m(hH)	T_m(ice)	T_h(L-V)	T_m(NaCl)
LV	Range	-26.4 to -19.5	- -	-25.3 to -19.5	92.7 to 125.5	- -
	Average	-24	- -	-21.1	112.6	- -
LVH	Range	-54.8 to -46.2	-13.1 to -12.48	-39 to -37.8	101.7 to 121.9	144.3 to 148.7
	Average	-51.1	-12.8	-38.4	107.5	146.6

Footnotes:
All data reported in °C.
- - Indicates not applicable or not observed.

All of the primary L-V inclusions hosted by purple, white and colourless fluorite exhibit similar behavior of phase assemblages during heating and cooling. Upon heating, the L-V inclusions homogenize to the liquid phase at temperatures ranging from 81 to 114°C. The range of homogenization temperatures for an individual fluid inclusion assemblage (FIA) was less than 5°C. Upon heating after freezing, first melting (i.e., the eutectic temperature) was observed at between -46 and -34°C. The temperatures of final melting of hydrohalite range from -43 to -25°C (individual FIA < 9°C). Ice was the last phase to melt at temperatures ranging from -9.1 to -5.6°C indicating that the

fluorite-hosted L-V fluid inclusions have salinities ranging from 9.2 to 12.8 equivalent wt. % NaCl.

Upon heating, the vapour bubble in white fluorite-hosted L-V-H fluid inclusions disappear at temperatures of 104 to 108°C (individual FIA < 4°C). Homogenization by halite dissolution was observed in two inclusions at a temperature of 137°C, indicating a salinity of 29% NaCl equiv. Upon cooling, the inclusions froze to a mixture of ice, hydrates and halite; upon subsequent heating, first melting was observed at -58 to -22°C. The final temperatures of final ice melting range from -34.2 to -7.4°C.

Quartz-hosted, secondary L-V inclusions homogenized to the liquid phase at temperatures ranging from 93 to 126°C (individual FIA < 1°C). Upon cooling, the inclusions froze to a homogeneous solid and, upon subsequent heating, first melting was observed at approximately -26 to -20°C. Final temperatures of ice melting ranged from -25.3 to -19.5°C, indicating that the quartz-hosted L-V fluid inclusions have salinities ranging from 22.4 to 25.6% NaCl equiv.

When heated, the vapour bubble in quartz-hosted L-V-H fluid inclusions disappears at 102 to 122°C (individual FIA < 5°C). Homogenization of the inclusions occurred by halite dissolution at temperatures ranging from 144 to 149°C, indicating salinities of 29.5 ± 0.1% NaCl equiv. The narrow range of halite-dissolution temperatures (5°C) of all the quartz-hosted secondary L-V-H inclusions supports the interpretation that this is a daughter mineral and not a trapped phase. Upon cooling, the inclusions froze to a mixture of ice, hydrates and halite and, upon subsequent heating, first melting was observed at -55 to -46°C. Final temperatures of hydrohalite melting range from -13.1 to -12.5°C and ice melting range from -39.0 to -37.8°C.

The microthermometric analyses indicate that three fluids occur within the Oregon No. 3 pegmatites: 1) a relatively low-salinity (9 to 12 wt. % NaCl equiv.) fluid represented by the primary, aqueous, L-V inclusions within purple, white and colourless fluorite, 2) a moderate-salinity (22 to 25 wt. % NaCl equiv.) fluid represented by the secondary, aqueous, L-V inclusions within quartz, and 3) a relatively high-salinity (29 wt. % NaCl equiv.) fluid represented by the primary,

aqueous, L-V-H inclusions in white fluorite and secondary or pseudosecondary, aqueous, L-V-H inclusions in quartz.

LA-ICP-MS Analysis

Instrumentation

Laser-ablation ICP-MS analysis of fluorite- and quartz-hosted fluid inclusions was conducted at the Great Lakes Institute for Environmental Research at the University of Windsor. The facility is equipped with a non-homogenized, solid-state, 266 nm Nd-doped Y-Al garnet (Nd:YAG) laser. Analyses were performed on chips taken from doubly-polished wafers and bonded to glass slides. All samples were cleaned prior to analysis by washing with distilled, deionized water and ethanol. Sample ablation was conducted in an Ar gas-filled sampling cell mounted to the stage of a modified polarizing microscope. The ablated material was transported from the ablation cell to the ICP-MS using Ar carrier gas. Whenever possible, fluid inclusions that occurred in assemblages, but sufficiently separated to enable analysis of individual inclusions, were selected so that replicate analyses could be performed. The ablation process was observed throughout, and the time of initiation and duration of fluid inclusion opening were recorded for use during data reduction.

Elemental analysis was performed using a ThermoElemental PQ3 ICP-MS, and instrument calibration was accomplished using NIST glass standard 610 (cf. Heinrich et al. 2003). The elements sought included the major elements most likely to be present in the inclusions, which are also required for calculations in the internal standardization (Na, K, Ca), and trace elements that are of interest in characterizing and potentially differentiating the hydrothermal fluids responsible for the formation of these deposits (Be, Sr, Y, Zr, Nb, Ba, Ce, Sm, Ho, Th and U). The analyte list was minimized in order to maximize (optimize) the number of sweeps that could be obtained across the selected masses for a given time-interval. For example, limiting the analyte list to 11 masses resulted in sweep times of approximately 140 ms, enabling the collection of approximately 35 mass scans for a 5-s-long signal. A summary of the

equipment specifications and general instrument operating conditions used during analysis of the fluid inclusions is provided in Table 4-3. Additional details pertaining to the instrument specifications, operation and calibration are presented in Gagnon et al. (2003a).

Table 4-3. Summary of instrument specifications and operating conditions – Great Lakes Institute, University of Windsor

Laser-sampling System	ICP-MS
Manufacturer: Continuum	**Manufacturer:** ThermoElemental
Model: Surelite I	**Model:** PQ3
Wavelength: 266 nm	**Mode:** Peak-jumping
Energy/Pulse: 1 mJ	**Dwell Time/Isotope:** 10 ms
Mode: Q-switched	**Sensitivity (Solution):** 3 x 10^8 counts/s/ppm
Frequency: 20 Hz	**Scan Time:** Approximately 150 ms/scan
Pulsewidth: 4 to 6 ns	
Laser Spot Diameter (at sample): 10 to 15 um	

Sampling Technique

Relatively large fluid inclusions hosted by minerals that a) readily absorb laser energy, b) have relatively high tensile strengths, and c) lack structural discontinuities, such as cleavages, can generally be sampled using laser ablation without significant difficulty. Fluid inclusions hosted by minerals that do not have these characteristics, such as fluorite, however, may require specialized sampling procedures to ensure representative sampling of the fluid inclusion's contents. Furthermore, most authors of previous LA-ICP-MS studies of fluid inclusions have used homogenized, 193 nm ArF Excimer lasers and a stepwise opening technique to conduct quantitative analyses of individual, relatively large, quartz-hosted fluid inclusions (e.g., Audétat et al. 1998, 2000, Günther et al. 1998, Heinrich et al. 1999, Ulrich et al. 1999). In contrast, our facility is equipped with a non-homogenized 266 nm Nd-YAG laser and, when sampling some minerals, the Gaussian energy distribution of the laser beam can result in differential ablation characteristics across the diameter of the beam, potentially causing fracturing of the sample at the low-energy edge of the beam, and resulting in uncontrolled opening of the fluid inclusions and non-representative sampling of the contents (Gagnon et al. 2003a). Beam homogenization is not an

option for this system owing to the significant reduction in laser power and coherence associated with homogenization.

To overcome the drawbacks of the non-homogenized 266 nm Nd:YAG laser for the analysis of individual fluid inclusions in fluorite, fixed-diameter beam constrictors (i.e., pinholes) are used to reduce the size of the laser beam. If precisely centered on the laser beam, the constrictors trim the beam to a size that is appropriate for the analysis of smaller inclusions. This trimming also is important because it removes the lower-energy, outer portion of the laser beam that may contribute to the differential ablation characteristics of the Gaussian energy distribution, and preserves the high-energy core of the beam, which improves ablation characteristics of poorly absorbing minerals such as fluorite. The system is relatively simple (Fig. 4-4) and does not experience the losses in coherence and reflectance inherent in expanding and homogenizing laser beams using complex arrays of lenses.

Two pinholes arranged in series enable stepwise opening of the fluid inclusions. However, the fluorite-hosted fluid inclusions analyzed in this study are relatively small (generally 10 to 15 μm in maximum diameter) and, consequently, stepwise opening of the inclusions was neither necessary nor desirable, as the lowest possible limits of detection were desired. Direct opening of the fluorite-hosted fluid inclusions (i.e., initiating ablation directly over the inclusion to be analyzed) was initially attempted; however, the sudden thermal and mechanical shock to the sample resulting from initiation of ablation over the inclusions commonly resulted in fracturing of the sample, premature decrepitation of the fluid inclusions, and loss of the contents of the fluid inclusion. Greater success was achieved by conducting 'traversed opening' of the fluid inclusions. In a traversed opening, ablation was initiated at a distance of approximately 50 to 100 μm from the fluid inclusion using a beam diameter approximately equal to the diameter of the fluid inclusion to be analyzed. After a stable ablation process was established, the surface of the sample was traversed using a computer-controlled, motorized X-Y-Z stage until the laser was immediately over the fluid inclusion, at which time traversing was discontinued, and the beam was allowed

to 'drill' into the sample. Fluid inclusions up to 150 μm below the surface of the sample could be analyzed; however, most inclusions were 30 to 100 μm deep. This method of analysis was designed to provide the most controlled ablation for the design of the system, the primary objective being representative sampling of the entire contents of the fluid inclusion. Through integration of the entire fluid-inclusion signal, the resultant analyses reflect the bulk composition of the fluid, inclusive of all solid, liquid and gas phases present in the inclusions, and the lowest possible detection limits.

The combination of beam constriction and traversed opening significantly improved the proportion of fluorite-hosted fluid inclusions that could be successfully analyzed using our non-homogenized 266 nm laser beam, from less than 50% using direct opening to 80 to 90% using beam constriction and traversed opening.

Data reduction

Conversion of the transient ICP-MS output data (integrated counts/second) to concentration units (μg/g) was accomplished using the method described in Gagnon et al. (2003a). In general, the method differs from that used by others for the analysis of melt and fluid inclusions (e.g., Halter et al. 2002, Heinrich et al. 2003) in that: a) rather than applying a single relative sensitivity factor (RSF) calculated for Na to all elements, correction factors are calculated for each element in the fluid inclusion, and b) a ratioing procedure is applied to the data from fluorite-hosted inclusions to remove host-mineral contributions to the fluid-inclusion signal that are not removed by simple subtraction of background. The data reduction procedure for fluorite- and quartz-hosted inclusions consists of: 1) calculation and subtraction of the average background (i.e., instrument and host mineral) from the spectra, 2) determination of the significance of the fluid-inclusion spectra (i.e., detection-limit screening), 3) spectral peak area integration, and 4) calculation of the fluid-inclusion composition. Data from fluorite-hosted fluid inclusions are also ratioed against

Ca after background subtraction to remove host-mineral contributions (Gagnon et al. 2003a).

For elemental spectra that exhibit non-zero backgrounds, the average count-rates obtained during measurement of the pre-ablation signal (i.e., combined instrument and gas-blank background) or the pre-inclusion host mineral (i.e., host-mineral background) were subtracted from the count rates obtained during fluid-inclusion analysis. The spectra were then evaluated to determine whether the count rates obtained for Na over the duration of the fluid-inclusion analysis exceed the mean background plus 3σ count rates obtained for the host mineral (i.e., whether the count rates obtained for Na in the fluid-inclusion signal are statistically significantly different from the background host-mineral count rates) (cf. Longerich et al. 1996). If the Na count rates were determined to be statistically insignificant from the host, the analytical data were discarded; otherwise, all other elemental spectra for the fluid inclusion were evaluated in a similar manner and, if the count rates during fluid-inclusion analysis were found to be statistically significant, further data-reduction procedures were applied.

It is impossible to conduct laser-ablation sampling of fluid inclusions without some of the host mineral being included in the sample that is introduced to the ICP-MS. For fluorite-hosted fluid inclusions, background subtraction often is inadequate to remove a host-mineral contribution to the fluid-inclusion signal. Therefore, the background-subtracted data obtained from fluorite-hosted fluid inclusions were further corrected by dividing the count rate obtained for each element for a single mass scan by the count rate obtained for Ca for the same mass scan. Calcium was selected because it is a major constituent of the host fluorite and is expected to have low concentrations due to the low solubility of fluorite in fluids with salinities comparable to the fluorite-hosted inclusions (Richardson & Holland 1979).

Uncorrected and corrected spectra, obtained for an approximately 12 μm, primary, L-V inclusion in purple fluorite, are illustrated in Figure 4-5. Subtraction of the instrumental and background count-rates of the host mineral was

inadequate to correct for the host-mineral contribution in the early part of the spectra, as indicated by the residual Ca spectral peak (Fig. 4-5a). A fluid inclusion hosted by fluorite cannot have a higher concentration of Ca than the host; therefore, the part of the Ca spectrum corresponding to the fluid inclusion should not exhibit a positive peak. The uncorrected spectra suggest that this fluid inclusion contained Na, K, Ca, Sr, Y, Ba, Ce, Sm, Th and U; however, the corrected spectra show that Ca and Y were contributed to the fluid-inclusion signal by the host fluorite (Fig. 4-5b). The differences between the areas of corrected and uncorrected spectral peaks indicate that determination of element concentrations without initially carrying out a host-mineral correction will result in erroneous results (Gagnon et al. 2003a).

To obtain quantitative data on the composition of an inclusion it is first necessary to obtain, as accurately as possible, an estimate of the concentration of Na in the inclusion using microthermometric analysis. The concentration of Na, as determined from microthermometric analysis (Na_{MT}), was used as an internal standard for the calculation of the abundances of all other elements within the fluid inclusions. Ideally, interpretation of the microthermometric data to obtain Na_{MT} will account for the abundance of other major electrolytes in the inclusions, i.e., those electrolytes that would have a significant effect on measurements such as T_m(ice) and T_m(NaCl) (cf. Heinrich et al. 1992). The abundance of K in all fluid inclusions in this study is negligible relative to the abundance of Na or Ca. Therefore, the phase relationships exhibited by the fluid inclusions are best interpreted using the system H_2O-NaCl (for Ca-free inclusions) or the system H_2O-NaCl-$CaCl_2$ (for Ca-bearing inclusions). It is possible to carry out such a correction and determine a more accurate Na_{MT} value for Ca-bearing, quartz-hosted inclusions. However, a similar correction cannot be applied to fluorite-hosted inclusions because the fluid-inclusion Ca signal is masked by the host-mineral Ca signal.

Figure 4-5. **A.** LA-ICP-MS spectra of a fluorite-hosted LV fluid inclusion that have had instrument and host mineral backgrounds subtracted. These spectra suggest that this inclusion contained Na, K, Ca, Sr, Y, Ba, Ce, Sm, Th and U. **B.** The same spectra after individual element count rates have been ratioed against the count rates obtained for Ca. These spectra show that Ca and Y in the uncorrected spectra were contributed to the fluid inclusion signal from the host fluorite. Calculation of fluid inclusion compositions from the uncorrected data would therefore result in erroneous results.

A

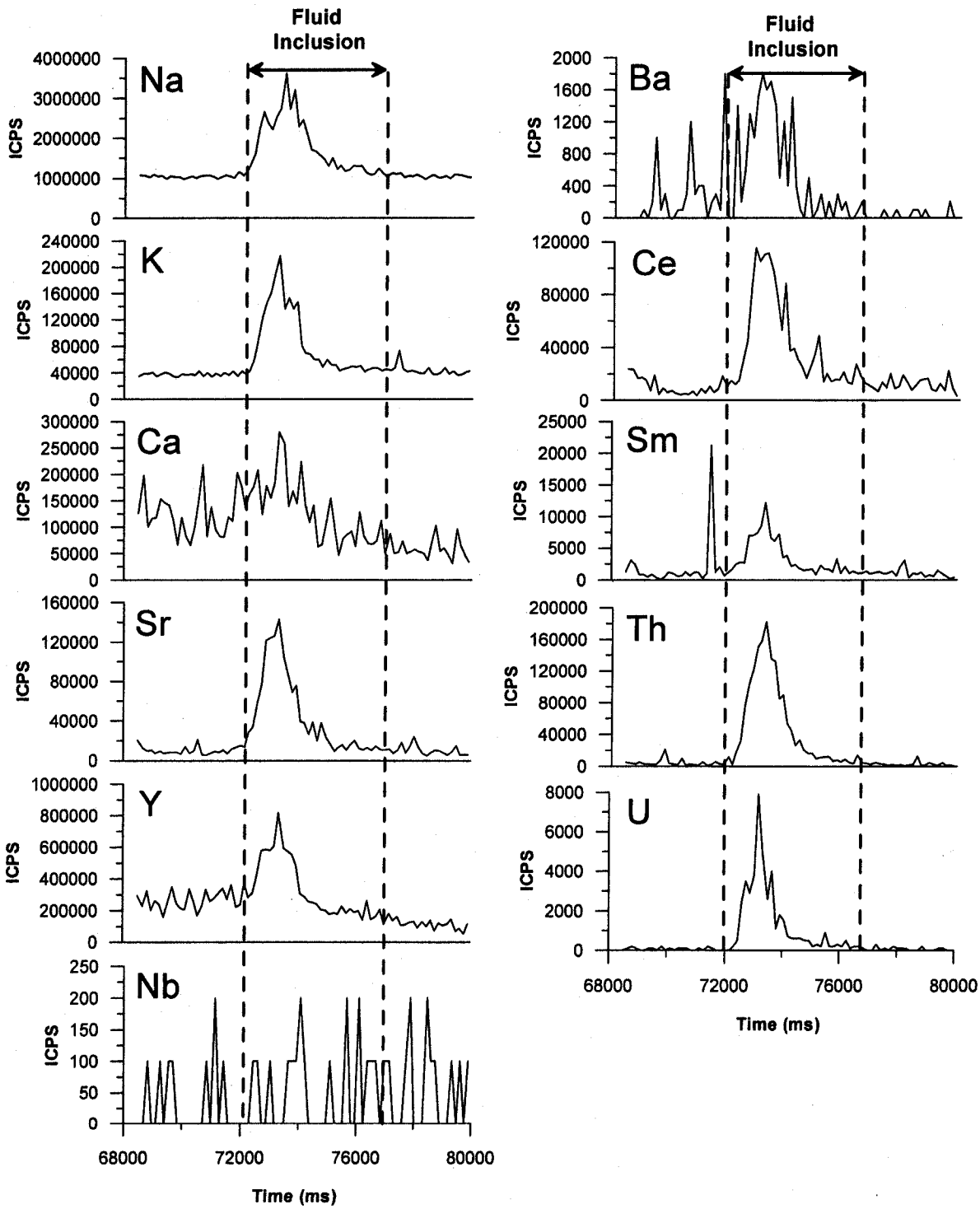
Fluid Inclusion
Na
K
Ca
Sr
Y
Nb
Ba
Ce
Sm
Th
U
ICPS
Time (ms)
68000
72000
76000
80000

B

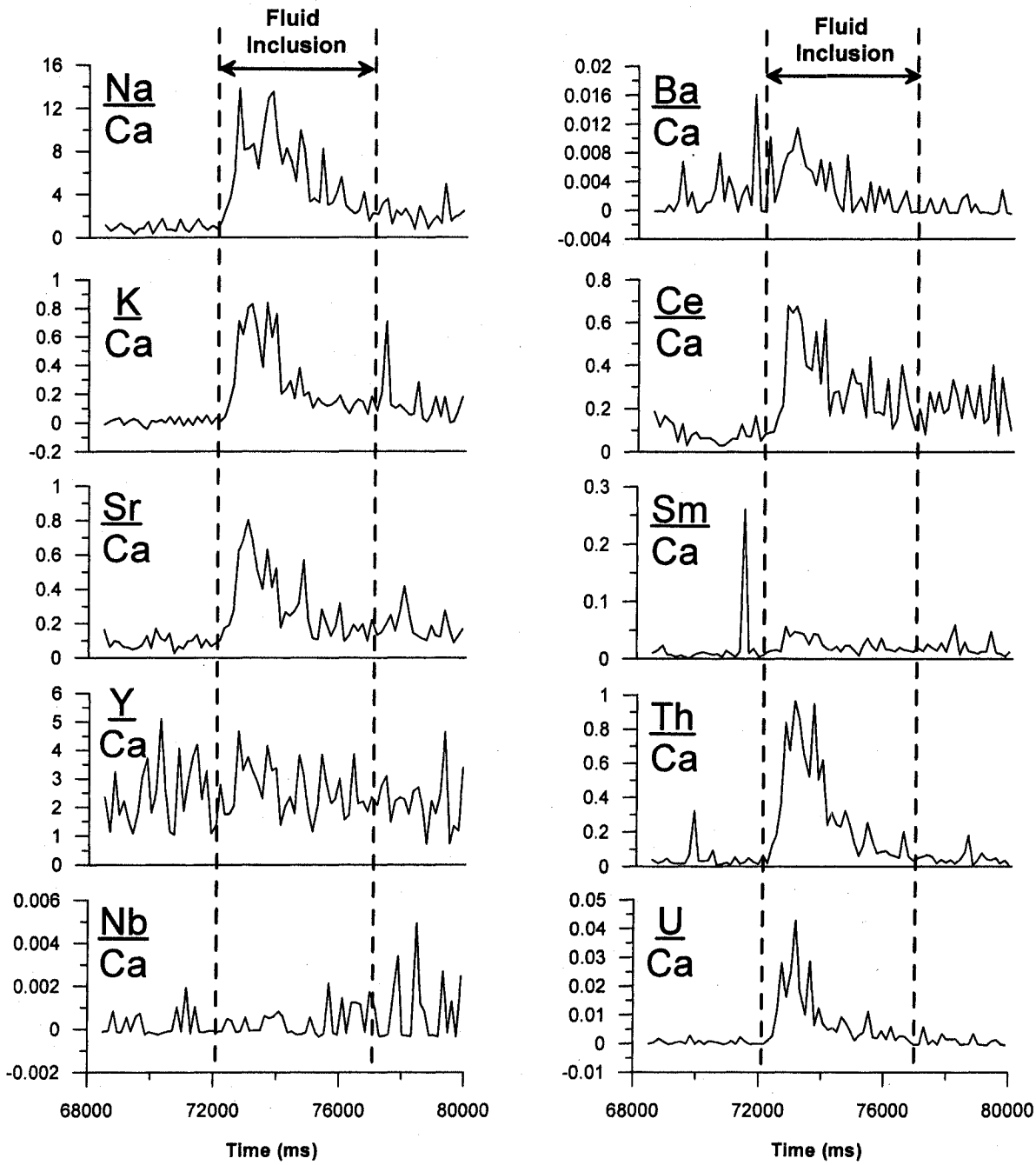
Fluid Inclusion
Na/Ca
K/Ca
Sr/Ca
Y/Ca
Nb/Ca
Ba/Ca
Ce/Ca
Sm/Ca
Th/Ca
U/Ca
68000
72000
76000
80000
Time (ms)

The Na_{MT} value for Ca-free inclusions was calculated using the equation of Bodnar (1993) for L-V inclusions and from the data of Sterner et al. (1988) for L-V-H inclusions. For quartz-hosted, Ca-bearing, L-V inclusions, total salinity can be calculated using equation (2) of Oakes et al. (1990) and the Ca:Na ratio measured from LA-ICP-MS analyses. Heinrich et al. (1992) presented the following equation, based on the data of Vanko et al. (1988), that relates the apparent salinity of an inclusion (equivalent weight percent NaCl calculated from T_m(NaCl) according to Sterner et al. 1988) to the concentrations of NaCl and $CaCl_2$ in L-V-H inclusions:

$$Salinity_{MT} = NaCl_{MT} + 0.5 \bullet CaCl_{2MT} \qquad (1)$$

This equation is, however, only valid at temperatures above 300°C. At lower temperatures, the NaCl solubility isotherms are not normal to the NaCl-H_2O binary join, which is the basis for equation (1). Furthermore, the calculations of Williams-Jones & Samson (1990) suggest that below 300°C, the isotherms are curved. Therefore, for quartz-hosted L-V-H inclusions with T_m(NaCl) < 300°C, NaCl and $CaCl_2$ contents have to be estimated graphically using the isotherms presented by Vanko et al. (1988) or Williams-Jones & Samson (1990). In this case, the isotherms of Williams-Jones & Samson (1990) were used because they are better defined in the temperature range of T_m(NaCl) observed in this study (140 to 150°C).

The effect of apportioning a fraction of the salinity to electrolytes other than Na is a reduction in the Na_{MT} value, which results in a decrease in the concentrations of all other elements determined to be present in the fluid inclusion. For example, if Na_{MT} is corrected for the presence of Ca in the most Ca-rich, quartz-hosted, L-V-H fluid inclusions measured in this study, the concentrations of all electrolytes detected in the inclusion (Na, K, Ca and Sr) decrease by approximately 39%. This reduction represents an extreme case, because it is based on the most Ca-rich fluid inclusion analyzed. Other inclusions containing less Ca exhibit smaller decreases in the calculated concentrations of the elements.

Results

Quartz-Hosted Fluid Inclusions

Results of the LA-ICP-MS analyses of secondary, quartz-hosted L-V and L-V-H inclusions are summarized in Table 4-4. Sodium and K were detected in all quartz-hosted inclusions. Strontium was detected in the majority, Ca and Ba were detected in approximately half, and Y, Nb, Ce, Sm, Th and U were detected in two or three of these inclusions, typically in concentrations less than 10 µg/g. Beryllium, Zr and Ho were not detected in quartz-hosted inclusions, although only four analyses included Be and only five included Zr.

The common occurrence of Na, K, Ca, Sr and Ba in quartz-hosted inclusions makes these elements useful in illustrating the different compositional groups and trends within these inclusions. Approximately half of the quartz-hosted L-V and L-V-H inclusions in this study do not contain detectable concentrations of Ca. Therefore, quartz-hosted inclusions can be divided into two compositional subgroups based on the presence or absence of Ca (Table 4-4).

Calcium-bearing, quartz-hosted inclusions have Ca concentrations ranging from 51,100 to 101,000 µg/g and K concentrations ranging from 395 to 2,270 µg/g (Fig. 4-6a). In inclusions that contain detectable amounts of both elements, the concentration of K appears to increase with increasing Ca concentration (Fig. 4-6a). In contrast, Ca-free (below detection) quartz-hosted inclusions have K concentrations ranging from 12 to 5,110 µg/g (Fig. 4-6a). These relationships allow us to define three types of fluid (Fig. 4-6a): F1 comprise Ca-free, low-K inclusions, F2 comprise Ca-bearing inclusions, and F3 comprise Ca-free, high-K inclusions.

Table 4-4. Summary of quartz-hosted fluid inclusion compositions – Oregon No. 3 pegmatite, South Platte, Colorado

Element	Range (ppm)	Average (ppm)	Number (n)
All Inclusions			
Be	- -	nd	4
Na	51,111 to 117,000	95,994	27
K	12 to 5,110	1,617	27
Ca	nd to 80,630	19,450	27
Sr	nd to 1,303	256	27
Y	nd to 169	6	27
Zr	- -	nd	4
Nb	nd to 17	1	27
Ba	nd to 1,119	146	23
Ce	nd to 86	3	27
Sm	nd to 5	nd	17
Ho	- -	nd	10
Th	nd to 6	0	27
U	nd to 96	4	27
Ca-bearing			
Be	- -	nd	1
Na	51,111 to 101,279	80,477	11
K	395 to 2,271	1,507	11
Ca	6,201 to 80,630	47,741	11
Sr	57 to 1,303	608	11
Y	0 to 5	nd	11
Zr	- -	nd	2
Nb	0 to 3	nd	11
Ba	5 to 1,119	364	9
Ce	0 to 5	1	11
Sm	0 to 5	1	7
Ho	- -	nd	4
Th	0 to 4	nd	11
U	0 to 11	1	11
Ca-free			
Be	- -	nd	3
Na	91,300 to 117,000	106,663	16
K	12 to 5,110	1,692	16
Ca	- -	nd	16
Sr	0 to 66	14	16
Y	0 to 169	11	16
Zr	- -	nd	2
Nb	0 to 17	1	16
Ba	0 to 69	7	14
Ce	0 to 96	5	16
Sm	- -	nd	10
Ho	- -	nd	6
Th	0 to 6	nd	16
U	0 to 96	6	16

Figure 4-6. Ca and K contents of quartz-hosted fluid inclusions (Fig. 4-6a) indicate three fluid types: F1 has Ca concentrations below detection and variable, but relatively low, K concentrations; F2 has variable Ca concentrations and a more restricted range of K concentrations than F1; and F3 has approximately twice the K concentrations of F1, and Ca concentrations below detection. Na contents (Fig. 4-6b) further distinguish the three fluid types: F1 and F3 have a relatively restricted range of Na; and F2 has a wider range, and generally lower, Na concentrations than F1 and F3. The range of Na and K concentrations of F1 and F2 overlap, and each fluid type contains examples of L-V and L-V-H inclusions despite having similar compositions. The absence of halite in some fluid inclusions is therefore interpreted to be related to kinetic effects that apparently have prevented nucleation of halite in some fluid inclusions. Variable Na and Ca contents of F2 fluid inclusions define a trend with a negative slope from relatively low Na and high Ca to relatively high Na and low Ca (Fig. 4-6c). In contrast, F1 and F3 have a restricted range of Na concentrations, with Ca concentrations that are below detection.

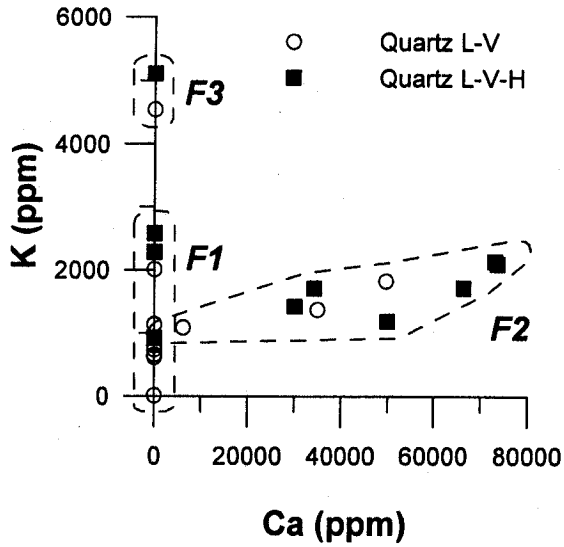
6000
4000
2000
0
K (ppm)
Quartz L-V
Quartz L-V-H
F3
F1
F2
0
20000
40000
60000
80000
Ca (ppm)

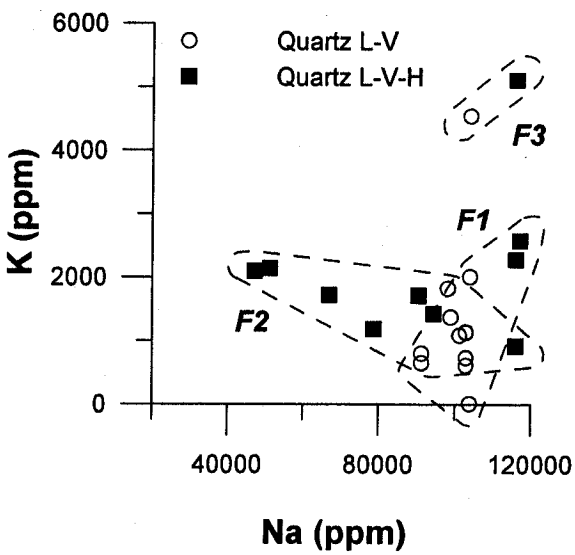
6000
4000
2000
0
K (ppm)
Quartz L-V
Quartz L-V-H
F3
F1
F2
40000
80000
120000
Na (ppm)

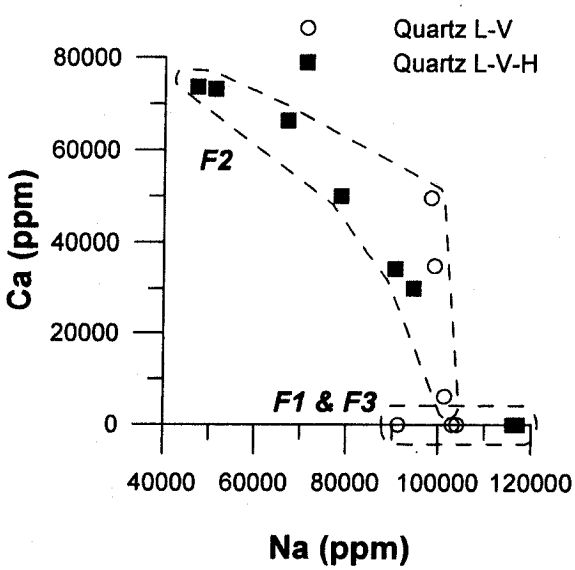
80000
60000
40000
20000
0
Ca (ppm)
Quartz L-V
Quartz L-V-H
F2
F1 & F3
40000
60000
80000
100000
120000
Na (ppm)

The majority of quartz-hosted inclusions have Na concentrations between 85,000 and 120,000 µg/g and K concentrations between 500 and 2,500 µg/g (Fig. 4-6b). Some quartz-hosted L-V-H inclusions, however, have lower Na, and one L-V and one L-V-H inclusion have higher K concentrations than the other quartz-hosted inclusions (Fig. 4-6b). Inclusions of the F2 type of fluid show a decrease in Na with increasing K and Ca (Figs. 4-6b, c). Calcium-bearing, quartz-hosted L-V and L-V-H inclusions (F2) exhibit a continuum in composition between L-V-H inclusions, which have Ca concentrations up to approximately 75,000 µg/g and Na concentrations as low as approximately 50,000 µg/g, to predominantly L-V inclusions, which have Na concentrations up to approximately 102,000 µg/g and Ca concentrations as low as approximately 6,200 µg/g (Fig. 4-6c). Ca-bearing L-V inclusions have a restricted range of Na concentrations (99,400 to 101,300 µg/g) and generally lower concentrations of Ca relative to Ca-bearing L-V-H inclusions suggesting that the continuum of compositions exhibited by these inclusions may comprise two separate compositional trends: 1) relatively constant Na and variable Ca, and 2) high Ca and low Na to low Ca and high Na.

Quartz-hosted, F2 inclusions also exhibit a positive correlation between the concentrations of Ca and Sr (Fig. 4-7a) and Ca and Ba (Fig. 4-7b). In the absence of data on Ca for fluorite-hosted fluid inclusions, the positive correlation among these elements, particularly Sr, is useful in inferring whether quartz-hosted and fluorite-hosted fluid inclusions have similar compositions. Comparison of quartz- and fluorite-hosted fluid inclusions is discussed below.

Although fluid F1 is represented predominantly by L-V inclusions and fluid F2 is represented predominantly by L-V-H inclusions, it is significant that both L-V and L-V-H inclusions occur within each type of fluid. These data suggest that the absence of halite is not reflective of compositional differences, but rather is due to the failure of halite to nucleate in some fluid inclusions.

Figure 4-7. Strontium (Fig. 4-7a) and Ba (Fig. 4-7b) concentrations exhibit positive relationships to Ca concentrations in Ca-bearing, quartz-hosted fluid inclusions (F2). In contrast, F1 and F3, which have Ca concentrations below detection, plot as a cluster near the origin.

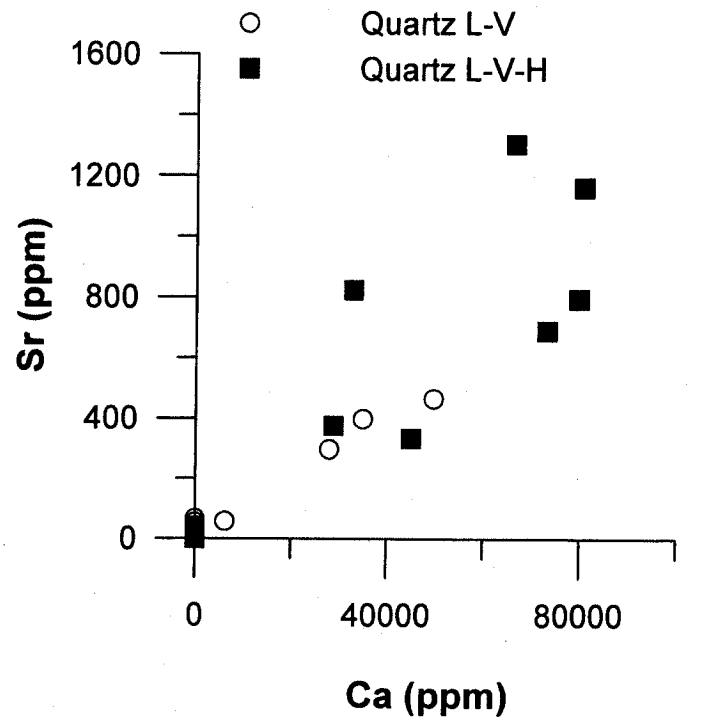
Quartz L-V
Quartz L-V-H
1600
1200
800
400
0
Sr (ppm)
0
40000
80000
Ca (ppm)

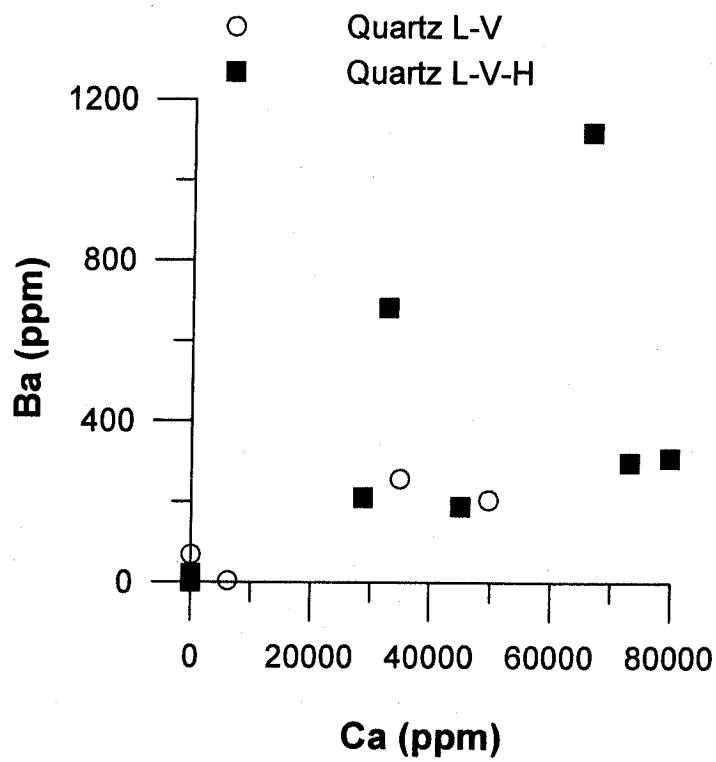
Quartz L-V
Quartz L-V-H
1200
800
400
0
Ba (ppm)
0
20000
40000
60000
80000
Ca (ppm)

Fluorite-Hosted Fluid Inclusions

The LA-ICP-MS analyses of purple, white and colourless fluorite-hosted L-V inclusions and white fluorite-hosted L-V-H inclusions are summarized in Tables 4-5 and 4-6, respectively. Sodium and K were detected in all fluorite-hosted inclusions (Fig. 4-8). Strontium and Ba were detected in the majority, and Y, Nb, Ce, Sm, Th and U were detected in only a few inclusions. As was the case for quartz-hosted inclusions, Be, Zr and Ho were not detected in fluorite-hosted inclusions, although only a limited number of analyses were performed for Be and Zr.

Fluorite-hosted L-V inclusions have Na concentrations ranging from 41,300 to 48,400 µg/g, K concentrations ranging from below detection to 851 µg/g, Sr concentrations ranging from below detection to 652 µg/g, and Ba concentrations ranging from below detection to 11 µg/g. The two fluorite-hosted L-V-H inclusions have a Na concentration of 95,200 µg/g [both inclusions had the same T_m(NaCl)], K concentrations of 1,210 and 1,590 µg/g, Sr concentrations of 546 and 786 µg/g and Ba concentrations either below detection or 353 µg/g.

The T_m(ice) data indicate that all purple, white and colourless fluorite-hosted L-V inclusions have comparable salinities. These data, combined with the results of LA-ICP-MS analyses, indicate that Na, K, Sr and Ba concentrations in L-V inclusions hosted in white, colourless and purple fluorite are all similar, but that in purple fluorite, L-V inclusions have higher concentrations of Ce, Sm, Th and U. As the sequence of fluorite crystallization is purple, white and then colourless, there was thus a temporal evolution in fluid composition toward lower Ce, Sm, Th and U concentrations at relatively constant salinity. Homogenization temperatures of L-V inclusions in the three types of fluorite are essentially the same (80 to 115°C), indicating that the evolution in fluid composition occurred isothermally.

Table 4-5. Summary of fluorite-hosted L-V fluid inclusion compositions – Oregon No. 3 pegmatite, South Platte, Colorado

Element	Range (ppm)	Average (ppm)	Number (n)
Purple Fluorite			
Be	- -	- -	- -
Na	41,300 to 43,200	42,250	2
K	286 to 375	331	2
Ca	- -	- -	- -
Sr	136 to 240	188	2
Y	nd to 1,590	795	2
Zr	- -	- -	- -
Nb	nd to 1	1	2
Ba	nd to 8	4	2
Ce	152 to 173	163	2
Sm	61 to 105	83	2
Ho	- -	- -	- -
Th	271 to 1,930	1,101	2
U	5 to 13	9	2
White Fluorite			
Be	- -	nd	3
Na	42,100 to 48,400	44,700	5
K	nd to 851	231	5
Ca	- -	- -	- -
Sr	nd to 652	199	5
Y	nd to 54	11	5
Zr	- -	nd	3
Nb	- -	nd	5
Ba	3 to 7	5	2
Ce	nd to 10	2	5
Sm	nd to 4	1	3
Ho	- -	nd	2
Th	nd to 12	6	5
U	nd to 1	nd	5
Colourless Fluorite			
Be	- -	- -	- -
Na	- -	42,900	3
K	123 to 150	139	3
Ca	- -	- -	- -
Sr	207 to 313	262	3
Y	- -	nd	3
Zr	- -	- -	- -
Nb	- -	nd	3
Ba	4 to 11	8	3
Ce	nd to 420	140	3
Sm	- -	- -	- -
Ho	- -	nd	2
Th	nd to 26	9	3
U	- -	nd	3

Table 4-6. Summary of white fluorite-hosted L-V-H fluid inclusion compositions – Oregon No. 3 pegmatite, South Platte, Colorado

Element	Range (ppm)	Average (ppm)	Number (n)
Be	- -	- -	- -
Na	- -	95,200	2
K	1,210 to 1,590	1,400	2
Ca	- -	- -	- -
Sr	546 to 786	666	2
Y	- -	nd	2
Zr	- -	- -	- -
Nb	- -	nd	2
Ba	nd to 353	177	2
Ce	- -	nd	2
Sm	- -	- -	- -
Ho	- -	nd	2
Th	- -	nd	2
U	- -	nd	2

Comparison of Quartz- and Fluorite-Hosted Fluid Inclusions

Sodium, K, Ca, Sr and Ba concentrations can be used to illustrate the relationships between the various types of quartz- and fluorite-hosted inclusions (Figs. 4-8, 4-9, 4-10). In order to plot the fluorite-hosted inclusions on Figure 4-9, we have assumed that the fluorite-hosted inclusions contain little or no Ca. This is a reasonable assumption based on the low solubility of fluorite at the salinities represented by the fluorite-hosted inclusions (Richardson & Holland 1979). The compositions of fluorite-hosted inclusions have not been corrected for the effect of Ca on Na_{MT}, as discussed above; if the correction was performed, and assuming that there is significant Ca in the fluorite-hosted inclusions, the concentration of Na would decrease, and concentrations of other elements (K, Sr, and Ba) would decrease proportionally. The effect that correcting Na_{MT} would have on the data in Figure 4-9 would be to cause the fluorite-hosted L-V and L-V-H inclusions to move from the Na-K binary join toward the Ca apex and away from the Na apex. Because K, Ba and Sr would change proportionally, the effect on Figure 4-10 would be negligible. Understanding the potential effect that the Ca correction would have on Na_{MT} enables direct comparison of corrected data from quartz-hosted fluid inclusions with uncorrected data from fluorite-hosted fluid inclusions.

Figure 4-8. Sodium and K concentrations of white fluorite-hosted L-V-H inclusions are similar to quartz-hosted, Ca-bearing LVH inclusions (F2). Purple, white, and colorless fluorite-hosted L-V inclusions, however, have lower Na and K concentrations than all quartz-hosted LV and LVH inclusions (F1, F2 and F3) and white fluorite-hosted L-V-H inclusions (F2?), indicating that a different fluid (F4) was responsible for the hydrothermal fluorite-REE mineralization.

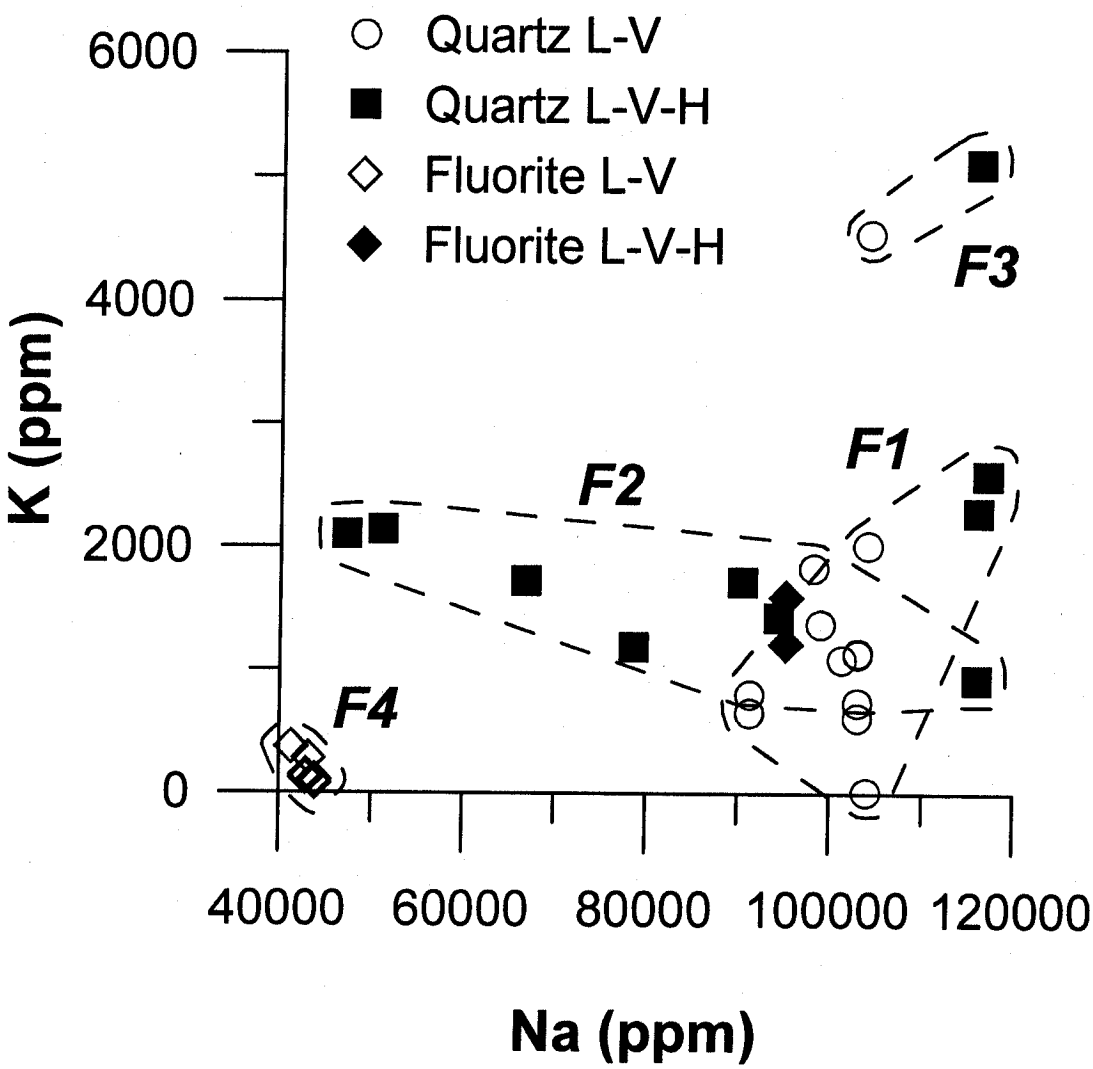
Quartz L-V
Quartz L-V-H
Fluorite L-V
Fluorite L-V-H
6000
4000
2000
0
K (ppm)
F1
F2
F3
F4
40000
60000
80000
100000
120000
Na (ppm)

Figure 4-9. Na-K-Ca relationships of quartz- and fluorite-hosted fluid inclusions. Concentrations of Ca that are below detection in some quartz-hosted inclusions (F1 and F3), and the inability to quantify Ca concentrations in fluorite-hosted inclusions (F4), cause these inclusions to plot along the Na-K binary join. Correction of some fluorite-hosted fluid inclusion compositions for the presence of Ca, however, would cause them to plot with F2 inclusions, suggesting that these inclusions may have the same composition as quartz-hosted F2.

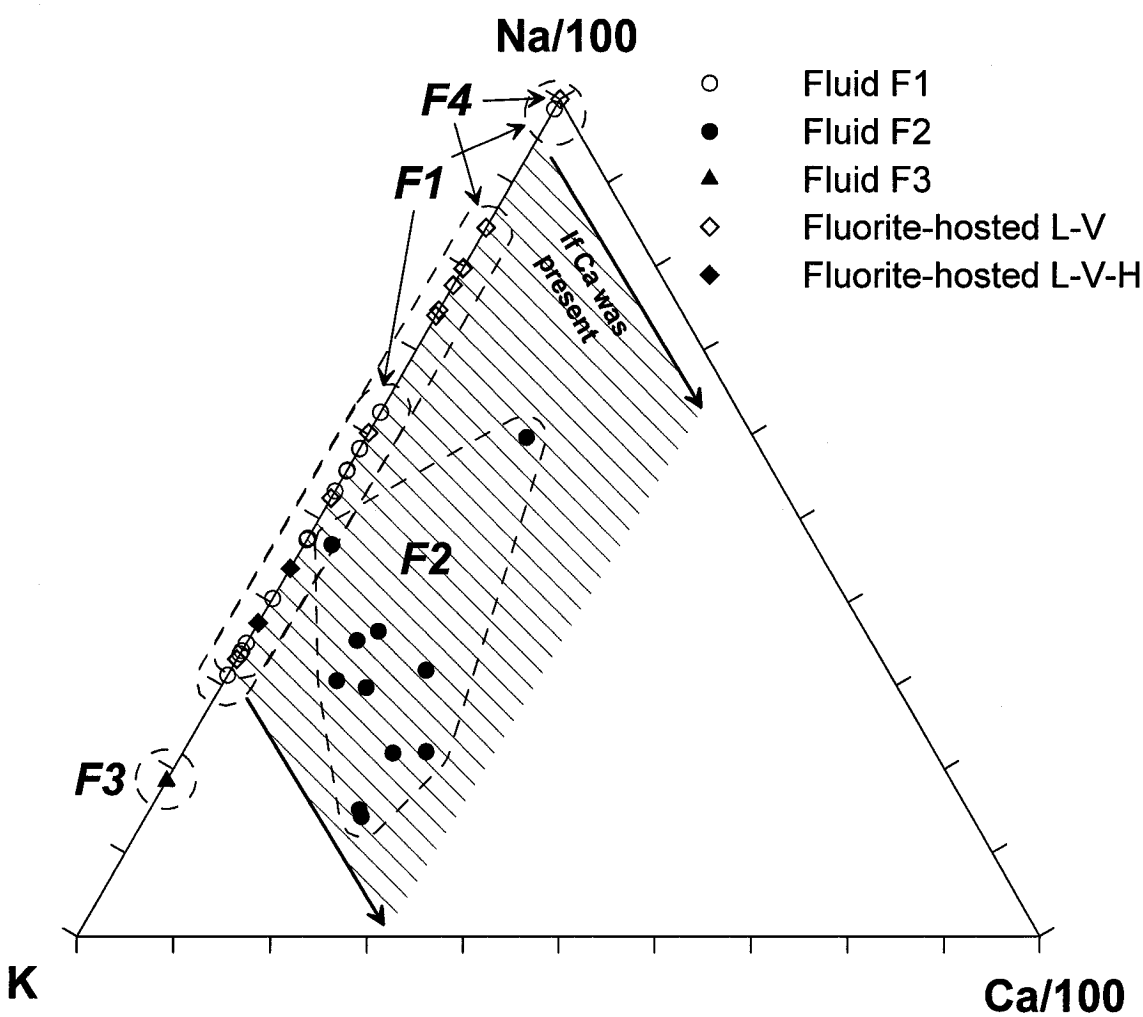
Na/100
F4
F1
F2
F3
If Ca was present
Fluid F1
Fluid F2
Fluid F3
Fluorite-hosted L-V
Fluorite-hosted L-V-H
K
Ca/100

Figure 4-10. Sr-K-Ba relationships of quartz- and fluorite-hosted fluid inclusions. Fluorite-hosted L-V inclusions plot near the Sr apex, indicting that these inclusions have a composition that is unique from other fluorite- and quartz-hosted inclusions.

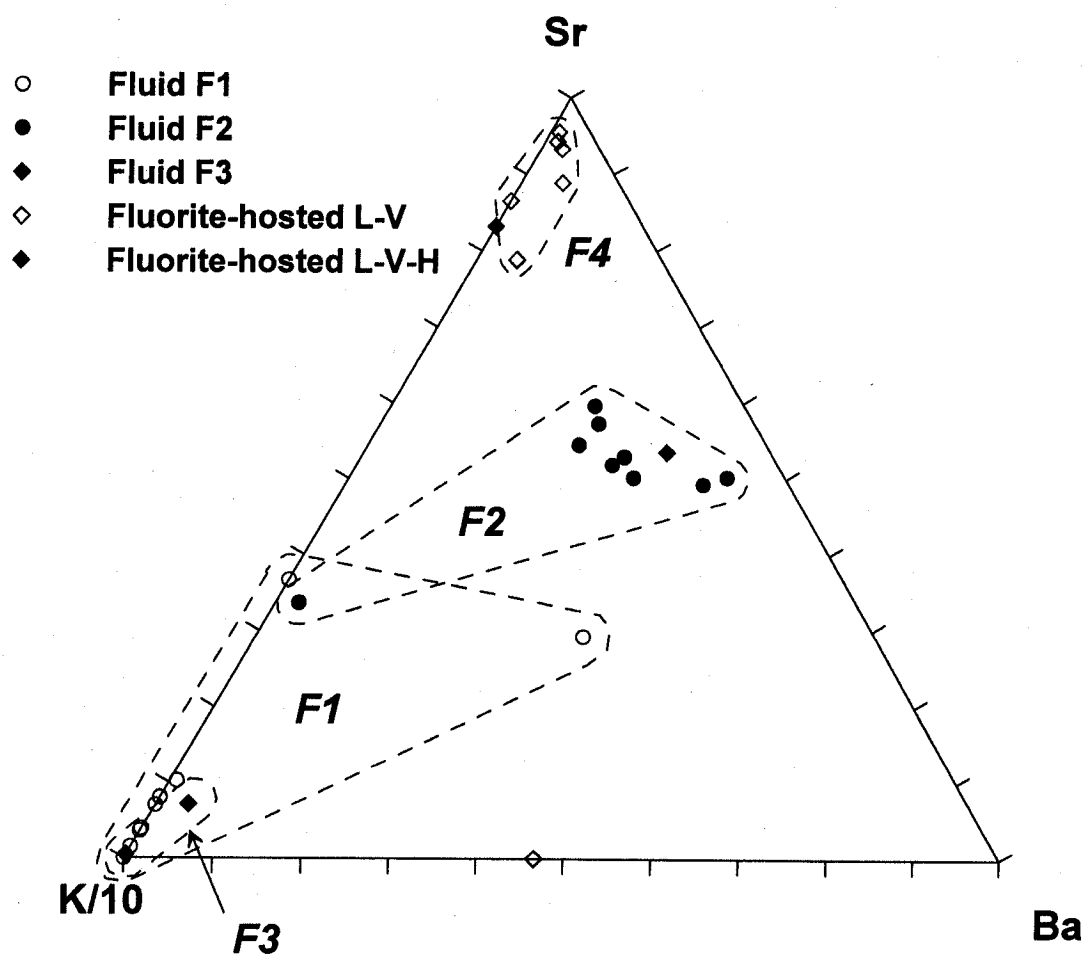
Fluid F1
Fluid F2
Fluid F3
Fluorite-hosted L-V
Fluorite-hosted L-V-H
Sr
F4
F2
F1
K/10
F3
Ba

Fluorite-hosted L-V inclusions have lower Na and K concentrations than fluorite-hosted L-V-H or quartz-hosted inclusions. Fluorite-hosted L-V-H inclusions have compositions similar to quartz-hosted, Ca-free inclusions (F1) (Figs. 4-8, 4-9). If the Na_{MT} of the fluorite-hosted LV inclusions was corrected, the inclusions would plot in an area of Na-K-Ca diagram that, with the exception of one quartz-hosted L-V inclusion, is devoid of other fluid inclusions (arrows on Fig. 4-9). However, if the fluorite-hosted L-V-H inclusions were Ca-bearing and Na_{MT} was corrected, the inclusions would potentially plot in an area of the Na-K-Ca diagram where quartz-hosted, Ca-bearing inclusions plot. Fluorite-hosted L-V-H inclusions thus would have similar major-element compositions to either quartz-hosted Ca-bearing (F2) or Ca-free inclusions (F1).

Fluorite-hosted L-V inclusions have proportionally higher Sr and lower K and Ba concentrations than fluorite-hosted L-V-H and quartz-hosted inclusions (Fig. 4-10). These inclusions plot near the Sr apex of the Sr-K-Ba diagram (Fig. 4-10) because K and Ba concentrations are relatively low and not because Sr concentrations are particularly high. Furthermore, correction of Na_{MT} would have a negligible effect on the element relationships in Figure 4-10. One of the fluorite-hosted L-V-H inclusions plots with the quartz-hosted, Ca-bearing inclusions (F2), and the other plots on the K-Sr binary join because Ba was not detected in this inclusion. These two inclusions plot together on Figure 4-8 along with quartz-hosted L-V-H inclusions, suggesting that both inclusion assemblages represent the same type of fluid.

White fluorite-hosted L-V-H inclusions have higher Na, K, Sr and Ba concentrations than fluorite-hosted L-V inclusions (F4). White fluorite-hosted L-V-H inclusions have similar K:Na, Sr:Na and Ba:Na ratios to quartz-hosted, Ca-bearing inclusions (F2) (Fig. 4-11). Quartz-hosted, Ca-free inclusions (F1 and F3) have variable K:Na and generally lower Sr:Na and Ba:Na ratios than quartz-hosted, Ca-bearing (F2) and white fluorite-hosted L-V-H inclusions. The similarity between the element concentrations and ratios of white fluorite-hosted

L-V-H and quartz-hosted, Ca-bearing inclusions (Figs. 4-8, 4-11) suggests that these two fluid-inclusion assemblages represent that same type of fluid (F2).

We conclude that: 1) fluorite-hosted L-V inclusions have a different composition from quartz-hosted inclusions and fluorite-hosted L-V-H inclusions and represent a different type of fluid (F4), and 2) fluorite-hosted L-V-H inclusions have compositions and element ratios that are similar to quartz-hosted, Ca-bearing inclusions and likely correspond to the same type of fluid (F2). Furthermore, we infer from these similarities that white fluorite-hosted L-V-H inclusions may also be Ca-bearing. The average Sr:Ca ratio of quartz-hosted, Ca-bearing inclusions is 0.013. If the average Sr:Ca ratio of quartz-hosted, Ca-bearing fluid inclusions and the Sr concentration of white fluorite-hosted L-V-H inclusions are used to calculate a hypothetical concentration of Ca, the white-fluorite-hosted inclusions would contain approximately 51,200 μg/g Ca. It is possible that Ca concentrations in the fluorite-hosted fluids were affected by equilibration with, or precipitation of fluorite; the observation that Sr and Ba contents are similar to the quartz-hosted inclusions suggests that this is not the case, however, as those elements are readily incorporated into fluorite (Gagnon et al. 2003b). The inference that white-fluorite-hosted L-V-H inclusions are Ca-bearing and are the same type of fluid as quartz-hosted, Ca-bearing inclusions has implications for the origin and timing of the hydrothermal fluid events, which are discussed below.

Figure 4-11. Element ratios by fluid type. Fluorite-hosted L-V-H inclusions have K:Na and Sr:Na ratios that plot at approximately the center of the range of K:Na and Sr:Na ratios exhibited by Ca-bearing, quartz-hosted inclusions (F2). The Ba:Na ratios of these fluorite-hoisted inclusions also overlap with the ratios of the quart-hosted inclusions. These relationships indicate that these two fluid inclusion assemblages represent the same fluid type.

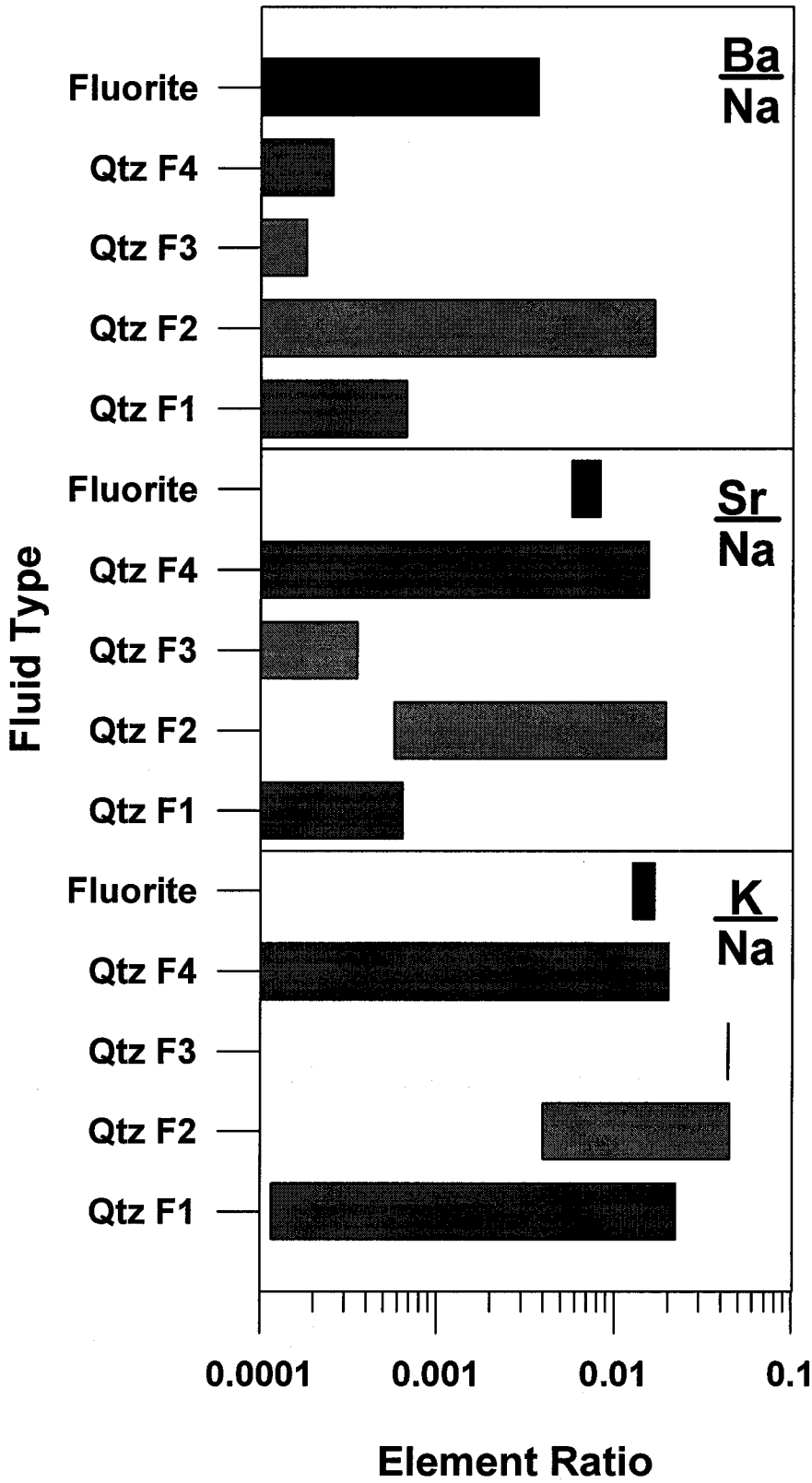
Ba
Na
Sr
Na
K
Na
Fluorite
Qtz F4
Qtz F3
Qtz F2
Qtz F1
Fluorite
Qtz F4
Qtz F3
Qtz F2
Qtz F1
Fluorite
Qtz F4
Qtz F3
Qtz F2
Qtz F1
Fluid Type
0.0001
0.001
0.01
0.1
Element Ratio

Discussion

Sources of Fluid

Microthermometric and LA-ICP-MS analyses indicate that at least four compositionally distinct types of hydrothermal fluid (F1 through F4) occur within the Oregon No. 3 pegmatite. Only F4, which is a Na-K-Ca-Sr-Ba-bearing and relatively low-salinity (9 to 12 wt. % NaCl equiv.) fluid, seems to have caused the secondary hydrothermal fluorite-REE mineralization. Potential sources of hydrothermal fluids in the Oregon No. 3 pegmatite are fluids derived internally, late in the crystallization history of the pegmatite, and fluid(s) derived from outside the pegmatite, either from the Pikes Peak granite or the enclosing country-rocks. The pegmatite is presently situated approximately 5 km from the nearest country rocks, however, Simmons & Heinrich (1980) interpreted the occurrence of country rock xenoliths in granite proximal to the pegmatite to indicate emplacement of the pegmatite near the top of the granite. Although it is possible that fluid from the country rocks could have been involved, migration of any formation waters through the granite would have resulted in compositional modification as a result of varying degrees of equilibration with the granite. Furthermore, extensive, secondary fluorite-REE mineralization selectively replaces the upper parts of the pegmatites, particularly the top of the quartz core and upper core-margin zone of the Oregon No. 3 pegmatite, suggesting that there is an intimate link between the secondary mineralization and pegmatite crystallization (Simmons & Heinrich 1980). Fluid and mineral composition data and fluid-rock reaction modeling (discussed below) indicate that the introduction of elements (e.g., Ca) into the pegmatite from the country rocks, as has occurred in some other cases of hydrothermal REE mineralization (e.g., Salvi & Williams-Jones 1990, Williams-Jones et al. 2000), was not necessary to form the hydrothermal fluorite-REE mineralization in the Oregon No. 3 pegmatite. Therefore, the most plausible sources of the hydrothermal fluids are the pegmatite itself or a late phase of the Pikes Peak granite.

The hydrothermal fluids responsible for the fluorite-REE mineralization (F4), whether internally or externally derived, were out of chemical equilibrium with wall-zone K-feldspar and magmatic core-margin fluorite at the P-T-X conditions of formation of the fluorite-REE mineralization, as evidenced by the extensive albitization associated with fluorite-REE mineralization, and by the replacement of primary, magmatic green fluorite by purple, white and colourless fluorite (Simmons & Heinrich 1980). If the source of fluid F4 was the Pikes Peak granite, the fluid represented by the fluorite-hosted L-V inclusions would be in chemical equilibrium with the granite at the prevailing condition in the granite. Questions that arise are: 1) would such a fluid, upon interaction with the pegmatite wall and core-margin zones, cause albitization and dissolution of fluorite, and 2) how would the composition of such a fluid compare to the observed fluid-inclusion compositions? In order to address these questions, we have used the HCh software package (Shvarov & Bastrakov 1999) and the SUPCRT database (Johnson et al. 1992), modified by Shock (1998), to react a hypothetical fluid in chemical equilibrium with the Pikes Peak granite with the pegmatite wall-zone to determine whether the fluid would cause albitization. A hypothetical composition was determined for aqueous brine in equilibrium with an average composition of the Pikes Peak granite, calculated using data presented in Hutchinson (1960) and Smith et al. (1999). The aqueous brine was then reacted with the pegmatite wall-zone, the composition of which was calculated by averaging 13 compositions reported in Simmons et al. (1987). Fluid-rock reaction was conducted at a temperature and pressure of 200°C and 2000 bars, respectively, which are reasonable estimates based on pressure-corrected temperatures obtained from our microthermometric analysis and the pressure estimates of Simmons et al. (1987), which are based on phase equilibria in the systems Q-Ab-Or-An-H_2O (Simmons & Heinrich 1980) and Q-Ab-Or-H_2O (Barker et al. 1975).

Fluid-rock interaction was modeled by reacting 100 grams of pegmatite wall-zone with incrementally increasing volumes of fluid. The starting fluid:rock ratio was arbitrarily set at 0.03, which is considered to be a low, but geologically

reasonable value. The fluid:rock ratio was incrementally increased until the final ratio was between approximately 3 and 8. At the start of the model, the equilibrium speciation of the fluid was calculated from the initial composition of the fluid and log K values for all plausible reactions involving the different aqueous species that could theoretically form. After each incremental addition of fluid, the rock and fluid were brought to chemical equilibrium by considering all possible reactions governing speciation, mineral deposition, and mineral dissolution. The compositions of rock and fluid were then recomputed and the fluid respeciated.

The average Na, K, Ca, Sr and Ba concentrations of type F1, F2, F3 and F4 fluids and the hypothetical fluid in compositional equilibrium with the Pikes Peak granite are presented in Table 4-7. The results of the modeling are presented graphically in Figure 4-12. The hypothetical, granite-equilibrated fluid has a lower Na concentration relative to type F1 through F4 fluids, a K content that lies within the range of that for the F1 through F4 fluids, and a lower concentration of Ca than type F2 fluid, the only other Ca-bearing fluid identified (Table 4-8). Reaction of the granite-equilibrated fluid with the wall-zone results in alteration of the rock to K-feldspar (Fig. 4-12a). At fluid:rock ratios greater than approximately 0.1, perthite is altered to microcline, and at ratios of approximately 3, perthite is replaced entirely by microcline. Therefore, a fluid that had equilibrated with the Pikes Peak granite would have had a different composition from type F1 through F4 fluids, could <u>not</u> have caused the observed albitization of the wall-zone and, by itself, could not have been responsible for the hydrothermal fluorite-REE mineralization. Therefore, it appears most likely that a hydrothermal fluid derived within the pegmatite was responsible for the secondary fluorite-REE mineralization.

The lack of Ca data for fluid F4 makes it difficult to quantitatively model interaction of this fluid with the wall-zone and test whether or not it would cause albitization. Although the fluids represented by the quartz-hosted fluid inclusions do not appear to have been directly associated with the fluorite-REE mineralization, their origins are of interest in constraining potential sources of

fluids within the pegmatite. Therefore, the average composition of each of the three quartz-hosted fluids (F1, F2 and F3) was reacted with the wall-zone to determine whether the fluids would cause albitization. Modeling was conducted under the same P-T conditions as for the granite fluid and wall-zone reaction.

Table 4-7. Comparison of fluid inclusion and modeled fluid compositions

Element	Quartz F1	Quartz F2	Fluorite F2	Quartz F3	Fluorite F4	Pikes Peak Granite
Na	106,000	112,000	95,200	110,000	43,700	27,000
K	1,250	2,415	1,400	4,800	224	2,600
Ca	nd	81,000	nd	nd	- -	6,560
Sr	13	1,000	670	22	220	- -
Ba	6	600	180	11	6	- -

Footnotes:
All concentrations reported as ppm (mg/g)
- - Indicates sample was not analyzed for this element
nd Indicates concentration of element was below limit of detection

Table 4-8. Fluid-fluorite partition coefficients

Element	Purple Fluorite	White Fluorite	Colourless Fluorite
Na	0.05	0.09	0.04
K	0.63	0.95	0.14
Sr	0.79	0.23	0.79
Ba	1.2	0.94	0.4

The results of the modeling are presented graphically in Figure 4-12 (b, c, d) and indicate that reaction of any of the three quartz-hosted fluid inclusion compositions with pegmatite wall-zone would result in albitization. At water:rock ratios greater than approximately 0.1, microcline is ion-exchanged to albite and at ratios ranging from 4 (Fig. 4-12d) to 8 (Fig. 4-12b), microcline is replaced entirely by albite, a reaction that causes secondary porosity. It is implied by the dissimilarity between the hypothetical granite-equilibrated and quartz-hosted fluid compositions and the fluid and wall-zone reaction modeling that the quartz-hosted fluids, although apparently not directly involved in the fluorite-REE mineralization, were derived internally to the pegmatites and could also have caused albitization of the wall-zone.

Figure 4-12. Fluid-mineral reactions generated using HCh software (Shvarov & Bastrakov 1999). A. This graph represents the reaction of a fluid that was calculated to be in chemical equilibrium with the Pikes Peak granite with the pegmatite wall-zone. Such an interaction would result in alteration of wall-zone perthite to microcline rather than albite, which is the predominant alteration mineral associated with the hydrothermal fluorite-REE mineralization. B, C and D. In contrast, reaction of quartz-hosted fluid compositions (F1, F2 and F3) with the wall-zone would result in alteration of the wall-zone to albite. Some quartz-hosted fluid compositions (i.e., F2), although not directly associated with the fluorite-REE mineralization, apparently reflect compositions that are consistent with the alteration that accompanies the fluorite-REE mineralization.

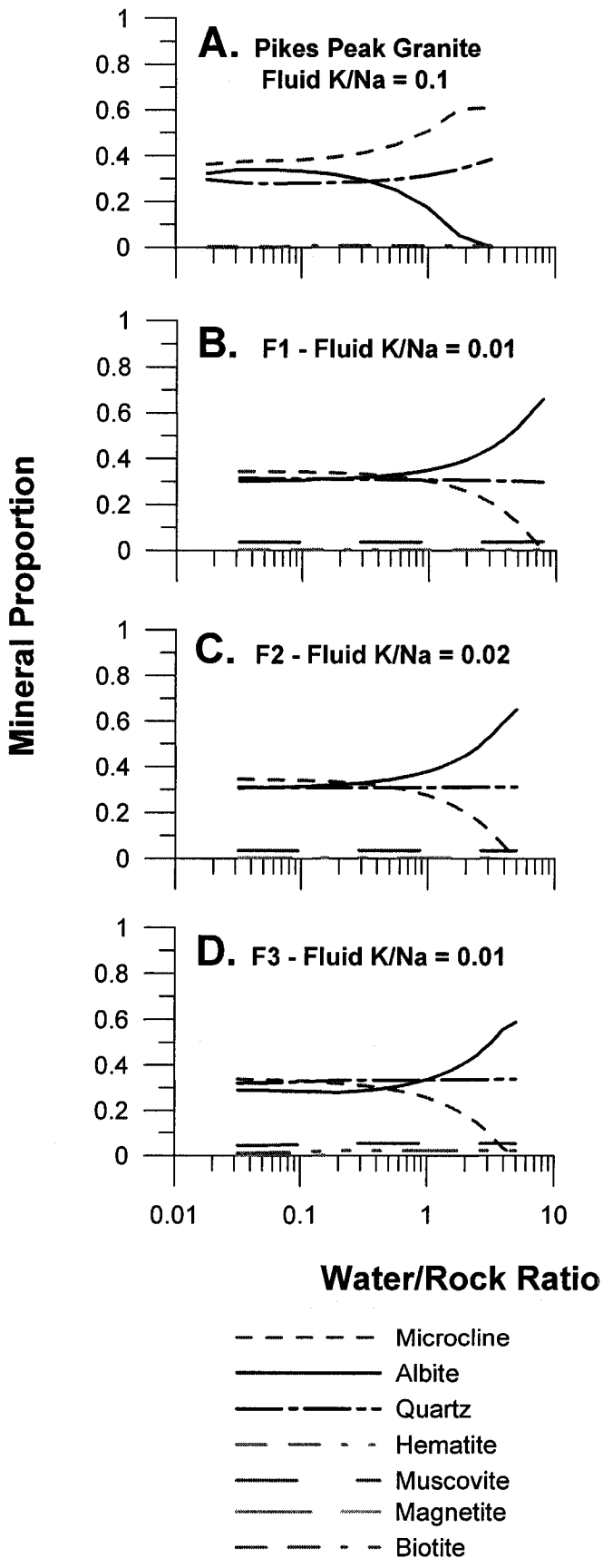
A. Pikes Peak Granite
Fluid K/Na = 0.1
B. F1 - Fluid K/Na = 0.01
C. F2 - Fluid K/Na = 0.02
D. F3 - Fluid K/Na = 0.01
Mineral Proportion
1
0.8
0.6
0.4
0.2
0
0.01
0.1
1
10
Water/Rock Ratio
Microcline
Albite
Quartz
Hematite
Muscovite
Magnetite
Biotite

The fluid-rock reaction modeling indicates that the most significant factor controlling whether wall-zone albitization or K-feldspar alteration occurs is the K:Na ratio of the hydrothermal fluid. The hypothetical fluid in compositional equilibrium with the Pikes Peak granite has a K:Na ratio of approximately 0.1. In contrast, quartz-hosted fluid inclusion compositions have K:Na ratios ranging from 0.01 to 0.03. Fluorite-hosted fluid inclusions have even lower K:Na ratios (approximately 0.005) indicating that if this fluid composition had reacted with the wall-zone, albitization would likely occur at even lower fluid:rock ratios than the quartz-hosted fluid inclusion compositions. The results of the fluid-rock reaction modeling are consistent with models in which albitization, and by association the fluorite-REE mineralization, was caused by fluids derived within the pegmatite.

Fluid Relationships

LA-ICP-MS analyses indicate that four types of fluid occur within the Oregon No. 3 pegmatite and fluid-rock reaction modeling indicates that these fluids were likely derived internally, within the pegmatite. If so, the questions that arise are what may have caused the compositional variations within F1 and F2 (Figs. 4-6, 4-7, 4-8) and what are the possible relationships among F1, F2, F3 and F4 (Figs. 4-8, 4-9, 4-10)? It is implied from the overlap in the compositions of F1 and F2 fluid inclusions and the trends in the data (Figs. 4-6, 4-7) that either two different processes caused evolution of a single fluid (F1) into two different compositions (F2 and F3), or two different fluids (F2 and F3) evolved toward a single composition of fluid (F1). Compositional trends between the fluid mainly responsible for the fluorite-REE mineralization (F4) and the other potentially related fluids (F1 through F3) are not readily apparent (Figs. 4-9, 4-10).

Processes known to have occurred within the pegmatite at the temperature of mineralization that have the potential to cause systematic variations in fluid composition are: 1) dissolution of green, magmatic fluorite, 2) precipitation of purple, white and colourless fluorite, and 3) reaction of fluids with the pegmatite wall-zone (albitization). Although other processes may have been involved (e.g., precipitation of other minerals, reaction with another rock-type, or

introduction of an externally derived fluid other than one in chemical equilibrium with the Pikes Peak granite), the observed variations in the fluid compositions are evaluated below to determine whether the trends can be explained in the context of the three processes that are known to have occurred within the pegmatite.

Data presented by Gagnon et al. (2003b) indicate that the green fluorite has higher average concentrations of Ca and Sr and lower concentrations of Na, K and Ba than F1. Therefore, dissolution of green fluorite by F1 would lead to greater relative increases in the concentrations of Ca and Sr in the fluid than Na, K and Ba. Although F1 does exhibit a trend of increasing Na and K that could be attributed to dissolution of fluorite (Fig. 4-13a), a concomitant change in Ca concentrations is not evident (Fig. 4-13b). Similarly, with the exception of K, compositional variation within F2 could be explained through dissolution of primary green fluorite or, alternatively, secondary hydrothermal purple, white or colourless fluorite (Fig. 4-13c). Compositional variation within and between Ca-free fluids (F1 and F3) cannot be entirely explained by reaction of either fluid with fluorite.

Data from Gagnon et al. (2003b) on the chemical composition of purple, white and colourless fluorite and analysis of primary fluid inclusions in fluorite from this study were used to calculate mineral-fluid partition coefficients (K_d) for Na, K, Sr and Ba (Table 4-8). Because these elements are incorporated into fluorite, fluorite precipitation will deplete the fluid in all these components. The partition coefficients, however, indicate that the precipitation of purple fluorite would cause greater depletion in Ca and Ba in the fluid than in Na, K and Sr, the precipitation of white fluorite would cause greater depletion in Ca, K and Ba in the fluid than in Na and Sr, and the precipitation of colourless fluorite would cause greater depletion in Ca in the fluid than in Na, K, Sr and Ba. The positive trend exhibited by Ca and K concentrations in F2 (Fig. 4-13c) is consistent with fluorite deposition, however, the negative trends in the Na and Ca concentrations (Fig. 4-13b) and Na and K concentrations of F2 (Fig. 4-13a) cannot be explained by fluorite precipitation. The lack of a trend in Ca concentrations, due to concentrations of Ca below detection, implies that progressive precipitation of

Figure 4-13. The inverse relationship exhibited by Na and Ca concentrations in Ca-bearing, quartz-hosted fluid inclusions (F2) (Fig. 4-13a) can potentially be explained by progressive albitization of the pegmatite wall-zone. This is consistent with the inverse relationship exhibited by Na and K concentrations (Fig. 4-13b) and the positive relationship exhibited by Ca and K concentrations (Fig. 4-13c). Fluorite precipitation or dissolution can explain some of the trends exhibited by the quartz-hosted inclusions; however, the compositional variation exhibited by F2 inclusions is most consistent with albitization of the pegmatite wall-zone, which accompanies fluorite-REE mineralization.

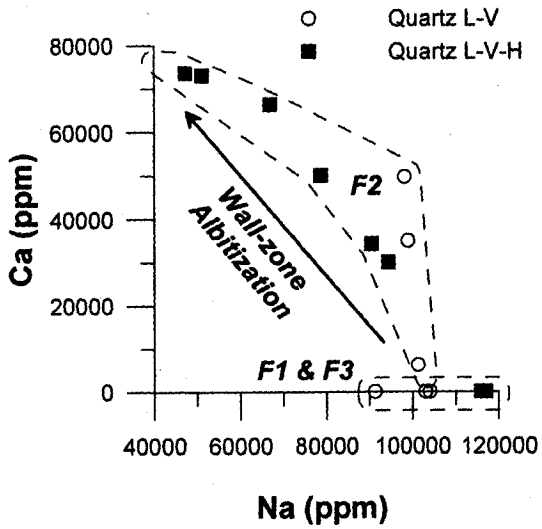
Quartz L-V
Quartz L-V-H
80000
60000
40000
20000
0
Ca (ppm)
F2
Wall-zone Albitization
F1 & F3
40000
60000
80000
100000
120000
Na (ppm)

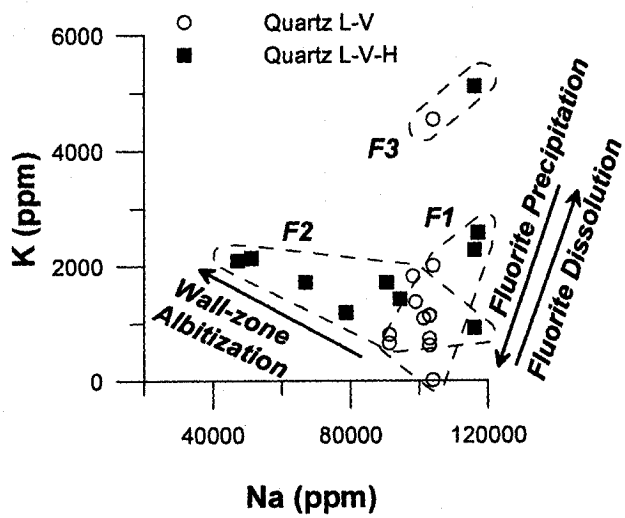
Quartz L-V
Quartz L-V-H
6000
4000
2000
0
K (ppm)
F3
F2
F1
Fluorite Precipitation
Fluorite Dissolution
Wall-zone Albitization
40000
80000
120000
Na (ppm)

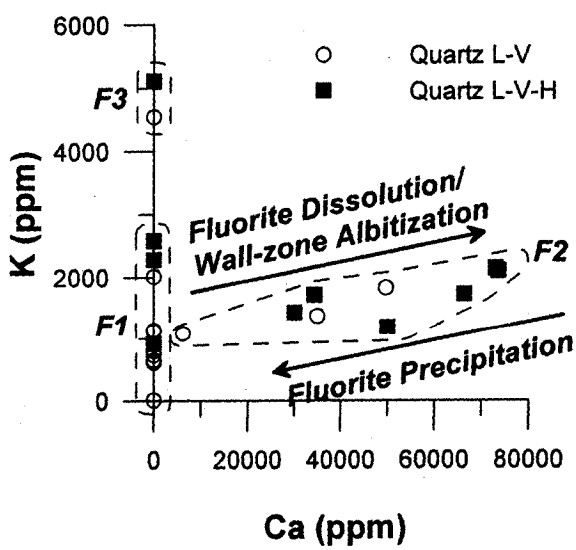
Quartz L-V
Quartz L-V-H
6000
4000
2000
0
K (ppm)
F3
F1
F2
Fluorite Dissolution/
Wall-zone Albitization
Fluorite Precipitation
0
20000
40000
60000
80000
Ca (ppm)

fluorite was not responsible for the compositional variation exhibited by F1 and cannot explain potential relationships between F1 and F3 (Fig. 4-13). The possibility exists, however, that F1 and F3 represent residual fluids that have been depleted in Ca and other elements as a result of fluorite precipitation. The K_d values indicate that fluorite deposition would result in a fluid with lower Na, K, Ca, Sr and Ba than the starting composition of the fluid. Primary fluorite-hosted fluid inclusions (F4), however, have lower salinities than type F1 and F3 fluids. Precipitation of fluorite from such fluids, although resulting in lower concentrations of cations, would not affect the bulk salinity of the hydrothermal fluid owing to the anhydrous nature and the lack of chlorine consumption during progressive fluorite precipitation. Therefore, the differences in the compositions of F1 and F3 relative to F4 cannot be explained by precipitation of purple, white or colourless fluorite.

Progressive dissolution of pre-existing primary green or secondary purple, white or colourless fluorite is expected to result in similar variations in fluid composition to those likely to occur during fluorite precipitation. The direction of the trends, however, would be toward higher concentrations of Na, K, Ca, Sr and Ba in the fluid with increasing amounts of fluorite dissolution rather than the lower concentrations that would result from fluorite precipitation. The negative trend exhibited by Na and Ca concentrations for type F2 fluid (Fig. 4-13b) and the lack of detectable concentrations of Ca in types F1 and F3 fluids are inconsistent with fluorite dissolution.

Fluid-rock reaction modeling of the interaction of the fluids represented by quartz-hosted inclusions (F1, F2 and F3) with the pegmatite wall-zone, in addition to causing albitization of the wall-zone, causes an evolution in the co-existing fluid composition. Progressive reaction of hydrothermal fluid with the wall-zone causes an increase in the concentrations of Ca and K in the fluid due to replacement of microcline by albite. Significant increases in Ca and K concentrations in the fluid occur at relatively low fluid:rock ratios (less than 0.1). In contrast, the Na concentration in the fluid is reduced owing to the precipitation of albite. Compositional trends observed in F2 are characterized by increasing K

(Fig. 4-13b) and Ca (Fig. 4-13a) and decreasing Na or in F1 by increasing K at relatively constant Na (Fig. 4-13a) and lacking Ca (Figs. 4-13b, c). Therefore, the compositional variation exhibited by F2 can be explained through progressive reaction of fluid(s) with the pegmatite wall-zone. Compositional variation within F1, or the potential relationship between F1 and F3, cannot be explained by the same process.

In summary, some of the compositional variation in the fluid types found as inclusions within the quartz core (F1, F2 and F3) can be explained by processes related to the secondary hydrothermal fluorite-REE mineralization. These fluids inclusions are, however, secondary in origin, different in composition from the primary fluid inclusions hosted by fluorite (F4) and, with the exception of L-V-H inclusions in white fluorite (F2), whose provenance is equivocal, have not been observed as primary fluid inclusions within fluorite. Therefore, the interpretation of the variations in the compositions of quartz-hosted fluid inclusions in the context of the fluorite-REE mineralization must be regarded as speculative in nature.

Timing and Cause of Fluorite-REE Mineralization

Four distinct types of fluid have been identified within the Oregon No. 3 pegmatite. Fluid F4, which was responsible for the fluorite-REE mineralization, was not observed in the quartz core. Fluid compositions similar to those observed in secondary, quartz-hosted fluid inclusions (F1 and F3) were not observed in fluorite with the exception of L-V-H inclusions hosted by white fluorite (F2?). Therefore, the relative timing of the four fluid-circulation events is not readily apparent based on fluid-inclusion petrography and compositions alone.

L-V-H fluid inclusions hosted by white fluorite have similar compositions to that of secondary, quartz-hosted, Ca-bearing fluid inclusions (F2). The origin of white-fluorite-hosted L-V-H inclusions, however, is equivocal, and they have been identified as primary in origin only tentatively. If white-fluorite-hosted L-V-H inclusions are primary in origin, represent fluid type F2, and the compositional variation in F2 is reflective of wall-zone albitization at 200°C, then precipitation of

white fluorite occurred contemporaneously with wall-zone albitization. The alteration of primary, pegmatite core-margin zone and wall-zone and the occurrence of vein and replacement-type fluorite-REE mineralization within the upper portions of the pegmatites (Simmons & Heinrich 1980) indicate that late-stage hydrothermal fluids derived within the pegmatite migrated from other portions of the pegmatite (likely underneath the mineralized zones) and reacted with the core-margin zone and wall-zone.

The most likely causes of fluorite deposition from hydrothermal solutions are decreasing temperature, increasing pH, and solution mixing (Richardson & Holland 1979). Fluid-inclusion microthermometric analyses indicate that temperature was approximately constant over the period of time that purple, white and colourless fluorite precipitated. Therefore, it is unlikely that decreasing temperature was the principal cause of fluorite precipitation. Modeling the reaction of pegmatite wall-zone with quartz-hosted fluids indicates that, with the exception of very high water:rock ratios (greater than 10:1), where a slight increase in pH (1 pH unit) was observed, fluid and wall-zone reaction occurs at approximately constant pH. The absence of hydration or dehydration reactions associated with the fluorite-REE mineralization, which would be indicative of considerable changes in hydrothermal fluid pH, support relatively constant pH. Therefore, an increase in solution pH resulting from reaction with the pegmatite wall-zone does not appear to be the principal cause of fluorite precipitation. Fluid-rock reaction modeling and variation in the compositions of quartz-hosted fluid inclusions (F2) suggest that cation exchange involving Na for K and Ca occurred, which is most readily explained by pegmatite wall-zone reaction. Potassium and Ca would be liberated from the pegmatite wall-zone during albitization associated with fluorite-REE mineralization, which would react with fluorine dissolved in the hydrothermal fluid and result in fluorite precipitation. Fluorite precipitation would occur even at low concentrations of Ca and F owing to the low solubility of fluorite (Richardson & Holland 1979). Therefore, the most likely cause of hydrothermal fluorite deposition in albitized pegmatite wall-zone was cation exchange resulting from reaction of late fluids with the wall-zone

which resulted in the addition to the fluid of cations liberated as a result of wall-zone albitization.

Conclusions

The following conclusions can be made based on the microthermometric and LA-ICP-MS analyses of quartz- and fluorite-hosted fluid inclusions and modeling of fluid-rock reaction associated with pegmatite-hosted fluorite-REE mineralization in the South Platte District, Colorado:

- Quantitative LA-ICP-MS analysis of individual, relatively small (less than 15 μm) fluid inclusions in compositionally complex minerals such as fluorite is possible using a non-homogenized 266 nm Nd:YAG laser. Alternate opening strategies (traversed opening) are necessary to overcome difficulties associated with poor absorbance of laser energy and mineral cleavages. Subtraction of instrument and host mineral backgrounds is inadequate to remove contributions to the fluid inclusion signal from the host mineral. The count rates obtained for elements potentially present within the fluid inclusions had to be ratioed against Ca count rates to quantitatively correct for the host mineral contribution to the fluid inclusion signal.
- Four compositional fluid types (F1, F2, F3 and F4) were identified in the Oregon No. 3 pegmatite; however, only one (F4) appears to have been directly involved in the secondary hydrothermal fluorite-REE mineralization. The fluids appear to have been derived internally to the pegmatite and fluorite precipitation appears to have occurred from F4 at relatively constant temperatures (81 to 114 °C) and pH, largely as a result of mixing of Ca liberated from pegmatite wall-zone as a result of albitization with F-bearing hydrothermal fluid. The addition of elements, such as Ca, into the pegmatite through introduction of a fluid derived externally to the Pikes Peak granite was not necessary to cause the hydrothermal fluorite-REE mineralization.

- Compositional variation exhibited by one of the quartz-hosted fluids (F2), which does not appear to have been directly responsible for fluorite deposition, may be the result of fluorite dissolution or pegmatite wall-zone albitization. The lack of a direct association of F2 with fluorite precipitation, however, makes this association speculative.
- The approach used by Heinrich et al. (1992, 2003) for correcting Na_{MT} using halite dissolution temperatures is valid only for temperatures in excess of approximately 300 °C. At lower temperatures, a graphical solution using the data of Vanko et al. (1988) or Williams-Jones & Samson (1990) is necessary; the selection of which is based on how well the isotherms are defined in the range of T relevant to the study. Improvements in the topology of the liquidus surface in the range of T from 100 to 300 °C would improve the accuracy of the determinations made using this graphical solution.

Acknowledgements

The authors thank Mr. R.L. Levasseur for assistance with field sampling and Ms. I. Drouin-Brisebois and Ms. M. Flore for assistance with microthermometry. Drs. D.J. Kontak and A.J. Anderson are thanked for their insightful reviews of an earlier version of this manuscript. Dr. R.F. Martin is thanked for his editorial handling of the manuscript. This research was funded by NSERC discovery grants to AEW-J, IMS and BJF and by a McGill Graduate Student Fellowship and SEG Student Travel Grant to JEG.

References

Audétat, A., Günther, D. and Heinrich, C.A. (1998): Formation of a Magmatic-Hydrothermal Ore Deposits: Insights with LA-ICP-MS Analysis of Fluid Inclusions. *Science*, **279**, 2091-2094.

Audétat, A., Günther, D. and Heinrich, C.A. (2000): Causes for large-scale metal zonation around mineralization plutons: Fluid inclusion LA-ICP-MS evidence from the Mole Granite, Australia. *Economic Geology*, **95**, 1563-1581.

Barker, F., Wones, D.R., Sharp, W.N. and Desborough, G.A. (1975): The Pikes Peak batholith, Colorado Front Range, and a model for the origin of the gabbro-anorthosite-syenite-potassic granite suite. *Precambrian Research*, **2**, 97-160.

Bodnar, R.J. (1993): Revised equation and table for determining the freezing point depression of H2O-NaCl solutions. *Geochimica et Cosmochimica Acta*, **57**, 683-684.

Brewster, R.H. (1986): The distribution and chemistry of rare-earth minerals in the South Platte pegmatite district, Colorado, and their genetic implications. M.S. thesis, University of New Orleans, 139 p.

Bühn, B., Schneider, J., Dulski, P. and Rankin, A.H. (2003): Fluid-rock interaction during progressive migration of carbonatitic fluids, derived from small-scale trace element and Sr, Pb isotope distribution in hydrothermal fluorite. *Geochimica et Cosmochimica Acta*, **67**, 4577-4595.

Gagnon, J.E., Samson, I.M., Fryer, B.J. and Williams-Jones, A.E. (2002): Hydrothermal Fluids in NYF Pegmatites, South Platte, Colorado – Preliminary Insights from LA-ICP-MS Analysis of Quartz- and Fluorite-hosted Fluid Inclusions. 8th Biennial Pan-American Conference on Research on Fluid Inclusions, Program with Abstracts, 25-27.

Gagnon, J.E., Samson, I.M., and Fryer, B.J. (2003a). LA-ICP-MS Analysis of Fluid Inclusions. *In* I. Samson, A. Anderson & D. Marshall (eds.), *The Analysis and Interpretation of Fluid Inclusions*, Mineralogical Association of Canada Short Course **32**, pp. 12-1 to 12-32.

Gagnon, J.E., Samson, I.M., Fryer, B.J., and Williams-Jones, A.E. (2003b). Compositional heterogeneity in fluorite and the genesis of fluorite deposits: insights from LA-ICP-MS analysis. *Canadian Mineralogist*, **41**, pp. 365-382.

Günther, D., Audétat, A., Frischknecht, R. and Heinrich, C.A. (1998): Quantitative analysis of major, minor and trace elements in fluid inclusions using laser ablation-inductively coupled plasma-mass spectrometry (LA-ICP-MS). *Journal of Analytical Atomic Spectrometry*, **13**, 263-270.

Halter, W. E., Pettke, T., Heinrich, C.A., and Rothen-Rutishauser, B. (2002): Major to trace element analysis of melt inclusions by laser-ablation ICP-MS: methods of quantification. *Chemical Geology*, **183**, 63-86.

Hedge, C.E. (1970): Whole rock Rb-Sr age of the Pikes Peak Batholith, Colorado. U.S. Geological Survey, Professional Paper 700B, p. 86-89.

Heinrich, C.A., Ryan, C.G., Mernagh, T.P. and Eadington, P.J. (1992): Segregation of Ore Metals between Magmatic Brine and Vapor: A Fluid Inclusion Study Using PIXE Microanalysis. *Economic Geology*, **87**, 1566-1583.

Heinrich, C.A., Günther, D., Audétat, A., Ulrich, T. and Frischknecht, R. (1999): Metal fractionation between magmatic brine and vapor, determined by microanalysis of fluid inclusions. *Geology*, **27**, 755-758.

Heinrich, C.A., Pettke, T., Halter, W., Aigner, M., Audétat, A., Günther, D., Hattendorf, B., Bleiner, D., Guillong, M., and Horn, I. (2003): Quantitative multi-element analysis of minerals, fluid and melt inclusions by laser-ablation inductively-coupled-plasma mass-spectrometry. *Geochimica et Cosmochimica Acta*, **67** (18), 3473-3496.

Hutchinson, R.M. (1960): Structure and petrology of north end of Pikes Peak batholith, Colorado. *In* Guide to the Geology of Colorado (eds. R.J. Weimer and J.D. Haun), Geological Society of America, Rocky Mountain Association of Geologists and Colorado Scientific Society, 170-180.

Johnson, J.W., Oelkers, E.H. and Helgeson, H.C. (1992): SUPCRT92: A software package for calculating the standard molal thermodynamic properties of minerals, gases, aqueous species and reactions from 1 to 5000 bars and 0° to 1000°C. *Computers and Geosciences*, **18**, 899-947.

Landtwing, M.R., Redmond, P.B., Einaudi, M.T., Heinrich, C.A., Halter, W.E., and Pettke, T. (2002): Veining, Timing of Sulphide Deposition and Fluid Evolution at the Bingham Cu-Au-Mo-Ag Porphyry Deposit – Fluid Inclusion LA-ICP-MS Results. 8th Biennial Pan-American Conference on Research on Fluid Inclusions, Program with Abstracts, 49-50.

Levasseur, R.L. (1997): Fluid Inclusion Studies of Rare Element Pegmatites, South Platte District, Colorado. Unpublished M.Sc. thesis, University of Windsor, 105 p.

Levasseur, R.L. and Samson, I.M. (1996): Fluid inclusion characteristics of REE-Y-Nb pegmatites, South Platte district, Colorado. *Geological Association of Canada – Mineralogical Association of Canada, Program with Abstracts* **21**, A56.

Longerich, H.P., Jackson, S.E., and Günther, D. (1996): Laser ablation inductively coupled plasma mass spectrometric transient signal data acquisition and analyte concentration calculation. *Journal of Analytical Atomic Spectrometry*, **11** (9), 899-904.

Müller, B., Frischknecht, R., Seward, T.M., Heinrich, C.A., and Gallegos, W.C. (2001): A fluid inclusion reconnaissance study of the Huanuni tin deposit (Bolivia), using LA-ICP-MS micro-analysis. *Mineralium Deposita*, **36**, 680-688.

Oakes, C.S., Bodnar, R.J. and Simonson, J.M. (1990): The system NaCl-$CaCl_2$-H_2O. I. The vapour-saturated ice liquidus. *Geochimica et Cosmochimica Acta*, **54**, 603-610.

Richardson C.K. and Holland, H.D., (1979): Fluorite deposition in hydrothermal systems. *Geochimica et Cosmochimica Acta*, **43**, 1327-1335.

Salvi, S., and Williams-Jones, A.E. (1990): The role of hydrothermal processes in the granite-hosted Zr, Y, REE deposit at Strange Lake, Quebec/Labrador: evidence from fluid inclusions. *Geochimica et Cosmochimica Acta*, **54**, 2403-2418.

Salvi, S., and Williams-Jones, A.E. (1992): Reduced orthomagmatic C-O-H-NaCl fluids in the Strange Lake rare-metal granitic complex, Quebec/Labrador, Canada. *European Journal of Mineralogy*, **4**, p. 1155-1174.

Samson, I.M., Kerr, I.D. and Graf, C. (2001): The Rock Canyon Creek fluorite-REE deposit, British Columbia. *In* Industrial Minerals in Canada. *Canadian Institute of Mining and Metallurgy, Special Volume* **53**, 1-10.

Shepherd, T.J., Ayora, C., Cendon, D.I., Chenery, S.R., and Moissette, A. (1998): Quantitative solute analysis of single fluid inclusions in halite by LA-ICP-MS and cryo-SEM-EDS: Complimentary microbeam techniques. *European Journal of Mineralogy*, **10** (6), 1097-1108.

Shock, E. L. (1998): Sequential access thermodynamic datafile for SUPCRIT92. Arizona State University, Department of Geological Sciences, GEOPIG database.

Shvarov Yu. V. and Bastrakov E.N. (1999): HCh: a software package for geochemical equilibrium modelling. User's Guide. AGSO Record 1999/25, Canberra

Simmons, W.B., and Heinrich, E.W. (1970): Rare-earth-fluorine pegmatites of the South Platte district, Jefferson County, Colorado. Geological Association of Canada-Mineralogical Association of Canada, Joint Annual Meeting, Abstracts of Papers, p. 48-49.

Simmons, W.B., and Heinrich, E.W. (1980): Rare-earth pegmatites of the South Platte district, Colorado, Colorado Geological Survey, Department of Natural Resources, Resource Series 11, 131 p.

Simmons, W.B., Lee, M.T., and Brewster, R.H. (1987): Geochemistry and evolution of the South Platte granite-pegmatite system, Jefferson County, Colorado. *Geochimica et Cosmochimica Acta*, **51**, p. 455-471.

Smith, D.R., Noblett, J. Wobus, R.A., Unruh, D., Douglass, J., Beane, R., Davis, C., Goldman, S., Kay, G., Gustavson, B., Saltoun, B. and Stewart, J. (1999): Petrology and geochemistry of late-stage intrusions of the A-type, mid-Proterozoic Pikes Peak batholith (Central Colorado, USA): implications for petrographic models. *Precambrian Research*, **98**, 271-305.

Sterner, S.M., Hall, D.L. and Bodnar, R.J. (1988): Synthetic fluid inclusions. V. Solubility relations in the system NaCl-KCl-H2O under vapor-saturated conditions. *Geochimica et Cosmochimica Acta*, **52**, p. 989-1005.

Ulrich, T., Günther, D. and Heinrich, C.A. (1999): Gold concentrations of magmatic brines and the metal budget of porphyry copper deposits. *Nature*, **399**, 676-679.

Vanko, D.A., Bodnar, R.J. and Sterner, S.M. (1988): Synthetic fluid inclusions: VIII. Vapor-saturated halite solubility in part of the system NaCl-$CaCl_2$-H_20, with application to fluid inclusions from oceanic hydrothermal systems. *Geochimica et Cosmochimica Acta*, **52**, 2451-2456.

Williams-Jones, A.E. and Samson, I.M. (1990): Theoretical estimation of halite solubility in the system NaCl-$CaCl_2$-H_2O: Applications to fluid inclusions. *Canadian Mineralogist*, **28**, 299-304.

Williams-Jones, A.E., Samson, I.M., and Olivo, G.R. (2000): The Genesis of Hydrothermal Fluorite-REE Deposits in the Gallinas Mountains, New Mexico. *Economic Geology*, **95**, p. 327-342.

Chapter 5

Quantitative analysis of silicates by LA-ICPMS with and without an internal standard

Preface

Analysis of minerals by LA-ICPMS historically has required the use of an element of known concentration as an internal standard. The internal standard is used to correct for differences in the rate of ablation of an unknown sample relative to an external calibration standard (e.g., Chapter 2). The need for an internal standard limits the use of LA-ICPMS for the determination of unknown materials. This is particularly problematic when minerals have been partially altered on a micrometer scale (i.e., along fractures) and it is desirable to quantitatively determine the compositions of the unaltered mineral and alteration products in a single analysis without using an internal standard (e.g., Chapter 6). Chapter 5 presents a method for obtaining quantitative major, minor and trace element analyses of silicates by LA-ICPMS without using an internal standard. The accuracy of the technique is demonstrated using silicate glass standard reference materials. The applicability of the technique to natural materials is demonstrated by the analysis of a compositionally complex, silicate mineral (i.e., arfvedsonite) from a major hydrothermal HFSE deposit (Strange Lake).

Quantitative analysis of silicates by LA-ICPMS with and without an internal standard

Joel E. Gagnon[1], Iain M. Samson[2], Brian J. Fryer[2]
and Anthony E. Williams-Jones[1]

[1]*Department of Earth and Planetary Sciences, McGill University, Montreal, Quebec, H3A 2A7*
[2]*Department of Earth Sciences, University of Windsor, Windsor, Ontario, N9B 3P4*

Abstract

Quantitative analysis by laser ablation inductively-coupled plasma mass spectrometry (LA-ICPMS) has relied on the use of an internal standard estimated from mineral stoichiometry or obtained using an alternative analytical technique (e.g., microthermometry, electron microprobe). Major, minor and trace element analysis of silicates can be conducted by LA-ICPMS without using an internal standard by analyzing for a comprehensive list of elements, converting the elements to equivalent oxide concentrations, scaling the oxides to 100 %, and converting the scaled oxide concentrations back into element concentrations. In general, the quantitative results obtained from analysis of silicate glass standard reference materials using oxide scaling are equally or more accurate than using any one of three elements (Si, Ca or Fe) as internal standards. Application of the technique to a natural, compositionally complex silicate mineral (i.e., arfvedsonite) yielded quantitative data comparable to those obtained using the concentration of Si estimated from mineral stoichiometry as an internal standard and by electron microprobe analysis. This method demonstrates that quantitative element concentrations can be obtained from synthetic and natural silicate materials having a wide range of compositions without using an internal standard. The technique expands the application of LA-ICPMS to the analysis of unknowns and is superior to electron microprobe due to its ability to quantify trace elements that are present at concentrations below the limit of detection of electron microprobe analysis.

Introduction

Quantitative analysis of silicates by laser ablation inductively-coupled plasma mass spectrometry (LA-ICPMS) typically has been limited to the determination of minor and trace element concentrations using an internal standard. Two approaches are typically used to obtain an estimate of the concentration of the internal standard: 1) the estimate is based on the proportion of an element in an 'ideal' mineral formula (i.e., stoichiometry, see Chapter 2), or 2) the concentration is estimated using another analytical method (e.g., microthermometry, see Chapter 4). Alternative methods of standardization, such as simultaneous addition of desolvated liquid standards (Leach et al., 1999; Halicz & Günther, 2004), also have been used. These quantification techniques require that the concentration of at least one element in unknown samples be analyzed independently, add a degree of complexity to LA-ICPMS analyses, potentially contribute to problematic molecular ion interferences (e.g., oxides, hydrides), or may preclude quantitative analysis of some elements (e.g., Cu, Halicz & Günther, 2004). Precise and accurate methods for determining major, minor and trace element concentrations in silicates are required that are simple, do not necessarily rely on internal standards, and do not contribute to problematic interferences. This would allow LA-ICPMS analysis of chemically complex, unknown materials.

This paper presents a method for conducting quantitative major, minor and trace element analyses of silicates by LA-ICPMS without using an internal standard. The applicability of the technique is demonstrated by the analysis of six synthetic silicate standard reference materials (SRMs) (NIST 610, NIST 612, NIST 614, BCR-2G, BHVO-2 and BIR-1). The accuracy of the technique is evaluated by comparing the results of analyses obtained for one reference material (NIST 610), which was treated as an unknown, with published values, and by comparing the results obtained for the six reference materials without using an internal standard with those obtained using up to three

different internal standards (Si, Ca and Fe). The precision of the technique is evaluated by conducting ten replicate analyses of each of the reference materials. Finally, the results of the analyses of the reference materials, calculated using the most accurate standardization technique obtained from NIST 610, are presented. These data provide quantitative determinations for some elements for which certified, reference or information (CRI) values were not previously available.

Application of the technique to natural materials is demonstrated by analysis of chemically complex silicate minerals from the Strange Lake peralkaline granite pluton, Quebec/Labrador, Canada. LA-ICPMS analysis of alkali amphibole (arfvedsonite) was conducted and concentration data calculated with and without using an internal standard; the element employed as the internal standard was Si. In order to demonstrate the accuracy of LA-ICPMS analysis of chemically complex, natural silicate minerals without using an internal standard, the latter concentration data are compared with data obtained on the same mineral grains using an electron microprobe.

Standard Reference Material Analysis

Preparation

The standard reference materials included in this study were obtained from the National Institute of Standards and Technology (NIST) and the United States Geological Survey (USGS). The NIST reference materials were synthesized using a silicate glass matrix and contain approximately 500 ppm (NIST 610), 50 ppm (NIST 612) and 1 ppm (NIST 614) of a large number of trace elements. The USGS reference materials are silicate glasses prepared from natural basaltic materials obtained from type localities in Oregon (BCR-2), Hawaii (BHVO-2) and Iceland (BIR-1).

The reference materials, as obtained from NIST and USGS, were cut into approximately 4 mm by 4 mm by 2 mm wafers using a low speed diamond saw (Buehler Isomet®) and cleaned by sonicating them for 15

minutes in MilliQ® water. The fragments were bonded to a glass slide with approximate dimensions of 27 mm by 46 mm by 1 mm using water-soluble glue (Weldbond®), and were stored in covered plastic Petrie dishes within a fume hood until LA-ICPMS analyses were conducted. Immediately before being introduced into the laser cell, the tops of the reference material fragments were wiped with ultrapure ethanol and blown dry with clean, compressed air. The slide was then placed in the laser sample cell under an Ar gas flow.

LA-ICPMS Instrumentation

The LA-ICPMS analyses were conducted in the Great Lakes Institute for Environmental Research at the University of Windsor, Windsor, Ontario, Canada. The laser ablation system comprises a non-homogenized Continuum Surelite I® solid state, 266 nm Nd:YAG laser, an Oriel® optical bench, an Olympus® BX-51 polarizing light microscope equipped with a Prior® computer-controlled stage, and miscellaneous devices for beam size and power manipulation and attenuation. Details regarding the construction of the laser ablation system were presented previously in Gagnon et al. (2003). A summary of the system specifications and operating conditions used during this study is presented in Table 5-1.

Laser-generated sample aerosols were transported from the ablation cell directly to the torch of a ThermoElectron® X7® ICPMS by routing all of the ICPMS nebulizer gas flow (~ 1.04 L/min) through the cell. This configuration facilitates ICPMS tuning and maximizes sample aerosol transport to the ICPMS. A summary of the ICPMS specifications and operating conditions used during this study are presented in Table 5-2.

Table 5-1. Laser ablation system specifications and operating conditions

Manufacturer	Continuum®
Model	Surelite® I
Frequency	20 Hz
Wavelengths	Fundamental: 1064 nm Output: 266 nm
Lamp voltage	Maximum: 1.3 kV Experiment: 1.12 kV
Pulse energy	Maximum: 2 mJ/pulse (100% power) Experiment: ~ 0.8 mJ/pulse (~ 40% power)
Iris	1 mm diameter
Objective Lens	10X
Traverse rate	5 µm/sec

Table 5-2. ICPMS instrumentation and operating conditions

Manufacturer	ThermoElectron®
Model	X7®
Detector type	ETP® dual mode (pulse and analogue)
Dynamic range	~ 1 x 10^9 ICPS
Sensitivity (solution)	~ 350 x 10^6 ICPS/ppm
Cone type	High performance interface (HPI)
Plasma conditions	Standard
Instrument tuning	Lens & torch position: Autotune then manual optimization RF power: 1200 W Resolution: Standard – 125, High – 145 Ar Cool gas: 14 L/min Ar Auxiliary gas: 0.9 L/min Ar Nebulizer gas: 1.04 L/min Quadrupole bias: 0.5 Hexapole bias: -1.5
Data acquisition	Dwell time/mass: 10 ms Masses analyzed: 81 Elements quantified: 64 Mass sweeps/acquisition: 250

Experimental Conditions and Data Acquisition

The high sensitivity of current ICPMS instruments can make it difficult to analyze elements that occur in high concentrations (i.e., weight %) in silicates without count rates exceeding the upper limit of the instrument detector. Tunable mass resolution enables the ThermoElectron® X7® ICPMS to conduct simultaneous quantitative analysis of element concentrations ranging from ppb to weight percent. The high mass resolution setting is manually adjusted during the pre-experiment instrument setup to ensure that relatively abundant, monoisotopic major elements (e.g., Na) are measured exclusively using the pulse mode of the detector. This eliminates any imprecision that may result from the cross-calibration between detector modes if sample data are collected in one mode (e.g., analogue) and initial instrument calibration is carried out in another mode (e.g., pulse). Through a combination of selecting low abundance isotopes (e.g., ^{29}Si) and selectively tuning the high mass resolution of the ICPMS, the concentrations of 64 of the 65 elements (from a total of 81 masses measured) for which certified, reference or information values could be found in the literature for NIST 610 were determined during a single analysis. The remaining element (Cl) was excluded because its determination was problematic using the instrument configuration used in this study.

Five experiments, each consisting of 16 analyses, were conducted. Each experiment included two replicate analyses of each of the six silicate glass standard reference materials, and these analyses were preceded and followed by two replicate analyses of NIST 610 (i.e., the external calibration standard). The sequence of analysis was NIST 610, NIST 612, NIST 614, NIST 610, BCR-2, BHVO-2, BIR-1 and NIST 610. The five experiments resulted in a total of 80 analyses, comprising 10 replicates of each reference material (including NIST 610), that were being treated as unknowns, and 20 additional analyses of NIST 610, which was used as the external calibration standard for the determination of the instrumental drift and element sensitivity factors (SFs) (i.e., integrated counts/s/ppm – ICPS/ppm). All five experiments

were conducted during a single operating session to ensure that the same instrument operating and tuning conditions were used throughout the study. The quadrupole analyzer of the ICPMS was mass calibrated, the detector plateau determined, and the detector modes cross-calibrated at the beginning of the operating session.

Ablation was conducted in a sampling cell through which all of the ICPMS nebulizer gas was routed, which enabled relatively easy ICPMS tuning to simultaneously achieve maximum sensitivity and formation of low oxides (CeO/Ce and UO/O < 0.1 %). Each analysis consisted of traversing the reference material with the laser beam at a constant rate (5 µm/s) using a computer-controlled, programmable stage for a duration of 2.5 min. Before each analysis, data were collected for 1 min on combined instrument and gas background and then again for 0.5 min after the analysis.

The analyte list included all major elements as well as the majority of the minor and trace elements present in the reference materials. The various matrix and molecular ions necessary to assess ICPMS tuning conditions and to correct for various interferences (e.g., ArCl on As) were also included in the analyte list. A comprehensive analyte list was used in order to improve the accuracy of the element concentrations calculated without using an internal standard (i.e., by oxide scaling, see below). The list of masses that were measured, and the elements that were quantified during each analysis, are presented in Table 5-3.

Data Reduction

Data Selection and Correction

Integration regions for each standard reference material analysis were selected from the time-resolved data (i.e., ICPS/time) using ThermoElectron® PlasmaLab® software. One integration region was selected from the approximately 1 min of pre-ablation background, and one region was selected from the stable portion of the signal corresponding to the approximately 2.5

min of reference material ablation. The output data (average ICPS) were transferred to commercial spreadsheet software, which was used to convert the ICPS data into concentration units (ppm).

Table 5-3. Measured masses and quantified elements

Masses Measured (81)	Elements Quantified (64)
^{7}Li, ^{9}Be, ^{11}B, ^{23}Na, ^{25}Mg, ^{27}Al, ^{29}Si, ^{31}P, ^{33}S, ^{39}K, ^{43}Ca, ^{44}Ca, ^{45}Sc, ^{47}Ti, ^{51}V, ^{52}Cr, ^{53}Cr, ^{55}Mn, ^{57}Fe, ^{59}Co, ^{60}Ni, ^{62}Ni, ^{65}Cu, ^{66}Zn, ^{68}Zn, ^{69}Ga, ^{72}Ge, ^{75}As, ^{77}ArCl, ^{82}Se, ^{83}Kr, ^{85}Rb, ^{86}Sr, ^{88}Sr, ^{89}Y, ^{90}Zr, ^{93}Nb, ^{95}Mo, ^{103}Rh, ^{105}Pd, ^{107}Ag, ^{110}Cd, ^{111}Cd, ^{115}In, ^{118}Sn, ^{120}Sn, ^{121}Sb, ^{133}Cs, ^{136}Ba, ^{137}Ba, ^{139}La, ^{140}Ce, ^{141}Pr, ^{146}Nd, ^{147}Sm, ^{153}Eu, ^{155}Gd, ^{156}CeO, ^{157}Gd, ^{159}Tb, ^{163}Dy, ^{165}Ho, ^{166}Er, ^{169}Tm, ^{172}Yb, ^{175}Lu, ^{178}Hf, ^{181}Ta, ^{182}W, ^{185}Re, ^{195}Pt, ^{197}Au, ^{205}Tl, ^{206}Pb, ^{207}Pb, ^{208}Pb, ^{209}Bi, ^{220}Background, ^{232}Th, ^{238}U and ^{254}UO	Li, Be, B, Na, Mg, Al, Si, P, K, Ca, Sc, Ti, V, Cr, Mn, Fe, Co, Ni, Cu, Zn, Ga, Ge, As, Se, Rb, Sr, Y, Zr, Nb, Mo, Rh, Pd, Ag, Cd, In, Sn, Sb, Cs, Ba, La, Ce, Pr, Nd, Sm, Eu, Gd, Tb, Dy, Ho, Er, Tm, Yb, Lu, Hf, Ta, W, Re, Pt, Au, Tl, Pb, Bi, Th and U

The reference material ablation signal was corrected by subtracting the average background ICPS from the average reference material ICPS for each sample (i.e., $ICPS_{Corr} = ICPS_{SRM} - ICPS_{Background}$). Background-corrected data were then drift-corrected using two different procedures. Where NIST 610 was treated as an unknown, drift corrections were calculated based on the first and last two samples (i.e., external calibration standards) in each experiment. To improve analytical accuracy for the remaining reference materials, each experiment was divided into two halves and the two NIST 610 analyses conducted in the middle of the experiment were used to calculate separate drift corrections for the first and second halves of the experiment.

Drift corrections were performed by constructing matrices of sensitivity factors (i.e., ICPS/ppm) for each element based on the sensitivity factors calculated from the external calibration standard (NIST 610). The background-corrected ICPS for the first and last two NIST 610 analyses were averaged and divided by the NIST 610 certified, reference or information values ($CRI_{NIST\ 610}$) to determine external calibration standard element sensitivity factors for the beginning and end of the sample set using:

$$SF_{NIST\,610} = \frac{\left(\frac{ICPS_{Corr_{NIST\,610\#1}} + ICPS_{Corr_{NIST\,610\#2}}}{2} \right)}{CRI_{NIST\,610}}$$

NIST 610 was used as the external calibration standard because it has the greatest number of certified, reference or information values of all the standard reference materials analyzed. Application of the NIST 610 elemental sensitivity factors to the other reference materials enabled calculation of the greatest number of elements for the remaining reference materials, including several elements currently without certified, reference or information values.

Element sensitivity factors for unknown samples (SF_{Unk}), which were used to simultaneously correct for instrumental drift and convert ICPS for each sample to unscaled concentration units (X_{Raw}), were determined for the remaining samples by interpolating between the sensitivity factors determined for NIST 610 at the beginning ($SF_{NIST\,610\,\#1\&2}$) and end ($SF_{NIST\,610\,\#3\&4}$) of each sample set. The drift correction was apportioned based on the time of sample analysis (ΔT) relative to the experiment duration (T) using:

$$SF_{Unk} = SF_{NIST\,610\#1\&2} - \left[\left(\frac{SF_{NIST\,610\#1\&2} - SF_{NIST\,610\#3\&4}}{T} \right) * \Delta T \right]$$

Unscaled element concentrations (X_{Raw}) were calculated for each unknown sample by dividing the sample average ICPS ($ICPS_{Unk}$) by the corresponding element sensitivity factor (SF_{Unk}):

$$X_{Raw} = \frac{ICPS_{Unk}}{SF_{Unk}}$$

Correction of the raw element concentrations for differences in the amount of unknown sample ablated relative to NIST 610 was accomplished by scaling the results using either: 1) an internal standard, or 2) by oxide scaling.

Internal Standard Method

For calculations using an internal standard, scaling factors were calculated by dividing the unscaled element concentrations (X_{Raw}) obtained for the internal standard element (e.g., Si, Ca or Fe) by the standard reference material certified, reference or information value. For example, internal standard scaling factors for NIST 612 were calculated using:

$$SC_{NIST\,612} = \frac{X_{Raw}}{CRI_{NIST\,612}}$$

Unscaled concentrations (X_{Raw}) for all other elements in the sample were subsequently converted to scaled (i.e., quantitative) element concentrations (X_{Scaled}) by dividing by the appropriate scaling factor:

$$X_{Scaled} = \frac{X_{Raw}}{SC_{NIST\,612}}$$

These data reduction protocols were applied to the raw data using each of the three internal standard elements (i.e., Si, Ca and Fe), which is similar to the method used in LA data reduction software (e.g., LAMTRACE, van Achterbergh et al., 2001). The resulting data are reported in parts per million (ppm) concentration units,

Oxide Scaling Method

Element concentrations were also calculated without an internal standard using an oxide scaling method. This consisted of converting the

unscaled element concentrations (X_{Raw}) into unscaled oxide concentrations by dividing by the proportion of the cation in the oxide formula (P_{Oxide}), scaling to 100 % (i.e., 1,000,000 ppm), and converting the scaled oxide concentrations back to scaled element concentrations (X_{Scaled}) using:

$$X_{Scaled} = \left\{ \left[\left(\sum \frac{X_{Raw}}{P_{Oxide}} \right) / 1000000 \right] * X_{Raw} \right\} * P_{Oxide}$$

The oxide formulas used in calculating the cation proportions are presented in Table 5-4.

An oxide scaling approach to quantification was previously used on silicate reference materials by Halicz & Günther (2004). The approach presented in this study differs from that used by Halicz & Günther (2004) in that a more extensive analyte list is used and all element abundances are simultaneously calculated by direct scaling of oxide concentrations, without using a desolvated standard solution for calibration.

Limit of Detection Calculation

Following calculation of the element concentrations, all results were filtered for the limit of detection (LOD_{Raw}) using the method presented in Longerich et al. (1996). The raw data (ICPS versus time) were used to calculate three times the standard deviation (σ) of the background signal using:

$$LOD_{Raw} = 3\left(\frac{\sigma}{\sqrt{n}} * \sqrt{2} \right)$$

The LOD_{Raw} were then adjusted by multiplying them by the scaling factors determined using either an internal standard or by oxide scaling to obtain scaled LODs (LOD_{Scaled}).

Results and Discussion

NIST 610

Concentration data for ten analyses of NIST 610 (treated as an unknown) calculated using Si, Ca and Fe as internal standards and by oxide scaling are presented in Table 5-5. The differences between the measured element concentrations and the certified, reference or information values (expressed as percentages) are included in the table. The method of standardization yielding the lowest percentage difference between the measured element concentration and the certified, reference or information value is indicated in bold italics. The results are presented graphically in Figure 5-1 as ratios of the measured concentrations relative to the NIST 610 certified, reference or information values.

The measured NIST 610 concentrations are generally different from the certified, reference or information values despite using NIST 610 as the external calibration standard (Table 5-5). Therefore, the differences between the measured and certified, reference or information values must result from changing analytical conditions (e.g., ICPMS tuning, laser output) during the analytical session because the calibration standard was 100 % matrix-matched to the unknowns (i.e., NIST 610) and all other variables were constant throughout the 5 experiments.

Table 5-4. List of oxide formulae and cation proportions

Oxide Formula	Cation Proportion	Oxide Formula	Cation Proportion	Oxide Formula	Cation Proportion
Li_2O	0.4646	As_2O_3	0.7574	Sm_2O_3	0.8624
BeO	0.3603	SeO	0.8315	Eu_2O_3	0.8636
B_2O_3	0.3106	Rb_2O	0.9144	Gd_2O_3	0.8676
Na_2O	0.7419	SrO	0.8456	Tb_2O_3	0.8688
MgO	0.6030	Y_2O_3	0.7874	Dy_2O_3	0.8713
Al_2O_3	0.5293	ZrO_2	0.7403	Ho_2O_3	0.8730
SiO_2	0.4674	Nb_2O_3	0.7947	Er_2O_3	0.8745
P_2O_5	0.4364	Mo_2O_3	0.7999	Tm_2O_3	0.8756
K_2O	0.8301	Rh_2O_3	0.8109	Yb_2O_3	0.8782
CaO	0.7147	PdO	0.8693	Lu_2O_3	0.8794
Sc_2O_3	0.6520	Ag_2O	0.9310	HfO_2	0.8480
TiO_2	0.5993	CdO	0.8754	Ta_2O_5	0.8190
V_2O_5	0.5602	In_2O_3	0.8271	WO_3	0.7930
Cr_2O_3	0.6842	SnO	0.8812	Re	1
MnO	0.7745	Sb_2O_3	0.8354	PtO	0.9242
FeO	0.7773	Cs_2O	0.9432	Au_2O	0.9610
CoO	0.7865	BaO	0.8957	Tl_2O_3	0.8949
NiO	0.7858	La_2O_3	0.8527	PbO	0.9283
CuO	0.7989	Ce_2O_3	0.8538	Bi_2O_3	0.8970
ZnO	0.8035	Pr_2O_3	0.8545	ThO_2	0.8788
GaO	0.8134	Nd_2O_3	0.8574	UO_2	0.8815
GeO_2	0.6942				

Table 5-5. Calculated concentrations – NIST 610

Element	*CRI*	Si Internal		Ca Internal		Fe Internal		Oxide Scaled	
		X_{Scaled}	%	X_{Scaled}	%	X_{Scaled}	%	X_{Scaled}	%
Li	484.6	491.1	1.34	496.9	2.54	488.4	***0.78***	492.6	1.65
Be	465.5	470.5	1.07	475.7	2.18	467.6	***0.44***	471.9	1.37
B	356.4	359.0	0.72	363.0	1.85	356.8	***0.10***	360.0	1.02
Na	99053	98567	0.49	99792	0.75	98057	1.01	98866	***0.19***
Mg	465.3	467.8	0.54	473.0	1.65	465.1	0.05	469.2	0.83
Al	10790	10830	0.38	10950	1.51	10770	0.20	10860	0.68
Si	327090	327090	0.00	330910	1.17	325280	0.55	328070	***0.30***
P	342.5	342.7	***0.06***	346.8	1.25	340.7	0.53	343.7	0.36
K	486	482	0.78	487	***0.13***	479	1.50	484	0.51
Ca	81830	81170	0.81	81830	0.00	80520	1.60	81380	***0.55***
Sc	441.1	441.9	***0.18***	446.1	1.12	438.7	0.55	443.1	0.46
Ti	434	434	***0.09***	438	0.87	430	0.83	435	0.18
V	441.7	435.2	1.47	439.3	***0.53***	432.1	2.18	436.4	1.19
Cr	405.2	400.9	1.07	404.8	***0.10***	397.8	1.82	402.0	0.79
Mn	433.3	434.2	***0.20***	439.0	1.21	431.0	0.52	435.4	0.48
Fe	457.1	461.0	***0.86***	465.3	1.79	457.1	0.00	462.3	1.13
Co	405	404	0.26	408	0.74	401	1.00	405	***0.02***
Ni	443.9	442.6	0.28	447.2	0.74	439.5	1.00	443.9	***0.00***
Cu	430.3	428.9	0.33	433.2	0.67	425.8	1.04	430.1	***0.05***
Zn	456.3	458.8	0.55	463.2	1.51	455.7	***0.13***	462.1	1.28
Ga	438.1	437.7	***0.09***	442.2	0.93	434.7	0.77	439.0	0.19
Ge	426.3	430.7	1.03	435.1	2.06	427.6	***0.31***	431.9	1.31
As	317.4	320.8	1.08	324.1	2.11	318.6	***0.38***	321.7	1.36
Se	109	110	0.87	111	1.83	109	***0.08***	110	1.14
Rb	431.1	421.2	2.30	425.4	***1.31***	418.3	2.96	422.4	2.03
Sr	497.4	497.9	***0.10***	503.2	1.17	494.5	0.58	499.3	0.39
Y	449.9	447.7	0.50	452.4	0.56	444.7	1.16	448.9	***0.21***
Zr	439.9	438.5	0.32	443.2	0.76	435.6	0.97	439.8	***0.03***
Nb	419.4	419.2	***0.06***	423.7	1.02	416.4	0.72	420.4	0.23
Mo	376.8	375.8	0.26	379.9	0.82	373.3	0.94	376.9	***0.03***
Rh	1.31	1.32	0.75	1.33	1.87	1.31	***0.07***	1.32	1.04
Pd	1.05	1.09	3.48	1.10	4.88	1.08	***2.90***	1.09	3.81
Ag	239.4	242.3	1.19	244.7	2.23	240.7	***0.53***	242.9	1.48
Cd	259.4	265.6	2.40	268.4	3.47	264.0	***1.78***	266.4	2.69
In	441.4	438.8	0.59	443.4	0.44	436.1	1.19	440.0	***0.31***
Sn	396.3	397.4	***0.28***	401.5	1.31	394.7	0.41	398.6	0.57

Table 5-5 (continued). Calculated concentrations – NIST 610

Element	*CRI*	Si Internal		Ca Internal		Fe Internal		Oxide Scaled	
		X_{Scaled}	%	X_{Scaled}	%	X_{Scaled}	%	X_{Scaled}	%
Sb	368.5	376.1	2.06	380.0	3.12	373.5	***1.36***	377.2	2.35
Cs	360.9	358.5	0.65	362.3	0.39	356.5	1.23	359.6	***0.37***
Ba	424.1	431.2	1.68	435.9	2.78	428.5	***1.05***	432.5	1.97
La	457.4	465.0	1.65	470.0	2.76	462.2	***1.04***	466.3	1.95
Ce	447.8	453.0	1.16	457.7	2.22	450.0	***0.50***	454.3	1.45
Pr	429.8	437.5	1.79	442.2	2.89	434.8	***1.17***	438.8	2.09
Nd	430.8	437.7	1.60	442.5	2.72	435.1	***0.99***	439.0	1.90
Sm	450.5	458.4	1.76	463.4	2.85	455.5	***1.11***	459.8	2.06
Eu	461.1	466.0	1.06	471.1	2.16	463.1	***0.43***	467.4	1.35
Gd	419.9	424.5	1.10	429.2	2.22	421.9	***0.48***	425.8	1.40
Tb	442.8	447.1	0.98	452.0	2.08	444.4	***0.35***	448.4	1.27
Dy	426.5	430.6	0.95	435.4	2.09	428.0	***0.34***	431.9	1.25
Ho	449.4	453.7	0.95	458.7	2.07	450.9	***0.32***	455.0	1.25
Er	426	430	0.86	434	1.99	427	***0.24***	431	1.16
Tm	420.1	423.4	0.79	428.1	1.91	420.8	***0.17***	424.7	1.08
Yb	461.5	463.8	0.50	469.0	1.62	461.0	***0.12***	465.2	0.80
Lu	434.7	438.4	0.86	443.4	2.00	435.8	***0.26***	439.7	1.15
Hf	417.7	423.0	1.28	427.8	2.42	420.6	***0.68***	424.3	1.58
Ta	376.6	382.4	1.55	386.8	2.71	380.2	***0.96***	383.6	1.85
W	445.3	447.0	0.39	452.1	1.52	444.2	***0.25***	448.4	0.69
Re	103.7	105.0	1.23	106.2	2.36	104.3	***0.57***	105.3	1.52
Pt	3.15	3.24	2.83	3.28	4.11	3.22	***2.30***	3.25	3.14
Au	22.5	23.0	2.28	23.3	3.44	22.9	***1.62***	23.1	2.58
Tl	61.2	62.8	2.55	63.4	3.56	62.3	***1.82***	62.9	2.83
Pb	413.3	418.4	1.22	422.8	2.30	415.7	***0.58***	419.6	1.51
Bi	357.7	367.7	2.80	371.6	3.90	365.5	***2.18***	368.8	3.10
Th	450.6	461.0	2.30	466.0	3.42	458.1	***1.67***	462.3	2.60
U	457.1	455.2	0.41	460.1	0.65	452.3	1.05	456.5	***0.12***

Figure 5-1. NIST 610 – Measured versus CRI values. The upper portion of the figure presents the data at a scale consistent with subsequent figures. The scale of the ordinate axis for the lower portion of the figure has been expanded to better illustrate the differences between the measured and CRI values.

NIST 610
Measured/CRI value
0.1
1
10
100
Si Internal
Ca Internal
Fe Internal
Scaled
Measured/CRI value
0.95
1
1.05
Element
Li Be Be Na Mg Al Si P K Ca Sc Te V Cr Mn Fe Co Ni Cu Zn Ga Ge As Se Rb Sr Y Zr Nb Mo Rh Pd Ag Cd In Sn Sb Cs Ba La Ce Pr Nd Sm Eu Gd Tb Dy Ho Er Tm Yb Lu Hf Ta W Re Pt Au Tl Pb Bi Th U

No one method of standardization produced the most accurate results for all elements. Despite differences in estimated concentrations resulting from the various standardization methods used, these differences are approximately constant, yielding approximately parallel lines when the data are plotted relative to the certified, reference or information values (Figure 5-1). This indicates that none of the standardization methods (including scaling) resulted in different degrees of apparent inter-element fractionation, and the differences in concentration between the various standardization methods approximately equal a common factor for all elements (Table 5-6). With respect to NIST 610, the average difference between scaling and using Si as an internal standard was 0 %, whereas use of Ca and Fe as internal standards resulted in average differences relative to scaling of 1 % and -1 %, respectively. The relatively constant average difference between the standardization techniques indicates that correction factors potentially could be applied to normalize data obtained using one internal standard to those obtained using another. Notwithstanding the similarity in the shapes of the data plots, results obtained using various internal standards or by scaling can differ by greater than ± 1σ, indicating that a statistically significant difference occurs among the results at this screening level.

Deviation from the NIST 610 certified, reference or information values (i.e., analytical accuracy) of less than approximately ± 5 % for all elements was observed for all 64 elements included in the analyses. Furthermore, the majority of elements (57 of 64) had analytical accuracies of less than approximately ± 3 %. Six of the seven elements (Pd, Cd, Pt, Au, Tl and Bi) that had analytical accuracies greater than ± 3 % are either present in NIST 610 at low concentrations (< 5 ppm) or have high (> 2) fractionation factors according to the relative fractionation index of Fryer et al. (1995). The remaining element (Th) has neither a low concentration nor high fractionation index, and its behavior relative to the other elements with relatively high analytical accuracies is anomalous.

Table 5-6. Average Difference between Internal Standard and Scaled Methods

SRM	Si vs. Scaled	Ca vs. Scaled	Fe vs. Scaled
NIST 610	***0 %***	1 %	- 1%
NIST 612	***-1 %***	8 %	- -
NIST 614	***-1 %***	15 %	- -
BCR-2G	-3 %	12 %	***0 %***
BHVO-2	***0 %***	6 %	-3 %
BIR-1	-6 %	35 %	***-1 %***

One method of standardization did not produce the most accurate results for all elements analyzed. Using Fe as an internal standard resulted in the most accurate results for the greatest number (39) of elements (Li, Be, B, Mg, Al, Zn, Ge, As, Se, Rh, Pd, Ag, Cd, Sb, Ba, La, Ce, Pr, Nd, Sm, Eu, Gd, Tb, Dy, Ho, Er, Tm, Yb, Lu, Hf, Ta, W, Re, Pt, Au, Tl, Pb, Bi and Th). Scaling the oxide concentrations resulted in the most accurate results for 12 elements (Na, Si, Ca, Co, Ni, Cu, Y, Zr, Mo, In, Cs and U). Using Si as an internal standard resulted in the most accurate results for 9 elements (P, Sc, Ti, Mn, Fe, Ga, Sr, Nb and Sn). Using Ca as an internal standard resulted in the most accurate results for only 4 elements (K, V, Cr and Rb). Calculation of element concentrations using oxide scaling provided equal or better accuracy for most elements than using Si or Ca as an internal standard. It is notable, at least in the case of NIST 610, that using a low abundance isotope (^{57}Fe, 2.119 %) of a trace element (457.1 ppm) yields the most accurate results for the majority of elements.

Other Standard Reference Materials

Concentration data for NIST 612, NIST 614, BCR-2G, BHVO-2 and BIR-1 are presented in Tables 5-7 to 5-11, respectively. Concentrations for NIST 612 and 614 were calculated using Si and Ca as internal standards, and by oxide scaling, only because Fe was not detected at concentrations in excess of the LODs for these reference materials. Concentrations for BCR-

2G, BHVO-2 and BIR-1 were calculated using Si, Ca and Fe as internal standards and by oxide scaling. The method of standardization yielding the lowest percentage difference between the measured element concentration and the certified, reference or information value is indicated in bold italics. The results are presented graphically in Figures 5-2 to 5-6 as ratios of the measured values relative to the certified, reference or information values for these reference materials.

As with NIST 610, measured concentrations for the five standard reference materials (NIST 612, NIST 614, BCR-2G, BHVO and BIR-1) are generally different from the certified, reference or information values (Tables 5-7 through 5-11) and one method of standardization did not produce the most accurate results for all elements analyzed. The likely causes of the observed differences between the measured and certified, reference or information values are differences in the composition of the external calibration standard (NIST 610) relative to the five reference materials (i.e., matrix effects) and changing analytical conditions during the analytical session.

Relative concentration differences estimated from the various standardization methods are approximately constant for most elements (Figures 5-2 through 5-6, Table 5-6). For NIST 612, the average difference between scaling and using Si and Ca as internal standards was -1 % and 8%, respectively. For NIST 614, the average difference between scaling and using Si and Ca as internal standards was -1 % and 15%, respectively. For BCR-2G, the average difference between scaling and using Si, Ca and Fe as internal standards was -3 %, 12 % and 0 %, respectively. For BHVO-2, the average difference between scaling and using Si, Ca and Fe as internal standards was 0 %, 6 % and -3 %, respectively. For BIR-1, the average difference between scaling and using Si, Ca and Fe as internal standards was -6 %, 35 % and -1 %, respectively. Using Si or Fe as an internal standard consistently resulted in a zero or a negative average difference in measured versus certified, reference or information values relative to scaling.

Table 5-7. Calculated concentrations – NIST 612

Element	CRI	Si Internal		Ca Internal		Oxide Scaled	
		X_{Scaled}	%	X_{Scaled}	%	X_{Scaled}	%
Li	41.54	41.94	***0.96***	46.30	11.46	42.62	2.61
Be	37.73	38.06	***0.86***	41.97	11.24	38.68	2.51
B	34.73	54.64	***57.32***	60.61	74.51	55.57	60.02
Na	103700	98900	4.62	109400	5.48	100500	***3.05***
Mg	77.44	60.46	21.93	65.67	***15.19***	60.75	21.55
Al	11200	10800	3.81	11900	6.04	10900	***2.23***
Si	336100	336100	0.00	371200	10.46	341600	***1.65***
P	55.16	35.81	35.07	39.55	***28.29***	36.41	34.00
K	66.26	< DL	- -	< DL	- -	< DL	- -
Ca	85260	77470	9.13	85260	0.00	78730	***7.66***
Sc	41.05	35.11	14.46	38.66	***5.83***	35.68	13.07
Ti	48.11	37.22	22.63	41.08	***14.61***	37.84	21.35
V	39.22	35.56	9.33	39.28	***0.15***	36.15	7.84
Cr	39.88	37.29	6.48	41.36	***3.72***	34.53	13.42
Mn	38.43	35.53	7.56	39.22	***2.06***	36.11	6.03
Fe	56.33	< DL	- -	< DL	- -	< DL	- -
Co	35.26	33.66	4.53	37.20	5.52	34.22	***2.96***
Ni	38.44	38.14	***0.77***	42.16	9.69	38.77	0.87
Cu	36.71	36.79	***0.20***	40.68	10.80	37.39	1.86
Zn	37.92	36.49	***3.77***	40.27	6.20	40.62	7.13
Ga	36.24	35.44	2.20	39.16	8.07	36.03	***0.58***
Ge	34.64	36.71	***5.97***	40.54	17.04	37.31	7.71
As	37.33	26.94	27.84	29.73	***20.36***	27.38	26.66
Se	- -	15.22	- -	16.84	- -	15.47	- -
Rb	31.63	29.24	7.56	32.31	***2.15***	29.72	6.03
Sr	76.15	70.93	6.86	78.28	***2.80***	72.09	5.33
Y	38.25	33.00	13.73	36.38	***4.88***	33.54	12.32
Zr	35.99	34.06	5.35	37.57	4.39	34.62	***3.79***
Nb	38.06	33.09	13.05	36.54	***3.99***	33.64	11.62
Mo	38.3	32.02	16.39	35.38	***7.63***	32.55	15.02
Rh	0.896	0.910	***1.58***	1.005	12.13	0.925	3.25
Pd	1.09	1.10	***0.47***	1.21	11.12	1.11	2.10
Ag	21.92	18.60	15.17	20.54	***6.28***	18.90	13.77
Cd	28.32	24.36	13.97	26.89	***5.03***	24.76	12.56
In	42.93	33.42	22.15	36.92	***13.99***	33.97	20.87
Sn	37.96	35.03	7.72	38.70	***1.95***	35.60	6.21
Sb	38.44	29.79	22.50	32.91	***14.38***	30.28	21.22
Cs	41.64	36.68	11.90	40.54	***2.65***	37.29	10.45

Footnote:

- - Calculation not possible due to lack of CRI value or measured concentration less than DL

Table 5-7 (continued). Calculated concentrations – NIST 612

Element	CRI	Si Internal		Ca Internal		Oxide Scaled	
		X_{Scaled}	%	X_{Scaled}	%	X_{Scaled}	%
Ba	37.74	34.58	8.37	38.17	***1.14***	35.15	6.87
La	35.77	34.51	3.52	38.07	6.43	35.08	***1.94***
Ce	38.35	35.66	7.02	39.38	***2.67***	36.24	5.49
Pr	37.16	33.92	8.72	37.44	***0.75***	34.48	7.22
Nd	35.24	32.91	6.63	36.33	***3.09***	33.45	5.09
Sm	36.72	34.42	6.26	37.97	***3.40***	34.98	4.73
Eu	34.44	33.94	1.45	37.44	8.72	34.50	***0.17***
Gd	36.95	31.66	14.31	34.91	***5.51***	32.18	12.91
Tb	35.92	33.06	7.97	36.46	***1.49***	33.60	6.46
Dy	35.97	31.14	13.42	34.33	***4.55***	31.65	12.00
Ho	37.87	33.28	12.11	36.70	***3.10***	33.83	10.67
Er	37.43	31.73	15.24	34.97	***6.57***	32.25	13.85
Tm	37.55	31.17	16.98	34.38	***8.45***	31.69	15.62
Yb	39.95	34.93	12.57	38.52	***3.57***	35.50	11.14
Lu	37.71	31.83	15.59	35.10	***6.92***	32.35	14.21
Hf	34.77	31.73	8.76	34.99	***0.62***	32.25	7.26
Ta	39.77	28.87	27.42	31.84	***19.95***	29.34	26.23
W	39.55	37.26	5.79	41.15	***4.05***	37.87	4.25
Re	8.12	13.63	***67.80***	15.04	85.25	13.85	70.54
Pt	2.59	2.47	4.66	2.73	5.44	2.51	***3.08***
Au	5.09	4.39	13.74	4.85	***4.75***	4.46	12.33
Tl	15.07	14.39	4.51	15.88	5.38	14.63	***2.94***
Pb	38.96	34.25	12.08	37.86	***2.82***	34.82	10.62
Bi	29.84	29.19	2.16	32.25	8.09	29.68	***0.55***
Th	37.23	33.60	9.74	37.07	***0.43***	34.15	8.26
U	37.15	33.35	10.22	36.89	***0.71***	33.91	8.73

Figure 5-2. NIST 612 – Measured versus CRI values.

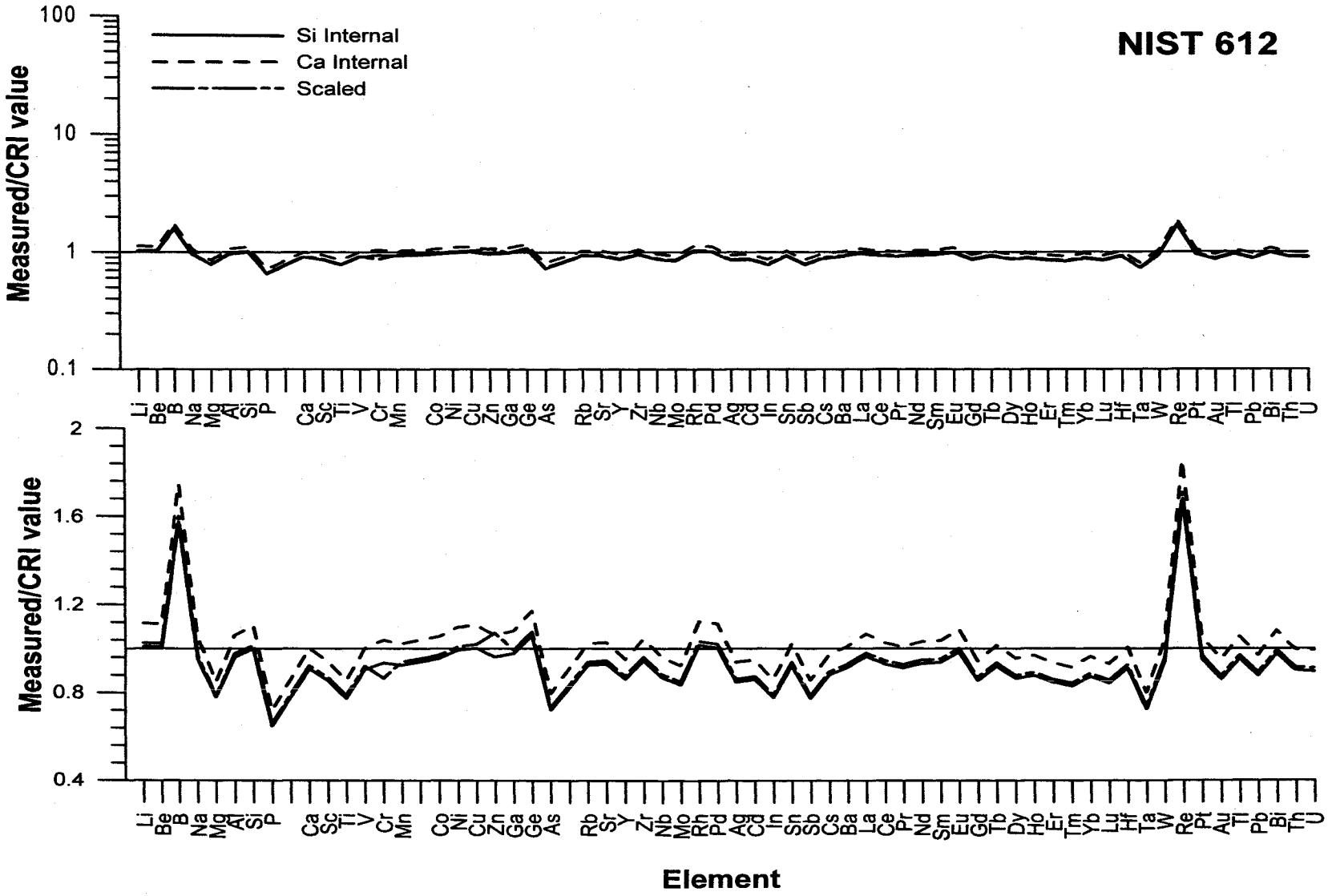
NIST 612
Si Internal
Ca Internal
Scaled
Measured/CRI value
100
10
1
0.1
2
1.6
1.2
0.8
0.4
Element

Using Ca as an internal standard consistently resulted in positive average differences in measured versus certified, reference or information values relative to scaling. In general, scaling produced similar or equal results to using either Si or Fe as an internal standard, whereas using Ca produced consistently higher values than scaling.

Analytical accuracies were less than approximately ± 25 % for the majority of elements included in the analyses of NIST 612. Five elements (B, P, As, Ta and Re) had analytical accuracies greater than ± 25 %, despite having relative high (> 5 ppm) concentrations. Four of the elements (P, As, Ta and Re) have moderate (1.5 to 2) or high (> 2) fractionation factors, whereas B does not have a fractionation factor (Fryer et al., 1995). It is implied from the relatively high analytical error that B would likely have a relatively high fractionation factor. Using Ca as an internal standard resulted in the most accurate results for the greatest number (39) of elements (Mg, P, Sc, Ti, V, Cr, Mn, As, Rb, Sr, Y, Nb, Mo, Ag, Cd, In, Sn, Sb, Cs, Ba, Ce, Pr, Nd, Sm, Gd, Tb, Dy, Ho, Er, Tm, Yb, Lu, Hf, Ta, W, Au, Pb, Th and U). Scaling the oxide concentrations resulted in the most accurate results for 12 elements (Na, Al, Si, Ca, Co, Ga, Zr, La, Eu, Pt, Tl and Bi). Using Si as an internal standard resulted in the most accurate results for 10 elements (Li, Be, B, Ni, Cu, Zn, Ge, Rh, Pd and Re). Calculation of element concentrations using oxide scaling provided better accuracy for more elements than using Si as an internal standard, and the results were, on average, within approximately 6 % of the results obtained using Ca as an internal standard.

Table 5-8. Calculated concentrations – NIST 614

Element	CRI	Si Internal		Ca Internal		Oxide Scaled	
		X_{Scaled}	%	X_{Scaled}	%	X_{Scaled}	%
Li	--	1.82	--	2.09	--	1.85	--
Be	--	< DL	--	< DL	--	< DL	--
B	1.3	19.8	***1420***	22.8	1660	20.1	1450
Na	103860	103550	***0.30***	118740	14.33	105110	1.21
Mg	--	34.60	--	36.28	--	35.11	--
Al	10585	10476	1.03	12014	13.50	10637	***0.49***
Si	336550	336550	0.00	385930	14.67	341740	***1.54***
P	30	11	62.46	13	***56.88***	11	61.87
K	--	< DL	--	< DL	--	< DL	--
Ca	85760	75130	12.40	85760	0.00	76250	***11.09***
Sc	0.59	< DL	--	< DL	--	< DL	--
Ti	3.1	< DL	--	7.5	***140.54***	< DL	--
V	--	1.0	--	1.1	--	1.0	--
Cr	--	38.4	--	42.9	--	< DL	--
Mn	--	1.3	--	1.5	--	1.3	--
Fe	13.3	< DL	--	< DL	--	< DL	--
Co	0.73	< DL	--	0.85	***17.12***	< DL	--
Ni	0.95	< DL	--	< DL	--	< DL	--
Cu	1.37	< DL	--	< DL	--	< DL	--
Zn	--	3.32	--	3.78	--	6.80	--
Ga	--	1.19	--	1.37	--	1.21	--
Ge	--	1.12	--	1.19	--	1.12	--
As	--	< DL	--	< DL	--	< DL	--
Se	--	0.48	--	0.56	--	0.61	--
Rb	0.855	< DL	--	1.14	***33.48***	< DL	--
Sr	45.8	40.66	11.23	46.57	***1.69***	41.27	9.88
Y	--	0.63	--	0.72	--	0.64	--
Zr	--	0.85	--	0.97	--	0.86	--
Nb	--	0.69	--	0.78	--	0.70	--
Mo	--	0.76	--	0.84	--	0.77	--
Rh	1.67	1.63	2.21	1.87	12.06	1.66	***0.71***
Pd	1.98	2.25	***13.76***	2.58	30.23	2.29	15.50
Ag	0.42	0.43	***2.65***	0.49	17.65	0.44	4.22
Cd	0.55	0.86	56.95	1.03	87.14	0.88	***59.75***
In	--	0.70	--	0.80	--	0.71	--
Sn	--	2.82	--	3.23	--	2.86	--
Sb	1.06	0.70	34.01	0.80	***24.44***	0.71	33.00
Cs	--	0.61	--	0.70	--	0.62	--

Table 5-8 (continued). Calculated concentrations – NIST 614

Element	*CRI*	Si Internal		Ca Internal		Oxide Scaled	
		X_{Scaled}	%	X_{Scaled}	%	X_{Scaled}	%
Ba	--	2.91	--	3.34	--	2.96	--
La	0.83	0.66	19.91	0.76	***8.10***	0.67	18.68
Ce	--	0.73	--	0.83	--	0.74	--
Pr	--	0.68	--	0.78	--	0.69	--
Nd	--	0.73	--	0.83	--	0.74	--
Sm	--	0.72	--	0.82	--	0.73	--
Eu	0.99	0.72	26.83	0.83	***16.25***	0.74	25.72
Gd	--	0.74	--	0.81	--	0.75	--
Tb	--	0.63	--	0.72	--	0.64	--
Dy	--	0.63	--	0.72	--	0.64	--
Ho	--	0.65	--	0.74	--	0.66	--
Er	--	0.58	--	0.66	--	0.59	--
Tm	--	0.58	--	0.66	--	0.59	--
Yb	--	0.66	--	0.75	--	0.67	--
Lu	--	0.59	--	0.68	--	0.60	--
Hf	--	0.61	--	0.69	--	0.62	--
Ta	--	0.57	--	0.66	--	0.58	--
W	--	0.78	--	0.89	--	0.79	--
Re	0.179	0.37	***104.19***	0.42	133.54	0.37	107.29
Pt	2.26	2.40	***6.22***	2.75	21.66	2.44	7.84
Au	0.5	0.50	0.85	0.57	13.14	0.50	***0.62***
Tl	0.269	0.27	***2.17***	0.32	17.11	0.28	3.72
Pb	2.32	2.56	***10.53***	2.94	26.61	2.60	12.18
Bi	--	0.60	--	0.68	--	0.61	--
Th	0.748	0.66	11.63	0.76	***1.43***	0.67	10.27
U	0.823	0.78	5.46	0.89	8.30	0.79	***4.04***

Figure 5-3. NIST 614 – Measured versus CRI values.

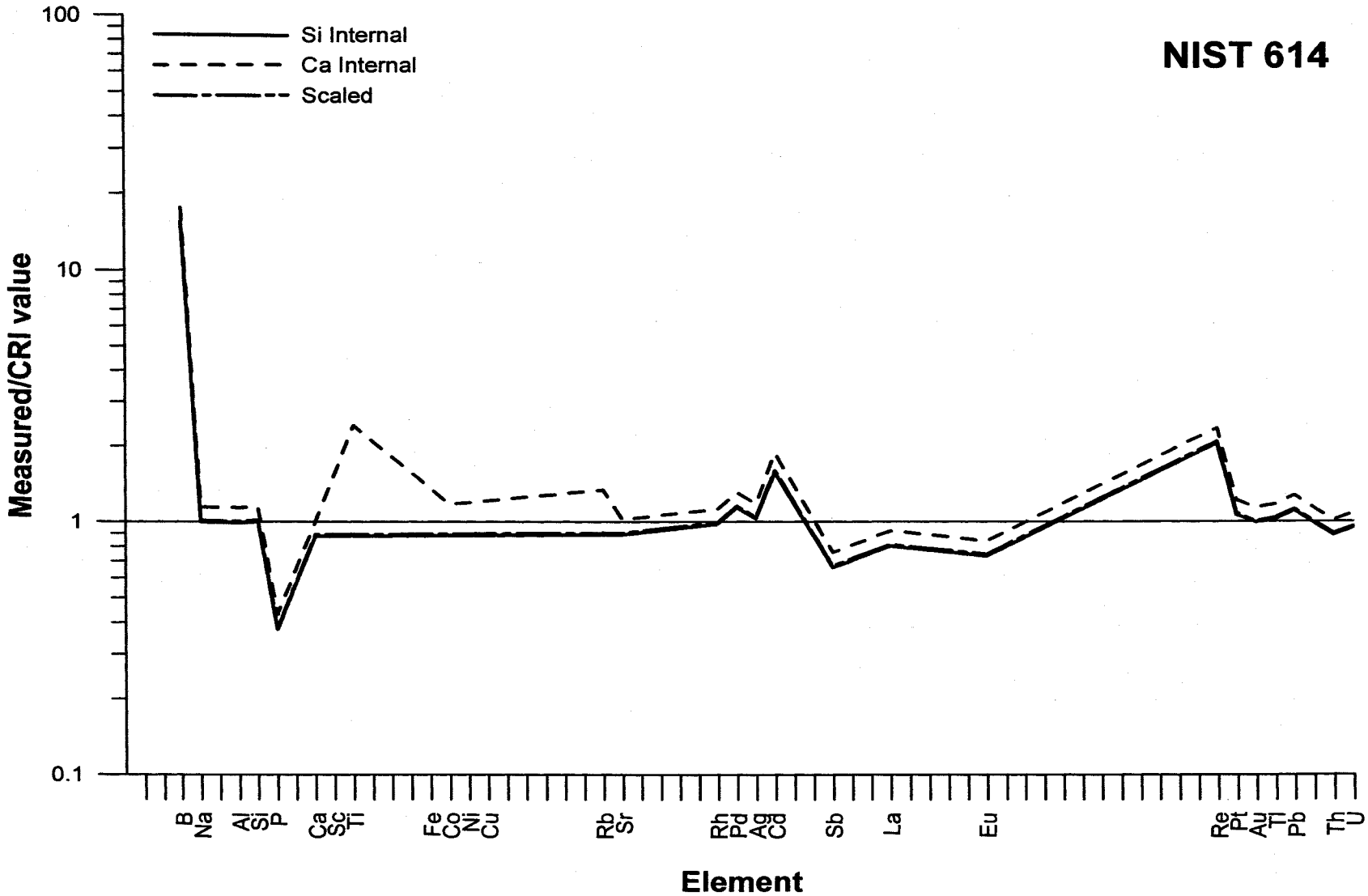
Si Internal
Ca Internal
Scaled
NIST 614
100
10
1
0.1
Measured/CRI value
B
Na
Al
Si
P
Ca
Sc
Ti
Fe
Co
Ni
Cu
Rb
Sr
Rh
Pd
Ag
Cd
Sb
La
Eu
Re
Pt
Au
Tl
Pb
Th
U
Element

Table 5-9. Calculated concentrations – BCR-2G

Element	*CRI*	Si Internal		Ca Internal		Fe Internal		Oxide Scaled	
		X_{Scaled}	%	X_{Scaled}	%	X_{Scaled}	%	X_{Scaled}	%
Li	--	9.4	--	11.8	--	9.8	--	9.8	--
Be	--	2.3	--	2.7	--	2.4	--	2.4	--
B	--	15.4	--	19.1	--	15.9	--	16.0	--
Na	23400	17845	23.74	22268	***4.84***	18500	20.94	18596	20.53
Mg	21600	19684	8.87	24504	13.44	20400	5.56	20511	***5.04***
Al	71400	73192	***2.51***	91034	27.50	75803	6.17	76239	6.78
Si	253000	253000	0.00	315458	24.69	262519	***3.76***	263784	4.26
P	1500	1186	20.91	1482	***1.22***	1233	17.80	1238	17.48
K	14900	15665	***5.13***	19524	31.04	16272	9.21	16342	9.67
Ca	50900	40994	19.46	50900	0.00	42455	16.59	42700	***16.11***
Sc	33	28.1	14.75	33.0	***5.97***	29.1	11.68	29.3	11.18
Ti	13500	11765	12.85	14633	***8.39***	12190	9.71	12258	9.20
V	416	354.7	14.74	441.1	***6.02***	367.4	11.68	369.5	11.18
Cr	18	13.5	24.88	16.5	***8.36***	13.7	23.69	13.8	23.16
Mn	1520	1439.2	5.32	1791.0	17.83	1491.1	1.90	1499.7	***1.34***
Fe	96600	93240	3.48	116038	20.12	96600	0.00	97152	***0.57***
Co	37	34	7.82	42	14.80	35	4.42	36	***3.92***
Ni	--	< DL	--	< DL	--	< DL	--	< DL	--
Cu	19	< DL	--	< DL	--	< DL	--	< DL	--
Zn	127	143.2	***12.76***	178.8	40.79	148.8	17.16	156.7	23.40
Ga	23	30.0	***30.45***	37.4	62.46	31.1	35.24	31.3	35.96
Ge	--	2.9	--	3.5	--	3.0	--	3.0	--
As	--	< DL	--	2.4	--	< DL	--	< DL	--
Se	--	< DL	--	< DL	--	< DL	--	< DL	--
Rb	48	40.4	15.79	50.3	***4.82***	41.9	12.73	42.1	12.25
Sr	346	281.5	18.64	350.0	***1.16***	291.4	15.77	293.2	15.26
Y	37	26.6	28.13	33.0	***10.71***	27.5	25.64	27.7	25.17
Zr	188	149.7	20.35	186.1	***1.03***	155.0	17.57	155.9	17.06
Nb	--	10.1	--	12.6	--	10.5	--	10.5	--
Mo	248	211.8	14.58	264.0	***6.44***	219.7	11.42	220.8	10.96
Rh	--	< DL	--	< DL	--	< DL	--	< DL	--
Pd	--	< DL	--	< DL	--	< DL	--	< DL	--
Ag	--	0.66	--	0.70	--	0.59	--	0.59	--
Cd	--	< DL	--	< DL	--	< DL	--	< DL	--
In	--	0.13	--	0.16	--	0.14	--	0.14	--
Sn	--	2.57	--	2.99	--	2.55	--	2.57	--
Sb	--	0.31	--	0.37	--	0.32	--	0.32	--
Cs	1.1	0.91	16.89	1.30	17.76	1.08	1.62	1.08	***1.49***

Table 5-9 (continued). Calculated concentrations – BCR-2G

Element	*CRI*	Si Internal		Ca Internal		Fe Internal		Oxide Scaled	
		X_{Scaled}	%	X_{Scaled}	%	X_{Scaled}	%	X_{Scaled}	%
Ba	693	558.3	19.44	694.2	***0.17***	578.1	16.58	591.7	14.61
La	25.4	22.0	13.44	27.4	***7.67***	22.8	10.36	22.9	9.84
Ce	53	43.0	18.92	53.5	***0.85***	44.5	16.02	44.8	15.54
Pr	6.5	5.4	16.96	6.7	***3.30***	5.6	14.01	5.6	13.50
Nd	29	24.1	16.91	30.0	***3.29***	25.0	13.97	25.1	13.46
Sm	6.6	5.7	14.23	7.1	***6.83***	5.9	11.13	5.9	10.62
Eu	2	1.9	5.83	2.3	16.76	1.9	3.05	2.0	***2.06***
Gd	7	5.2	26.29	6.4	***8.42***	5.3	23.73	5.4	23.25
Tb	1.1	1.0	7.40	1.3	15.42	1.1	4.05	1.1	***3.38***
Dy	6.4	5.1	20.33	6.3	***1.04***	5.3	17.55	5.3	17.03
Ho	1.25	1.2	5.08	1.58	18.50	1.23	1.62	1.24	***0.96***
Er	3.6	2.8	23.18	3.4	***4.46***	2.9	20.44	2.9	19.96
Tm	0.57	0.42	25.84	0.72	25.85	0.44	23.37	0.44	***22.67***
Yb	3.4	2.9	15.96	3.6	***4.75***	3.0	12.90	3.0	12.41
Lu	0.51	0.45	12.41	0.73	43.80	0.46	9.51	0.47	***8.71***
Hf	4.8	3.9	18.47	4.9	***1.30***	4.1	15.57	4.1	15.07
Ta	--	0.63	--	0.88	--	0.76	--	0.76	--
W	--	0.72	--	0.92	--	0.75	--	0.76	--
Re	--	< DL	--	< DL	--	< DL	--	< DL	--
Pt	--	0.31	--	0.38	--	0.32	--	0.32	--
Au	--	< DL	--	0.03	--	< DL	--	< DL	--
Tl	--	0.25	--	0.31	--	0.26	--	0.26	--
Pb	11	9.4	14.28	11.8	***7.13***	9.8	10.96	9.8	10.58
Bi	--	0.10	--	0.11	--	0.10	--	0.10	--
Th	6.2	5.0	19.21	6.2	***0.61***	5.2	16.29	5.2	15.81
U	1.79	1.54	9.14	1.91	13.10	1.59	6.21	1.60	***5.40***

Figure 5-4. BCR-2G – Measured versus CRI values.

Measured/CRI value
0.1
1
10
100
Si Internal
Ca Internal
Fe Internal
Scaled
BCR-2G
Measured/CRI value
0.6
0.8
1
1.2
1.4
1.6
1.8
Na
Mg
Al
Si
P
K
Ca
Sc
Ti
V
Cr
Mn
Fe
Co
Cu
Zn
Ga
Rb
Sr
Y
Zr
Mo
Cs
Ba
La
Ce
Pr
Nd
Sm
Eu
Gd
Tb
Dy
Ho
Er
Tm
Yb
Lu
Hf
Pb
Th
U
Element

Analytical accuracies were less than approximately ± 30 % for the majority of elements included in the analyses of NIST 614. Seven elements (B, P, Ti, Rb, Cd, Sb and Re) had analytical accuracies greater than ± 30 %. Six of the elements (B, Ti, Rb, Cd, Sb and Re) are present in NIST 614 at relatively low concentrations (< 5 ppm) and four of the elements (P, Cd, Sb and Re) have moderate (1.5 to 2) to high (> 2) fractionation factors. Using Ca as an internal standard resulted in the most accurate results for the greatest number (9) of elements (P, Ti, Co, Rb, Sr, Sb, La, Eu and Th). Using Si as an internal standard resulted in the most accurate results for 8 elements (B, Na, Pd, Ag, Re, Pt, Tl and Pb). Scaling the oxide concentrations resulted in the most accurate results for 7 elements (Al, Si, Ca, Rh, Cd, Au and U). Calculation of element concentrations using oxide scaling provided comparable accuracy to using Si as an internal standard, and the results were, on average, within approximately 15 % of the results obtained using Ca as an internal standard.

Analytical accuracies were less than approximately ± 30 % for the majority of elements included in the analyses of BCR-2G. Two elements (Ga and Lu) had analytical accuracies greater than ± 30 %. Ga has a moderate fractionation factor and Lu is present in BCR-2G at a relatively low concentration. Using Ca as an internal standard resulted in the most accurate results for the greatest number (24) of elements (Na, P, Sc, Ti, V, Cr, Rb, Sr, Y, Zr, Mo, Ba, La, Ce, Pr, Nd, Sm, Gd, Dy, Er, Yb, Hf, Pb and Bi). Scaling the oxide concentrations resulted in the most accurate results for 12 elements (Mg, Ca, Mn, Fe, Co, Cs, Eu, Tb, Ho, Tm, Lu and U). Using Si and Fe as internal standards resulted in the most accurate results for 4 elements (Al, K, Zn and Ga) and 1 element (Si), respectively. Calculation of element concentrations using oxide scaling provided better accuracy than using Si and Fe as internal standards, and the results were, on average, within approximately 12 % of the results obtained using Ca as an internal standard.

Table 5-10. Calculated concentrations – BHVO-2

Element	CRI	Si Internal		Ca Internal		Fe Internal		Oxide Scaled	
		X_{Scaled}	%	X_{Scaled}	%	X_{Scaled}	%	X_{Scaled}	%
Li	5	4.2	16.47	4.6	***8.06***	4.0	20.17	4.2	16.16
Be	--	< DL	--	1.6	--	< DL	--	< DL	--
B	--	14.0	--	15.4	--	13.4	--	14.1	--
Na	16400	12147	25.93	13446	***18.01***	11622	29.13	12211	25.54
Mg	43600	49117	12.65	54238	24.40	46937	***7.65***	49339	13.16
Al	71600	75694	5.72	83525	16.66	72426	***1.15***	76038	6.20
Si	233000	233000	0.00	257754	10.62	223082	4.26	234282	***0.55***
P	1200	852.7	28.94	946.7	***21.10***	817.2	31.90	858.6	28.45
K	4300	4515	5.00	4997	16.20	4325	***0.58***	4542	5.62
Ca	81700	74093	9.31	81700	0.00	70916	13.20	74434	***8.89***
Sc	32	27.8	13.15	30.6	***4.23***	26.6	16.86	27.9	12.76
Ti	16300	14510	10.98	16022	***1.71***	13883	14.83	14579	10.56
V	317	268.3	15.36	296.8	***6.39***	256.5	19.07	269.7	14.93
Cr	280	250.8	10.44	277.3	***0.96***	239.9	14.34	257.0	8.23
Mn	1290	1369.8	6.18	1513.8	17.35	1308.5	***1.43***	1376.3	6.69
Fe	86300	90349	***4.69***	99920	15.78	86300	0.00	90794	5.21
Co	45	41.4	8.10	45.7	***1.62***	39.6	12.09	41.6	7.62
Ni	119	108.5	8.87	120.1	***0.91***	103.8	12.75	109.1	8.34
Cu	127	106.0	16.51	117.4	***7.53***	101.7	19.90	106.7	15.98
Zn	103	95.3	7.44	105.5	***2.42***	91.5	11.12	96.6	6.18
Ga	21.7	19.9	8.35	22.0	***1.36***	19.1	12.13	20.0	7.82
Ge	--	2.2	--	2.4	--	2.2	--	2.2	--
As	--	< DL	--	< DL	--	< DL	--	< DL	--
Se	--	< DL	--	< DL	--	< DL	--	< DL	--
Rb	9.8	7.8	20.90	8.6	***12.60***	7.4	24.28	7.8	20.49
Sr	389	347.6	10.65	383.3	***1.48***	332.2	14.60	349.0	10.28
Y	26	19.5	25.20	21.4	***17.64***	18.6	28.47	19.5	24.91
Zr	172	137.1	20.32	151.0	***12.20***	131.1	23.78	137.6	19.99
Nb	18	14.4	20.16	15.9	***11.94***	13.8	23.63	14.4	19.81
Mo	--	3.2	--	3.6	--	3.1	--	3.2	--
Rh	--	< DL	--	< DL	--	< DL	--	< DL	--
Pd	--	< DL	--	< DL	--	< DL	--	< DL	--
Ag	--	0.36	--	0.38	--	0.34	--	0.36	--
Cd	--	< DL	--	< DL	--	< DL	--	< DL	--
In	--	0.08	--	0.08	--	0.08	--	0.08	--
Sn	1.9	1.9	2.01	2.0	7.01	1.8	6.12	1.9	***1.80***
Sb	--	0.10	--	0.11	--	0.11	--	0.11	--
Cs	--	< DL	--	< DL	--	< DL	--	< DL	--

Table 5-10 (continued). Calculated concentrations – BHVO-2

Element	*CRI*	Si Internal		Ca Internal		Fe Internal		Oxide Scaled	
		X_{Scaled}	%	X_{Scaled}	%	X_{Scaled}	%	X_{Scaled}	%
Ba	130	117.4	9.73	129.4	***0.49***	112.2	13.72	117.8	9.36
La	15.5	13.5	12.82	14.9	***4.05***	12.9	16.65	13.6	12.50
Ce	37.4	32.5	13.18	35.8	***4.28***	31.0	17.02	32.6	12.82
Pr	5	4.3	13.80	4.7	***5.17***	4.1	17.58	4.3	13.49
Nd	25	21.2	15.13	23.4	***6.53***	20.3	18.86	21.3	14.79
Sm	6.1	5.2	14.60	5.7	***6.07***	5.0	18.34	5.2	14.29
Eu	2.1	1.9	9.81	2.1	***1.84***	1.8	13.72	1.9	9.71
Gd	6.5	4.7	28.03	5.1	***20.91***	4.5	31.18	4.7	27.79
Tb	0.96	0.73	24.04	0.79	***17.47***	0.70	27.29	0.73	23.98
Dy	5.2	4.0	22.33	4.4	***14.67***	3.9	25.73	4.1	22.08
Ho	0.93	0.80	13.94	0.86	***7.01***	0.77	17.08	0.80	13.92
Er	2.5	1.9	24.53	2.1	***17.88***	1.8	27.71	1.9	24.43
Tm	0.36	0.26	27.40	0.28	***23.18***	0.25	30.02	0.26	27.15
Yb	2	1.6	18.18	1.8	***10.94***	1.6	21.68	1.6	18.09
Lu	0.28	0.22	20.41	0.24	***13.49***	0.21	23.28	0.22	20.11
Hf	4.1	3.4	17.17	3.7	***9.12***	3.3	20.74	3.4	16.91
Ta	1.4	0.79	43.72	0.86	***38.74***	0.76	46.06	0.79	43.64
W	--	0.21	--	0.23	--	0.21	--	0.21	--
Re	--	< DL	--	< DL	--	< DL	--	< DL	--
Pt	--	0.10	--	0.11	--	0.10	--	0.10	--
Au	--	0.27	--	0.29	--	0.26	--	0.27	--
Tl	--	0.03	--	0.03	--	0.03	--	0.03	--
Pb	--	1.43	--	1.56	--	1.38	--	1.44	--
Bi	--	0.02	--	0.02	--	0.02	--	0.02	--
Th	1.2	1.02	14.98	1.11	***7.47***	0.98	18.54	1.02	14.87
U	--	0.35	--	0.38	--	0.33	--	0.35	--

Figure 5-5. BHVO-2 – Measured versus CRI values.

Measured/CRI value
0.1
1
10
100
Si Internal
Ca Internal
Fe Internal
Scaled
BHVO-2
Measured/CRI value
0.4
0.6
0.8
1
1.2
1.4
Li
Na
Mg
Al
Si
P
K
Ca
Sc
Ti
V
Cr
Mn
Fe
Co
Ni
Cu
Zn
Ga
Rb
Sr
Y
Zr
Nb
Sn
Ba
La
Ce
Pr
Nd
Sm
Eu
Gd
Tb
Dy
Ho
Er
Tm
Yb
Lu
Hf
Ta
Th
Element

Table 5-11. Calculated concentrations – BIR-1

Element	CRI	Si Internal		Ca Internal		Fe Internal		Oxide Scaled	
		X_{Scaled}	%	X_{Scaled}	%	X_{Scaled}	%	X_{Scaled}	%
Li	3.6	2.5	29.90	3.5	***3.33***	2.7	25.79	2.7	25.30
Be	0.58	< DL	--	< DL	--	< DL	--	< DL	--
B	0.53	12.6	***2276***	17.2	3135	13.3	2402	13.4	2422
Na	13500	9692	28.21	13369	***0.97***	10263	23.98	10327	23.51
Mg	58000	57464	***0.92***	79017	36.24	60728	4.70	61161	5.45
Al	82000	77485	5.51	106273	29.60	81827	***0.21***	82421	0.51
Si	224200	224200	0.00	309295	37.95	237429	***5.90***	238962	6.58
P	92	79.9	13.19	110.5	20.09	84.8	7.87	85.2	***7.36***
K	250	152.5	39.02	211.0	***15.59***	165.0	33.98	165.2	33.90
Ca	95100	69579	26.84	95100	0.00	73408	22.81	73960	***22.23***
Sc	44	32.1	27.05	43.9	***0.16***	33.9	23.03	34.1	22.44
Ti	5800	4439	23.46	6090	***5.00***	4688.6	19.16	4723	18.57
V	310	241.3	22.17	331.8	***7.02***	254.9	17.76	256.9	17.15
Cr	370	303.3	18.02	417.8	12.93	320.7	13.33	329.4	***10.97***
Mn	1360	1255.8	7.66	1726.3	26.93	1326.4	2.47	1336.7	***1.71***
Fe	79000	74811	5.30	102821	30.15	79000	0.00	79628	***0.80***
Co	52	47.7	8.37	65.6	26.14	50.4	3.07	50.8	***2.39***
Ni	170	154.5	9.14	212.4	24.93	163.2	3.98	164.5	***3.24***
Cu	125	99.9	20.06	137.4	***9.90***	105.7	15.44	106.4	14.85
Zn	70	91.3	***30.47***	125.5	79.27	96.6	38.00	97.8	39.69
Ga	16	15.5	3.40	21.3	32.95	16.4	***2.25***	16.5	2.95
Ge	--	2.4	--	3.3	--	2.6	--	2.6	--
As	0.44	< DL	--	2.31	***425.22***	< DL	--	< DL	--
Se	--	< DL	--	< DL	--	< DL	--	< DL	--
Rb	--	< DL	--	< DL	--	< DL	--	< DL	--
Sr	110	85.3	22.47	116.9	***6.27***	90.0	18.17	90.7	17.55
Y	16	10.3	35.64	14.1	***11.78***	10.9	32.07	11.0	31.56
Zr	18	10.8	39.81	14.9	***17.41***	11.4	36.47	11.5	35.98
Nb	0.6	0.39	35.15	0.53	***12.37***	0.41	31.92	0.41	31.15
Mo	--	< DL	--	< DL	--	< DL	--	< DL	--
Rh	--	0.04	--	0.04	--	0.03	--	0.04	--
Pd	--	< DL	--	< DL	--	< DL	--	< DL	--
Ag	--	0.38	--	0.50	--	0.40	--	0.40	--
Cd	--	0.36	--	0.40	--	0.40	--	0.39	--
In	--	0.06	--	0.08	--	0.06	--	0.06	--
Sn	--	1.19	--	1.63	--	1.26	--	1.27	--
Sb	0.58	0.48	17.47	0.66	13.25	0.51	12.75	0.51	***12.16***
Cs	--	< DL	--	< DL	--	< DL	--	< DL	--

Table 5-11 (continued). Calculated concentrations – BIR-1

Element	CRI	Si Internal		Ca Internal		Fe Internal		Oxide Scaled	
		X_{Scaled}	%	X_{Scaled}	%	X_{Scaled}	%	X_{Scaled}	%
Ba	7	5.4	22.26	7.5	***6.77***	5.8	17.85	6.0	14.93
La	0.71	0.51	28.61	0.67	***5.47***	0.52	27.01	0.52	26.41
Ce	2.1	1.5	28.57	2.1	***1.97***	1.6	24.60	1.6	24.01
Pr	0.42	0.30	27.95	0.41	***2.60***	0.32	24.63	0.32	23.68
Nd	2.5	1.9	23.64	2.6	***4.66***	2.0	19.33	2.0	18.80
Sm	1.1	0.9	22.53	1.2	***6.22***	0.9	18.18	0.9	17.63
Eu	0.58	0.43	25.29	0.59	***2.57***	0.46	21.15	0.46	20.49
Gd	2	1.3	34.92	1.8	***10.90***	1.4	31.32	1.4	30.79
Tb	0.43	0.26	38.75	0.35	***18.57***	0.27	36.26	0.28	35.41
Dy	2.7	1.8	33.34	2.5	***8.94***	1.9	29.73	1.9	29.17
Ho	0.59	0.39	33.61	0.53	***10.43***	0.41	30.51	0.41	29.69
Er	1.7	1.2	32.52	1.6	***7.53***	1.2	28.82	1.2	28.25
Tm	0.33	0.18	45.54	0.24	***28.77***	0.19	43.20	0.19	42.57
Yb	1.7	1.3	25.16	1.7	***2.56***	1.3	21.01	1.4	20.41
Lu	0.26	0.18	31.74	0.23	***10.44***	0.19	28.01	0.19	27.67
Hf	0.6	0.41	32.00	0.6	***6.54***	0.43	28.12	0.43	27.63
Ta	--	0.06	--	0.06	--	0.04	--	0.04	--
W	--	< DL	--	0.08	--	< DL	--	< DL	--
Re	--	< DL	--	0.06	--	< DL	--	< DL	--
Pt	--	0.72	--	1.01	--	0.76	--	0.77	--
Au	--	0.09	--	0.12	--	0.09	--	0.10	--
Tl	--	< DL	--	< DL	--	< DL	--	< DL	--
Pb	3	4.2	***39.49***	5.8	92.25	4.4	47.69	4.5	48.77
Bi	--	< DL	--	0.03	--	< DL	--	< DL	--
Th	--	< DL	--	< DL	--	< DL	--	< DL	--
U	--	< DL	--	< DL	--	< DL	--	< DL	--

Figure 5-6. BIR-1 – Measured versus CRI values.

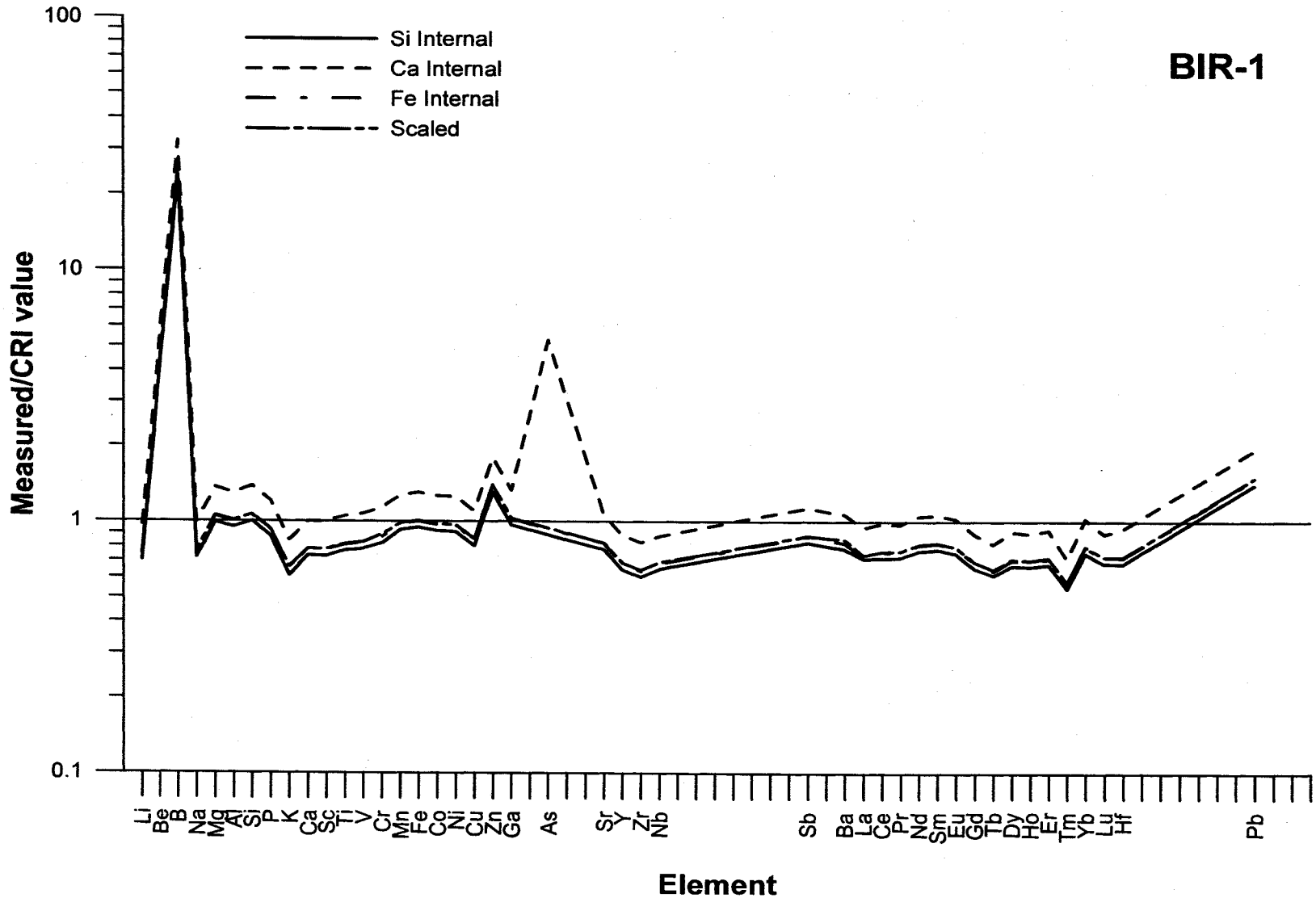
Si Internal
Ca Internal
Fe Internal
Scaled
BIR-1
100
10
1
0.1
Measured/CRI value
Li Be B Na Mg Al Si P K Ca Sc Ti V Cr Mn Fe Co Ni Cu Zn Ga As Sr Y Zr Nb Sb Ba La Ce Pr Nd Sm Eu Gd Tb Dy Ho Er Tm Yb Lu Hf Pb
Element

Analytical accuracies were less than approximately ± 30 % for the majority of elements included in the analyses of BHVO-2. Two elements (P and Ta) had analytical accuracies greater than ± 30 %. P has a moderate fractionation factor and Ta is present in BHVO-2 at a relatively low concentration. Using Ca as an internal standard resulted in the most accurate results for the greatest number (35) of elements (Li, Na, P, Sc, Ti, V, Cr, Co, Ni, Cu, Zn, Ga, Rb, Sr, Y, Zr, Nb, Ba, La, Ce, Pr, Nd, Sm, Eu, Gd, Tb, Dy, Ho, Er, Tm, Yb, Lu, Hf, Ta and Th). Using Fe as an internal standard resulted in the most accurate results for 4 elements (Mg, Al, K and Mn). Scaling the oxide concentrations and using Si as an internal standard resulted in the most accurate results for 3 elements (Si, Ca and Sn) and 1 element (Fe), respectively. Calculation of element concentrations using oxide scaling provided better accuracy than using Si and approximately equal accuracy than using Fe as internal standards, and the results were, on average, within approximately 6 % of the results obtained using Ca as an internal standard.

Analytical accuracies of less than approximately ± 30 % were observed for the majority of elements included in the analyses of BIR-1. Seven elements (B, Zn, As, Zr, Tb, Tm and Pb) had analytical accuracies greater than ± 30 %. Zn, As and Pb have moderate fractionation factors and B, As, Tb, Tm and Pb are present in BIR-1 at relatively low concentrations. Zr has neither a low concentration nor high fractionation index and its behavior relative to the other elements with relatively high ranges of analytical accuracies is anomalous. Using Ca as an internal standard resulted in the most accurate results for the greatest number (28) of elements (Li, Na, K, Sc, Ti, V, Cu, As, Sr, Y, Zr, Nb, Ba, La, Ce, Pr, Nd, Sm, Eu, Gd, Tb, Dy, Ho, Er, Tm, Yb, Lu and Hf). Scaling the oxide concentrations resulted in the most accurate results for 8 elements (P, Ca, Cr, Mn, Fe, Co, Ni and Sb). Using Si and Fe as internal standards resulted in the most accurate results for 4 elements (B, Mg, Zn and Pb) and 3 elements (Al, Si and Ga), respectively. Calculation of element concentrations using oxide scaling provided better

accuracy than using Si and Fe and the results were, on average, within approximately 35 % of the results obtained using Ca as an internal standard.

Use of an internal standard element (Si, Ca or Fe) or oxide scaling typically yielded excellent (± 3 %) to acceptable (± 30 %) analytical accuracies for all of the reference materials considered in this study. Deviations from the more typical accuracies appear to result largely from low concentrations (< 5 ppm) and/or moderate (1.5 to 2) to high (> 2) fractionation indices or a combination of the two. Quantification of element concentrations from LA-ICPMS analysis using oxide scaling is, in general, as accurate and precise as using an internal standard for a range of silicate compositions and enables the determination of element concentrations without the concentration of one or more elements being known beforehand.

Not surprisingly, analytical accuracy was best for NIST 610 (typically < ± 3 %), as it was used as the external calibration standard (i.e., 100 % matrix-matched). The range of analytical accuracy varied depending on the reference material analyzed, indicating that LA-ICPMS analysis using a 266 nm Nd:YAG laser exhibits some matrix effects, even for materials that are quite similar (silicate reference glass standards). Matrix effects exhibited by some elements can be explained by either their presence in relatively low concentrations in the reference material or moderate to high fractionation factors. Not all elements with low concentrations or moderate to high fractionation indices, however, deviated from the analytical accuracies exhibited by most elements, indicating that the matrix effects are more complex than can be explained by these two factors alone.

Tentative Concentrations for Elements without CRI Values

In addition to providing a measure of analytical accuracy for elements with certified, reference or information values, data obtained during this study were used to calculate tentative concentrations for elements that currently do not have certified, reference or information values (Table 5-12). For NIST

612, the concentration for Se obtained using Si as an internal standard was used because it was not possible to use the internal standard that provided the best accuracy for Se for NIST 610 (i.e., Fe). For NIST 614, BCR-2G, BHVO-2 and BIR-1, the standardization method that yielded the most accurate results for NIST 612 was used to select the tentative value. This assumes that the other reference materials would have comparable analytical accuracies to NIST 612, which is reasonable for the majority of the reference materials, based on a comparison of the analytical accuracies of NIST 612 (Figure 5-2) with NIST 614 (Figure 5-3), BCR-2G (Figure 5-4), BHVO-2 (Figure 5-5) and BIR-1 (Figure 5-6). All of these reference materials show comparable, systematic differences in concentrations for most elements relative to the certified, reference or information values, suggesting that elements that do not have these values would likely behave similarly to those in NIST 612.

Table 5-12. Standard Reference Materials Tentative Values

SRM	Element = Tentative Value$^{\text{Standardization Method Used}}$
NIST 612	Se = 15.22 ppm^{Si}
NIST 614	Li = 1.82 ppm^{Si}, Mg = 36.28 ppm^{Ca}, V = 1.1 ppm^{Ca}, Cr = 42.9 ppm^{Ca}, Zn = 3.32 ppm^{Si}, Ga = 1.19 ppm^{Si}, Ge = 1.12 ppm^{Si}, Se = 0.48 ppm^{Si}, Y = 0.72 ppm^{Ca}, Zr = 0.97 ppm^{Ca}, Nb = 0.78 ppm^{Ca}, Mo = 0.84 ppm^{Ca}, In = 0.80 ppm^{Ca}, Sn = 3.23 ppm^{Ca}, Cs = 0.70 ppm^{Ca}, Ba = 3.34 ppm^{Ca}, Ce = 0.83 ppm^{Ca}, Pr = 0.78 ppm^{Ca}, Nd = 0.83 ppm^{Ca}, Sm = 0.82 ppm^{Ca}, Gd = 0.81 ppm^{Ca}, Tb = 0.72 ppm^{Ca}, Dy = 0.72 ppm^{Ca}, Ho = 0.74 ppm^{Ca}, Er = 0.66 ppm^{Ca}, Tm = 0.66 ppm^{Ca}, Yb = 0.75 ppm^{Ca}, Lu = 0.68 ppm^{Ca}, Hf = 0.69 ppm^{Ca}, Ta = 0.66 ppm^{Ca}, W = 0.89 ppm^{Ca}, Bi = 0.61 ppm^{OS}
BCR-2G	Li = 9.4 ppm^{Si}, Be = 2.3 ppm^{Si}, B = 15.4 ppm^{Si}, Ge = 2.9 ppm^{Si}, As = 2.4 ppm^{Ca}, Nb = 12.6 ppm^{Ca}, Ag = 0.70 ppm^{Ca}, In = 0.16 ppm^{Ca}, Sn = 2.99 ppm^{Ca}, Sb = 0.37 ppm^{Ca}, Ta = 0.88 ppm^{Ca}, W = 0.92 ppm^{Ca}, Pt = 0.32 ppm^{OS}, Au = 0.03 ppm^{Ca}, Tl = 0.26 ppm^{OS}, Bi = 0.10 ppm^{OS}
BHVO-2	Be = 1.6 ppm^{Ca}, B = 14.0 ppm^{Si}, Ge = 2.2 ppm^{Si}, Mo = 3.6 ppm^{Ca}, Ag = 0.38 ppm^{Ca}, In = 0.08 ppm^{Ca}, Sb = 0.11^{Ca}, W = 0.23^{Ca}, Pt = 0.10ppm^{OS}, Au = 0.29 ppm^{Ca}, Tl = 0.03 ppm^{OS}, Pb = 1.56 ppm^{Ca}, Bi = 0.02 ppm^{OS}, U = 0.38 ppm^{Ca}
BIR-1	Ge = 2.4 ppm^{Si}, Rh = 0.04 ppm^{Si}, Ag = 0.50 ppm^{Ca}, Cd = 0.40 ppm^{Ca}, In = 0.08 ppm^{Ca}, Sn = 1.63 ppm^{Ca}, Ta = 0.06 ppm^{Ca}, W = 0.08 ppm^{Ca}, Re = 0.06 ppm^{Ca}, Pt = 0.77 ppm^{OS}, Au = 0.12 ppm^{Ca}, Bi = 0.03 ppm^{Ca}

Application to Unknown Silicates

Introduction

The accuracy of conducting analyses of chemically complex, natural silicate minerals without using an internal standard was evaluated by performing LA-ICPMS and electron microprobe analyses of alkali amphibole (arfvedsonite) from the Strange Lake peralkaline granite, Quebec/Labrador. Arfvedsonite from Strange Lake was selected because it is an important mineral in understanding the magmatic and hydrothermal evolution of this intrusion. Arfvedsonite also has a complex composition, with numerous elemental substitutions (e.g., Ca, Na, Mg, Fe^{2+}, Mn^{2+}, Li, Al, Fe^{3+} and Ti), which significantly impairs the usefulness of some elements as internal standards for LA-ICPMS analysis based solely on mineral stoichiometry. Furthermore, arfvedsonite is a hydrous silicate mineral with elements in hydroxyl crystallographic sites (e.g., OH, F), the concentrations of which can not be determined directly using ICPMS. If these elements are not included during quantification by oxide scaling, this could potentially affect the accuracy of the concentration estimates. Quantitative data were obtained by LA-ICPMS (using Si from 'ideal' mineral stoichiometry as an internal standard and by oxide scaling) and were compared with quantitative data obtained using an electron microprobe.

Sample Suite

Arfvedsonite is the primary mafic phase in the Strange Lake peralkaline granite. Arfvedsonite-bearing samples included in this investigation were 56a-1a, TTR-26, SL-Cb, SL1-12a, and 46S-3a, which are representative of the hypersolvus (56a-1a), subsolvus (TTR-26) and subsolvus pegmatitic (SL-Cb and SL1-12a) phases of the granite. These rocks have been variably altered by two stages of hydrothermal alteration (Salvi & Williams-Jones, 1996); however, original magmatic arfvedsonite is preserved in all samples.

Instrumentation and Experimental Conditions

Arfvedsonite was analyzed using the LA-ICPMS instrumentation in the Great Lakes Institute for Environmental Research at the University of Windsor, Windsor, Ontario. The configuration, operating conditions and methods for LA-ICPMS analyses were the same as those used for the analysis of the reference materials described above. Electron microprobe analyses were conducted in the Department of Earth Sciences at the University of Western Ontario, London, Ontario. A summary of the electron microprobe system specifications and operating conditions used during this study are presented in Table 5-13.

Table 5-13. Electron microprobe system specifications and operating conditions

Manufacturer	JEOL®
Model	JXA-8600 Superprobe®
Quantitative analyzer	Wavelength dispersive system
Accelerating voltage	15 kV
Current	10 nA
Counting time	Na: 15 sec All other elements: 20 sec

Data Reduction

Data reduction protocols for LA-ICPMS analysis using Si as an internal standard and by oxide scaling were the same as those used for the standard reference material analyses. Due to potentially significant elemental substitutions within the A site (e.g., Na and K), T site (e.g., $Si^{4+}$and Al^{4+}), M(1,2 and 3) sites (e.g., Al, Fe^{3+}, Ti, Zr, Zn, Mg, Li, Fe^{2+} and Mn^{2+}) and M(4) site (e.g., Mn^{2+}, Ca and Na), Si is the only viable internal standard element for quantification of the LA-ICPMS data using an internal standard based on mineral stoichiometry. Although Al can substitute for Si in these minerals, the Al content of arfvedsonite from the Strange Lake granite was previously found to be low ($< 10^{-2}$ lower than Si) (Hawthorne et al., 2001).

The samples were analyzed for Si, Ti, Al, Cr, Fe, Mn, Mg, Ca, Na, K, Cl and F using the electron microprobe. The O content of the minerals was estimated on the basis of mineral stoichiometry. All elements were quantified by measuring K-alpha lines using wavelength-dispersive (WDS) analysis. Absorption corrections were applied using CITZAF (Armstrong, 1995) data reduction software.

Results and Discussion

The concentrations of 63 major, minor and trace elements were quantitatively determined using LA-ICPMS. Electron microprobe analysis was only capable of obtaining quantitative data on 13 elements. Data for 10 elements measured using both methods (Si, Ti, Al, Cr, Fe, Mn, Mg, Ca, Na and K) for samples 56-1a, TTR-26, SL-Cb, 46S-3a are summarized in Tables 5-14 through 5-17, respectively. The tables include concentration data obtained by LA-ICPMS using oxide scaling and Si as an internal standard, and by electron microprobe. The tables also include the difference between the scaled and Si internal standardized LA-ICPMS expressed as a percentage relative to the electron microprobe data. The results of the analyses for the 53 additional elements obtained using LA-ICPMS are discussed elsewhere (Chapter 6).

Table 5-14. Sample 56a-1a – LA-ICPMS versus Probe

Element	Scaled (n=7)	Si Internal (n=7)	Probe (n=4)	Scaled/Probe	Internal/Probe
Si	266373 ppm	234319 ppm	241675 ppm	110 %	***97 %***
Ti	6156 ppm	5422 ppm	7097 ppm	***87 %***	76 %
Al	2829 ppm	2491 ppm	2817 ppm	***100 %***	88 %
Cr	< DL	< DL	33 ppm	- -	- -
Fe	225655 ppm	198565 ppm	253050 ppm	***89 %***	78 %
Mn	5979 ppm	5265 ppm	5352 ppm	112 %	***98 %***
Mg	1691 ppm	1490 ppm	2420 ppm	***70 %***	62 %
Ca	< DL	< DL	2662 ppm	- -	- -
Na	65035 ppm	57255 ppm	69550 ppm	***94 %***	82 %
K	10660 ppm	9383 ppm	12253 ppm	***87 %***	77 %

The majority of LA-ICPMS results obtained using either oxide scaling or Si as an internal standard are within approximately ± 25 % of the electron microprobe results. Some elements (Fe, Mg and Ca), however, show consistently greater variability between the two analytical techniques. Differences between element compositions determined by LA-ICPMS using oxide scaling and Si as an internal standard, however, were between an average of approximately 14 % (56a-1a) and 33 % (SL-Cb) of concentrations calculated using Si as an internal standard. This degree of variability between LA-ICPMS results obtained using oxide scaling and an internal standard is the same as that observed for the reference materials, suggesting that the greater variability shown relative to the electron microprobe data is sample (i.e., chemical heterogeneity within individual crystals) or instrument related and not the result of the different methods of LA-ICPMS data reduction. Although both sets of data were acquired from the same sample and mostly from the same mineral grain, the two sets of analyses were not obtained from exactly the same location, suggesting that within sample or within grain compositional heterogeneity may explain some of the differences between the two data sets (see Chapter 6).

Table 5-15. Sample TTR-26 – LA-ICPMS versus Probe

Element	Scaled (n=15)	Si Internal (n=15)	Probe (n=4)	Scaled/Probe	Internal/Probe
Si	307454 ppm	234319 ppm	243375 ppm	126 %	***96 %***
Ti	5660 ppm	4324 ppm	6832 ppm	***83 %***	63 %
Al	3391 ppm	2592 ppm	1751 ppm	194 %	***148 %***
Cr	< DL	< DL	158 ppm	- -	- -
Fe	151922 ppm	116136 ppm	253275 ppm	***60 %***	46 %
Mn	4088 ppm	3115 ppm	5996 ppm	***68 %***	52 %
Mg	1407 ppm	1078 ppm	1027 ppm	137 %	***105 %***
Ca	2933 ppm	2247 ppm	1551 ppm	189 %	***145 %***
Na	72525 ppm	55411 ppm	67250 ppm	***108 %***	82 %
K	8066 ppm	6151 ppm	16425 ppm	***49 %***	37 %

Table 5-16. Sample SL-Cb – LA-ICPMS versus Probe

Element	Scaled (n=8)	Si Internal (n=8)	Probe (n=2)	Scaled/Probe	Internal/Probe
Si	311507 ppm	234319 ppm	241250 ppm	129 %	***97 %***
Ti	5419 ppm	4083 ppm	8437 ppm	***64 %***	48 %
Al	2242 ppm	1689 ppm	1639 ppm	137 %	***103 %***
Cr	< DL	< DL	0 ppm	- -	- -
Fe	150780 ppm	113570 ppm	252250 ppm	***60 %***	45 %
Mn	3931 ppm	2962 ppm	6152 ppm	***64 %***	48 %
Mg	< DL	< DL	244 ppm	- -	- -
Ca	2697 ppm	2028 ppm	498 ppm	542 %	***407 %***
Na	70293 ppm	52945 ppm	68350 ppm	***103 %***	77 %
K	7653 ppm	5773 ppm	15971 ppm	***48 %***	36 %

Table 5-17. Sample 46S-3a – LA-ICPMS versus Probe

Element	Scaled (n=5)	Si Internal (n=5)	Probe (n=4)	Scaled/Probe	Internal/Probe
Si	273957 ppm	234319 ppm	250575 ppm	109 %	***94 %***
Ti	1662 ppm	1230 ppm	2123 ppm	***78 %***	58 %
Al	1515 ppm	1849 ppm	1354 ppm	**112 %**	137 %
Cr	< DL	< DL	34 ppm	- -	- -
Fe	189402 ppm	138102 ppm	224925 ppm	***84 %***	61 %
Mn	21092 ppm	15333 ppm	18146 ppm	116 %	84 %
Mg	4612 ppm	6021 ppm	1993 ppm	***231 %***	302 %
Ca	3096 ppm	7674 ppm	158 ppm	***1962 %***	4865 %
Na	65060 ppm	57034 ppm	65500 ppm	***99 %***	87 %
K	20544 ppm	15640 ppm	23766 ppm	***86 %***	66 %

In general, data obtained using LA-ICPMS and electron microprobe are similar (i.e., generally within ± 25 %). Relative to the electron microprobe data, LA-ICPMS typically yielded higher Si, Al and Ca and lower Ti, Cr, Fe and K concentrations. Differences in Mn, Mg and Na concentrations were non-systematic between the two analytical techniques. The differences in element concentrations between those obtained by the LA-ICPMS analysis and those by electron microprobe analysis for different samples (some element concentrations were higher and others lower for the same technique) indicate that exclusion of the hydroxyl site elements (OH, F) in the calculation

of the LA-ICPMS concentrations without using an internal standard did not introduce a significant, systematic error. Inclusion of the approximately 2 % F, that was found to be present in the hydroxyl site of arfvedsonite using electron microprobe analyses, would have a negligible effect on the calculated element concentrations when the F abundance was apportioned across the remaining elements. Therefore, the differences between the LA-ICPMS and electron microprobe data reflect method limitations (e.g., detection limit for Cr for electron microprobe), analytical imprecision, or variations in sample composition, rather than systematic errors introduced by the data reduction algorithms.

Differences between the results of LA-ICPMS analyses calculated by oxide scaling and using Si as an internal standard (average ~ 14 to 33 %) are consistent with the differences exhibited by the reference materials, suggesting that analytical inaccuracies and possible matrix-related effects are comparable to those exhibited during reference material analyses. The relatively small difference in the results obtained using the two methods of LA-ICPMS data reduction indicates that either method could be used to obtain reasonably accurate determinations of arfvedsonite composition. The added benefit of conducting LA-ICPMS instead of electron microprobe analysis is the ability to quantify the concentrations of many more minor and trace elements, the concentrations of which are impossible to determine using the electron microprobe due to elevated detection limits relative to LA-ICPMS analysis.

Conclusions

Based on laboratory analyses, and interpretations of data resulting from these analyses, the following conclusions can be drawn:

- Quantitative analysis of synthetic silicate standard reference materials by LA-ICPMS without using a previously-determined or estimated internal standard element and without using alternative calibration

(e.g., liquid introduction) strategies is possible by conducting comprehensive elemental analyses and performing oxide scaling. Element concentrations calculated using oxide scaling typically have comparable or better analytical accuracy (typically less than ± 3 % to ± 30 %) than those obtained using common internal standard elements (e.g., Si, Ca or Fe).

- Analyses of NIST 612, NIST 614, BCR-2G, BHVO-2, and BIR-1 using NIST 610 as an external calibration standard, have larger ranges of analytical error (up to ± 30 %) than analyses of NIST 610 using NIST 610 as an external calibration standard (typically less than ± 3 %). The differences in analytical accuracy appear to be the result of matrix effects. Although some elements have atypical (high) analytical accuracies that appear to be related to relatively low abundances (< 5 ppm) in the reference material and/or moderate to high elemental fractionation factors (1.5 to greater than 2), the lack of coherent behaviour among all elements with low concentrations and high fractionation factors indicates that the observed matrix effects are more complex than can be explained by these two factors alone.

- LA-ICPMS analysis of arfvedsonite without using an internal standard yielded similar results (i.e., within 14 to 33 %) to LA-ICPMS analysis using Si but based on stoichiometry as an internal standard and to electron microprobe, with differences apparently resulting from fundamental differences in analytical methods. Regardless, the data indicate that quantitative analysis of chemically complex silicate minerals by LA-ICPMS without using an internal standard is possible. Analysis by LA-ICPMS is also superior to electron microprobe analysis due to its the ability to quantify the concentrations of many more minor and trace elements present in concentrations below the limits of detection of electron microprobe.

References

Armstrong J. T. (1995): CITZAF: A package of correction programs for the quantitative electron microbeam x-ray analysis of thick polished material, thin films, and particles. *Microbeam Analysis*, **4**, 177-200.

Gagnon, J.E., Samson, I.M., and Fryer, B.J. (2003): LA-ICP-MS Analysis of Fluid Inclusions. *In* I. Samson, A. Anderson & D. Marshall (eds.), The Analysis and Interpretation of Fluid Inclusions, *Mineralogical Association of Canada*, Short Course **32**, 12/1-12/32.

Halicz, L. and Günther, D. (2004): Quantitative analysis of silicates using LA-ICP-MS with liquid calibration. *Journal of Analytical Atomic Spectrometry*, **19**, 1539-1545.

Hawthorne, F.C., Oberti, R., Cannillo, E., Ottolini, L., Roelofsen, J.N. and Martin, R.F. (2001): Li-bearing arfvedsonite amphiboles from the Strange Lake peralkaline granite, Quebec. *The Canadian Mineralogist*, **39**, 1161-1170.

Leach, J.J., Allen, L.A., Aeschliman, D.B., and Houk, R.S. (1999): Calibration of Laser Ablation Inductively Coupled Plasma Mass Spectrometry Using Standard Additions with Dried Solution Aerosols. *Analytical Chemistry*, **71**, 440-445.

Leach A.M. and Hieftje, G.M. (2002): Identification of alloys using single shot laser ablation inductively coupled plasma time-of-flight mass spectrometry. *Journal of Analytical Atomic Spectrometry*, **17**, 852-857.

Longerich, H.P., Jackson, S.E. and Günther, D. (1996): Laser Ablation Inductively Coupled Plasma Mass Spectrometric Transient Signal Data Acquisition and Analyte Concentration Calculation. *Journal of Analytical Atomic Spectrometry*, **11**, 899-904.

Fryer, B.J., Jackson, S.E. and Longerich, H.P. (1995): The design, operation and role of the laser-ablation microprobe coupled with an inductively coupled plasma – mass spectrometer (LAM-ICP-MS) in the earth sciences. *The Canadian Mineralogist*, **33**, 303-312.

Salvi & Williams-Jones (1996): The role of hydrothermal processes in concentrating high-field strength elements in the Strange Lake peralkaline complex, northeastern Canada. *Geochimica et Cosmochimica Acta*, **60**, 1917-1932.

van Achterbergh, E., Ryan, C.G., Jackson, S.E., and Griffin, W.L. (2001): Data Reduction Software for LA-ICP-MS. *In* Laser-Ablation-ICPMS in the Earth Sciences, Mineralogical Association of Canada, Short Course Series, **29**, 239-243.

Chapter 6

Extreme hydrothermal HFSE mobility and enrichment in the Strange Lake peralkaline complex, northeastern Canada.

Preface

The method for obtaining quantitative analyses by LA-ICPMS without using an internal standard (Chapter 5) is applied to minerals from the Strange Lake hydrothermal HFSE deposit. The nature and complexity of some of the mineral intergrowths associated with secondary, hydrothermal HFSE mineralization required that an alternative approach be used for quantification of mineral compositions. Detailed petrographic and LA-ICPMS analyses of unaltered and altered rocks from the Strange Lake deposit are conducted to further characterize the mineralogical and chemical changes associated with hydrothermal HFSE enrichment.

Extreme hydrothermal HFSE mobility and enrichment in the Strange Lake peralkaline complex, northeastern Canada.

Joel E. Gagnon[1], Anthony E. Williams-Jones[1], Iain M. Samson[2], and Brian J. Fryer[2]

[1]*Department of Earth and Planetary Sciences, McGill University, Montreal, Quebec, H3A 2A7*
[2]*Department of Earth Sciences, University of Windsor, Windsor, Ontario, N9B 3P4*

Abstract

Three distinct hydrothermal events have locally affected rocks within the Strange Lake pluton. The first is characterized by replacement of magmatic arfvedsonite by aegirine. Extreme enrichment of high field strength elements (HFSE) by hydrothermal processes occurred during the second event, which is characterized by the replacement of mostly secondary aegirine and, to a lesser extent, magmatic elpidite and arfvedsonite by an assemblage comprising gittinsite, hematite and quartz (GHQ). The third hydrothermal event is characterized by veining and partial replacement of primarily GHQ alteration by quartz + fluorite. The HFSE enrichment accompanying GHQ alteration occurred as a result of the reaction of preexisting minerals with a Ca- and Zr-bearing aqueous fluid. Petrographic, mineral reaction and LA-ICPMS data indicate that whole rock changes in elemental concentrations accompanying low temperature alteration are largely explained by the alteration of aegirine to GHQ. The absence of significant quantities of precursor zirconosilicate minerals in unaltered rocks and the direct relationship between HFSE enrichment and GHQ alteration indicate that HFSE enrichment within the Strange Lake pluton resulted from secondary, subsolidus hydrothermal and not magmatic processes. The amount of HFSE enrichment is proportional to the degree to which the rocks have been affected by GHQ alteration and the abundance of aegirine in the rocks prior to alteration.

Introduction

High field strength elements (HFSE), which include Sc, Ti, V, Y, Zr, Nb, Hf, Ta and the rare earth elements (REE), have historically been considered to be immobile during metasomatic processes (e.g., metamorphism, hydrothermal alteration). This apparent immobility has led to their widespread use in classifying rocks (e.g., Pearce and Cann, 1973; Floyd and Winchester, 1975; 1978; Pearce and Norry, 1979), modelling geologic processes (e.g., Munker et al., 2004), and quantifying mass or volume changes during deformation and alteration (e.g., O'Hara and Blackburn, 1989; MacLean, 1990; Fujimoto et al., 2001). A growing body of evidence, however, indicates that HFSE have been mobilized in a variety of geologic environments ranging from those of hydrothermal ore deposits (e.g., MacLean, 1988; Salvi and Williams-Jones, 1996; Jiang, 2000; Samson and Wood, in press), to that of the mantle (e.g., Heaman et al., 2002). Despite this evidence, comparatively little is known about the factors controlling transport and deposition of HFSE in hydrothermal systems.

Evidence of hydrothermal HFSE mobility and enrichment is particularly convincing in some alkaline igneous systems (e.g., Trueman et al., 1988; Sørensen, 1992; Salvi and Williams-Jones, 1996; Salvi et al., 2000; Salvi and Williams-Jones, in press), where it is often associated spatially with hydrothermal alteration (e.g., fenitization, albitization, Ca-metasomatism, or hematization). Establishing the extent of secondary, hydrothermal enrichment in these systems, however, is further complicated by anomalously high, primary magmatic concentrations of HFSE in many of the intrusions that host these deposits (e.g., Strange Lake). This has led some investigators (e.g., Kovalenko et al., 1995; Miller, 1996) to question whether *significant* remobilization of HFSE by hydrothermal processes has occurred within these intrusions and whether there is a genetic link between hydrothermal alteration and HFSE mineralization. Despite the apparent association between HFSE enrichment and alteration in these intrusions, the genetic link remains equivocal. Determining the nature and magnitude of HFSE enrichment and its relationship with mineralogical alteration

is critical to understanding HFSE mobility in hydrothermal systems, and has important implications for the exploration and development of these deposits.

The Strange Lake peralkaline complex hosts one of the largest occurrences of Zr-REE-Y-Nb-Be mineralization in the world. Although the entire intrusion contains anomalously high concentrations of HFSE (Zajac et al., 1984; Miller, 1986; Salvi and Williams-Jones, 1996), the most enriched rocks occur in zones that are relatively small and exhibit mineralogical and chemical evidence of secondary, hydrothermal alteration (Salvi and Williams-Jones, 1990; 1995; 1996). Whole-rock mass-balance calculations conducted by Salvi and Williams-Jones (1996) indicate that hydrothermal processes resulted in HFSE enrichment that was typically greater than 20 % more than in unaltered rocks, and on a scale that was large enough to create a potential ore deposit comprising approximately 30 million tonnes grading 3.25 % ZrO_2, 0.66 % Y_2O_3, 0.56 % Nb_2O_5, 0.12 % BeO and 1.30 % REE (Iron Ore Company of Canada, unpublished data).

The primary mineralogical change associated with HFSE mineralization in the Strange Lake pluton has been reported to be the replacement of magmatic HFSE silicates by hydrothermal phases, e.g., elpidite by gittinsite, through a Na-Ca exchange reaction. Salvi and Williams-Jones (1995) described the zirconosilicate alteration using the following reaction:

$$Na_2ZrSi_6O_{15}\cdot 3H_2O + Ca^{2+} + 5\ H_2O \leftrightarrow CaZrSi_2O_7 + 2\ Na^+ + 4\ H_4SiO_4 \qquad (1)$$

$$Elpidite + Ca^{2+}_{(aq)} + 5\ H_2O \leftrightarrow Gittinsite + 2\ Na^+_{(aq)} + 4\ Silicic\ Acid_{(aq)}$$

This replacement was accompanied by hematization of the host granite and pegmatite (Miller, 1996; Salvi and Williams-Jones, 1996). Alteration of elpidite to gittinsite, however, approximately conserves Zr (i.e., alteration was isochemical). Therefore, this replacement alone does not explain the significant (i.e., 10's of %) increase in HFSE concentrations observed in the most strongly mineralized rocks, as indicated by whole-rock analyses (Salvi and Williams-Jones, 1996). Furthermore, although hematization appears to be associated with HFSE enrichment, Salvi and Williams-Jones (1996) demonstrated that this

alteration typically was not accompanied by significant addition of Fe to the altered rocks (i.e., Fe was approximately conserved). Therefore, although hydrothermal processes played a role in HFSE mobility and enrichment in the Strange Lake pluton, the processes causing extreme HFSE enrichment and the genetic link, if any, to hematization, are not completely understood.

This paper presents the results of an investigation into the petrography, mineralogy and mineral chemistry of unaltered, hydrothermally-altered, and HFSE-mineralized rocks from the Strange Lake pluton. The investigation was conducted to further understand the nature of hematization and its possible association with HFSE enrichment, determine mechanisms for HFSE enrichment, and identify possible sources of HFSE in hydrothermally altered rocks.

The Strange Lake Pluton

Geology

The Strange Lake pluton is located along the Quebec/Labrador border, approximately 150 km west of Nain, Labrador, and 250 km northeast of Schefferville, Quebec, in the eastern portion of the Rae tectonic province. The pluton and associated HFSE mineralization have been described by Zajac et al. (1984a; b), Currie (1985), Miller (1985; 1986; 1988; 1990; 1996), Pillet (1985), Pillet et al. (1989; 1992), Hill and Miller (1990), Salvi and Williams-Jones (1990; 1991; 1992; 1995; 1996; 1997; in press), Birkett and Miller (1991), Birkett et al. (1992), Nassif and Martin (1991), Nassif (1993), Boily and Williams-Jones (1994), and Miller et al. (1997).

Achaean to Paleoproterozoic gneisses of the Mistastin and Mistinibi-Raude Domains occur to the north and east, and a Mesoproterozoic quartz monzonite pluton occurs to the south and west of the Strange Lake pluton (Taylor, 1979; Belanger, 1984; Currie, 1985; Pillet, 1985; Miller, 1986; Ryan et al., 1988; Van der Leeden et al., 1990). Mistastin Domain rocks comprise granulite facies, pegmatoidal, white granitic gneiss, gabbronorite gneiss, biotite-

rich gneiss, augen gneiss and quartzofeldspathic migmatite (Ryan et al., 1988), and were metamorphosed during the Paleoproterozoic Hudsonian orogeny (Taylor, 1979; Belanger, 1984). Ryan et al. (1991) determined that the Mistastin Domain rocks are 2574 ± 8 Ma old using high-precision U-Pb dating of zircon. Mistinibi-Raude Domain rocks comprise amphibolite facies, migmatitic, semi-pelitic paragneiss, with two-mica granite in places (Belanger, 1984), and are thought to be Paleoproterozoic in age (Van der Leeden et al., 1990).

The Strange Lake pluton is circular in plan, approximately 6 km in diameter, cylindrical in cross-section, and comprises numerous phases of peralkaline granite (Miller, 1986; Nassif and Martin, 1991) (Fig. 6-1). Miller (1986) subdivided the granite into 'exotic-poor', 'exotic-rich' and 'exotic' varieties, based on the relative abundance of HFSE-bearing minerals. Nassif and Martin (1991) and Nassif (1993) used feldspar mineralogy to reclassify the pluton into hypersolvus, subsolvus and transsolvus granite, which approximately correspond with the respective major subdivisions of Miller (1986). The three main types of granite are concentrically distributed, with the earliest, hypersolvus granite in the core, the latest, subsolvus granite around the outside, and the transsolvus granite occurring as irregular, discontinuous units at the contact between hypersolvus and subsolvus granite (Miller, 1986; Nassif and Martin, 1991). Miller (1986; 1996) further subdivided each of the three main types of granite on the basis of textural features into fine-grained, porphyritic, aplitic, and pegmatitic varieties. The perimeter of the pluton is demarcated by an outwardly dipping ring fracture that contains a heterogeneous breccia in a fluorite-bearing matrix (Salvi and Williams-Jones, 1997). Most exposures of the pluton contain abundant, large, host-rock xenoliths and roof pendants and miarolitic cavities (Miller, 1986; Salvi and Williams-Jones, 1996).

Figure 6-1 Geology of the Strange Lake pluton.

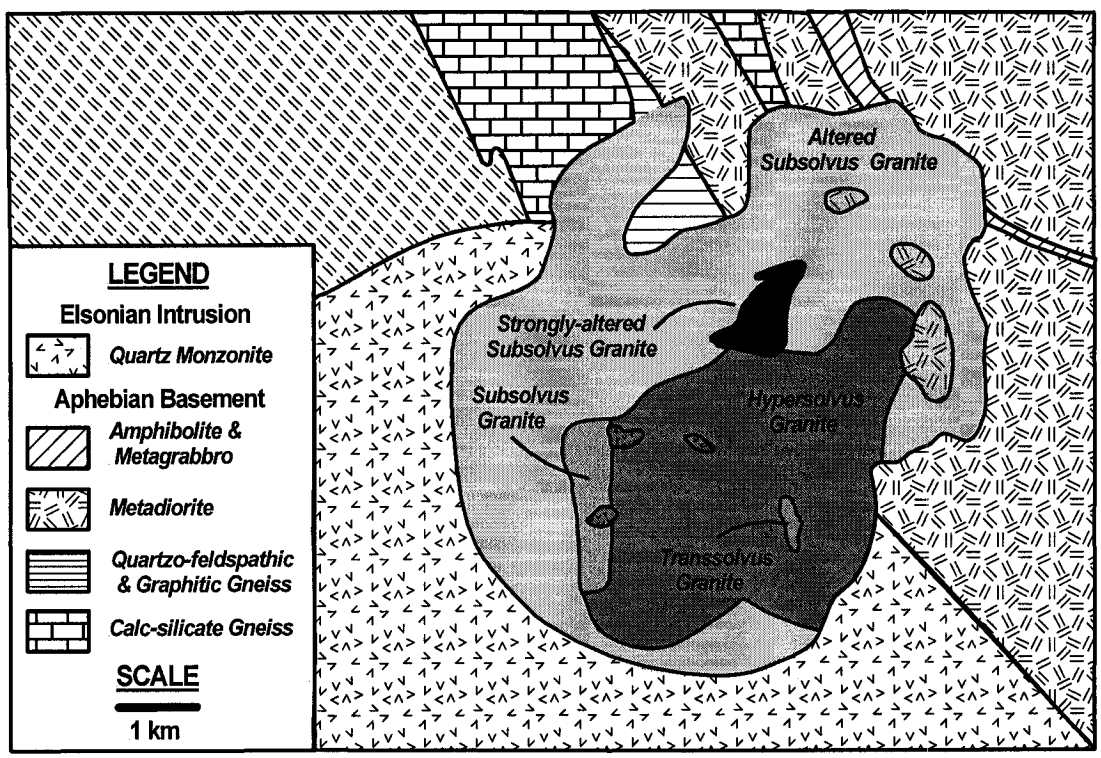

Modified from Salvi and Williams-Jones (1996)

Hypersolvus granite comprises early-crystallized perthitic alkali feldspar, interstitial quartz, and late-crystallized arfvedsonite with accessory albite, fluorite, zircon, thorite, aenigmatite, astrophyllite, vlasovite, dalyite and other exotic minerals (Miller, 1986; Nassif, 1993; Salvi and Williams-Jones, 1996). This is the oldest unit in the pluton and has been determined to be Mesoproterozoic in age (1240 ± 2 Ma) using high-precision U-Pb age dating of zircon (Miller et al., 1997). Transsolvus granite is similar to hypersolvus granite but contains microcline in addition to perthitic feldspar (Miller, 1986; Nassif, 1993; Salvi and Williams-Jones, 1996). Porphyritic varieties of hypersolvus and transsolvus granite contain phenocrysts of quartz and perthite (Miller, 1986; Nassif, 1993; Salvi and Williams-Jones, 1996).

Approximately 60 % of the exposed pluton comprises subsolvus granite, which consists of idiomorphic quartz, arfvedsonite, sodic and potassic feldspar, and accessory zircon, elpidite, armstrongite, gittinsite, kainosite, calcite, hematite, fluorite, thorite, bastnäsite, monazite, pyrochlore, allanite, yttrian milarite, and other unidentified phases (Miller, 1986; Nassif, 1993; Salvi and Williams-Jones, 1996). Some units of the subsolvus granite contain up to 20 % elpidite (Miller, 1996). Equigranular and arfvedsonite-phyric varieties of subsolvus granite have been observed.

The Strange Lake pluton hosts numerous pegmatites, the majority of which are concentrated in subsolvus granite (Miller, 1986; Salvi and Williams-Jones, 1992). The pegmatites comprise quartz, microcline, albite, arfvedsonite, aegirine, and HFSE minerals, have grain sizes ranging from 1 to 10 cm, and generally occur as 10 to 50 cm thick irregular bodies that generally strike east-west and dip subvertically (Miller, 1986; Salvi and Williams-Jones, 1992; 1997). Nassif (1993) and Boily and Williams-Jones (1994) concluded that pegmatite formation was penecontemporaneous with fluid exsolution from the subsolvus granite, which was emplaced as a volatile-saturated melt. HFSE-bearing minerals locally comprise up to 30 % of some pegmatites (Miller, 1986).

The presence of roof pendants and miarolitic cavities (Miller, 1986; Salvi and Williams-Jones, 1992), and the low trapping pressures estimated from

primary fluid inclusions containing orthomagmatic fluid (Salvi and Williams-Jones, 1992), has led to the conclusion that the pluton was emplaced at a relatively shallow depth.

Mineralization

The highest concentrations of HFSE occur in the north-central part of the pluton, within restricted zones at the contact between the hypersolvus and subsolvus granites (Miller, 1986; Salvi and Williams-Jones, 1990; 1996). The most significant individual occurrence of HFSE mineralization (the main lens, Miller, 1986) is a layered, approximately dome-shaped body that averages 6 to 10 meters in thickness, has an approximate area and volume of 0.75 km^2 and 0.175 km^3, respectively (Miller, 1996), and has been partly eroded. The main zone is characterized by well-developed internal textural zoning that Miller (1996) subdivided into an early, lower massive aplite layer, a central pegmatite-aplite layer, and a late, upper pegmatite layer. Miller (1986) concluded that the main lens formed from an incompatible element-enriched silicate melt that was emplaced into the upper portions of the subsolvus granite.

Alteration

Miller (1986) noted the presence of chemical zoning within the granite that is independent of the apparently primary magmatic layering, but did not interpret its origin. Salvi and Williams-Jones (1990; 1992; 1996) attributed this zoning to hydrothermal processes, and showed that most of the subsolvus granite underwent at least two episodes of alteration. Early, high temperature alteration, which is particularly well-developed in pegmatites, is characterized by the replacement of arfvedsonite by aegirine (Salvi and Williams-Jones, 1992; 1996). Elpidite and armstrongite were replaced by gittinsite during a later, low temperature alteration event, which also resulted in considerable enrichment of HFSE (Salvi and Williams-Jones, 1995; 1996). Salvi and Williams-Jones (1996) used whole-rock analyses to demonstrate that zones of HFSE enrichment are underlain in places by HFSE-depleted rocks.

Early alteration was caused by reaction of the granite with a reduced, saline (approximately 25 equiv. wt % NaCl), Ca-free and Na-, F- and HFSE-bearing fluid, which coexisted with an immiscible carbonic fluid (Salvi and Williams-Jones, 1992). This alteration occurred at relatively high temperature (≥ 350 °C) and low pressure (700 bars), and resulted in partial to complete replacement of arfvedsonite by aegirine and/or hematite, quartz and accessory Zr-Ti-Y-Be-REE-bearing minerals and, in places, by depletion of Zr, Y and HREE (Salvi and Williams-Jones, 1992; 1996). Replacement of arfvedsonite by aegirine is sporadic, varies in intensity, occurs with and without later alteration, is most intense in and adjacent to pegmatites, and is most prevalent in the north-central part of the intrusion (Salvi and Williams-Jones, 1996). This high-temperature alteration extends to greater depths than the later alteration (> 80 m from surface) and was caused by a hydrothermal fluid exsolved from the subsolvus granite (Salvi and Williams-Jones, 1992).

The later alteration event occurred at relatively low temperature (≤ 200 °C) and was caused by reaction of the granite with an oxidized, moderate salinity (approximately 13 to 24 equiv. wt. % NaCl), Ca-bearing, effectively F-free formation or meteoric water, which coexisted with an immiscible carbonic fluid (Salvi and Williams-Jones, 1990; 1992). This alteration is characterized by hematization, the addition of Mg, and by pseudomorphic replacement of Na-bearing HFSE minerals by Ca-bearing equivalents (i.e., gittinsite + quartz after elpidite, or titanite + quartz ± fluorite after narsarsukite) by exchange of Ca for Na. The fluid that caused this alteration is thought to have been in equilibrium with the calc-silicate gneisses and gabbros that host the Strange Lake granite (Salvi and Williams-Jones, 1992). The highest concentrations of HFSE, Be and F occur in the most intensely hematized subsolvus granite, which corresponds to the main lens (Salvi and Williams-Jones, 1996). Salvi and Williams-Jones (1990; 1996) concluded that formation of the most significant HFSE mineralization resulted from mixing of the Ca-poor, HFSE-rich fluid, exsolved from the granite, with the Ca-rich fluid introduced into the granite from the host rocks.

Methods

Sample Selection, Preparation and Petrographic Analysis

The samples used in this study comprise a subset of samples from the Strange Lake peralkaline complex and related HFSE mineralization that are part of a collection housed in the Department of Earth and Planetary Sciences, McGill University, Montreal, Quebec. A suite of twenty samples, including unaltered hypersolvus, subsolvus, and pegmatitic granite, and their altered equivalents, were selected for this study. Particular attention was paid to samples that, on the basis of petrographic analysis, exhibited evidence of high temperature (e.g., aegirine after arfvedsonite) and low temperature (e.g., gittinsite after elpidite) alteration or exhibited mineral textures (e.g., product-reactant associations) suggestive of possible HFSE mobility (e.g., hematization, high modal abundances of zirconosilicate minerals).

Polished thin sections and fluid inclusion wafers were prepared from each sample for petrographic, mineralogical and laser ablation inductively-coupled plasma mass spectrometry (LA-ICPMS) analysis. Particular care was exercised during cutting and preparation (i.e., slow cutting rates, large quantities of cooling water, low temperature bonding agents) to prevent heating of the samples and to preserve the integrity of fluid inclusions for possible future analysis. Detailed petrographic analyses were performed using a Nikon polarizing light microscope to identify the minerals comprising the rocks, evaluate mineral textures, and characterize mineral parageneses. The results of the petrographic analysis are presented below.

LA-ICPMS Analysis

Sample Selection and Preparation: Quantitative analysis of minerals was performed using LA-ICPMS. Polished thin sections used for petrographic analysis were also used for LA-ICPMS analysis. The approximately 27 mm by 46 mm by 1 mm glass slides were stored in covered plastic Petri dishes in a fume hood until LA-ICPMS analysis was conducted. Before LA-ICPMS analysis,

each slide was cleaned with ultra-pure ethanol, blown dry with clean, compressed air, and placed in the laser sample cell under an Ar gas flow.

LA-ICPMS Instrumentation: Laser ablation ICPMS analyses were conducted in the Great Lakes Institute for Environmental Research at the University of Windsor, Windsor, Ontario. The purpose-built laser ablation system comprises a non-homogenized Continuum Surelite® solid state, 266 nm Nd:YAG laser, Oriel® optical bench, Olympus® BX-51 polarizing light microscope equipped with a Prior® computer-controlled stage, and miscellaneous devices for beam size (e.g., multiple irises) and power attenuation (e.g., ½-wave plate and glan prism). Details of the laser ablation system construction were presented previously in Gagnon et al. (2003). A summary of the system specifications and operating conditions used during this study are presented in Table 6-1.

Table 6-1. Laser ablation system specifications and operating conditions

Manufacturer	Continuum®
Model	Surelite® I
Frequency	20 Hz
Wavelength	Fundamental: 1064 nm Output: 266 nm
Flashlamp voltage	Maximum: 1.3 kV Experiment: 1.12 kV
Pulse energy	System Maximum: 2 mJ/pulse Experiment: ~ 0.8 mJ/pulse
Iris	1 mm diameter
Objective Lens	10X
Traverse rate	5 µm/sec

Analysis of mineral grains was conducted by traversing the grains at a fixed rate (i.e., 5 µm/sec) using a motorized programmable stage. The traverse rate and laser power were adjusted to prevent the laser from burning through the polished thin section, and to provide the extended acquisition time necessary to obtain data for a long list of elements. Laser-generated sample aerosols were transported from the ablation cell directly to the torch of a ThermoElectron X7®

ICPMS by routing all of the ICPMS nebulizer gas flow (~ 1.0 L/min) through the cell. This configuration facilitates ICPMS tuning and maximizes sample aerosol transport to the ICPMS. A summary of the ICPMS specifications and operating conditions used during this study are presented in Table 6-2.

Table 6-2. ICPMS instrumentation specifications and operating conditions

Manufacturer	ThermoElectron®
Model	X7®
Detector type	ETP® dual mode (pulse and analogue)
Dynamic range	~ 1 x 10^9 ICPS
Sensitivity (solution)	~ 350 x 10^6 ICPS/ppm
Cone type	High performance interface (HPI)
Plasma conditions	Standard
Instrument tuning	Lenses & torch: Autotune followed by manual optimization RF power: 1200 W Standard mass resolution: 125 High mass resolution: 145 Ar Cool gas: 14 L/min Ar Auxiliary gas: 0.9 L/min Ar Nebulizer gas: 1.04 L/min Quadrupole bias: 0.5 Hexapole bias: -1.5
Data acquisition	Dwell time/mass: 10 ms Masses analyzed: 81 Elements quantified: 64 Mass sweeps/acquisition: 250

Experimental Conditions and Data Acquisition: By selecting low abundance isotopes (e.g., ^{29}Si) or manually adjusting the high mass resolution of the ICPMS during pre-experiment instrument setup to prevent count rates measured on high abundance isotopes from exceeding the dynamic range of the instrument, it was possible to simultaneously determine the concentrations of 62 elements (from a total of 81 masses measured) in concentrations ranging from parts per million (ppm) to weight percent. Mineral analyses were preceded and followed by two replicate analyses of NIST 610, which were used as external calibration standards for the determination of instrumental drift and element sensitivity factors (i.e., integrated counts/s/ppm – ICPS/ppm). At the beginning of each

operating session, the ICPMS quadrupole analyzer was mass calibrated, the detector plateau determined, and the two detector modes (pulse and analogue) were cross-calibrated to improve instrument accuracy and precision.

Ablation was conducted in a sampling cell through which all of the ICPMS nebulizer gas was routed, which enabled relatively easy ICPMS tuning to simultaneously achieve maximum sensitivity and low oxide concentrations (CeO/Ce and UO/O < 0.1 %). Each analysis involved traversing the selected mineral grain with the laser beam at a constant rate (5 μm/s) and was preceded by 60 s, and followed by 30 s, of data collection on combined instrument and gas background.

Each analysis included all of the major, minor and trace elements likely comprising the minerals, and the various matrix and molecular ions necessary to assess ICPMS tuning conditions and to correct for various molecular ion interferences (e.g., ArCl on As). A comprehensive analyte list was used to improve the accuracy of the element concentrations calculated without using an internal standard (i.e., by oxide scaling) (see Chapter 5). The list of masses that were measured and the elements that were quantified during each analysis are presented in Table 6-3.

Table 6-3. Measured masses and quantified elements

Masses Measured (81)	Elements Quantified (62)
^{7}Li, ^{9}Be, ^{11}B, ^{23}Na, ^{25}Mg, ^{27}Al, ^{29}Si, ^{31}P, ^{33}S, ^{39}K, ^{43}Ca, ^{44}Ca, ^{45}Sc, ^{47}Ti, ^{51}V, ^{52}Cr, ^{53}Cr, ^{55}Mn, ^{57}Fe, ^{59}Co, ^{60}Ni, ^{62}Ni, ^{65}Cu, ^{66}Zn, ^{68}Zn, ^{69}Ga, ^{72}Ge, ^{75}As, ^{77}ArCl, ^{82}Se, ^{83}Kr, ^{85}Rb, ^{86}Sr, ^{88}Sr, ^{89}Y, ^{90}Zr, ^{93}Nb, ^{95}Mo, ^{103}Rh, ^{105}Pd, ^{107}Ag, ^{110}Cd, ^{111}Cd, ^{115}In, ^{118}Sn, ^{120}Sn, ^{121}Sb, ^{133}Cs, ^{136}Ba, ^{137}Ba, ^{139}La, ^{140}Ce, ^{141}Pr, ^{146}Nd, ^{147}Sm, ^{153}Eu, ^{155}Gd, ^{156}CeO, ^{157}Gd, ^{159}Tb, ^{163}Dy, ^{165}Ho, ^{166}Er, ^{169}Tm, ^{172}Yb, ^{175}Lu, ^{178}Hf, ^{181}Ta, ^{182}W, ^{185}Re, ^{195}Pt, ^{197}Au, ^{205}Tl, ^{206}Pb, ^{207}Pb, ^{208}Pb, ^{209}Bi, ^{220}Background, ^{232}Th, ^{238}U and ^{254}UO	Li, Be, B, Na, Mg, Al, Si, P, K, Ca, Sc, Ti, V, Cr, Mn, Fe, Co, Ni, Cu, Zn, Ga, Ge, As, Se, Rb, Sr, Y, Zr, Nb, Mo, Rh, Pd, Ag, Cd, In, Sn, Sb, Cs, Ba, La, Ce, Pr, Nd, Sm, Eu, Gd, Tb, Dy, Ho, Er, Tm, Yb, Lu, Hf, Ta, W, Re, Pt, Au, Tl, Pb, Bi, Th and U

Data reduction: Integration regions for each analysis were selected from the time-resolved data (i.e., ICPS/time) using ThermoElectron® PlasmaLab® software. One integration region was selected from the approximately 60 s of pre-ablation background and one region was selected from the stable portion of the signal corresponding to the mineral. The output data (average ICPS/region) were transferred to commercial spreadsheet software and converted into concentration units (ppm). Concentrations were calculated from the time-resolved data using an oxide scaling method (see Chapter 5) so that quantitative analyses could be conducted without using an internal standard or standard addition (cf., Halicz and Günther, 2004). All concentrations were calculated on a dry weight basis (i.e., hydroxyl group ions in arfvedsonite were not factored into the calculation) and Fe was calculated entirely as Fe^{2+} for minerals likely to contain multiple oxidation states of Fe.

Results

Petrography

A listing and brief description of the samples used for petrographic analysis are presented in Table 6-4. These samples were selected because they include representatives of each of the two, major varieties of granite (hypersolvus and subsolvus), pegmatites and veins.

Granites and Pegmatites: Hypersolvus granite typically comprises perthitic feldspar, quartz, and arfvedsonite, and subsolvus granite typically comprises perthitic feldspar, microcline, quartz, arfvedsonite, and locally plagioclase. The granites are inequigranular, and in many cases are seriate, with a gradation in grain size from perthitic feldspar (coarsest), through quartz, microcline, and plagioclase (when present), to arfvedsonite (finest). Porphyritic examples with phenocrysts of perthitic feldspar or arfvedsonite are less common. Coarse arfvedsonite crystals commonly contain fine-grained quartz inclusions indicating that arfvedsonite formed late. Common accessory phases in hypersolvus and

subsolvus granite include fine-grained titanite, elpidite, zircon, and yellow fluorite. In the least altered granites, elpidite typically forms less than 5 % of the mode.

Table 6-4. Sample Descriptions

Rock Type	Sample Numbers
'Fresh' hypersolvus granite	56A-1, 46A-3
'Fresh' subsolvus granite	SL4-12, SL4-14, TTR-26
Altered subsolvus granite	SL1-16
'Fresh' pegmatite	SL2-4
Altered pegmatite	SL3-9, SL1-12, SL1-14, SL1-15, SL1-22, SL-A, SL-C
Quartz veins and silicified pegmatite	Vein 1, SL-B, 46G-1, TTR-22, TTR-23, SL1-22

The mineralogy of the pegmatites is similar to that of the subsolvus granite, except that the grain size of individual minerals can exceed 5 cm, aegirine is the dominant mafic mineral, and arfvedsonite is commonly absent, or present only as relicts within aegirine. The modal mineralogy of the relatively fresh granites and pegmatites observed during this study is similar to that observed by Miller (1996) and Salvi and Williams-Jones (1990; 1996).

High Temperature Alteration: Salvi and Williams-Jones (1990; 1996) showed that much of the Strange Lake pluton, particularly in the vicinity of pegmatites, underwent an alteration event at relatively high temperature (≥ 350 °C). The effect of this alteration was described by Salvi and Williams-Jones (1996) using the following reaction:

$$3Na_3Fe_4^{2+}Fe^{3+}Si_8O_{22}(OH)_2 + 2\ H_2O \leftrightarrow 9\ NaFe(SiO_3)_2 + 2\ Fe_3O_4 + 6\ SiO_2 + 5\ H_2 \quad \textbf{(2)}$$

3 Arfvedsonite + 2 H_2O ↔ 9 Aegirine + 2 Magnetite + 6 Quartz + 5 $H_{2\,(gas)}$

All samples of hypersolvus and subsolvus granite included in this study show evidence of high temperature alteration, consisting of the replacement of arfvedsonite by aegirine. This alteration ranges from partial replacement, manifested as irregular patches or as mantles along crystal edges, fractures or cleavages (Fig. 6-2a), to complete replacement by individual or, in the case of pegmatites, aggregates of aegirine crystals (Fig. 6-2b). In some pegmatites, fine-grained aegirine has completely pseudomorphed coarse-grained arfvedsonite. Coarse-grained arfvedsonite commonly contains inclusions of quartz but the aegirine that replaces it does not. Aegirine alteration tends to be more pervasive and complete in the pegmatites than in the granites and also is commonly accompanied by small, euhedral (tetragonal dipyramidal) crystals of pyrochlore (identified by crystal morphology and LA-ICPMS analysis; see below).

All samples exhibited this type of alteration with one exception, in which magnetite occurs with aegirine as an alteration product of arfvedsonite. This sample, however, also exhibits evidence of a second, later alteration event (see below). Therefore, based on this study, replacement of arfvedsonite by aegirine during high temperature alteration is best described by the following reaction:

$$Na_3Fe_4^{2+}Fe^{3+}Si_8O_{22}(OH)_2 + 2\ SiO_2 + 2\ Na^+ + O_2 \leftrightarrow 5\ NaFeSi_2O_6 + 2\ H^+ \quad \textbf{(3)}$$

$$\textit{Arfvedsonite} + 2\ \textit{Quartz} + 2\ Na^+_{(aq)} + O_{2\,(gas)} \leftrightarrow 5\ \textit{Aegirine} + 2\ H^+_{(aq)}$$

This reaction has been balanced conserving Fe and contrasts with that proposed by Salvi and Williams-Jones (1996) in that magnetite is not a reaction product. Reaction 2 is balanced for mass and charge, and the sum of the molar volumes of the solid reactants (320.56 cm^3/mole) is similar to the sum of the molar volumes of the solid products (325.25 cm^3/mole) indicating that this reaction conserves volume, which is consistent with petrographic observations.

Figure 6-2. Photomicrographs of high temperature alteration – partial replacement of outer edge of primary magmatic arfvedsonite by aegirine in subsolvus granite (Fig. 6-2A) and pervasive replacement of arfvedsonite by aegirine in pegmatite (Fig. 6-2B).

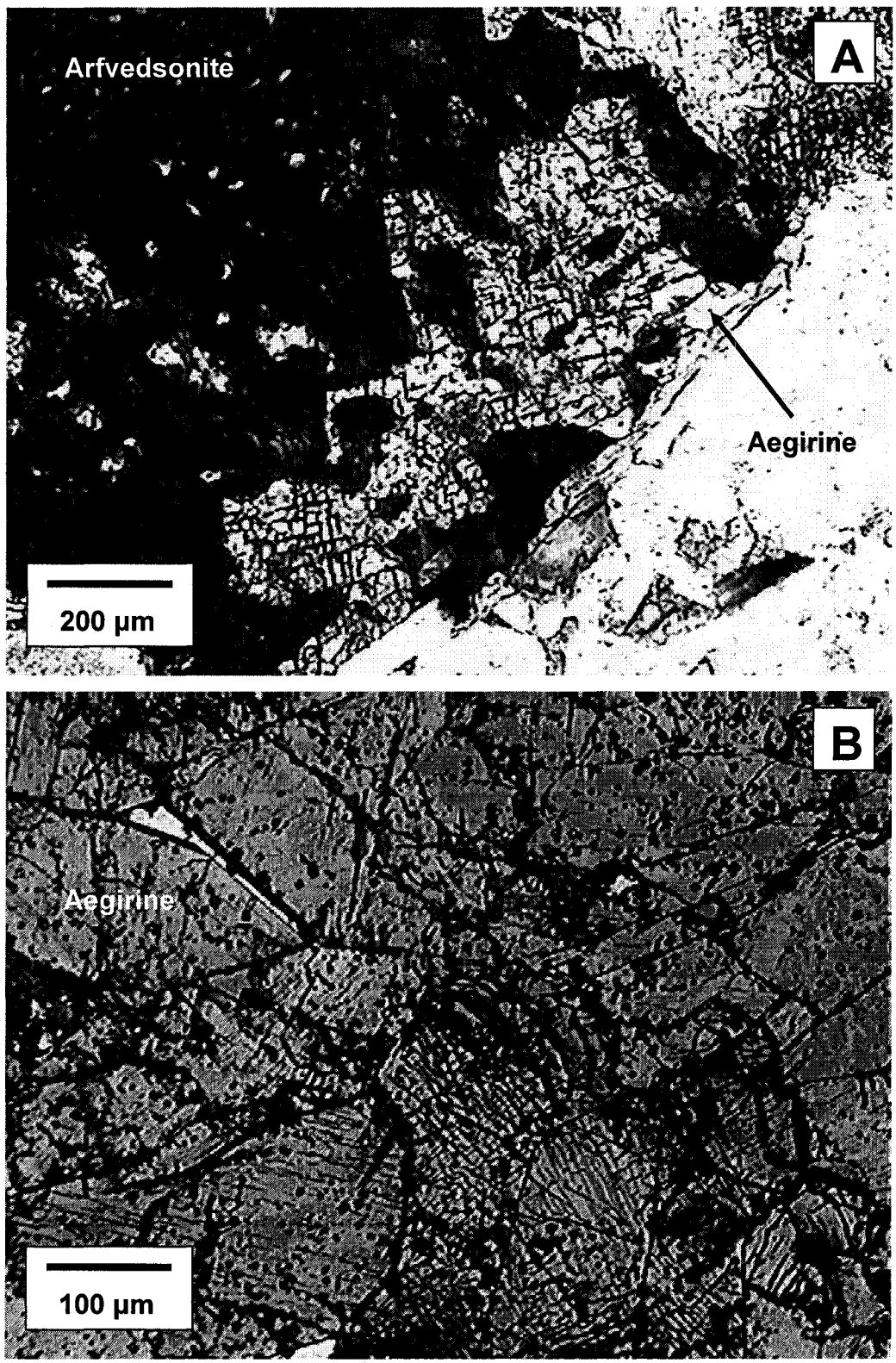
A
Arfvedsonite
Aegirine
200 µm
B
Aegirine
100 µm

Low Temperature Alteration: Subsolvus granite and, in particular, pegmatites underwent a second hydrothermal alteration event at relatively low temperatures (≤ 200 °C) (Salvi and Williams-Jones, 1990; 1995; 1996). This alteration, as described by Salvi and Williams-Jones (1990; 1996), is characterized primarily by the replacement of primary, magmatic elpidite by secondary, hydrothermal gittinsite, and is associated with hematization. Salvi and Williams-Jones (1995) described the alteration using the following Zr-conserving reaction:

$$Na_2ZrSi_6O_{15}\cdot 3H_2O + Ca^{2+} + 5\ H_2O \leftrightarrow CaZrSi_2O_7 + 2\ Na^+ + 4\ H_4SiO_4 \qquad (1)$$

$$Elpidite + Ca^{2+}_{(aq)} + 5\ H_2O \leftrightarrow Gittinsite + 2\ Na^+_{(aq)} + 4\ Silicic\ Acid_{(aq)}$$

Evidence of replacement of elpidite by gittinsite was observed during this study. Euhedral, boat-shaped crystals of elpidite have been entirely replaced by fine-grained, fibrous gittinsite in some altered rocks (Fig. 6-3).

Petrographic observations show that in this particular sample this replacement was not associated with the formation of significant void space, nor was the gittinsite accompanied by quartz and hematite, as reported by Salvi and Williams-Jones (1996). Low temperature alteration of elpidite to gittinsite is better described by the following Si-conserving reaction:

$$Na_2ZrSi_6O_{15}\cdot 3H_2O + 2\ Zr^{4+} + 3\ Ca^{2+} + 3\ H_2O \leftrightarrow 3\ CaZrSi_2O_7 + 2\ Na^+ + 12\ H^+ \qquad (4)$$

$$Elpidite + 2\ Zr^{4+}_{(aq)} + 3\ Ca^{2+}_{(aq)} + 3\ H_2O \leftrightarrow 3\ Gittinsite + 2\ Na^+_{(aq)} + 12\ H^+_{(aq)}$$

Figure 6-3. Photomicrograph of euhedral magmatic elpidite that has been pseudomorphed by fine-grained, fibrous gittinsite. Diagonal lines are approximately 30 μm diameter LA-ICPMS traverses.

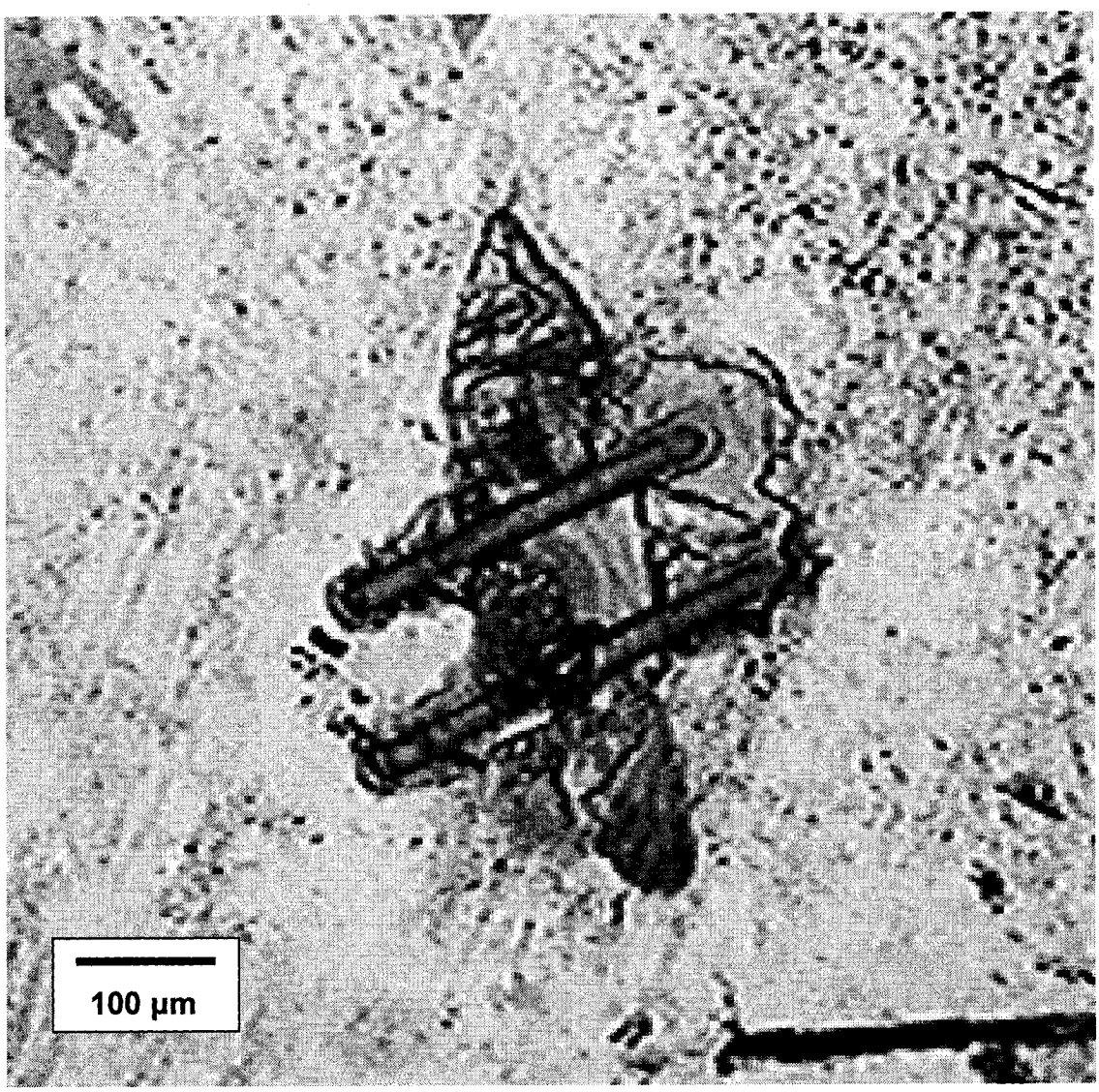
100 µm

Reaction 4 is balanced for mass and charge, and the sum of the molar volumes of the solid reactants (226.25 cm^3/mole) is similar to the sum of the molar volumes of the products (246.00 cm^3/mole) indicating that this reaction approximately conserves volume. Conservation of Si in this reaction rather than Zr (as proposed by Salvi and Williams-Jones, 1996), is supported by other mineralogical changes that accompanied low temperature alteration observed during this study. These changes indicate that Zr and Ca were introduced by the hydrothermal fluid (see below).

Something not recognized by Salvi and Williams-Jones (1990, 1995, 1996) is that hematite-bearing and zirconosilicate-enriched subsolvus granite and pegmatites show extensive replacement of aegirine, and to a lesser extent arfvedsonite, by an assemblage comprising fine-grained intergrowths of fibrous gittinsite (identified from LA-ICPMS analysis; see below), hematite and quartz (hereafter referred to as GHQ alteration). Alteration of aegirine to the GHQ assemblage varies from partial replacement along fractures or cleavages (Fig. 6-4a) to pervasive replacement of some or all of an aegirine crystal (Fig. 6-4b). Pervasive replacement by the GHQ assemblage is particularly well-developed in pegmatites, where fine-grained aggregates of aegirine (high temperature alteration) had previously completely replaced coarse-grained, magmatic arfvedsonite. In contrast, arfvedsonite is unaffected or only partially replaced by GHQ alteration and is commonly preserved as patchy relicts within pervasively-altered aegirine (Fig. 6-5).

Figure 6-4. Photomicrographs of low temperature GHQ alteration – partial replacement of aegirine (high temperature alteration product) along fractures and cleavage planes (Fig. 6-4A) and pervasive replacement of aegirine, which preserves the outline of magmatic arfvedsonite (Fig. 6-4B).

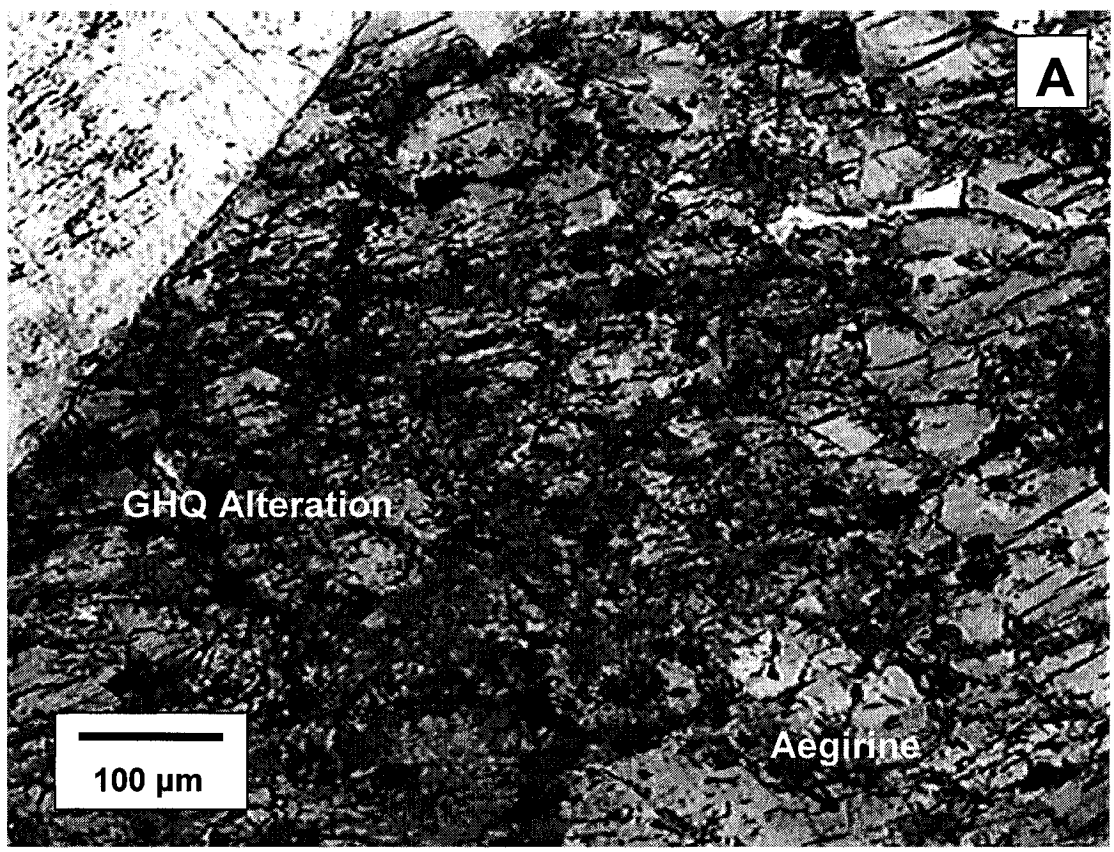
A
GHQ Alteration
Aegirine
100 µm

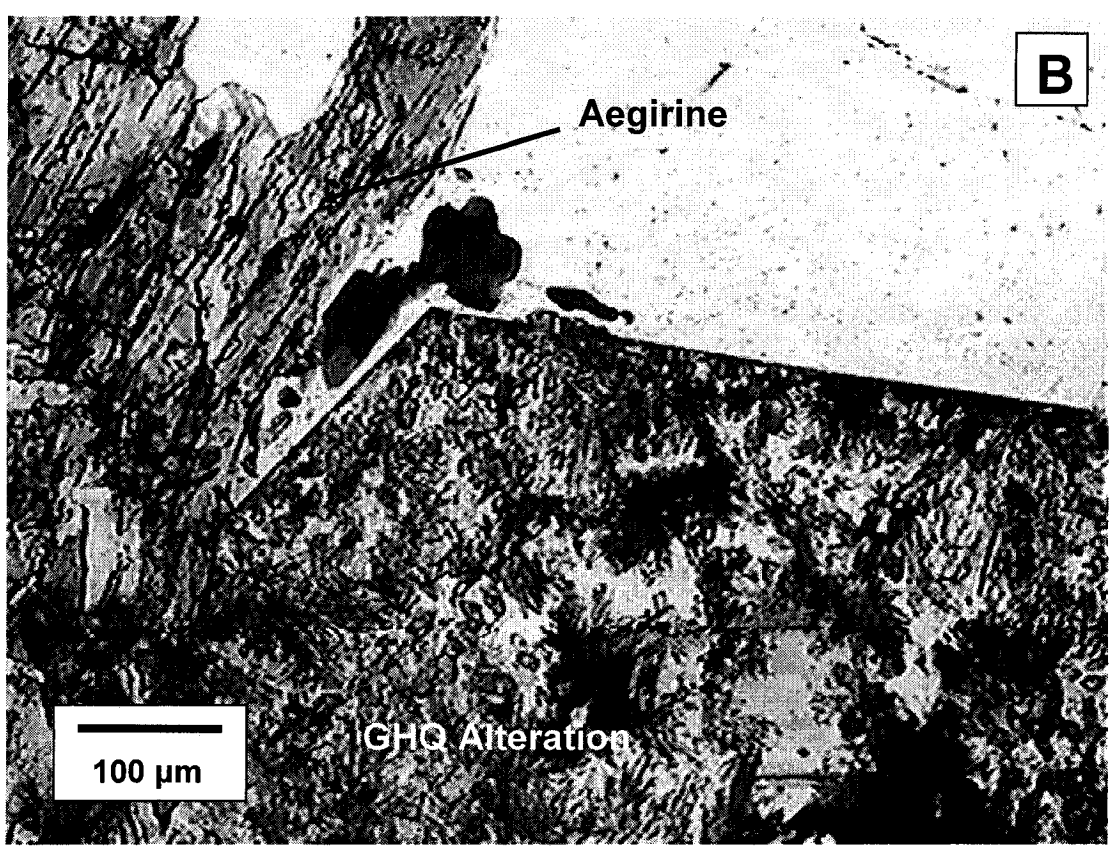
B
Aegirine
GHQ Alteration
100 µm

Figure 6-5. Photomicrographs of low temperature GHQ alteration. Figure 6-5A shows partial replacement of the outer edge of arfvedsonite by GHQ alteration. Figure 6-5B shows a single, coarse-grained, optically continuous arfvedsonite crystal that has been partially replaced by aegirine (high temperature alteration) and GHQ alteration.

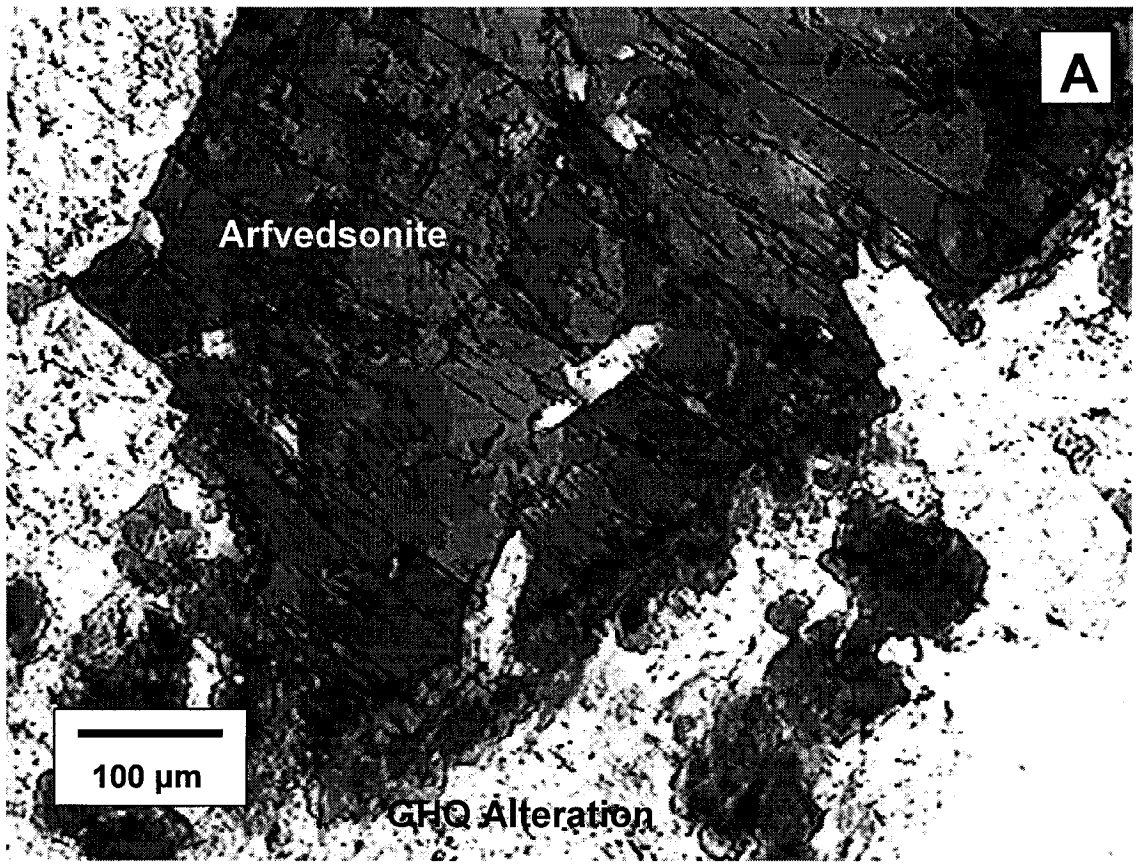
A
Arfvedsonite
100 µm
GHQ Alteration

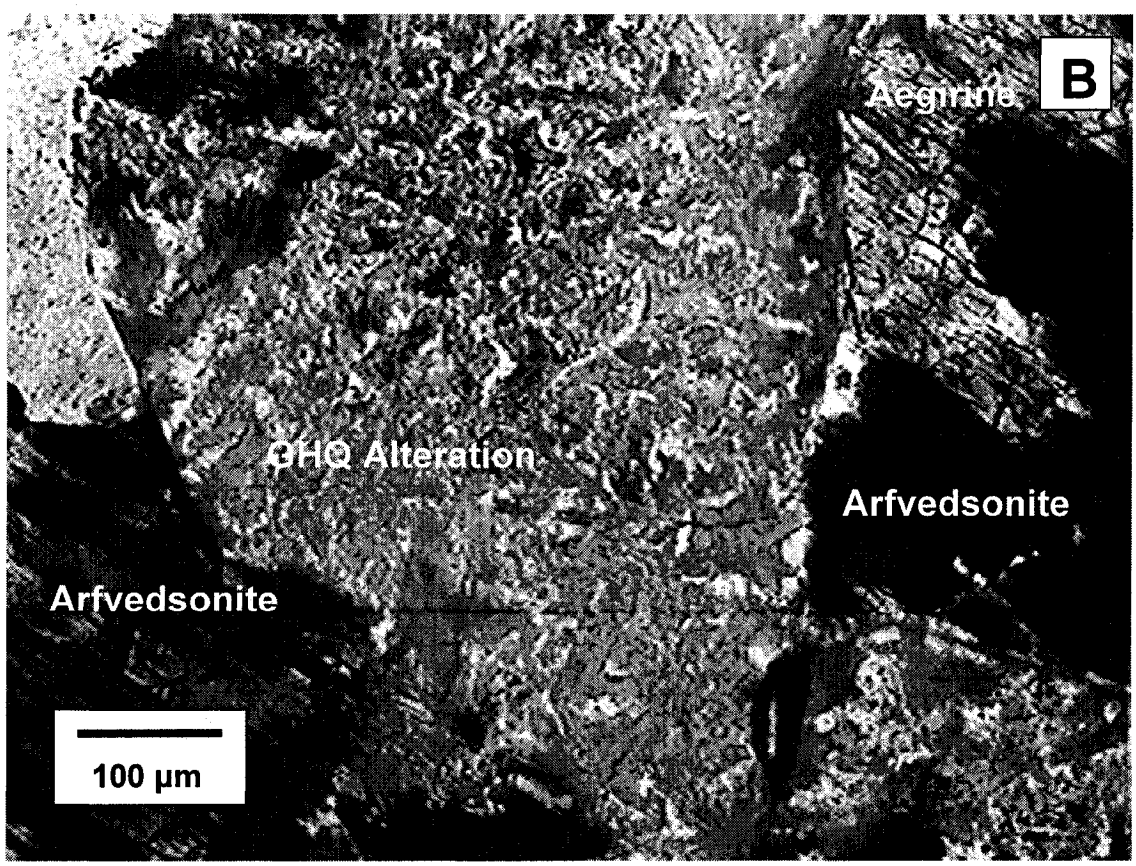
B
Aegirine
GHQ Alteration
Arfvedsonite
Arfvedsonite
100 µm

The most altered rocks, in which aegirine is completely replaced by GHQ alteration, are brick red in color and have a significantly increased modal abundance of gittinsite (approximately 20 %). An important point is that Miller (1986; 1996) and Salvi and Williams-Jones (1990; 1995; 1996) identified gittinsite and hematite solely as alteration products of primary, magmatic zirconosilicates (e.g., armstrongite, elpidite) and did not identify GHQ alteration as a replacement of aegirine. The significance of this will be discussed later. Despite localized, pervasive replacement of aegirine, primary textures (e.g., outlines of coarse arfvedsonite crystals) are preserved (Fig. 6-6a). Although replacement of magmatic elpidite by hydrothermal gittinsite was observed, low temperature alteration in all hematized rocks examined in this study is dominated by GHQ replacement of aegirine ± arfvedsonite. This resulted in significant increases in the abundance of gittinsite in GHQ-altered rocks. The abundance of gittinsite in strongly altered rocks (~ 20 % of the mode) greatly exceeds the typical abundance of primary, magmatic zirconosilicates in unaltered rocks (≤ 5 % of the mode).

Feldspar in strongly hematized rocks also shows evidence of alteration, ranging from patchy, cloudy mantles, to intense, pervasive clouding or alteration to sericite, which accentuates cleavage and perthitic exsolution lamellae. Inclusions of feldspar, quartz and pyrochlore, formerly hosted by arfvedsonite or aegirine, are commonly preserved as cloudy areas and relicts within GHQ alteration (Fig. 6-6b).

In places, GHQ alteration also includes fluorite and 'exotic' minerals, such as thorite. Minor amounts of fine-grained purple fluorite occur interspersed within GHQ alteration, however, most of the fluorite post-dates and along with quartz replaced GHQ alteration. Therefore, fluorite is considered mostly to be a product of a later alteration event (see below).

Figure 6-6. Photomicrographs of low temperature GHQ alteration. Figure 6-6A shows pervasive replacement of arfvedsonite and/or aegirine by GHQ alteration and thorite. The original outline of the amphibole crystal is preserved. Figure 6-6B shows that the alteration assemblage also contains relict, corroded pyrochlore crystals. The presence of pyrochlore relicts in the GHQ alteration assemblage indicates that, in this particular case, GHQ likely replaced aegirine which, with pyrochlore, replaced arfvedsonite in high temperature-altered pegmatite.

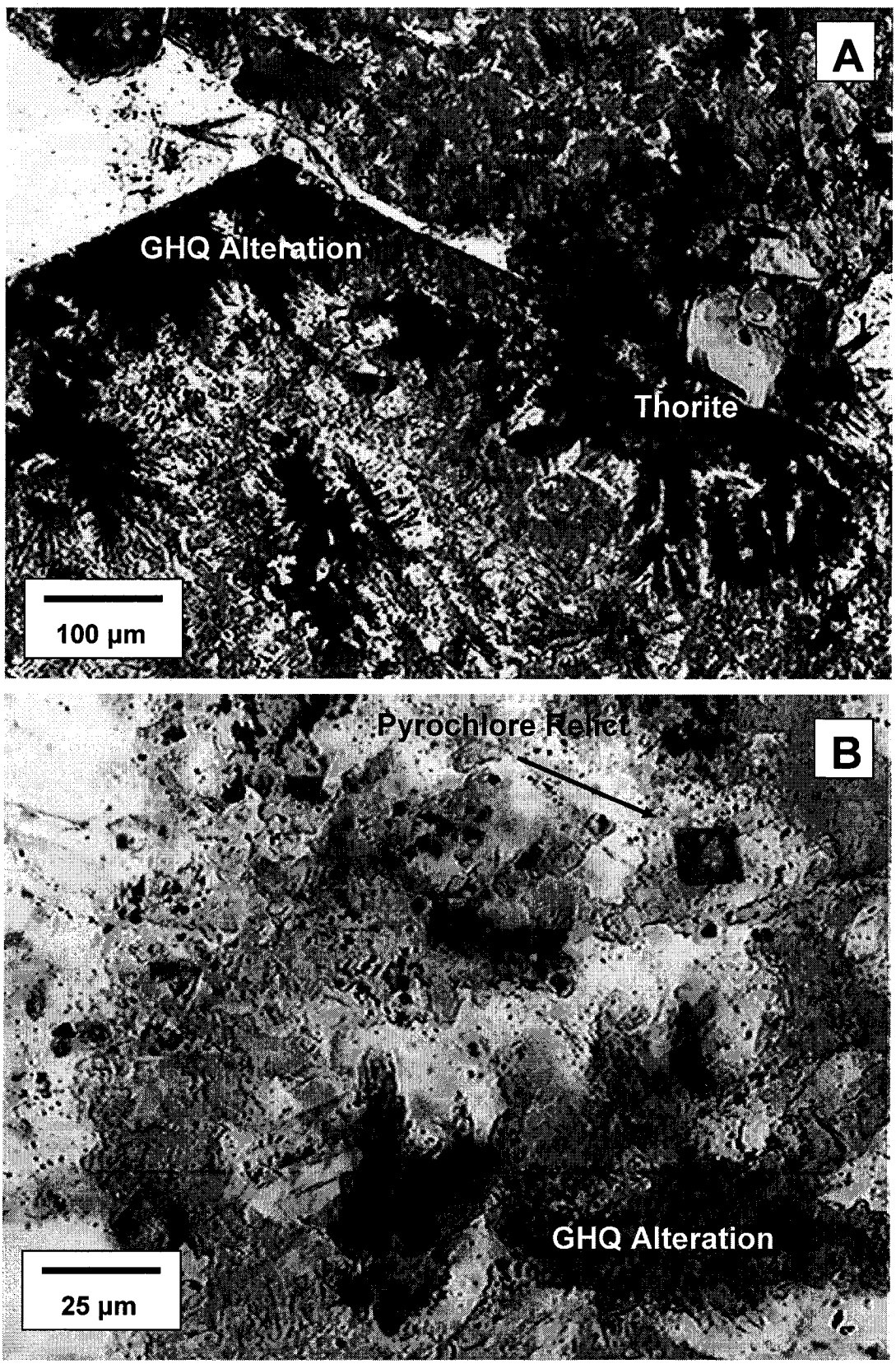
A
GHQ Alteration
Thorite
100 µm
B
Pyrochlore Relict
GHQ Alteration
25 µm

Replacement of arfvedsonite (magmatic) and aegirine (high temperature alteration) by low temperature, GHQ alteration can be represented by the following reactions:

$$2\ Na_3Fe_4^{2+}Fe^{3+}Si_8O_{22}(OH)_2 + 2\ Ca^{2+} + 2\ Zr^{4+} + 1\ H_2O + 2\ O_2 \leftrightarrow$$
$$2\ CaZrSi_2O_7 + 12\ SiO_2 + 5\ Fe_2O_3 + 6\ Na^+ + 6\ H^+ \qquad \textbf{(5)}$$

$$2\ Arfvedsonite + 2\ Ca^{2+}_{(aq)} + 2\ Zr^{4+}_{(aq)} + 1\ H_2O + 2\ O_{2(gas)} \leftrightarrow$$
$$2\ Gittinsite + 12\ Quartz + 5\ Hematite + 6\ Na^+_{(aq)} + 6\ H^+_{(aq)}$$

$$2\ NaFe^{3+}Si_2O_6 + Ca^{2+} + Zr^{4+} + 2\ H_2O \leftrightarrow$$
$$CaZrSi_2O_7 + 2\ SiO_2 + Fe_2O_3 + 2\ Na^+ + 4\ H^+ \qquad \textbf{(6)}$$

$$2\ Aegirine + Ca^{2+}_{(aq)} + Zr^{4+}_{(aq)} + 2\ H_2O \leftrightarrow$$
$$Gittinsite + 2\ Quartz + Hematite + 2\ Na^+_{(aq)} + 4\ H^+_{(aq)}$$

Reactions 5 and 6 are balanced for mass and charge, and the sums of the molar volumes of the solid reactants (281.74 cm^3/mole for reaction 5, and 130.1 cm^3/mole for reaction 6) are smaller than the sums of the molar volumes of the products (292.97 cm^3/mole and 157.01 cm^3/mole, for reactions 5 and 6, respectively). As there is no evidence of dilation, this requires that some components (e.g., SiO_2) were likely removed during replacement. Mobilization of SiO_2 during low-temperature alteration is indicated by the occurrence of silicification and quartz veins, which postdate and cross-cut GHQ alteration (see below).

Quartz-Fluorite Alteration: Purple fluorite and quartz occur in silicified rocks, infilling void space and interstices between GHQ alteration minerals, and in quartz + fluorite ± carbonate ± sulfide veins that cut GHQ alteration. In some samples, fluorite occurs with the GHQ assemblage, suggesting that, at least in places, it is part of the GHQ alteration assemblage. Most occurrences of fluorite and quartz (either as silicification or veins), however, partially replace or cross-

cut GHQ alteration minerals, indicating that fluorite and quartz precipitation continued after GHQ alteration ceased.

Most late, cross-cutting veins and veinlets comprise quartz and fluorite. In places, however, veins contain calcite and galena, which were the only occurrences of these minerals observed during this study. Quartz-fluorite alteration was not identified as a separate event by Salvi and Williams-Jones (1990; 1996), however, the cross-cutting nature of the veins and silicification of GHQ alteration indicate this mineralization represents a separate, later event.

Mineral Chemistry

A listing of the samples, rock types and the minerals analyzed using LA-ICPMS are presented in Table 6-5. The samples were selected because they include examples of least altered rocks as well as examples of high and low temperature alteration.

Table 6-5. Samples used for LA-ICPMS analyses

Sample Number	Rock Type	Mineral Analyzed
46S-3a	Hypersolvus granite with pegmatite vein	Arfvedsonite, Aegirine
56A-1a	Porphyritic hypersolvus granite	Arfvedsonite, Aegirine
SL-Ab	Hematized coarse pegmatite	Gittinsite (after Arfvedsonite or Aegirine)
SL1-12a	Hematized pegmatite	Gittinsite (after Elpidite), Thorite, Pyrochlore, Arfvedsonite, Aegirine
TTR-26	Subsolvus granite	Arfvedsonite, Aegirine
SL-Cb	Hematized subsolvus granite and pegmatite	Arfvedsonite, Aegirine, Gittinsite (after Arfvedsonite or Aegirine)

Magmatic Arfvedsonite: The compositions of primary, magmatic arfvedsonite and secondary, hydrothermal aegirine (high temperature alteration) from hypersolvus and subsolvus granites and a pegmatite hosted by subsolvus granite were determined using LA-ICPMS and are presented in Table 6-6. Arfvedsonite

that is hosted by subsolvus granite and pegmatite has similar composition, which differs from the composition of arfvedsonite hosted by hypersolvus granite. The concentrations of Li, Na and Si are consistently higher, and B, Mg, K, V, Mn, Fe, Zn, As, Ba, W, Pb and Th are consistently lower in arfvedsonite hosted by subsolvus granite and pegmatite than in hypersolvus granite. The remaining elements are either present in comparable concentrations or show no systematic difference in concentration for the different types of granite and pegmatite host.

Chondrite-normalized REE patterns for arfvedsonite in hypersolvus granite vary among samples. Concentrations range from approximately 1 to 400 times chondrite and the patterns vary from MREE depleted, with negative Ce and Eu, and positive Y anomalies to heavy REE enriched, with positive Ce, and negative Eu and Y anomalies (Figs. 6-7a and b). The concentrations of REE in arfvedsonite in pegmatite (Fig. 6-7c) range from approximately 0.7 to 250 times chondrite and the pattern is light REE depleted, with negative Ce and Eu, and positive Y anomalies. Chondrite-normalized REE patterns from the pegmatite (SL-Cb) are similar to one of the samples of hypersolvus granite (46S-3a).

High Temperature Alteration: The concentrations of Li, Mg, Al, Si, K, Ca, Mn, Ni, Cu, Zn, Rb, Sr, Nb, In, Sn, La, Ce and Ta are consistently higher, and those of B, P, Ti, V, Cr, Fe, Co, Zr, Hf, W, Pb, Th and U consistently lower in aegirine-hosted in subsolvus granite and pegmatite compared to aegirine-hosted in hypersolvus granite (Table 6-6). The remaining elements are either present in comparable concentrations or show no systematic differences in concentration among the different types of granite and pegmatite.

Table 6-6. Average Arfvedsonite and Aegirine Analyses (ppm)

Sample	46S-3a		56A-1a		TTR-26	SL-Cb	
Rock Type	Hypersolvus Granite		Hypersolvus Granite		Subsolvus Granite	Pegmatite	
Mineral	Arfvedsonite	Aegirine	Arfvedsonite	Aegirine	Arfvedsonite	Arfvedsonite	Aegirine
n	4	4	7	5	15	8	6
Li	591	21.5	292	31.4	2,350	2,590	63.5
Be	16.6	23.2	25.4	5.7	14.8	12.1	15.3
B	118	152	93.7	127	60.2	46.4	65.9
Na	64,800	95,400	65,200	98,300	72,700	70,300	97,800
Mg	4,680	848	1,700	332	1,410	683	2,500
Al	1,510	1,680	2,830	2,990	3,390	2,240	6,130
Si	272,000	271,000	267,000	264,000	307,000	311,000	305,000
P	2.0	28.6	9.7	19.2	7.0	7.8	5.6
K	20,700	619	10,500	726	8,070	7,670	1,070
Ca	2,360	1,290	3,090	1,640	2,930	2,690	3,000
Sc	7.9	8.5	11.9	13.2	7.4	4.2	2.8
Ti	1,700	7,770	6,220	6,500	5,650	5,420	4,980
V	0.8	2.3	4.6	4.0	0.6	0.5	0.1
Cr	0.4	1.2	2.6	1.1	0.2	0.4	0.6
Mn	21,300	1,620	5,970	1,680	4,080	3,940	2,140
Fe	192,000	205,000	225,000	212,000	152,000	151,000	138,000
Co	1.1	1.0	2.7	0.6	1.3	0.4	0.1
Ni	< DL	1.1	3.5	0.7	1.0	0.5	2.4
Cu	1.1	3.4	5.1	12.4	3.6	3.6	6.0
Zn	9,350	1,570	4,100	1,450	3,290	3,680	1,920
As	127	30.8	2.7	3.1	0.5	0.5	3.2
Rb	35.4	17.8	35.6	2.7	40.0	45.7	42.5
Sr	2.2	1.1	3.2	0.6	2.6	1.4	4.7
Y	9.2	22.1	138	92.3	45.0	25.8	56.7
Zr	184	1,440	1,400	2,110	1,320	1,140	998
Nb	28.1	131	83.0	169	77.9	77.0	206
Mo	0.9	0.1	0.2	0.1	0.3	0.2	0.1
Ag	0.1	0.1	0.1	0.1	0.1	0.1	0.1
Cd	0.1	0.3	1.9	1.0	1.8	2.0	1.1
In	0.9	1.4	1.9	1.9	1.5	1.2	5.2
Sn	103	171	76.8	130	79.7	111	1,040
Sb	0.1	1.0	0.1	0.2	0.1	0.1	0.1
Cs	0.1	3.8	0.2	0.1	< DL	0.1	0.2
Ba	9.8	60.8	2.2	3.0	1.1	1.1	6.3
La	1.2	2.8	88.2	31.2	7.0	1.7	14.4
Ce	3.0	12.7	41.8	39.4	12.2	2.7	19.3
Pr	0.3	0.9	8.0	9.0	2.7	0.5	3.4
Nd	1.6	4.5	31.6	41.5	11.5	2.0	12.6
Sm	0.8	2.4	9.9	9.7	3.0	0.6	3.2
Eu	0.1	0.3	0.5	0.7	0.1	0.1	0.1
Gd	1.1	3.5	17.2	10.2	2.5	0.7	3.5
Tb	0.3	0.8	1.7	2.8	0.6	0.2	0.9
Dy	1.9	5.6	13.3	17.2	6.2	2.8	7.2
Ho	0.5	1.6	4.3	5.1	2.1	1.3	2.0
Er	4.4	6.2	17.2	19.7	11.5	8.5	7.6
Tm	2.6	2.0	4.3	5.2	3.8	2.9	1.7
Yb	47.1	38.5	52.0	73.3	49.2	38.4	20.6
Lu	10.1	12.1	11.4	15.8	11.3	8.7	4.7
Hf	6.7	65.9	61.4	66.2	56.9	56.9	38.2
Ta	0.5	3.9	1.8	5.8	0.9	1.1	8.9
W	0.3	11.2	0.2	0.4	0.1	0.1	0.1
Au	< DL	< DL	< DL	< DL	< DL	< DL	< DL
Tl	0.1	3.1	0.8	0.4	0.1	0.4	0.8
Pb	21.2	117	26.9	43.4	13.2	9.3	6.7
Bi	0.1	0.1	0.3	1.4	0.1	0.2	0.2
Th	5.1	26.4	7.9	30.1	0.2	0.1	0.7
U	2.0	7.8	1.3	5.3	0.7	1.4	2.3

Aegirine in hypersolvus granite has consistently lower Li, Mg, K, Ca, Mn and Zn, higher Na, Pb, Th and U, and similar Al, Si and Fe concentrations than the magmatic arfvedsonite it has replaced (Fig. 6-8). Arsenic concentrations in aegirine exhibit non-systematic behavior, and are higher in one sample of hypersolvus granite and lower in another, relative to arfvedsonite. The composition of arfvedsonite and aegirine also vary among granite and pegmatite (Fig. 6-8). In the pegmatite, aegirine has lower Li, K, Mn, Zn and Pb, higher Na, Mg, Al, As, Th and U, and similar Si, Ca and Fe concentrations that arfvedsonite.

The distributions in the concentrations of HFSE and Be in arfvedsonite and aegirine also vary with rock type. In hypersolvus granite, HFSE concentrations (Sc, Ti, V, Y, Zr, Nb, Hf and Ta) in aegirine are typically similar to or greater than those in arfvedsonite (Fig. 6-9a and b). Only Be concentrations in arfvedsonite and aegirine exhibited non-systematic behavior among different samples of hypersolvus granite. In the pegmatite, the concentrations of the majority of HFSE were either similar (Be, Ti and Zr) or greater (Y, Nb and Ta) in aegirine than in arfvedsonite (Fig. 6-9c). The concentrations of Sc, V and Hf were lower in aegirine than in arfvedsonite.

The concentrations of light and middle REE in aegirine in samples of granite are either similar to (Fig. 6-7a) or greater than those in arfvedsonite (Fig. 6-7b). Increases in light and middle REE in aegirine ranged from approximately 5 to 10 times the concentrations in arfvedsonite from the same samples. In the pegmatite, the concentrations of heavy REE in aegirine are lower (approximately 3 times) than in arfvedsonite (Fig. 6-7c).

Petrographic evidence and mineral reactions (e.g., reaction 3) suggest that replacement of arfvedsonite by aegirine approximately conserved volume. This volume for volume replacement indicates that the observed differences in elemental concentrations between unaltered and altered samples approximately reflect the elemental enrichments or depletions that resulted from the high temperature alteration. The differences in the compositions of aegirine and arfvedsonite generally correspond with the changes in whole rock composition reported by Salvi and Williams-Jones (1996) as having resulted from the high

temperature alteration, which indicates that these differences do indeed reflect elemental depletions/enrichments (see below).

Low Temperature Alteration: The composition of aegirine, altered aegirine, gittinsite (after aegirine or elpidite), thorite, and pyrochlore in pegmatites, determined using LA-ICPMS, are presented in Table 6-7. Due to the indiscrete boundaries between mineral phases in partially altered aegirine and the inability to conduct discrete analysis of small mineral inclusions, the analyses in Table 6-7 may represent mixtures of minerals. Low temperature alteration of aegirine varied from minor replacement along fractures to pervasive replacement by the GHQ assemblage. Analysis of minor alteration zones along fractures resulted in complex, time-resolved spectra (e.g., Fig. 6-10) from which integration regions were selected that best represent each of the individual mineral phases (i.e., aegirine, altered aegirine). Similarly, small (< 50 μm) mineral inclusions within aegirine (i.e., pyrochlore) could not be sampled independently from the host mineral during LA-ICPMS analysis. Despite the limitations posed by LA-ICPMS analyses of fine mineral intergrowths, it is apparent from petrographic observations, spectral data for alteration along fractures (Fig. 6-10) and compositional data for more pervasive GHQ alteration (Table 6-7) that aegirine was replaced during low temperature alteration by a zirconosilicate mineral with a stoichiometry comparable to that of gittinsite.

Figure 6-7. Chondrite-normalized REE patterns – arfvedsonite and aegirine.

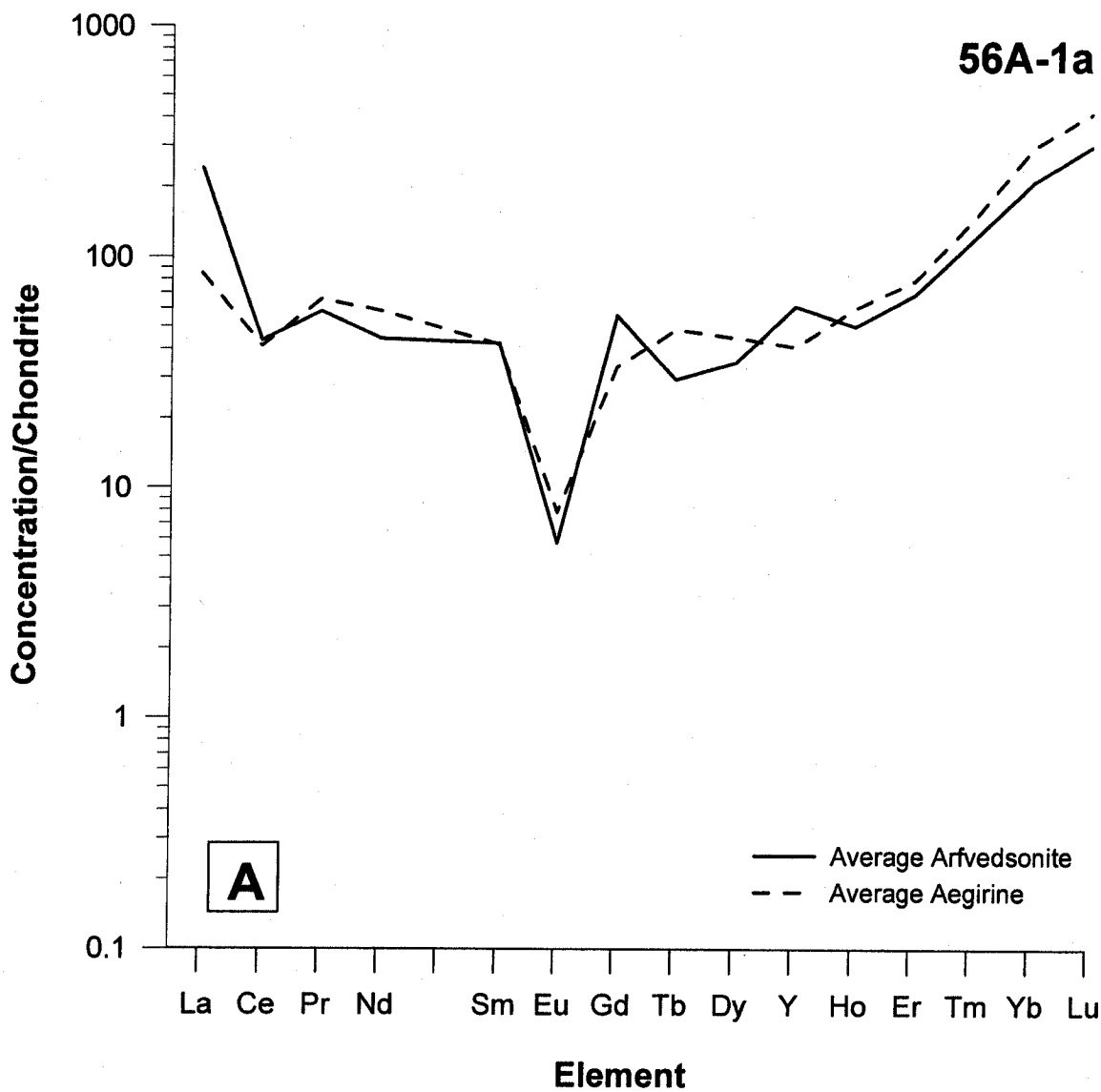
56A-1a
1000
100
10
1
0.1
Concentration/Chondrite
A
Average Arfvedsonite
Average Aegirine
La Ce Pr Nd Sm Eu Gd Tb Dy Y Ho Er Tm Yb Lu
Element

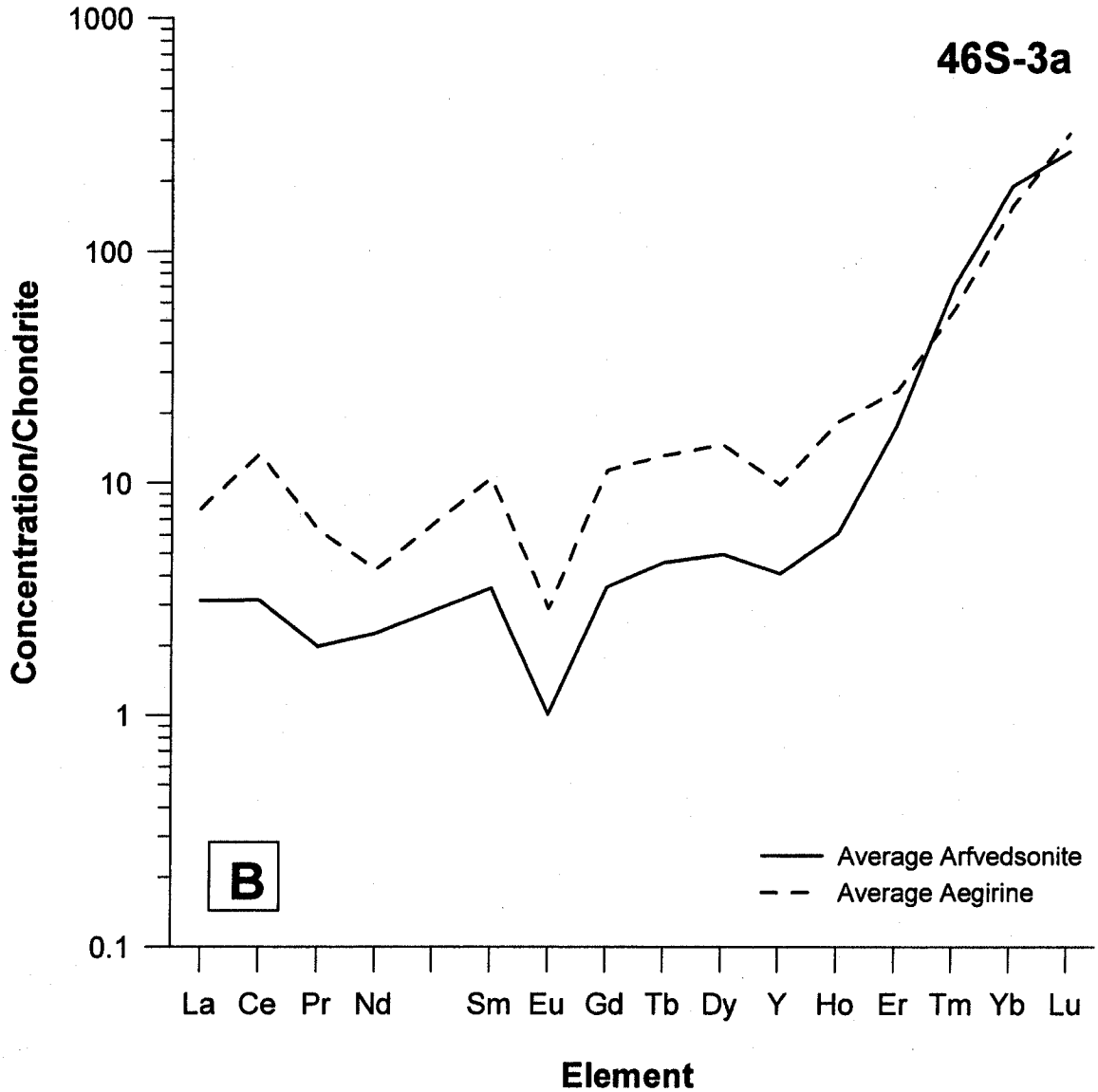
46S-3a
1000
100
10
1
0.1
Concentration/Chondrite
B
Average Arfvedsonite
Average Aegirine
La Ce Pr Nd Sm Eu Gd Tb Dy Y Ho Er Tm Yb Lu
Element

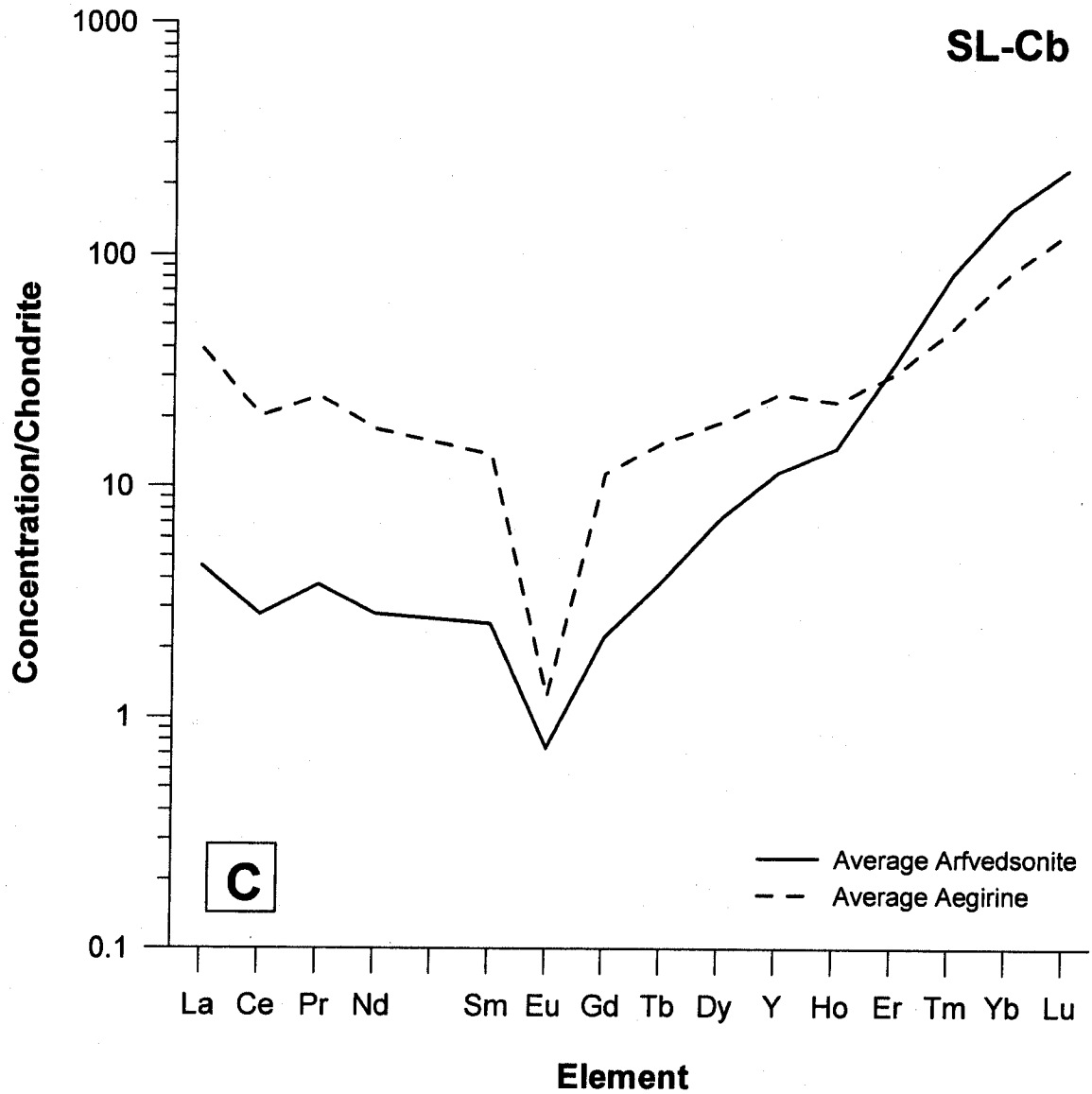
SL-Cb
1000
100
10
1
0.1
Concentration/Chondrite
C
Average Arfvedsonite
Average Aegirine
La Ce Pr Nd Sm Eu Gd Tb Dy Y Ho Er Tm Yb Lu
Element

Figure 6-8. Major element concentrations – aegirine/arfvedsonite.

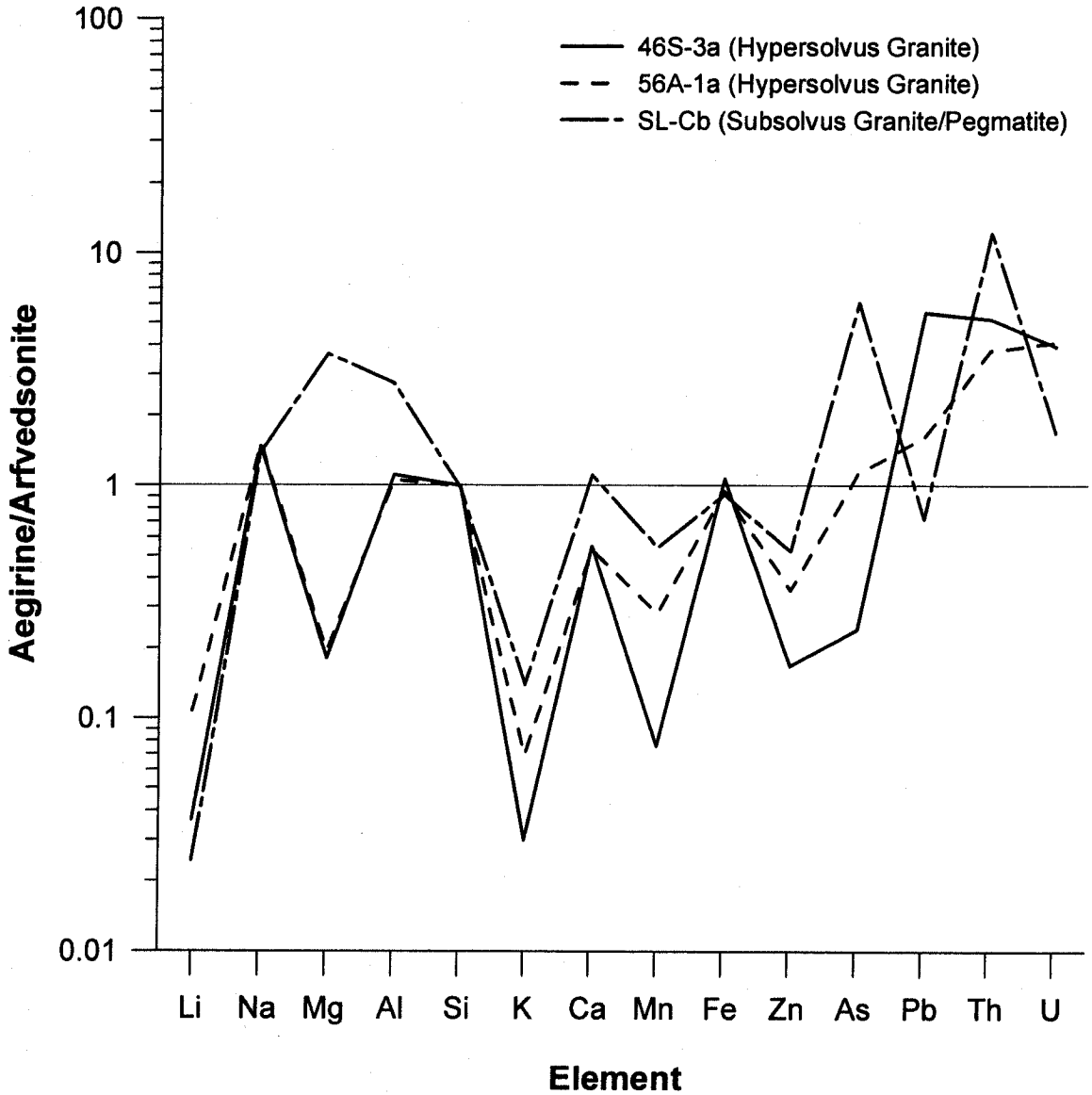
46S-3a (Hypersolvus Granite)
56A-1a (Hypersolvus Granite)
SL-Cb (Subsolvus Granite/Pegmatite)
100
10
1
0.1
0.01
Aegirine/Arfvedsonite
Li
Na
Mg
Al
Si
K
Ca
Mn
Fe
Zn
As
Pb
Th
U
Element

Figure 6-9. Be and HFSE – arfvedsonite and aegirine.

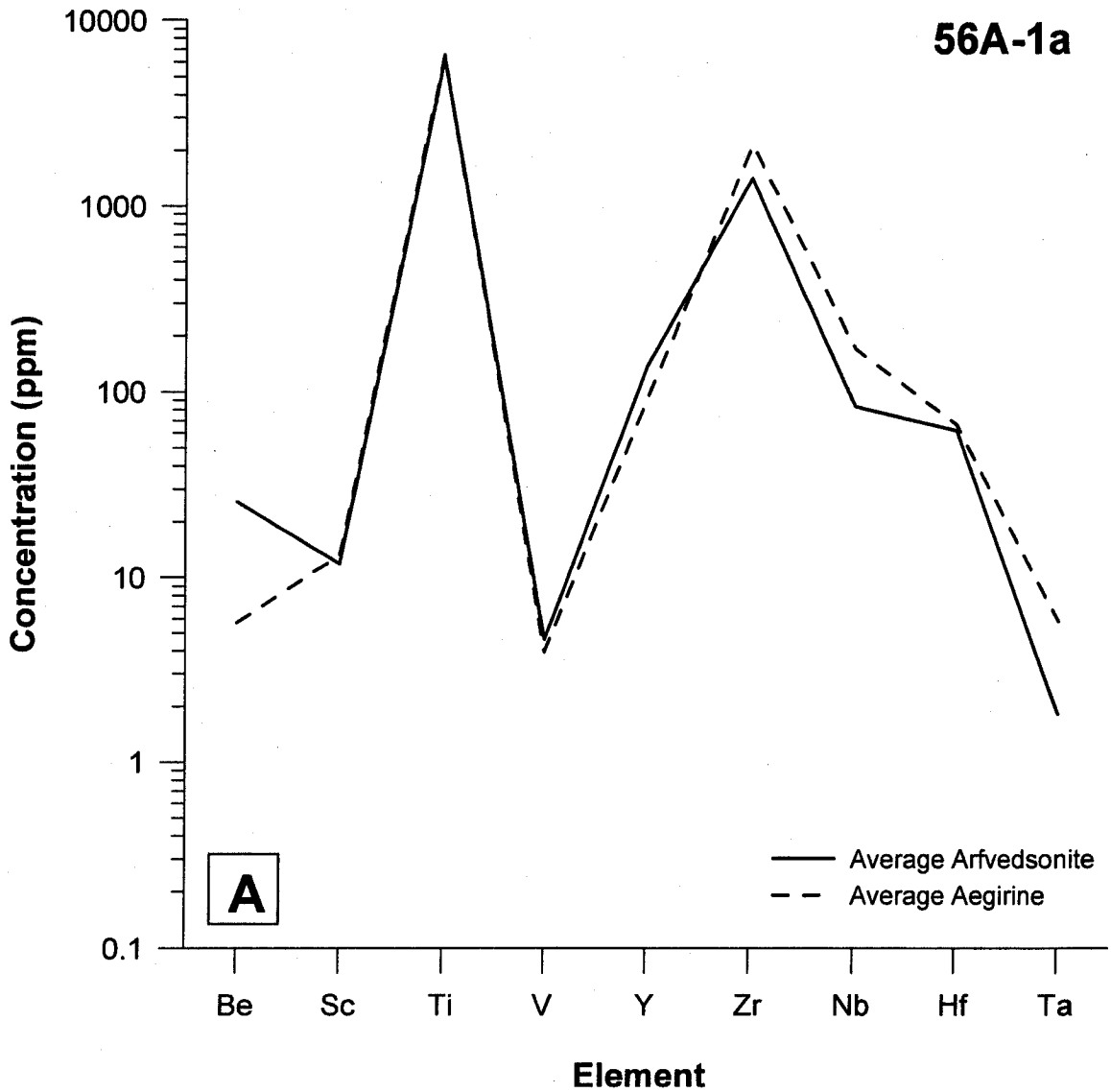
56A-1a
10000
1000
100
10
1
0.1
Concentration (ppm)
A
Average Arfvedsonite
Average Aegirine
Be
Sc
Ti
V
Y
Zr
Nb
Hf
Ta
Element

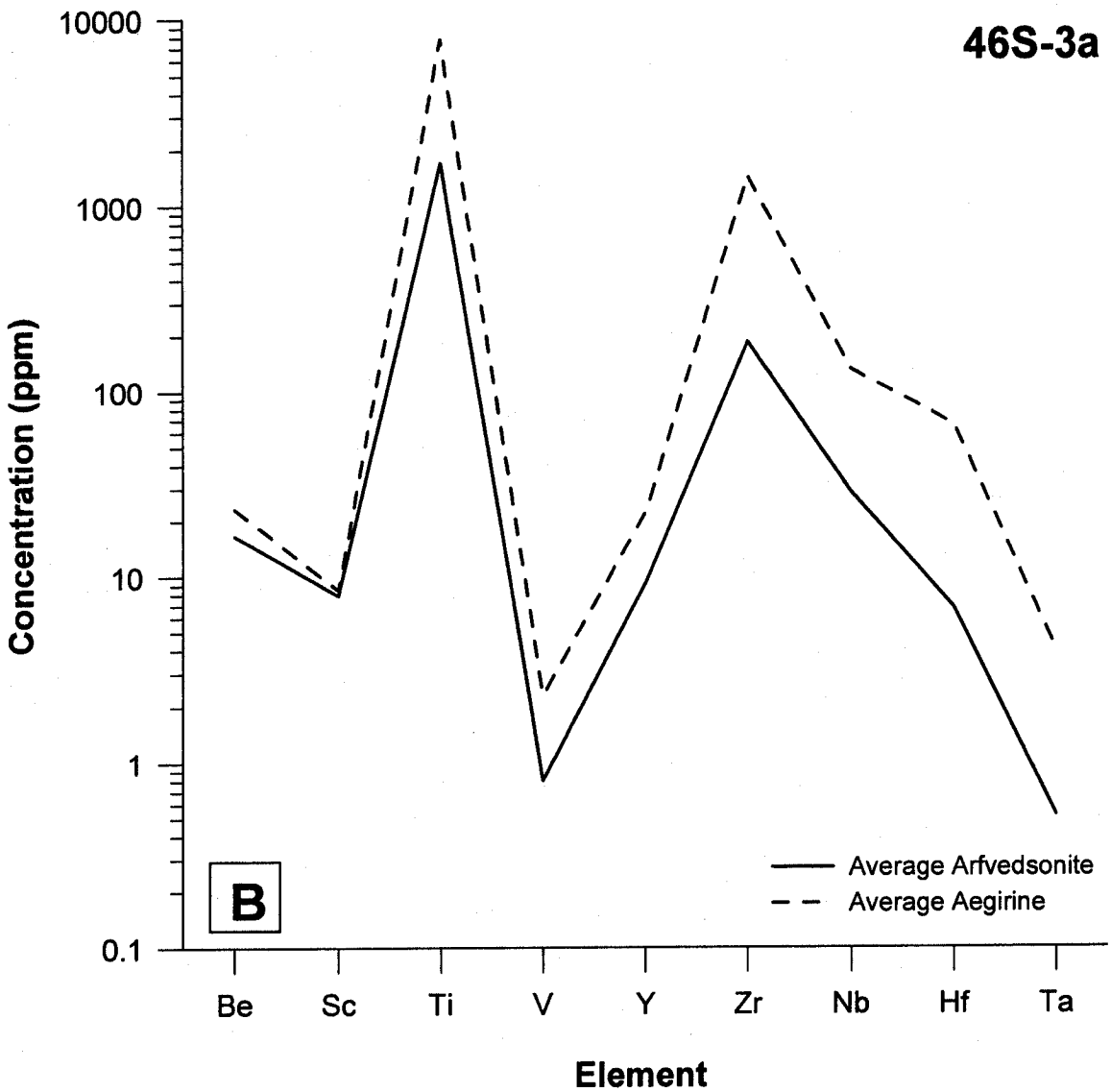
46S-3a
10000
1000
100
10
1
0.1
Concentration (ppm)
B
Average Arfvedsonite
Average Aegirine
Be
Sc
Ti
V
Y
Zr
Nb
Hf
Ta
Element

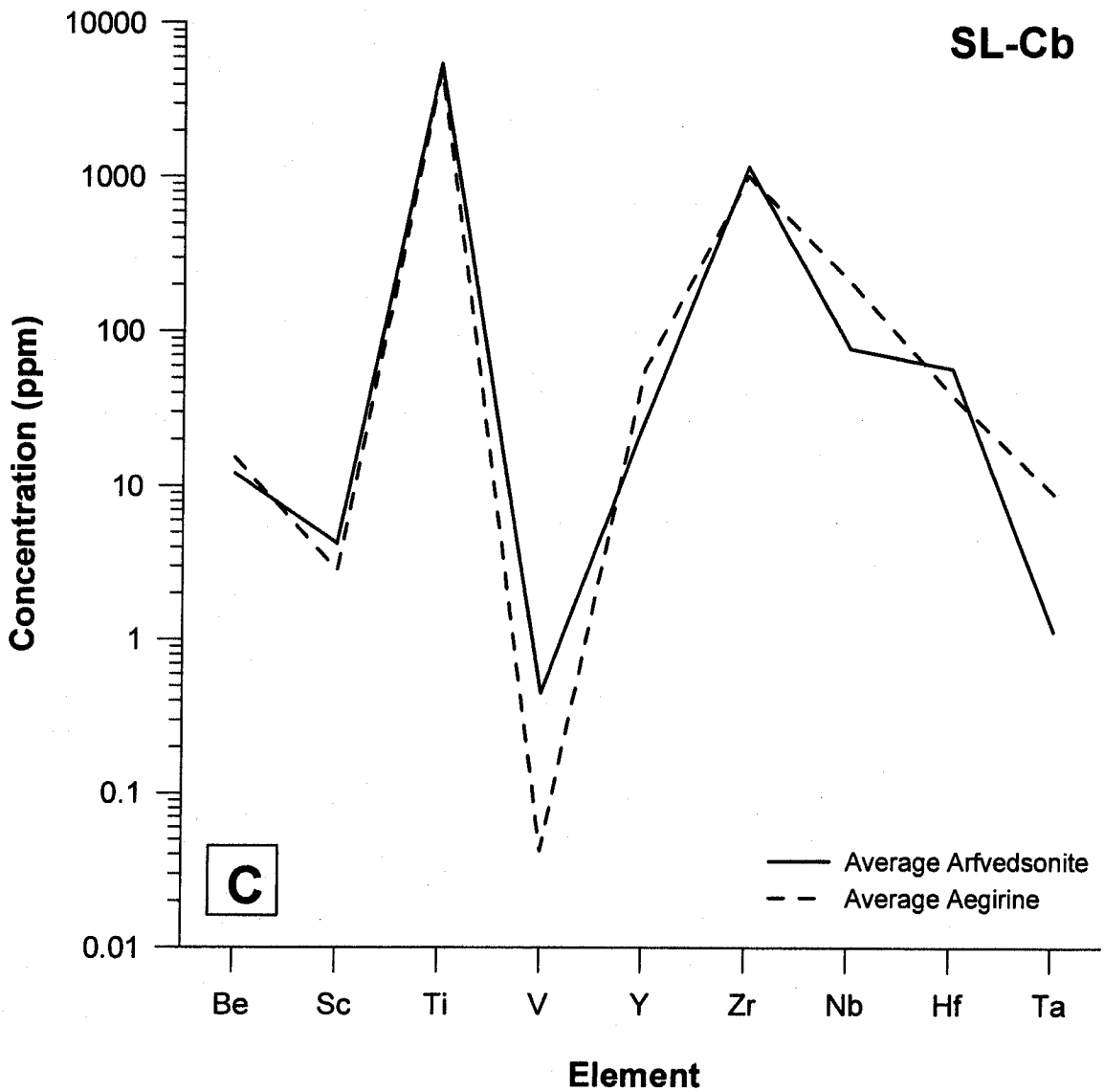
SL-Cb
10000
1000
100
10
1
0.1
0.01
Concentration (ppm)
C
Average Arfvedsonite
Average Aegirine
Be
Sc
Ti
V
Y
Zr
Nb
Hf
Ta
Element

Figure 6-10. Time-resolved analysis and photomicrograph of laser traverses – partial replacement of aegirine by GHQ alteration assemblage.

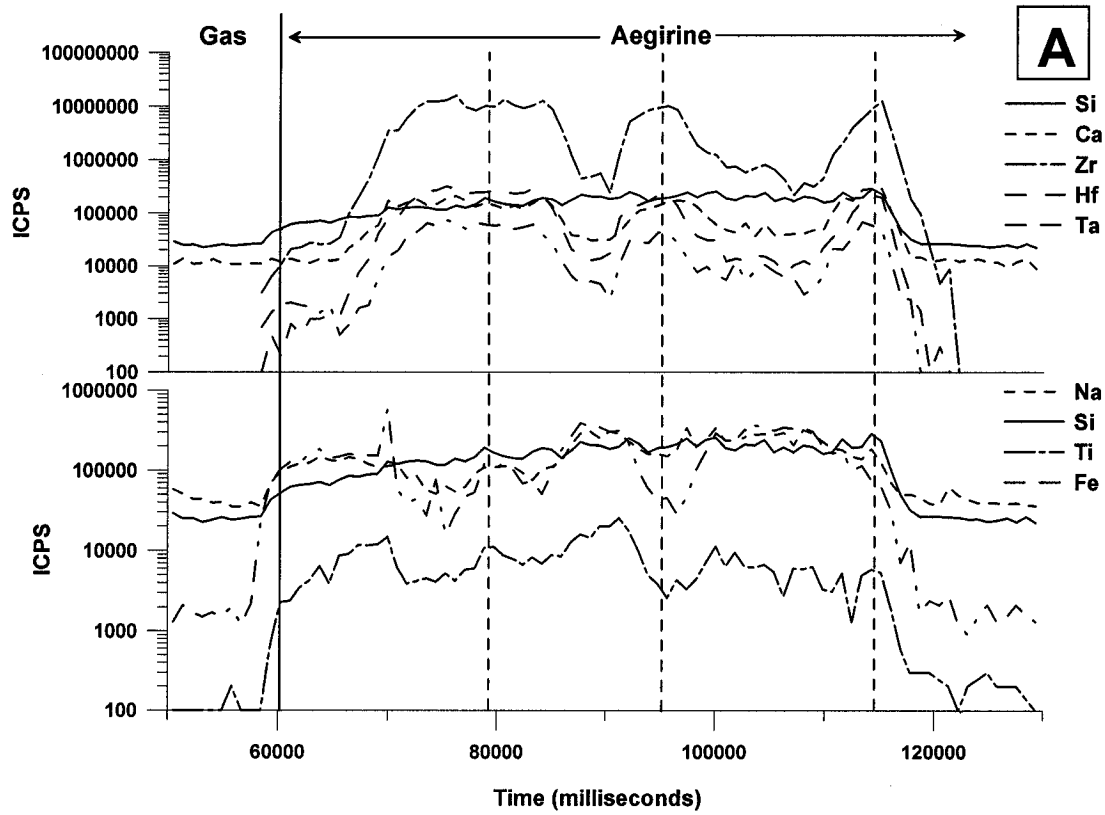
A
Gas
Aegirine
ICPS
100000000
10000000
1000000
100000
10000
1000
100
Si
Ca
Zr
Hf
Ta
ICPS
1000000
100000
10000
1000
100
Na
Si
Ti
Fe
60000
80000
100000
120000
Time (milliseconds)

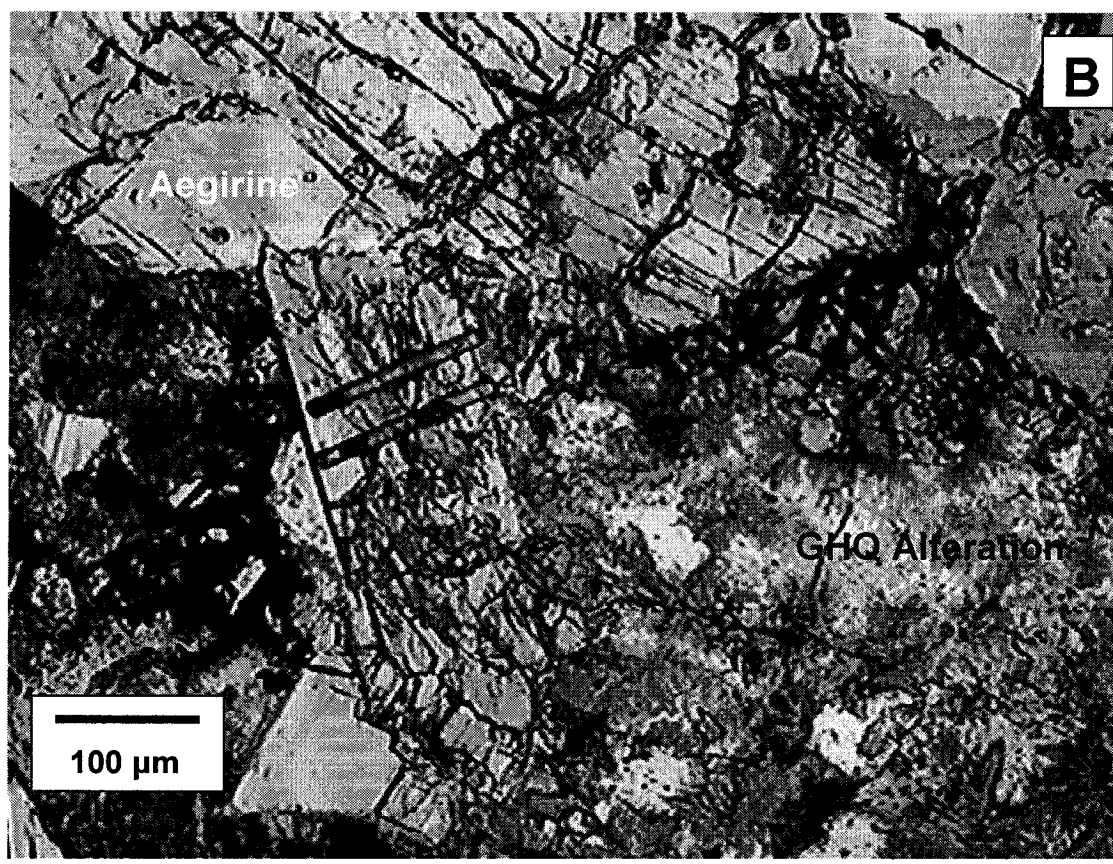
B
Aegirine
GHQ Alteration
100 µm

Aegirine that has been altered along fractures has a composition intermediate between aegirine (e.g., higher Fe and Na and lower Ca and Zr) and the varieties of gittinsite that pseudomorphed elpidite and pervasively replaced aegirine (i.e., GHQ alteration). Therefore, the LA-ICPMS analyses reflect incomplete replacement of aegirine by gittinsite (i.e., they are mineral mixtures). The composition of gittinsite after elpidite and in pervasive GHQ alteration has a composition closer to the stoichiometry of 'ideal' gittinsite ($CaZrSi_2O_7$). Aegirine that has been altered along fractures has higher average concentrations of Li, Be, B, Mg, Al, P, K, Ca, Sc, Cr, Mn, Co, Cu, As, Rb, Sr, Y, Zr, Nb, Ag, Cd, Sb, Cs, Ba, REE, Hf, Ta, W, Pb, Th and U, lower Na, Si, Ti, V, Fe and Zn, and similar Mo, In, Sn, Au, Tl and Bi than unaltered aegirine,. Altered aegirine also has higher average concentrations of Li, Be, B, Mg, Ti, Fe, Cu, Zn, Y, Nb, Sb, REE, Ta and W, lower P, K, Sc, V, Cr, Mn, Ni, As, Rb, Sr, Hf, Tl, Pb, Th and U, and similar Na, Al, Si, Ca, Co, Zr, Mo, Ag, Cd, In, Sn, Cs, Ba, Au and Bi relative to gittinsite pseudomorphs after elpidite.

Gittinsite in pervasive GHQ alteration differs from the other two varieties and is closer in composition to 'ideal' gittinsite. This indicates that the analyses of gittinsite after elpidite or of the alteration zones along fractures in aegirine either represent mineral mixtures or that the precursor elpidite or aegirine has influenced the composition of the alteration mineral (i.e., relatively low water-rock ratios).

Table 6-7. Average 'Exotic', Aegirine and Alteration Mineral Analyses (ppm)

Sample	SL1-12a					SL-Ab
Rock Type	Pegmatite					Pegmatite
Mineral	Aegirine	Altered Aegirine	Gittinsite (after Elpidite)	Thorite	Pyrochlore	Gittinsite (after Aegirine)
N	2	6	2	2	4	4
Li	17.8	24.7	3.8	12.4	6.3	2.4
Be	86.0	3,000	49.7	753	7.1	13.7
B	94.8	1,180	101.8	313	48.5	54.3
Na	105,000	33,200	33,900	18,600	40,100	20,500
Mg	1,460	19,000	6,380	14,900	664	5,020
Al	2,180	5,440	4,890	10,100	337	2,330
Si	262,000	220,000	258,000	196,000	26,900	246,000
P	< DL	73.4	262	239	73.8	136
K	96.1	799.	4,690	6,170	283	1,400
Ca	2,230	73,500	80,500	33,700	22,100	131,000
Sc	5.2	8.4	21.2	< DL	< DL	23.8
Ti	3,560	1,770	131	1,050	16,900	303
V	8.3	2.1	11.0	< DL	< DL	6.2
Cr	< DL	5.0	13.3	< DL	3.0	8.9
Mn	2,050	5,120	11,100	7,430	363	2,020
Fe	206,000	48,200	5,850	47,200	10,600	2,780
Co	< DL	0.9	0.8	161	1.1	1.4
Ni	< DL	< DL	127	< DL	< DL	45.5
Cu	18.0	54.3	20.2	1,070	7.5	6.9
Zn	3,870	2,800	437	1,380	295	214
As	16.2	282	448	581	36.0	301
Rb	5.0	14.8	150	157	3.1	16.4
Sr	3.1	230	369	577	442	114
Y	1,270	51,100	8,770	45,600	390	1,890
Zr	2,240	91,800	152,000	3,240	1,480	169,000
Nb	123	4,430	551	6,570	469,000	232
Mo	1.0	0.7	< DL	0.3	5.1	0.3
Ag	0.3	9.2	14.0	3.2	3.6	14.0
Cd	< DL	4.2	5.6	1.2	3.1	4.1
In	7.3	7.8	9.0	1.2	3.7	2.2
Sn	1,960	1,940	2,210	329	1,050	554
Sb	0.2	6.7	3.6	24.7	2.5	1.0
Cs	0.4	1.2	1.8	3.4	0.8	0.6
Ba	13.2	343	440	965	526	168
La	27.4	1,660	211	1,920	37,800	48.8
Ce	31.2	3,020	430	14,200	91,100	63.2
Pr	11.5	650	38.9	457	8,790	9.6
Nd	53.4	3,420	149	2,040	23,700	34.6
Sm	45.6	2,520	125	1,600	2,170	10.1
Eu	4.2	187	16.7	85.8	67.8	1.0
Gd	90.3	4,190	221	3,120	602	23.2
Tb	35.5	1,410	130	1,300	50.0	13.6
Dy	354.8	10,900	1,500	12,100	183	206
Ho	81.6	2,310.	427	2,830	24.9	83.7
Er	227.2	6,300	1,850	8,120	59.9	434
Tm	38.9	955	495	1,180	6.8	110
Yb	991	6,310	4,700	6,840	41.5	1,110
Lu	21.4	599	485	575	5.2	146
Hf	60.2	1,790	2,870	90.0	29.5	4,580
Ta	17.1	121	85.9	147	16,300	60.1
W	0.5	4.0	0.6	23.1	113	0.3
Au	< DL	0.2	0.1	0.1	7.1	0.2
Tl	< DL	0.3	1.4	0.7	0.3	0.2
Pb	31.1	1,100	2,300	4,030	1,270	242
Bi	< DL	0.1	< DL	< DL	0.1	< DL
Th	0.1	14.0	253	205,000	33.4	12.5
U	6.0	286	443	2,120	2,570	89.7

Figure 6-11. Major element concentrations - low temperature alteration/aegirine.

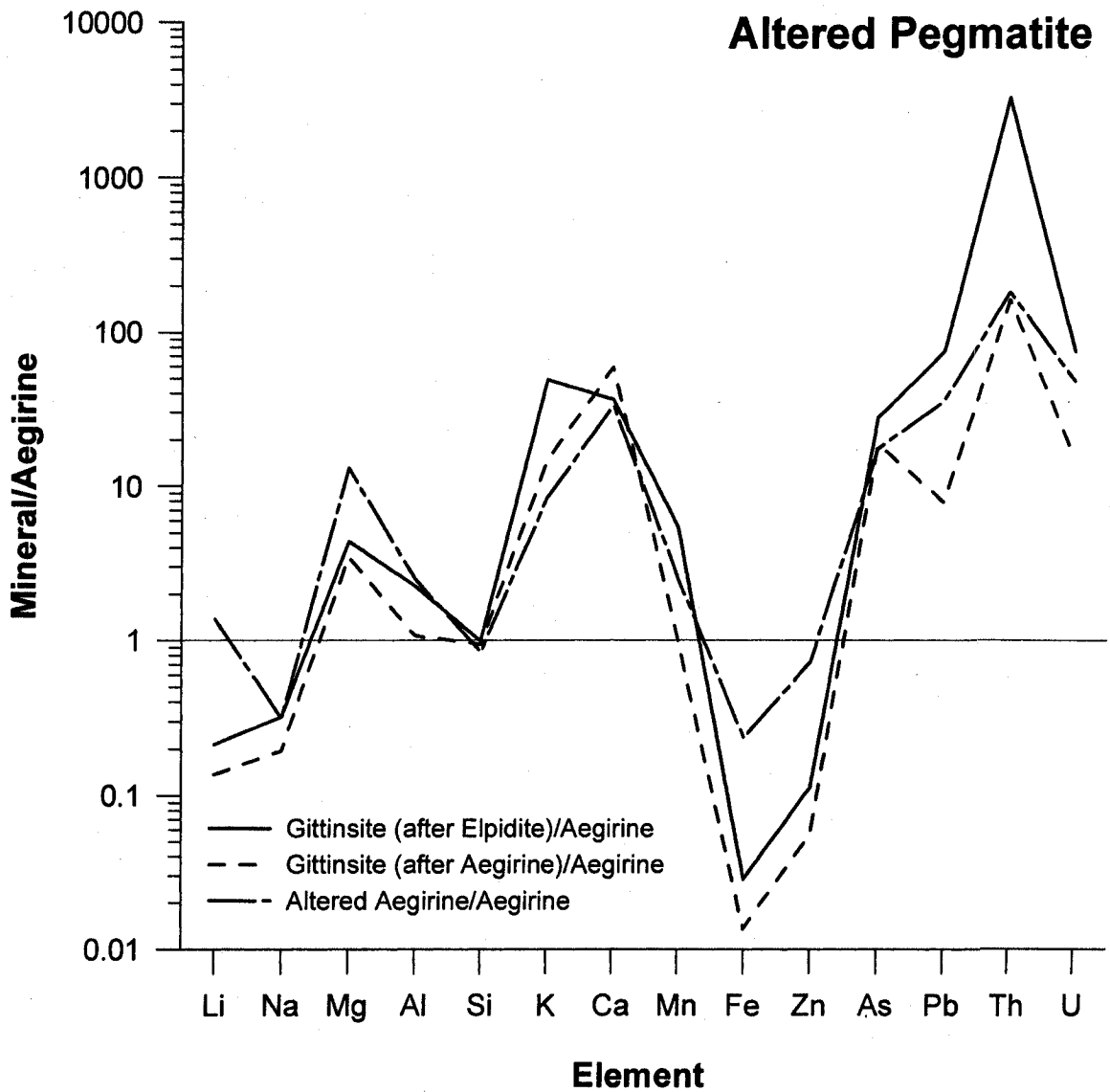
Altered Pegmatite
10000
1000
100
10
1
0.1
0.01
Mineral/Aegirine
Gittinsite (after Elpidite)/Aegirine
Gittinsite (after Aegirine)/Aegirine
Altered Aegirine/Aegirine
Li
Na
Mg
Al
Si
K
Ca
Mn
Fe
Zn
As
Pb
Th
U
Element

Figure 6-12. Be and HFSE – low temperature alteration/aegirine.

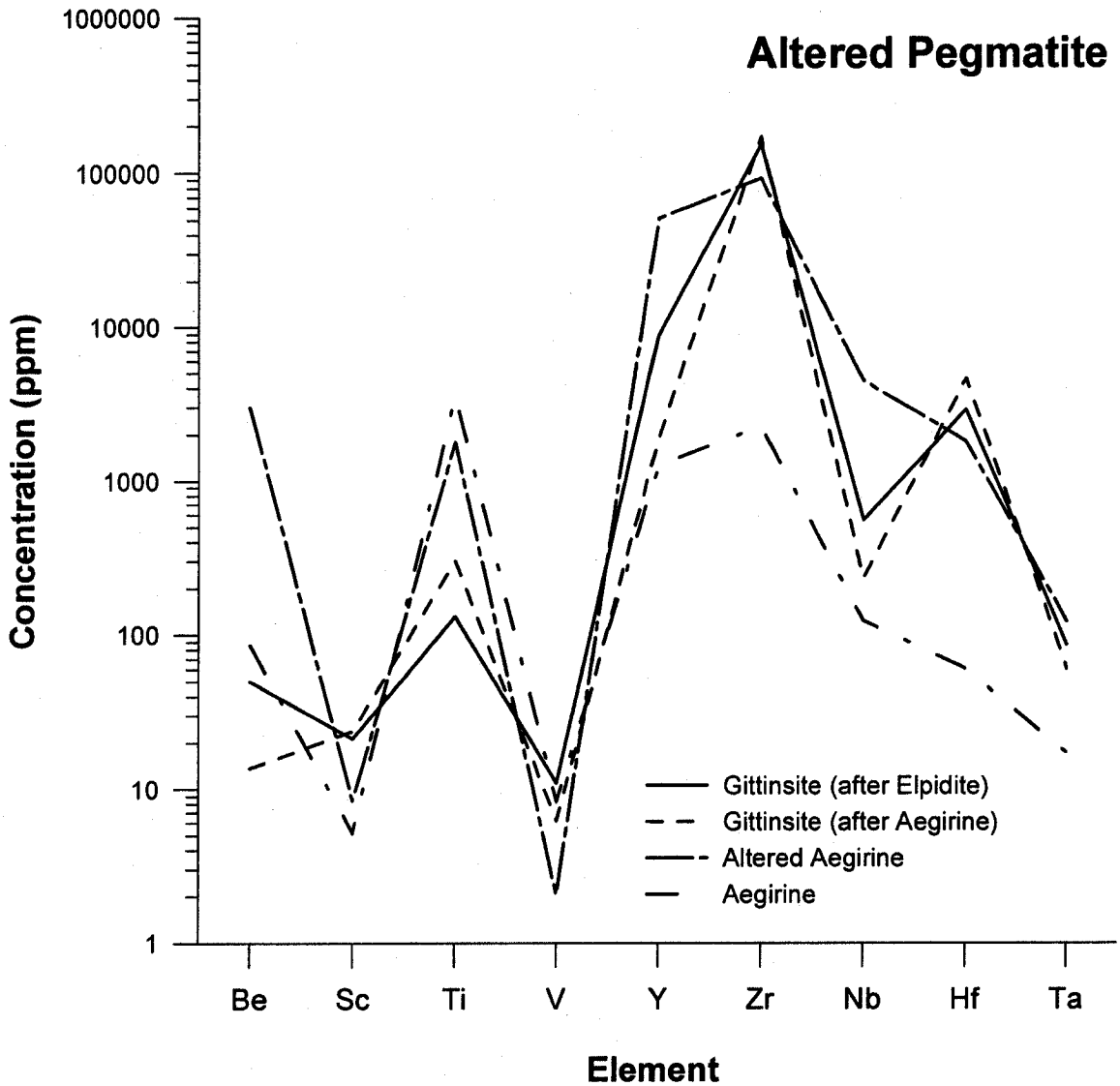
Altered Pegmatite
1000000
100000
10000
1000
100
10
1
Concentration (ppm)
Be
Sc
Ti
V
Y
Zr
Nb
Hf
Ta
Element
Gittinsite (after Elpidite)
Gittinsite (after Aegirine)
Altered Aegirine
Aegirine

The major element compositions of altered aegirine (i.e., GHQ alteration) and gittinsite (after elpidite) from different samples are closer than the compositions of altered aegirine and gittinsite (after aegirine) from different samples. In contrast, the differences in HFSE concentrations between altered aegirine and aegirine from the same rock, altered aegirine from different rocks, or gittinsite (after elpidite) tend to be more non-systematic (Fig. 6-11 and 6-12). The incoherent behavior of the HFSE may reflect localized controls on gittinsite composition reflective of precursor mineral composition, elemental partitioning or complexation, water-rock ratio, etc. Despite these localized differences, consistent replacement of aegirine by the GHQ assemblage, regardless of rock type, indicates that the critical factors causing this alteration were consistent throughout all rocks affected by low temperature alteration.

Concentrations of REE in aegirine, altered aegirine, and gittinsite (GHQ alteration and after elpidite) range from approximately 10 to 20,000 times chondrite (Fig. 6-13). Chondrite-normalized REE patterns for unaltered and altered aegirine are similar, however, the concentrations in altered aegirine are approximately 100 times higher than in unaltered aegirine. Aegirine and altered aegirine have heavy REE-enriched patterns with negative Ce, Eu and Y anomalies. The chondrite-normalized REE pattern for aegirine also has a positive Yb anomaly. Gittinsite that has pseudomorphed elpidite has light REE concentrations intermediate between those of aegirine and altered aegirine and heavy REE concentrations similar to those of altered aegirine. The chondrite-normalized REE pattern for gittinsite after elpidite does not have a negative Ce anomaly, but has negative Eu and Y anomalies and a positive Yb anomaly. Gittinsite from GHQ alteration in a second pegmatite has chondrite-normalized REE patterns similar to those of unaltered aegirine (Fig 6-13). Despite pervasive alteration by gittinsite, the REE pattern is remarkably similar to that of aegirine and similarly has negative Ce and Eu anomalies and a positive Yb anomaly.

'Exotic' Minerals: The major element compositions of the 'exotic' minerals that were analyzed are summarized in Table 6-8. The table includes analyses of aegirine, altered aegirine (along fractures), gittinsite (after elpidite), thorite (from GHQ alteration with gittinsite pseudomorphs after elpidite), and pyrochlore (inclusions in aegirine after arfvedsonite).

Table 6-8. Sample SL1-12a – Average Major Element Oxide Concentrations

Element	Aegirine	Altered Aegirine	Gittinsite (after Elpidite)	Thorite	Pyrochlore
Na	**14.22**	**4.48**	**4.56**	**2.51**	**5.40**
Mg	0.24	**3.14**	**1.06**	**2.48**	0.11
Si	**56.02**	**46.97**	**55.17**	**41.87**	**5.75**
Ca	0.31	**10.28**	**11.26**	**4.71**	**3.10**
Ti	0.59	0.30	0.02	0.18	**2.82**
Mn	0.26	0.66	**1.43**	0.96	0.05
Fe	**26.56**	**6.20**	0.75	**6.07**	**1.37**
Y	0.16	**6.49**	**1.11**	**5.79**	0.05
Zr	0.30	**12.40**	**20.55**	0.44	0.20
Nb	0.02	0.56	0.07	0.83	**59.07**
La	0.00	0.20	0.02	0.23	**4.44**
Ce	0.00	0.35	0.05	**1.67**	**10.66**
Pr	0.00	0.08	0.00	0.05	**1.03**
Nd	0.01	0.40	0.02	0.24	**2.76**
Dy	0.04	**1.25**	0.17	**1.39**	0.02
Ta	0.00	0.01	0.01	0.02	**1.99**
Th	0.00	0.00	0.03	**23.32**	0.00
Sum	**98.75**	**93.76**	**96.30**	**92.73**	**98.82**

The compositions of aegirine, altered aegirine, and pyrochlore represent, to varying degrees, altered minerals or mineral mixtures. Despite this, the compositions of altered aegirine and pyrochlore are similar to the 'ideal' stoichiometric compositions.

Figure 6-13. Chondrite-normalized REE patterns – low temperature alteration.

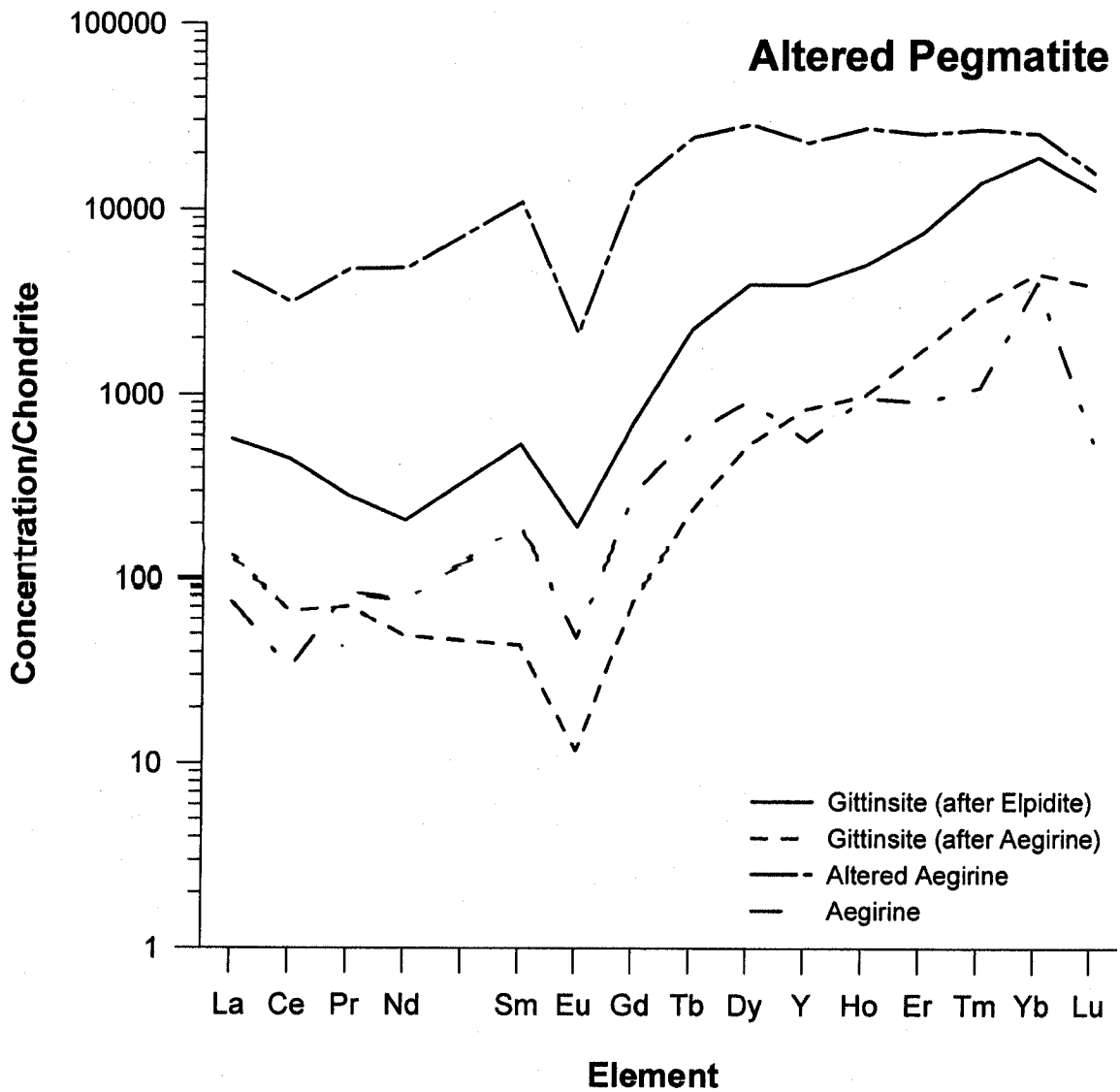
Altered Pegmatite
100000
10000
1000
100
10
1
Concentration/Chondrite
La Ce Pr Nd Sm Eu Gd Tb Dy Y Ho Er Tm Yb Lu
Element
Gittinsite (after Elpidite)
Gittinsite (after Aegirine)
Altered Aegirine
Aegirine

Figure 6-14. Chondrite-normalized REE patterns – exotic minerals.

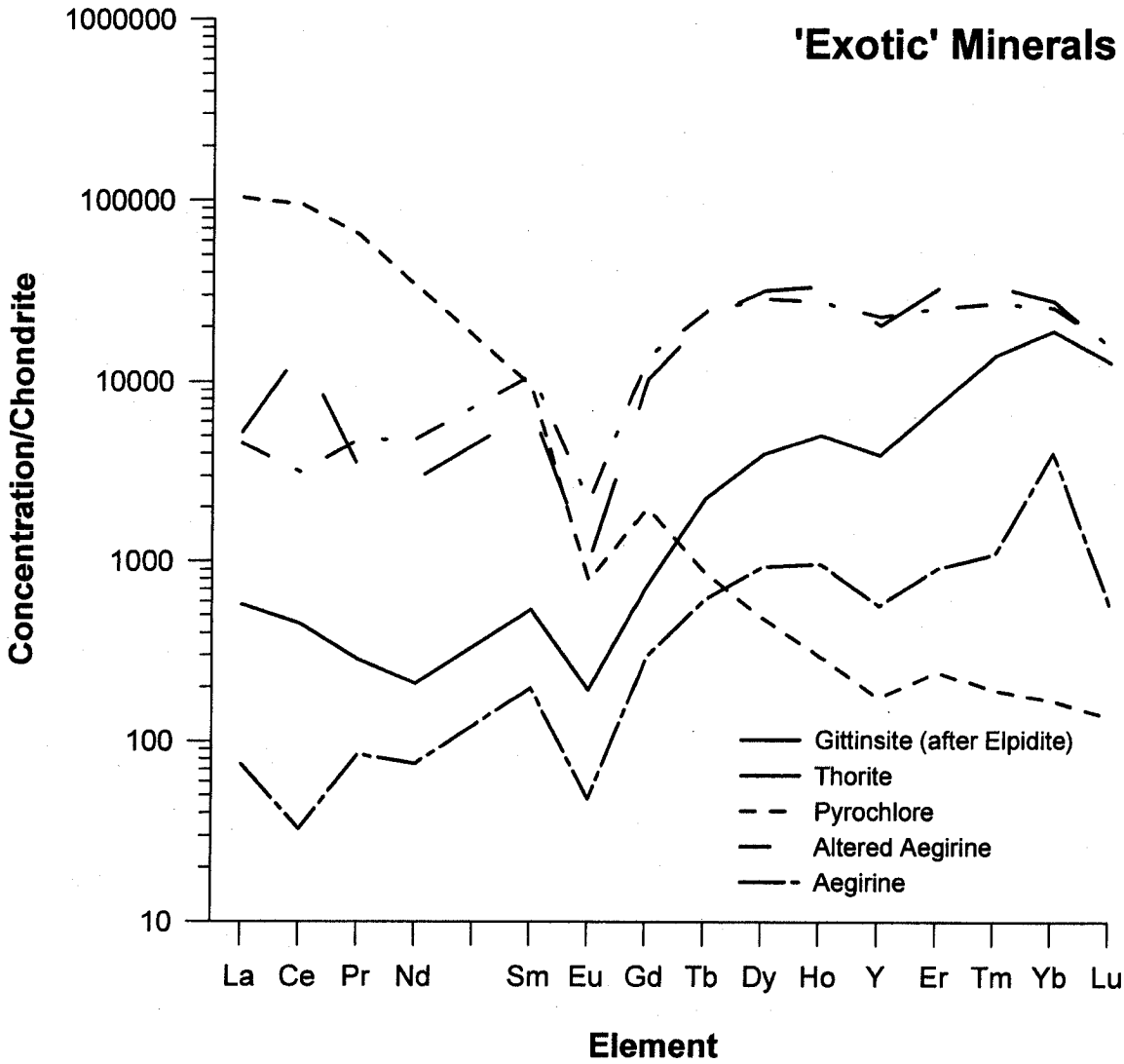
'Exotic' Minerals
1000000
100000
10000
1000
100
10
Concentration/Chondrite
La Ce Pr Nd Sm Eu Gd Tb Dy Ho Y Er Tm Yb Lu
Element
Gittinsite (after Elpidite)
Thorite
Pyrochlore
Altered Aegirine
Aegirine

On the basis of petrographic observations, low temperature alteration of aegirine and precipitation of thorite appear to have occurred contemporaneously. The REE concentrations and the chondrite-normalized patterns for thorite are nearly identical to those of altered aegirine from the same sample (Fig. 6-14). Thorite has a positive Ce anomaly and a more pronounced negative Y anomaly than altered aegirine. The similar REE concentrations and patterns (with the exception of Ce and Y) indicate that REE were not differentially partitioned into these two minerals during low temperature alteration. Pyrochlore has a very different, extremely light REE-enriched chondrite-normalized REE pattern from all of the other minerals studied. The chondrite-normalized REE pattern for pyrochlore also has negative Eu and Y anomalies but lacks Ce and Yb anomalies. Pyrochlore appears to have preferentially concentrated light REE during high temperature alteration of arfvedsonite to aegirine. Subsequent low temperature alteration of aegirine and pyrochlore to GHQ appears to have caused enrichment in the light REE in altered aegirine, resulting in similar middle REE concentrations and light REE concentrations that are intermediate between those of pyrochlore and aegirine. In general, altered aegirine has similar REE patterns and anomalies to unaltered aegirine indicating that, although alteration may have caused enrichment in most REE, significant inter-element fractionation of REE did not occur.

Discussion

Mineral Alteration

Mineralogical evidence for the hydrothermal enrichment of HFSE in excess of primary magmatic concentrations (i.e., elpidite) and the association of HFSE enrichment with hematization in the Strange Lake pluton has not been reported previously. Studies by Salvi and Williams-Jones (1990; 1992; 1995; 1996) resulted in the identification of two stages of hydrothermal alteration (high and low temperature). Mineral reactions proposed by Miller (1996) and Salvi and

Williams-Jones (1995) to explain the elevated modal abundances of zirconosilicate minerals and hematite in HFSE-enriched rocks affected by low temperature alteration (e.g., gittinsite + quartz after elpidite or armstrongite) do not explain either the association of hematization with HFSE mineralization or enrichment of HFSE in excess of magmatic concentrations.

Reevaluation of unaltered and altered rocks during this study has shown that the principal mineral reaction resulting in hematization and HFSE-enrichment during low temperature alteration was replacement of aegirine ± arfvedsonite by gittinsite + hematite + quartz (i.e., GHQ alteration). This alteration, which accompanied replacement of magmatic elpidite by hydrothermal gittinsite, was not previously identified in HFSE-mineralized rocks, and it demonstrates that HFSE mobility and enrichment by hydrothermal processes were more pervasive than previously thought. Therefore, hematization and HFSE enrichment are directly linked and the amount of HFSE enrichment is directly proportional to the degree to which the rocks have been affected by low temperature alteration, and the abundance of aegirine present in the rocks prior to alteration. Pegmatite, in which primary, coarse-grained arfvedsonite had previously been pervasively replaced by aggregations of aegirine crystals, and subsequently pervasively altered during the low temperature alteration event, shows the greatest HFSE enrichment.

The occurrence of hematization in the Strange Lake pluton is relatively widespread because it affects the majority of the rocks comprising the main lens (Miller, 1996). Whether or not the association between HFSE mineralization and hematization observed in this study applies to all hematized rocks, however, is not known. If hematization is exclusively associated with GHQ alteration, then hydrothermal enrichment of HFSE also could be more widespread than previously recognized.

Birkett and Miller (1991) and Miller (1996) concluded that all HFSE enrichment resulted from magmatic processes and secondary hydrothermal effects were insignificant. Unaltered (i.e., unhematized) rocks, however, contain modal abundances of zirconosilicates only in accessory amounts (< 5 %),

whereas rocks with higher modal abundances of zirconosilicates (up to 20 %) have been hematized. Furthermore, in hematized rocks, two types of gittinsite are present: 1) pseudomorphs after magmatic elpidite, and 2) replacements after aegirine. The abundance of pseudomorphs after elpidite in these rocks is consistent with magmatic abundances and increases in the amount of zirconosilicates resulted from replacement of minerals other than elpidite (e.g., aegirine ± arfvedsonite). The two occurrences of gittinsite also have distinctly different associations. Gittinsite alone replaced elpidite, however, gittinsite + hematite + quartz replace aegirine. It is clear from the mineral associations that hydrothermal processes caused significant increases in the HFSE content of the altered rocks through replacement of aegirine by gittinsite + hematite + quartz. The occurrence of low temperature alteration in all units comprising the pluton (including pegmatites) and the superimposition of this alteration upon an earlier, subsolidus high temperature alteration event (replacement of arfvedsonite by aegirine), clearly demonstrate the post-magmatic, hydrothermal nature of the mineralization. Although Miller (1986) observed rocks with modal abundances of up to 20 % gittinsite, neither Salvi and Williams-Jones (1990; 1995) nor this study identified gittinsite as a primary magmatic phase. Therefore, it is very doubtful that the high modal abundances reported by Miller (1986) represent primary, magmatic concentrations.

Birkett and Miller (1991) and Miller (1996) also concluded that the Strange Lake pluton did not undergo low-temperature Ca-metasomatism and HFSE mobility, and that the alteration is the result of late-stage, magmatic processes. This argument is based on the interpretation that gittinsite replaced armstrongite (both Ca zirconosilicates) rather than elpidite (Na zirconosilicate), as proposed by Salvi and Williams-Jones (1990; 1995; 1996). This study has shown that, in addition to replacement of elpidite by gittinsite, alteration of aegirine (Na pyroxene) to an assemblage of gittinsite (Ca zirconosilicate) + hematite + quartz is the predominant replacement mineral assemblage in rocks that were hematized during low temperature alteration. The textural evidence and mineral chemistry data clearly document the replacement of a Na-rich mineral (aegirine)

by a Ca-rich mineral (gittinsite) as a result of hydrothermal alteration. The fact that hematization and zirconosilicate alteration are also widespread in the pegmatitic layers of the subsolvus granite (Miller, 1996; Salvi and Williams-Jones, 1990; 1996) simply indicates that this alteration occurred on a large scale.

Mineral Chemistry versus Whole Rock Chemistry

High Temperature Alteration: Petrographic observations and mineral reactions indicate that high temperature alteration resulted in the addition of Na and water and removal of H and F from the rocks during replacement of arfvedsonite by aegirine. LA-ICPMS analyses indicate, assuming volume for volume replacement of arfvedsonite by aegirine, that Li, Mg, Al, Si, K, Ca, Mn, Ni, Cu, Zn, Rb, Sr, Nb, In, Sn, La, Ce and Ta were added, B, P, Ti, V, Cr, Fe, Co, Zr, Hf, W, Pb, Th and U were removed, and Na was approximately conserved during high temperature alteration. Whole rock analyses and mass balance calculations conducted by Salvi and Williams-Jones (1996) indicated that high temperature alteration produced no significant change in major element composition of the rocks but did cause significant HFSE depletion. The petrographic, mineral reaction, LA-ICPMS and whole rock data are in general agreement, with the following notable exceptions. The mineral reactions suggest that Na was removed from the rocks, however, the whole rock data indicate that Na was approximately conserved. Therefore, another mineral reaction may have occurred in rocks that were affected by high temperature alteration to off-set the addition of Na during alteration of arfvedsonite (e.g., loss of Na from plagioclase during alteration to sericite). The whole rock data of Salvi and Williams-Jones (1996) indicate that HFSE were depleted during high temperature alteration, however, LA-ICPMS analyses indicate that HFSE behavior was less systematic and, in many instances, these elements are higher in aegirine than arfvedsonite. Therefore, if whole rock mass balance calculations indicate that HFSE were consistently depleted in the rocks during high temperature alteration, this must have resulted from leaching of HFSE from other primary, magmatic HFSE-

bearing minerals (e.g., elpidite, gittinsite, narsarsukite, zircon, titanite, fluorite, pyrochlore).

Low Temperature Alteration: Petrographic observations and mineral reactions indicate that low temperature alteration resulted in the addition of Ca, Zr, H_2O, ± H and removal of Na, H ± F from the rocks during replacement of aegirine or arfvedsonite by GHQ alteration. LA-ICPMS analyses indicate, assuming volume for volume replacement of aegirine by gittinsite, that Li, Be, B, Mg, Al, P, K, Ca, Sc, Cr, Mn, Co, Cu, As, Rb, Sr, Y, Zr, Nb, Ag, Cd, Sb, Cs, Ba, REE, Hf, Ta, W, Pb, Th and U were added, Na, Si, Ti, V, Fe and Zn were removed, and Mo, In, Sn, Au, Tl and Bi were approximately conserved during low temperature alteration. Whole rock analyses and mass balance calculations conducted by Boily and Williams-Jones (1994) and Salvi and Williams-Jones (1996) indicated that low temperature alteration caused addition of Ca, Mg, Sr, Y, Zr and heavy REE and removal of Na ± F. In the case of the low temperature alteration event, the petrographic, mineral reaction, LA-ICPMS and whole rock data are all in excellent agreement, indicating that the changes in elemental concentrations observed on a whole rock basis are wholly or at least substantially explained by the alteration of aegirine to gittinsite. Addition of Ca and HFSE to rocks that had undergone GHQ alteration was extreme, resulting in the conversion of aegirine, which contains less than approximately 3000 ppm Ca and Zr, to gittinsite, which contains greater than approximately 110,000 ppm Ca and 124,000 ppm Zr (Table 6-8).

Implications for Hydrothermal Fluid Composition

Salvi and Williams-Jones (1996) concluded that hydrothermal HFSE mineralization within the Strange Lake granite resulted from a high salinity, Ca-free, F- and HFSE-bearing orthomagmatic fluid, exsolved from the granite. This fluid leached HFSE from HFSE minerals (principally elpidite) and subsequently mixed with Ca-bearing formation water. Precipitation of fluorite was proposed as

the principal cause of destabilization of HFSE-fluoride complexes and formation of the secondary HFSE mineralization.

Theoretical estimates of HFSE solubility in hydrothermal fluids indicate that HFSE are most likely transported as F complexes (Wood, 1990; Haas et al., 1995; Wood, 2003; Samson and Wood, in press). Experimental evidence for peraluminous melts, however, indicates that an orthomagmatic fluid exsolved from granite would likely have a low F content due to strong partitioning of F into the melt phase (London et al., 1988; Carroll and Webster, 1994; Johannes and Holtz, 1996; Chevychelov et al., 2004). Concentration of F in the silicate melt phase is suggested for the Strange Lake granite by the relatively high F contents (~ 2 %) of magmatic arfvedsonite (Chapter 5). Therefore, it is possible that, upon exsolution, the orthomagmatic fluid contained relatively low F and, by extension, HFSE. Despite the potentially low, initial F content, complexation of HFSE by F (Wood, 1990) and possibly other ligands, such as Cl (Gammons et al., 2002; Migdisov and Williams-Jones, 2002), by the orthomagmatic fluid could have occurred. Some HFSE (particularly light and middle REE), however, occur in higher concentrations in secondary aegirine than in primary arfvedsonite. This indicates that these elements must have been transported in the orthomagmatic fluid by either F or possibly other ligands during the high temperature alteration event. Regardless of the potential for the original orthomagmatic fluid to contain or transport HFSE, subsequent modification of the composition of the fluid through water-rock interaction would have increased the F content and, therefore, the ability of the fluid to leach and transport HFSE (see below).

Alteration of arfvedsonite, which contains approximately 2 % F (Chapter 5), to aegirine (reaction 2) would cause an increase in the activities of F and various cations, and a decrease in the pH of the orthomagmatic fluid. The modified orthomagmatic fluid composition would, therefore, have an increased capacity to mobilize and transport HFSE from primary magmatic minerals (e.g., elpidite) and F complexes. The majority of the granite shows evidence of alteration of arfvedsonite to aegirine and, therefore, a considerable amount of F could have been released into the orthomagmatic fluid during high temperature

alteration. Furthermore, the interval underlying the main mineralized zone shows evidence of leaching of HFSE (Salvi and Williams-Jones, 1996) and likely represents the source zone for many of the elements that were concentrated during later, low temperature GHQ alteration as a result of leaching by the modified orthomagmatic fluid.

Salvi and Williams-Jones (1990; 1996) also concluded that the orthomagmatic fluid that caused the high temperature alteration did not contain Ca. The lack of fluorite associated with high temperature alteration appears to support the absence of Ca in the orthomagmatic fluid. If the fluid had contained significant quantities of Ca, then it would have reacted with F liberated from the arfvedsonite during replacement by aegirine, and fluorite would have precipitated due to its low solubility product. High temperature alteration of the granite and pegmatite, with the exception of the minor, localized clouding of feldspar grains, is not associated with other mineralogical changes in the rocks (i.e., precipitation of another mineral that would preferentially concentrate elements liberated during alteration of arfvedsonite). Therefore, the absence of a mineral reaction that would have consumed F during high temperature alteration would have ensured that F remained in the hydrothermal fluid. This is also true for other elements released during alteration of arfvedsonite to aegirine. Although high temperature alteration of arfvedsonite to aegirine does not appear to have been a consistent source of HFSE, many elements liberated as a result of this alteration (e.g., F, Mg, K, Ca and Mn) were concentrated during later, low temperature alteration (Salvi and Williams-Jones, 1996). This suggests that the high temperature alteration event contributed elements to the hydrothermal fluid that were later concentrated during low temperature alteration.

Low temperature alteration resulted from introduction of a fluid containing Ca in concentrations sufficient to cause precipitation of Ca-bearing phases (e.g., gittinsite, fluorite and calcite). Circulation of this Ca-bearing fluid though the Strange Lake pluton continued after cessation of low temperature alteration, as evidenced by the predominance of fluorite and the presence of calcite in veins that cut the low temperature alteration mineral assemblage. Salvi and Williams-

Jones (1990; 1996) concluded that this fluid was a Ca-bearing, meteoric or formation water derived externally to the granite. The mineral reactions and the results of chemical analyses presented above support introduction of Ca from sources other than the minerals within the granite itself. Therefore, in light of the data and interpretations made in this study, introduction of Ca by a fluid from a source external to the granite continues to be most likely source for the elevated concentrations of Ca that occur in rocks affected by low temperature and quartz-fluorite alteration.

Critical Factors Controlling HFSE Mineralization

Fluorite precipitation was proposed by Salvi and Williams-Jones (1996) to be the dominant mechanism controlling destabilization of HFSE-fluoride complexes and precipitation of HFSE minerals. The greatest HFSE enrichment, however, occurs in rocks that have undergone low temperature GHQ alteration, which may or may not contain hydrothermal fluorite. In most instances, where hydrothermal fluorite is present, it precipitated late, and cross-cuts or replaces GHQ alteration. Additionally, replacement of elpidite by gittinsite, the main mechanism proposed by Salvi and Williams-Jones (1995; 1996) for formation of the hydrothermal HFSE mineralization does not include F. Therefore, observations made in this study suggest that fluorite precipitation was not the critical mechanism controlling formation of HFSE mineralization in rocks affected by low temperature alteration.

Alteration of arfvedsonite to aegirine (high temperature alteration) or the GHQ assemblage (low temperature alteration) released F into the hydrothermal fluid. Since F was not consumed during low temperature GHQ alteration, it would have remained in the hydrothermal fluid. Mineralogical evidence indicates that the residual (i.e., post low temperature alteration) hydrothermal fluid contained sufficient F to precipitate fluorite in cross-cutting quartz-fluorite veins and as a replacement of GHQ alteration. Mineralogical evidence and molar volume data also indicate that, in order to preserve volume, Si was likely removed from the rocks during low temperature alteration (e.g., reactions 5 and

6), transported by the hydrothermal fluid, and precipitated as quartz in the late, cross-cutting veins or caused localized silicification. The lack of HFSE minerals (e.g., gittinsite) associated with the main fluorite precipitation event indicates that these elements had already been preferentially removed from the hydrothermal fluid (relative to F) into earlier-formed phases (i.e., gittinsite) during GHQ alteration, which would have caused a drop in the concentrations of HFSE in the residual fluid. Mixing of a Ca-bearing fluid with a high salinity, F- and HFSE-bearing fluid (that had previously reacted with arfvedsonite) in the presence of aegirine appears to have caused GHQ alteration. Destabilization of HFSE-fluoride or possibly HFSE-chloride complexes occurred as a result of this reaction. HFSE were concentrated in minerals (primarily gittinsite but also thorite) and F remained in the fluid phase.

Sources of HFSE

Mineral analyses conducted during this study indicate that secondary, hydrothermal aegirine typically has similar or higher concentrations of HFSE than primary magmatic arfvedsonite. Whole rock analyses and mass balance calculations conducted by Salvi and Williams-Jones (1996), however, show that rocks that have undergone high temperature alteration have significantly depleted HFSE. Therefore, the most likely source of the HFSE that were subsequently concentrated in rocks that underwent low temperature alteration is primary, magmatic, HFSE and HFSE-bearing minerals (e.g., elpidite, narsarsukite, zircon, fluorite, pyrochlore).

Revisions to the Model for the Formation of the Strange Lake HFSE Deposit

The model proposed for the formation of the Strange Lake HFSE mineralization by Salvi and Williams-Jones (1996) retains validity with the following important changes. First, on the basis of theoretical data, the fluid exsolved from the granite may or may not have contained significant F ± HFSE. These components, however, were either introduced or their concentrations were enhanced in the orthomagmatic fluid as a result of the high temperature

alteration event. Second, the primary product of low temperature alteration in hematized rocks is replacement of aegirine ± arfvedsonite by an assemblage comprising gittinsite + hematite + quartz, which represents the most significant HFSE enrichment process in the Strange Lake pluton. Third, a late stage of mineralization comprising quartz + fluorite ± calcite ± galena veins and replacement occurred after the low temperature alteration stage. Based on the results of this study, a revised model for the deposit consists of the following major events:

1. A high salinity, low Ca, ± F, ± HFSE, Na-bearing orthomagmatic fluid is exsolved from the granite.
2. The orthomagmatic fluid reacts with arfvedsonite in the granite which causes an increase in the F content and a decrease in the pH of the fluid.
3. The modified hydrothermal fluid leaches HFSE from primary, magmatic HFSE and HFSE-bearing minerals in the volume of rocks situated below the current location of the main lens.
4. The F- and HFSE-bearing modified orthomagmatic fluid encounters a low salinity, Ca-bearing, low-F formation water.
5. A mixing zone is established in the current location of the main lens, where modified orthomagmatic fluid and formation water mix in the presence of aegirine.
6. Aegirine in the mixing zone is altered to gittinsite + hematite + quartz and primary, magmatic elpidite is pseudomorphed by gittinsite. This alteration causes HFSE loss, F addition and a reduction in the pH of the fluid.
7. Residual, F-bearing orthomagmatic fluid continues to mix with formation water resulting in the formation of quartz + fluorite ± calcite ± galena veins and localized silicification.

Conclusions

The following conclusions can be made on the basis of the petrographic and LA-ICPMS data obtained and the interpretations made during this investigation of the HFSE mineralization hosted by the Strange Lake peralkaline complex:

- Subsolvus granite and pegmatite have been affected in places by three hydrothermal events. The first and second, which were previously identified as discrete events by Salvi and Williams-Jones (1996), are characterized by the replacement of arfvedsonite by aegirine (high temperature alteration) and the replacement of elpidite by gittinsite (low temperature alteration). This investigation has shown that aegirine and, to a lesser extent, arfvedsonite were also replaced by gittinsite, hematite and quartz (GHQ) during the low temperature alteration event. The third event commenced during the latter part of the low temperature alteration event but continued after its cessation and consists of quartz and fluorite, which vein and replace all minerals but has particularly affected the GHQ alteration assemblage.
- The replacement of Na-Fe silicate minerals (aegirine and arfvedsonite) by a Ca-Zr silicate mineral (gittinsite) indicates that the hydrothermal enrichment of HFSE during the low temperature alteration event was more extreme than previously identified by Salvi and Williams-Jones (1996). The GHQ alteration mineral assemblage explains the enrichment of HFSE in rocks affected by low temperature alteration above the concentrations resulting solely from the largely isochemical replacement of magmatic elpidite by hydrothermal gittinsite. Additionally, identification of hematite as a direct product of low temperature alteration (with gittinsite and quartz) explains the association of HFSE enrichment with hematization.
- Replacement of minerals with relatively low Ca and Zr contents (arfvedsonite and aegirine; < 0.5 wt. % CaO and < 2000 ppm Zr), by gittinsite (~ 15.5 wt. % CaO and ~ 14.7 wt. % Zr) requires extreme

enrichment of these elements in the rocks affected by GHQ alteration relative to unaltered granite and pegmatite. The absence of significant amounts of precursor Ca-Zr silicate minerals in these altered rocks indicates that extreme HFSE enrichment occurred as a result of hydrothermal processes, rather than localized redistribution of elements from previous magmatic concentrations, as suggested by Miller (1996).

- On the basis of mineral reactions, replacement of aegirine or arfvedsonite by the GHQ mineral assemblage resulted from a Ca- and Zr- bearing aqueous fluid. This is consistent with the fluid composition proposed by Salvi and Williams-Jones (1996) for the low temperature alteration event.
- Replacement of arfvedsonite and aegirine by the GHQ mineral assemblage affected subsolvus granite and pegmatite, however, it is best represented in pegmatite, in which coarse-grained arfvedsonite had been pervasively replaced by aggregates of fine-grained aegirine during the earlier, high temperature alteration event.
- The direct association of hematization with HFSE enrichment indicates that the presence and relative abundance of hematite may be a simple indicator for conducting exploration and development within the Strange Lake pluton.

References

Belanger, M. (1984): Region du lac Brisson. *Ministere Energie Resources, Quebec;* Document **DP 84-20** (carte annotee, scale 1:50,000).

Birkett, T.C. and Miller, R.R. (1991): The role of hyrothermal processes in the granite-hosted Zr, Y, REE deposit at Strange Lake, Quebec/Labrador; evidence from fluid inclusions; discussion. *Geochimica et Cosmochimica Acta*, **55**. 3433-3449.

Birkett, T. C., Miller, R.R., Roberts, A.C., and Mariano, A.N. (1992): Zirconium-bearing minerals of the Strange Lake Intrusive Complex, Quebec-Labrador. *Canadian Mineralogist*, **30**, 191-205.

Boily, M. and Williams-Jones, A.E. (1994): The role of magmatic and hydrothermal processes in the chemical evolution of the Strange Lake plutonic complex, Quebec-Labrador. *Contributions to Mineralogy and Petrology*, **118**, 33-47.

Carroll, M.R. and Webster, J.D. (1994): Solubilities of sulfur, noble gases, nitrogen, chlorine, and fluorine in magmas. *Reviews in Mineralogy and Geochemistry,* **30**, 231-279.

Chevychelov, V.Yu., Zaraisky, G., Borisovsky, S., and Borkov, D. (2004): Partitioning of Ta and Nb between magmatic melt and aqueous (K,Na,H)F-containing fluid: Effects of temperature and chemical composition of the melt. *EMPG-X Symposium Abstracts*, Lithos supplement to v. 73, Nos. 1-2, S17.

Currie, K.L. (1985): An unusual peralkaline granite near Lac Brisson, Quebec-Labrador. *Geological Survey of Canada Paper* **85-1A**, 73-80.

Floyd, P.A. and Winchester, J.A. (1975): Magma type and tectonic setting discrimination using immobile elements. *Earth and Planetary Science Letters*, **27**, 211-218.

Floyd, P.A. and Winchester, J.A. (1978): Identification and discrimination of altered and metamorphosed volcanic rocks using immobile elements. *Chemical Geology*, **21**, 291-306.

Fujimoto, K., Tanaka, H., Higuchi, T., Tomida, N., Ohtani, T., and Ito, H. (2001): Alteration and mass transfer inferred from the Hirabayashi GSJ drill penetrating the Nojima Fault, Japan. *The Island Arc*, **10**, 401-410.

Gagnon, J.E., Samson, I.M., and Fryer, B.J. (2003): LA-ICP-MS Analysis of Fluid Inclusions. *In* I. Samson, A. Anderson & D. Marshall (eds.), The Analysis and Interpretation of Fluid Inclusions, *Mineralogical Association of Canada*, Short Course **32**, 12/1-12/32.

Gammons, C.H., Wood, S.A., and Li, Y. (2002): Complexation of the rare earth elements with aqueous chloride at 200 °C and 300 °C and saturated water vapor pressure, *In* Hellmann, R., and Wood, S.A., eds., Water-Rock Interactions, Ore Deposits, and Environmental Geochemistry: A Tribute to David A. Crerar. *The Geochemical Society*, Special Publication **7**, 191-207.

Haas, J.R., Shock, E.L., and Sassani, D.C. (1995): Rare earth elements in hydrothermal systems: Estimates of standard partial molal thermodynamic properties of aqueous complexes of the rare earth elements at high pressures and temperatures. *Geochimica et Cosmochimica Acta*, **59**, 4329-4250.

Halicz, L. and Günther, D. (2004): Quantitative analysis of silicates using LA-ICP-MS with liquid calibration. *Journal of Analytical Atomic Spectrometry*, **19**, 1539-1545.

Heaman, L.M., Creaser, R.A., and Cookenboo, H.O. (2002): Extreme enrichment of high field strength elements in Jericho eclogite xenoliths: A cryptic record of Paleoproterozoic subduction, partial melting, and metasomatism beneath the Slave craton, Canada.

Hill, J.D. and Miller, R.R. (1990): A review of Middle Proterozoic epigenic felsic magmatism in Labrador. *In* Mid-Proterozoic Laurentia – Baltica (C.F. Gower, T. Rivers and B. Ryan, eds.), *Geological Association of Canada Special Paper* **38**, 417-431.

Jiang, S-Y (2000): Controls on the mobility of high field strength elements (HFSE), U, and Th in an ancient submarine hydrothermal system of the Proterozoic Sullivan Pb-Zn-Ag deposit, British Columbia, Canada. *Geochemical Journal*, **34**, 341-348.

Johannes, W. and Holtz, F. (1996): Petrogenesis and experimental petrology of granitic rocks. *Springer-Verlag*, Berlin, 335 p.

Kovalenko, V.I., Tsaryeva, G.M., Goreglyad, A.V., Yarmoluk, V.V., and Troitsky, V.A. (1995): The peralkaline-granite related Khaldzan-Buregtey Rare metal (Zr, Nb, REE) deposit, Western Mongolia. *Economic Geology*, **90**, 530-547.

London, D., Hervig, R.L., and Morgan, G.B. VI., (1988): Melt-vapor solubilities and elemental partitioning in peraluminous granite-pegmatite systems: experimental results with Macusani glass at 200 MPa. *Contributions to Mineralogy and Petrology*, **99**, 360-373.

MacLean, W.H. (1988): Rare earth mobility at constant inter-REE ratios in the alteration zone at the Phelps Dodge Massive Sulfide Deposit, Mattagami, Quebec. *Mineralium Deposita*, **23**, 231-238.

MacLean, W.H. (1990): Mass change calculations in altered rock series. *Mineralium Deposita*, **25**, 44-49.

Migdisov, A.A. and Williams-Jones, A.E. (2002): A spectrophotometric study of neodymium(III) complexation in chloride solutions. *Geochimica et Cosmichimica Acta*, **66**, 4311-4323.

Miller, R.R. (1985): Geology of the Strange Lake alkalic complex and the associated Zr-Y-Nb-Be-REE mineralization. *In* Granite-Related Mineral Deposits: Geology, Petrogenesis and Tectonic Setting (R.P. Taylor and D.F. Strong, eds.), *Canadian Institute for Mining and Metallurgy, Extended Abstract,* 193-196.

Miller, R.R. (1986): Geology of the Strange Lake Alkalic Complex and the associated Zr-Y-Nb-Be-REE mineralization. *Newfoundland Department of Mines, Mineral Development Division,* Report **86-1**, 11-19.

Miller, R.R. (1988): Yttrium (Y) and other rare metals (Be, Nb, REE, Ta, Zr) in Labrador. *Newfoundland Department of Mines, Mineral Development Division,* Report **88-1**, 229-245.

Miller, R.R. (1990): The Strange Lake pegmatite-aplite hosted rare-metal deposit, Labrador, *Newfoundland Department of Mines and Energy, Geological Survey Branch*, Report **90-1**, 171-182.

Miller, R.R. (1996): Structural and textural evolution of the Strange Lake peralkaline rare-element (NYF) granitic pegmatite, Quebec-Labrador, *The Canadian Mineralogist*, **34**, 349-371.

Miller, R.R., Heaman, L.M., and Birkett, T.C. (1997): U-Pb zircon age of the Strange Lake peralkaline complex: implications for Mesoproterzoic peralkaline magmatism in north-central Labrador. *Precambrian Research*, **81**, 67-92.

Munker, C., Wömer, G., Yogodzinski, G., and Churikova, T. (2004): Behavior of high field strength elements in subduction zones: constraints from Kamchatka-Aleutian arc lavas. *Earth and Planetary Science Letters*, **224**, 275-293.

Nassif, G.J. (1993): *The Strange Lake Peralkaline Complex, Quebec-Labrador: the Hypersolvus-Subsolvus Granite Transition and Feldspar Mineralogy.* M.Sc. thesis, McGill University, Montreal, Quebec.

Nassif, G.J., and Martin, R.F. (1991): The hypersolvus granite-subsolvus granite transition at Strange Lake, Quebec-Labrador. , *GAC-MAC-CSPG Annual Meeting Toronto,* **A89** (abstract).

O'Hara, K. and Blackburn, W.H. (1989): Volume-loss model for trace-element enrichments in mylonites. *Geology*, **17**, 524-527.

Pearce, J.A. and Cann, J.R. (1973): Tectonic setting of basic volcanic rocks determined using trace element analysis. *Earth and Planetary Science Letters*, **19**, 290-300.

Pearce, J.A. and Norry, M.J. (1979): Petrogenetic implications of Ti, Zr, Y, and Nb variations in volcanic rocks. *Contributions to Mineralogy and Petrology*, **69**, 33-47.

Pillet, D. (1985): Le granite peralcaline du Lac Brisson, Territoire du Nouveau-Quebec: resultats preliminaries. Ministere de l'Energie et des Resources, Quebec, **MB 85-37**, SNRC 024A/08.

Pillet, D., Bonhomme, M.G., Duthou, J.L., and Chenevoy, M. (1989): Chronologie Rb/Sr et K/Ar du granite peralcalin du lac Brisson, Labrador central, Nouveau-Quebec. *Canadian Journal of Earth Science*, **26**, 328-332.

Pillet, D., Chenevoy, M., and Belanger, M. (1992): Petrologie du granite peralcalin du Lac Brisson, Labrador central, Nouveau-Quebec. I. Mode de mise en place et evolution chimique. *Canadian Journal of Earth Science*, **29**, 353-372.

Ryan, B., Lee, D., and Dunphy, D. (1988): The discovery of probably Archean rocks within the Labrador arm of the Trans-Hudson Orogen near the Labrador-Quebec border (NTS 14D/3,4,5 and 24A/1,8). *Newfoundland Department of Mines and Energy, Mineral Development Division*, Report **88-1**, 1-14.

Ryan, B., Krogh, T.E., Heaman, L., Schärer, U., Philippe, S., and Oliver, G. (1991): On recent geochronological studies in the Nain Province, Churchill Province and Nain Plutonic Suite, north-central Labrador. *Newfoundland Department of Mines and Energy, Geological Survey Branch*, Report **91-1**, 257-261.

Salvi, S. and Williams-Jones, A.E. (1990): The role of hydrothermal processes in the granite-hosted Zr, Y, REE deposit at Strange Lake, Quebec/Labrador: evidence from fluid inclusions. *Geochimica et Cosmochimica Acta*, **54**, 2403-2418.

Salvi S. and Williams-Jones, A.E. (1991): The role of hyrothermal processes in the granite-hosted Zr, Y, REE deposit at Strange Lake, Quebec/Labrador; evidence from fluid inclusions; reply. *Geochimica et Cosmochimica Acta*, **55**. 3433-3449.

Salvi, S. and Williams-Jones, A.E. (1992): Reduced orthomagmatic C-O-H-N-NaCl fluids in the Strange Lake rare-metal granitic complex, Quebec/Labrador, Canada. *European Journal of Mineralogy*, **4**, 1155-11

Salvi, S. and Williams-Jones, A.E. (1995): Zirconosilicate phase relations in the Strange Lake (Lac Brisson) pluton, Quebec-Labrador, Canada. *American Mineralogist*, **80**, 1031-1040.

Salvi, S. and Williams-Jones, A.E. (1996): The role of hydrothermal processes in concentrating HFSE in the Strange Lake peralkaline complex, northeastern Canada. *Geochimica et Cosmochimica Acta*, **60**,1917-1932.

Salvi, S. and Williams-Jones, A.E. (1997): Fischer-Tropsch synthesis of hydrocarbons during sub-solidus alteration of the Strange Lake peralkaline granite, Quebec/Labrador, Canada. *Geochimica et Cosmochimica Acta*, **61**, 83-99.

Salvi, S., and Williams-Jones, A.E., (in press): Alkaline granite-syenite hosted deposits: in Linnen, R.L., and Samson, I.M., eds., *Rare-Element Geochemistry and Mineral Deposits*, Geological Association of Canada Short Course Notes, **17**, 315-341.

Salvi, S., Fontan, F., Monchoux, P., Williams-Jones, A.E., and Moine, B. (2000): Hydrothermal Mobilization of High Field Strength Elements in Alkaline Igneous Systems: Evidence from the Tamazeght Complex (Morocco). *Economic Geology*, **95**, 559-576.

Samson, I.M., and Wood, S.A., (in press): The rare-earth elements: Behaviour in hydrothermal fluids and concentration in hydrothermal mineral deposits, exclusive of alkaline settings: in Linnen, R.L., and Samson, I.M., eds., *Rare-Element Geochemistry and Mineral Deposits*, Geological Association of Canada Short Course Notes, **17**, 269-297.

Sørensen, H. (1992): Agpaitic nepheline syenites: a potential source of rare elements. *Applied Geochemistry*, **7**, 417-427.

Taylor, F.C. (1979): Reconnaissance geology of a part of the Precambrian Shield, northeastern Quebec, northern Labrador and Northwest Territories. *Geological Survey of Canada*, Memoir **393**.

Trueman, D.L. Pedersen, J.C. de St. Jorre, L., and Smith, D.G.W. (1988): The Thor Lake, N.W.T. rare-metal deposit. In Granite-Related Mineral Deposits: Geology, Petrogenesis and Tectonic Settings (eds. R.P. Taylor and D.F. Strong), *Canadian Institute for Mining and Metallurgy*, Special Volume **39**, 279-284.

Van der Leeden, J., Belanger, M., Danis, D., Girard, R., and Martelain, J. (1990): Lithotectonic domains in the high-grade terrain east of the Labrador Trough (Quebec). *In* Lewry, L.F. and Stauffer, M.R. (eds.), The Early Proterozoic

Trans-Hudson Orogen of North America, *Geological Association of Canada*, Special Paper **37**, 371-386.

Williams-Jones, A.E., Samson, I.M., and Olivo, G.R. (2000): The genesis of hydrothermal fluorite-REE mineralization in the Gallinas Mountains, New Mexico. *Economic Geology*, **95**, 327-342.

Wood, S.A. (1990): The aqueous geochemistry of the rare-earth elements and yttrium 2. Theoretical predictions of speciation in hydrothermal solutions to 350 °C at saturation water vapor pressure. *Chemical Geology*, **88**, 99-125.

Wood, S.A. (2003): The geochemistry of rare earth elements and yttrium in geothermal waters. *In* Simmons, S.F. and Graham, E., eds., Volcanic, Geothermal and Ore-Forming Fluids: Rulers and Witnesses of Processes within the Earth. *Society of Economic Geologists*, Special Publication **10**, 133-158.

Zajac, I.S., Miller, R.R., Birkett, T.C., and Nantel, S. (1984a): The Strange Lake deposit, Quebec-Labrador. *Canadian Institute for Mining and Metallurgy Bulletin*, **77**, 60 (abstract).

Zajac, I.S., Miller, R.R., Birkett, T.C., and Nantel, S. (1984b): Le gite de Zr, Y, Nb, et Be du complexe alcalin de Strange Lake, Quebec-Labrador. *Ministere de l'Energie et des Resources, Quebec*, **DV 84-18**, 127-142.

Chapter 7

Conclusions

The following conclusions can be made on the basis of the data collected and interpretations made during preparation of this thesis:

- LA-ICP-MS is an effective method for determining elemental concentrations in fluorite and has enabled the identification of compositional heterogeneities and trends in fluorite not previously documented. These variations in composition can result from temporal and spatial influences and may reflect replacement of preexisting minerals in a relatively 'closed' system or progressive mixing of hydrothermal fluids or interaction of hydrothermal fluid with wall rocks in a relatively 'open' system. Distinctive compositional ranges that might be indicative of a particular geologic setting, and which could be used as an exploration tool, were not identified, and Tb/Ca and Tb/La ratios in fluorite do not appear to be reliable indicators of the affinity of fluorite. The small-scale variation in the composition of fluorite (10s of micrometers) indicates that bulk analysis is inadequate to fully characterize the compositional heterogeneity of fluorite. The use of bulk analyses of fluorite that may be compositionally zoned to make inferences about the affinity or ore potential of a deposit or district is, therefore, strongly cautioned.

- Quantitative LA-ICP-MS analysis of individual fluid inclusions in compositionally complex minerals such as fluorite can be accomplished using a non-homogenized 266 nm Nd:YAG laser, traversed opening technique, and by ratioing the count rates obtained for elements potentially contained within a fluid inclusion against the count rates obtained for an element present in significant quantities in the host mineral (e.g., Ca for fluorite). Use of the traversed opening technique can overcome difficulties associated with the poor absorbance of laser energy

and mineral cleavage and ratioing of the count rates can correct for the host mineral contribution to the fluid inclusion signal that is not addressed by subtraction of instrument and host mineral backgrounds alone. These combined techniques enable representative and quantitative analyses of fluid inclusions in compositionally complex host minerals.

- Microthermometric and LA-ICPMS analysis of fluid inclusions from the Oregon No. 3 pegmatite in the South Platte district, Colorado identified four compositional fluid types (F1, F2, F3 and F4). Only one (F4), however, appears to have been directly involved in the secondary hydrothermal fluorite-REE mineralization. Differentiation of two of the fluid types (F1 and F2) was only possible using LA-ICPMS. The fluids appear to have been derived internally to the pegmatite and fluorite precipitation appears to have occurred from F4 fluid at relatively constant temperatures (81 to 114 °C) and pH, largely as a result of mixing of Ca liberated from pegmatite wall-zone during albitization with an F-bearing hydrothermal fluid. The addition of elements, such as Ca, into the pegmatite by introduction of a fluid derived externally to the Pikes Peak granite was not necessary to cause the hydrothermal fluorite-REE mineralization.

- Quantitative analysis of synthetic silicate standard reference materials and silicate minerals by LA-ICPMS is possible without using a previously-determined or estimated internal standard element and without using alternative calibration (e.g., liquid introduction) strategies by conducting comprehensive elemental analyses and performing oxide scaling. The element concentrations calculated using oxide scaling typically have comparable or better analytical accuracy (less than ± 3 % to ± 30 %) than those obtained using common internal standard elements (e.g., Si, Ca or Fe). The differences in analytical accuracy observed between standard reference materials appear to be the result of matrix effects and can be explained in most, but not all instances, by relatively low abundances (< 5 ppm) and/or moderate to high elemental fractionation indices (1.5 to

greater than 2). This indicates that the matrix effects are more complex than can be explained by these two factors alone. Analysis of arfvedsonite without using an internal standard yielded similar results to the silicate standard reference materials, indicating that accurate, quantitative analysis of chemically complex silicate minerals by LA-ICPMS without using an internal standard is possible.

- Subsolvus granite and pegmatite within the Strange Lake pluton have been locally affected by three hydrothermal events. Extreme HFSE enrichment is associated with the second, low temperature alteration event, which is characterized by the replacement of aegirine and, to a lesser extent, arfvedsonite by gittinsite, hematite and quartz (GHQ). The replacement of Na-Fe silicate minerals (aegirine and arfvedsonite), which have relatively low Ca and Zr contents (< 0.5 wt. % CaO and < 2000 ppm Zr), by gittinsite (~ 15.5 wt. % CaO and ~ 14.7 wt. % Zr) indicates that secondary, hydrothermal enrichment of HFSE was more extreme than previously identified. Identification of GHQ alteration explains the association of HFSE enrichment with hematization and demonstrates that secondary, hydrothermal, not magmatic processes (as suggested by Miller, 1996), were responsible for the extreme HFSE enrichment shown by hematized rocks from the Strange Lake pluton. Replacement of arfvedsonite and aegirine by the GHQ mineral assemblage is best represented in pegmatite, in which coarse-grained arfvedsonite had been pervasively replaced by aggregates of fine-grained aegirine during the earlier, high temperature alteration event.

Summary of Contributions to Knowledge

The significant contributions to knowledge that are a direct result of the research activities conducted as part of this thesis are:

- Compositional heterogeneity in fluorite is greater than previously documented using bulk analytical techniques and element discrimination diagrams used to make inferences regarding fluorite provenance are not always accurate. These are significant observations considering the widespread use of bulk analysis of fluorite as an indicator of either the geologic affinity of an individual deposit or the ore potential of a region.
- Quantitative analysis of individual fluid inclusions in compositionally complex host minerals (i.e., fluorite) using LA-ICPMS is possible by ratioing count rates to correct for host mineral contributions that are not removed by simple background subtraction. This method expands the application of LA-ICPMS analysis of fluid inclusions to many more host minerals than have been considered thus far (e.g., pyroxene, sphalerite, garnet).
- One hydrothermal fluid, which was derived internally to the pegmatite, appears to have caused the fluorite-REE mineralization hosted by the Oregon No. 3 pegmatite in the South Platte district. Precipitation of fluorite-REE mineralization occurred at relatively constant temperature and pH, due to wallrock interaction.
- Quantitative analysis of silicate minerals using LA-ICPMS without using an internal or added standard is possible by analyzing for a comprehensive list of elements and oxide scaling. This method expands the use of LA-ICPMS into the analysis of unknown materials.
- The identification of GHQ alteration within the Strange Lake pluton demonstrates that extreme HFSE mobility has resulted from hydrothermal processes and documents the genetic link between mineralogical alteration (i.e., hematization) and HFSE mineralization. The association between hematization and HFSE mineralization provides a potential

means of readily conducting exploration and development activities within the pluton.

Recommendations for Future Work

To further improve our understanding of the formation of hydrothermal HFSE mineral deposits and the application of LA-ICPMS to the analysis of minerals and fluid inclusions from these deposits, the following research activities are recommended on the basis of the results of the investigations conducted as part of this thesis:

- The majority of these deposits have formed at temperatures less than approximately 350 °C. Therefore, it is necessary to use a graphical solution to correct for Na_{MT} using halite dissolution temperatures. Improvements in the topology of the liquidus surface in the range of T from 100 to 300 °C are necessary to improve the accuracy of the determinations made using this graphical solution. Additional experimentation is needed to better define the liquidus surface in this temperature range.
- Quantitative analysis of individual fluid inclusions within fluorite is possible using a 266 nm Nd:YAG-based LA-ICPMS system. A large proportion of fluid inclusions, however, were either too small or did not provide quantitative data due to leakage of the inclusions prior to analysis. Therefore, an alternative approach (ultrafast LA-ICPMS) should be applied to fluid inclusions from these deposits in order to provide additional data that can be used to evaluate trends in fluid composition and possible controls on mineral precipitation. This is particularly relevant for evaluating GHQ alteration within the Strange Lake pluton.
- The latest hydrothermal event identified at Strange Lake (quartz-fluorite veins and replacement) would provide an ideal opportunity to conduct a similar type of comparative study of quartz- and fluorite-hosted fluid inclusions that was conducted using samples from the Oregon No. 3

pegmatite. Use of ultrafast LA-ICPMS instrumentation would improve the ability to conduct quantitative analysis of individual fluid inclusions within fluorite.

- Petrographic analysis shows that GHQ alteration replaced arfvedsonite and aegirine, however, the causes of precipitation of GHQ alteration are not known. Additional evaluation (e.g., LA-ICPMS analysis of fluid inclusions and water/rock reaction modeling) is required to evaluate the factors controlling the formation of GHQ alteration.
- This thesis has demonstrated that quantitative analysis of fluid inclusions in compositionally complex host minerals is possible using count rate ratios. This technique, however, needs to be evaluated to determine what effect ratioing the count rates has on precision, accuracy and limits of detection of analysis.
- It is possible that much of the compositional variation exhibited by fluorite from South Platte, Colorado; St. Lawrence, Newfoundland; Rock Canyon Creek, British Columbia; and Gallinas Mountains, New Mexico could be controlled by only a few intensive variables (i.e., temperature). To better understand the potential effect of intensive variables on the composition of fluorite, additional data (i.e., microthermometry) on the hydrothermal systems responsible for these deposits are required.
- This study has demonstrated that extreme HFSE enrichment in the Strange Lake pluton occurred as a result of hydrothermal processes accompanying low temperature alteration of subsolvus granite and pegmatite. Although some bulk compositional data have been obtained from fluid inclusions present within low temperature altered rocks, discrete sampling of individual fluid inclusions has not been conducted. Consequently, the nature of the fluids responsible for the extreme HFSE mobility remains poorly understood. Identification, characterization and analysis of these fluids by LA-ICPMS are required.

Appendix A

Appendix to Chapter 2 – "Compositional Heterogeneity in Fluorite and the Genesis of Fluorite Deposits – Insights from LA-ICP-MS Analysis"

South Platte Fluorite Analyses

Analysis Number:			De15A06	De15A07	De15A08	De15A09	De15A10
Type:			Green	Green	Green	Purple	Purple
Element	Mass	Unit					
Na2O	23	wt%	0.343	0.336	0.327	0.311	0.175
MgO	25	wt%	0.005	0.004	0.005	0.004	0.002
K2O	39	wt%	0	0	0	0.001	0
CaO	43	wt%	71.821	71.821	71.821	71.821	71.821
Mn	55	ppm					
Cu	65	ppm	0.534	0.86	<0.695	1.485	16.253
Zn	66	ppm	0.543	<0.232	<0.293	0.292	1.121
Rb	85	ppm	0.126	0.14	0.157	0.212	0.108
Sr	86	ppm	173.799	189.241	180.632	186.594	125.278
Y	89	ppm	3237.176	3296.567	3255.283	3330.847	2036.993
Nb	93	ppm	<0.051	0.22	<0.051	<0.073	1.205
Ba	137	ppm	5.202	5.247	4.651	3.868	4.297
Pb	208	ppm	2.693	2.566	2.382	3.547	4.318
Th	232	ppm	66.625	63.928	59.199	70.076	46.196
U	238	ppm	1.027	0.948	1.075	0.983	0.558

Chondrite Normalized

Analysis Number:			De15A06	De15A07	De15A08	De15A09	De15A10
Type:			Green	Green	Green	Purple	Purple
Element	Mass	Unit					
La	139	ppm	457.2247	437.4329	440.0807	546.0775	278.3906
Ce	140	ppm	282.3994	279.046	271.6319	325.5076	198.5339
Pr	141	ppm	361.878	361.5717	349.2956	417.3076	219.6011
Nd	145	ppm	448.8176	432.9154	423.6107	472.1168	256.8137
Pm	145	ppm					
Sm	147	ppm	708.846	699.1665	666.8085	740.4768	354.199
Eu	151	ppm	206.0609	199.7499	201.3457	217.3569	99.58814
Gd	157	ppm					
Tb	159	ppm	1887.794	1799.339	1756.12	1902.05	806.1119
Dy	163	ppm					
Y	89	ppm	1438.745	1465.141	1446.793	1480.377	905.3303
Ho	165	ppm	2978.268	2875.144	2773.882	2957.696	1262.035
Er	167	ppm	3434.329	3328.076	3202.089	3443.719	1439.537
Tm	169	ppm					
Yb	173	ppm	4224.007	4046.963	3855.619	4280.256	1871.068
Lu	175	ppm	3736.394	3562.28	3468.723	3812.152	1677.836

South Platte Fluorite Analyses

Analysis Number:			De15A11	De15A12	De15A13	De15A14	De15A15
Type:			Clear	Clear	Purple	Clear	Purple
Element	Mass	Unit					
Na2O	23	wt%	0.371	0.367	0.11	0.296	1.262
MgO	25	wt%	0.005	0.005	0.017	0.005	0.096
K2O	39	wt%	0.001	0	0.001	<0.000	0.129
CaO	43	wt%	71.821	71.821	71.821	71.821	71.821
Mn	55	ppm					
Cu	65	ppm	1.087	<0.733	2.426	<1.188	3.846
Zn	66	ppm	0.581	<0.275	0.445	<0.426	15.653
Rb	85	ppm	0.245	0.192	0.104	0.188	0.511
Sr	86	ppm	187.581	208.277	175.19	167.22	81.248
Y	89	ppm	3647.465	3077.811	296.25	3525.509	101.25
Nb	93	ppm	0.078	0.105	2.093	<0.066	1.654
Ba	137	ppm	4.649	4.312	4.252	3.183	4.775
Pb	208	ppm	3.427	5.918	3.219	5.126	3.035
Th	232	ppm	77.855	137.423	72.267	92.681	1.081
U	238	ppm	1.114	0.925	0.455	0.592	0.157

Chondrite Normalized

Analysis Number:			De15A11	De15A12	De15A13	De15A14	De15A15
Type:			Clear	Clear	Purple	Clear	Purple
Element	Mass	Unit					
La	139	ppm	591.2502	553.0512	128.1804	425.1539	8.461886
Ce	140	ppm	361.1352	354.3313	70.75854	269.0195	4.815867
Pr	141	ppm	455.8357	470.8728	90.72241	350.2276	8.003683
Nd	145	ppm	526.5743	575.1781	82.55086	420.499	8.084542
Pm	145	ppm					
Sm	147	ppm	803.9707	964.6887	76.08788	696.912	11.97702
Eu	151	ppm	241.0354	232.0417	13.33744	170.6119	2.409434
Gd	157	ppm					
Tb	159	ppm	2123.812	2096.373	69.40328	1513.564	18.50769
Dy	163	ppm					
Y	89	ppm	1621.096	1367.916	131.6664	1566.893	45.0002
Ho	165	ppm	3271.028	2813.313	65.2276	2095.074	22.59844
Er	167	ppm	3866.702	3139.688	65.2601	2459.813	26.92696
Tm	169	ppm					
Yb	173	ppm	4760.627	3995.804	62.8773	3002.206	37.45054
Lu	175	ppm	4342.215	3537.46	57.80308	2591.874	34.71105

South Platte Fluorite Analyses

	Analysis Number:		De15A16	De15A17	De15A18
	Type:		White	White	White
Element	Mass	Unit			
Na2O	23	wt%	2.164	0.215	0.274
MgO	25	wt%	0.223	0.003	0.002
K2O	39	wt%	0.141	0.001	0.001
CaO	43	wt%	71.821	71.821	71.821
Mn	55	ppm			
Cu	65	ppm	5.231	1.136	<0.454
Zn	66	ppm	15.275	0.391	0.274
Rb	85	ppm	2.501	0.138	0.307
Sr	86	ppm	50.143	42.193	38.398
Y	89	ppm	1622.623	1513.621	2513.201
Nb	93	ppm	60.591	0.373	0.889
Ba	137	ppm	4.977	4.79	5.19
Pb	208	ppm	23.335	9.033	20.389
Th	232	ppm	3.391	278.826	228.235
U	238	ppm	59.759	4.884	2.786

Chondrite Normalized

	Analysis Number:		De15A16	De15A17	De15A18
	Type:		White	White	White
Element	Mass	Unit			
La	139	ppm	14.03087	158.703	241.3736
Ce	140	ppm	8.066234	100.8216	144.6756
Pr	141	ppm	16.27302	137.3599	197.9547
Nd	145	ppm	16.77888	151.6011	186.2426
Pm	145	ppm			
Sm	147	ppm	29.76003	189.2985	252.9602
Eu	151	ppm	5.843202	21.36988	40.45702
Gd	157	ppm			
Tb	159	ppm	85.36118	222.9472	779.0612
Dy	163	ppm			
Y	89	ppm	721.1658	672.7202	1116.978
Ho	165	ppm	165.9488	377.7373	2015.771
Er	167	ppm	224.2051	480.9585	3044.64
Tm	169	ppm			
Yb	173	ppm	349.2511	833.4241	5609.999
Lu	175	ppm	285.1261	801.4472	4814.874

South Platte Fluorite Analyses

Element	Mass	Unit	Analysis Number: Type	n Green	Maximum Green	Minimum Green	Mean Green	Sigma Green
Na2O	23	wt%		3	0.343	0.327	0.335333	0.008021
MgO	25	wt%		3	0.005	0.004	0.004667	0.000577
K2O	39	wt%		3	0	0	0	0
CaO	43	wt%		3	71.821	71.821	71.821	0
Mn	55	ppm						
Cu	65	ppm		3	0.86	0.534	0.697	0.230517
Zn	66	ppm		3	0.543	0.543	0.543	
Rb	85	ppm		3	0.157	0.126	0.141	0.015524
Sr	86	ppm		3	189.241	173.799	181.224	7.738003
Y	89	ppm		3	3296.567	3237.176	3263.009	30.43989
Nb	93	ppm		3	0.22	0.22	0.22	
Ba	137	ppm		3	5.247	4.651	5.033333	0.331874
Pb	208	ppm		3	2.693	2.382	2.547	0.156368
Th	232	ppm		3	66.625	59.199	63.25067	3.75905
U	238	ppm		3	1.075	0.948	1.016667	0.064127

Chondrite Normalized

Element	Mass	Unit	Analysis Number: Type:	n Green	Maximum Green	Minimum Green	Mean Green	Sigma Green
La	139	ppm		3	457.2247	437.4329	444.9128	10.74435
Ce	140	ppm		3	282.3994	271.6319	277.6924	5.509863
Pr	141	ppm		3	361.878	349.2956	357.5818	7.177626
Nd	145	ppm		3	448.8176	423.6107	435.1146	12.74652
Pm	145	ppm						
Sm	147	ppm		3	708.846	666.8085	691.607	22.0147
Eu	151	ppm		3	206.0609	199.7499	202.3855	3.281501
Gd	157							
Tb	159	ppm		3	1887.794	1756.12	1814.418	67.11935
Dy	163							
Y	89	ppm		3	1465.141	1438.745	1450.226	13.52861
Ho	165	ppm		3	2978.268	2773.882	2875.764	102.1944
Er	167	ppm		3	3434.329	3202.089	3321.498	116.2599
Tm	169							
Yb	173	ppm		3	4224.007	3855.619	4042.197	184.2407
Lu	175	ppm		3	3736.394	3468.723	3589.132	135.8409

South Platte Fluorite Analyses

Element	Analysis Number: Type Mass	Unit	n Purple	Maximum Purple	Minimum Purple	Mean Purple	Sigma Purple
Na2O	23	wt%	4	1.262	0.11	0.4645	0.538222
MgO	25	wt%	4	0.096	0.002	0.02975	0.044664
K2O	39	wt%	4	0.129	0	0.03275	0.064168
CaO	43	wt%	4	71.821	71.821	71.821	0
Mn	55	ppm					
Cu	65	ppm	4	16.253	1.485	6.0025	6.902232
Zn	66	ppm	4	15.653	0.292	4.37775	7.525458
Rb	85	ppm	4	0.511	0.104	0.23375	0.191476
Sr	86	ppm	4	186.594	81.248	142.0775	48.51325
Y	89	ppm	4	3330.847	101.25	1441.335	1531.025
Nb	93	ppm	4	2.093	1.205	1.650667	0.444009
Ba	137	ppm	4	4.775	3.868	4.298	0.371728
Pb	208	ppm	4	4.318	3.035	3.52975	0.566562
Th	232	ppm	4	72.267	1.081	47.405	33.06291
U	238	ppm	4	0.983	0.157	0.53825	0.341797

Chondrite Normalized

Element	Analysis Number: Type: Mass	Unit	n Purple	Maximum Purple	Minimum Purple	Mean Purple	Sigma Purple
La	139	ppm	4	546.0775	8.461886	240.2776	231.8552
Ce	140	ppm	4	325.5076	4.815867	149.904	142.0283
Pr	141	ppm	4	417.3076	8.003683	183.9087	178.3024
Nd	145	ppm	4	472.1168	8.084542	204.8915	206.4021
Pm	145	ppm					
Sm	147	ppm	4	740.4768	11.97702	295.6852	331.6508
Eu	151	ppm	4	217.3569	2.409434	83.17299	99.45609
Gd	157						
Tb	159	ppm	4	1902.05	18.50769	699.0182	879.0646
Dy	163						
Y	89	ppm	4	1480.377	45.0002	640.5934	680.4556
Ho	165	ppm	4	2957.696	22.59844	1076.889	1379.215
Er	167	ppm	4	3443.719	26.92696	1243.861	1607.036
Tm	169						
Yb	173	ppm	4	4280.256	37.45054	1562.913	2004.666
Lu	175	ppm	4	3812.152	34.71105	1395.626	1785.226

South Platte Fluorite Analyses

Element	Analysis Number: Type Mass	Unit	n Clear	Maximum Clear	Minimum Clear	Mean Clear	Sigma Clear
Na2O	23	wt%	3	0.371	0.296	0.344667	0.042194
MgO	25	wt%	3	0.005	0.005	0.005	8.23E-11
K2O	39	wt%	3	0.001	0	0.0005	0.000707
CaO	43	wt%	3	71.821	71.821	71.821	0
Mn	55	ppm					
Cu	65	ppm	3	1.087	1.087	1.087	
Zn	66	ppm	3	0.581	0.581	0.581	
Rb	85	ppm	3	0.245	0.188	0.208333	0.031817
Sr	86	ppm	3	208.277	167.22	187.6927	20.52873
Y	89	ppm	3	3647.465	3077.811	3416.928	299.9479
Nb	93	ppm	3	0.105	0.078	0.0915	0.019092
Ba	137	ppm	3	4.649	3.183	4.048	0.767829
Pb	208	ppm	3	5.918	3.427	4.823667	1.272723
Th	232	ppm	3	137.423	77.855	102.653	31.01076
U	238	ppm	3	1.114	0.592	0.877	0.26429

Chondrite Normalized

Element	Analysis Number: Type: Mass	Unit	n Clear	Maximum Clear	Minimum Clear	Mean Clear	Sigma Clear
La	139	ppm	3	591.2502	425.1539	523.1518	86.99123
Ce	140	ppm	3	361.1352	269.0195	328.162	51.33176
Pr	141	ppm	3	470.8728	350.2276	425.6454	65.74506
Nd	145	ppm	3	575.1781	420.499	507.4171	79.09897
Pm	145	ppm					
Sm	147	ppm	3	964.6887	696.912	821.8571	134.7814
Eu	151	ppm	3	241.0354	170.6119	214.563	38.3275
Gd	157						
Tb	159	ppm	3	2123.812	1513.564	1911.25	344.6793
Dy	163						
Y	89	ppm	3	1621.096	1367.916	1518.635	133.3102
Ho	165	ppm	3	3271.028	2095.074	2726.472	592.767
Er	167	ppm	3	3866.702	2459.813	3155.401	703.5759
Tm	169						
Yb	173	ppm	3	4760.627	3002.206	3919.546	881.6875
Lu	175	ppm	3	4342.215	2591.874	3490.516	876.1141

South Platte Fluorite Analyses

Element	Mass	Unit	n White	Maximum White	Minimum White	Mean White	Sigma White
Analysis Number: Type							
Na2O	23	wt%	3	2.164	0.215	0.884333	1.108616
MgO	25	wt%	3	0.223	0.002	0.076	0.127307
K2O	39	wt%	3	0.141	0.001	0.047667	0.080829
CaO	43	wt%	3	71.821	71.821	71.821	0
Mn	55	ppm					
Cu	65	ppm	3	5.231	1.136	3.1835	2.895602
Zn	66	ppm	3	15.275	0.274	5.313333	8.627255
Rb	85	ppm	3	2.501	0.138	0.982	1.318204
Sr	86	ppm	3	50.143	38.398	43.578	5.99374
Y	89	ppm	3	2513.201	1513.621	1883.148	548.3568
Nb	93	ppm	3	60.591	0.373	20.61767	34.61888
Ba	137	ppm	3	5.19	4.79	4.985667	0.200141
Pb	208	ppm	3	23.335	9.033	17.58567	7.551875
Th	232	ppm	3	278.826	3.391	170.1507	146.6167
U	238	ppm	3	59.759	2.786	22.47633	32.30477

Chondrite Normalized

Element	Mass	Unit	n White	Maximum White	Minimum White	Mean White	Sigma White
Analysis Number: Type:							
La	139	ppm	3	241.3736	14.03087	138.0358	115.0718
Ce	140	ppm	3	144.6756	8.066234	84.52117	69.7482
Pr	141	ppm	3	197.9547	16.27302	117.1958	92.50402
Nd	145	ppm	3	186.2426	16.77888	118.2075	89.53121
Pm	145	ppm					
Sm	147	ppm	3	252.9602	29.76003	157.3396	114.9809
Eu	151	ppm	3	40.45702	5.843202	22.5567	17.3374
Gd	157						
Tb	159	ppm	3	779.0612	85.36118	362.4565	367.2902
Dy	163						
Y	89	ppm	3	1116.978	672.7202	836.9548	243.7143
Ho	165	ppm	3	2015.771	165.9488	853.1522	1012.41
Er	167	ppm	3	3044.64	224.2051	1249.935	1559.553
Tm	169						
Yb	173	ppm	3	5609.999	349.2511	2264.225	2907.621
Lu	175	ppm	3	4814.874	285.1261	1967.149	2479.678

St. Lawrence Fluorite

	Analysis Number:		gnv8a-c-1	gnv8a-c-2	gnv8a-c-3	gnv8a-c-4	gnv8a-c-5
	Type:		GNV-C	GNV-C	GNC-C	GNV-C	GNV-C
Element	**Mass**	**Unit**					
Na2O	23	wt%					
MgO	25	wt%	-1.800641	-1.958151	-1.332213	0.510419	0.106864
K2O	39	wt%					
CaO	43	wt%	72	72	72	72	72
Mn	55	ppm	-1.256533	0.039439	0.458491	-0.089414	0.076989
Cu	65	ppm					
Zn	66	ppm					
Rb	85	ppm					
Sr	86	ppm	71.32615	80.12078	71.28394	69.96534	63.95394
Y	89	ppm	1214.688	766.7642	55.22843	48.56956	1434.842
Nb	93	ppm					
Ba	137	ppm	3.038024	4.283198	25.96039	4.202273	3.201005
Pb	208	ppm					
Th	232	ppm	0	-0.027227	0.00171	0.006972	0.00053
U	238	ppm	0.012165	0.269812	0.275971	-0.001921	0.005232

Chondrite Normalized

	Analysis Number:		gnv8a-c-1	gnv8a-c-2	gnv8a-c-3	gnv8a-c-4	gnv8a-c-5
	Type:		GNV-C	GNV-C	GNC-C	GNV-C	GNV-C
Element	**Mass**	**Unit**					
La	139	ppm	98.11705	110.7619	77.45158	81.61815	86.66575
Ce	140	ppm	100.5502	133.0394	98.46139	102.8017	85.66909
Pr	141	ppm	112.7961	158.3308	126.6197	125.513	96.26963
Nd	145	ppm	117.8153	174.0833	105.2206	102.9215	89.72546
Pm	145	ppm					
Sm	147	ppm	101.4998	156.4642	45.82849	52.00851	83.96847
Eu	151	ppm	34.42012	53.50814	22.67541	26.15298	24.31829
Gd	157	ppm	126.9389	123.4824	45.45811	35.64176	101.62
Tb	159	ppm	125.3553	103.0651	15.14878	15.85338	102.417
Dy	163	ppm	123.1525	78.05778	7.181763	6.215641	112.4685
Y	89	ppm	539.8614	340.7841	24.54597	21.58647	637.7073
Ho	165	ppm	115.6178	53.54791	4.828318	4.012673	113.0443
Er	167	ppm	98.98646	38.58289	1.707585	1.721838	99.81623
Tm	169	ppm	70.33163	20.31712	0.256166	1.316508	68.01892
Yb	173	ppm	37.81325	8.636303	0.429051	0.138215	53.85217
Lu	175	ppm	28.47189	8.052386	-0.418772	0.236955	30.70887

St. Lawrence Fluorite

Analysis Number:			gnv8a-d-1	gnv8a-d-2	gnv8a-d-3	gnv8a-d-4	gnv8a-d-5
Type:			GNV-D	GNV-D	GNV-D	GNV-D	GNV-D
Element	**Mass**	**Unit**					
Na2O	23	wt%					
MgO	25	wt%	4.585296	0.688583	5.99525	0.948414	1.221654
K2O	39	wt%					
CaO	43	wt%	72	72	72	72	72
Mn	55	ppm	0.183117	0.068014	-0.587239	0.287156	1.188916
Cu	65	ppm					
Zn	66	ppm					
Rb	85	ppm					
Sr	86	ppm	63.86703	61.22596	74.32462	98.19798	93.81687
Y	89	ppm	1182.732	454.3023	1835.693	1928.497	1056.002
Nb	93	ppm					
Ba	137	ppm	2.866631	4.795814	6.427569	4.81824	3.558435
Pb	208	ppm					
Th	232	ppm	-0.00626	-0.005444	-0.010937	0.014068	0.017729
U	238	ppm	0.137814	0.008054	0.008853	0.863137	0.017623

Chondrite Normalized

Analysis Number:			gnv8a-d-1	gnv8a-d-2	gnv8a-d-3	gnv8a-d-4	gnv8a-d-5
Type:			GNV-D	GNV-D	GNV-D	GNV-D	GNV-D
Element	**Mass**	**Unit**					
La	139	ppm	80.68891	64.50431	87.03406	95.72738	92.13799
Ce	140	ppm	88.44134	66.80327	68.99813	86.07977	100.031
Pr	141	ppm	89.21163	78.87953	77.23277	97.88174	124.2001
Nd	145	ppm	83.42168	76.13461	71.10079	98.13532	135.1242
Pm	145	ppm					
Sm	147	ppm	84.55875	71.2542	67.36983	106.4091	125.0839
Eu	151	ppm	20.51959	26.86572	18.90006	39.06403	54.12412
Gd	157	ppm	99.91932	80.79962	91.15116	133.1764	141.1284
Tb	159	ppm	102.224	68.2043	129.4985	160.1068	129.1981
Dy	163	ppm	115.1828	51.51169	145.4284	161.9474	96.61913
Y	89	ppm	525.6589	201.9121	815.8636	857.1098	469.334
Ho	165	ppm	111.9812	41.89814	168.1097	157.9462	81.62011
Er	167	ppm	89.89164	23.60067	155.7193	130.7093	47.23355
Tm	169	ppm	65.32858	11.79872	123.5387	80.89796	20.78099
Yb	173	ppm	44.50722	6.112731	95.20679	39.12663	8.589217
Lu	175	ppm	30.36925	6.346627	61.63774	22.8558	8.724263

St. Lawrence Fluorite

	Analysis Number:		gnv8a-e-1	isv1l-f-1	isv1l-f-2	isv1l-g-1	isv1l-g-2
	Type:		GNV-E	ISV-F	ISV-F	ISV-G	ISV-G
Element	**Mass**	**Unit**					
Na2O	23	wt%					
MgO	25	wt%	1.350682	0.220588	0.127974	-0.437385	0.501679
K2O	39	wt%					
CaO	43	wt%	72	72	72	72	72
Mn	55	ppm	-0.115468	0.181327	0.032542	0.36552	0.107585
Cu	65	ppm					
Zn	66	ppm					
Rb	85	ppm					
Sr	86	ppm	52.81881	34.64352	27.89509	11.94319	16.76388
Y	89	ppm	1021.673	283.8116	226.3793	251.8241	782.0522
Nb	93	ppm					
Ba	137	ppm	2.816996	2.971124	2.5183	1.913376	2.005365
Pb	208	ppm					
Th	232	ppm	-0.000874	0.005835	0.019022	0.00733	0.005244
U	238	ppm	0.005831	0.017575	-0.000376	0.002881	-0.00284

Chondrite Normalized

	Analysis Number:		gnv8a-e-1	isv1l-f-1	isv1l-f-2	isv1l-g-1	isv1l-g-2
	Type:		GNV-E	ISV-F	ISV-F	ISV-G	ISV-G
Element	**Mass**	**Unit**					
La	139	ppm	57.99941	13.48192	1.805208	3.164019	0.380192
Ce	140	ppm	54.08565	13.46774	2.533547	2.869431	0.346107
Pr	141	ppm	55.66847	13.86497	3.454739	3.170555	0.619894
Nd	145	ppm	47.4751	13.53694	4.396375	1.965963	0.615807
Pm	145	ppm					
Sm	147	ppm	35.97543	18.91769	10.17672	2.507253	2.000846
Eu	151	ppm	16.26929	2.819607	1.116578	0.340834	0.350739
Gd	157	ppm	57.80815	23.20902	13.68051	6.992117	11.20073
Tb	159	ppm	70.23177	24.03937	15.05425	10.09525	26.88693
Dy	163	ppm	84.36007	26.8354	15.64169	14.43462	42.99471
Y	89	ppm	454.077	126.1385	100.613	111.9218	347.5788
Ho	165	ppm	82.8542	31.02541	13.72673	16.39649	51.94091
Er	167	ppm	90.82215	32.72949	14.63866	18.11905	55.36533
Tm	169	ppm	81.90003	37.38715	10.26196	15.69331	47.61093
Yb	173	ppm	59.00962	40.21838	8.965854	13.49438	37.43604
Lu	175	ppm	47.66427	30.7271	7.094407	11.33874	23.66473

St. Lawrence Fluorite

	Analysis Number:		isv1l-g-3	lbv7a-1	lbv7a-2	lbv7a-3	lbv7a-4
	Type:		ISV-G	LBV-F/G	LBV-F/G	LBV-F/G	LBV-F/G
Element	**Mass**	**Unit**					
Na2O	23	wt%					
MgO	25	wt%	0.75743				
K2O	39	wt%					
CaO	43	wt%	72	72	72	72	72
Mn	55	ppm	0.106435				
Cu	65	ppm					
Zn	66	ppm					
Rb	85	ppm					
Sr	86	ppm	12.42255	215.5238	307.8741	260.6345	178.8198
Y	89	ppm	811.3004	1403.51	1719.737	1584.092	967.079
Nb	93	ppm					
Ba	137	ppm	1.948837	80.41781	<16.0	<15.6	<49.1
Pb	208	ppm		<1.4	<0.9	2.040078	<0.6
Th	232	ppm		<1.0	<0.5	<0.2	<0.2
U	238	ppm		<0.4	<0.5	<0.3	<0.4

Chondrite Normalized

	Analysis Number:		isv1l-g-3	lbv7a-1	lbv7a-2	lbv7a-3	lbv7a-4
	Type:		ISV-G	LBV-F/G	LBV-F/G	LBV-F/G	LBV-F/G
Element	**Mass**	**Unit**					
La	139	ppm	0.198588	97.10575	119.8868	99.62799	49.32191
Ce	140	ppm	0.210102	82.90303	117.347	91.23383	47.77348
Pr	141	ppm	0.357587	86.76158	110.9107	100.5279	55.81876
Nd	145	ppm	0.34206	88.80973	102.9928	128.1464	45.71342
Pm	145	ppm					
Sm	147	ppm	1.363034	103.2257	143.825	184.1689	97.34474
Eu	151	ppm	0.309074	38.81203	45.71946	48.77057	23.36817
Gd	157	ppm	6.77877	124.3832	198.1121	163.0876	101.7113
Tb	159	ppm	19.06304	195.7416	217.185	241.9625	112.3832
Dy	163	ppm	36.27833	198.2925	278.7645	267.5558	128.0847
Y	89	ppm	360.5779	623.7824	764.3276	704.0408	429.8129
Ho	165	ppm	48.97107	236.5162	307.8348	237.0295	117.755
Er	167	ppm	58.3332	251.8125	317.6539	284.2257	112.8048
Tm	169	ppm	47.80101	251.2919	349.3993	251.4505	99.39186
Yb	173	ppm	34.75078	221.626	245.9967	274.2002	49.49201
Lu	175	ppm	25.08889	113.8574	185.8337	133.9991	47.72111

St. Lawrence Fluorite

	Analysis Number:		lbv7a-5	lbv7a-6	lbv7a-7	lbv7a-8	lbv7a-10
	Type:		LBV-F/G	LBV-F/G	LBV-F/G	LBV-D	LBV-D
Element	**Mass**	**Unit**					
Na2O	23	wt%					
MgO	25	wt%					
K2O	39	wt%					
CaO	43	wt%	72	72	72	72	72
Mn	55	ppm					
Cu	65	ppm					
Zn	66	ppm					
Rb	85	ppm					
Sr	86	ppm	156.2111	194.5342	189.407	115.9257	2530.124
Y	89	ppm	716.4633	959.159	922.3568	945.3452	796.854
Nb	93	ppm					
Ba	137	ppm	<37.0	82.36889	<13.9	17.09961	239114.1
Pb	208	ppm	17749.81	1026.228	95.6423	<3.6	4.129553
Th	232	ppm	<0.3	<0.2	<0.4	<0.7	<0.3
U	238	ppm	<0.3	<0.2	<0.4	0	<0.6

Chondrite Normalized

	Analysis Number:		lbv7a-5	lbv7a-6	lbv7a-7	lbv7a-8	lbv7a-9
	Type:		LBV-F/G	LBV-F/G	LBV-F/G	LBV-D	LBV-D
Element	**Mass**	**Unit**					
La	139	ppm	39.97678	39.47977	45.42457	69.28481	55.50572
Ce	140	ppm	36.68316	43.54398	39.60361	55.52949	65.28341
Pr	141	ppm	37.63416	56.42617	48.29978	60.6613	69.03004
Nd	145	ppm	45.23119	34.99123	45.21785	70.07276	62.20646
Pm	145	ppm					
Sm	147	ppm	56.27893	73.571	91.95624	52.19147	77.63292
Eu	151	ppm	14.3351	28.09037	16.60518	50.38812	32.18508
Gd	157	ppm	92.65361	99.83841	103.3291	163.3051	108.6721
Tb	159	ppm	101.8857	116.5476	104.9648	104.6337	122.6502
Dy	163	ppm	103.9727	120.1445	135.7463	161.7402	130.066
Y	89	ppm	318.4281	426.2929	409.9363	420.1534	441.1867
Ho	165	ppm	93.36661	118.4199	134.3948	117.7695	116.2814
Er	167	ppm	65.50782	82.52281	133.8605	92.6029	94.79581
Tm	169	ppm	51.65205	60.741	67.62502	82.30187	85.39134
Yb	173	ppm	31.75574	44.06045	50.67196	34.29136	49.85029
Lu	175	ppm	20.74363	33.16234	45.39234	10.7673	35.18746

St. Lawrence Fluorite

	Analysis Number:		lbv7a-11	lbv7a-12	lbv7a-13	lbv7a-14
	Type:		LBV-D	LBV-D	LBV-D	LBV-D
Element	**Mass**	**Unit**				
Na2O	23	wt%				
MgO	25	wt%				
K2O	39	wt%				
CaO	43	wt%	72	72	72	72
Mn	55	ppm				
Cu	65	ppm				
Zn	66	ppm				
Rb	85	ppm				
Sr	86	ppm	190.0859	221.7068	133.8073	91.68019
Y	89	ppm	1052.663	1205.812	1188.595	872.7213
Nb	93	ppm				
Ba	137	ppm	<9.6	20.16231	213.2488	<66.2
Pb	208	ppm	<0.6	1.575363	4.792938	1.239099
Th	232	ppm	<0.2	<0.4	<0.1	<1.4
U	238	ppm	<0.2	<0.5	<0.1	<0.8

Chondrite Normalized

	Analysis Number:		lbv7a-11	lbv7a-12	lbv7a-13	lbv7a-14
	Type:		LBV-D	LBV-D	LBV-D	LBV-D
Element	**Mass**	**Unit**				
La	139	ppm	86.6157	76.55083	61.33244	67.2922
Ce	140	ppm	65.6055	55.62898	64.24994	61.50053
Pr	141	ppm	83.4559	63.85543	60.79165	54.8254
Nd	145	ppm	70.16555	82.52391	67.91341	45.21538
Pm	145	ppm				
Sm	147	ppm	113.5597	140.8243	83.76608	77.94447
Eu	151	ppm	50.96419	58.32311	34.80029	31.64877
Gd	157	ppm	120.9527	142.7896	123.638	79.20377
Tb	159	ppm	137.0183	128.6766	136.536	50.25708
Dy	163	ppm	173.5251	135.011	133.0087	79.89969
Y	89	ppm	467.85	535.9167	528.2643	387.8761
Ho	165	ppm	143.1734	142.731	132.3653	68.68142
Er	167	ppm	132.648	97.73921	124.3936	76.89841
Tm	169	ppm	83.86404	80.74681	82.17561	49.12089
Yb	173	ppm	59.62509	71.69956	55.8007	35.73144
Lu	175	ppm	45.09624	18.863	32.98617	29.91731

St. Lawrence Fluorite

Analysis Number: / Type: / Element	Mass	Unit	n GNV	Maximum GNV	Minimum GNV	Mean GNV	Sigma GNV
Na2O	23	wt%					
MgO	25	wt%	11	5.99525	-1.958151	0.937833	2.471982
K2O	39	wt%					
CaO	43	wt%	11	72	72	72	0
Mn	55	ppm	11	1.188916	-1.256533	0.023043	0.60754
Cu	65	ppm					
Zn	66	ppm					
Rb	85	ppm					
Sr	86	ppm	11	98.19798	52.81881	72.80922	13.5884
Y	89	ppm	11	1928.497	48.56956	999.9083	631.0834
Nb	93	ppm					
Ba	137	ppm	11	25.96039	2.816996	5.997143	6.709279
Pb	208	ppm					
Th	232	ppm	11	0.017729	-0.027227	-0.000885	0.01219
U	238	ppm	11	0.863137	-0.001921	0.145688	0.260796

Chondrite Normalized

Analysis Number: / Type: / Element	Mass	Unit	n GNV	Maximum GNV	Minimum GNV	Mean GNV	Sigma GNV
La	139	ppm	11	110.7619	57.99941	84.7915	14.98099
Ce	140	ppm	11	133.0394	54.08565	89.5419	21.45471
Pr	141	ppm	11	158.3308	55.66847	103.873	29.00152
Nd	145	ppm	11	174.0833	47.4751	100.1053	34.0919
Pm	145	ppm					
Sm	147	ppm	11	156.4642	35.97543	84.5837	36.01363
Eu	151	ppm	11	54.12412	16.26929	30.6198	13.207
Gd	157	ppm	11	141.1284	35.64176	94.28401	36.13376
Tb	159	ppm	11	160.1068	15.14878	92.84573	46.48986
Dy	163	ppm	11	161.9474	6.215641	89.28416	51.04847
Y	89	ppm	11	857.1098	21.58647	444.4037	280.4815
Ho	165	ppm	11	168.1097	4.012673	85.04187	55.25372
Er	167	ppm	11	155.7193	1.707585	70.79923	51.54498
Tm	169	ppm	11	123.5387	0.256166	49.49867	40.48356
Yb	173	ppm	11	95.20679	0.138215	32.1292	30.36271
Lu	175	ppm	11	61.63774	-0.418772	22.24084	20.02427

St. Lawrence Fluorite

Analysis Number: / Type:			n	Maximum	Minimum	Mean	Sigma
Element	**Mass**	**Unit**	**ISV**	**ISV**	**ISV**	**ISV**	**ISV**
Na2O	23	wt%					
MgO	25	wt%	5	0.75743	-0.437385	0.234057	0.449391
K2O	39	wt%					
CaO	43	wt%	5	72	72	72	0
Mn	55	ppm	5	0.36552	0.032542	0.158682	0.12703
Cu	65	ppm					
Zn	66	ppm					
Rb	85	ppm					
Sr	86	ppm	5	34.64352	11.94319	20.73365	10.08559
Y	89	ppm	5	811.3004	226.3793	471.0735	298.1085
Nb	93	ppm					
Ba	137	ppm	5	2.971124	1.913376	2.2714	0.461946
Pb	208	ppm					
Th	232	ppm	4	0.019022	0.005244	0.009358	0.006503
U	238	ppm	4	0.017575	-0.00284	0.00431	0.009148

Chondrite Normalized

Analysis Number: / Type:			n	Maximum	Minimum	Mean	Sigma
Element	**Mass**	**Unit**	**ISV**	**ISV**	**ISV**	**ISV**	**ISV**
La	139	ppm	5	13.48192	0.198588	3.805986	5.540496
Ce	140	ppm	5	13.46774	0.210102	3.885386	5.493528
Pr	141	ppm	5	13.86497	0.357587	4.293549	5.535441
Nd	145	ppm	5	13.53694	0.34206	4.171429	5.475719
Pm	145	ppm					
Sm	147	ppm	5	18.91769	1.363034	6.993108	7.5676
Eu	151	ppm	5	2.819607	0.309074	0.987366	1.079025
Gd	157	ppm	5	23.20902	6.77877	12.37223	6.722209
Tb	159	ppm	5	26.88693	10.09525	19.02777	6.753936
Dy	163	ppm	5	42.99471	14.43462	27.23695	12.5356
Y	89	ppm	5	360.5779	100.613	209.366	132.4927
Ho	165	ppm	5	51.94091	13.72673	32.41212	17.77034
Er	167	ppm	5	58.3332	14.63866	35.83715	20.37392
Tm	169	ppm	5	47.80101	10.26196	31.75087	17.752
Yb	173	ppm	5	40.21838	8.965854	26.97309	14.58886
Lu	175	ppm	5	30.7271	7.094407	19.58277	9.938549

St. Lawrence Fluorite

Analysis Number: / Type:			n	Maximum	Minimum	Mean	Sigma
Element	**Mass**	**Unit**	**LBV**	**LBV**	**LBV**	**LBV**	**LBV**
Na2O	23	wt%					
MgO	25	wt%					
K2O	39	wt%					
CaO	43	wt%	14	72	72	72	0
Mn	55	ppm					
Cu	65	ppm					
Zn	66	ppm					
Rb	85	ppm					
Sr	86	ppm	14	2530.124	91.68019	499.3398	694.6551
Y	89	ppm	14	1719.737	716.4633	950.0704	302.2486
Nb	93	ppm					
Ba	137	ppm	14	239114.1	17.09961	70022.52	103760.9
Pb	208	ppm	14	17749.81	1.239099	2362.173	5878.252
Th	232	ppm	14	0	0	#DIV/0!	#DIV/0!
U	238	ppm	14	0	0	0	#DIV/0!

Chondrite Normalized

Analysis Number: / Type:			n	Maximum	Minimum	Mean	Sigma
Element	**Mass**	**Unit**	**LBV**	**LBV**	**LBV**	**LBV**	**LBV**
La	139	ppm	13	119.8868	39.47977	69.80041	25.1283
Ce	140	ppm	13	117.347	36.68316	63.60661	22.58022
Pr	141	ppm	13	110.9107	37.63416	68.38452	21.17093
Nd	145	ppm	13	128.1464	34.99123	68.40001	26.87844
Pm	145	ppm					
Sm	147	ppm	13	184.1689	52.19147	99.71458	37.72994
Eu	151	ppm	13	58.32311	14.3351	36.46234	13.8279
Gd	157	ppm	13	198.1121	79.20377	124.7444	33.73036
Tb	159	ppm	13	241.9625	50.25708	136.1879	52.45605
Dy	163	ppm	13	278.7645	79.89969	157.3701	59.32612
Y	89	ppm	13	764.3276	318.4281	496.7591	130.2737
Ho	165	ppm	13	307.8348	68.68142	151.2553	67.47673
Er	167	ppm	13	317.6539	65.50782	143.6512	84.00196
Tm	169	ppm	13	349.3993	49.12089	122.704	95.88046
Yb	173	ppm	13	274.2002	31.75574	94.2155	88.57066
Lu	175	ppm	13	185.8337	10.7673	57.96363	52.73424

Rock Canyon Creek Fluorite

Analysis Number:		MR15C03	MR15C04	MR15C05	MR15C06	MR15C07	MR15C08
Group:		B/V	B/V	B/V	B/V	B/V	B/V
Type:		Core	Core	Core	Core	Core	Core
Element	Unit						
Na2O	wt%	0.094	0.073	0.052	0.054	0.064	0.057
MgO	wt%	0.001	0.001	0.001	0.000	0.041	0.007
SiO2	wt%	0.438	0.116	0.088	0.128	0.176	0.157
K2O	wt%	0.002	<0.000	<0.000	<0.000	0.001	0.002
CaO	wt%	71.821	71.821	71.821	71.821	71.821	71.821
Cu	ppm	0.684	0.879	0.681	0.673	1.451	2.716
Zn	ppm	0.279	0.299	0.290	0.469	1.070	3.426
Rb	ppm	0.188	0.132	0.069	<0.069	0.345	0.405
Sr	ppm	1215.893	1286.679	1542.909	1637.958	1063.673	3624.649
Nb	ppm	<0.066	<0.050	<0.036	0.043	2.723	1.265
Ba	ppm	6.903	4.934	5.051	4.166	14.874	59.427
La	ppm	30.944	33.802	32.177	30.959	83.528	313.189
Ce	ppm	66.260	80.648	75.749	73.737	202.306	884.711
Pr	ppm	12.144	17.778	14.447	12.182	40.485	124.168
Nd	ppm	66.119	95.776	62.282	50.119	192.599	663.448
Sm	ppm	27.336	42.933	19.128	14.346	94.397	340.339
Eu	ppm	13.671	18.578	7.181	5.321	55.410	204.254
Gd	ppm	31.557	50.121	15.167	11.267	134.347	549.222
Tb	ppm	10.512	15.577	4.882	3.706	53.470	182.209
Dy	ppm	90.497	139.418	42.634	34.100	396.233	1521.580
Y	ppm	175.043	218.300	84.186	87.198	1579.279	2686.555
Ho	ppm	22.965	34.309	10.518	8.550	71.994	262.712
Er	ppm	81.394	117.454	40.176	32.359	192.676	631.567
Tm	ppm	15.376	22.755	9.675	8.205	29.617	71.490
Yb	ppm	102.832	153.370	74.610	63.381	170.431	318.792
Lu	ppm	15.457	22.059	12.716	10.680	22.355	35.136
Pb	ppm	5.878	6.543	4.141	4.696	14.702	55.044
Th	ppm	1574.044	2146.741	1189.776	1427.699	5290.974	15308.204
U	ppm	0.596	0.326	0.177	0.182	1.698	5.926

Rock Canyon Creek Fluorite

Analysis Number:		MR15C09	MR15C10	MR15C11	MR15C12	MR15C13	MR15C14
Group:		B/V	B/V	B/V	B/V	B/V	B/V
Type:		Core	Ppl Rim	Ppl Rim	Ppl Rim	Ppl Rim	Ppl Rim
Element	Unit						
Na2O	wt%	0.072	0.070	0.086	0.086	0.053	0.056
MgO	wt%	0.000	0.001	0.002	0.002	0.000	0.001
SiO2	wt%	0.243	0.098	0.125	0.100	0.162	0.201
K2O	wt%	<0.000	<0.000	0.002	0.002	<0.000	<0.000
CaO	wt%	71.821	71.821	71.821	71.821	71.821	71.821
Cu	ppm	1.011	0.871	0.750	0.729	0.751	1.353
Zn	ppm	<0.176	0.564	0.379	0.569	0.172	1.836
Rb	ppm	0.198	0.142	0.164	0.200	<0.106	<0.132
Sr	ppm	744.986	797.347	1097.362	1065.048	1393.473	1087.374
Nb	ppm	<0.037	0.074	0.130	0.080	<0.025	0.034
Ba	ppm	4.421	6.195	18.167	18.350	3.489	4.087
La	ppm	22.374	30.878	98.560	100.990	32.837	24.331
Ce	ppm	62.479	81.368	130.467	131.964	80.605	58.743
Pr	ppm	15.570	25.194	16.379	15.544	14.152	10.432
Nd	ppm	101.913	119.188	57.294	55.245	62.591	47.189
Sm	ppm	63.517	73.280	11.977	11.644	18.180	13.916
Eu	ppm	35.529	39.540	4.284	4.255	6.951	5.276
Gd	ppm	113.557	129.347	16.022	16.438	13.973	10.953
Tb	ppm	36.031	40.168	2.795	2.775	4.437	3.342
Dy	ppm	289.742	336.252	21.990	22.641	38.537	30.411
Y	ppm	1937.499	2129.901	79.412	78.610	69.541	75.473
Ho	ppm	70.150	82.002	5.860	5.767	9.894	7.907
Er	ppm	210.151	237.950	21.021	19.914	37.026	29.072
Tm	ppm	32.501	37.950	4.304	4.477	9.041	7.664
Yb	ppm	187.112	221.729	32.253	33.072	70.413	60.885
Lu	ppm	24.158	29.223	5.282	5.344	11.968	10.459
Pb	ppm	3.413	5.852	9.972	11.308	4.216	3.984
Th	ppm	696.889	1763.680	4630.429	4864.044	1119.988	826.502
U	ppm	0.106	0.206	2.554	2.619	0.226	0.149

Rock Canyon Creek Fluorite

Analysis Number:		MR15C15	MR15C16	MR15C17	MR15C18	MR15D03	MR15D04
Group:		B/V	B/V	B/V	B/V	B/V	B/V
Type:		Ppl Rim	Ppl	Ppl	Ppl	Ppl	Ppl
Element	Unit						
Na2O	wt%	0.058	0.064	0.072	0.050	0.072	0.037
MgO	wt%	0.023	0.040	0.002	0.001	0.013	0.003
SiO2	wt%	0.257	0.176	0.249	0.146	0.196	0.161
K2O	wt%	0.000	0.000	0.000	<0.000	0.001	<0.000
CaO	wt%	71.821	71.821	71.821	71.821	71.821	71.821
Cu	ppm	1.938	1.787	1.388	<11.097	9.136	1.583
Zn	ppm	2.941	5.827	1.155	0.397	5.508	1.652
Rb	ppm	0.244	0.161	0.186	0.149	<0.132	<0.095
Sr	ppm	244.716	281.575	531.871	171.757	57.215	35.253
Nb	ppm	6.702	2.050	0.080	0.365	0.290	0.061
Ba	ppm	9.671	5.672	5.937	6.018	11.024	8.339
La	ppm	113.364	10.542	19.237	9.476	8.601	0.874
Ce	ppm	325.220	25.450	68.866	21.934	13.590	1.705
Pr	ppm	53.801	4.954	14.031	5.510	1.774	0.350
Nd	ppm	378.239	25.661	94.431	33.081	5.551	2.061
Sm	ppm	178.038	14.655	60.103	21.989	1.713	1.089
Eu	ppm	104.283	8.158	32.689	11.707	0.653	0.754
Gd	ppm	276.285	25.689	103.588	41.547	3.130	4.888
Tb	ppm	99.759	10.013	30.652	18.611	0.621	1.222
Dy	ppm	811.365	107.295	256.106	133.090	6.891	16.226
Y	ppm	2451.434	1727.576	1673.600	1696.647	132.489	392.145
Ho	ppm	170.570	35.757	59.828	48.546	2.538	5.794
Er	ppm	348.370	136.996	168.867	133.691	9.359	23.649
Tm	ppm	42.098	24.990	26.058	24.530	1.897	4.525
Yb	ppm	250.690	169.245	145.167	162.225	14.556	33.511
Lu	ppm	25.397	21.382	18.690	20.830	2.125	4.584
Pb	ppm	26.424	53.667	5.491	2.807	2.388	0.625
Th	ppm	10263.444	744.080	1191.224	795.082	7.668	5.021
U	ppm	3.127	0.560	0.176	0.230	<0.066	<0.034

Rock Canyon Creek Fluorite

Analysis Number:		MR15D05	MR15D06	MR15D07	MR15D08	MR15D09	MR15D10
Group:		B/V	B/V	B/V	B/V	B/V	B/V
Type:		Ppl	Ppl	Ppl	Ppl	Ppl	Ppl
Element	Unit						
Na2O	wt%	0.023	0.036	0.095	0.052	0.063	0.071
MgO	wt%	0.001	0.000	0.002	0.001	0.583	0.078
SiO2	wt%	0.099	0.119	0.162	0.187	0.194	0.181
K2O	wt%	<0.000	<0.000	0.000	0.000	0.001	0.001
CaO	wt%	71.821	71.821	71.821	71.821	71.821	71.821
Cu	ppm	0.965	1.141	1.461	1.655	2.039	1.336
Zn	ppm	0.431	0.455	0.774	0.706	4.201	1.355
Rb	ppm	<0.094	<0.132	0.086	<0.087	0.083	0.103
Sr	ppm	38.762	302.066	501.566	1014.100	932.354	951.863
Nb	ppm	<0.038	<0.044	<0.053	0.023	0.873	0.711
Ba	ppm	3.707	3.799	3.134	5.700	7.749	10.628
La	ppm	2.219	0.702	0.892	40.657	39.480	43.829
Ce	ppm	4.472	2.362	2.394	91.087	81.285	82.316
Pr	ppm	0.820	0.467	0.534	16.324	12.943	12.684
Nd	ppm	3.947	2.364	3.057	71.731	52.341	51.282
Sm	ppm	1.491	1.367	1.598	23.019	15.785	14.781
Eu	ppm	0.674	0.793	0.840	9.550	6.486	5.980
Gd	ppm	2.282	2.338	2.274	24.698	17.140	16.569
Tb	ppm	0.842	0.615	0.634	6.591	4.402	4.150
Dy	ppm	10.851	5.354	5.112	59.017	35.664	35.614
Y	ppm	155.344	42.023	19.967	174.340	125.716	114.057
Ho	ppm	3.548	1.492	1.255	14.017	9.562	9.054
Er	ppm	14.004	5.065	4.179	45.238	30.089	30.241
Tm	ppm	2.834	0.948	0.768	9.637	6.316	6.311
Yb	ppm	19.644	7.454	6.092	66.715	45.009	47.380
Lu	ppm	2.989	1.229	0.956	10.347	7.472	7.662
Pb	ppm	0.327	0.248	0.718	6.889	10.077	10.881
Th	ppm	9.484	6.383	8.038	2759.231	3492.814	4535.721
U	ppm	<0.019	0.025	<0.027	0.222	0.632	0.730

Rock Canyon Creek Fluorite

Analysis Number:		MR15D11	MR15D12	MR15D13	MR15D14	MR15D15	MR15D16
Group:		B/V	B/V	B/V	B/V	B/V	B/V
Type:		Ppl	Ppl	Ppl	Ppl	Ppl	Clear
Element	Unit						
Na2O	wt%	0.089	0.072	0.038	0.029	0.024	0.025
MgO	wt%	2.081	0.146	0.016	0.007	0.013	0.001
SiO2	wt%	3.306	0.249	0.115	0.159	0.219	0.169
K2O	wt%	0.016	0.003	<0.000	0.000	0.001	<0.000
CaO	wt%	71.821	71.821	71.821	71.821	71.821	71.821
Cu	ppm	53.373	52.095	1.261	2.079	2.231	1.475
Zn	ppm	381.239	26.638	2.071	5.059	2.772	0.661
Rb	ppm	1.178	0.133	<0.070	<0.066	<0.076	<0.084
Sr	ppm	1286.140	1123.400	394.511	68.356	146.169	49.587
Nb	ppm	9.402	0.100	0.030	0.034	0.053	<0.031
Ba	ppm	406.077	6.171	8.676	6.379	107.771	3.877
La	ppm	882.474	50.136	2.911	2.452	86.271	0.766
Ce	ppm	1922.132	119.393	5.449	3.396	141.747	1.602
Pr	ppm	260.704	19.785	1.032	0.801	13.735	0.250
Nd	ppm	1085.978	88.885	4.646	3.844	15.825	1.437
Sm	ppm	254.988	26.403	2.365	1.806	3.356	1.276
Eu	ppm	94.708	11.136	1.103	1.085	1.422	0.956
Gd	ppm	300.505	28.110	3.531	5.938	5.572	4.539
Tb	ppm	34.409	7.442	0.912	1.770	1.302	2.169
Dy	ppm	185.937	59.625	7.380	24.483	14.320	27.133
Y	ppm	498.623	178.388	38.350	336.326	210.807	279.035
Ho	ppm	30.481	13.856	1.884	7.895	4.220	8.713
Er	ppm	64.220	45.140	5.658	31.195	14.805	32.257
Tm	ppm	8.370	9.268	1.171	6.406	2.677	6.330
Yb	ppm	43.758	64.920	8.827	45.954	18.782	44.527
Lu	ppm	5.748	9.800	1.411	6.372	2.469	6.476
Pb	ppm	217.701	21.089	1.225	0.968	1.091	0.430
Th	ppm	14294.381	2117.470	47.174	36.874	66.790	13.477
U	ppm	2.093	0.725	0.041	<0.019	0.019	<0.012

Rock Canyon Creek Fluorite

Analysis Number:		MR15D17	MR15D18	MR22A03	MR22A04	MR22A05	MR22A06
Group:		B/V	B/V	B/V	B/V	B/V	B/V
Type:		Clear	Clear	White	W. Vein	Clear Vein	Clear Vein
Element	Unit						
Na2O	wt%	0.020	0.046	0.019	0.015	0.063	0.065
MgO	wt%	0.001	0.314	0.014	0.011	0.468	0.339
SiO2	wt%	0.117	0.254	0.238	0.046	0.379	0.37
K2O	wt%	<0.000	0.001	0.004	<0.000	0.001	0.001
CaO	wt%	71.821	71.821	71.821	71.821	71.821	71.821
Cu	ppm	1.060	4.393	2.036	1.13	2.364	1.884
Zn	ppm	0.857	7.137	1.393	0.351	2.517	3.097
Rb	ppm	<0.044	0.083	0.04	<0.021	0.076	0.058
Sr	ppm	38.653	956.074	87.513	50.676	1058.063	1085.412
Nb	ppm	<0.018	0.356	0.03	0.02	0.124	0.065
Ba	ppm	4.357	6.941	5.843	4.741	12.918	14.997
La	ppm	0.533	41.253	4.605	3.332	32.219	16.089
Ce	ppm	0.699	96.757	8.575	6.054	61.656	39.538
Pr	ppm	0.204	16.616	1.222	0.812	8.524	6.093
Nd	ppm	1.144	70.688	4.324	2.649	29.52	24.222
Sm	ppm	1.293	22.199	0.786	0.405	4.668	5.607
Eu	ppm	1.018	9.034	0.359	0.139	1.516	2.151
Gd	ppm	5.874	23.429	1.374	0.572	4.924	5.388
Tb	ppm	2.346	5.870	0.264	0.092	0.902	1.477
Dy	ppm	27.330	50.830	2.51	0.735	7.305	14.506
Y	ppm	356.774	194.543	73.316	37.013	61.457	129.883
Ho	ppm	8.043	12.644	0.727	0.219	1.802	4.012
Er	ppm	27.034	42.109	2.386	0.679	6.309	14.808
Tm	ppm	5.040	8.453	0.357	0.083	1.241	2.966
Yb	ppm	33.153	60.126	1.995	0.547	10.045	22.36
Lu	ppm	4.571	9.416	0.219	0.06	1.661	3.382
Pb	ppm	0.383	7.467	0.365	0.211	1.473	2.217
Th	ppm	33.367	1406.979	4.047	2.083	5.64	1.09
U	ppm	<0.010	0.492	0.046	0.029	0.093	0.286

Rock Canyon Creek Fluorite

Analysis Number:		MR22A07	MR22A08	MR22A09	MR22A10	MR22A11	MR22A12
Group:		B/V	B/V	B/V	B/V	B/V	B/V
Type:		Clr & Ppl	Clr & Ppl	Purple	Purple	Purple	Purple
Element	Unit						
Na2O	wt%	0.027	0.025	0.052	0.04	0.013	0.036
MgO	wt%	0.002	0	0.022	0.004	0.003	0.689
SiO2	wt%	0.125	0.108	0.268	0.122	0.064	0.152
K2O	wt%	0.001	0	0	0	<0.000	0
CaO	wt%	71.821	71.821	71.821	71.821	71.821	71.821
Cu	ppm	2.203	1.131	1.952	1.852	2.806	4.763
Zn	ppm	0.794	0.622	0.705	1.009	2.337	4.341
Rb	ppm	0.052	0.018	0.049	0.063	0.021	0.043
Sr	ppm	34.336	34.047	39.094	39.115	16.908	245.128
Nb	ppm	0.195	0.066	0.028	0.099	0.018	0.065
Ba	ppm	4.539	4.171	4.68	4.807	6.105	441.185
La	ppm	1.806	4.443	2.017	0.8	2.407	6.18
Ce	ppm	2.518	8.463	3.225	1.486	7.255	11.606
Pr	ppm	0.361	0.919	0.402	0.225	0.566	1.664
Nd	ppm	1.076	3.079	1.442	0.809	2.497	5.989
Sm	ppm	0.124	0.313	0.181	0.168	0.546	1.483
Eu	ppm	0.044	0.092	0.063	0.054	0.261	0.817
Gd	ppm	0.183	0.363	0.289	0.316	1.81	159.689
Tb	ppm	0.034	0.05	0.038	0.05	0.21	0.549
Dy	ppm	0.158	0.399	0.332	0.425	1.761	5.268
Y	ppm	16.677	21.271	17.257	23.742	57.333	109.365
Ho	ppm	0.071	0.116	0.08	0.127	0.447	1.424
Er	ppm	0.209	0.36	0.289	0.389	1.41	5.18
Tm	ppm	0.032	0.045	0.048	0.052	0.203	0.783
Yb	ppm	0.171	0.236	0.315	0.293	1.074	4.943
Lu	ppm	0.024	0.036	0.037	0.032	0.104	0.596
Pb	ppm	8.099	0.184	0.332	0.449	2.255	1.526
Th	ppm	0.049	0.921	0.273	0.319	0.95	1.512
U	ppm	<0.006	0.008	0.007	0.05	0.047	0.033

Rock Canyon Creek Fluorite

Analysis Number:		MR22A13	MR22A14	MR22A15	MR22A16	MR22A17	MR22A18
Group:		B/V	B/V	Dissem'd	Dissem'd	Dissem'd	Dissem'd
Type:		Purple	Purple	Rose	Rose	Rose	Rose
Element	Unit						
Na2O	wt%	0.02	0.054	0.019	0.029	0.027	0.019
MgO	wt%	0.001	0.002	0.005	0.098	0.021	0.059
SiO2	wt%	0.119	0.117	0.127	0.127	0.115	2.138
K2O	wt%	<0.000	<0.000	0	0	<0.000	0
CaO	wt%	71.821	71.821	71.821	71.821	71.821	71.821
Cu	ppm	1.122	1.789	2.928	3.988	7.972	2.189
Zn	ppm	0.352	0.733	1.696	1.81	1.646	2.454
Rb	ppm	<0.028	<0.023	0.036	<0.028	0.025	0.14
Sr	ppm	54.097	93.509	92.909	46.632	58.086	71.472
Nb	ppm	0.031	0.117	0.098	0.02	0.029	0.086
Ba	ppm	4.024	4.667	6.482	6.302	65.471	4.618
La	ppm	4.07	5.303	11.242	2.823	2.035	7.967
Ce	ppm	6.011	8.694	55.707	4.264	2.886	12.862
Pr	ppm	1.417	1.38	2.684	0.672	0.377	1.757
Nd	ppm	3.291	4.015	11.443	2.397	1.143	6.381
Sm	ppm	0.444	0.481	1.515	0.293	0.251	0.854
Eu	ppm	0.156	0.169	0.425	0.143	0.076	0.335
Gd	ppm	0.403	1.926	2.667	1.512	23.646	1.438
Tb	ppm	0.074	0.129	0.234	0.094	0.073	0.169
Dy	ppm	0.667	0.99	1.19	0.722	0.625	1.238
Y	ppm	40.994	54.572	59.713	40.205	39.917	45.328
Ho	ppm	0.164	0.236	0.354	0.208	0.164	0.318
Er	ppm	0.53	0.709	1.013	0.654	0.448	0.763
Tm	ppm	0.067	0.105	0.157	0.109	0.092	0.111
Yb	ppm	0.386	0.51	0.929	0.834	0.398	0.722
Lu	ppm	0.03	0.061	0.126	0.084	0.039	0.068
Pb	ppm	0.193	0.304	25.004	0.742	2.708	0.93
Th	ppm	1.165	1.173	3.246	0.439	0.7	2.598
U	ppm	0.011	0.012	0.02	<0.007	0.02	0.021

Rock Canyon Creek Fluorite

Analysis Number:		MR22B04	MR22B05	MR22B06	MR22B07	MR22B08	MR22B09
Group:		Dissem'd	Dissem'd	Dissem'd	Dissem'd	Dissem'd	Dissem'd
Type:		Rose	Rose	Rose	Rose	Rose	Clear
Element	Unit						
Na2O	wt%	0.116	0.091	0.063	0.078	0.025	0.021
MgO	wt%	0.098	0.897	0.213	0.094	0.029	0.278
SiO2	wt%	0.504	0.414	0.156	0.143	0.185	0.133
K2O	wt%	0.004	0.004	0.002	0.003	0	0
CaO	wt%	71.821	71.821	71.821	71.821	71.821	71.821
Cu	ppm	4.805	8.068	4.446	7.297	1.739	2.23
Zn	ppm	1.925	9.608	1.802	7.662	2.569	1.011
Rb	ppm	0.098	0.091	0.059	0.091	0.463	<0.032
Sr	ppm	358.009	331.648	305.955	168.037	25.257	34.311
Nb	ppm	4.278	2.501	5.845	2.8	0.091	0.422
Ba	ppm	8683.803	17562.048	996.999	1130.054	227.174	23.943
La	ppm	66.325	43.285	33.882	30.452	15.917	14.114
Ce	ppm	58.981	45.453	31.684	31.735	16.547	16.135
Pr	ppm	4.652	4.329	2.747	2.965	1.947	1.793
Nd	ppm	13.181	11.035	8.401	9.657	5.808	5.167
Sm	ppm	2.675	2.554	2.094	2.225	1.598	1.068
Eu	ppm	1.847	2.524	1.345	1.271	0.635	0.607
Gd	ppm	1966.156	5898.687	298.339	132.293	17.996	10.697
Tb	ppm	0.882	0.986	0.915	0.84	0.531	0.456
Dy	ppm	6.236	7.105	6.326	6.846	3.913	3.617
Y	ppm	107.878	131.901	119.097	145.345	96.92	95.369
Ho	ppm	1.52	1.88	1.532	1.596	1.023	0.855
Er	ppm	4.203	5.378	4.336	4.53	2.529	2.184
Tm	ppm	0.663	0.822	0.701	0.681	0.326	0.278
Yb	ppm	3.736	4.777	4.001	4.034	1.764	1.481
Lu	ppm	0.486	0.755	0.496	0.588	0.151	0.168
Pb	ppm	0.623	5.331	1.755	1.175	0.636	0.888
Th	ppm	7.142	6.845	6.829	8.155	5.59	3.243
U	ppm	0.046	0.123	0.101	0.052	0.104	0.011

Rock Canyon Creek Fluorite

Analysis Number:		MR22B10	MR22B11	MR22B12	MR22B13	MR22B14	MR22B16
Group:		Dissem'd	Dissem'd	Dissem'd	Dissem'd	Dissem'd	Dissem'd
Type:		Clear	Clear	Clear	Clear	Clear	Clear
Element	Unit						
Na2O	wt%	0.056	0.034	0.063	0.065	0.052	0.057
MgO	wt%	0.24	0.102	0.1	0.078	0.957	4.789
SiO2	wt%	0.185	0.186	0.172	0.162	0.175	0.296
K2O	wt%	0.001	0	0.006	0.002	0.003	0.001
CaO	wt%	71.821	71.821	71.821	71.821	71.821	71.821
Cu	ppm	2.933	5.191	4.836	4.26	5.822	3.129
Zn	ppm	1.984	1.05	5.208	2.294	4.206	28.278
Rb	ppm	<0.030	<0.039	0.08	0.102	0.053	0.072
Sr	ppm	253.005	26.388	585.565	769.456	328.616	467.772
Nb	ppm	4.245	0.089	1.183	6.915	1.078	2.54
Ba	ppm	17.325	4.778	100.331	706.833	63.197	20.968
La	ppm	35.195	15.43	12.682	53.591	110.495	58.316
Ce	ppm	37.639	13.648	18.13	55.529	145.849	69.624
Pr	ppm	3.457	1.407	2.278	6.242	10.191	7.021
Nd	ppm	10.372	4.131	8.185	20.714	27.007	18.67
Sm	ppm	2.332	0.993	3.11	6.083	4.898	3.053
Eu	ppm	1.287	0.525	2.101	2.846	2.174	1.311
Gd	ppm	10.185	2.838	46.987	59.809	33.202	14.426
Tb	ppm	0.98	0.438	1.61	1.894	1.259	0.734
Dy	ppm	7.566	3.275	12.882	14.615	8.94	5.231
Y	ppm	158.868	92.772	198.659	216.26	159.81	141.155
Ho	ppm	1.93	0.739	2.912	3.461	2.172	1.347
Er	ppm	6.095	2.128	8.675	9.959	6.272	3.923
Tm	ppm	0.924	0.266	1.312	1.536	0.918	0.579
Yb	ppm	5.743	1.251	7.852	8.671	5.235	3.317
Lu	ppm	0.763	0.21	1.044	1.026	0.679	0.434
Pb	ppm	0.605	0.437	0.967	2.161	1.779	2.08
Th	ppm	5.811	1.189	53.642	66.368	19.501	2.491
U	ppm	0.032	0.041	0.858	0.969	0.188	0.027

Rock Canyon Creek Fluorite

Analysis Number:		MR22B17	MR22B18	MR22C03	MR22C04	MR22C05
Group:		Dissem'd	Dissem'd	Dissem'd	Rplcment	Rplcment
Type:		Clear	Clear	White	Patchy	Patchy
Element	Unit					
Na2O	wt%	0.047	0.026	0.186	0.144	0.138
MgO	wt%	0.07	0.103	5.241	0.114	1.094
SiO2	wt%	0.151	0.137	0.665	1.711	0.38
K2O	wt%	0.001	0	0.002	0.003	0.004
CaO	wt%	71.821	71.821	71.821	71.821	71.821
Cu	ppm	4.081	1.669	9.378	61.09	64.038
Zn	ppm	1.057	0.647	28.89	43.565	65.029
Rb	ppm	0.056	<0.036	0.195	0.202	0.312
Sr	ppm	333.982	123.637	7537.225	7343.323	9412.158
Nb	ppm	1.409	12.534	296.856	1132.27	2528.383
Ba	ppm	23.734	5.989	20653.438	649048.398	712366.005
La	ppm	21.829	24.597	482328.958	276302.873	417958.491
Ce	ppm	20.102	24.328	365083.473	216991.209	296984.08
Pr	ppm	2.054	2.366	30791.2	19295.204	24273.105
Nd	ppm	5.468	6.83	69399.373	43007.606	56311.039
Sm	ppm	1.442	1.274	2186.515	1612.875	1923.707
Eu	ppm	0.69	0.568	500.91	369.243	459.03
Gd	ppm	9.844	3.43	8466.383	174259.109	195855.325
Tb	ppm	0.534	0.463	135.339	70.933	91.898
Dy	ppm	4.208	3.939	328.703	199.874	242.263
Y	ppm	142.687	119.732	1894.043	1380.391	1562.02
Ho	ppm	1.089	0.939	60.629	35.568	42.852
Er	ppm	3.319	2.621	167.603	78.506	97.75
Tm	ppm	0.49	0.352	32.651	9.934	13.515
Yb	ppm	2.788	1.762	264.281	53.84	81.243
Lu	ppm	0.33	0.205	38.271	6.947	10.632
Pb	ppm	0.778	1.427	72.332	50.179	70.075
Th	ppm	2.179	6.286	12591.222	6953.769	10859.701
U	ppm	<0.011	0.184	0.965	0.745	0.972

Rock Canyon Creek Fluorite

Analysis Number:		MR22C08	MR22C09	MR22C10	MR22C12	MR22C13
Group:		Rplcment	Rplcment	Rplcment	Rplcment	Rplcment
Type:		Patchy	Patchy	Patchy	Patchy	Patchy
Element	Unit					
Na2O	wt%	0.103	0.446	0.074	0.267	0.398
MgO	wt%	1.531	0.218	1.105	0.139	0.054
SiO2	wt%	0.28	3.148	0.274	0.675	0.986
K2O	wt%	0.002	0.228	0.004	0.032	0.013
CaO	wt%	71.821	71.821	71.821	71.821	71.821
Cu	ppm	3.761	142.188	4.211	103.414	29.496
Zn	ppm	6.025	118.198	5.572	65.603	61.122
Rb	ppm	0.1	10.996	0.206	1.025	0.518
Sr	ppm	1000.384	20594.668	509.599	1066.745	2584.942
Nb	ppm	14.556	378.047	8.111	5.766	3.944
Ba	ppm	48.66	862638.019	4010.296	722.548	2328.123
La	ppm	266706.658	1830708.984	39947.691	344273.345	860425.668
Ce	ppm	239177.285	1735048.282	35584.145	335790.929	801973.607
Pr	ppm	24033.532	178506.95	3303.211	34813.652	83914.678
Nd	ppm	60611.668	452919.997	6765.558	89251.592	220334.426
Sm	ppm	2248.657	19529.675	331.371	3591.993	9042.509
Eu	ppm	510.105	5048.315	78.281	833.65	2148.948
Gd	ppm	1431.67	243011.179	1692.838	2731.836	6997.559
Tb	ppm	120.234	733.825	17.437	197.031	500.293
Dy	ppm	235.626	1668.716	40.305	402.713	972.508
Y	ppm	1073.862	6950.44	373.852	1486.762	3282.618
Ho	ppm	34.928	238.711	7.016	58.611	134.938
Er	ppm	61.314	383.06	17.783	94.687	207.728
Tm	ppm	7.109	36.767	2.597	8.759	18.819
Yb	ppm	30.52	156.652	14.085	33.582	68.265
Lu	ppm	3.501	16.044	1.73	3.177	6.837
Pb	ppm	24.788	228.975	6.273	65.147	102.256
Th	ppm	3053.986	24637.845	308.103	3249.599	5226.853
U	ppm	0.416	3.095	0.109	0.615	1.749

Rock Canyon Creek Fluorite

Statistic:		n	Minimum	Maximum	Mean	Sigma
Type:		B/V	B/V	B/V	B/V	B/V
Element	Unit					
Na2O	wt%	44	0.013	0.095	0.052	0.022
MgO	wt%	44	0.000	2.081	0.112	0.339
SiO2	wt%	44	0.046	3.306	0.247	0.473
K2O	wt%	44	0.000	0.016	0.002	0.002
CaO	wt%	44	71.821	71.821	71.821	0.000
Cu	ppm	44	0.673	53.373	4.186	10.711
Zn	ppm	44	0.172	381.239	11.150	56.625
Rb	ppm	44	0.018	1.178	0.167	0.189
Sr	ppm	44	16.908	3624.649	648.210	684.867
Nb	ppm	44	0.018	9.402	0.775	1.736
Ba	ppm	44	3.134	441.185	29.417	87.798
La	ppm	44	0.533	882.474	51.693	136.942
Ce	ppm	44	0.699	1922.132	116.045	308.436
Pr	ppm	44	0.204	260.704	17.713	42.227
Nd	ppm	44	0.809	1085.978	83.020	190.061
Sm	ppm	44	0.124	340.339	31.716	66.939
Eu	ppm	44	0.044	204.254	16.116	36.438
Gd	ppm	44	0.183	549.222	49.253	101.725
Tb	ppm	44	0.034	182.209	13.593	31.620
Dy	ppm	44	0.158	1521.580	110.880	259.601
Y	ppm	44	16.677	2686.555	469.138	740.023
Ho	ppm	44	0.071	262.712	23.903	47.931
Er	ppm	44	0.209	631.567	65.822	114.295
Tm	ppm	44	0.032	71.490	10.401	14.346
Yb	ppm	44	0.171	318.792	64.079	75.989
Lu	ppm	44	0.024	35.136	8.659	9.134
Pb	ppm	44	0.184	217.701	11.779	33.519
Th	ppm	44	0.049	15308.204	1879.384	3461.570
U	ppm	44	0.007	5.926	0.679	1.117

Rock Canyon Creek Fluorite

Statistic:		n	Minimum	Maximum	Mean	Sigma
Type:		Dissem'd	Dissem'd	Dissem'd	Dissem'd	Dissem'd
Element	Unit					
Na2O	wt%	19	0.019	0.186	0.057	0.040
MgO	wt%	19	0.005	5.241	0.709	1.501
SiO2	wt%	19	0.115	2.138	0.325	0.451
K2O	wt%	19	0.000	0.006	0.002	0.002
CaO	wt%	19	71.821	71.821	71.821	0.000
Cu	ppm	19	1.669	9.378	4.577	2.202
Zn	ppm	19	0.647	28.890	5.568	8.215
Rb	ppm	19	0.025	0.463	0.112	0.103
Sr	ppm	19	25.257	7537.225	627.261	1641.060
Nb	ppm	19	0.020	296.856	18.054	65.787
Ba	ppm	19	4.618	20653.438	2647.552	5982.694
La	ppm	19	2.035	482328.958	25415.218	107695.605
Ce	ppm	19	2.886	365083.473	19249.715	81513.805
Pr	ppm	19	0.377	30791.200	1623.692	6874.848
Nd	ppm	19	1.143	69399.373	3661.861	15494.481
Sm	ppm	19	0.251	2186.515	117.096	487.769
Eu	ppm	19	0.076	500.910	27.454	111.598
Gd	ppm	19	1.438	8466.383	894.765	2238.929
Tb	ppm	19	0.073	135.339	7.812	30.062
Dy	ppm	19	0.625	328.703	22.483	72.271
Y	ppm	19	39.917	1894.043	210.824	399.659
Ho	ppm	19	0.164	60.629	4.456	13.268
Er	ppm	19	0.448	167.603	12.454	36.658
Tm	ppm	19	0.092	32.651	2.261	7.174
Yb	ppm	19	0.398	264.281	17.030	58.324
Lu	ppm	19	0.039	38.271	2.417	8.456
Pb	ppm	19	0.437	72.332	6.440	16.430
Th	ppm	19	0.439	12591.222	673.341	2809.125
U	ppm	19	0.011	0.969	0.221	0.323

Rock Canyon Creek Fluorite

Statistic: Type: Element	Unit	n Replace't	Minimum Replace't	Maximum Replace't	Mean Replace't	Sigma Replace't
Na2O	wt%	7	0.074	0.446	0.224	0.138
MgO	wt%	7	0.054	1.531	0.608	0.568
SiO2	wt%	7	0.274	3.148	1.065	0.973
K2O	wt%	7	0.002	0.228	0.041	0.077
CaO	wt%	7	71.821	71.821	71.821	0.000
Cu	ppm	7	3.761	142.188	58.314	47.574
Zn	ppm	7	5.572	118.198	52.159	36.175
Rb	ppm	7	0.100	10.996	1.908	3.721
Sr	ppm	7	509.599	20594.668	6073.117	6735.350
Nb	ppm	7	3.944	2528.383	581.582	882.394
Ba	ppm	7	48.660	862638.019	318737.436	370663.624
La	ppm	7	39947.691	1830708.984	576617.673	561464.552
Ce	ppm	7	35584.145	1735048.282	523078.505	540474.478
Pr	ppm	7	3303.211	178506.950	52591.476	56451.448
Nd	ppm	7	6765.558	452919.997	132743.127	144935.750
Sm	ppm	7	331.371	19529.675	5468.684	6304.198
Eu	ppm	7	78.281	5048.315	1349.653	1632.740
Gd	ppm	7	1431.670	243011.179	89425.645	101321.765
Tb	ppm	7	17.437	733.825	247.379	247.120
Dy	ppm	7	40.305	1668.716	537.429	538.057
Y	ppm	7	373.852	6950.440	2301.421	2065.265
Ho	ppm	7	7.016	238.711	78.946	74.995
Er	ppm	7	17.783	383.060	134.404	114.763
Tm	ppm	7	2.597	36.767	13.929	10.442
Yb	ppm	7	14.085	156.652	62.598	43.959
Lu	ppm	7	1.730	16.044	6.981	4.624
Pb	ppm	7	6.273	228.975	78.242	67.991
Th	ppm	7	308.103	24637.845	7755.694	7555.108
U	ppm	7	0.109	3.095	1.100	0.943

Gallinas Mountains Fluorite

	Analysis Number:		De14A03	De14A04	De14A05	De14A06	De14A07
	Type:		P1	P1	P2	P2	P2
Element	**Mass**	**Unit**					
Na2O	23	wt%	0.50962	0.631983	0.702661	7.842664	0.893816
MgO	25	wt%					
K2O	39	wt%	0.027572	0.016832	0.025024	0.178521	0.008634
CaO	43	wt%	71.821	71.821	71.821	71.821	71.821
MnO	55	wt%	0.001071	0.00078	0.000925	0.006429	0.000708
Cu	65	ppm					
Zn	66	ppm					
Rb	85	ppm	0.127309	0.142249	0.286435	2.567791	0.816627
Sr	86	ppm	293.0297	291.497	315.7483	619.2418	1304.935
Y	89	ppm	174.4419	271.6968	885.8783	616.8658	273.6325
Nb	93	ppm	0.069359	0.090601	0.182272	0.122754	0.028516
Ba	137	ppm	7.164111	3.137831	6.306644	5.067861	72.77834
Pb	208	ppm	0.671044	0.08703	0.240593	1.057806	0.155582
Th	232	ppm					
U	238	ppm	0.213676	0.042228	9.924017	0.458206	0.142171

Chondrite Normalized

	Analysis Number:		De14A03	De14A04	De14A05	De14A06	De14A07
	Type:		P1	P1	P2	P2	P2
Element	**Mass**	**Unit**					
La	139	ppm	36.44026	45.96709	336.3972	7219.949	1025.113
Ce	140	ppm	23.91006	34.55938	124.5409	2925.96	514.4136
Pr	141	ppm	39.42446	39.08874	172.8778	4088.037	414.4265
Nd	145	ppm	33.89865	41.05996	125.2064	2379.615	230.4659
Pm	145	ppm					
Sm	147	ppm	17.7955	25.50591	97.09339	800.264	96.09401
Eu	151	ppm	11.48029	17.77633	90.5835	428.093	63.46173
Gd	157	ppm	20.57002	38.44433	161.8279	475.2348	215.5145
Tb	159	ppm	14.38808	19.87313	159.2628	265.5274	60.81773
Dy	163	ppm					
Y	89	ppm	77.52974	120.7542	393.7237	274.1626	121.6144
Ho	165	ppm	16.75736	23.30109	241.0444	185.0695	54.27981
Er	167	ppm	17.72465	27.01939	333.086	187.2666	61.41891
Tm	169	ppm					
Yb	173	ppm	14.24248	20.7594	401.6354	165.71	68.33331
Lu	175	ppm	9.05879	14.18462	290.6622	113.1073	46.76881

Gallinas Mountains Fluorite

	Analysis Number:		De14A08	De14A09	De14A11	De14A12	De14A13
	Type:		P1	P2	P1	P1	P3
Element	**Mass**	**Unit**					
Na2O	23	wt%	0.404282	0.519221	0.039989	0.035839	0.683784
MgO	25	wt%					
K2O	39	wt%	0.002989	0.004446	0.000582	0.000698	0.012898
CaO	43	wt%	71.821	71.821	71.821	71.821	71.821
MnO	55	wt%	0.003415	0.046395	0.00387	0.001352	0.322262
Cu	65	ppm					
Zn	66	ppm					
Rb	85	ppm	0.263481	1.329765	0.020545	0.030639	1.269238
Sr	86	ppm	304.1317	399.9911	303.5711	309.9268	1787.913
Y	89	ppm	318.1962	536.7431	253.9885	245.1731	1168.993
Nb	93	ppm	0.560242	1.059326	0.085353	0.096818	10.59942
Ba	137	ppm	7.774201	45.05871	13.11836	4.669255	1664.997
Pb	208	ppm	167.8776	415.6747	66.04105	22.16775	5102.193
Th	232	ppm					
U	238	ppm	3.217934	10.22136	0.445309	0.103927	203.9568

Chondrite Normalized

	Analysis Number:		De14A08	De14A09	De14A11	De14A12	De14A13
	Type:		P1	P2	P1	P1	P3
Element	**Mass**	**Unit**					
La	139	ppm	114.055	1932.101	106.2205	42.67691	20266.48
Ce	140	ppm	211.347	874.9791	56.72032	32.08717	8714.565
Pr	141	ppm	123.7158	591.8551	41.88759	42.13533	6836.762
Nd	145	ppm	148.1315	444.088	42.94734	37.64053	7154.64
Pm	145	ppm					
Sm	147	ppm	38.3884	142.2529	24.39187	25.00328	2685.687
Eu	151	ppm	30.24722	112.3079	20.50299	16.58325	1592.557
Gd	157	ppm	42.50495	151.4221	34.90309	25.80308	3599.025
Tb	159	ppm	24.47495	74.74473	18.50658	18.21182	949.5159
Dy	163	ppm					
Y	89	ppm	141.4205	238.5525	112.8838	108.9658	519.5524
Ho	165	ppm	29.24142	71.33692	22.19034	21.79464	463.6267
Er	167	ppm	30.99773	79.84839	24.42415	24.95896	414.4026
Tm	169	ppm					
Yb	173	ppm	22.83814	67.88954	20.77786	21.04935	336.5074
Lu	175	ppm	17.45251	41.36366	13.32273	13.28448	213.4136

Gallinas Mountains Fluorite

Analysis Number:			De14A14	De14A15	De14A16	De14A17	De14A18
Type:			P3	P3	P3	P2	P3
Element	**Mass**	**Unit**					
Na2O	23	wt%	0.342542	0.594514	0.292398	0.166631	0.383881
MgO	25	wt%					
K2O	39	wt%	0.003421	0.013451	0.003485	0.000504	0.003283
CaO	43	wt%	71.821	71.821	71.821	71.821	71.821
MnO	55	wt%	0.103362	0.48039	0.089336	0.004522	0.178894
Cu	65	ppm					
Zn	66	ppm					
Rb	85	ppm	0.403813	0.355572	0.487746	0.091563	0.39571
Sr	86	ppm	3651.858	5070.043	3296.681	563.7704	4348.769
Y	89	ppm	1708.399	2194.379	1518.577	571.1633	1805.248
Nb	93	ppm	15.76985	53.23253	63.53544	0.286588	17.6115
Ba	137	ppm	640.853	497.0909	4979.513	11.23411	13388.2
Pb	208	ppm	3113.271	6141.321	2154.474	44.10919	5583.937
Th	232	ppm					
U	238	ppm	382.3335	400.6443	165.2446	10.78949	485.5337

Chondrite Normalized

Analysis Number:			De14A14	De14A15	De14A16	De14A17	De14A18
Type:			P3	P3	P3	P2	P3
Element	**Mass**	**Unit**					
La	139	ppm	45079.19	49007.16	23224.52	1290.565	43549.2
Ce	140	ppm	17836.97	19213.1	9199.592	469.1133	17224.58
Pr	141	ppm	13273.67	21128.74	9155.538	565.8742	13088.43
Nd	145	ppm	14612.17	14423.85	7758.676	364.7245	14552.02
Pm	145	ppm					
Sm	147	ppm	4867.961	5090.92	2651.546	156.8398	4986.92
Eu	151	ppm	2883.895	2959.561	1574.186	100.5125	2926.376
Gd	157	ppm	3718.342	3652.194	8319.903	140.9591	20272.46
Tb	159	ppm	1614.093	1663.308	980.8689	121.4251	1617.273
Dy	163	ppm					
Y	89	ppm	759.2886	975.2794	674.923	253.8503	802.3325
Ho	165	ppm	626.6017	811.9227	560.6903	137.8721	683.59
Er	167	ppm	507.9997	658.036	549.9632	167.9583	566.7418
Tm	169	ppm					
Yb	173	ppm	387.9824	436.8591	551.4694	202.8276	441.0314
Lu	175	ppm	255.5873	313.2239	369.4027	140.0972	277.0161

Gallinas Mountains Fluorite

	Analysis Number:		De15A03	De15A04	De15A05
	Type:		P1	P3	P2
Element	Mass	Unit			
Na2O	23	wt%	0.195757	0.399328	0.443386
MgO	25	wt%	0.003467	0.019658	0.012861
K2O	39	wt%	0.015648	0.003873	0.003094
CaO	43	wt%	71.821	71.821	71.821
MnO	55	wt%			
Cu	65	ppm	3.241922	38.63175	1.882398
Zn	66	ppm	3.41927	21.28962	0.993026
Rb	85	ppm	0.591217	0.480513	0.384039
Sr	86	ppm	300.9785	2872.25	427.8899
Y	89	ppm	208.4092	1693.404	450.1294
Nb	93	ppm	0.088859	4.082159	0.111318
Ba	137	ppm	6.858641	162.2748	23.70677
Pb	208	ppm	14.59846	1545.57	1.144925
Th	232	ppm	0.100538	241.9683	0.487773
U	238	ppm	0.30874	294.3801	0.457308

Chondrite Normalized

	Analysis Number:		De15A03	De15A04	De15A05
	Type:		P1	P3	P2
Element	Mass	Unit			
La	139	ppm	55.582	63500.8	1182.871
Ce	140	ppm	33.75917	21656.41	457.2711
Pr	141	ppm	40.72576	16847.55	588.9255
Nd	145	ppm	38.83814	18718.12	445.7234
Pm	145	ppm			
Sm	147	ppm	21.00028	4911.561	161.1811
Eu	151	ppm	14.84754	2569.127	100.1745
Gd	157	ppm			
Tb	159	ppm	15.95789	1580.571	102.3155
Dy	163	ppm			
Y	89	ppm	92.62633	752.6241	200.0575
Ho	165	ppm	18.48425	574.1005	101.8449
Er	167	ppm	21.71384	470.4439	126.924
Tm	169	ppm			
Yb	173	ppm	17.45804	346.0954	161.6682
Lu	175	ppm	11.88696	215.0353	115.158

Gallinas Mountains Fluorite

Analysis Number: / Type:			n	Maximum	Minimum	Mean	Sigma
			P1	P1	P1	P1	P1
Element	**Mass**	**Unit**					
Na2O	23	wt%	6	0.631983	0.035839	0.302912	0.250292
MgO	25	wt%	1	0.003467	0.003467	0.003467	
K2O	39	wt%	6	0.027572	0.000582	0.01072	0.011033
CaO	43	wt%	6	71.821	71.821	71.821	0
MnO	55	wt%	5	0.00387	0.00078	0.002097	0.001434
Cu	65	ppm	1	3.241922	3.241922	3.241922	
Zn	66	ppm	1	3.41927	3.41927	3.41927	
Rb	85	ppm	6	0.591217	0.020545	0.195907	0.212832
Sr	86	ppm	6	309.9268	291.497	300.5225	7.050838
Y	89	ppm	6	318.1962	174.4419	245.3176	49.93586
Nb	93	ppm	6	0.560242	0.069359	0.165205	0.193746
Ba	137	ppm	6	13.11836	3.137831	7.1204	3.415916
Pb	208	ppm	6	167.8776	0.08703	45.24048	64.75967
Th	232	ppm	1	0.100538	0.100538	0.100538	
U	238	ppm	6	3.217934	0.042228	0.721969	1.231221

Chondrite Normalized

Analysis Number: / Type:			n	Maximum	Minimum	Mean	Sigma
			P1	P1	P1	P1	P1
Element	**Mass**	**Unit**					
La	139	ppm	6	114.055	36.44026	66.82363	34.20673
Ce	140	ppm	6	211.347	23.91006	65.39719	72.33162
Pr	141	ppm	6	123.7158	39.08874	54.49628	33.93316
Nd	145	ppm	6	148.1315	33.89865	57.08602	44.70969
Pm	145	ppm					
Sm	147	ppm	6	38.3884	17.7955	25.34754	7.029267
Eu	151	ppm	6	30.24722	11.48029	18.57294	6.462068
Gd	157	ppm					
Tb	159	ppm	6	24.47495	14.38808	18.56874	3.49315
Dy	163	ppm					
Y	89	ppm	6	141.4205	77.52974	109.0301	22.19371
Ho	165	ppm	6	29.24142	16.75736	21.96152	4.336964
Er	167	ppm	6	30.99773	17.72465	24.47312	4.526542
Tm	169	ppm					
Yb	173	ppm	6	22.83814	14.24248	19.52088	3.116767
Lu	175	ppm	6	17.45251	9.05879	13.19835	2.754967

Gallinas Mountains Fluorite

Analysis Number:							
Type:			n	Maximum	Minimum	Mean	Sigma
Element	Mass	Unit	P2	P2	P2	P2	P2
Na2O	23	wt%	6	7.842664	0.166631	1.761396	2.989276
MgO	25	wt%	1	0.012861	0.012861	0.012861	
K2O	39	wt%	6	0.178521	0.000504	0.036704	0.070024
CaO	43	wt%	6	71.821	71.821	71.821	0
MnO	55	wt%	5	0.046395	0.000708	0.011796	0.019493
Cu	65	ppm	1	1.882398	1.882398	1.882398	
Zn	66	ppm	1	0.993026	0.993026	0.993026	
Rb	85	ppm	6	2.567791	0.091563	0.912703	0.923954
Sr	86	ppm	6	1304.935	315.7483	605.2627	360.2428
Y	89	ppm	6	885.8783	273.6325	555.7354	202.0221
Nb	93	ppm	6	1.059326	0.028516	0.298462	0.382445
Ba	137	ppm	6	72.77834	5.067861	27.35874	26.79419
Pb	208	ppm	6	415.6747	0.155582	77.0638	166.7937
Th	232	ppm	1	0.487773	0.487773	0.487773	
U	238	ppm	6	10.78949	0.142171	5.332092	5.463103

Chondrite Normalized

Analysis Number:							
Type:			n	Maximum	Minimum	Mean	Sigma
Element	Mass	Unit	P2	P2	P2	P2	P2
La	139	ppm	6	7219.949	336.3972	2164.499	2528.996
Ce	140	ppm	6	2925.96	124.5409	894.3796	1023.39
Pr	141	ppm	6	4088.037	172.8778	1070.333	1487.101
Nd	145	ppm	6	2379.615	125.2064	664.9705	849.3704
Pm	145	ppm					
Sm	147	ppm	6	800.264	96.09401	242.2875	274.8375
Eu	151	ppm	6	428.093	63.46173	149.1888	137.625
Gd	157	ppm					
Tb	159	ppm	6	265.5274	60.81773	130.6822	74.70005
Dy	163	ppm					
Y	89	ppm	6	393.7237	121.6144	246.9935	89.78761
Ho	165	ppm	6	241.0444	54.27981	131.908	71.23378
Er	167	ppm	6	333.086	61.41891	159.417	97.97966
Tm	169	ppm					
Yb	173	ppm	6	401.6354	67.88954	178.0107	122.6361
Lu	175	ppm	6	290.6622	41.36366	124.5262	90.58035

Gallinas Mountains Fluorite

Analysis Number: Type: Element	Mass	Unit	n P3	Maximum P3	Minimum P3	Mean P3	Sigma P3
Na2O	23	wt%	6	0.683784	0.292398	0.449408	0.154183
MgO	25	wt%	1	0.019658	0.019658	0.019658	
K2O	39	wt%	6	0.013451	0.003283	0.006735	0.004995
CaO	43	wt%	6	71.821	71.821	71.821	0
MnO	55	wt%	5	0.48039	0.089336	0.234849	0.165473
Cu	65	ppm	1	38.63175	38.63175	38.63175	
Zn	66	ppm	1	21.28962	21.28962	21.28962	
Rb	85	ppm	6	1.269238	0.355572	0.565432	0.348585
Sr	86	ppm	6	5070.043	1787.913	3504.586	1146.737
Y	89	ppm	6	2194.379	1168.993	1681.5	337.1738
Nb	93	ppm	6	63.53544	4.082159	27.47181	24.61753
Ba	137	ppm	6	13388.2	162.2748	3555.488	5131.214
Pb	208	ppm	6	6141.321	1545.57	3940.128	1923.742
Th	232	ppm	1	241.9683	241.9683	241.9683	
U	238	ppm	6	485.5337	165.2446	322.0155	123.1565

Chondrite Normalized

Analysis Number: Type: Element	Mass	Unit	n P3	Maximum P3	Minimum P3	Mean P3	Sigma P3
La	139	ppm	6	63500.8	20266.48	40771.22	16365.03
Ce	140	ppm	6	21656.41	8714.565	15640.87	5398.932
Pr	141	ppm	6	21128.74	6836.762	13388.45	5154.082
Nd	145	ppm	6	18718.12	7154.64	12869.91	4500.45
Pm	145	ppm					
Sm	147	ppm	6	5090.92	2651.546	4199.099	1187.966
Eu	151	ppm	6	2959.561	1574.186	2417.617	661.0612
Gd	157	ppm					
Tb	159	ppm	6	1663.308	949.5159	1400.938	338.6981
Dy	163	ppm					
Y	89	ppm	6	975.2794	519.5524	747.3333	149.855
Ho	165	ppm	6	811.9227	463.6267	620.0887	119.1625
Er	167	ppm	6	658.036	414.4026	527.9312	84.27305
Tm	169	ppm					
Yb	173	ppm	6	551.4694	336.5074	416.6575	79.24866
Lu	175	ppm	6	369.4027	213.4136	273.9465	60.22599

Appendix B

Appendix to Chapter 3 – "LA-ICP-MS Analysis of Fluid Inclusions" Example of a Quantitative Fluid Inclusion Calculation

Appendix B

Example of a Quantitative Fluid Inclusion Calculation

Introduction

Fluid inclusion data collected by an ICP-MS typically is too complex to be interpreted using the software included with the ICP-MS or currently available from third parties. Therefore, a method of reducing the raw data (integrated counts/second - icps) to concentration units (µg/g) is required. The following section presents a worked example in which raw data is converted to concentration units using readily available commercial spreadsheet (e.g., Microsoft® Excel®) and spectral analysis (e.g., PeakFit®) software. The procedure can be used for evaluating either relatively simple or complex (e.g., stepwise opened) fluid inclusion signals as well as data obtained from fluid inclusions hosted by compositionally complex host minerals (e.g., fluorite). The data correction procedures are quantitative; however, the effect on analytical precision has not been fully evaluated at this time. Once a spreadsheet has been developed that includes the described operations, calculation of fluid inclusion compositions can be carried out relatively quickly. Use of spreadsheet macros or related applications development software (e.g., Microsoft® Visual Basic® or Lotus Script®) to automate many of the procedures described below can significantly increase the efficiency of data reduction.

Step 1

The first step in the process is to extract the raw data (i.e., icps) obtained during LA-ICP-MS analysis of the fluid inclusions from the ICP-MS. The raw data are typically included in the ICP-MS software in a form that can be readily copied and pasted into a spreadsheet program. If it is not possible to copy the data directly, the data can usually be exported from the ICP-MS experiment file in a format that can be imported into the spreadsheet program (e.g., comma-separated values).

Step 2

Prior to integrating the spectral peaks, it is necessary to subtract the instrumental or gas background from the raw data. This is particularly relevant for elements that may have high backgrounds (e.g., K) relative to the fluid inclusion signal and host mineral background. In cases where the instrumental or gas background is high and a correction is ***not*** performed prior to host mineral data correction (subtraction), the fluid inclusion signal may be obscured.

To obtain an instrumental/gas background correction factor, data should be acquired for a period of time prior to host mineral or fluid inclusion ablation to establish an average count rate that is characteristic of instrumental/gas background for each of the selected isotopes. Typically, a period of 30 to 60 seconds of data acquisition, without conducting ablation, is adequate to establish background. The data obtained for this period of time are averaged, and the calculated average count rates are subtracted from the data collected for each isotope analyzed. Although it is only necessary to subtract backgrounds from the isotopes that have non-zero instrumental/gas backgrounds, configuring the spreadsheet to treat all isotopes in a consistent manner (i.e., calculate and subtract average instrumental/gas backgrounds for all isotopes) will lead to fewer data reduction errors.

Step 3

After the data have been exported from the ICP-MS and corrected for instrumental/gas background, it may be necessary to reformat the data for compatibility with the selected spectral analysis software. To minimize potential software conflicts, select a spectral analysis software package that interfaces seamlessly with the selected spreadsheet program (e.g., PeakFit® and Microsoft® Excel®). This minimizes the amount of data reformatting that may be required and contributes to the stability of the data reduction procedure.

Once the data are in the appropriate form, the spectra obtained for each fluid inclusion and calibration standard can be viewed and the peak areas determined. The output is expressed as total icps integrated over the time

interval represented by each fluid inclusion. If the peak areas are determined relative to the background host mineral, then further background correction is not necessary. For the complex fluid inclusion signals obtained using a stepwise opening procedure, each of the segments of the spectrum is integrated and the icps obtained from each segment summed to obtain the total number of counts for the entire fluid inclusion analysis.

Step 4

Next, the slopes of the calibration lines for each isotope of interest contained within the calibration standard that was used during the LA-ICP-MS analysis are calculated using Equation 1. Table B-1 documents how the slopes of the calibration curves (i.e., the correction factors) are calculated from the total counts obtained using the spectral analysis software.

The concentrations presented in Column 2 of Table B-1 are the published values for NIST 610 synthetic glass. The concentration ratios presented in Column 3 are calculated by dividing the concentration of the selected isotope in the standard by the concentration of sodium in the standard (e.g., 463.1/135000 = 0.00343 for potassium). The total standard icps presented in Column 4 are obtained from the spectra using a commercial peak integration software package (e.g., 1.81×10^9 icps for K). The standard count ratios presented in Column 5 are calculated by dividing the standard icps obtained for the selected isotope by the standard icps obtained for Na (e.g., $1.81 \times 10^9 / 8.48 \times 10^{10} = 0.213$ for K). Finally, the correction factor presented in Column 6, which defines the slope of the calibration line for each element in the standard, is calculated by dividing the concentration ratio by the standard count ratio (e.g., 0.00343/0.0213 = 0.161 for K).

Step 5

Once the correction factor has been calculated for each element of interest in the standard, the icps obtained from the spectra for a single fluid inclusion analysis can be used to calculate elemental concentrations using

Equation 2. Table B-2 presents the results of an analysis performed on an approximately 12 µm, primary, liquid-vapor inclusion in purple fluorite from South Platte, Colorado. The equivalent weight percent NaCl obtained from this fluid inclusion from microthermometry was 252,000 µg/g, which converts to an elemental Na concentration of 99,100 µg/g. In this particular example, the concentration of Ca in the fluid inclusion can not be determined due to the predominance of Ca in the signal from the host fluorite which masks the fluid inclusion Ca concentration. The data evaluation was conducted ***without*** correction for host mineral contribution to the fluid inclusion signal. In the case of compositionally complex host minerals, this can significantly affect the outcome of the data reduction procedure.

The correction factors presented in Table B-2 are copied directly from Table B-1. The sample counts are obtained from the fluid inclusion spectra using the spectral analysis software (e.g., 8.45×10^7 for K). The sample count ratios are calculated by dividing the sample icps obtained for the selected isotope by the sample icps obtained for Na (e.g., $8.45 \times 10^7 / 3.03 \times 10^9 = 0.0279$ for K). Finally, the concentrations are calculated by multiplying the correction factor by the sample count ratio, and then multiplying by the concentration of Na determined from microthermometry (e.g., (0.161 x 0.0279) x 99,100 = 444 µg/g for K).

Step 6

It is impossible to conduct LA-ICP-MS analysis of fluid inclusions without including some of the host mineral in the sample that is introduced to the ICP-MS. Some sampling strategies can reduce, but not eliminate, this host mineral contribution and, therefore, correction of the data is necessary to reduce or eliminate the effect that the host mineral contribution may have on the calculated fluid inclusion composition. The need to conduct data filtering is particularly relevant when sampling fluid inclusions that have relatively small volumes compared to the diameter of the laser beam (i.e., a relatively high host mineral to fluid inclusion signal contribution) or that have complex compositions. It is

important to note that although the contributions to the fluid inclusion signal can be corrected for some elements, it may not be possible to correct for all host mineral contributions for all elements (e.g., Ca in fluid inclusions hosted by calcite or fluorite).

The data can be corrected by dividing the icps obtained for all of the selected elements by the icps obtained for an element that is a significant constituent of the host mineral (e.g., Ca in calcite or fluorite) and is likely to have low or zero concentration in the fluid inclusion. This procedure should be applied to both the standards used during the analysis and the unknowns, and is conducted after correction for the instrumental/gas background. The remaining steps of the data reduction procedure are then followed (i.e., between Steps 2 and 3 described above).

The fluid inclusion analysis presented above in Tables B-1 and B-2 was not corrected for host mineral contribution. However, it is evidence from the spectra obtained for this inclusion (Figures 3-6a and 3-6b) that the LA-ICP-MS analysis of the fluid inclusion has been significantly affected by a host mineral contribution, particularly during the early part of the signal. Tables B-3 and B-4 present the data from the same fluid inclusion; however, the data has been corrected to adjust for the contribution from the host fluorite.

It is apparent from the spectra that data correction is required for this inclusion, and the results obtained using the uncorrected and corrected data are dramatically different. The concentrations of K and Sm increased, and Sr, Y, Ba, Ce, Th and U decreased as a result of data correction. Furthermore, the concentration of Y detected in the uncorrected data was entirely the result of a host mineral contribution.

Table B-1. Calculation of correction factors for NIST 610 standard – uncorrected data

Element	Concentration (µg/g)	Concentration Ratio	Total Standard icps	Standard icps Ratios	Correction Factor
Na	135,000	1	8.48×10^{10}	1	1
K	463.1	0.00343	1.81×10^{9}	0.0213	0.161
Ca	114,000	0.844	3.62×10^{8}	0.00427	198
Sr	505.3	0.00375	3.56×10^{9}	0.0421	0.0890
Y	452.6	0.00335	2.98×10^{9}	0.0352	0.0952
Ba	415.9	0.00308	5.51×10^{8}	0.00650	0.474
Ce	462	0.00342	4.62×10^{9}	0.0545	0.0627
Sm	458	0.00339	7.73×10^{8}	0.00912	0.372
Th	463.1	0.00343	2.23×10^{9}	0.0263	0.130
U	462.9	0.00343	3.57×10^{9}	0.0421	0.0815

Table B-2. Calculation of elemental concentrations in primary LV inclusion – uncorrected data

Element	Correction Factor	Total Sample icps	Sample icps Ratios	Element Concentration µg/g
Na	1	3.03×10^{9}	1	99,100
K	0.161	8.45×10^{7}	0.0279	444
Ca	198	--	--	--
Sr	0.0890	7.38×10^{8}	0.243	2,150
Y	0.0952	2.97×10^{8}	0.0977	922
Ba	0.474	6.63×10^{5}	0.000219	10.3
Ce	0.0627	9.99×10^{7}	0.0329	206
Sm	0.372	5.68×10^{6}	0.00187	68.9
Th	0.130	9.00×10^{8}	0.297	3,840
U	0.0815	9.96×10^{6}	0.00328	26.5

Table B-3. Calculation of correction factors for NIST 610 standard – corrected data

Element	Concentration (µg/g)	Concentration Ratio	Total Standard icps*	Standard icps Ratios	Correction Factor
Na	135,000	1	1.49×10^7	1	1
K	463.1	0.00343	2.85×10^5	0.0191	0.18
Ca	114,000	0.844	5.41×10^4	0.00362	233
Sr	505.3	0.00375	5.57×10^5	0.0373	0.101
Y	452.6	0.00335	4.67×10^5	0.0313	0.107
Ba	415.9	0.00308	8.67×10^5	0.058	0.0531
Ce	462	0.00342	7.34×10^5	0.049	0.007
Sm	458	0.00339	1.22×10^5	0.00815	0.416
Th	463.1	0.00343	3.52×10^5	0.0235	0.146
U	462.9	0.00343	5.67×10^5	0.038	0.09

* Ratioed against Ca.

Table B-4. Calculation of elemental concentrations in primary LV inclusion – corrected data

Element	Correction Factor	Total Sample icps*	Sample icps Ratios	Element Concentration µg/g
Na	1	3.37×10^4	1	99,100
K	0.18	1.38×10^3	0.041	731
Ca	233	--	--	--
Sr	0.101	1.6×10^3	0.0476	476
Y	0.107	0	0	ND
Ba	0.0531	12	0.000356	2
Ce	0.007	1.37×10^3	0.0407	28
Sm	0.416	83	0.00246	101
Th	0.146	1.53×10^3	0.0453	655
U	0.09	41	0.00123	11

* Ratioed against Ca.

Appendix C

Appendix to Chapter 4 – "The composition and origin of hydrothermal fluids in an NYF-type granitic pegmatite, South Platte District, Colorado: Evidence from LA-ICP-MS analysis of fluorite- and quartz-hosted fluid inclusions"

White Fluorite - Secondary

Run Number:	Ju08B03	NaCl (ppm):	242053	Na (ppm):	95166
Analysis of:	Sec LVS in white fluorite				

Element	**Isotope**	**Corr. Fact.**	**Counts**	**Count Ratios**	**Conc.**
Be	9	1.0262	0	0.0000	0.0000
Na	23	1.0000	31227	1.0000	95166.1368
K	39	0.1002	2763	0.0885	843.6360
Ca	43	- -		0.0000	- -
Sr	86	0.5896	303	0.0097	544.4228
Y	89	0.0779	0	0.0000	0.0000
Zr	90	0.1615	0	0.0000	0.0000
Nb	93	0.0705	0	0.0000	0.0000
Ce	140	0.0633	43296	1.3865	8350.2208
Sm	147	0.3865	0	0.0000	0.0000
Th	232	0.1738	213	0.0068	112.8247
U	238	0.1106	11	0.0004	3.7068

White Fluorite - Secondary

Run Number:	Ju15C06	NaCl (ppm):	242100	Na (ppm):	95185
Analysis of:	Sec? LVS in white fluorite				

Element	**Isotope**	**Corr. Fact.**	**Counts**	**Count Ratios**	**Conc.**
Na	23	1.0000	217560	1.0000	95184.6154
K	39	0.0784	35330	0.1624	1212.3307
Ca	43	- -		0.0000	- -
Sr	86	0.0388	32185	0.1479	545.9123
Y	89	0.0434	0	0.0000	0.0000
Nb	93	0.0405	15	0.0001	0.2661
Ba	137	0.1971	4092	0.0188	352.8983
Ce	140	0.0277	0	0.0000	0.0000
Ho	165	0.0261	0	0.0000	0.0000
Th	232	0.0525	0	0.0000	0.0000
U	238	0.0311	0	0.0000	0.0000

White Fluorite - Secondary

Run Number:	Ju15C07	NaCl (ppm):	242100	Na (ppm):	95185
Analysis of:	Sec? LVS in white fluorite				

Element	**Isotope**	**Corr. Fact.**	**Counts**	**Count Ratios**	**Conc.**
Na	23	1.0000	114065	1.0000	95184.6154
K	39	0.0784	24297	0.2130	1590.2184
Ca	43	- -		0.0000	- -
Sr	86	0.0388	24286	0.2129	785.6914
Y	89	0.0434	0	0.0000	0.0000
Nb	93	0.0405	0	0.0000	0.0000
Ba	137	0.1971	0	0.0000	0.0000
Ce	140	0.0277	0	0.0000	0.0000
Ho	165	0.0261	0	0.0000	0.0000
Th	232	0.0525	0	0.0000	0.0000
U	238	0.0311	0	0.0000	0.0000

White Fluorite - Primary

Run Number: Ju15C15 NaCl (ppm): 109000 Na (ppm): 42855

Analysis of: Pri LV in white fluorite

Element	Isotope	Corr. Fact.	Counts	Count Ratios	Conc.
Na	23	1.0000	139748	1.0000	42854.7009
K	39	0.0784	4633	0.0332	111.4307
Ca	43	- -		0.0000	- -
Sr	86	0.0388	24981	0.1788	296.9917
Y	89	0.0434	0	0.0000	0.0000
Nb	93	0.0405	0	0.0000	0.0000
Ba	137	0.1971	46	0.0003	2.7806
Ce	140	0.0277	0	0.0000	0.0000
Ho	165	0.0261	0	0.0000	0.0000
Th	232	0.0525	476	0.0034	7.6675
U	238	0.0311	0	0.0000	0.0000

White Fluorite - Primary

Run Number: Ju15C16 NaCl (ppm): 109000 Na (ppm): 42855

Analysis of: Pri LV in white fluorite

Element	Isotope	Corr. Fact.	Counts	Count Ratios	Conc.
Na	23	1.0000	30486	1.0000	42854.7009
K	39	0.0784	724	0.0237	79.8227
Ca	43	- -		0.0000	- -
Sr	86	0.0388	0	0.0000	0.0000
Y	89	0.0434	0	0.0000	0.0000
Nb	93	0.0405	7	0.0002	0.3989
Ba	137	0.1971	25	0.0008	6.9273
Ce	140	0.0277	0	0.0000	0.0000
Ho	165	0.0261	0	0.0000	0.0000
Th	232	0.0525	149	0.0049	11.0022
U	238	0.0311	12	0.0004	0.5241

Quartz - Secondary

Run Number: Ju15B10 NaCl (ppm): 304100 Na (ppm): 119561

Analysis of: Sec LVS in quartz

Element	Isotope	Corr. Fact.	Counts	Count Ratios	Conc.
Na	23	1.0000	3610000000	1.0000	119560.6838
K	39	0.1172	793000000	0.2197	3079.1128
Ca	43	319.3877	11220907	0.0031	118693.5928
Sr	86	0.0887	793000000	0.2197	2330.2634
Y	89	0.1097	108740	0.0000	0.3952
Nb	93	0.0955	1423103	0.0004	4.5014
Ba	137	0.3147	192000000	0.0532	2001.3458
Ce	140	0.0489	825820	0.0002	1.3365
Ho	165	0.0398	0	0.0000	0.0000
Th	232	0.0760	0	0.0000	0.0000
U	238	0.0368	0	0.0000	0.0000

Quartz - Secondary

Run Number: Ju14A08b NaCl (ppm): 263000 Na (ppm): 103402

Analysis of: Sec LV in quartz

Element	Isotope	Corr. Fact.	Counts	Count Ratios	Conc.
Na	23	1.0000	1450000000	1.0000	103401.7094
K	39	0.0638	423000000	0.2917	1924.6601
Ca	43	79.5562	9230769	0.0064	52368.6795
Sr	86	0.0293	234000000	0.1614	489.2953
Y	89	0.0329	2285116	0.0016	5.3563
Nb	93	0.0299	577304	0.0004	1.2325
Ba	137	0.1508	20144204	0.0139	216.6179
Ce	140	0.0210	679019	0.0005	1.0177
Sm	147	0.1220	561518	0.0004	4.8860
Th	232	0.0466	1403237	0.0010	4.6653
U	238	0.0277	5970857	0.0041	11.8069

Quartz - Secondary

Run Number: Ju14A09a NaCl (ppm): 263000 Na (ppm): 103402

Analysis of: Sec LV in quartz

Element	Isotope	Corr. Fact.	Counts	Count Ratios	Conc.
Na	23	1.0000	3730000000	1.0000	103401.7094
K	39	0.0638	627000000	0.1681	1109.0226
Ca	43	79.5562	2870633	0.0008	6330.9748
Sr	86	0.0293	72062384	0.0193	58.5764
Y	89	0.0329	0	0.0000	0.0000
Nb	93	0.0299	0	0.0000	0.0000
Ba	137	0.1508	1107803	0.0003	4.6309
Ce	140	0.0210	0	0.0000	0.0000
Sm	147	0.1220	0	0.0000	0.0000
Th	232	0.0466	0	0.0000	0.0000
U	238	0.0277	0	0.0000	0.0000

Quartz - Secondary

Run Number: Ju14A09b NaCl (ppm): 263000 Na (ppm): 103402

Analysis of: Sec LV in quartz

Element	Isotope	Corr. Fact.	Counts	Count Ratios	Conc.
Na	23	1.0000	746000000	1.0000	103401.7094
K	39	0.0638	69560987	0.0932	615.1890
Ca	43	79.5562	0	0.0000	0.0000
Sr	86	0.0293	13245996	0.0178	53.8355
Y	89	0.0329	0	0.0000	0.0000
Nb	93	0.0299	0	0.0000	0.0000
Ba	137	0.1508	3317633	0.0044	69.3429
Ce	140	0.0210	0	0.0000	0.0000
Sm	147	0.1220	0	0.0000	0.0000
Th	232	0.0466	0	0.0000	0.0000
U	238	0.0277	0	0.0000	0.0000

White Fluorite - Primary

Run Number: Ju08A06 NaCl (ppm): 123000 Na (ppm): 48359

Analysis of: Pri LV in white fluorite

Element	Isotope	Corr. Fact.	Counts	Count Ratios	Conc.
Be	9	1.1433	0	0.0000	0.0000
Na	23	1.0000	7498	1.0000	48358.9744
K	39	0.1171	0	0.0000	0.0000
Ca	43	- -		0.0000	- -
Sr	86	0.5894	0	0.0000	0.0000
Y	89	0.0816	0	0.0000	0.0000
Zr		0.1679	0	0.0000	0.0000
Nb	93	0.0701	0	0.0000	0.0000
Ce	140	0.0628	0	0.0000	0.0000
Sm	147	0.3929	0	0.0000	0.0000
Th	232	0.1903	0	0.0000	0.0000
U	238	0.1146	0	0.0000	0.0000

White Fluorite - Primary

Run Number: Ju08a08 NaCl (ppm): 107000 Na (ppm): 42068

Analysis of: Primary LV in white fluorite

Element	Isotope	Corr. Fact.	Counts	Count Ratios	Conc.
Be	9	1.1433	0	0.0000	0.0000
Na	23	1.0000	12200	1.0000	42068.3761
K	39	0.1171	2108	0.1728	851.0766
Ca	43	- -		0.0000	- -
Sr	86	0.5894	321	0.0263	652.3995
Y	89	0.0816	0	0.0000	0.0000
Zr		0.1679	0	0.0000	0.0000
Nb	93	0.0701	0	0.0000	0.0000
Ce	140	0.0628	0	0.0000	0.0000
Sm	147	0.3929	0	0.0000	0.0000
Th	232	0.1903	0	0.0000	0.0000
U	238	0.1146	0	0.0000	0.0000

White Fluorite - Primary

Run Number: Ju12J10 NaCl (ppm): 115000 Na (ppm): 45214

Analysis of: LV in white fluorite

Element	Isotope	Corr. Fact.	Counts	Count Ratios	Conc.
Be	9	2.9852	0	0.0000	0.0000
Na	23	1.0000	530033	1.0000	45213.6752
K	39	0.1443	9276	0.0175	114.1810
Ca	43	- -		0.0000	- -
Sr	86	0.9024	573	0.0011	44.1078
Y	89	0.1108	5713	0.0108	54.0157
Zr	90	0.2150	0	0.0000	0.0000
Nb	93	0.0917	76.3	0.0001	0.5968
Ce	140	0.0493	2311	0.0044	9.7260
Sm	147	0.3247	135	0.0003	3.7395
Th	232	0.0926	1557	0.0029	12.3031
U	238	0.0501	21	0.0000	0.0898

Clear Fluorite - Primary

Run Number:	Ju15C04	NaCl (ppm):	109000	Na (ppm):	42855
Analysis of:	Pri LV in fluorite				
Element	**Isotope**	**Corr. Fact.**	**Counts**	**Count Ratios**	**Conc.**
Na	23	1.0000	75961	1.0000	42854.7009
K	39	0.0784	3268	0.0430	144.6038
Ca	43	- -		0.0000	- -
Sr	86	0.0388	14314	0.1884	313.0765
Y	89	0.0434	0	0.0000	0.0000
Nb	93	0.0405	0	0.0000	0.0000
Ba	137	0.1971	72	0.0009	8.0069
Ce	140	0.0277	0	0.0000	0.0000
Ho	165	0.0261	0	0.0000	0.0000
Th	232	0.0525	887	0.0117	26.2861
U	238	0.0311	0	0.0000	0.0000

Clear Fluorite - Primary

Run Number:	Ju15C05	NaCl (ppm):	109000	Na (ppm):	42855
Analysis of:	Pri LV in fluorite				
Element	**Isotope**	**Corr. Fact.**	**Counts**	**Count Ratios**	**Conc.**
Na	23	1.0000	76925	1.0000	42854.7009
K	39	0.0784	2822	0.0367	123.3042
Ca	43	- -		0.0000	- -
Sr	86	0.0388	12378	0.1609	267.3395
Y	89	0.0434	0	0.0000	0.0000
Nb	93	0.0405	0	0.0000	0.0000
Ba	137	0.1971	37	0.0005	4.0631
Ce	140	0.0277	27280	0.3546	420.4242
Ho	165	0.0261	0	0.0000	0.0000
Th	232	0.0525	0	0.0000	0.0000
U	238	0.0311	0	0.0000	0.0000

Quartz - Secondary

Run Number:	Ju14A09c	NaCl (ppm):	263000	Na (ppm):	103402
Analysis of:	Sec LV in quartz				
Element	**Isotope**	**Corr. Fact.**	**Counts**	**Count Ratios**	**Conc.**
Na	23	1.0000	8080000000	1.0000	103401.7094
K	39	0.0638	1380000000	0.1708	1126.8066
Ca	43	79.5562	0	0.0000	0.0000
Sr	86	0.0293	34096875	0.0042	12.7946
Y	89	0.0329	0	0.0000	0.0000
Nb	93	0.0299	0	0.0000	0.0000
Ba	137	0.1508	236209	0.0000	0.4558
Ce	140	0.0210	0	0.0000	0.0000
Sm	147	0.1220	0	0.0000	0.0000
Th	232	0.0466	0	0.0000	0.0000
U	238	0.0277	0	0.0000	0.0000

Quartz - Secondary

Run Number:	Ju14A07	NaCl (ppm):	263000	Na (ppm):	103402
Analysis of:	Sec LV in quartz				
Element	**Isotope**	**Corr. Fact.**	**Counts**	**Count Ratios**	**Conc.**
Na	23	1.0000	825000000	1.0000	103401.7094
K	39	0.0638	92061339	0.1116	736.2156
Ca	43	79.5562	0	0.0000	0.0000
Sr	86	0.0293	722518.15	0.0009	2.6553
Y	89	0.0329	0	0.0000	0.0000
Nb	93	0.0299	0	0.0000	0.0000
Ba	137	0.1508	0	0.0000	0.0000
Ce	140	0.0210	0	0.0000	0.0000
Sm	147	0.1220	0	0.0000	0.0000
Th	232	0.0466	0	0.0000	0.0000
U	238	0.0277	0	0.0000	0.0000

Quartz - Secondary

Run Number:	Ju14A10a	NaCl (ppm):	263000	Na (ppm):	103402
Analysis of:	Sec LV in quartz				
Element	**Isotope**	**Corr. Fact.**	**Counts**	**Count Ratios**	**Conc.**
Na	23	1.0000	341000000	1.0000	103401.7094
K	39	0.0638	58829494	0.1725	1138.2100
Ca	43	79.5562	0	0.0000	0.0000
Sr	86	0.0293	7413630	0.0217	65.9174
Y	89	0.0329	0	0.0000	0.0000
Nb	93	0.0299	0	0.0000	0.0000
Ba	137	0.1508	0	0.0000	0.0000
Ce	140	0.0210	0	0.0000	0.0000
Sm	147	0.1220	0	0.0000	0.0000
Th	232	0.0466	0	0.0000	0.0000
U	238	0.0277	0	0.0000	0.0000

Purple Fluorite - Primary

Run Number:	De18A17	NaCl (ppm):	252000	Na (ppm):	99077
Analysis of:	Pri LV in purple fluorite				
Element	**Isotope**	**Corr. Fact.**	**Counts**	**Count Ratios**	**Conc.**
Na	23	1.0000	3404	1.0000	99076.9231
Mg		25.7077	35.4	0.0104	26488.0527
K	39	0.7869	0	0.0000	0.0000
Ca	43	- -		0.0000	- -
Cu		2.3476	0	0.0000	0.0000
Zn		1.7506	0	0.0000	0.0000
Rb		0.3529	0	0.0000	0.0000
Y	89	0.6368	0	0.0000	0.0000
Nb	93	0.7309	0	0.0000	0.0000
Ce	140	0.5694	0	0.0000	0.0000
Pb		0.3490	0	0.0000	0.0000

Purple Fluorite - Primary

Run Number:	Ju14B07	NaCl (ppm):	110000	Na (ppm):	43248
Analysis of:	Pri LV in c/p fluorite				
Element	**Isotope**	**Corr. Fact.**	**Counts**	**Count Ratios**	**Conc.**
Na	23	1.0000	90211	1.0000	43247.8632
K	39	0.1873	3183	0.0353	285.7988
Ca	43	- -		0.0000	- -
Sr	86	0.1002	2822	0.0313	135.5867
Y	89	0.1065	31081	0.3445	1587.4180
Nb	93	0.0953	24.3	0.0003	1.1103
Ba	137	0.5362	29.4	0.0003	7.5569
Ce	140	0.0698	4555	0.0505	152.4535
Sm	147	0.4162	307	0.0034	61.2539
Th	232	0.1457	27666	0.3067	1932.6303
U	238	0.0910	309	0.0034	13.4739

Purple Fluorite - Primary

Run Number:	Ju14B08	NaCl (ppm):	105000	Na (ppm):	41282
Analysis of:	Pri LV in c/p fluorite				
Element	**Isotope**	**Corr. Fact.**	**Counts**	**Count Ratios**	**Conc.**
Na	23	1.0000	38461	1.0000	41282.0513
K	39	0.1873	1866	0.0485	375.1206
Ca	43	- -		0.0000	- -
Sr	86	0.1002	2233	0.0581	240.2063
Y	89	0.1065	0	0.0000	0.0000
Nb	93	0.0953	0	0.0000	0.0000
Ba	137	0.5362	0	0.0000	0.0000
Ce	140	0.0698	2315	0.0602	173.4744
Sm	147	0.4162	235	0.0061	104.9781
Th	232	0.1457	1730	0.0450	270.5727
U	238	0.0910	45.6	0.0012	4.4518

Quartz - Secondary

Run Number: Ju12I10 NaCl (ppm): 294600 Na (ppm): 115826

Analysis of: Sec LVS in quartz

Element	Isotope	Corr. Fact.	Counts	Count Ratios	Conc.
Be	9	2.6232	0	0.0000	0.0000
Na	23	1.0000	6020000000	1.0000	115825.6410
K	39	0.0908	1590000000	0.2641	2777.2339
Ca	43	229.2689	29915944	0.0050	131964.1588
Sr	86	0.6858	144000000	0.0239	1899.9908
Y	89	0.0901	0	0.0000	0.0000
Zr	90	0.1815	0	0.0000	0.0000
Nb	93	0.0768	0	0.0000	0.0000
Ce	140	0.0444	0	0.0000	0.0000
Sm	147	0.2934	0	0.0000	0.0000
Th	232	0.0899	0	0.0000	0.0000
U	238	0.0498	0	0.0000	0.0000

Quartz - Secondary

Run Number: Ju12J04 NaCl (ppm): 295400 Na (ppm): 116140

Analysis of: Sec LV in quartz

Element	Isotope	Corr. Fact.	Counts	Count Ratios	Conc.
Be	9	2.9103	0	0.0000	0.0000
Na	23	1.0000	1920000000	1.0000	116140.1709
K	39	0.1406	201000000	0.1047	1709.3919
Ca	43	280.2727	0	0.0000	0.0000
Sr	86	0.8843	0	0.0000	0.0000
Y	89	0.1093	0	0.0000	0.0000
Zr	90	0.2116	0	0.0000	0.0000
Nb	93	0.0900	0	0.0000	0.0000
Ce	140	0.0483	0	0.0000	0.0000
Sm	147	0.3231	0	0.0000	0.0000
Th	232	0.0919	0	0.0000	0.0000
U	238	0.0496	0	0.0000	0.0000

Quartz - Secondary

Run Number: Ju14A03a NaCl (ppm): 295400 Na (ppm): 116140

Analysis of: Sec LVS in quartz

Element	Isotope	Corr. Fact.	Counts	Count Ratios	Conc.
Na	23	1.0000	794000000	1.0000	116140.1709
K	39	0.0638	547000000	0.6889	5105.0881
Ca	43	79.5562	0	0.0000	0.0000
Sr	86	0.0293	9667592	0.0122	41.4644
Y	89	0.0329	35157367	0.0443	169.0332
Nb	93	0.0299	3797786	0.0048	16.6303
Ba	137	0.1508	974263	0.0012	21.4893
Ce	140	0.0210	28063566	0.0353	86.2756
Sm	147	0.1220	0	0.0000	0.0000
Th	232	0.0466	812102	0.0010	5.5381
U	238	0.0277	23654769	0.0298	95.9443

Quartz - Secondary

Run Number:	Ju15A03	NaCl (ppm):	265000	Na (ppm):	104188
Analysis of:	Sec LV in quartz				
Element	**Isotope**	**Corr. Fact.**	**Counts**	**Count Ratios**	**Conc.**
Na	23	1.0000	3870000000	1.0000	104188.0342
K	39	0.2624	643000000	0.1661	4541.7331
Ca	43	363.0140	0	0.0000	0.0000
Sr	86	0.0838	703284	0.0002	1.5871
Y	89	0.1045	0	0.0000	0.0000
Nb	93	0.0871	0	0.0000	0.0000
Ba	137	0.2616	0	0.0000	0.0000
Ce	140	0.0420	0	0.0000	0.0000
Ho	165	0.0305	0	0.0000	0.0000
Th	232	0.0575	0	0.0000	0.0000
U	238	0.0275	0	0.0000	0.0000

Quartz - Secondary

Run Number:	Ju15A04	NaCl (ppm):	265000	Na (ppm):	104188
Analysis of:	Sec LV in quartz				
Element	**Isotope**	**Corr. Fact.**	**Counts**	**Count Ratios**	**Conc.**
Na	23	1.0000	43500000000	1.0000	104188.0342
K	39	0.2624	18974134	0.0004	11.9232
Ca	43	363.0140	0	0.0000	0.0000
Sr	86	0.0838	0	0.0000	0.0000
Y	89	0.1045	0	0.0000	0.0000
Nb	93	0.0871	0	0.0000	0.0000
Ba	137	0.2616	0	0.0000	0.0000
Ce	140	0.0420	0	0.0000	0.0000
Ho	165	0.0305	0	0.0000	0.0000
Th	232	0.0575	0	0.0000	0.0000
U	238	0.0275	0	0.0000	0.0000

Quartz - Secondary

Run Number:	Ju15A05	NaCl (ppm):	265000	Na (ppm):	104188
Analysis of:	Sec LV in quartz				
Element	**Isotope**	**Corr. Fact.**	**Counts**	**Count Ratios**	**Conc.**
Na	23	1.0000	216000000	1.0000	104188.0342
K	39	0.2624	15851574	0.0734	2006.0430
Ca	43	363.0140	0	0.0000	0.0000
Sr	86	0.0838	0	0.0000	0.0000
Y	89	0.1045	0	0.0000	0.0000
Nb	93	0.0871	0	0.0000	0.0000
Ba	137	0.2616	0	0.0000	0.0000
Ce	140	0.0420	0	0.0000	0.0000
Ho	165	0.0305	0	0.0000	0.0000
Th	232	0.0575	0	0.0000	0.0000
U	238	0.0275	0	0.0000	0.0000

Clear Fluorite - Primary

Run Number: Ju14B05 NaCl (ppm): 115000 Na (ppm): 45214

Analysis of: Pri LV in w/c fluorite

Element	Isotope	Corr. Fact.	Counts	Count Ratios	Conc.
Na	23	1.0000	45070	1.0000	45213.6752
K	39	0.1873	733	0.0163	137.7225
Ca	43	- -		0.0000	- -
Sr	86	0.1002	8880	0.1970	892.7918
Y	89	0.1065	54861	1.2172	5863.2327
Nb	93	0.0953	0	0.0000	0.0000
Ba	137	0.5362	38	0.0008	20.4388
Ce	140	0.0698	42879	0.9514	3003.1064
Sm	147	0.4162	3815	0.0846	1592.8207
Th	232	0.1457	3	0.0001	0.4385
U	238	0.0910	0	0.0000	0.0000

Clear Fluorite - Primary

Run Number: Ju14B06 NaCl (ppm): 111000 Na (ppm): 43641

Analysis of: Pri LV in w/c fluorite

Element	Isotope	Corr. Fact.	Counts	Count Ratios	Conc.
Na	23	1.0000	40328	1.0000	43641.0256
K	39	0.1873	2713	0.0673	549.8657
Ca	43	- -		0.0000	- -
Sr	86	0.1002	5797	0.1437	628.7045
Y	89	0.1065	88664	2.1986	10221.7850
Nb	93	0.0953	10.5	0.0003	1.0829
Ba	137	0.5362	14.7	0.0004	8.5289
Ce	140	0.0698	2176	0.0540	164.3959
Sm	147	0.4162	344	0.0085	154.9305
Th	232	0.1457	0	0.0000	0.0000
U	238	0.0910	0	0.0000	0.0000

Clear Fluorite - Primary

Run Number: Ju15C03 NaCl (ppm): 109000 Na (ppm): 42855

Analysis of: Pri LV in c/w fluorite

Element	Isotope	Corr. Fact.	Counts	Count Ratios	Conc.
Na	23	1.0000	52595	1.0000	42854.7009
K	39	0.0784	2344	0.0446	149.7964
Ca	43	- -		0.0000	- -
Sr	86	0.0388	6567	0.1249	207.4448
Y	89	0.0434	0	0.0000	0.0000
Nb	93	0.0405	0	0.0000	0.0000
Ba	137	0.1971	67	0.0013	10.7611
Ce	140	0.0277	0	0.0000	0.0000
Ho	165	0.0261	0	0.0000	0.0000
Th	232	0.0525	0	0.0000	0.0000
U	238	0.0311	0	0.0000	0.0000

Quartz - Secondary

Run Number: Ju14A03b NaCl (ppm): 295400 Na (ppm): 116140

Analysis of: Sec LVS in quartz

Element	Isotope	Corr. Fact.	Counts	Count Ratios	Conc.
Na	23	1.0000	625000000	1.0000	116140.1709
K	39	0.0638	148000000	0.2368	1754.7616
Ca	43	79.5562	2501901	0.0040	36986.7855
Sr	86	0.0293	88240450	0.1412	480.8013
Y	89	0.0329	0	0.0000	0.0000
Nb	93	0.0299	0	0.0000	0.0000
Ba	137	0.1508	9671892	0.0155	271.0182
Ce	140	0.0210	0	0.0000	0.0000
Sm	147	0.1220	0	0.0000	0.0000
Th	232	0.0466	0	0.0000	0.0000
U	238	0.0277	0	0.0000	0.0000

Quartz - Secondary

Run Number: Ju14A04 NaCl (ppm): 295400 Na (ppm): 116140

Analysis of: Sec LVS in quartz

Element	Isotope	Corr. Fact.	Counts	Count Ratios	Conc.
Na	23	1.0000	4220000000	1.0000	116140.1709
K	39	0.0638	999000000	0.2367	1754.2418
Ca	43	79.5562	33740031	0.0080	73873.6421
Sr	86	0.0293	676000000	0.1602	545.5219
Y	89	0.0329	0	0.0000	0.0000
Nb	93	0.0299	0	0.0000	0.0000
Ba	137	0.1508	74692858	0.0177	309.9799
Ce	140	0.0210	265576	0.0001	0.1536
Sm	147	0.1220	36864	0.0000	0.1238
Th	232	0.0466	0	0.0000	0.0000
U	238	0.0277	0	0.0000	0.0000

Quartz - Secondary

Run Number: Ju14A05a NaCl (ppm): 295400 Na (ppm): 116140

Analysis of: Sec LV in quartz

Element	Isotope	Corr. Fact.	Counts	Count Ratios	Conc.
Na	23	1.0000	5760000000	1.0000	116140.1709
K	39	0.0638	1770000000	0.3073	2277.1267
Ca	43	79.5562	0	0.0000	0.0000
Sr	86	0.0293	34523879	0.0060	20.4115
Y	89	0.0329	0	0.0000	0.0000
Nb	93	0.0299	0	0.0000	0.0000
Ba	137	0.1508	0	0.0000	0.0000
Ce	140	0.0210	0	0.0000	0.0000
Sm	147	0.1220	0	0.0000	0.0000
Th	232	0.0466	0	0.0000	0.0000
U	238	0.0277	0	0.0000	0.0000

Quartz - Secondary

Run Number: Ju15A07 NaCl (ppm): 298600 Na (ppm): 117398

Analysis of: Sec LVS in quartz

Element	Isotope	Corr. Fact.	Counts	Count Ratios	Conc.
Na	23	1.0000	2200000000	1.0000	117398.2906
K	39	0.2624	177000000	0.0805	2478.0845
Ca	43	363.0140	0	0.0000	0.0000
Sr	86	0.0838	23700	0.0000	0.1060
Y	89	0.1045	0	0.0000	0.0000
Nb	93	0.0871	0	0.0000	0.0000
Ba	137	0.2616	0	0.0000	0.0000
Ce	140	0.0420	0	0.0000	0.0000
Ho	165	0.0305	0	0.0000	0.0000
Th	232	0.0575	0	0.0000	0.0000
U	238	0.0275	0	0.0000	0.0000

Quartz - Secondary

Run Number: Ju15A08 NaCl (ppm): 298600 Na (ppm): 117398

Analysis of: Sec LVS in quartz

Element	Isotope	Corr. Fact.	Counts	Count Ratios	Conc.
Na	23	1.0000	1060000000	1.0000	117398.2906
K	39	0.2624	169000000	0.1594	4910.7335
Ca	43	363.0140	4175123	0.0039	167860.5396
Sr	86	0.0838	170000000	0.1604	1578.2489
Y	89	0.1045	0	0.0000	0.0000
Nb	93	0.0871	0	0.0000	0.0000
Ba	137	0.2616	23713443	0.0224	686.9599
Ce	140	0.0420	0	0.0000	0.0000
Ho	165	0.0305	0	0.0000	0.0000
Th	232	0.0575	0	0.0000	0.0000
U	238	0.0275	0	0.0000	0.0000

Quartz - Secondary

Run Number: Ju15A09 NaCl (ppm): 298600 Na (ppm): 117398

Analysis of: Sec LVS in quartz

Element	Isotope	Corr. Fact.	Counts	Count Ratios	Conc.
Na	23	1.0000	1960000000	1.0000	117398.2906
K	39	0.2624	332000000	0.1694	5217.3208
Ca	43	363.0140	8423253	0.0043	183150.8674
Sr	86	0.0838	363000000	0.1852	1822.5648
Y	89	0.1045	0	0.0000	0.0000
Nb	93	0.0871	0	0.0000	0.0000
Ba	137	0.2616	45498513	0.0232	712.8264
Ce	140	0.0420	0	0.0000	0.0000
Ho	165	0.0305	0	0.0000	0.0000
Th	232	0.0575	0	0.0000	0.0000
U	238	0.0275	0	0.0000	0.0000

Quartz - Secondary

Run Number: Ju08B06 NaCl (ppm): 203000 Na (ppm): 79812

Analysis of: Sec LV(carb) in quartz

Element	Isotope	Corr. Fact.	Counts	Count Ratios	Conc.
Be	9	1.0654	0	0.0000	0.0000
Na	23	1.0000	241000000	1.0000	79811.9658
K	39	0.0958	0	0.0000	0.0000
Ca	43	109.6554	0	0.0000	0.0000
Sr	86	0.6176	0	0.0000	0.0000
Y	89	0.0799	0	0.0000	0.0000
Zr	90	0.1650	0	0.0000	0.0000
Nb	93	0.0704	0	0.0000	0.0000
Ce	140	0.0647	0	0.0000	0.0000
Sm	147	0.3989	0	0.0000	0.0000
Th	232	0.1830	0	0.0000	0.0000
U	238	0.1130	0	0.0000	0.0000

Quartz - Secondary

Run Number: Ju12I06 NaCl (ppm): 263000 Na (ppm): 103402

Analysis of: Sec LV in quartz

Element	Isotope	Corr. Fact.	Counts	Count Ratios	Conc.
Be	9	2.6232	0	0.0000	0.0000
Na	23	1.0000	5740000000	1.0000	103401.7094
K	39	0.0908	1170000000	0.2038	1913.4133
Ca	43	229.2689	0	0.0000	0.0000
Sr	86	0.6858	0	0.0000	0.0000
Y	89	0.0901	0	0.0000	0.0000
Zr	90	0.1815	0	0.0000	0.0000
Nb	93	0.0768	0	0.0000	0.0000
Ce	140	0.0444	64800	0.0000	0.0518
Sm	147	0.2934	0	0.0000	0.0000
Th	232	0.0899	0	0.0000	0.0000
U	238	0.0498	0	0.0000	0.0000

Quartz - Secondary

Run Number: Ju12I09 NaCl (ppm): 263000 Na (ppm): 103402

Analysis of: Sec LV in quartz

Element	Isotope	Corr. Fact.	Counts	Count Ratios	Conc.
Be	9	2.6232	0	0.0000	0.0000
Na	23	1.0000	295000000	1.0000	103401.7094
K	39	0.0908	12900000	0.0437	410.4899
Ca	43	229.2689	361119	0.0012	29020.2469
Sr	86	0.6858	1283451	0.0044	308.5075
Y	89	0.0901	0	0.0000	0.0000
Zr	90	0.1815	0	0.0000	0.0000
Nb	93	0.0768	0	0.0000	0.0000
Ce	140	0.0444	0	0.0000	0.0000
Sm	147	0.2934	0	0.0000	0.0000
Th	232	0.0899	0	0.0000	0.0000
U	238	0.0498	0	0.0000	0.0000

Quartz - Secondary

Run Number:	Ju14A05b	NaCl (ppm):	295400	Na (ppm):	116140
Analysis of:	Sec LV in quartz				
Element	**Isotope**	**Corr. Fact.**	**Counts**	**Count Ratios**	**Conc.**
Na	23	1.0000	1610000000	1.0000	116140.1709
K	39	0.0638	201000000	0.1248	925.1382
Ca	43	79.5562	0	0.0000	0.0000
Sr	86	0.0293	3324943	0.0021	7.0329
Y	89	0.0329	0	0.0000	0.0000
Nb	93	0.0299	0	0.0000	0.0000
Ba	137	0.1508	0	0.0000	0.0000
Ce	140	0.0210	0	0.0000	0.0000
Sm	147	0.1220	0	0.0000	0.0000
Th	232	0.0466	0	0.0000	0.0000
U	238	0.0277	0	0.0000	0.0000

Quartz - Secondary

Run Number:	Ju14A05c	NaCl (ppm):	295400	Na (ppm):	116140
Analysis of:	Sec LV in quartz				
Element	**Isotope**	**Corr. Fact.**	**Counts**	**Count Ratios**	**Conc.**
Na	23	1.0000	5670000000	1.0000	116140.1709
K	39	0.0638	705000000	0.1243	921.3878
Ca	43	79.5562	0	0.0000	0.0000
Sr	86	0.0293	12605633	0.0022	7.5711
Y	89	0.0329	0	0.0000	0.0000
Nb	93	0.0299	0	0.0000	0.0000
Ba	137	0.1508	0	0.0000	0.0000
Ce	140	0.0210	0	0.0000	0.0000
Sm	147	0.1220	0	0.0000	0.0000
Th	232	0.0466	0	0.0000	0.0000
U	238	0.0277	0	0.0000	0.0000

Quartz - Secondary

Run Number:	Ju14A06	NaCl (ppm):	263000	Na (ppm):	103402
Analysis of:	Sec LV in quartz				
Element	**Isotope**	**Corr. Fact.**	**Counts**	**Count Ratios**	**Conc.**
Na	23	1.0000	4690000000	1.0000	103401.7094
K	39	0.0638	1020000000	0.2175	1434.8583
Ca	43	79.5562	20843317	0.0044	36559.1200
Sr	86	0.0293	642000000	0.1369	415.0356
Y	89	0.0329	0	0.0000	0.0000
Nb	93	0.0299	0	0.0000	0.0000
Ba	137	0.1508	80837739	0.0172	268.7531
Ce	140	0.0210	0	0.0000	0.0000
Sm	147	0.1220	0	0.0000	0.0000
Th	232	0.0466	0	0.0000	0.0000
U	238	0.0277	0	0.0000	0.0000

Quartz - Secondary

Run Number:	Ju15B03	NaCl (ppm):	232300	Na (ppm):	91332
Analysis of:	Sec LV in quartz				

Element	**Isotope**	**Corr. Fact.**	**Counts**	**Count Ratios**	**Conc.**
Na	23	1.0000	1290000000	1.0000	91331.6239
K	39	0.1172	96601719	0.0749	801.8397
Ca	43	319.3877	0	0.0000	0.0000
Sr	86	0.0887	532336	0.0004	3.3440
Y	89	0.1097	0	0.0000	0.0000
Nb	93	0.0955	0	0.0000	0.0000
Ba	137	0.3147	0	0.0000	0.0000
Ce	140	0.0489	0	0.0000	0.0000
Ho	165	0.0398	0	0.0000	0.0000
Th	232	0.0760	0	0.0000	0.0000
U	238	0.0368	0	0.0000	0.0000

Quartz - Secondary

Run Number:	Ju15B04	NaCl (ppm):	232300	Na (ppm):	91332
Analysis of:	Sec LV in quartz				

Element	**Isotope**	**Corr. Fact.**	**Counts**	**Count Ratios**	**Conc.**
Na	23	1.0000	703000000	1.0000	91331.6239
K	39	0.1172	42925694	0.0611	653.8143
Ca	43	319.3877	0	0.0000	0.0000
Sr	86	0.0887	116008	0.0002	1.3372
Y	89	0.1097	0	0.0000	0.0000
Nb	93	0.0955	0	0.0000	0.0000
Ba	137	0.3147	0	0.0000	0.0000
Ce	140	0.0489	0	0.0000	0.0000
Ho	165	0.0398	0	0.0000	0.0000
Th	232	0.0760	0	0.0000	0.0000
U	238	0.0368	0	0.0000	0.0000

Quartz - Secondary

Run Number:	Ju15B09	NaCl (ppm):	293300	Na (ppm):	115315
Analysis of:	Sec LVS in quartz				

Element	**Isotope**	**Corr. Fact.**	**Counts**	**Count Ratios**	**Conc.**
Na	23	1.0000	1120000000	1.0000	115314.5299
K	39	0.1172	181000000	0.1616	2184.8207
Ca	43	319.3877	1328549	0.0012	43687.9546
Sr	86	0.0887	120000000	0.1071	1096.2204
Y	89	0.1097	0	0.0000	0.0000
Nb	93	0.0955	0	0.0000	0.0000
Ba	137	0.3147	28079169	0.0251	909.8923
Ce	140	0.0489	1200104	0.0011	6.0378
Ho	165	0.0398	0	0.0000	0.0000
Th	232	0.0760	0	0.0000	0.0000
U	238	0.0368	0	0.0000	0.0000

Quartz-hosted Fluid Inclusions

Mineral	Zone	Sample	Analysis:	Type:	Phases:	Prov:	Be	Na	K	Ca	Sr	Y	Zr
Quartz	Core	RL-94-60-3	Ju12I09	Aq.	LV	Sec.	0	99391	395	27895	297	0	0
Quartz	Core	RL-94-60-3	Ju14A06	Aq.	LV	Sec.		98920	1373	34974	397	0	
Quartz	Core	RL-94-60-3	Ju14A08b	Aq.	LV	Sec.		98133	1827	49700	464	5	
Quartz	Core	RL-94-60-3	Ju14A09a	Aq.	LV	Sec.		101279	1086	6201	57	0	
Quartz	Core	RL-94-60-3	Ju12I06	Aq.	LV	Sec.	0	103000	1910	0	0	0	0
Quartz	Core	RL-94-60-3	Ju14A09b	Aq.	LV	Sec.	0	103000	615	0	54	0	
Quartz	Core	RL-94-60-3	Ju14A09c	Aq.	LV	Sec.		103000	1130	0	13	0	
Quartz	Core	RL-94-60-3	Ju14A09d	Aq.	LV	Sec.		103000	736	0	3	0	
Quartz	Core	RL-94-60-3	Ju14A10a	Aq.	LV	Sec.		103000	1140	0	66	0	
Quartz	Core	RL-94-60	Ju15A03	Aq.	LV	Sec.		104000	4540	0	2	0	
Quartz	Core	RL-94-60	Ju15A04	Aq.	LV	Sec.		104000	12	0	0	0	
Quartz	Core	RL-94-60	Ju15A05	Aq.	LV	Sec.		104000	2010	0	0	0	
Quartz	Core	RL-94-60	Ju15B03	Aq.	LV	Sec.		91300	802	0	3	0	
Quartz	Core	RL-94-60	Ju15B04	Aq.	LV	Sec.		91300	654	0	1	0	
Quartz	Core	RL-94-60-3	Ju12I10	Aq.	LVH	Sec.		70769	1697	80630	1161	0	0
Quartz	Core	RL-94-60-3	Ju14A03b	Aq.	LVH	Sec.		90427	1366	28798	374	0	
Quartz	Core	RL-94-60-3	Ju14A04	Aq.	LVH	Sec.		70769	1069	45014	332	0	
Quartz	Core	RL-94-60	Ju15A08	Aq.	LVH	Sec.		51111	2138	73081	687	0	
Quartz	Core	RL-94-60	Ju15A09	Aq.	LVH	Sec.		51111	2271	79737	793	0	
Quartz	Core	RL-94-60	Ju15B09	Aq.	LVH	Sec.		86496	1639	32770	822	0	
Quartz	Core	RL-94-60	Ju15B10	Aq.	LVH	Sec.		66838	1721	66353	1303	0	
Quartz	Core	RL-94-60-3	Ju12J04	Aq.	LVH	Sec.	0	116000	1710	0	0	0	0
Quartz	Core	RL-94-60-3	Ju14A03a	Aq.	LVH	Sec.		116000	5110	0	41	169	
Quartz	Core	RL-94-60-3	Ju14A05a	Aq.	LVH	Sec.		116000	2280	0	20	0	
Quartz	Core	RL-94-60-3	Ju14A05b	Aq.	LVH	Sec.		116000	925	0	7	0	
Quartz	Core	RL-94-60-3	Ju14A05c	Aq.	LVH	Sec.		116000	921	0	8	0	
Quartz	Core	RL-94-60	Ju15A07	Aq.	LVH	Sec.		117000	2580	0	0	0	

Quartz-hosted Fluid Inclusions

Mineral	Zone	Sample	Analysis:	Type:	Phases:	Prov:	Nb	Ba	Ce	Sm	Ho	Th	U
Quartz	Core	RL-94-60-3	Ju12I09	Aq.	LV	Sec.	0		0	0		0	0
Quartz	Core	RL-94-60-3	Ju14A06	Aq.	LV	Sec.	0	257	0	0		0	0
Quartz	Core	RL-94-60-3	Ju14A08b	Aq.	LV	Sec.	1	206	1	5		4	11
Quartz	Core	RL-94-60-3	Ju14A09a	Aq.	LV	Sec.	0	5	0	0		0	0
Quartz	Core	RL-94-60-3	Ju12I06	Aq.	LV	Sec.	0		0	0		0	0
Quartz	Core	RL-94-60-3	Ju14A09b	Aq.	LV	Sec.	0	69	0	0		0	0
Quartz	Core	RL-94-60-3	Ju14A09c	Aq.	LV	Sec.	0	1	0	0		0	0
Quartz	Core	RL-94-60-3	Ju14A09d	Aq.	LV	Sec.	0	0	0	0		0	0
Quartz	Core	RL-94-60-3	Ju14A10a	Aq.	LV	Sec.	0	0	0	0		0	0
Quartz	Core	RL-94-60	Ju15A03	Aq.	LV	Sec.	0	0	0		0	0	0
Quartz	Core	RL-94-60	Ju15A04	Aq.	LV	Sec.	0	0	0		0	0	0
Quartz	Core	RL-94-60	Ju15A05	Aq.	LV	Sec.	0	0	0		0	0	0
Quartz	Core	RL-94-60	Ju15B03	Aq.	LV	Sec.	0	0	0		0	0	0
Quartz	Core	RL-94-60	Ju15B04	Aq.	LV	Sec.	0	0	0		0	0	0
Quartz	Core	RL-94-60-3	Ju12I10	Aq.	LVH	Sec.	0		0	0		0	0
Quartz	Core	RL-94-60-3	Ju14A03b	Aq.	LVH	Sec.	0	211	0	0		0	0
Quartz	Core	RL-94-60-3	Ju14A04	Aq.	LVH	Sec.	0	189	0	0		0	0
Quartz	Core	RL-94-60	Ju15A08	Aq.	LVH	Sec.	0	299	0		0	0	0
Quartz	Core	RL-94-60	Ju15A09	Aq.	LVH	Sec.	0	310	0		0	0	0
Quartz	Core	RL-94-60	Ju15B09	Aq.	LVH	Sec.	0	682	5		0	0	0
Quartz	Core	RL-94-60	Ju15B10	Aq.	LVH	Sec.	3	1119	1		0	0	0
Quartz	Core	RL-94-60-3	Ju12J04	Aq.	LVH	Sec.	0		0	0		0	0
Quartz	Core	RL-94-60-3	Ju14A03a	Aq.	LVH	Sec.	17	21	86	0		6	96
Quartz	Core	RL-94-60-3	Ju14A05a	Aq.	LVH	Sec.	0	0	0	0		0	0
Quartz	Core	RL-94-60-3	Ju14A05b	Aq.	LVH	Sec.	0	0	0	0		0	0
Quartz	Core	RL-94-60-3	Ju14A05c	Aq.	LVH	Sec.	0	0	0	0		0	0
Quartz	Core	RL-94-60	Ju15A07	Aq.	LVH	Sec.	0	0	0		0	0	0

Quartz-hosted Fluid Inclusions

Mineral	Peg. Zone	Sample	Analysis:	Type:	Phases:	Prov:		Be	Na	K	Ca	Sr	Y	Zr
Quartz	Core	RL-94-60-3	**Ju14A03b**	Aqueous	LVH	Sec.	**Orig.**		116000	1750	37000	481	0	
							Recalc.		94359	1426	30050	391	0	
Quartz	Core	RL-94-60-3	**Ju14A04**	Aqueous	LVH	Sec.	**Orig.**		116000	1750	73900	546	0	
							Recalc.		78632	1188	50016	369	0	
Quartz	Core	RL-94-60	**Ju15A08**	Aqueous	LVH	Sec.	**Orig.**		117000	4910	178000	1580	0	
							Recalc.		51111	2138	73081	687	0	
Quartz	Core	RL-94-60	**Ju15A09**	Aqueous	LVH	Sec.	**Orig.**		117000	5220	183000	1820	0	
							Recalc.		47179	2097	73604	732	0	
Quartz	Core	RL-94-60	**Ju15B09**	Aqueous	LVH	Sec.	**Orig.**		115000	2180	43700	1100	0	
							Recalc.		90427	1713	34259	860	0	
Quartz	Core	RL-94-60	**Ju15B10**	Aqueous	LVH	Sec.	**Orig.**		120000	3100	119000	2330	0	
							Recalc.		66838	1721	66353	1303	0	

Quartz-hosted Fluid Inclusions

Mineral	Peg. Zone	Sample	Analysis:	Type:	Phases:	Prov:		Nb	Ba	Ce	Sm	Ho	Th	U
Quartz	Core	RL-94-60-3	**Ju14A03b**	Aqueous	LVH	Sec.	**Orig.**	0	271	0	0		0	0
							Recalc.	0	220	0	0	0		
Quartz	Core	RL-94-60-3	**Ju14A04**	Aqueous	LVH	Sec.	**Orig.**	0	310	0	0		0	0
							Recalc.	0	210	0	0		0	0
Quartz	Core	RL-94-60	**Ju15A08**	Aqueous	LVH	Sec.	**Orig.**	0	687	0		0	0	0
							Recalc.	0	299	0		0	0	0
Quartz	Core	RL-94-60	**Ju15A09**	Aqueous	LVH	Sec.	**Orig.**	0	713	0		0	0	0
							Recalc.	0	286	0		0	0	0
Quartz	Core	RL-94-60	**Ju15B09**	Aqueous	LVH	Sec.	**Orig.**	0	910	6		0	0	0
							Recalc.	0	714	5		0	0	0
Quartz	Core	RL-94-60	**Ju15B10**	Aqueous	LVH	Sec.	**Orig.**	5	2000	1		0	0	0
							Recalc.	3	1119	1		0	0	0

Fluorite-hosted Fluid Inclusions

Host Mineral	Peg. Zone	Sample	Analysis:	Type:	Phases:	Provenance:	Be	Na	K	Ca	Sr	Y	Zr
White Fluorite	Core-margin	RL-94-63	Ju08A06	Aqueous	LV	Primary	0	48,400	0		0	0	0
White Fluorite	Core-margin	RL-94-63	Ju08a08	Aqueous	LV	Primary	0	42,100	851		652	0	0
White Fluorite	Core-margin	RL-94-63-jg	Ju12J10	Aqueous	LV	Primary	0	45,200	115		44	54	0
White Fluorite	Core-margin	RL-9455b	Ju15C15	Aqueous	LV	Primary		43,900	111		297	0	
White Fluorite	Core-margin	RL-94-55b	Ju15C16	Aqueous	LV	Primary		43,900	80		0	0	
Purple Fluorite	Core-margin	RL-94-63-jg	Ju14B07	Aqueous	LV	Primary		43,200	286		136	1,590	
Purple Fluorite	Core-margin	RL-94-63-jg	Ju14B08	Aqueous	LV	Primary		41,300	375		240	0	
Clear Fluorite	Core-margin	RL-94-55b	Ju15C03	Aqueous	LV	Primary		42,900	150		207	0	
Clear Fluorite	Core-margin	RL-94-55b	Ju15C04	Aqueous	LV	Primary		42,900	145		313	0	
Clear Fluorite	Core-margin	RL-9455b	Ju15C05	Aqueous	LV	Primary		42,900	123		267	0	
White Fluorite	Core-margin	RL-94-55b	Ju15C06	Aqueous	LVH	Secondary?		95,200	1,210		546	0	
White Fluorite	Core-margin	RL-94-55b	Ju15C07	Aqueous	LVH	Secondary?		95,200	1,590		786	0	

Host Mineral	Peg. Zone	Sample	Analysis:	Type:	Phases:	Provenance:	Nb	Ba	Ce	Sm	Ho	Th	U
White Fluorite	Core-margin	RL-94-63	Ju08A06	Aqueous	LV	Primary	0		0	0		0	0
White Fluorite	Core-margin	RL-94-63	Ju08a08	Aqueous	LV	Primary	0		0	0		0	0
White Fluorite	Core-margin	RL-94-63-jg	Ju12J10	Aqueous	LV	Primary	0		10	4		12	0
White Fluorite	Core-margin	RL-9455b	Ju15C15	Aqueous	LV	Primary	0	3	0		0	8	0
White Fluorite	Core-margin	RL-94-55b	Ju15C16	Aqueous	LV	Primary	0	7	0		0	11	1
Purple Fluorite	Core-margin	RL-94-63-jg	Ju14B07	Aqueous	LV	Primary	1	8	152	61		1,930	13
Purple Fluorite	Core-margin	RL-94-63-jg	Ju14B08	Aqueous	LV	Primary	0	0	173	105		271	5
Clear Fluorite	Core-margin	RL-94-55b	Ju15C03	Aqueous	LV	Primary	0	11	0			0	0
Clear Fluorite	Core-margin	RL-94-55b	Ju15C04	Aqueous	LV	Primary	0	8	0		0	26	0
Clear Fluorite	Core-margin	RL-9455b	Ju15C05	Aqueous	LV	Primary	0	4	420		0	0	0
White Fluorite	Core-margin	RL-94-55b	Ju15C06	Aqueous	LVH	Secondary?	0	353	0		0	0	0
White Fluorite	Core-margin	RL-94-55b	Ju15C07	Aqueous	LVH	Secondary?	0	0	0		0	0	0

Appendix D

Appendix to Chapter 5 – "Quantitative analysis of silicates by LA-ICPMS with and without an internal standard"

NIST 610 (Average)

Isotope	Element	Pub. Conc.	Si Internal	Ca Internal	Fe Internal	Scaled
7Li	Li	484.6	491.09	496.89	488.40	492.57
9Be	Be	465.5	470.48	475.67	467.55	471.86
11B	B	356.4	358.96	363.01	356.76	360.02
23Na	Na	99053	98567.33	99791.74	98056.83	98865.89
25Mg	Mg	465.3	467.79	472.99	465.08	469.16
27Al	Al	10790	10831.07	10953.39	10768.23	10862.93
29Si	Si	327090	327090.00	330913.33	325282.92	328065.22
31P	P	342.5	342.72	346.77	340.69	343.74
39K	K	486	482.21	486.65	478.73	483.53
44Ca	Ca	81830	81169.06	81830.00	80523.12	81382.84
45Sc	Sc	441.1	441.91	446.05	438.66	443.12
47Ti	Ti	434	433.59	437.79	430.42	434.80
51V	V	441.7	435.22	439.34	432.08	436.42
52Cr	Cr	405.2	400.87	404.79	397.84	401.99
55Mn	Mn	433.3	434.16	438.53	431.04	435.38
57Fe	Fe	457.1	461.02	465.30	457.10	462.27
59Co	Co	405	403.93	407.99	400.95	405.07
60Ni	Ni	443.9	442.64	447.20	439.48	443.89
65Cu	Cu	430.3	428.87	433.18	425.84	430.07
66Zn	Zn	456.3	458.79	463.21	455.70	462.14
69Ga	Ga	438.1	437.70	442.16	434.72	438.95
72Ge	Ge	426.3	430.67	435.08	427.61	431.89
75As	As	317.4	320.83	324.09	318.59	321.73
82Se	Se	109	109.94	111.00	109.08	110.25
85Rb	Rb	431.1	421.17	425.44	418.32	422.36
88Sr	Sr	497.4	497.88	503.24	494.54	499.32
89Y	Y	449.9	447.65	452.40	444.68	448.94
90Zr	Zr	439.9	438.48	443.23	435.63	439.75
93Nb	Nb	419.4	419.16	423.66	416.40	420.37
95Mo	Mo	376.8	375.83	379.88	373.27	376.91
103Rh	Rh	1.31	1.32	1.33	1.31	1.32
105Pd	Pd	1.05	1.09	1.10	1.08	1.09
107Ag	Ag	239.4	242.25	244.74	240.67	242.93
111Cd	Cd	259.4	265.64	268.41	264.03	266.39
115In	In	441.4	438.78	443.35	436.13	440.03
118Sn	Sn	396.3	397.41	401.51	394.67	398.55
121Sb	Sb	368.5	376.08	380.01	373.52	377.16
133Cs	Cs	360.9	358.54	362.30	356.46	359.57
137Ba	Ba	424.1	431.21	435.91	428.54	432.47
139La	La	457.4	464.96	470.04	462.15	466.32
140Ce	Ce	447.8	452.99	457.73	450.04	454.29
141Pr	Pr	429.8	437.51	442.23	434.81	438.78
146Nd	Nd	430.8	437.70	442.54	435.05	438.99
147Sm	Sm	450.5	458.43	463.36	455.49	459.76
153Eu	Eu	461.1	465.99	471.06	463.09	467.35
157Gd	Gd	419.9	424.52	429.23	421.91	425.77
159Tb	Tb	442.8	447.12	452.03	444.36	448.43
163Dy	Dy	426.5	430.57	435.43	427.96	431.85
165Ho	Ho	449.4	453.66	458.71	450.86	455.00

NIST 610 (Average)

Isotope	Element	Pub. Conc.	Si Internal	Ca Internal	Fe Internal	Scaled
166Er	Er	426	429.68	434.48	427.04	430.95
169Tm	Tm	420.1	423.40	428.13	420.82	424.65
172Yb	Yb	461.5	463.81	468.98	460.96	465.17
175Lu	Lu	434.7	438.42	443.37	435.83	439.72
178Hf	Hf	417.7	423.04	427.82	420.56	424.29
181Ta	Ta	376.6	382.42	386.81	380.22	383.56
182W	W	445.3	447.03	452.08	444.18	448.36
185Re	Re	103.7	104.97	106.15	104.29	105.28
195Pt	Pt	3.15	3.24	3.28	3.22	3.25
197Au	Au	22.5	23.01	23.27	22.86	23.08
205Tl	Tl	61.2	62.76	63.38	62.31	62.93
208Pb	Pb	413.3	418.35	422.82	415.70	419.56
209Bi	Bi	357.7	367.71	371.64	365.49	368.77
232Th	Th	450.6	460.96	466.01	458.14	462.31
238U	U	457.1	455.23	460.07	452.31	456.54

NIST 612 (Average)

Isotope	Element	Pub. Conc.	Si Internal	Ca Internal	Fe Internal	Scaled
7Li	Li	41.54	41.79	46.16	50.53	42.48
9Be	Be	37.73	38.14	42.08	45.56	38.77
11B	B	34.73	54.74	60.63	70.21	55.68
23Na	Na	103700	98745.15	109294.33	118722.96	100379.58
25Mg	Mg	77.44	59.97	65.95	69.93	60.93
27Al	Al	11200	10792.87	11898.30	12868.17	10969.99
29Si	Si	336100	336100.00	371376.71	404789.94	341667.72
31P	P	55.16	35.79	39.52	43.61	36.39
39K	K	66.26	84.96	92.23	106.89	86.19
44Ca	Ca	85260	77535.00	85260.00	93183.46	78791.45
45Sc	Sc	41.05	35.18	38.72	42.00	35.76
47Ti	Ti	48.11	37.21	41.04	45.41	37.83
51V	V	39.22	35.46	39.16	43.07	36.45
52Cr	Cr	39.88	37.13	41.23	43.72	34.42
55Mn	Mn	38.43	35.54	39.23	42.78	36.13
57Fe	Fe	56.33	58.29	64.39	56.33	59.20
59Co	Co	35.26	33.61	37.15	40.71	34.17
60Ni	Ni	38.44	38.10	42.13	46.03	38.74
65Cu	Cu	36.71	36.78	40.68	44.26	37.39
66Zn	Zn	37.92	36.70	40.50	44.15	40.88
69Ga	Ga	36.24	35.43	39.16	42.82	36.02
72Ge	Ge	34.64	36.79	40.65	44.33	37.40
75As	As	37.33	27.04	29.85	32.76	27.48
82Se	Se	- -	15.26	16.89	18.52	15.51
85Rb	Rb	31.63	29.07	32.12	35.19	29.55
88Sr	Sr	76.15	70.87	78.25	84.78	72.04
89Y	Y	38.25	32.95	36.34	39.19	33.49
90Zr	Zr	35.99	34.02	37.53	40.50	34.58
93Nb	Nb	38.06	33.07	36.53	39.61	33.62
95Mo	Mo	38.3	31.96	35.32	38.70	32.49
103Rh	Rh	0.896	0.91	1.01	1.10	0.93
105Pd	Pd	1.09	1.10	1.22	1.31	1.12
107Ag	Ag	21.92	18.71	20.68	22.56	19.02
111Cd	Cd	28.32	24.62	27.20	29.56	25.03
115In	In	42.93	33.45	36.97	40.37	34.01
118Sn	Sn	37.96	35.04	38.73	42.34	35.62
121Sb	Sb	38.44	29.96	33.12	36.17	30.45
133Cs	Cs	41.64	36.71	40.57	44.30	37.32
137Ba	Ba	37.74	34.73	38.36	41.59	35.30
139La	La	35.77	34.66	38.26	41.25	35.23
140Ce	Ce	38.35	35.76	39.52	42.89	36.36
141Pr	Pr	37.16	34.08	37.64	40.72	34.64
146Nd	Nd	35.24	33.03	36.49	39.41	33.58
147Sm	Sm	36.72	34.56	38.15	41.10	35.13
153Eu	Eu	34.44	34.03	37.56	40.48	34.59
157Gd	Gd	36.95	31.74	35.01	37.74	32.26
159Tb	Tb	35.92	33.13	36.55	39.39	33.68
163Dy	Dy	35.97	31.19	34.40	36.97	31.70
165Ho	Ho	37.87	33.34	36.78	39.56	33.89

NIST 612 (Average)

Isotope	Element	Pub. Conc.	Si Internal	Ca Internal	Fe Internal	Scaled
166Er	Er	37.43	31.76	35.03	37.69	32.29
169Tm	Tm	37.55	31.21	34.44	37.05	31.73
172Yb	Yb	39.95	34.94	38.56	41.52	35.52
175Lu	Lu	37.71	31.88	35.17	37.79	32.40
178Hf	Hf	34.77	31.82	35.11	37.77	32.34
181Ta	Ta	39.77	28.96	31.97	34.35	29.44
182W	W	39.55	37.21	41.13	44.80	37.82
185Re	Re	8.12	13.64	15.07	16.43	13.87
195Pt	Pt	2.59	2.49	2.75	2.99	2.53
197Au	Au	5.09	4.41	4.88	5.34	4.49
205Tl	Tl	15.07	14.52	16.03	17.54	14.77
208Pb	Pb	38.96	34.40	38.05	41.71	34.97
209Bi	Bi	29.84	29.47	32.59	35.68	29.97
232Th	Th	37.23	33.79	37.31	40.28	34.35
238U	U	37.15	33.31	36.85	40.65	33.86

NIST 614 (Average)

Isotope	Element	Pub. Conc.	Si Internal	Ca Internal	Fe Internal	Scaled
7Li	Li	- -	1.81	2.07	11.41	1.84
9Be	Be	- -	0.96	1.06	18.68	0.98
11B	B	1.3	19.89	22.80	197.37	20.21
23Na	Na	103860	103218.70	118169.87	640728.95	104821.43
25Mg	Mg	- -	31.09	35.54	139.90	31.59
27Al	Al	10585	10505.52	12034.68	65407.82	10671.79
29Si	Si	336553.2	336553.20	385284.58	2118591.99	341880.15
31P	P	30	11.24	12.88	72.87	11.43
39K	K	- -	76.39	86.85	428.13	77.56
44Ca	Ca	85764.1	75103.51	85764.10	463216.00	76273.29
45Sc	Sc	0.59	2.81	3.20	18.80	2.86
47Ti	Ti	3.1	3.84	4.11	36.51	3.90
51V	V	- -	0.96	1.09	6.08	1.47
52Cr	Cr	- -	6.37	7.14	11.68	1.30
55Mn	Mn	- -	1.29	1.47	8.41	1.31
57Fe	Fe	13.3	30.90	34.95	#DIV/0!	31.44
59Co	Co	0.73	0.62	0.71	5.66	0.63
60Ni	Ni	0.95	3.16	3.62	30.75	3.22
65Cu	Cu	1.37	4.05	4.65	35.25	4.11
66Zn	Zn	- -	3.35	3.82	17.42	6.88
69Ga	Ga	- -	1.19	1.37	8.28	1.21
72Ge	Ge	- -	0.95	1.09	6.89	0.97
75As	As	- -	0.83	0.95	0.48	0.84
82Se	Se	- -	0.88	1.02	8.29	0.90
85Rb	Rb	0.855	0.85	0.97	6.51	0.87
88Sr	Sr	45.8	40.61	46.48	255.01	41.24
89Y	Y	- -	0.63	0.72	4.05	0.64
90Zr	Zr	- -	0.85	0.97	5.01	0.86
93Nb	Nb	- -	0.68	0.78	3.99	0.70
95Mo	Mo	- -	0.73	0.84	4.68	0.74
103Rh	Rh	1.67	1.64	1.87	10.14	1.66
105Pd	Pd	1.98	2.26	2.58	13.54	2.29
107Ag	Ag	0.42	0.44	0.50	3.33	0.44
111Cd	Cd	0.55	0.75	0.89	2.34	0.76
115In	In	- -	0.70	0.80	4.48	0.71
118Sn	Sn	- -	2.82	3.23	18.71	2.86
121Sb	Sb	1.06	0.71	0.81	4.55	0.72
133Cs	Cs	- -	0.61	0.70	4.03	0.62
137Ba	Ba	- -	2.94	3.36	18.94	2.98
139La	La	0.83	0.67	0.77	4.48	0.68
140Ce	Ce	- -	0.73	0.84	4.40	0.74
141Pr	Pr	- -	0.69	0.79	4.22	0.70
146Nd	Nd	- -	0.70	0.80	4.10	0.71
147Sm	Sm	- -	0.72	0.83	4.42	0.73
153Eu	Eu	0.99	0.73	0.83	4.25	0.74
157Gd	Gd	- -	0.68	0.77	4.38	0.69
159Tb	Tb	- -	0.63	0.72	3.93	0.64
163Dy	Dy	- -	0.63	0.72	4.41	0.64
165Ho	Ho	- -	0.65	0.75	4.06	0.66

NIST 614 (Average)

Isotope	Element	Pub. Conc.	Si Internal	Ca Internal	Fe Internal	Scaled
166Er	Er	- -	0.58	0.66	3.64	0.59
169Tm	Tm	- -	0.58	0.66	3.71	0.59
172Yb	Yb	- -	0.66	0.75	4.15	0.67
175Lu	Lu	- -	0.59	0.68	3.86	0.60
178Hf	Hf	- -	0.61	0.70	3.65	0.62
181Ta	Ta	- -	0.58	0.66	3.58	0.58
182W	W	- -	0.78	0.89	5.05	0.79
185Re	Re	0.179	0.37	0.42	2.72	0.37
195Pt	Pt	2.26	2.43	2.78	16.11	2.47
197Au	Au	0.5	0.50	0.57	3.16	0.51
205Tl	Tl	0.269	0.28	0.32	1.70	0.28
208Pb	Pb	2.32	2.59	2.96	17.11	2.63
209Bi	Bi	- -	0.61	0.69	3.92	0.62
232Th	Th	0.748	0.67	0.77	4.73	0.68
238U	U	0.823	0.78	0.89	5.50	0.79

BCR-2G (Average)

Isotope	Element	Pub. Conc.	Si Internal	Ca Internal	Fe Internal	Scaled
7Li	Li	- -	9.37	11.67	9.73	9.72
9Be	Be	- -	2.04	2.58	2.14	2.13
11B	B	- -	15.42	19.12	15.97	15.97
23Na	Na	23400	17753.34	22121.47	18435.69	18410.02
25Mg	Mg	21600	19759.20	24578.72	20516.28	20492.99
27Al	Al	71400	73342.46	91111.45	76076.92	76026.83
29Si	Si	253000	253000.00	315351.14	263107.36	262648.17
31P	P	1500	1181.62	1474.93	1230.56	1227.67
39K	K	14900	15622.79	19480.28	16274.55	16230.97
44Ca	Ca	50900	41075.81	50900.00	42569.34	42566.95
45Sc	Sc	33	28.23	35.04	29.28	29.26
47Ti	Ti	13500	11758.96	14604.97	12198.69	12190.97
51V	V	416	353.00	438.29	366.06	367.60
52Cr	Cr	18	13.14	16.34	13.64	13.66
55Mn	Mn	1520	1438.86	1789.06	1493.35	1492.53
57Fe	Fe	96600	93152.01	115704.50	96600.00	96577.08
59Co	Co	37	33.94	42.23	35.25	35.22
60Ni	Ni	- -	11.63	14.60	12.29	12.22
65Cu	Cu	19	16.62	21.12	17.58	17.46
66Zn	Zn	127	144.36	180.15	150.32	157.74
69Ga	Ga	23	29.97	37.29	31.11	31.09
72Ge	Ge	- -	2.79	3.49	2.91	2.90
75As	As	- -	1.79	2.27	1.89	1.88
82Se	Se	- -	-0.77	-0.92	-0.75	0.00
85Rb	Rb	48	39.96	49.69	41.48	41.45
88Sr	Sr	346	280.85	348.64	291.08	291.01
89Y	Y	37	26.47	32.83	27.42	27.42
90Zr	Zr	188	149.06	184.98	154.48	154.45
93Nb	Nb	- -	10.08	12.53	10.46	10.45
95Mo	Mo	248	210.83	262.35	218.93	218.71
103Rh	Rh	- -	- -	0.02	0.02	0.02
105Pd	Pd	- -	- -	- -	- -	- -
107Ag	Ag	- -	0.53	0.66	0.55	0.55
111Cd	Cd	- -	0.66	0.64	0.71	0.69
115In	In	- -	0.25	0.32	0.26	0.26
118Sn	Sn	- -	2.39	2.99	2.49	2.48
121Sb	Sb	- -	0.42	0.53	0.44	0.44
133Cs	Cs	1.1	0.97	1.21	1.02	1.02
137Ba	Ba	693	573.89	712.43	594.92	594.64
139La	La	25.4	22.22	27.60	23.04	23.03
140Ce	Ce	53	43.32	53.80	44.92	44.90
141Pr	Pr	6.5	5.46	6.78	5.66	5.66
146Nd	Nd	29	24.32	30.19	25.21	25.20
147Sm	Sm	6.6	5.71	7.11	5.93	5.93
153Eu	Eu	2	1.82	2.27	1.90	1.89
157Gd	Gd	7	5.19	6.44	5.37	5.38
159Tb	Tb	1.1	1.02	1.18	0.98	0.98
163Dy	Dy	6.4	5.12	6.35	5.31	5.30
165Ho	Ho	1.25	1.10	1.33	1.15	1.14

BCR-2G (Average)

Isotope	Element	Pub. Conc.	Si Internal	Ca Internal	Fe Internal	Scaled
166Er	Er	3.6	2.77	3.45	2.88	2.88
169Tm	Tm	0.57	0.54	0.69	0.57	0.57
172Yb	Yb	3.4	2.86	3.56	2.97	2.97
175Lu	Lu	0.51	0.58	0.74	0.61	0.61
178Hf	Hf	4.8	3.94	4.90	4.09	4.09
181Ta	Ta	- -	0.70	0.88	0.77	0.73
182W	W	- -	0.71	0.91	0.75	0.75
185Re	Re	- -	0.19	0.18	0.21	0.20
195Pt	Pt	- -	0.31	0.39	0.32	0.32
197Au	Au	- -	0.04	0.05	0.04	0.04
205Tl	Tl	- -	0.24	0.30	0.25	0.25
208Pb	Pb	11	9.51	11.87	9.89	9.87
209Bi	Bi	- -	0.21	0.27	0.22	0.22
232Th	Th	6.2	5.08	6.32	5.27	5.27
238U	U	1.69	1.45	1.81	1.51	1.51

BHVO-2 (Average)

Isotope	Element	Pub. Conc.	Si Internal	Ca Internal	Fe Internal	Scaled
7Li	Li	5	4.17	4.59	4.00	4.16
9Be	Be	- -	1.18	1.29	1.18	1.14
11B	B	- -	13.99	15.42	13.43	13.97
23Na	Na	16400	12116.84	13410.35	11613.77	12114.02
25Mg	Mg	43600	49222.25	54396.32	47167.89	49202.59
27Al	Al	71600	75800.34	83667.16	72698.20	75752.09
29Si	Si	233000	233000.00	257703.76	223461.72	233081.18
31P	P	1200	850.26	942.99	815.34	851.72
39K	K	4300	4500.13	4981.69	4318.17	4505.41
44Ca	Ca	81700	74035.76	81700.00	71040.74	74021.08
45Sc	Sc	32	27.81	30.69	26.69	27.80
47Ti	Ti	16300	14484.70	16000.66	13889.66	14479.58
51V	V	317	267.29	295.76	256.14	268.72
52Cr	Cr	280	249.22	275.74	238.90	254.16
55Mn	Mn	1290	1368.82	1513.88	1311.01	1368.83
57Fe	Fe	86300	90143.64	99752.92	86300.00	90145.64
59Co	Co	45	41.21	45.57	39.50	41.22
60Ni	Ni	119	108.08	119.63	103.63	108.14
65Cu	Cu	127	105.73	117.01	101.55	105.86
66Zn	Zn	103	95.87	105.98	92.15	96.84
69Ga	Ga	21.7	19.86	21.95	19.07	19.87
72Ge	Ge	- -	2.16	2.38	2.07	2.16
75As	As	- -	1.14	1.26	1.09	1.14
82Se	Se	- -	-0.82	-0.91	-0.77	0.00
85Rb	Rb	9.8	7.70	8.51	7.38	7.70
88Sr	Sr	389	346.78	382.61	332.30	346.38
89Y	Y	26	19.38	21.35	18.58	19.35
90Zr	Zr	172	136.62	150.65	131.05	136.49
93Nb	Nb	18	14.34	15.82	13.75	14.33
95Mo	Mo	- -	3.21	3.55	3.08	3.21
103Rh	Rh	- -	- -	- -	- -	- -
105Pd	Pd	- -	- -	- -	- -	- -
107Ag	Ag	- -	0.36	0.35	0.35	0.36
111Cd	Cd	- -	0.17	0.19	0.17	0.17
115In	In	- -	0.07	0.08	0.07	0.07
118Sn	Sn	1.9	1.76	1.93	1.69	1.75
121Sb	Sb	- -	0.10	0.10	0.09	0.10
133Cs	Cs	- -	0.09	0.09	0.08	0.09
137Ba	Ba	130	117.97	130.10	113.03	117.82
139La	La	15.5	13.59	14.96	13.03	13.57
140Ce	Ce	37.4	32.60	35.95	31.23	32.56
141Pr	Pr	5	4.34	4.77	4.16	4.33
146Nd	Nd	25	21.33	23.50	20.44	21.30
147Sm	Sm	6.1	5.24	5.76	5.02	5.23
153Eu	Eu	2.1	1.78	1.95	1.71	1.77
157Gd	Gd	6.5	4.69	5.16	4.50	4.68
159Tb	Tb	0.96	0.73	0.80	0.70	0.73
163Dy	Dy	5.2	4.05	4.45	3.88	4.04
165Ho	Ho	0.93	0.77	0.84	0.74	0.77

BHVO-2 (Average)

Isotope	Element	Pub. Conc.	Si Internal	Ca Internal	Fe Internal	Scaled
166Er	Er	2.5	1.76	1.92	1.69	1.75
169Tm	Tm	0.36	0.24	0.26	0.23	0.24
172Yb	Yb	2	1.64	1.65	1.57	1.50
175Lu	Lu	0.28	0.21	0.23	0.20	0.21
178Hf	Hf	4.1	3.41	3.74	3.27	3.40
181Ta	Ta	1.4	0.79	0.86	0.76	0.79
182W	W	- -	0.21	0.22	0.20	0.20
185Re	Re	- -	- -	- -	- -	- -
195Pt	Pt	- -	0.09	0.10	0.09	0.09
197Au	Au	- -	0.27	0.30	0.26	0.27
205Tl	Tl	- -	0.02	0.03	0.02	0.02
208Pb	Pb	- -	1.37	1.50	1.32	1.37
209Bi	Bi	- -	0.02	0.02	0.02	0.02
232Th	Th	1.2	0.95	1.04	0.92	0.95
238U	U	- -	0.33	0.35	0.31	0.32

BIR-1 (Average)

Isotope	Element	Pub. Conc.	Si Internal	Ca Internal	Fe Internal	Scaled
7Li	Li	3.6	2.52	3.48	2.67	2.68
9Be	Be	0.58	- -	0.77	- -	- -
11B	B	0.53	12.60	17.15	13.27	13.34
23Na	Na	13500	9678.80	13368.44	10264.07	10295.36
25Mg	Mg	58000	57531.39	79173.44	60869.80	61115.78
27Al	Al	82000	77552.89	106415.38	81967.45	82326.64
29Si	Si	224200	224200.00	309635.11	237734.84	238554.51
31P	P	92	79.74	110.44	84.73	84.96
39K	K	250	150.70	210.75	162.75	162.59
44Ca	Ca	95100	69638.18	95100.00	73483.99	73847.06
45Sc	Sc	44	32.14	43.97	33.92	34.09
47Ti	Ti	5800	4436.54	6086.26	4689.08	4709.95
51V	V	310	240.87	331.28	254.74	256.34
52Cr	Cr	370	302.36	416.74	320.03	327.77
55Mn	Mn	1360	1255.78	1727.02	1327.87	1334.10
57Fe	Fe	79000	74742.20	102729.40	79000.00	79389.47
59Co	Co	52	47.57	65.50	50.37	50.57
60Ni	Ni	170	154.18	212.08	163.09	163.87
65Cu	Cu	125	99.77	137.20	105.62	106.07
66Zn	Zn	70	91.61	125.89	96.95	97.96
69Ga	Ga	16	15.44	21.26	16.36	16.43
72Ge	Ge	- -	2.41	3.34	2.56	2.57
75As	As	0.44	1.07	1.47	1.14	1.14
82Se	Se	- -	-0.69	-0.82	-0.67	0.00
85Rb	Rb	- -	0.22	0.27	0.23	0.23
88Sr	Sr	110	85.20	116.83	90.01	90.43
89Y	Y	16	10.28	14.10	10.86	10.91
90Zr	Zr	18	10.82	14.85	11.43	11.49
93Nb	Nb	0.6	0.38	0.53	0.40	0.41
95Mo	Mo	- -	0.24	0.27	0.26	0.26
103Rh	Rh	- -	0.04	0.03	0.03	0.04
105Pd	Pd	- -	0.17	0.25	0.19	0.19
107Ag	Ag	- -	0.37	0.51	0.39	0.39
111Cd	Cd	- -	0.26	0.33	0.26	0.26
115In	In	- -	0.06	0.07	0.06	0.06
118Sn	Sn	- -	1.19	1.63	1.26	1.26
121Sb	Sb	0.58	0.48	0.66	0.51	0.51
133Cs	Cs	- -	0.07	0.10	0.08	0.08
137Ba	Ba	7	5.60	7.75	5.94	5.96
139La	La	0.71	0.49	0.67	0.52	0.52
140Ce	Ce	2.1	1.50	2.06	1.59	1.60
141Pr	Pr	0.42	0.28	0.38	0.30	0.30
146Nd	Nd	2.5	1.91	2.62	2.02	2.03
147Sm	Sm	1.1	0.85	1.17	0.90	0.91
153Eu	Eu	0.58	0.43	0.60	0.46	0.46
157Gd	Gd	2	1.30	1.79	1.38	1.38
159Tb	Tb	0.43	0.24	0.32	0.25	0.25
163Dy	Dy	2.7	1.80	2.46	1.90	1.91
165Ho	Ho	0.59	0.37	0.51	0.39	0.40

BIR-1 (Average)

Isotope	Element	Pub. Conc.	Si Internal	Ca Internal	Fe Internal	Scaled
166Er	Er	1.7	1.15	1.57	1.21	1.22
169Tm	Tm	0.33	0.18	0.22	0.18	0.19
172Yb	Yb	1.7	1.27	1.75	1.34	1.35
175Lu	Lu	0.26	0.17	0.23	0.18	0.18
178Hf	Hf	0.6	0.41	0.56	0.43	0.43
181Ta	Ta	--	0.04	0.06	0.05	0.05
182W	W	--	0.05	0.06	0.05	0.06
185Re	Re	--	0.05	0.07	0.05	0.06
195Pt	Pt	--	0.72	1.01	0.77	0.77
197Au	Au	--	0.09	0.11	0.09	0.09
205Tl	Tl	--	--	--	--	--
208Pb	Pb	3	4.19	5.78	4.44	4.46
209Bi	Bi	--	0.02	0.03	0.02	0.02
232Th	Th	--	0.04	0.05	0.04	0.04
238U	U	--	0.04	0.04	0.03	0.03

Si Internal Isotope	NIST 610 Pub. Conc.	Ap16A07	Ap16A08	Ap16B07	Ap16B08	Ap16C07
7Li	**484.6**	463.3	504.3	492.9	508.8	473.1
9Be	**465.5**	474.9	482.3	479.0	472.7	455.9
11B	**356.4**	362.2	369.0	360.0	361.4	347.2
23Na	**99053**	96241.3	98029.4	96819.4	96918.6	102004.7
25Mg	**465.3**	472.6	467.5	473.0	474.7	472.4
27Al	**10790**	10815.2	10663.7	11041.3	11072.8	10765.0
29Si	**327090**	327090.0	327090.0	327090.0	327090.0	327090.0
31P	**342.5**	340.3	345.6	337.2	344.0	345.8
33S	**25**	< DL	< DL	< DL	< DL	< DL
39K	**486**	538.6	502.5	495.1	490.1	483.8
43Ca	**81830**	88570.6	83557.1	89789.0	88264.4	82845.6
44Ca	**81830**	87639.9	82994.6	88561.3	87089.1	80181.4
45Sc	**441.1**	466.7	446.3	468.3	462.0	440.1
47Ti	**434**	455.5	444.1	450.5	447.1	425.9
51V	**441.7**	446.5	441.6	466.0	461.2	428.3
52Cr	**405.2**	411.9	401.5	418.1	419.6	404.6
53Cr	**405.2**	409.1	414.8	421.6	416.8	398.8
55Mn	**433.3**	434.5	432.9	455.5	460.2	433.0
57Fe	**457.1**	474.0	468.9	494.4	481.1	460.2
59Co	**405**	409.6	405.5	419.6	423.8	403.6
60Ni	**443.9**	449.2	447.4	454.8	461.7	444.3
62Ni	**443.9**	458.0	456.3	433.3	464.0	455.2
65Cu	**430.3**	444.2	429.1	437.5	451.9	431.1
66Zn	**456.3**	476.8	458.4	485.4	482.6	478.4
68Zn	**456.3**	481.8	467.0	486.5	473.9	474.7
69Ga	**438.1**	453.0	446.9	444.3	459.2	423.0
72Ge	**426.3**	438.1	441.5	446.3	441.5	429.8
75As	**317.4**	327.9	337.4	326.9	330.8	324.3
77Ar Cl	**0**	--	--	--	--	--
82Se	**109**	112.1	117.1	114.6	116.0	108.3
83Kr	**0**	--	--	--	--	--
85Rb	**431.1**	426.7	413.8	435.4	449.7	425.2
86Sr	**497.4**	497.2	510.0	506.6	514.0	483.6
88Sr	**497.4**	502.3	499.4	507.7	509.6	497.2
89Y	**449.9**	447.6	446.8	461.8	466.9	441.5
90Zr	**439.9**	435.0	434.2	453.1	454.3	431.1
93Nb	**419.4**	423.8	420.2	426.7	432.9	413.8
95Mo	**376.8**	381.7	386.0	379.1	381.9	373.3
103Rh	**1.31**	1.3	1.3	1.3	1.4	1.3
105Pd	**1.05**	1.1	1.1	0.9	1.1	1.1
107Ag	**239.4**	246.8	248.4	247.9	253.7	251.8
110Cd	**259.4**	267.9	273.8	279.7	274.0	288.1
111Cd	**259.4**	272.1	273.0	274.4	266.7	287.5
115In	**441.4**	453.4	448.2	443.0	459.0	446.0
118Sn	**396.3**	413.4	421.1	396.7	410.7	386.4
120Sn	**396.3**	410.7	422.4	397.6	412.2	388.6
121Sb	**368.5**	393.0	405.1	372.9	380.5	371.7
133Cs	**360.9**	350.6	364.9	371.0	385.5	358.1
136Ba	**424.1**	445.4	447.4	428.7	438.7	420.1

Si Internal Isotope	NIST 610 Pub. Conc.	Ap16A07	Ap16A08	Ap16B07	Ap16B08	Ap16C07
137Ba	**424.1**	441.6	443.1	430.5	439.8	423.9
139La	**457.4**	472.9	485.0	464.5	473.8	447.5
140Ce	**447.8**	466.1	471.6	455.3	470.1	440.2
141Pr	**429.8**	445.8	455.3	439.2	445.7	424.7
146Nd	**430.8**	440.7	450.0	439.2	447.9	424.5
147Sm	**450.5**	466.9	475.7	458.4	471.6	446.8
153Eu	**461.1**	469.9	488.3	465.5	476.7	456.0
155Gd	**419.9**	426.5	442.2	428.7	434.3	413.8
156Ce O	**0**	--	--	--	--	--
157Gd	**419.9**	422.7	441.1	427.7	432.4	412.1
159Tb	**442.8**	449.7	465.6	449.7	455.1	435.8
163Dy	**426.5**	429.3	446.7	429.9	435.3	419.1
165Ho	**449.4**	449.3	470.6	455.5	462.9	446.1
166Er	**426**	428.0	448.2	429.7	436.8	416.6
169Tm	**420.1**	421.2	442.7	425.4	428.2	411.2
172Yb	**461.5**	466.0	485.8	461.8	469.5	451.5
175Lu	**434.7**	437.8	458.4	436.2	443.0	424.2
178Hf	**417.7**	424.0	442.6	421.2	426.9	409.0
181Ta	**376.6**	385.0	403.4	376.3	382.5	368.3
182W	**445.3**	452.5	485.1	437.3	444.6	425.7
185Re	**103.7**	106.6	113.8	102.5	104.7	100.9
195Pt	**3.15**	3.4	3.4	2.9	3.2	3.3
197Au	**22.5**	23.1	24.7	22.7	23.0	22.9
205Tl	**61.2**	63.8	67.6	64.5	65.6	64.3
206Pb	**413.3**	426.7	458.2	413.5	416.0	424.9
207Pb	**413.3**	439.1	465.8	420.3	417.7	425.4
208Pb	**413.3**	434.8	452.5	409.8	419.3	424.4
209Bi	**357.7**	385.4	404.1	359.3	363.8	374.5
220Bkg	**0**	--	--	--	--	--
232Th	**450.6**	478.6	495.7	456.0	453.6	452.2
238U	**457.1**	477.6	497.3	444.4	457.0	448.8
254U O	**0**	--	--	--	--	--

Si Internal Isotope	NIST 610 Pub. Conc.	Ap16C08	Ap16D07	Ap16D08	Ap16E07	Ap16E08
7Li	484.6	486.5	508.3	489.2	492.6	492.0
9Be	465.5	449.8	477.3	464.3	474.1	474.4
11B	356.4	349.1	364.1	349.2	360.6	366.7
23Na	99053	100504.3	96480.4	99820.5	98842.4	100012.3
25Mg	465.3	459.2	470.4	464.3	467.2	456.7
27Al	10790	10829.5	10751.7	10769.7	10853.8	10747.9
29Si	327090	327090.0	327090.0	327090.0	327090.0	327090.0
31P	342.5	343.4	334.0	335.5	349.8	351.6
33S	25	< DL	< DL	< DL	< DL	< DL
39K	486	450.6	466.6	458.0	463.3	473.6
43Ca	81830	75370.1	77362.4	74478.9	80906.8	75985.4
44Ca	81830	74860.0	77441.3	76764.9	79951.4	76206.6
45Sc	441.1	417.8	427.1	420.2	438.0	432.6
47Ti	434	399.1	428.7	415.0	439.7	430.4
51V	441.7	407.9	429.9	418.1	424.2	428.3
52Cr	405.2	371.3	385.8	381.6	400.6	393.4
53Cr	405.2	373.6	385.6	379.2	401.7	407.5
55Mn	433.3	408.1	429.0	414.3	437.6	436.6
57Fe	457.1	420.1	429.4	426.7	478.7	476.7
59Co	405	373.5	393.9	387.3	413.8	408.8
60Ni	443.9	415.9	435.1	420.7	444.1	453.1
62Ni	443.9	426.7	454.4	405.7	439.4	448.3
65Cu	430.3	405.5	423.4	405.0	433.0	427.9
66Zn	456.3	442.9	458.6	429.7	433.1	442.0
68Zn	456.3	442.8	459.6	442.0	442.7	437.6
69Ga	438.1	408.2	437.4	427.5	438.7	438.8
72Ge	426.3	400.7	431.2	407.9	433.3	436.5
75As	317.4	302.9	315.4	304.3	319.0	319.3
77Ar Cl	0	--	--	--	--	--
82Se	109	101.1	107.5	101.3	107.9	113.6
83Kr	0	--	--	--	--	--
85Rb	431.1	393.9	419.6	413.2	416.2	417.9
86Sr	497.4	475.9	497.3	482.3	503.4	498.5
88Sr	497.4	468.2	498.0	483.1	506.3	507.1
89Y	449.9	426.2	448.2	435.5	452.1	449.9
90Zr	439.9	419.2	443.4	427.4	443.9	443.0
93Nb	419.4	398.8	422.8	404.6	422.7	425.2
95Mo	376.8	354.9	373.7	359.8	380.8	387.1
103Rh	1.31	1.3	1.3	1.2	1.3	1.4
105Pd	1.05	1.1	1.1	1.0	1.2	1.2
107Ag	239.4	240.0	237.9	225.7	232.9	237.5
110Cd	259.4	261.8	269.5	248.5	250.9	255.1
111Cd	259.4	262.8	267.6	248.8	248.4	255.0
115In	441.4	419.4	439.3	438.1	411.0	430.4
118Sn	396.3	378.5	392.0	375.4	397.2	402.7
120Sn	396.3	385.9	396.2	373.0	387.5	395.2
121Sb	368.5	364.8	370.2	347.3	375.2	380.0
133Cs	360.9	349.6	375.7	348.4	338.1	343.5
136Ba	424.1	417.1	427.9	419.2	429.0	429.9

Si Internal Isotope	NIST 610 Pub. Conc.	Ap16C08	Ap16D07	Ap16D08	Ap16E07	Ap16E08
137Ba	**424.1**	417.9	436.5	416.3	431.4	431.1
139La	**457.4**	450.5	479.8	449.6	465.5	460.5
140Ce	**447.8**	431.4	459.6	434.7	448.3	452.7
141Pr	**429.8**	419.3	451.9	422.1	437.7	433.4
146Nd	**430.8**	424.4	455.1	418.9	438.7	437.6
147Sm	**450.5**	439.3	467.4	437.8	460.6	459.9
153Eu	**461.1**	448.1	477.9	447.3	465.8	464.5
155Gd	**419.9**	414.4	439.1	407.5	424.1	429.7
156Ce O	**0**	--	--	--	--	--
157Gd	**419.9**	412.5	437.0	406.5	426.7	426.4
159Tb	**442.8**	433.2	459.4	427.5	448.1	447.3
163Dy	**426.5**	418.0	444.0	413.2	434.8	435.4
165Ho	**449.4**	437.2	466.3	435.7	457.3	455.7
166Er	**426**	411.7	444.2	414.8	432.2	434.8
169Tm	**420.1**	408.8	432.9	411.8	426.6	425.2
172Yb	**461.5**	445.5	475.4	449.2	463.8	469.5
175Lu	**434.7**	426.2	453.4	425.2	441.0	438.8
178Hf	**417.7**	410.7	437.6	412.1	420.3	426.1
181Ta	**376.6**	372.6	394.9	373.9	381.2	386.1
182W	**445.3**	427.1	449.8	431.4	452.7	464.1
185Re	**103.7**	100.6	104.6	100.8	105.8	109.2
195Pt	**3.15**	3.2	3.3	3.2	3.1	3.5
197Au	**22.5**	22.4	23.0	21.5	23.1	23.8
205Tl	**61.2**	64.0	59.3	55.3	61.9	61.4
206Pb	**413.3**	425.9	412.2	398.3	413.8	419.2
207Pb	**413.3**	424.3	435.0	407.3	414.6	420.1
208Pb	**413.3**	410.9	413.5	391.3	416.1	411.0
209Bi	**357.7**	361.5	361.5	352.0	359.2	355.9
220Bkg	**0**	--	--	--	--	--
232Th	**450.6**	445.2	458.2	451.8	458.4	459.9
238U	**457.1**	431.4	437.6	454.6	446.5	457.1
254U O	**0**	--	--	--	--	--

Si Internal Isotope	NIST 610 Pub. Conc.	Count	Min	Max	Average	Sigma	SDOM
7Li	**484.6**	10.0	463.3	508.8	491.1	13.8	1.6
9Be	**465.5**	10.0	449.8	482.3	470.5	9.9	1.1
11B	**356.4**	10.0	347.2	369.0	359.0	7.3	0.9
23Na	**99053**	10.0	96241.3	102004.7	98567.3	1874.3	219.4
25Mg	**465.3**	10.0	456.7	474.7	467.8	5.8	0.7
27Al	**10790**	10.0	10663.7	11072.8	10831.1	123.6	14.7
29Si	**327090**	10.0	327090.0	327090.0	327090.0	0.0	0.0
31P	**342.5**	10.0	334.0	351.6	342.7	5.6	0.7
33S	**25**	0.0	0.0	0.0	--	0.0	0.0
39K	**486**	10.0	450.6	538.6	482.2	24.7	3.0
43Ca	**81830**	10.0	74478.9	89789.0	81713.0	5520.9	679.6
44Ca	**81830**	10.0	74860.0	88561.3	81169.1	4848.5	601.4
45Sc	**441.1**	10.0	417.8	468.3	441.9	17.6	2.2
47Ti	**434**	10.0	399.1	455.5	433.6	16.5	2.1
51V	**441.7**	10.0	407.9	466.0	435.2	17.5	2.2
52Cr	**405.2**	10.0	371.3	419.6	398.8	15.1	1.9
53Cr	**405.2**	10.0	373.6	421.6	400.9	15.6	2.0
55Mn	**433.3**	10.0	408.1	460.2	434.2	15.0	2.0
57Fe	**457.1**	10.0	420.1	494.4	461.0	24.8	3.3
59Co	**405**	10.0	373.5	423.8	403.9	14.5	1.9
60Ni	**443.9**	10.0	415.9	461.7	442.6	14.0	1.9
62Ni	**443.9**	10.0	405.7	464.0	444.1	17.0	2.3
65Cu	**430.3**	10.0	405.0	451.9	428.9	14.2	1.9
66Zn	**456.3**	10.0	429.7	485.4	458.8	20.0	2.8
68Zn	**456.3**	10.0	437.6	486.5	460.9	17.5	2.4
69Ga	**438.1**	10.0	408.2	459.2	437.7	14.2	2.0
72Ge	**426.3**	10.0	400.7	446.3	430.7	14.1	2.0
75As	**317.4**	10.0	302.9	337.4	320.8	10.5	1.5
77Ar Cl	**0**	0.0	--	--	--	--	--
82Se	**109**	10.0	101.1	117.1	109.9	5.4	0.8
83Kr	**0**	0.0	--	--	--	--	--
85Rb	**431.1**	10.0	393.9	449.7	421.2	14.0	2.0
86Sr	**497.4**	10.0	475.9	514.0	496.9	12.0	1.8
88Sr	**497.4**	10.0	468.2	509.6	497.9	12.3	1.8
89Y	**449.9**	10.0	426.2	466.9	447.6	11.2	1.7
90Zr	**439.9**	10.0	419.2	454.3	438.5	10.6	1.6
93Nb	**419.4**	10.0	398.8	432.9	419.2	9.9	1.5
95Mo	**376.8**	10.0	354.9	387.1	375.8	10.2	1.6
103Rh	**1.31**	10.0	1.2	1.4	1.3	0.0	0.0
105Pd	**1.05**	10.0	0.9	1.2	1.1	0.1	0.0
107Ag	**239.4**	10.0	225.7	253.7	242.3	8.5	1.4
110Cd	**259.4**	10.0	248.5	288.1	266.9	12.2	2.0
111Cd	**259.4**	10.0	248.4	287.5	265.6	11.6	1.9
115In	**441.4**	10.0	411.0	459.0	438.8	14.1	2.4
118Sn	**396.3**	10.0	375.4	421.1	397.4	14.2	2.4
120Sn	**396.3**	10.0	373.0	422.4	396.9	13.9	2.4
121Sb	**368.5**	10.0	347.3	405.1	376.1	14.8	2.6
133Cs	**360.9**	10.0	338.1	385.5	358.5	14.5	2.6
136Ba	**424.1**	10.0	417.1	447.4	430.3	10.0	1.8

Si Internal Isotope	NIST 610 Pub. Conc.	Count	Min	Max	Average	Sigma	SDOM
137Ba	**424.1**	10.0	416.3	443.1	431.2	9.0	1.7
139La	**457.4**	10.0	447.5	485.0	465.0	12.4	2.3
140Ce	**447.8**	10.0	431.4	471.6	453.0	13.6	2.6
141Pr	**429.8**	10.0	419.3	455.3	437.5	11.9	2.3
146Nd	**430.8**	10.0	418.9	455.1	437.7	11.3	2.3
147Sm	**450.5**	10.0	437.8	475.7	458.4	12.5	2.5
153Eu	**461.1**	10.0	447.3	488.3	466.0	12.4	2.6
155Gd	**419.9**	10.0	407.5	442.2	426.0	10.8	2.3
156Ce O	**0**	0.0	--	--	--	--	--
157Gd	**419.9**	10.0	406.5	441.1	424.5	10.7	2.3
159Tb	**442.8**	10.0	427.5	465.6	447.1	11.3	2.5
163Dy	**426.5**	10.0	413.2	446.7	430.6	10.5	2.4
165Ho	**449.4**	10.0	435.7	470.6	453.7	11.0	2.6
166Er	**426**	10.0	411.7	448.2	429.7	11.6	2.8
169Tm	**420.1**	10.0	408.8	442.7	423.4	10.0	2.5
172Yb	**461.5**	10.0	445.5	485.8	463.8	11.8	3.0
175Lu	**434.7**	10.0	424.2	458.4	438.4	10.9	2.9
178Hf	**417.7**	10.0	409.0	442.6	423.0	10.5	2.9
181Ta	**376.6**	10.0	368.3	403.4	382.4	10.1	2.9
182W	**445.3**	10.0	425.7	485.1	447.0	17.3	5.2
185Re	**103.7**	10.0	100.6	113.8	105.0	4.0	1.3
195Pt	**3.15**	10.0	2.9	3.5	3.2	0.1	0.0
197Au	**22.5**	10.0	21.5	24.7	23.0	0.8	0.3
205Tl	**61.2**	10.0	55.3	67.6	62.8	3.3	1.3
206Pb	**413.3**	10.0	398.3	458.2	420.9	14.8	6.0
207Pb	**413.3**	10.0	407.3	465.8	427.0	15.7	7.0
208Pb	**413.3**	10.0	391.3	452.5	418.4	15.6	7.8
209Bi	**357.7**	10.0	352.0	404.1	367.7	15.2	8.8
220Bkg	**0**	0.0	--	--	--	--	--
232Th	**450.6**	10.0	445.2	495.7	461.0	14.2	10.1
238U	**457.1**	10.0	431.4	497.3	455.2	18.4	18.4
254U O	**0**	0.0	--	--	--	--	--

Ca Internal Isotope	NIST 610 Pub. Conc.	Ap16A07	Ap16A08	Ap16B07	Ap16B08	Ap16C07
7Li	484.6	432.6	497.2	455.5	478.0	482.9
9Be	465.5	443.4	475.5	442.6	444.2	465.3
11B	356.4	338.2	363.8	332.6	339.6	354.4
23Na	99053	89861.2	96653.8	89460.4	91065.9	104102.0
25Mg	465.3	441.2	461.0	437.0	446.0	482.1
27Al	10790	10098.2	10514.0	10202.1	10404.1	10986.3
29Si	327090	305406.3	322500.1	302228.6	307337.7	333815.4
31P	342.5	317.8	340.7	311.6	323.2	352.9
33S	25	< DL	< DL	< DL	< DL	< DL
39K	486	502.9	495.5	457.4	460.5	493.7
43Ca	81830	82699.0	82384.6	82964.3	82934.3	84549.0
44Ca	81830	81830.0	81830.0	81830.0	81830.0	81830.0
45Sc	441.1	435.7	440.0	432.7	434.1	449.1
47Ti	434	425.3	437.9	416.3	420.1	434.6
51V	441.7	416.9	435.4	430.6	433.4	437.1
52Cr	405.2	384.6	395.8	386.3	394.3	412.9
53Cr	405.2	382.0	409.0	389.6	391.6	407.0
55Mn	433.3	405.7	426.8	420.9	432.4	441.9
57Fe	457.1	442.6	462.3	456.9	452.0	469.7
59Co	405	382.4	399.8	387.7	398.2	411.9
60Ni	443.9	419.4	441.2	420.2	433.8	453.4
62Ni	443.9	427.6	449.9	400.3	436.0	464.5
65Cu	430.3	414.7	423.1	404.2	424.6	439.9
66Zn	456.3	445.2	452.0	448.5	453.4	488.2
68Zn	456.3	449.8	460.5	449.5	445.3	484.5
69Ga	438.1	423.0	440.6	410.5	431.5	431.7
72Ge	426.3	409.1	435.3	412.3	414.8	438.6
75As	317.4	306.2	332.7	302.0	310.8	331.0
77Ar Cl	0	--	--	--	--	--
82Se	109	104.6	115.5	105.8	109.0	110.5
83Kr	0	--	--	--	--	--
85Rb	431.1	398.4	408.0	402.3	422.6	433.9
86Sr	497.4	464.2	502.8	468.1	482.9	493.5
88Sr	497.4	469.0	492.4	469.1	478.8	507.4
89Y	449.9	417.9	440.5	426.7	438.7	450.6
90Zr	439.9	406.2	428.1	418.7	426.9	440.0
93Nb	419.4	395.7	414.3	394.3	406.8	422.3
95Mo	376.8	356.4	380.6	350.3	358.9	380.9
103Rh	1.31	1.2	1.3	1.2	1.3	1.4
105Pd	1.05	1.1	1.1	0.8	1.0	1.1
107Ag	239.4	230.4	244.9	229.1	238.4	257.0
110Cd	259.4	250.2	269.9	258.4	257.5	294.0
111Cd	259.4	254.1	269.2	253.6	250.6	293.4
115In	441.4	423.3	441.9	409.3	431.3	455.2
118Sn	396.3	386.0	415.2	366.6	385.9	394.3
120Sn	396.3	383.4	416.5	367.4	387.3	396.6
121Sb	368.5	367.0	399.4	344.6	357.5	379.4
133Cs	360.9	327.4	359.8	342.8	362.2	365.5
136Ba	424.1	415.8	441.2	396.1	412.2	428.7

Ca Internal Isotope	NIST 610 Pub. Conc.	Ap16A07	Ap16A08	Ap16B07	Ap16B08	Ap16C07
137Ba	**424.1**	412.3	436.9	397.8	413.2	432.7
139La	**457.4**	441.5	478.2	429.2	445.1	456.7
140Ce	**447.8**	435.2	465.0	420.7	441.7	449.2
141Pr	**429.8**	416.3	448.9	405.9	418.8	433.4
146Nd	**430.8**	411.4	443.7	405.8	420.9	433.2
147Sm	**450.5**	435.9	469.0	423.5	443.1	456.0
153Eu	**461.1**	438.7	481.4	430.1	447.9	465.4
155Gd	**419.9**	398.2	436.0	396.1	408.1	422.3
156Ce O	**0**	--	--	--	--	--
157Gd	**419.9**	394.7	434.9	395.2	406.3	420.6
159Tb	**442.8**	419.9	459.1	415.5	427.6	444.7
163Dy	**426.5**	400.8	440.4	397.2	409.0	427.7
165Ho	**449.4**	419.5	464.0	420.9	434.9	455.2
166Er	**426**	399.6	441.9	397.1	410.4	425.1
169Tm	**420.1**	393.3	436.5	393.1	402.4	419.7
172Yb	**461.5**	435.1	479.0	426.7	441.2	460.8
175Lu	**434.7**	408.7	452.0	403.0	416.3	432.9
178Hf	**417.7**	395.9	436.4	389.2	401.1	417.4
181Ta	**376.6**	359.5	397.8	347.7	359.4	375.8
182W	**445.3**	422.5	478.3	404.1	417.7	434.4
185Re	**103.7**	99.5	112.2	94.7	98.4	102.9
195Pt	**3.15**	3.2	3.3	2.7	3.0	3.3
197Au	**22.5**	21.6	24.3	21.0	21.6	23.3
205Tl	**61.2**	59.5	66.6	59.6	61.7	65.6
206Pb	**413.3**	398.5	451.8	382.0	390.9	433.6
207Pb	**413.3**	410.0	459.3	388.3	392.5	434.1
208Pb	**413.3**	406.0	446.2	378.6	394.0	433.2
209Bi	**357.7**	359.8	398.4	332.0	341.8	382.2
220Bkg	**0**	--	--	--	--	--
232Th	**450.6**	446.9	488.8	421.3	426.2	461.5
238U	**457.1**	445.9	490.4	410.6	429.4	458.1
254U O	**0**	--	--	--	--	--

Ca Internal Isotope	NIST 610 Pub. Conc.	Ap16C08	Ap16D07	Ap16D08	Ap16E07	Ap16E08
7Li	484.6	531.8	537.1	521.5	504.2	528.3
9Be	465.5	491.7	504.4	495.0	485.2	509.4
11B	356.4	381.6	384.7	372.2	369.1	393.8
23Na	99053	109862.0	101948.0	106406.9	101164.9	107392.3
25Mg	465.3	501.9	497.0	494.9	478.2	490.4
27Al	10790	11837.8	11361.0	11480.3	11108.9	11541.0
29Si	327090	357544.5	345626.5	348672.2	334775.5	351226.3
31P	342.5	375.4	352.9	357.7	358.0	377.5
33S	25	< DL	< DL	< DL	< DL	< DL
39K	486	492.5	493.1	488.3	474.2	508.5
43Ca	81830	82387.7	81746.6	79393.2	82807.9	81592.4
44Ca	81830	81830.0	81830.0	81830.0	81830.0	81830.0
45Sc	441.1	456.7	451.3	448.0	448.3	464.6
47Ti	434	436.2	453.0	442.3	450.1	462.2
51V	441.7	445.9	454.3	445.7	434.1	459.9
52Cr	405.2	405.8	407.6	406.8	410.0	422.4
53Cr	405.2	408.4	407.4	404.2	411.1	437.6
55Mn	433.3	446.1	453.3	441.6	447.9	468.8
57Fe	457.1	459.2	453.7	454.9	489.9	511.8
59Co	405	408.3	416.3	412.9	423.5	439.0
60Ni	443.9	454.6	459.8	448.4	454.6	486.6
62Ni	443.9	466.4	480.2	432.5	449.7	481.3
65Cu	430.3	443.3	447.4	431.7	443.2	459.5
66Zn	456.3	484.1	484.6	458.1	443.3	474.6
68Zn	456.3	484.0	485.7	471.1	453.1	469.8
69Ga	438.1	446.2	462.2	455.7	449.0	471.2
72Ge	426.3	438.0	455.6	434.8	443.5	468.7
75As	317.4	331.1	333.2	324.3	326.5	342.9
77Ar Cl	0	- -	- -	- -	- -	- -
82Se	109	110.5	113.6	108.0	110.4	122.0
83Kr	0	- -	- -	- -	- -	- -
85Rb	431.1	430.6	443.4	440.5	426.0	448.8
86Sr	497.4	520.3	525.5	514.1	515.3	535.3
88Sr	497.4	511.8	526.2	514.9	518.2	544.5
89Y	449.9	465.8	473.6	464.3	462.7	483.1
90Zr	439.9	458.3	468.5	455.6	454.4	475.7
93Nb	419.4	436.0	446.7	431.3	432.6	456.6
95Mo	376.8	387.9	394.8	383.5	389.7	415.7
103Rh	1.31	1.4	1.4	1.3	1.4	1.5
105Pd	1.05	1.2	1.2	1.1	1.2	1.3
107Ag	239.4	262.3	251.4	240.6	238.3	255.0
110Cd	259.4	286.1	284.8	264.8	256.8	273.9
111Cd	259.4	287.2	282.8	265.3	254.3	273.8
115In	441.4	458.4	464.2	467.0	420.7	462.1
118Sn	396.3	413.7	414.2	400.2	406.5	432.4
120Sn	396.3	421.9	418.6	397.7	396.6	424.4
121Sb	368.5	398.8	391.2	370.2	384.0	408.1
133Cs	360.9	382.1	396.9	371.3	346.1	368.8
136Ba	424.1	455.9	452.1	446.8	439.1	461.7

Ca Internal Isotope	NIST 610 Pub. Conc.	Ap16C08	Ap16D07	Ap16D08	Ap16E07	Ap16E08
137Ba	**424.1**	456.9	461.2	443.8	441.5	462.9
139La	**457.4**	492.5	506.9	479.3	476.5	494.5
140Ce	**447.8**	471.5	485.6	463.4	458.8	486.1
141Pr	**429.8**	458.3	477.5	449.9	448.0	465.4
146Nd	**430.8**	464.0	480.9	446.6	449.0	469.9
147Sm	**450.5**	480.2	493.9	466.7	471.5	493.8
153Eu	**461.1**	489.8	505.0	476.9	476.7	498.7
155Gd	**419.9**	453.0	464.0	434.3	434.1	461.5
156Ce O	**0**	--	--	--	--	--
157Gd	**419.9**	450.9	461.7	433.3	436.7	457.9
159Tb	**442.8**	473.5	485.5	455.7	458.6	480.3
163Dy	**426.5**	456.9	469.2	440.5	445.0	467.6
165Ho	**449.4**	478.0	492.7	464.5	468.1	489.3
166Er	**426**	450.0	469.4	442.2	442.3	466.8
169Tm	**420.1**	446.8	457.4	438.9	436.6	456.5
172Yb	**461.5**	487.0	502.3	478.9	474.7	504.1
175Lu	**434.7**	465.9	479.1	453.2	451.3	471.2
178Hf	**417.7**	449.0	462.4	439.2	430.1	457.5
181Ta	**376.6**	407.3	417.3	398.5	390.2	414.6
182W	**445.3**	466.8	475.3	459.9	463.3	498.4
185Re	**103.7**	110.0	110.6	107.4	108.3	117.3
195Pt	**3.15**	3.5	3.5	3.5	3.2	3.7
197Au	**22.5**	24.5	24.3	22.9	23.7	25.6
205Tl	**61.2**	69.9	62.7	58.9	63.4	65.9
206Pb	**413.3**	465.5	435.6	424.5	423.5	450.2
207Pb	**413.3**	463.8	459.6	434.2	424.3	451.1
208Pb	**413.3**	449.1	436.9	417.1	425.9	441.3
209Bi	**357.7**	395.2	382.0	375.3	367.7	382.1
220Bkg	**0**	--	--	--	--	--
232Th	**450.6**	486.6	484.2	481.6	469.1	493.8
238U	**457.1**	471.6	462.4	484.6	457.0	490.8
254U O	**0**	--	--	--	--	--

Ca Internal Isotope	NIST 610 Pub. Conc.	Count	Min	Max	Average	Sigma	SDOM
7Li	**484.6**	10.0	432.6	537.1	496.9	33.0	3.8
9Be	**465.5**	10.0	442.6	509.4	475.7	24.3	2.8
11B	**356.4**	10.0	332.6	393.8	363.0	20.1	2.3
23Na	**99053**	10.0	89460.4	109862.0	99791.7	7206.9	843.5
25Mg	**465.3**	10.0	437.0	501.9	473.0	23.4	2.8
27Al	**10790**	10.0	10098.2	11837.8	10953.4	582.0	69.1
29Si	**327090**	10.0	302228.6	357544.5	330913.3	19434.6	2322.9
31P	**342.5**	10.0	311.6	377.5	346.8	21.8	2.6
33S	**25**	0.0	0.0	0.0	--	0.0	0.0
39K	**486**	10.0	457.4	508.5	486.7	16.2	2.0
43Ca	**81830**	10.0	79393.2	84549.0	82345.9	1247.8	153.6
44Ca	**81830**	10.0	81830.0	81830.0	81830.0	0.0	0.0
45Sc	**441.1**	10.0	432.7	464.6	446.0	9.8	1.2
47Ti	**434**	10.0	416.3	462.2	437.8	13.9	1.8
51V	**441.7**	10.0	416.9	459.9	439.3	11.8	1.5
52Cr	**405.2**	10.0	384.6	422.4	402.7	11.5	1.5
53Cr	**405.2**	10.0	382.0	437.6	404.8	14.4	1.9
55Mn	**433.3**	10.0	405.7	468.8	438.5	16.9	2.2
57Fe	**457.1**	10.0	442.6	511.8	465.3	19.6	2.6
59Co	**405**	10.0	382.4	439.0	408.0	15.9	2.1
60Ni	**443.9**	10.0	419.4	486.6	447.2	18.9	2.5
62Ni	**443.9**	10.0	400.3	481.3	448.8	24.1	3.3
65Cu	**430.3**	10.0	404.2	459.5	433.2	15.8	2.2
66Zn	**456.3**	10.0	443.3	488.2	463.2	16.9	2.3
68Zn	**456.3**	10.0	445.3	485.7	465.3	15.0	2.1
69Ga	**438.1**	10.0	410.5	471.2	442.2	17.6	2.5
72Ge	**426.3**	10.0	409.1	468.7	435.1	18.0	2.5
75As	**317.4**	10.0	302.0	342.9	324.1	12.6	1.8
77Ar Cl	**0**	0.0	--	--	--	--	--
82Se	**109**	10.0	104.6	122.0	111.0	4.8	0.7
83Kr	**0**	0.0	--	--	--	--	--
85Rb	**431.1**	10.0	398.4	448.8	425.4	16.6	2.4
86Sr	**497.4**	10.0	464.2	535.3	502.2	23.1	3.4
88Sr	**497.4**	10.0	469.0	544.5	503.2	23.9	3.6
89Y	**449.9**	10.0	417.9	483.1	452.4	20.0	3.0
90Zr	**439.9**	10.0	406.2	475.7	443.2	21.6	3.3
93Nb	**419.4**	10.0	394.3	456.6	423.7	19.8	3.1
95Mo	**376.8**	10.0	350.3	415.7	379.9	18.8	2.9
103Rh	**1.31**	10.0	1.2	1.5	1.3	0.1	0.0
105Pd	**1.05**	10.0	0.8	1.3	1.1	0.1	0.0
107Ag	**239.4**	10.0	229.1	262.3	244.7	10.8	1.7
110Cd	**259.4**	10.0	250.2	294.0	269.7	14.0	2.3
111Cd	**259.4**	10.0	250.6	293.4	268.4	14.7	2.5
115In	**441.4**	10.0	409.3	467.0	443.4	19.8	3.4
118Sn	**396.3**	10.0	366.6	432.4	401.5	18.0	3.1
120Sn	**396.3**	10.0	367.4	424.4	401.0	17.9	3.1
121Sb	**368.5**	10.0	344.6	408.1	380.0	19.2	3.4
133Cs	**360.9**	10.0	327.4	396.9	362.3	19.0	3.4
136Ba	**424.1**	10.0	396.1	461.7	435.0	20.2	3.7

Ca Internal Isotope	NIST 610 Pub. Conc.	Count	Min	Max	Average	Sigma	SDOM
137Ba	**424.1**	10.0	397.8	462.9	435.9	21.1	3.9
139La	**457.4**	10.0	429.2	506.9	470.0	24.4	4.6
140Ce	**447.8**	10.0	420.7	486.1	457.7	20.2	3.9
141Pr	**429.8**	10.0	405.9	477.5	442.2	21.9	4.3
146Nd	**430.8**	10.0	405.8	480.9	442.5	23.7	4.7
147Sm	**450.5**	10.0	423.5	493.9	463.4	22.5	4.6
153Eu	**461.1**	10.0	430.1	505.0	471.1	24.0	5.0
155Gd	**419.9**	10.0	396.1	464.0	430.8	23.3	5.0
156Ce O	**0**	0.0	--	--	--	--	--
157Gd	**419.9**	10.0	394.7	461.7	429.2	23.2	5.1
159Tb	**442.8**	10.0	415.5	485.5	452.0	23.5	5.2
163Dy	**426.5**	10.0	397.2	469.2	435.4	24.9	5.7
165Ho	**449.4**	10.0	419.5	492.7	458.7	24.8	5.8
166Er	**426**	10.0	397.1	469.4	434.5	24.4	5.9
169Tm	**420.1**	10.0	393.1	457.4	428.1	23.4	5.8
172Yb	**461.5**	10.0	426.7	504.1	469.0	25.8	6.7
175Lu	**434.7**	10.0	403.0	479.1	443.4	25.4	6.8
178Hf	**417.7**	10.0	389.2	462.4	427.8	24.6	6.8
181Ta	**376.6**	10.0	347.7	417.3	386.8	23.5	6.8
182W	**445.3**	10.0	404.1	498.4	452.1	29.1	8.8
185Re	**103.7**	10.0	94.7	117.3	106.2	6.7	2.1
195Pt	**3.15**	10.0	2.7	3.7	3.3	0.3	0.1
197Au	**22.5**	10.0	21.0	25.6	23.3	1.4	0.5
205Tl	**61.2**	10.0	58.9	69.9	63.4	3.4	1.3
206Pb	**413.3**	10.0	382.0	465.5	425.6	26.3	10.7
207Pb	**413.3**	10.0	388.3	463.8	431.7	26.3	11.8
208Pb	**413.3**	10.0	378.6	449.1	422.8	22.3	11.2
209Bi	**357.7**	10.0	332.0	398.4	371.6	20.6	11.9
220Bkg	**0**	0.0	--	--	--	--	--
232Th	**450.6**	10.0	421.3	493.8	466.0	25.0	17.7
238U	**457.1**	10.0	410.6	490.8	460.1	24.9	24.9
254U O	**0**	0.0	--	--	--	--	--

Fe Internal Isotope	NIST 610 Pub. Conc.	Ap16A07	Ap16A08	Ap16B07	Ap16B08	Ap16C07
7Li	484.6	446.8	491.6	455.7	483.4	469.9
9Be	465.5	457.9	470.1	442.8	449.1	452.8
11B	356.4	349.3	359.7	332.8	343.4	344.9
23Na	99053	92810.2	95564.0	89507.8	92083.4	101314.5
25Mg	465.3	455.7	455.8	437.3	451.0	469.2
27Al	10790	10429.6	10395.5	10207.5	10520.4	10692.1
29Si	327090	315428.9	318863.8	302388.7	310771.6	324876.9
31P	342.5	328.2	336.9	311.7	326.8	343.5
33S	25	< DL	< DL	< DL	< DL	< DL
39K	486	519.4	489.9	457.7	465.6	480.5
43Ca	81830	85412.9	81455.7	83008.3	83860.9	82285.0
44Ca	81830	84515.4	80907.3	81873.3	82744.3	79638.9
45Sc	441.1	450.0	435.0	432.9	439.0	437.1
47Ti	434	439.2	432.9	416.5	424.8	423.0
51V	441.7	430.6	430.5	430.8	438.2	425.4
52Cr	405.2	397.2	391.4	386.5	398.7	401.8
53Cr	405.2	394.6	404.4	389.8	396.0	396.1
55Mn	433.3	419.0	422.0	421.1	437.2	430.1
57Fe	457.1	457.1	457.1	457.1	457.1	457.1
59Co	405	395.0	395.3	387.9	402.6	400.8
60Ni	443.9	433.1	436.2	420.4	438.7	441.3
62Ni	443.9	441.7	444.8	400.6	440.8	452.1
65Cu	430.3	428.3	418.3	404.4	429.4	428.2
66Zn	456.3	459.8	446.9	448.7	458.5	475.2
68Zn	456.3	464.6	455.3	449.8	450.2	471.5
69Ga	438.1	436.9	435.6	410.7	436.3	420.1
72Ge	426.3	422.5	430.4	412.6	419.4	426.9
75As	317.4	316.2	328.9	302.2	314.3	322.1
77Ar Cl	0	--	--	--	--	--
82Se	109	108.1	114.2	105.9	110.2	107.5
83Kr	0	--	--	--	--	--
85Rb	431.1	411.4	403.4	402.6	427.3	422.3
86Sr	497.4	479.5	497.1	468.3	488.3	480.3
88Sr	497.4	484.4	486.8	469.4	484.2	493.8
89Y	449.9	431.6	435.6	427.0	443.6	438.5
90Zr	439.9	419.5	423.2	418.9	431.7	428.2
93Nb	419.4	408.7	409.7	394.5	411.3	411.0
95Mo	376.8	368.1	376.3	350.5	362.9	370.7
103Rh	1.31	1.2	1.3	1.2	1.3	1.3
105Pd	1.05	1.1	1.1	0.8	1.0	1.0
107Ag	239.4	238.0	242.1	229.2	241.0	250.1
110Cd	259.4	258.4	266.9	258.5	260.4	286.1
111Cd	259.4	262.4	266.2	253.7	253.4	285.5
115In	441.4	437.2	437.0	409.5	436.1	443.0
118Sn	396.3	398.7	410.5	366.8	390.2	383.7
120Sn	396.3	396.0	411.8	367.5	391.7	386.0
121Sb	368.5	379.0	394.9	344.8	361.5	369.2
133Cs	360.9	338.1	355.8	343.0	366.2	355.7
136Ba	424.1	429.5	436.2	396.3	416.8	417.2

Fe Internal Isotope	NIST 610 Pub. Conc.	Ap16A07	Ap16A08	Ap16B07	Ap16B08	Ap16C07
137Ba	**424.1**	425.9	431.9	398.0	417.8	421.1
139La	**457.4**	456.0	472.8	429.4	450.1	444.5
140Ce	**447.8**	449.5	459.8	420.9	446.7	437.2
141Pr	**429.8**	429.9	443.9	406.1	423.4	421.8
146Nd	**430.8**	425.0	438.7	406.0	425.6	421.6
147Sm	**450.5**	450.2	463.7	423.7	448.0	443.8
153Eu	**461.1**	453.1	476.0	430.3	452.9	452.9
155Gd	**419.9**	411.3	431.1	396.3	412.6	411.0
156Ce O	**0**	--	--	--	--	--
157Gd	**419.9**	407.6	430.0	395.4	410.9	409.3
159Tb	**442.8**	433.6	453.9	415.7	432.4	432.8
163Dy	**426.5**	414.0	435.4	397.5	413.6	416.3
165Ho	**449.4**	433.3	458.7	421.1	439.8	443.1
166Er	**426**	412.7	436.9	397.3	415.0	413.8
169Tm	**420.1**	406.2	431.6	393.3	406.9	408.4
172Yb	**461.5**	449.4	473.6	427.0	446.1	448.4
175Lu	**434.7**	422.2	446.9	403.2	420.9	421.3
178Hf	**417.7**	408.9	431.5	389.4	405.6	406.2
181Ta	**376.6**	371.3	393.3	347.8	363.4	365.8
182W	**445.3**	436.4	472.9	404.3	422.4	422.8
185Re	**103.7**	102.8	111.0	94.8	99.5	100.2
195Pt	**3.15**	3.3	3.3	2.7	3.0	3.2
197Au	**22.5**	22.3	24.0	21.0	21.8	22.7
205Tl	**61.2**	61.5	65.9	59.6	62.3	63.9
206Pb	**413.3**	411.5	446.7	382.2	395.2	422.0
207Pb	**413.3**	423.5	454.1	388.5	396.8	422.5
208Pb	**413.3**	419.3	441.1	378.8	398.4	421.6
209Bi	**357.7**	371.6	393.9	332.1	345.6	371.9
220Bkg	**0**	--	--	--	--	--
232Th	**450.6**	461.5	483.3	421.5	431.0	449.2
238U	**457.1**	460.6	484.8	410.9	434.2	445.8
254U O	**0**	--	--	--	--	--

Fe Internal Isotope	NIST 610 Pub. Conc.	Ap16C08	Ap16D07	Ap16D08	Ap16E07	Ap16E08
7Li	**484.6**	529.3	541.1	524.1	470.4	471.8
9Be	**465.5**	489.4	508.2	497.4	452.7	454.9
11B	**356.4**	379.9	387.6	374.0	344.4	351.7
23Na	**99053**	109353.0	102715.9	106930.6	94382.0	95907.0
25Mg	**465.3**	499.6	500.8	497.4	446.1	437.9
27Al	**10790**	11782.9	11446.6	11536.9	10364.0	10306.7
29Si	**327090**	355887.9	348229.9	350388.3	312329.6	313663.5
31P	**342.5**	373.7	355.6	359.4	334.0	337.1
33S	**25**	< DL	< DL	< DL	< DL	< DL
39K	**486**	490.2	496.8	490.7	442.4	454.1
43Ca	**81830**	82005.9	82362.4	79783.9	77255.8	72866.3
44Ca	**81830**	81450.9	82446.4	82232.7	76343.5	73078.5
45Sc	**441.1**	454.6	454.7	450.2	418.3	414.9
47Ti	**434**	434.2	456.4	444.5	419.9	412.7
51V	**441.7**	443.9	457.7	447.9	405.0	410.7
52Cr	**405.2**	404.0	410.7	408.8	382.6	377.2
53Cr	**405.2**	406.5	410.5	406.2	383.6	390.8
55Mn	**433.3**	444.0	456.7	443.8	417.8	418.7
57Fe	**457.1**	457.1	457.1	457.1	457.1	457.1
59Co	**405**	406.4	419.4	414.9	395.1	392.0
60Ni	**443.9**	452.5	463.2	450.6	424.1	434.5
62Ni	**443.9**	464.2	483.8	434.6	419.6	429.9
65Cu	**430.3**	441.2	450.8	433.9	413.5	410.4
66Zn	**456.3**	481.9	488.3	460.3	413.6	423.9
68Zn	**456.3**	481.8	489.3	473.4	422.7	419.6
69Ga	**438.1**	444.2	465.7	457.9	418.9	420.8
72Ge	**426.3**	436.0	459.1	437.0	413.7	418.6
75As	**317.4**	329.6	335.7	325.9	304.6	306.2
77Ar Cl	**0**	--	--	--	--	--
82Se	**109**	110.0	114.5	108.5	103.0	109.0
83Kr	**0**	--	--	--	--	--
85Rb	**431.1**	428.6	446.7	442.7	397.4	400.8
86Sr	**497.4**	517.8	529.4	516.6	480.7	478.0
88Sr	**497.4**	509.4	530.2	517.5	483.4	486.3
89Y	**449.9**	463.7	477.1	466.6	431.7	431.5
90Zr	**439.9**	456.2	472.0	457.9	423.9	424.8
93Nb	**419.4**	433.9	450.1	433.4	403.6	407.7
95Mo	**376.8**	386.1	397.8	385.4	363.6	371.2
103Rh	**1.31**	1.4	1.4	1.3	1.3	1.3
105Pd	**1.05**	1.1	1.2	1.1	1.1	1.2
107Ag	**239.4**	261.1	253.3	241.8	222.4	227.8
110Cd	**259.4**	284.8	287.0	266.2	239.6	244.6
111Cd	**259.4**	285.9	284.9	266.6	237.2	244.5
115In	**441.4**	456.3	467.7	469.3	392.5	412.7
118Sn	**396.3**	411.8	417.4	402.2	379.3	386.2
120Sn	**396.3**	419.9	421.8	399.6	370.0	379.0
121Sb	**368.5**	396.9	394.1	372.0	358.3	364.4
133Cs	**360.9**	380.4	399.9	373.2	322.9	329.4
136Ba	**424.1**	453.8	455.5	449.0	409.6	412.3

Fe Internal Isotope	NIST 610 Pub. Conc.	Ap16C08	Ap16D07	Ap16D08	Ap16E07	Ap16E08
137Ba	424.1	454.7	464.7	446.0	411.9	413.4
139La	457.4	490.2	510.8	481.6	444.5	441.6
140Ce	447.8	469.3	489.3	465.6	428.0	434.1
141Pr	429.8	456.2	481.1	452.1	417.9	415.7
146Nd	430.8	461.8	484.6	448.8	418.9	419.7
147Sm	450.5	478.0	497.6	469.0	439.9	441.0
153Eu	461.1	487.5	508.8	479.2	444.7	445.4
155Gd	419.9	450.9	467.5	436.5	405.0	412.1
156Ce O	0	--	--	--	--	--
157Gd	419.9	448.8	465.2	435.5	407.5	408.9
159Tb	442.8	471.3	489.1	457.9	427.9	428.9
163Dy	426.5	454.8	472.7	442.6	415.2	417.6
165Ho	449.4	475.7	496.4	466.8	436.7	437.0
166Er	426	447.9	472.9	444.3	412.7	416.9
169Tm	420.1	444.8	460.9	441.1	407.4	407.7
172Yb	461.5	484.7	506.1	481.2	442.9	450.2
175Lu	434.7	463.7	482.7	455.4	421.1	420.8
178Hf	417.7	446.9	465.8	441.4	401.3	408.6
181Ta	376.6	405.4	420.5	400.5	364.0	370.3
182W	445.3	464.7	478.9	462.2	432.3	445.1
185Re	103.7	109.5	111.4	108.0	101.1	104.7
195Pt	3.15	3.5	3.5	3.5	2.9	3.3
197Au	22.5	24.4	24.5	23.0	22.1	22.9
205Tl	61.2	69.6	63.1	59.2	59.1	58.9
206Pb	413.3	463.3	438.8	426.6	395.1	402.0
207Pb	413.3	461.7	463.1	436.3	395.9	402.8
208Pb	413.3	447.0	440.2	419.2	397.3	394.1
209Bi	357.7	393.3	384.8	377.1	343.0	341.3
220Bkg	0	--	--	--	--	--
232Th	450.6	484.4	487.8	483.9	437.7	441.0
238U	457.1	469.4	465.8	487.0	426.3	438.3
254U O	0	--	--	--	--	--

Fe Internal Isotope	NIST 610 Pub. Conc.	Count	Min	Max	Average	Sigma	SDOM
7Li	484.6	10.0	446.8	541.1	488.4	30.8	3.5
9Be	465.5	10.0	442.8	508.2	467.6	21.6	2.5
11B	356.4	10.0	332.8	387.6	356.8	17.1	2.0
23Na	99053	10.0	89507.8	109353.0	98056.8	6319.1	739.6
25Mg	465.3	10.0	437.3	500.8	465.1	24.0	2.8
27Al	10790	10.0	10207.5	11782.9	10768.2	556.1	66.0
29Si	327090	10.0	302388.7	355887.9	325282.9	18081.8	2161.2
31P	342.5	10.0	311.7	373.7	340.7	17.1	2.1
33S	25	0.0	0.0	0.0	--	0.0	0.0
39K	486	10.0	442.4	519.4	478.7	22.2	2.7
43Ca	81830	10.0	72866.3	85412.9	81029.7	3436.1	422.9
44Ca	81830	10.0	73078.5	84515.4	80523.1	3224.9	400.0
45Sc	441.1	10.0	414.9	454.7	438.7	13.4	1.7
47Ti	434	10.0	412.7	456.4	430.4	12.9	1.6
51V	441.7	10.0	405.0	457.7	432.1	15.2	1.9
52Cr	405.2	10.0	377.2	410.7	395.9	10.6	1.4
53Cr	405.2	10.0	383.6	410.5	397.8	8.3	1.1
55Mn	433.3	10.0	417.8	456.7	431.0	13.0	1.7
57Fe	457.1	10.0	457.1	457.1	457.1	0.0	0.0
59Co	405	10.0	387.9	419.4	400.9	9.6	1.3
60Ni	443.9	10.0	420.4	463.2	439.5	12.4	1.7
62Ni	443.9	10.0	400.6	483.8	441.2	21.8	2.9
65Cu	430.3	10.0	404.4	450.8	425.8	13.6	1.9
66Zn	456.3	10.0	413.6	488.3	455.7	22.6	3.1
68Zn	456.3	10.0	419.6	489.3	457.8	22.1	3.1
69Ga	438.1	10.0	410.7	465.7	434.7	16.8	2.4
72Ge	426.3	10.0	412.6	459.1	427.6	13.2	1.9
75As	317.4	10.0	302.2	335.7	318.6	11.1	1.6
77Ar Cl	0	0.0	--	--	--	--	--
82Se	109	10.0	103.0	114.5	109.1	3.3	0.5
83Kr	0	0.0	--	--	--	--	--
85Rb	431.1	10.0	397.4	446.7	418.3	16.9	2.5
86Sr	497.4	10.0	468.3	529.4	493.6	19.7	2.9
88Sr	497.4	10.0	469.4	530.2	494.5	17.6	2.6
89Y	449.9	10.0	427.0	477.1	444.7	16.9	2.5
90Zr	439.9	10.0	418.9	472.0	435.6	18.1	2.8
93Nb	419.4	10.0	394.5	450.1	416.4	16.1	2.5
95Mo	376.8	10.0	350.5	397.8	373.3	13.0	2.0
103Rh	1.31	10.0	1.2	1.4	1.3	0.1	0.0
105Pd	1.05	10.0	0.8	1.2	1.1	0.1	0.0
107Ag	239.4	10.0	222.4	261.1	240.7	11.4	1.9
110Cd	259.4	10.0	239.6	287.0	265.2	15.8	2.6
111Cd	259.4	10.0	237.2	285.9	264.0	16.5	2.7
115In	441.4	10.0	392.5	469.3	436.1	23.9	4.0
118Sn	396.3	10.0	366.8	417.4	394.7	15.4	2.6
120Sn	396.3	10.0	367.5	421.8	394.3	18.3	3.2
121Sb	368.5	10.0	344.8	396.9	373.5	16.6	2.9
133Cs	360.9	10.0	322.9	399.9	356.5	22.8	4.1
136Ba	424.1	10.0	396.3	455.5	427.6	19.4	3.5

Fe Internal Isotope	NIST 610 Pub. Conc.	Count	Min	Max	Average	Sigma	SDOM
137Ba	**424.1**	10.0	398.0	464.7	428.5	19.8	3.7
139La	**457.4**	10.0	429.4	510.8	462.2	24.4	4.6
140Ce	**447.8**	10.0	420.9	489.3	450.0	20.0	3.9
141Pr	**429.8**	10.0	406.1	481.1	434.8	21.9	4.3
146Nd	**430.8**	10.0	406.0	484.6	435.0	22.5	4.5
147Sm	**450.5**	10.0	423.7	497.6	455.5	20.5	4.2
153Eu	**461.1**	10.0	430.3	508.8	463.1	22.7	4.7
155Gd	**419.9**	10.0	396.3	467.5	423.4	21.3	4.5
156Ce O	**0**	0.0	--	--	--	--	--
157Gd	**419.9**	10.0	395.4	465.2	421.9	21.0	4.6
159Tb	**442.8**	10.0	415.7	489.1	444.4	21.8	4.9
163Dy	**426.5**	10.0	397.5	472.7	428.0	21.8	5.0
165Ho	**449.4**	10.0	421.1	496.4	450.9	21.9	5.2
166Er	**426**	10.0	397.3	472.9	427.0	21.6	5.2
169Tm	**420.1**	10.0	393.3	460.9	420.8	20.9	5.2
172Yb	**461.5**	10.0	427.0	506.1	461.0	23.0	5.9
175Lu	**434.7**	10.0	403.2	482.7	435.8	23.7	6.3
178Hf	**417.7**	10.0	389.4	465.8	420.6	23.1	6.4
181Ta	**376.6**	10.0	347.8	420.5	380.2	21.9	6.3
182W	**445.3**	10.0	404.3	478.9	444.2	23.4	7.1
185Re	**103.7**	10.0	94.8	111.4	104.3	5.3	1.7
195Pt	**3.15**	10.0	2.7	3.5	3.2	0.2	0.1
197Au	**22.5**	10.0	21.0	24.5	22.9	1.1	0.4
205Tl	**61.2**	10.0	58.9	69.6	62.3	3.3	1.2
206Pb	**413.3**	10.0	382.2	463.3	418.4	24.5	10.0
207Pb	**413.3**	10.0	388.5	463.1	424.5	26.9	12.0
208Pb	**413.3**	10.0	378.8	447.0	415.7	21.8	10.9
209Bi	**357.7**	10.0	332.1	393.9	365.5	21.8	12.6
220Bkg	**0**	0.0	--	--	--	--	--
232Th	**450.6**	10.0	421.5	487.8	458.1	24.0	17.0
238U	**457.1**	10.0	410.9	487.0	452.3	24.0	24.0
254U O	**0**	0.0	--	--	--	--	--

Scaled Isotope	NIST 610 Pub. Conc.	Ap16A07	Ap16A08	Ap16B07	Ap16B08	Ap16C07
7Li	484.6	461.7	504.5	490.1	506.6	473.2
9Be	465.5	473.2	482.5	476.2	470.7	456.0
11B	356.4	361.0	369.1	357.9	359.9	347.3
23Na	99053	95903.7	98071.6	96252.2	96499.9	102025.9
25Mg	465.3	470.9	467.8	470.2	472.6	472.5
27Al	10790	10777.3	10668.3	10976.7	11025.0	10767.2
29Si	327090	325942.6	327230.6	325173.9	325677.0	327158.3
31P	342.5	339.1	345.7	335.2	342.5	345.9
33S	25	27.8	28.2	21.7	21.0	25.5
39K	486	536.7	502.8	492.2	488.0	483.9
44Ca	81830	87332.5	83030.3	88042.5	86712.9	80198.1
45Sc	441.1	465.0	446.4	465.5	460.0	440.2
47Ti	434	453.9	444.3	447.9	445.1	426.0
51V	441.7	453.9	444.3	463.3	459.2	428.4
52Cr	405.2	407.7	415.0	419.1	415.0	398.9
55Mn	433.3	433.0	433.1	452.8	458.2	433.1
57Fe	457.1	472.3	469.1	491.5	479.0	460.3
59Co	405	408.1	405.7	417.1	421.9	403.7
60Ni	443.9	447.6	447.6	452.1	459.7	444.4
65Cu	430.3	442.6	429.3	434.9	450.0	431.2
68Zn	456.3	480.1	467.2	483.7	471.8	474.8
69Ga	438.1	451.4	447.1	441.6	457.3	423.1
72Ge	426.3	436.6	441.7	443.6	439.6	429.9
75As	317.4	326.7	337.6	325.0	329.4	324.4
82Se	109	111.7	117.2	113.9	115.5	108.3
85Rb	431.1	425.2	414.0	432.9	447.8	425.3
88Sr	497.4	500.5	499.6	504.7	507.4	497.3
89Y	449.9	446.0	447.0	459.1	464.9	441.6
90Zr	439.9	433.5	434.3	450.5	452.4	431.2
93Nb	419.4	422.4	420.4	424.2	431.1	413.9
95Mo	376.8	380.4	386.1	376.9	380.3	373.3
103Rh	1.31	1.3	1.3	1.3	1.4	1.3
105Pd	1.05	1.1	1.1	0.9	1.1	1.1
107Ag	239.4	245.9	248.5	246.4	252.6	251.8
111Cd	259.4	271.2	273.1	272.8	265.5	287.5
115In	441.4	451.8	448.4	440.4	457.0	446.1
118Sn	396.3	412.0	421.3	394.4	408.9	386.4
121Sb	368.5	391.7	405.3	370.8	378.8	371.8
133Cs	360.9	349.4	365.1	368.9	383.8	358.2
137Ba	424.1	440.1	443.3	428.0	437.9	424.0
139La	457.4	471.2	485.2	461.8	471.7	447.6
140Ce	447.8	464.4	471.8	452.6	468.1	440.3
141Pr	429.8	444.3	455.5	436.7	443.7	424.7
146Nd	430.8	439.1	450.2	436.6	446.0	424.6
147Sm	450.5	465.3	475.9	455.7	469.5	446.9
153Eu	461.1	468.2	488.5	462.7	474.6	456.1
157Gd	419.9	421.2	441.3	425.2	430.6	412.2
159Tb	442.8	448.1	465.8	447.0	453.1	435.9
163Dy	426.5	427.8	446.8	427.4	433.4	419.2

Scaled Isotope	NIST 610 Pub. Conc.	Ap16A07	Ap16A08	Ap16B07	Ap16B08	Ap16C07
165Ho	**449.4**	447.8	470.8	452.8	460.9	446.2
166Er	**426**	426.5	448.4	427.2	434.9	416.7
169Tm	**420.1**	419.7	442.9	422.9	426.4	411.3
172Yb	**461.5**	464.4	486.0	459.1	467.5	451.6
175Lu	**434.7**	436.2	458.6	433.6	441.1	424.3
178Hf	**417.7**	422.5	442.8	418.7	425.1	409.0
181Ta	**376.6**	383.6	403.6	374.1	380.8	368.3
182W	**445.3**	451.0	485.3	434.8	442.6	425.8
185Re	**103.7**	106.2	113.9	101.9	104.3	100.9
195Pt	**3.15**	3.4	3.4	2.9	3.2	3.3
197Au	**22.5**	23.0	24.7	22.6	22.9	22.9
205Tl	**61.2**	63.5	67.6	64.1	65.3	64.3
208Pb	**413.3**	433.3	452.7	407.4	417.5	424.5
209Bi	**357.7**	384.0	404.3	357.2	362.2	374.6
232Th	**450.6**	476.9	496.0	453.3	451.7	452.3
238U	**457.1**	475.9	497.6	441.8	455.0	448.9

Scaled Isotope	NIST 610 Pub. Conc.	Ap16C08	Ap16D07	Ap16D08	Ap16E07	Ap16E08
7Li	**484.6**	491.6	513.9	493.5	494.7	496.0
9Be	**465.5**	454.6	482.7	468.4	476.1	478.3
11B	**356.4**	352.8	368.1	352.2	362.2	369.7
23Na	**99053**	101566.0	97554.2	100688.0	99264.8	100821.4
25Mg	**465.3**	464.0	475.6	468.3	469.2	460.4
27Al	**10790**	10943.9	10871.4	10863.3	10900.2	10834.9
29Si	**327090**	330545.2	330730.6	329932.7	328487.8	329736.3
31P	**342.5**	347.0	337.7	338.4	351.3	354.4
33S	**25**	18.1	27.2	21.1	30.1	23.1
39K	**486**	455.3	471.8	462.0	465.3	477.4
44Ca	**81830**	75650.8	78303.3	77432.0	80293.1	76823.2
45Sc	**441.1**	422.2	431.9	423.9	439.9	436.1
47Ti	**434**	403.3	433.4	418.6	441.6	433.9
51V	**441.7**	412.2	434.7	421.8	426.0	431.8
52Cr	**405.2**	377.6	389.9	382.5	403.4	410.8
55Mn	**433.3**	412.4	433.8	417.9	439.5	440.1
57Fe	**457.1**	424.5	434.1	430.4	480.7	480.5
59Co	**405**	377.4	398.3	390.7	415.6	412.1
60Ni	**443.9**	420.3	440.0	424.3	446.0	456.8
65Cu	**430.3**	409.8	428.1	408.5	434.9	431.4
68Zn	**456.3**	447.5	464.7	445.8	444.6	441.1
69Ga	**438.1**	412.5	442.3	431.2	440.5	442.4
72Ge	**426.3**	404.9	436.0	411.5	435.1	440.1
75As	**317.4**	306.1	318.9	306.9	320.4	321.9
82Se	**109**	102.1	108.7	102.2	108.4	114.5
85Rb	**431.1**	398.1	424.2	416.8	418.0	421.3
88Sr	**497.4**	473.1	503.6	487.2	508.4	511.2
89Y	**449.9**	430.7	453.1	439.3	454.1	453.6
90Zr	**439.9**	423.7	448.3	431.2	445.8	446.6
93Nb	**419.4**	403.0	427.5	408.1	424.5	428.6
95Mo	**376.8**	358.6	377.8	362.9	382.4	390.3
103Rh	**1.31**	1.3	1.3	1.2	1.3	1.4
105Pd	**1.05**	1.1	1.1	1.0	1.2	1.2
107Ag	**239.4**	242.5	240.5	227.7	233.9	239.4
111Cd	**259.4**	265.5	270.6	251.0	249.5	257.0
115In	**441.4**	423.8	444.2	441.9	412.8	433.9
118Sn	**396.3**	382.5	396.4	378.7	398.9	406.0
121Sb	**368.5**	368.7	374.3	350.3	376.8	383.1
133Cs	**360.9**	353.3	379.8	351.4	339.6	346.2
137Ba	**424.1**	422.4	441.3	419.9	433.2	434.6
139La	**457.4**	455.3	485.1	453.5	467.5	464.2
140Ce	**447.8**	435.9	464.7	438.5	450.2	456.4
141Pr	**429.8**	423.7	456.9	425.7	439.6	437.0
146Nd	**430.8**	428.9	460.2	422.6	440.6	441.2
147Sm	**450.5**	444.0	472.6	441.6	462.6	463.6
153Eu	**461.1**	452.8	483.3	451.2	467.7	468.2
157Gd	**419.9**	416.9	441.8	410.0	428.5	429.8
159Tb	**442.8**	437.8	464.6	431.2	450.0	450.9
163Dy	**426.5**	422.4	448.9	416.8	436.7	439.0

Scaled Isotope	NIST 610 Pub. Conc.	Ap16C08	Ap16D07	Ap16D08	Ap16E07	Ap16E08
165Ho	**449.4**	441.9	471.5	439.5	459.3	459.4
166Er	**426**	416.0	449.1	418.4	434.0	438.3
169Tm	**420.1**	413.1	437.7	415.3	428.4	428.6
172Yb	**461.5**	450.2	480.7	453.1	465.8	473.2
175Lu	**434.7**	430.7	458.5	428.9	442.9	442.4
178Hf	**417.7**	415.1	442.4	415.6	422.1	429.5
181Ta	**376.6**	376.5	399.3	377.1	382.9	389.2
182W	**445.3**	431.6	454.8	435.2	454.6	467.9
185Re	**103.7**	101.7	105.8	101.7	106.3	110.1
195Pt	**3.15**	3.2	3.3	3.3	3.1	3.5
197Au	**22.5**	22.7	23.3	21.6	23.2	24.0
205Tl	**61.2**	64.6	60.0	55.7	62.2	61.9
208Pb	**413.3**	415.2	418.1	394.7	417.9	414.3
209Bi	**357.7**	365.3	365.5	355.1	360.8	358.7
232Th	**450.6**	449.9	463.3	455.7	460.3	463.6
238U	**457.1**	436.0	442.4	458.5	448.4	460.8

Scaled Isotope	NIST 610 Pub. Conc.	Count	Min	Max	Average	Sigma	SDOM
7Li	484.6	10.0	461.7	513.9	492.6	14.7	1.8
9Be	465.5	10.0	454.6	482.7	471.9	9.3	1.2
11B	356.4	10.0	347.3	369.7	360.0	7.3	0.9
23Na	99053	10.0	95903.7	102025.9	98864.8	2194.0	278.6
25Mg	465.3	10.0	460.4	475.6	469.2	4.2	0.5
27Al	10790	10.0	10668.3	11025.0	10862.8	101.2	13.1
29Si	327090	10.0	325173.9	330730.6	328061.5	1995.0	259.7
31P	342.5	10.0	335.2	354.4	343.7	5.9	0.8
33S	25	10.0	18.1	30.1	24.4	3.7	0.5
39K	486	10.0	455.3	536.7	483.5	22.5	3.0
44Ca	81830	10.0	75650.8	88042.5	81381.9	4384.1	591.2
45Sc	441.1	10.0	422.2	465.5	443.1	15.1	2.1
47Ti	434	10.0	403.3	453.9	434.8	14.5	2.0
51V	441.7	10.0	412.2	463.3	437.6	16.1	2.2
52Cr	405.2	10.0	377.6	419.1	402.0	13.7	1.9
55Mn	433.3	10.0	412.4	458.2	435.4	13.1	1.9
57Fe	457.1	10.0	424.5	491.5	462.3	22.8	3.3
59Co	405	10.0	377.4	421.9	405.1	12.7	1.8
60Ni	443.9	10.0	420.3	459.7	443.9	12.1	1.8
65Cu	430.3	10.0	408.5	450.0	430.1	12.2	1.8
68Zn	456.3	10.0	441.1	483.7	462.1	15.2	2.3
69Ga	438.1	10.0	412.5	457.3	438.9	12.6	1.9
72Ge	426.3	10.0	404.9	443.6	431.9	12.5	1.9
75As	317.4	10.0	306.1	337.6	321.7	9.1	1.4
82Se	109	10.0	102.1	117.2	110.2	5.0	0.8
85Rb	431.1	10.0	398.1	447.8	422.4	12.2	1.9
88Sr	497.4	10.0	473.1	511.2	499.3	10.8	1.7
89Y	449.9	10.0	430.7	464.9	448.9	9.6	1.6
90Zr	439.9	10.0	423.7	452.4	439.7	9.5	1.6
93Nb	419.4	10.0	403.0	431.1	420.4	8.7	1.5
95Mo	376.8	10.0	358.6	390.3	376.9	9.3	1.6
103Rh	1.31	10.0	1.2	1.4	1.3	0.0	0.0
105Pd	1.05	10.0	0.9	1.2	1.1	0.1	0.0
107Ag	239.4	10.0	227.7	252.6	242.9	7.5	1.3
111Cd	259.4	10.0	249.5	287.5	266.4	10.9	2.0
115In	441.4	10.0	412.8	457.0	440.0	12.6	2.3
118Sn	396.3	10.0	378.7	421.3	398.5	13.0	2.4
121Sb	368.5	10.0	350.3	405.3	377.2	13.8	2.6
133Cs	360.9	10.0	339.6	383.8	359.6	13.8	2.7
137Ba	424.1	10.0	419.9	443.3	432.5	8.0	1.6
139La	457.4	10.0	447.6	485.2	466.3	11.9	2.4
140Ce	447.8	10.0	435.9	471.8	454.3	12.3	2.5
141Pr	429.8	10.0	423.7	456.9	438.8	11.3	2.3
146Nd	430.8	10.0	422.6	460.2	439.0	11.0	2.3
147Sm	450.5	10.0	441.6	475.9	459.8	11.6	2.5
153Eu	461.1	10.0	451.2	488.5	467.3	11.7	2.6
157Gd	419.9	10.0	410.0	441.8	425.8	10.4	2.4
159Tb	442.8	10.0	431.2	465.8	448.4	10.8	2.5
163Dy	426.5	10.0	416.8	448.9	431.8	10.5	2.5

Scaled Isotope	NIST 610 Pub. Conc.	Count	Min	Max	Average	Sigma	SDOM
165Ho	**449.4**	10.0	439.5	471.5	455.0	10.7	2.7
166Er	**426**	10.0	416.0	449.1	430.9	11.5	3.0
169Tm	**420.1**	10.0	411.3	442.9	424.6	9.8	2.6
172Yb	**461.5**	10.0	450.2	486.0	465.2	11.6	3.2
175Lu	**434.7**	10.0	424.3	458.6	439.7	11.0	3.2
178Hf	**417.7**	10.0	409.0	442.8	424.3	10.6	3.2
181Ta	**376.6**	10.0	368.3	403.6	383.6	10.5	3.3
182W	**445.3**	10.0	425.8	485.3	448.4	17.4	5.8
185Re	**103.7**	10.0	100.9	113.9	105.3	4.0	1.4
195Pt	**3.15**	10.0	2.9	3.5	3.2	0.2	0.1
197Au	**22.5**	10.0	21.6	24.7	23.1	0.8	0.3
205Tl	**61.2**	10.0	55.7	67.6	62.9	3.1	1.4
208Pb	**413.3**	10.0	394.7	452.7	419.6	14.6	7.3
209Bi	**357.7**	10.0	355.1	404.3	368.8	14.4	8.3
232Th	**450.6**	10.0	449.9	496.0	462.3	13.6	9.6
238U	**457.1**	10.0	436.0	497.6	456.5	17.4	17.4

Si Internal Isotope	NIST 612 Pub. Conc.	Ap16A03	Ap16A04	Ap16B03	Ap16B04	Ap16C03
7Li	**41.54**	44.9	41.3	41.5	41.7	41.0
9Be	**37.73**	37.6	35.1	39.0	40.1	38.1
11B	**34.73**	77.5	74.3	54.9	52.9	47.2
23Na	**103700**	99137.2	99184.2	90903.8	92401.6	96314.9
25Mg	**77.44**	< DL	54.9	64.5	60.0	60.4
27Al	**11200**	10160.1	9935.5	11611.1	11634.6	10702.9
29Si	**336100**	336100.0	336100.0	336100.0	336100.0	336100.0
31P	**55.16**	37.4	37.4	34.9	38.1	35.1
33S	**16**	< DL	< DL	14.7	20.5	9.1
39K	**66.26**	< DL	< DL	99.4	79.0	84.2
43Ca	**85260**	76164.8	71508.1	91047.7	86931.8	76838.3
44Ca	**85260**	75066.6	71319.8	87670.3	84670.7	73703.8
45Sc	**41.05**	33.3	31.5	38.8	39.1	35.1
47Ti	**48.11**	38.1	39.4	39.5	39.9	39.8
51V	**39.22**	37.2	36.4	36.1	33.9	35.9
52Cr	**39.88**	36.7	35.3	36.0	32.3	35.1
53Cr	**39.88**	35.6	34.0	34.4	33.4	33.1
55Mn	**38.43**	35.4	35.0	37.4	34.8	36.8
57Fe	**56.33**	< DL	< DL	51.1	44.9	62.2
59Co	**35.26**	34.1	35.1	34.6	31.3	34.4
60Ni	**38.44**	38.8	38.8	36.8	37.0	40.2
62Ni	**38.44**	< DL	< DL	50.7	38.1	38.6
65Cu	**36.71**	39.3	36.0	36.1	35.4	38.9
66Zn	**37.92**	36.3	35.9	39.2	34.9	41.1
68Zn	**39.13**	39.8	40.0	42.8	36.9	43.8
69Ga	**36.24**	36.5	36.1	36.0	33.6	36.6
72Ge	**34.64**	37.4	36.4	37.2	34.3	38.7
75As	**37.33**	28.4	26.7	26.3	25.0	29.6
77Ar Cl	**0**	- -	- -	- -	- -	- -
82Se	**- -**	15.3	16.6	14.9	14.3	16.9
83Kr	**0**	- -	- -	- -	- -	- -
85Rb	**31.63**	30.3	29.6	29.5	28.4	30.3
86Sr	**76.15**	66.5	67.3	74.5	71.1	75.1
88Sr	**120.67**	67.4	68.2	74.1	71.6	73.0
89Y	**38.25**	30.7	30.0	35.6	35.2	35.0
90Zr	**35.99**	31.5	31.5	36.5	36.0	36.4
93Nb	**38.06**	31.7	32.4	34.4	33.5	34.5
95Mo	**38.3**	32.6	32.8	31.8	30.5	32.8
103Rh	**0.896**	1.0	0.9	0.9	0.9	0.9
105Pd	**1.09**	1.2	1.0	0.9	0.9	1.1
107Ag	**21.92**	19.0	18.7	18.7	18.1	20.0
110Cd	**28.32**	25.2	24.2	25.5	23.8	27.5
111Cd	**28.32**	24.6	23.7	25.0	22.5	26.9
115In	**42.93**	33.9	34.0	34.3	32.1	34.9
118Sn	**37.96**	36.7	35.1	34.2	33.7	35.6
120Sn	**32.99**	35.6	35.6	34.0	33.3	35.4
121Sb	**38.44**	30.6	30.3	29.5	27.9	32.1
133Cs	**41.64**	37.0	37.1	36.9	34.1	38.4
136Ba	**37.74**	35.0	33.1	35.8	34.8	36.1

Si Internal Isotope	NIST 612 Pub. Conc.	Ap16A03	Ap16A04	Ap16B03	Ap16B04	Ap16C03
137Ba	**37.74**	33.8	33.4	35.1	34.7	35.4
139La	**35.77**	33.1	31.9	35.6	35.4	35.9
140Ce	**38.35**	35.4	34.8	36.1	35.3	36.9
141Pr	**37.16**	33.2	32.3	34.7	34.3	34.9
146Nd	**35.24**	32.1	31.1	32.9	34.0	34.6
147Sm	**36.72**	32.9	31.3	35.4	35.3	36.5
153Eu	**34.44**	32.9	31.0	35.1	35.0	36.1
155Gd	**36.95**	30.6	26.9	33.2	33.7	33.0
156Ce O	**0**	--	--	--	--	--
157Gd	**36.95**	30.4	28.7	33.7	33.5	33.4
159Tb	**35.92**	31.9	29.9	34.8	34.9	35.2
163Dy	**35.97**	29.5	27.6	32.8	33.0	33.1
165Ho	**37.87**	31.3	29.7	35.2	35.3	35.4
166Er	**37.43**	29.9	28.3	34.0	33.7	33.6
169Tm	**37.55**	29.9	27.9	32.8	32.9	33.1
172Yb	**39.95**	33.3	31.6	36.0	36.7	37.0
175Lu	**37.71**	30.5	28.3	33.7	33.4	33.9
178Hf	**34.77**	30.4	28.5	33.0	33.5	33.6
181Ta	**39.77**	27.5	26.0	30.0	29.7	30.7
182W	**39.55**	38.7	36.3	36.1	35.3	38.2
185Re	**8.12**	13.8	13.4	13.4	13.1	13.7
195Pt	**2.59**	2.5	2.5	2.3	2.2	2.6
197Au	**5.09**	4.6	4.4	4.4	4.3	4.6
205Tl	**15.07**	14.6	14.5	15.5	14.8	15.5
206Pb	**38.96**	36.9	35.2	34.0	32.6	37.1
207Pb	**38.96**	36.1	36.2	34.6	33.1	37.3
208Pb	**38.96**	36.6	35.5	33.7	31.6	37.0
209Bi	**29.84**	31.2	30.1	29.4	27.6	31.5
220Bkg	**0**	--	--	--	--	--
232Th	**37.23**	32.3	31.7	35.6	34.6	34.9
238U	**37.15**	36.2	35.9	32.0	31.8	33.3
254U O	**0**	--	--	--	--	--

Si Internal Isotope	NIST 612 Pub. Conc.	Ap16C04	Ap16D03	Ap16D04	Ap16E03	Ap16E04
7Li	**41.54**	43.7	38.8	40.8	43.6	40.5
9Be	**37.73**	39.8	39.7	35.9	39.3	36.9
11B	**34.73**	51.0	46.4	45.5	49.5	48.1
23Na	**103700**	98932.0	101850.5	103279.2	103991.8	101456.4
25Mg	**77.44**	60.4	60.3	60.9	56.6	61.8
27Al	**11200**	10821.1	10840.7	10856.3	10657.1	10709.4
29Si	**336100**	336100.0	336100.0	336100.0	336100.0	336100.0
31P	**55.16**	34.2	34.0	33.9	36.8	36.3
33S	**16**	17.4	10.8	15.4	17.7	19.3
39K	**66.26**	84.8	78.3	76.9	88.9	88.1
43Ca	**85260**	78054.3	75229.6	73219.7	82019.9	87705.8
44Ca	**85260**	76898.9	73198.2	71139.1	79315.2	82367.5
45Sc	**41.05**	36.1	33.7	33.1	36.0	35.2
47Ti	**48.11**	35.3	34.6	32.2	37.7	35.6
51V	**39.22**	35.6	33.3	33.0	36.8	36.4
52Cr	**39.88**	33.9	42.0	49.9	35.6	34.6
53Cr	**39.88**	33.7	31.8	31.6	35.9	35.3
55Mn	**38.43**	35.8	34.0	34.4	36.3	35.4
57Fe	**56.33**	59.1	71.9	83.7	49.4	43.9
59Co	**35.26**	33.4	33.0	32.3	34.8	33.2
60Ni	**38.44**	37.9	39.1	35.7	38.6	38.3
62Ni	**38.44**	42.3	25.2	38.3	51.7	54.8
65Cu	**36.71**	35.3	36.1	37.4	38.0	35.4
66Zn	**37.92**	36.9	34.5	33.8	38.0	36.5
68Zn	**39.13**	41.4	39.1	38.0	41.2	39.0
69Ga	**36.24**	35.2	34.4	34.6	36.5	34.9
72Ge	**34.64**	37.0	35.3	35.4	39.3	37.1
75As	**37.33**	27.5	24.4	24.0	29.5	29.0
77Ar Cl	**0**	--	--	--	--	--
82Se	**--**	14.7	16.0	14.0	15.3	14.6
83Kr	**0**	--	--	--	--	--
85Rb	**31.63**	29.4	27.7	27.6	29.7	28.3
86Sr	**76.15**	74.2	69.3	70.7	72.8	66.4
88Sr	**120.67**	73.9	69.3	70.8	72.8	67.5
89Y	**38.25**	34.6	31.8	32.5	33.8	30.3
90Zr	**35.99**	36.2	32.9	33.5	34.7	31.1
93Nb	**38.06**	34.2	32.3	33.3	33.4	30.9
95Mo	**38.3**	31.8	30.7	30.6	33.7	32.2
103Rh	**0.896**	0.9	0.9	0.8	0.9	0.9
105Pd	**1.09**	1.1	1.0	1.3	1.2	1.2
107Ag	**21.92**	19.9	17.5	18.0	18.8	18.3
110Cd	**28.32**	26.3	25.2	23.8	27.2	25.1
111Cd	**28.32**	25.4	23.3	23.5	26.2	25.1
115In	**42.93**	33.5	32.7	32.8	33.9	32.4
118Sn	**37.96**	35.1	34.3	33.9	36.9	34.9
120Sn	**32.99**	34.5	32.6	33.8	36.4	34.5
121Sb	**38.44**	30.5	28.6	28.8	31.5	29.7
133Cs	**41.64**	36.9	35.7	35.3	39.0	36.8
136Ba	**37.74**	35.2	34.8	37.3	37.0	34.3

Si Internal Isotope	NIST 612 Pub. Conc.	Ap16C04	Ap16D03	Ap16D04	Ap16E03	Ap16E04
137Ba	**37.74**	35.9	32.9	35.6	36.4	34.0
139La	**35.77**	36.6	34.0	35.1	36.0	33.0
140Ce	**38.35**	36.8	34.7	36.1	37.1	34.5
141Pr	**37.16**	35.2	33.4	34.8	35.4	32.5
146Nd	**35.24**	34.6	32.7	33.3	34.1	30.9
147Sm	**36.72**	36.1	33.4	34.6	37.6	32.6
153Eu	**34.44**	35.6	33.3	34.1	35.0	32.1
155Gd	**36.95**	33.0	31.0	31.9	32.2	30.0
156Ce O	**0**	--	--	--	--	--
157Gd	**36.95**	33.7	29.9	32.2	32.6	29.2
159Tb	**35.92**	35.2	32.0	32.9	34.1	30.3
163Dy	**35.97**	33.5	30.9	30.7	32.3	28.4
165Ho	**37.87**	35.4	32.5	33.3	34.4	30.8
166Er	**37.43**	33.8	30.6	31.7	32.7	29.4
169Tm	**37.55**	33.3	30.2	31.5	31.7	28.8
172Yb	**39.95**	37.1	34.0	35.2	35.9	32.6
175Lu	**37.71**	34.1	31.1	32.1	33.0	28.9
178Hf	**34.77**	33.8	31.2	32.0	32.5	29.5
181Ta	**39.77**	31.2	28.3	29.4	29.6	27.2
182W	**39.55**	36.9	36.3	36.6	40.1	37.5
185Re	**8.12**	13.9	13.1	13.4	14.9	13.6
195Pt	**2.59**	2.6	2.6	2.5	2.5	2.4
197Au	**5.09**	4.6	4.3	4.1	4.6	4.4
205Tl	**15.07**	14.4	13.4	13.7	14.6	14.1
206Pb	**38.96**	35.4	33.4	32.7	36.8	34.3
207Pb	**38.96**	34.9	33.3	33.0	35.9	34.5
208Pb	**38.96**	34.6	32.5	32.7	35.7	33.9
209Bi	**29.84**	30.2	28.0	28.1	30.0	28.6
220Bkg	**0**	--	--	--	--	--
232Th	**37.23**	34.7	33.1	34.9	34.9	31.3
238U	**37.15**	33.1	31.5	32.3	34.5	32.3
254U O	**0**	--	--	--	--	--

Si Internal Isotope	NIST 612 Pub. Conc.	Count	Min	Max	Average	Sigma
7Li	**41.54**	10.0	38.8	44.9	41.8	1.7
9Be	**37.73**	10.0	35.1	40.1	38.1	1.7
11B	**34.73**	10.0	45.5	77.5	54.7	11.0
23Na	**103700**	10.0	90903.8	103991.8	98745.2	4160.5
25Mg	**77.44**	9.0	54.9	64.5	60.0	18.2
27Al	**11200**	10.0	9935.5	11634.6	10792.9	505.4
29Si	**336100**	10.0	336100.0	336100.0	336100.0	0.0
31P	**55.16**	10.0	33.9	38.1	35.8	1.5
33S	**16**	8.0	9.1	20.5	15.6	7.1
39K	**66.26**	8.0	76.9	99.4	85.0	34.5
43Ca	**85260**	10.0	71508.1	91047.7	79872.0	6346.1
44Ca	**85260**	10.0	71139.1	87670.3	77535.0	5474.4
45Sc	**41.05**	10.0	31.5	39.1	35.2	2.3
47Ti	**48.11**	10.0	32.2	39.9	37.2	2.5
51V	**39.22**	10.0	33.0	37.2	35.5	1.4
52Cr	**39.88**	10.0	32.3	49.9	37.1	4.9
53Cr	**39.88**	10.0	31.6	35.9	33.9	1.4
55Mn	**38.43**	10.0	34.0	37.4	35.5	1.0
57Fe	**56.33**	8.0	43.9	83.7	58.3	26.1
59Co	**35.26**	10.0	31.3	35.1	33.6	1.1
60Ni	**38.44**	10.0	35.7	40.2	38.1	1.2
62Ni	**38.44**	8.0	25.2	54.8	42.5	18.8
65Cu	**36.71**	10.0	35.3	39.3	36.8	1.4
66Zn	**37.92**	10.0	33.8	41.1	36.7	2.1
68Zn	**39.13**	10.0	36.9	43.8	40.2	2.0
69Ga	**36.24**	10.0	33.6	36.6	35.4	1.0
72Ge	**34.64**	10.0	34.3	39.3	36.8	1.5
75As	**37.33**	10.0	24.0	29.6	27.0	2.0
77Ar Cl	**0**	0.0	--	--	--	--
82Se	**--**	10.0	14.0	16.9	15.3	0.9
83Kr	**0**	0.0	--	--	--	--
85Rb	**31.63**	10.0	27.6	30.3	29.1	1.0
86Sr	**76.15**	10.0	66.4	75.1	70.8	3.2
88Sr	**120.67**	10.0	67.4	74.1	70.9	2.5
89Y	**38.25**	10.0	30.0	35.6	33.0	2.0
90Zr	**35.99**	10.0	31.1	36.5	34.0	2.1
93Nb	**38.06**	10.0	30.9	34.5	33.1	1.2
95Mo	**38.3**	10.0	30.5	33.7	32.0	1.0
103Rh	**0.896**	10.0	0.8	1.0	0.9	0.0
105Pd	**1.09**	10.0	0.9	1.3	1.1	0.1
107Ag	**21.92**	10.0	17.5	20.0	18.7	0.8
110Cd	**28.32**	10.0	23.8	27.5	25.4	1.2
111Cd	**28.32**	10.0	22.5	26.9	24.6	1.3
115In	**42.93**	10.0	32.1	34.9	33.5	0.9
118Sn	**37.96**	10.0	33.7	36.9	35.0	1.0
120Sn	**32.99**	10.0	32.6	36.4	34.6	1.1
121Sb	**38.44**	10.0	27.9	32.1	30.0	1.3
133Cs	**41.64**	10.0	34.1	39.0	36.7	1.4
136Ba	**37.74**	10.0	33.1	37.3	35.3	1.2

Si Internal Isotope	NIST 612 Pub. Conc.	Count	Min	Max	Average	Sigma
137Ba	**37.74**	10.0	32.9	36.4	34.7	1.1
139La	**35.77**	10.0	31.9	36.6	34.7	1.5
140Ce	**38.35**	10.0	34.5	37.1	35.8	0.9
141Pr	**37.16**	10.0	32.3	35.4	34.1	1.1
146Nd	**35.24**	10.0	30.9	34.6	33.0	1.3
147Sm	**36.72**	10.0	31.3	37.6	34.6	1.9
153Eu	**34.44**	10.0	31.0	36.1	34.0	1.6
155Gd	**36.95**	10.0	26.9	33.7	31.6	1.9
156Ce O	**0**	0.0	--	--	--	--
157Gd	**36.95**	10.0	28.7	33.7	31.7	1.9
159Tb	**35.92**	10.0	29.9	35.2	33.1	1.9
163Dy	**35.97**	10.0	27.6	33.5	31.2	2.0
165Ho	**37.87**	10.0	29.7	35.4	33.3	2.0
166Er	**37.43**	10.0	28.3	34.0	31.8	2.0
169Tm	**37.55**	10.0	27.9	33.3	31.2	1.8
172Yb	**39.95**	10.0	31.6	37.1	34.9	1.9
175Lu	**37.71**	10.0	28.3	34.1	31.9	2.0
178Hf	**34.77**	10.0	28.5	33.8	31.8	1.8
181Ta	**39.77**	10.0	26.0	31.2	29.0	1.6
182W	**39.55**	10.0	35.3	40.1	37.2	1.4
185Re	**8.12**	10.0	13.1	14.9	13.6	0.5
195Pt	**2.59**	10.0	2.2	2.6	2.5	0.1
197Au	**5.09**	10.0	4.1	4.6	4.4	0.2
205Tl	**15.07**	10.0	13.4	15.5	14.5	0.6
206Pb	**38.96**	10.0	32.6	37.1	34.8	1.6
207Pb	**38.96**	10.0	33.0	37.3	34.9	1.4
208Pb	**38.96**	10.0	31.6	37.0	34.4	1.7
209Bi	**29.84**	10.0	27.6	31.5	29.5	1.3
220Bkg	**0**	0.0	--	--	--	--
232Th	**37.23**	10.0	31.3	35.6	33.8	1.5
238U	**37.15**	10.0	31.5	36.2	33.3	1.6
254U O	**0**	0.0	--	--	--	--

Ca Internal Isotope	NIST 612 Pub. Conc.	Ap16A03	Ap16A04	Ap16B03	Ap16B04	Ap16C03
7Li	**41.54**	51.1	49.4	40.4	42.0	47.4
9Be	**37.73**	42.7	41.9	37.9	40.4	44.1
11B	**34.73**	88.0	88.8	53.4	53.3	54.6
23Na	**103700**	112599.1	118570.8	88404.6	93044.7	111416.3
25Mg	**77.44**	< DL	65.6	62.7	60.4	69.8
27Al	**11200**	11539.7	11877.5	11291.9	11715.5	12381.0
29Si	**336100**	381739.5	401794.5	326859.7	338439.2	388797.8
31P	**55.16**	42.5	44.7	34.0	38.3	40.6
33S	**16**	< DL	< DL	14.3	20.6	10.6
39K	**66.26**	< DL	< DL	96.7	79.6	97.4
43Ca	**85260**	86507.3	85485.2	88544.6	87536.9	88885.9
44Ca	**85260**	85260.0	85260.0	85260.0	85260.0	85260.0
45Sc	**41.05**	37.9	37.6	37.8	39.3	40.6
47Ti	**48.11**	43.3	47.0	38.4	40.1	46.1
51V	**39.22**	42.2	43.5	35.1	34.2	41.5
52Cr	**39.88**	41.6	42.2	35.0	32.5	40.6
53Cr	**39.88**	40.4	40.6	33.4	33.6	38.3
55Mn	**38.43**	40.2	41.8	36.3	35.1	42.5
57Fe	**56.33**	< DL	< DL	49.7	45.2	72.0
59Co	**35.26**	38.7	41.9	33.6	31.5	39.8
60Ni	**38.44**	44.1	46.3	35.7	37.2	46.4
62Ni	**38.44**	< DL	< DL	49.3	38.4	44.6
65Cu	**36.71**	44.6	43.1	35.1	35.7	45.0
66Zn	**37.92**	41.2	42.9	38.1	35.1	47.5
68Zn	**39.13**	45.2	47.8	41.6	37.2	50.6
69Ga	**36.24**	41.4	43.1	35.0	33.8	42.3
72Ge	**34.64**	42.5	43.5	36.2	34.5	44.7
75As	**37.33**	32.3	31.9	25.6	25.2	34.2
77Ar Cl	**0**	--	--	--	--	--
82Se	**--**	17.4	19.8	14.5	14.4	19.5
83Kr	**0**	--	--	--	--	--
85Rb	**31.63**	34.4	35.4	28.7	28.6	35.0
86Sr	**76.15**	75.5	80.4	72.4	71.6	86.9
88Sr	**120.67**	76.5	81.6	72.1	72.1	84.5
89Y	**38.25**	34.9	35.9	34.6	35.4	40.4
90Zr	**35.99**	35.8	37.7	35.5	36.2	42.1
93Nb	**38.06**	36.0	38.7	33.5	33.7	39.9
95Mo	**38.3**	37.1	39.2	30.9	30.7	37.9
103Rh	**0.896**	1.1	1.1	0.9	0.9	1.1
105Pd	**1.09**	1.3	1.2	0.9	0.9	1.3
107Ag	**21.92**	21.6	22.4	18.1	18.3	23.2
110Cd	**28.32**	28.6	28.9	24.8	24.0	31.8
111Cd	**28.32**	28.0	28.4	24.3	22.7	31.2
115In	**42.93**	38.5	40.7	33.4	32.3	40.3
118Sn	**37.96**	41.7	42.0	33.3	33.9	41.2
120Sn	**32.99**	40.5	42.5	33.1	33.5	40.9
121Sb	**38.44**	34.8	36.2	28.7	28.1	37.1
133Cs	**41.64**	42.0	44.3	35.8	34.3	44.5
136Ba	**37.74**	39.8	39.6	34.8	35.0	41.8

Ca Internal Isotope	NIST 612 Pub. Conc.	Ap16A03	Ap16A04	Ap16B03	Ap16B04	Ap16C03
137Ba	**37.74**	38.4	39.9	34.1	35.0	41.0
139La	**35.77**	37.6	38.1	34.7	35.7	41.5
140Ce	**38.35**	40.2	41.6	35.1	35.6	42.7
141Pr	**37.16**	37.8	38.6	33.8	34.6	40.4
146Nd	**35.24**	36.5	37.1	32.0	34.2	40.0
147Sm	**36.72**	37.3	37.4	34.4	35.6	42.2
153Eu	**34.44**	37.4	37.1	34.1	35.3	41.7
155Gd	**36.95**	34.7	32.2	32.3	34.0	38.1
156Ce O	**0**	--	--	--	--	--
157Gd	**36.95**	34.5	34.3	32.8	33.8	38.7
159Tb	**35.92**	36.2	35.7	33.9	35.2	40.7
163Dy	**35.97**	33.5	33.0	31.9	33.2	38.3
165Ho	**37.87**	35.6	35.6	34.3	35.6	41.0
166Er	**37.43**	34.0	33.8	33.1	33.9	38.8
169Tm	**37.55**	34.0	33.3	31.9	33.1	38.3
172Yb	**39.95**	37.9	37.8	35.0	37.0	42.8
175Lu	**37.71**	34.6	33.8	32.7	33.6	39.2
178Hf	**34.77**	34.6	34.0	32.1	33.7	38.9
181Ta	**39.77**	31.2	31.1	29.2	29.9	35.6
182W	**39.55**	44.0	43.4	35.1	35.6	44.2
185Re	**8.12**	15.7	16.0	13.1	13.2	15.9
195Pt	**2.59**	2.9	3.0	2.3	2.2	3.0
197Au	**5.09**	5.3	5.3	4.2	4.3	5.3
205Tl	**15.07**	16.6	17.4	15.1	14.9	18.0
206Pb	**38.96**	41.9	42.1	33.0	32.8	42.9
207Pb	**38.96**	41.1	43.3	33.6	33.3	43.2
208Pb	**38.96**	41.6	42.5	32.8	31.9	42.9
209Bi	**29.84**	35.5	36.0	28.6	27.8	36.4
220Bkg	**0**	--	--	--	--	--
232Th	**37.23**	36.7	37.9	34.6	34.8	40.4
238U	**37.15**	41.1	43.0	31.1	32.0	38.5
254U O	**0**	--	--	--	--	--

Ca Internal Isotope	NIST 612 Pub. Conc.	Ap16C04	Ap16D03	Ap16D04	Ap16E03	Ap16E04
7Li	**41.54**	48.5	45.2	48.9	46.9	41.9
9Be	**37.73**	44.1	46.2	43.0	42.2	38.2
11B	**34.73**	56.6	54.0	54.5	53.2	49.8
23Na	**103700**	109688.7	118633.7	123779.9	111786.2	105019.2
25Mg	**77.44**	66.9	70.3	73.0	60.9	63.9
27Al	**11200**	11997.7	12627.1	13011.3	11455.8	11085.5
29Si	**336100**	372643.9	391483.5	402815.1	361291.4	347902.7
31P	**55.16**	37.9	39.6	40.6	39.5	37.5
33S	**16**	19.3	12.6	18.5	19.0	19.9
39K	**66.26**	94.0	91.2	92.2	95.5	91.2
43Ca	**85260**	86541.1	87626.1	87753.7	88167.5	90785.7
44Ca	**85260**	85260.0	85260.0	85260.0	85260.0	85260.0
45Sc	**41.05**	40.0	39.2	39.7	38.7	36.4
47Ti	**48.11**	39.1	40.3	38.6	40.5	36.9
51V	**39.22**	39.5	38.8	39.5	39.6	37.7
52Cr	**39.88**	37.5	49.0	59.8	38.3	35.8
53Cr	**39.88**	37.4	37.0	37.9	38.6	36.5
55Mn	**38.43**	39.7	39.6	41.3	39.1	36.6
57Fe	**56.33**	65.5	83.8	100.3	53.2	45.5
59Co	**35.26**	37.0	38.4	38.7	37.4	34.3
60Ni	**38.44**	42.1	45.5	42.8	41.5	39.7
62Ni	**38.44**	46.9	29.4	45.9	55.6	56.7
65Cu	**36.71**	39.1	42.0	44.9	40.8	36.7
66Zn	**37.92**	40.9	40.1	40.6	40.8	37.7
68Zn	**39.13**	45.9	45.6	45.6	44.3	40.4
69Ga	**36.24**	39.0	40.0	41.5	39.2	36.1
72Ge	**34.64**	41.0	41.1	42.4	42.2	38.4
75As	**37.33**	30.5	28.4	28.8	31.8	30.0
77Ar Cl	**0**	--	--	--	--	--
82Se	--	16.3	18.6	16.8	16.4	15.2
83Kr	**0**	--	--	--	--	--
85Rb	**31.63**	32.6	32.3	33.1	31.9	29.3
86Sr	**76.15**	82.3	80.7	84.7	78.3	68.7
88Sr	**120.67**	81.9	80.7	84.8	78.2	69.9
89Y	**38.25**	38.3	37.0	39.0	36.4	31.4
90Zr	**35.99**	40.1	38.3	40.1	37.3	32.2
93Nb	**38.06**	37.9	37.6	39.9	35.9	32.0
95Mo	**38.3**	35.3	35.8	36.7	36.2	33.4
103Rh	**0.896**	1.0	1.0	1.0	1.0	1.0
105Pd	**1.09**	1.3	1.2	1.6	1.3	1.2
107Ag	**21.92**	22.1	20.4	21.6	20.2	18.9
110Cd	**28.32**	29.2	29.3	28.5	29.2	26.0
111Cd	**28.32**	28.2	27.1	28.1	28.1	25.9
115In	**42.93**	37.2	38.0	39.3	36.5	33.6
118Sn	**37.96**	38.9	39.9	40.6	39.6	36.1
120Sn	**32.99**	38.2	38.0	40.5	39.1	35.7
121Sb	**38.44**	33.8	33.3	34.5	33.9	30.8
133Cs	**41.64**	40.9	41.5	42.3	42.0	38.1
136Ba	**37.74**	39.0	40.6	44.6	39.8	35.5

Ca Internal Isotope	NIST 612 Pub. Conc.	Ap16C04	Ap16D03	Ap16D04	Ap16E03	Ap16E04
137Ba	**37.74**	39.8	38.3	42.7	39.2	35.2
139La	**35.77**	40.6	39.6	42.0	38.7	34.1
140Ce	**38.35**	40.8	40.5	43.2	39.9	35.7
141Pr	**37.16**	39.0	38.9	41.7	38.0	33.6
146Nd	**35.24**	38.4	38.1	39.9	36.6	31.9
147Sm	**36.72**	40.1	38.9	41.5	40.4	33.7
153Eu	**34.44**	39.5	38.8	40.9	37.7	33.2
155Gd	**36.95**	36.6	36.1	38.2	34.6	31.1
156Ce O	**0**	--	--	--	--	--
157Gd	**36.95**	37.3	34.8	38.5	35.1	30.2
159Tb	**35.92**	39.1	37.3	39.5	36.6	31.4
163Dy	**35.97**	37.1	36.0	36.8	34.7	29.4
165Ho	**37.87**	39.3	37.8	39.9	36.9	31.9
166Er	**37.43**	37.5	35.7	38.0	35.1	30.4
169Tm	**37.55**	36.9	35.2	37.7	34.1	29.8
172Yb	**39.95**	41.2	39.6	42.2	38.6	33.7
175Lu	**37.71**	37.8	36.3	38.4	35.4	29.9
178Hf	**34.77**	37.5	36.4	38.3	35.0	30.6
181Ta	**39.77**	34.6	33.0	35.3	31.8	28.1
182W	**39.55**	41.0	42.3	43.9	43.1	38.8
185Re	**8.12**	15.4	15.3	16.0	16.0	14.1
195Pt	**2.59**	2.9	3.0	3.0	2.7	2.5
197Au	**5.09**	5.1	5.0	4.9	5.0	4.5
205Tl	**15.07**	15.9	15.6	16.5	15.7	14.6
206Pb	**38.96**	39.2	38.9	39.1	39.6	35.6
207Pb	**38.96**	38.7	38.7	39.6	38.6	35.7
208Pb	**38.96**	38.4	37.8	39.2	38.4	35.1
209Bi	**29.84**	33.5	32.6	33.6	32.2	29.6
220Bkg	**0**	--	--	--	--	--
232Th	**37.23**	38.5	38.6	41.8	37.5	32.4
238U	**37.15**	36.7	36.7	38.8	37.1	33.5
254U O	**0**	--	--	--	--	--

Ca Internal Isotope	NIST 612 Pub. Conc.	Count	Min	Max	Average	Sigma
7Li	**41.54**	10.0	40.4	51.1	46.2	3.5
9Be	**37.73**	10.0	37.9	46.2	42.1	2.5
11B	**34.73**	10.0	49.8	88.8	60.6	14.0
23Na	**103700**	10.0	88404.6	123779.9	109294.3	10600.0
25Mg	**77.44**	9.0	60.4	73.0	66.0	20.2
27Al	**11200**	10.0	11085.5	13011.3	11898.3	583.0
29Si	**336100**	10.0	326859.7	402815.1	371376.7	25396.4
31P	**55.16**	10.0	34.0	44.7	39.5	2.8
33S	**16**	8.0	10.6	20.6	16.9	7.5
39K	**66.26**	8.0	79.6	97.4	92.2	37.2
43Ca	**85260**	10.0	85485.2	90785.7	87783.4	1396.3
44Ca	**85260**	10.0	85260.0	85260.0	85260.0	0.0
45Sc	**41.05**	10.0	36.4	40.6	38.7	1.2
47Ti	**48.11**	10.0	36.9	47.0	41.0	3.2
51V	**39.22**	10.0	34.2	43.5	39.2	2.8
52Cr	**39.88**	10.0	32.5	59.8	41.2	7.6
53Cr	**39.88**	10.0	33.4	40.6	37.4	2.3
55Mn	**38.43**	10.0	35.1	42.5	39.2	2.4
57Fe	**56.33**	8.0	45.2	100.3	64.4	30.7
59Co	**35.26**	10.0	31.5	41.9	37.1	3.0
60Ni	**38.44**	10.0	35.7	46.4	42.1	3.5
62Ni	**38.44**	8.0	29.4	56.7	45.8	19.8
65Cu	**36.71**	10.0	35.1	45.0	40.7	3.7
66Zn	**37.92**	10.0	35.1	47.5	40.5	3.1
68Zn	**39.13**	10.0	37.2	50.6	44.4	3.6
69Ga	**36.24**	10.0	33.8	43.1	39.2	3.0
72Ge	**34.64**	10.0	34.5	44.7	40.6	3.1
75As	**37.33**	10.0	25.2	34.2	29.9	2.8
77Ar Cl	**0**	0.0	--	--	--	--
82Se	**--**	10.0	14.4	19.8	16.9	1.8
83Kr	**0**	0.0	--	--	--	--
85Rb	**31.63**	10.0	28.6	35.4	32.1	2.4
86Sr	**76.15**	10.0	68.7	86.9	78.2	5.7
88Sr	**120.67**	10.0	69.9	84.8	78.2	5.1
89Y	**38.25**	10.0	31.4	40.4	36.3	2.4
90Zr	**35.99**	10.0	32.2	42.1	37.5	2.7
93Nb	**38.06**	10.0	32.0	39.9	36.5	2.6
95Mo	**38.3**	10.0	30.7	39.2	35.3	2.7
103Rh	**0.896**	10.0	0.9	1.1	1.0	0.1
105Pd	**1.09**	10.0	0.9	1.6	1.2	0.2
107Ag	**21.92**	10.0	18.1	23.2	20.7	1.7
110Cd	**28.32**	10.0	24.0	31.8	28.0	2.3
111Cd	**28.32**	10.0	22.7	31.2	27.2	2.3
115In	**42.93**	10.0	32.3	40.7	37.0	2.8
118Sn	**37.96**	10.0	33.3	42.0	38.7	3.0
120Sn	**32.99**	10.0	33.1	42.5	38.2	3.0
121Sb	**38.44**	10.0	28.1	37.1	33.1	2.9
133Cs	**41.64**	10.0	34.3	44.5	40.6	3.2
136Ba	**37.74**	10.0	34.8	44.6	39.1	3.0

Ca Internal Isotope	NIST 612 Pub. Conc.	Count	Min	Max	Average	Sigma
137Ba	**37.74**	10.0	34.1	42.7	38.4	2.6
139La	**35.77**	10.0	34.1	42.0	38.3	2.6
140Ce	**38.35**	10.0	35.1	43.2	39.5	2.8
141Pr	**37.16**	10.0	33.6	41.7	37.6	2.6
146Nd	**35.24**	10.0	31.9	40.0	36.5	2.8
147Sm	**36.72**	10.0	33.7	42.2	38.1	2.8
153Eu	**34.44**	10.0	33.2	41.7	37.6	2.7
155Gd	**36.95**	10.0	31.1	38.2	34.8	2.4
156Ce O	**0**	0.0	--	--	--	--
157Gd	**36.95**	10.0	30.2	38.7	35.0	2.5
159Tb	**35.92**	10.0	31.4	40.7	36.6	2.6
163Dy	**35.97**	10.0	29.4	38.3	34.4	2.6
165Ho	**37.87**	10.0	31.9	41.0	36.8	2.6
166Er	**37.43**	10.0	30.4	38.8	35.0	2.4
169Tm	**37.55**	10.0	29.8	38.3	34.4	2.5
172Yb	**39.95**	10.0	33.7	42.8	38.6	2.8
175Lu	**37.71**	10.0	29.9	39.2	35.2	2.7
178Hf	**34.77**	10.0	30.6	38.9	35.1	2.6
181Ta	**39.77**	10.0	28.1	35.6	32.0	2.4
182W	**39.55**	10.0	35.1	44.2	41.1	3.3
185Re	**8.12**	10.0	13.1	16.0	15.1	1.1
195Pt	**2.59**	10.0	2.2	3.0	2.8	0.3
197Au	**5.09**	10.0	4.2	5.3	4.9	0.4
205Tl	**15.07**	10.0	14.6	18.0	16.0	1.0
206Pb	**38.96**	10.0	32.8	42.9	38.5	3.4
207Pb	**38.96**	10.0	33.3	43.3	38.6	3.3
208Pb	**38.96**	10.0	31.9	42.9	38.0	3.6
209Bi	**29.84**	10.0	27.8	36.4	32.6	2.9
220Bkg	**0**	0.0	--	--	--	--
232Th	**37.23**	10.0	32.4	41.8	37.3	2.7
238U	**37.15**	10.0	31.1	43.0	36.9	3.6
254U O	**0**	0.0	--	--	--	--

Fe Internal Isotope	NIST 612 Pub. Conc.	Ap16A03	Ap16A04	Ap16B03	Ap16B04	Ap16C03
7Li	**41.54**	72.0	97.0	45.7	52.4	37.1
9Be	**37.73**	60.3	82.4	43.0	50.3	34.5
11B	**34.73**	124.2	174.5	60.5	66.5	42.8
23Na	**103700**	158801.0	232911.9	100146.6	116023.4	87185.1
25Mg	**77.44**	79.9	128.9	71.0	75.3	54.6
27Al	**11200**	16274.8	23331.2	12791.7	14608.8	9688.4
29Si	**336100**	538375.5	789255.7	370273.7	422021.7	304240.5
31P	**55.16**	59.9	87.8	38.5	47.8	31.8
33S	**16**	< DL	< DL	16.2	25.7	8.3
39K	**66.26**	< DL	268.8	109.6	99.2	76.2
43Ca	**85260**	122003.2	167920.8	100305.2	109155.4	69554.7
44Ca	**85260**	120244.0	167478.5	96584.4	106316.2	66717.3
45Sc	**41.05**	53.4	73.9	42.8	49.0	31.8
47Ti	**48.11**	61.0	92.4	43.5	50.1	36.1
51V	**39.22**	59.5	85.4	39.7	42.6	32.5
52Cr	**39.88**	58.7	82.8	39.7	40.5	31.8
53Cr	**39.88**	57.0	79.8	37.8	41.9	30.0
55Mn	**38.43**	56.8	82.1	41.2	43.8	33.3
57Fe	**56.33**	< DL	< DL	56.3	56.3	56.3
59Co	**35.26**	54.6	82.4	38.1	39.3	31.2
60Ni	**38.44**	62.2	91.0	40.5	46.4	36.3
62Ni	**38.44**	< DL	< DL	55.9	47.8	34.9
65Cu	**36.71**	62.9	84.6	39.7	44.5	35.2
66Zn	**37.92**	58.1	84.2	43.2	43.8	37.2
68Zn	**39.13**	63.8	94.0	47.2	46.4	39.6
69Ga	**36.24**	58.4	84.7	39.7	42.2	33.1
72Ge	**34.64**	60.0	85.4	41.0	43.0	35.0
75As	**37.33**	45.5	62.7	28.9	31.4	26.8
77Ar Cl	**0**	--	--	--	--	--
82Se	**--**	24.5	38.9	16.5	18.0	15.3
83Kr	**0**	--	--	--	--	--
85Rb	**31.63**	48.5	69.5	32.6	35.6	27.4
86Sr	**76.15**	106.5	158.0	82.0	89.3	68.0
88Sr	**120.67**	107.9	160.2	81.7	89.9	66.1
89Y	**38.25**	49.2	70.5	39.2	44.2	31.7
90Zr	**35.99**	50.5	74.0	40.2	45.2	32.9
93Nb	**38.06**	50.8	76.1	37.9	42.1	31.3
95Mo	**38.3**	52.3	77.1	35.0	38.3	29.7
103Rh	**0.896**	1.5	2.1	1.0	1.2	0.8
105Pd	**1.09**	1.9	2.4	1.0	1.1	1.0
107Ag	**21.92**	30.5	44.0	20.6	22.8	18.1
110Cd	**28.32**	40.4	56.7	28.1	29.9	24.9
111Cd	**28.32**	39.5	55.8	27.6	28.2	24.4
115In	**42.93**	54.3	79.9	37.8	40.3	31.5
118Sn	**37.96**	58.8	82.5	37.7	42.3	32.2
120Sn	**32.99**	57.1	83.5	37.5	41.8	32.0
121Sb	**38.44**	49.1	71.2	32.5	35.0	29.1
133Cs	**41.64**	59.3	87.0	40.6	42.8	34.8
136Ba	**37.74**	56.1	77.8	39.5	43.7	32.7

Fe Internal Isotope	NIST 612 Pub. Conc.	Ap16A03	Ap16A04	Ap16B03	Ap16B04	Ap16C03
137Ba	**37.74**	54.1	78.4	38.7	43.6	32.1
139La	**35.77**	53.0	74.9	39.3	44.5	32.5
140Ce	**38.35**	56.7	81.6	39.7	44.3	33.4
141Pr	**37.16**	53.3	75.9	38.2	43.1	31.6
146Nd	**35.24**	51.4	72.9	36.2	42.7	31.3
147Sm	**36.72**	52.6	73.5	39.0	44.3	33.0
153Eu	**34.44**	52.7	72.8	38.6	44.0	32.7
155Gd	**36.95**	49.0	63.2	36.6	42.4	29.8
156Ce O	**0**	--	--	--	--	--
157Gd	**36.95**	48.7	67.5	37.1	42.1	30.3
159Tb	**35.92**	51.0	70.2	38.4	43.8	31.8
163Dy	**35.97**	47.3	64.9	36.1	41.4	30.0
165Ho	**37.87**	50.2	69.8	38.8	44.4	32.1
166Er	**37.43**	47.9	66.4	37.5	42.3	30.4
169Tm	**37.55**	47.9	65.5	36.2	41.3	30.0
172Yb	**39.95**	53.4	74.2	39.7	46.1	33.5
175Lu	**37.71**	48.8	66.4	37.1	41.9	30.7
178Hf	**34.77**	48.8	66.9	36.3	42.1	30.4
181Ta	**39.77**	44.0	61.0	33.0	37.3	27.8
182W	**39.55**	62.0	85.3	39.8	44.3	34.6
185Re	**8.12**	22.1	31.5	14.8	16.4	12.4
195Pt	**2.59**	4.1	5.9	2.6	2.8	2.4
197Au	**5.09**	7.4	10.4	4.8	5.3	4.1
205Tl	**15.07**	23.4	34.1	17.1	18.6	14.1
206Pb	**38.96**	59.1	82.7	37.4	40.9	33.6
207Pb	**38.96**	57.9	85.0	38.1	41.6	33.8
208Pb	**38.96**	58.7	83.4	37.1	39.7	33.5
209Bi	**29.84**	50.0	70.7	32.4	34.7	28.5
220Bkg	**0**	--	--	--	--	--
232Th	**37.23**	51.7	74.5	39.2	43.4	31.6
238U	**37.15**	58.0	84.4	35.2	39.9	30.1
254U O	**0**	--	--	--	--	--

Fe Internal Isotope	NIST 612 Pub. Conc.	Ap16C04	Ap16D03	Ap16D04	Ap16E03	Ap16E04
7Li	**41.54**	41.7	30.4	27.4	49.7	51.9
9Be	**37.73**	38.0	31.1	24.2	44.7	47.3
11B	**34.73**	48.7	36.3	30.6	56.4	61.7
23Na	**103700**	94373.7	79743.6	69523.9	118461.7	130058.8
25Mg	**77.44**	57.6	47.2	41.0	64.5	79.2
27Al	**11200**	10322.5	8487.7	7308.1	12139.9	13728.6
29Si	**336100**	320614.3	263148.5	226250.7	382866.3	430852.6
31P	**55.16**	32.6	26.6	22.8	41.9	46.5
33S	**16**	16.6	8.5	10.4	20.2	24.7
39K	**66.26**	80.9	61.3	51.8	101.2	113.0
43Ca	**85260**	74458.0	58900.8	49289.0	93432.5	112431.6
44Ca	**85260**	73355.8	57310.3	47888.3	90351.4	105588.4
45Sc	**41.05**	34.4	26.4	22.3	41.0	45.1
47Ti	**48.11**	33.7	27.1	21.7	42.9	45.7
51V	**39.22**	34.0	26.1	22.2	41.9	46.7
52Cr	**39.88**	32.3	32.9	33.6	40.5	44.3
53Cr	**39.88**	32.2	24.9	21.3	40.9	45.2
55Mn	**38.43**	34.2	26.6	23.2	41.4	45.3
57Fe	**56.33**	56.3	56.3	56.3	56.3	56.3
59Co	**35.26**	31.9	25.8	21.7	39.6	42.5
60Ni	**38.44**	36.2	30.6	24.0	44.0	49.1
62Ni	**38.44**	40.3	19.8	25.8	58.9	70.2
65Cu	**36.71**	33.7	28.2	25.2	43.2	45.4
66Zn	**37.92**	35.2	27.0	22.8	43.2	46.7
68Zn	**39.13**	39.5	30.6	25.6	47.0	50.0
69Ga	**36.24**	33.6	26.9	23.3	41.5	44.8
72Ge	**34.64**	35.3	27.6	23.8	44.7	47.5
75As	**37.33**	26.2	19.1	16.2	33.7	37.2
77Ar Cl	**0**	--	--	--	--	--
82Se	**--**	14.0	12.5	9.4	17.4	18.8
83Kr	**0**	--	--	--	--	--
85Rb	**31.63**	28.0	21.7	18.6	33.8	36.2
86Sr	**76.15**	70.8	54.2	47.6	82.9	85.1
88Sr	**120.67**	70.5	54.3	47.7	82.9	86.6
89Y	**38.25**	33.0	24.9	21.9	38.5	38.9
90Zr	**35.99**	34.5	25.7	22.5	39.6	39.8
93Nb	**38.06**	32.6	25.3	22.4	38.1	39.6
95Mo	**38.3**	30.4	24.0	20.6	38.4	41.3
103Rh	**0.896**	0.9	0.7	0.6	1.1	1.2
105Pd	**1.09**	1.1	0.8	0.9	1.4	1.5
107Ag	**21.92**	19.0	13.7	12.1	21.4	23.4
110Cd	**28.32**	25.1	19.7	16.0	31.0	32.2
111Cd	**28.32**	24.2	18.2	15.8	29.8	32.1
115In	**42.93**	32.0	25.6	22.1	38.6	41.6
118Sn	**37.96**	33.5	26.9	22.8	42.0	44.7
120Sn	**32.99**	32.9	25.5	22.8	41.4	44.2
121Sb	**38.44**	29.1	22.4	19.4	35.9	38.1
133Cs	**41.64**	35.2	27.9	23.7	44.5	47.2
136Ba	**37.74**	33.6	27.3	25.1	42.1	44.0

Fe Internal Isotope	NIST 612 Pub. Conc.	Ap16C04	Ap16D03	Ap16D04	Ap16E03	Ap16E04
137Ba	**37.74**	34.2	25.8	24.0	41.5	43.6
139La	**35.77**	34.9	26.6	23.6	41.0	42.2
140Ce	**38.35**	35.1	27.2	24.3	42.2	44.3
141Pr	**37.16**	33.6	26.1	23.4	40.3	41.6
146Nd	**35.24**	33.1	25.6	22.4	38.8	39.6
147Sm	**36.72**	34.5	26.1	23.3	42.8	41.8
153Eu	**34.44**	34.0	26.1	23.0	39.9	41.1
155Gd	**36.95**	31.5	24.3	21.5	36.7	38.5
156Ce O	**0**	--	--	--	--	--
157Gd	**36.95**	32.1	23.4	21.7	37.2	37.4
159Tb	**35.92**	33.6	25.1	22.2	38.8	38.9
163Dy	**35.97**	31.9	24.2	20.6	36.8	36.4
165Ho	**37.87**	33.8	25.4	22.4	39.1	39.5
166Er	**37.43**	32.3	24.0	21.3	37.2	37.6
169Tm	**37.55**	31.8	23.6	21.2	36.1	36.9
172Yb	**39.95**	35.4	26.6	23.7	40.9	41.8
175Lu	**37.71**	32.5	24.4	21.6	37.6	37.0
178Hf	**34.77**	32.3	24.4	21.5	37.1	37.9
181Ta	**39.77**	29.8	22.2	19.8	33.7	34.8
182W	**39.55**	35.2	28.4	24.6	45.6	48.0
185Re	**8.12**	13.3	10.3	9.0	17.0	17.5
195Pt	**2.59**	2.5	2.0	1.7	2.9	3.1
197Au	**5.09**	4.4	3.3	2.8	5.3	5.6
205Tl	**15.07**	13.7	10.5	9.2	16.7	18.1
206Pb	**38.96**	33.8	26.1	22.0	41.9	44.0
207Pb	**38.96**	33.3	26.0	22.2	40.9	44.2
208Pb	**38.96**	33.0	25.4	22.0	40.7	43.5
209Bi	**29.84**	28.8	21.9	18.9	34.2	36.6
220Bkg	**0**	--	--	--	--	--
232Th	**37.23**	33.1	25.9	23.5	39.8	40.1
238U	**37.15**	31.6	24.7	21.8	39.3	41.4
254U O	**0**	--	--	--	--	--

Fe Internal Isotope	NIST 612 Pub. Conc.	Count	Min	Max	Average	Sigma
7Li	**41.54**	10.0	27.4	97.0	50.5	19.6
9Be	**37.73**	10.0	24.2	82.4	45.6	15.7
11B	**34.73**	10.0	30.6	174.5	70.2	42.5
23Na	**103700**	10.0	69523.9	232911.9	118723.0	45446.4
25Mg	**77.44**	10.0	41.0	128.9	69.9	23.4
27Al	**11200**	10.0	7308.1	23331.2	12868.2	4382.7
29Si	**336100**	10.0	226250.7	789255.7	404789.9	154091.4
31P	**55.16**	10.0	22.8	87.8	43.6	18.0
33S	**16**	8.0	8.3	25.7	16.3	8.7
39K	**66.26**	9.0	51.8	268.8	106.9	65.9
43Ca	**85260**	10.0	49289.0	167920.8	95745.1	33223.5
44Ca	**85260**	10.0	47888.3	167478.5	93183.5	33211.6
45Sc	**41.05**	10.0	22.3	73.9	42.0	14.1
47Ti	**48.11**	10.0	21.7	92.4	45.4	19.0
51V	**39.22**	10.0	22.2	85.4	43.1	17.3
52Cr	**39.88**	10.0	31.8	82.8	43.7	15.1
53Cr	**39.88**	10.0	21.3	79.8	41.1	16.2
55Mn	**38.43**	10.0	23.2	82.1	42.8	16.0
57Fe	**56.33**	8.0	56.3	56.3	56.3	22.5
59Co	**35.26**	10.0	21.7	82.4	40.7	16.4
60Ni	**38.44**	10.0	24.0	91.0	46.0	18.0
62Ni	**38.44**	8.0	19.8	70.2	44.2	22.8
65Cu	**36.71**	10.0	25.2	84.6	44.3	16.8
66Zn	**37.92**	10.0	22.8	84.2	44.1	16.4
68Zn	**39.13**	10.0	25.6	94.0	48.4	18.2
69Ga	**36.24**	10.0	23.3	84.7	42.8	16.8
72Ge	**34.64**	10.0	23.8	85.4	44.3	16.8
75As	**37.33**	10.0	16.2	62.7	32.8	12.8
77Ar Cl	**0**	0.0	--	--	--	--
82Se	**--**	10.0	9.4	38.9	18.5	7.8
83Kr	**0**	0.0	--	--	--	--
85Rb	**31.63**	10.0	18.6	69.5	35.2	13.9
86Sr	**76.15**	10.0	47.6	158.0	84.5	29.4
88Sr	**120.67**	10.0	47.7	160.2	84.8	30.2
89Y	**38.25**	10.0	21.9	70.5	39.2	13.1
90Zr	**35.99**	10.0	22.5	74.0	40.5	13.7
93Nb	**38.06**	10.0	22.4	76.1	39.6	14.4
95Mo	**38.3**	10.0	20.6	77.1	38.7	15.4
103Rh	**0.896**	10.0	0.6	2.1	1.1	0.4
105Pd	**1.09**	10.0	0.8	2.4	1.3	0.5
107Ag	**21.92**	10.0	12.1	44.0	22.6	8.6
110Cd	**28.32**	10.0	16.0	56.7	30.4	10.9
111Cd	**28.32**	10.0	15.8	55.8	29.6	10.8
115In	**42.93**	10.0	22.1	79.9	40.4	15.7
118Sn	**37.96**	10.0	22.8	82.5	42.3	16.5
120Sn	**32.99**	10.0	22.8	83.5	41.9	16.7
121Sb	**38.44**	10.0	19.4	71.2	36.2	14.1
133Cs	**41.64**	10.0	23.7	87.0	44.3	17.2
136Ba	**37.74**	10.0	25.1	77.8	42.2	14.7

Fe Internal Isotope	NIST 612 Pub. Conc.	Count	Min	Max	Average	Sigma
137Ba	**37.74**	10.0	24.0	78.4	41.6	14.9
139La	**35.77**	10.0	23.6	74.9	41.3	13.9
140Ce	**38.35**	10.0	24.3	81.6	42.9	15.7
141Pr	**37.16**	10.0	23.4	75.9	40.7	14.3
146Nd	**35.24**	10.0	22.4	72.9	39.4	13.7
147Sm	**36.72**	10.0	23.3	73.5	41.1	13.6
153Eu	**34.44**	10.0	23.0	72.8	40.5	13.5
155Gd	**36.95**	10.0	21.5	63.2	37.3	11.6
156Ce O	**0**	0.0	--	--	--	--
157Gd	**36.95**	10.0	21.7	67.5	37.7	12.6
159Tb	**35.92**	10.0	22.2	70.2	39.4	13.0
163Dy	**35.97**	10.0	20.6	64.9	37.0	11.9
165Ho	**37.87**	10.0	22.4	69.8	39.6	12.8
166Er	**37.43**	10.0	21.3	66.4	37.7	12.2
169Tm	**37.55**	10.0	21.2	65.5	37.0	12.1
172Yb	**39.95**	10.0	23.7	74.2	41.5	13.7
175Lu	**37.71**	10.0	21.6	66.4	37.8	12.2
178Hf	**34.77**	10.0	21.5	66.9	37.8	12.3
181Ta	**39.77**	10.0	19.8	61.0	34.3	11.1
182W	**39.55**	10.0	24.6	85.3	44.8	16.9
185Re	**8.12**	10.0	9.0	31.5	16.4	6.2
195Pt	**2.59**	10.0	1.7	5.9	3.0	1.2
197Au	**5.09**	10.0	2.8	10.4	5.3	2.1
205Tl	**15.07**	10.0	9.2	34.1	17.5	6.7
206Pb	**38.96**	10.0	22.0	82.7	42.2	16.6
207Pb	**38.96**	10.0	22.2	85.0	42.3	17.1
208Pb	**38.96**	10.0	22.0	83.4	41.7	16.9
209Bi	**29.84**	10.0	18.9	70.7	35.7	14.2
220Bkg	**0**	0.0	--	--	--	--
232Th	**37.23**	10.0	23.5	74.5	40.3	13.9
238U	**37.15**	10.0	21.8	84.4	40.7	17.5
254U O	**0**	0.0	--	--	--	--

Scaled Isotope	NIST 612 Pub Data	Ap16A03	Ap16A04	Ap16B03	Ap16B04	Ap16C03
7Li	41.54	45.9	42.4	42.0	42.3	42.0
9Be	37.73	38.4	36.0	39.5	40.6	39.1
11B	34.73	79.1	76.3	55.6	53.7	48.4
23Na	103700	101196.4	101830.1	91917.1	93641.7	98784.1
25Mg	77.44	< DL	56.4	65.2	60.8	61.9
27Al	11200	10371.1	10200.5	11740.6	11790.7	10977.3
29Si	336100	343081.2	345066.0	339846.7	340610.8	344716.3
31P	55.16	38.2	38.4	35.3	38.6	36.0
33S	16	< DL	< DL	14.9	20.7	9.4
39K	66.26	< DL	< DL	100.6	80.1	86.4
44Ca	85260	76625.8	73222.3	88647.6	85807.1	75593.3
45Sc	41.05	34.0	32.3	39.3	39.6	36.0
47Ti	48.11	38.9	40.4	40.0	40.4	40.9
51V	39.22	38.9	40.4	36.5	34.4	36.8
53Cr	39.88	36.3	34.9	34.7	33.8	34.0
55Mn	38.43	36.2	35.9	37.8	35.3	37.7
57Fe	56.33	< DL	< DL	51.7	45.5	63.8
59Co	35.26	34.8	36.0	35.0	31.8	35.3
60Ni	38.44	39.7	39.8	37.2	37.4	41.2
65Cu	36.71	40.1	37.0	36.5	35.9	39.9
68Zn	37.92	40.7	41.1	43.3	37.4	44.9
69Ga	36.24	37.2	37.0	36.4	34.1	37.5
72Ge	34.64	38.2	37.3	37.6	34.7	39.7
75As	37.33	29.0	27.4	26.6	25.3	30.3
82Se		15.6	17.0	15.1	14.5	17.3
85Rb	31.63	30.9	30.4	29.9	28.7	31.1
88Sr	76.15	68.8	70.1	75.0	72.6	74.9
89Y	38.25	31.3	30.8	36.0	35.7	35.9
90Zr	35.99	32.2	32.4	36.9	36.5	37.3
93Nb	38.06	32.4	33.3	34.8	33.9	35.4
95Mo	38.3	33.3	33.7	32.1	30.9	33.6
103Rh	0.896	1.0	0.9	0.9	0.9	0.9
105Pd	1.09	1.2	1.0	0.9	0.9	1.1
107Ag	21.92	19.4	19.2	18.9	18.4	20.5
111Cd	28.32	25.1	24.4	25.3	22.8	27.6
115In	42.93	34.6	34.9	34.7	32.5	35.7
118Sn	37.96	37.4	36.1	34.6	34.1	36.5
121Sb	38.44	31.3	31.1	29.8	28.2	32.9
133Cs	41.64	37.8	38.1	37.3	34.6	39.4
137Ba	37.74	34.5	34.3	35.5	35.2	36.3
139La	35.77	33.7	32.8	36.0	35.9	36.8
140Ce	38.35	36.1	35.7	36.5	35.8	37.8
141Pr	37.16	33.9	33.2	35.1	34.8	35.8
146Nd	35.24	32.8	31.9	33.3	34.5	35.5
147Sm	36.72	33.5	32.1	35.8	35.8	37.4
153Eu	34.44	33.6	31.8	35.4	35.5	37.0
157Gd	36.95	31.0	29.5	34.1	34.0	34.3
159Tb	35.92	32.5	30.7	35.2	35.4	36.1
163Dy	35.97	30.1	28.4	33.2	33.4	34.0

Scaled Isotope	NIST 612 Pub Data	Ap16A03	Ap16A04	Ap16B03	Ap16B04	Ap16C03
165Ho	**37.87**	32.0	30.5	35.6	35.8	36.3
166Er	**37.43**	30.5	29.0	34.4	34.1	34.4
169Tm	**37.55**	30.5	28.6	33.2	33.4	34.0
172Yb	**39.95**	34.0	32.5	36.4	37.2	37.9
175Lu	**37.71**	31.1	29.0	34.0	33.8	34.7
178Hf	**34.77**	31.1	29.2	33.4	34.0	34.5
181Ta	**39.77**	28.1	26.7	30.3	30.1	31.5
182W	**39.55**	39.5	37.3	36.5	35.8	39.2
185Re	**8.12**	14.1	13.8	13.6	13.3	14.1
195Pt	**2.59**	2.6	2.6	2.4	2.2	2.7
197Au	**5.09**	4.7	4.5	4.4	4.3	4.7
205Tl	**15.07**	14.9	14.9	15.7	15.0	15.9
208Pb	**38.96**	37.4	36.5	34.1	32.1	38.0
209Bi	**29.84**	31.9	30.9	29.8	28.0	32.3
232Th	**37.23**	32.9	32.6	36.0	35.0	35.8
238U	**37.15**	37.0	36.9	32.3	32.2	34.1

Scaled Isotope	NIST 612 Pub Data	Ap16C04	Ap16D03	Ap16D04	Ap16E03	Ap16E04
7Li	**41.54**	44.5	39.5	41.6	43.9	40.7
9Be	**37.73**	40.5	40.4	36.6	39.5	37.1
11B	**34.73**	51.9	47.2	46.4	49.8	48.4
23Na	**103700**	100620.9	103731.9	105282.9	104713.0	102077.7
25Mg	**77.44**	61.4	61.4	62.1	57.0	62.1
27Al	**11200**	11005.8	11041.0	11066.9	10731.0	10775.0
29Si	**336100**	341838.0	342308.4	342620.7	338430.8	338158.2
31P	**55.16**	34.8	34.6	34.6	37.0	36.5
33S	**16**	17.7	11.0	15.7	17.8	19.4
39K	**66.26**	86.2	79.8	78.4	89.5	88.7
44Ca	**85260**	78211.7	74550.3	72519.2	79865.2	82871.9
45Sc	**41.05**	36.7	34.3	33.8	36.2	35.4
47Ti	**48.11**	35.9	35.2	32.9	38.0	35.8
51V	**39.22**	36.3	33.9	33.6	37.1	36.6
53Cr	**39.88**	34.3	32.3	32.2	36.2	35.5
55Mn	**38.43**	36.5	34.6	35.1	36.6	35.6
57Fe	**56.33**	60.1	73.3	85.3	49.8	44.2
59Co	**35.26**	34.0	33.6	32.9	35.0	33.4
60Ni	**38.44**	38.6	39.8	36.4	38.9	38.5
65Cu	**36.71**	35.9	36.7	38.2	38.2	35.6
68Zn	**37.92**	42.1	39.8	38.8	41.5	39.2
69Ga	**36.24**	35.8	35.0	35.3	36.7	35.1
72Ge	**34.64**	37.6	35.9	36.1	39.5	37.3
75As	**37.33**	28.0	24.8	24.5	29.8	29.2
82Se		14.9	16.3	14.3	15.4	14.7
85Rb	**31.63**	29.9	28.2	28.1	29.9	28.4
88Sr	**76.15**	75.2	70.6	72.2	73.3	67.9
89Y	**38.25**	35.2	32.4	33.2	34.1	30.5
90Zr	**35.99**	36.8	33.5	34.1	35.0	31.3
93Nb	**38.06**	34.8	32.9	33.9	33.7	31.1
95Mo	**38.3**	32.4	31.3	31.2	33.9	32.4
103Rh	**0.896**	0.9	0.9	0.9	1.0	0.9
105Pd	**1.09**	1.2	1.0	1.3	1.2	1.2
107Ag	**21.92**	20.3	17.8	18.4	18.9	18.4
111Cd	**28.32**	25.9	23.7	23.9	26.4	25.2
115In	**42.93**	34.1	33.3	33.4	34.1	32.6
118Sn	**37.96**	35.7	34.9	34.5	37.1	35.1
121Sb	**38.44**	31.0	29.1	29.3	31.7	29.9
133Cs	**41.64**	37.5	36.3	35.9	39.3	37.0
137Ba	**37.74**	36.5	33.5	36.3	36.7	34.2
139La	**35.77**	37.2	34.6	35.8	36.3	33.2
140Ce	**38.35**	37.4	35.4	36.8	37.3	34.7
141Pr	**37.16**	35.8	34.0	35.4	35.6	32.7
146Nd	**35.24**	35.2	33.4	34.0	34.3	31.0
147Sm	**36.72**	36.8	34.0	35.3	37.9	32.8
153Eu	**34.44**	36.2	34.0	34.8	35.3	32.3
157Gd	**36.95**	34.2	30.4	32.8	32.9	29.4
159Tb	**35.92**	35.8	32.6	33.6	34.3	30.5
163Dy	**35.97**	34.1	31.5	31.3	32.6	28.5

Scaled Isotope	NIST 612 Pub Data	Ap16C04	Ap16D03	Ap16D04	Ap16E03	Ap16E04
165Ho	**37.87**	36.0	33.1	33.9	34.6	31.0
166Er	**37.43**	34.4	31.2	32.3	32.9	29.5
169Tm	**37.55**	33.9	30.8	32.1	31.9	28.9
172Yb	**39.95**	37.8	34.6	35.9	36.1	32.8
175Lu	**37.71**	34.6	31.7	32.7	33.2	29.1
178Hf	**34.77**	34.4	31.8	32.6	32.8	29.7
181Ta	**39.77**	31.7	28.8	30.0	29.8	27.4
182W	**39.55**	37.6	37.0	37.3	40.3	37.7
185Re	**8.12**	14.2	13.4	13.6	15.0	13.7
195Pt	**2.59**	2.7	2.7	2.5	2.5	2.4
197Au	**5.09**	4.6	4.3	4.2	4.7	4.4
205Tl	**15.07**	14.6	13.7	14.0	14.7	14.2
208Pb	**38.96**	35.2	33.1	33.4	35.9	34.1
209Bi	**29.84**	30.7	28.5	28.6	30.2	28.7
232Th	**37.23**	35.3	33.7	35.5	35.1	31.4
238U	**37.15**	33.7	32.1	33.0	34.7	32.5

Scaled Isotope	NIST 612 Pub Data	Count	Min	Max	Average	Sigma
7Li	**41.54**	10.0	39.5	45.9	42.5	1.8
9Be	**37.73**	10.0	36.0	40.6	38.8	1.6
11B	**34.73**	10.0	46.4	79.1	55.7	11.4
23Na	**103700**	10.0	91917.1	105282.9	100379.6	4234.7
25Mg	**77.44**	9.0	56.4	65.2	60.9	18.4
27Al	**11200**	10.0	10200.5	11790.7	10970.0	482.6
29Si	**336100**	10.0	338158.2	345066.0	341667.7	2267.5
31P	**55.16**	10.0	34.6	38.6	36.4	1.5
33S	**16**	8.0	9.4	20.7	15.8	7.1
39K	**66.26**	8.0	78.4	100.6	86.2	35.0
44Ca	**85260**	10.0	72519.2	88647.6	78791.5	5174.6
45Sc	**41.05**	10.0	32.3	39.6	35.8	2.2
47Ti	**48.11**	10.0	32.9	40.9	37.8	2.6
51V	**39.22**	10.0	33.6	40.4	36.4	2.0
53Cr	**39.88**	10.0	32.2	36.3	34.4	1.3
55Mn	**38.43**	10.0	34.6	37.8	36.1	1.0
57Fe	**56.33**	8.0	44.2	85.3	59.2	26.6
59Co	**35.26**	10.0	31.8	36.0	34.2	1.2
60Ni	**38.44**	10.0	36.4	41.2	38.7	1.4
65Cu	**36.71**	10.0	35.6	40.1	37.4	1.5
68Zn	**37.92**	10.0	37.4	44.9	40.9	2.1
69Ga	**36.24**	10.0	34.1	37.5	36.0	1.1
72Ge	**34.64**	10.0	34.7	39.7	37.4	1.5
75As	**37.33**	10.0	24.5	30.3	27.5	2.0
82Se		10.0	14.3	17.3	15.5	1.0
85Rb	**31.63**	10.0	28.1	31.1	29.6	1.0
88Sr	**76.15**	10.0	67.9	75.2	72.0	2.5
89Y	**38.25**	10.0	30.5	36.0	33.5	2.0
90Zr	**35.99**	10.0	31.3	37.3	34.6	2.1
93Nb	**38.06**	10.0	31.1	35.4	33.6	1.2
95Mo	**38.3**	10.0	30.9	33.9	32.5	1.1
103Rh	**0.896**	10.0	0.9	1.0	0.9	0.0
105Pd	**1.09**	10.0	0.9	1.3	1.1	0.1
107Ag	**21.92**	10.0	17.8	20.5	19.0	0.8
111Cd	**28.32**	10.0	22.8	27.6	25.0	1.3
115In	**42.93**	10.0	32.5	35.7	34.0	1.0
118Sn	**37.96**	10.0	34.1	37.4	35.6	1.1
121Sb	**38.44**	10.0	28.2	32.9	30.5	1.3
133Cs	**41.64**	10.0	34.6	39.4	37.3	1.4
137Ba	**37.74**	10.0	33.5	36.7	35.3	1.1
139La	**35.77**	10.0	32.8	37.2	35.2	1.5
140Ce	**38.35**	10.0	34.7	37.8	36.4	0.9
141Pr	**37.16**	10.0	32.7	35.8	34.6	1.1
146Nd	**35.24**	10.0	31.0	35.5	33.6	1.3
147Sm	**36.72**	10.0	32.1	37.9	35.1	1.9
153Eu	**34.44**	10.0	31.8	37.0	34.6	1.6
157Gd	**36.95**	10.0	29.4	34.3	32.3	1.9
159Tb	**35.92**	10.0	30.5	36.1	33.7	1.9
163Dy	**35.97**	10.0	28.4	34.1	31.7	2.0

Scaled Isotope	NIST 612 Pub Data	Count	Min	Max	Average	Sigma
165Ho	**37.87**	10.0	30.5	36.3	33.9	2.0
166Er	**37.43**	10.0	29.0	34.4	32.3	2.0
169Tm	**37.55**	10.0	28.6	34.0	31.7	1.9
172Yb	**39.95**	10.0	32.5	37.9	35.5	1.9
175Lu	**37.71**	10.0	29.0	34.7	32.4	2.0
178Hf	**34.77**	10.0	29.2	34.5	32.3	1.8
181Ta	**39.77**	10.0	26.7	31.7	29.4	1.6
182W	**39.55**	10.0	35.8	40.3	37.8	1.4
185Re	**8.12**	10.0	13.3	15.0	13.9	0.5
195Pt	**2.59**	10.0	2.2	2.7	2.5	0.1
197Au	**5.09**	10.0	4.2	4.7	4.5	0.2
205Tl	**15.07**	10.0	13.7	15.9	14.8	0.7
208Pb	**38.96**	10.0	32.1	38.0	35.0	1.8
209Bi	**29.84**	10.0	28.0	32.3	30.0	1.4
232Th	**37.23**	10.0	31.4	36.0	34.4	1.5
238U	**37.15**	10.0	32.1	37.0	33.9	1.7

Si Internal Isotope	NIST 614 Pub. Conc.	Ap16A05	Ap16A06	Ap16B05	Ap16B06	Ap16C05
7Li		1.8	1.8	2.1	1.7	1.8
9Be		< DL	< DL	0.6	< DL	1.3
11B	1.3	32.5	31.6	21.6	18.1	17.1
23Na	103860	101485.4	108150.7	93468.8	104418.6	107422.9
25Mg		< DL	< DL	26.9	25.7	30.2
27Al	10585	10367.9	10383.0	10484.6	10329.5	10438.7
29Si	336553.2	336553.2	336553.2	336553.2	336553.2	336553.2
31P	30	11.6	10.9	11.8	11.9	9.8
33S		< DL	< DL	20.4	17.6	16.4
39K		< DL	< DL	70.8	77.4	93.7
43Ca	85764.1	72006.8	73433.7	76877.6	70924.3	87769.1
44Ca	85764.1	73530.2	74818.0	75955.3	70574.9	81675.5
45Sc	0.59	< DL	< DL	2.8	2.9	3.3
47Ti	3.1	< DL	< DL	3.8	4.1	4.5
51V		1.0	1.0	0.8	1.2	1.0
52Cr		< DL	< DL	2.6	1.7	1.3
53Cr		< DL	< DL	1.6	< DL	1.5
55Mn		1.3	1.3	1.2	1.4	1.3
57Fe	13.3	< DL	< DL	48.5	32.9	24.4
59Co	0.73	< DL	< DL	0.7	0.6	0.7
60Ni	0.95	< DL	< DL	4.0	1.9	3.9
62Ni	0.95	< DL	< DL	< DL	21.0	< DL
65Cu	1.37	< DL	< DL	3.7	4.1	2.9
66Zn		2.7	3.1	3.0	3.2	4.6
68Zn		5.8	5.9	6.7	6.6	7.9
69Ga		1.3	1.2	1.2	1.1	1.2
72Ge		1.0	1.3	0.6	1.0	1.1
75As		< DL	< DL	0.7	0.9	< DL
77Ar Cl		--	--	--	--	--
82Se		0.7	0.8	0.7	< DL	0.6
83Kr		--	--	--	--	--
85Rb	0.855	< DL	1.0	1.0	0.8	0.9
86Sr	45.8	40.9	41.7	39.7	38.9	40.7
88Sr	45.8	40.5	42.7	40.2	39.4	42.3
89Y		0.6	0.7	0.6	0.6	0.7
90Zr		0.8	0.9	0.9	0.7	0.9
93Nb		0.6	0.7	0.7	0.6	0.7
95Mo		0.7	0.8	0.7	0.5	0.9
103Rh	1.67	1.6	1.6	1.7	1.7	1.7
105Pd	1.98	2.1	2.2	2.2	2.4	2.7
107Ag	0.42	0.5	0.4	0.4	0.5	0.4
110Cd	0.55	2.3	2.5	2.1	2.1	2.7
111Cd	0.55	< DL	0.7	0.6	0.4	0.4
115In		0.7	0.8	0.7	0.7	0.7
118Sn		3.0	3.1	2.7	3.2	2.8
120Sn		3.0	3.1	2.5	2.7	2.6
121Sb	1.06	0.7	0.7	0.7	0.6	0.7
133Cs		0.6	0.7	0.6	0.6	0.6
136Ba		3.1	2.9	2.7	3.0	2.9
137Ba		3.0	3.2	3.0	2.9	2.8

Si Internal Isotope	NIST 614 Pub. Conc.	Ap16A05	Ap16A06	Ap16B05	Ap16B06	Ap16C05
139La	0.83	0.7	0.7	0.7	0.6	0.7
140Ce		0.7	0.8	0.7	0.7	0.7
141Pr		0.7	0.7	0.6	0.7	0.7
146Nd		0.6	0.7	0.6	0.5	1.2
147Sm		0.7	0.8	0.9	0.7	0.7
153Eu	0.99	0.7	0.8	0.7	0.7	0.8
155Gd		< DL	< DL	1.0	0.6	0.7
156Ce O		--	--	--	--	--
157Gd		0.6	0.9	0.6	0.8	1.4
159Tb		0.6	0.7	0.6	0.6	0.6
163Dy		0.7	0.8	0.6	0.6	0.6
165Ho		0.6	0.7	0.6	0.7	0.6
166Er		0.6	0.6	0.6	0.5	0.6
169Tm		0.6	0.7	0.6	0.5	0.6
172Yb		0.7	0.7	0.7	0.6	0.6
175Lu		0.6	0.7	0.6	0.6	0.6
178Hf		0.6	0.6	0.6	0.7	0.6
181Ta		0.6	0.6	0.6	0.5	0.6
182W		0.8	0.9	0.8	0.7	0.8
185Re	0.179	0.4	0.4	0.4	0.3	0.5
195Pt	2.26	2.6	2.6	2.3	2.3	2.6
197Au	0.5	0.5	0.5	0.4	0.5	0.6
205Tl	0.269	0.3	0.3	0.3	0.3	0.3
206Pb	2.32	2.8	3.2	2.5	2.8	3.0
207Pb	2.32	2.8	2.9	2.3	2.5	2.9
208Pb	2.32	2.7	3.3	2.3	2.5	2.7
209Bi		0.6	0.7	0.6	0.6	0.6
220Bkg		--	--	--	--	--
232Th	0.748	0.8	0.8	0.6	0.6	0.6
238U	0.823	0.9	0.9	0.7	0.8	0.8
254U O		--	--	--	--	--

Si Internal Isotope	NIST 614 Pub. Conc.	Ap16C06	Ap16D05	Ap16D06	Ap16E05	Ap16E06
7Li		1.9	1.5	1.9	1.9	1.6
9Be		< DL	< DL	0.8	1.3	0.8
11B	1.3	16.6	15.1	16.6	15.1	14.5
23Na	103860	104653.3	106229.3	108265.8	100316.7	97775.5
25Mg		27.5	35.4	36.2	31.4	35.6
27Al	10585	10134.8	11172.5	10966.9	10265.1	10512.3
29Si	336553.2	336553.2	336553.2	336553.2	336553.2	336553.2
31P	30	11.6	10.7	12.1	9.2	12.8
33S		17.5	13.1	15.2	21.6	20.2
39K		66.8	61.7	83.4	70.6	86.8
43Ca	85764.1	81916.2	69130.2	82860.1	84941.8	80130.0
44Ca	85764.1	77638.2	67620.9	77184.7	76941.4	75096.0
45Sc	0.59	2.8	2.2	3.4	2.6	2.5
47Ti	3.1	< DL	6.0	3.1	3.5	2.0
51V		1.1	0.8	0.9	0.9	1.0
52Cr		1.8	1.2	1.8	38.4	2.1
53Cr		1.1	1.0	1.4	< DL	1.1
55Mn		1.5	1.2	1.3	1.2	1.2
57Fe	13.3	24.6	< DL	22.4	< DL	32.6
59Co	0.73	0.5	0.6	0.6	0.8	0.7
60Ni	0.95	3.1	3.5	< DL	< DL	2.5
62Ni	0.95	< DL	< DL	< DL	< DL	< DL
65Cu	1.37	3.3	4.8	5.0	3.5	5.1
66Zn		3.1	3.4	3.3	3.5	3.6
68Zn		7.1	6.6	7.6	7.2	6.3
69Ga		1.2	1.2	1.2	1.2	1.2
72Ge		0.8	0.9	1.1	0.8	0.8
75As		0.4	0.4	1.6	1.1	< DL
77Ar Cl		--	--	--	--	--
82Se		< DL	0.8	< DL	< DL	1.8
83Kr		--	--	--	--	--
85Rb	0.855	0.9	0.8	0.8	0.7	0.9
86Sr	45.8	39.4	40.2	40.3	38.9	38.8
88Sr	45.8	40.1	41.2	40.5	39.3	39.9
89Y		0.6	0.6	0.7	0.6	0.6
90Zr		0.8	0.9	0.8	1.0	0.8
93Nb		0.7	0.7	0.7	0.7	0.6
95Mo		0.7	0.7	0.7	0.7	0.9
103Rh	1.67	1.7	1.6	1.6	1.6	1.6
105Pd	1.98	2.3	2.1	2.1	2.6	2.0
107Ag	0.42	0.5	0.3	0.4	0.3	0.5
110Cd	0.55	2.5	2.0	2.0	2.0	1.9
111Cd	0.55	0.4	3.0	0.3	0.5	0.4
115In		0.7	0.7	0.7	0.7	0.6
118Sn		2.7	2.5	2.9	2.6	2.9
120Sn		2.6	2.5	2.9	2.6	2.6
121Sb	1.06	0.7	0.7	0.7	0.7	0.7
133Cs		0.7	0.6	0.6	0.6	0.6
136Ba		3.0	2.6	3.1	2.4	3.1
137Ba		3.2	2.9	3.0	2.3	3.0

Si Internal Isotope	NIST 614 Pub. Conc.	Ap16C06	Ap16D05	Ap16D06	Ap16E05	Ap16E06
139La	0.83	0.6	0.7	0.7	0.6	0.6
140Ce		0.7	0.7	0.8	0.7	0.7
141Pr		0.7	0.7	0.7	0.6	0.7
146Nd		0.4	0.7	0.9	0.6	0.8
147Sm		0.6	0.7	0.7	0.6	0.7
153Eu	0.99	0.7	0.8	0.7	0.7	0.7
155Gd		0.9	0.4	0.7	< DL	0.7
156Ce O		--	--	--	--	--
157Gd		0.4	0.4	0.5	0.5	0.7
159Tb		0.6	0.6	0.7	0.6	0.7
163Dy		0.5	0.6	0.7	0.5	0.6
165Ho		0.6	0.7	0.7	0.6	0.7
166Er		0.6	0.6	0.5	0.6	0.6
169Tm		0.5	0.6	0.5	0.5	0.6
172Yb		0.6	0.6	0.7	0.6	0.6
175Lu		0.5	0.6	0.6	0.5	0.5
178Hf		0.6	0.6	0.7	0.5	0.7
181Ta		0.6	0.6	0.5	0.5	0.6
182W		0.8	0.8	0.8	0.8	0.8
185Re	0.179	0.3	0.3	0.3	0.4	0.3
195Pt	2.26	2.4	2.3	2.5	2.5	2.4
197Au	0.5	0.5	0.4	0.5	0.5	0.5
205Tl	0.269	0.3	0.3	0.3	0.3	0.2
206Pb	2.32	2.6	2.6	2.7	2.6	2.7
207Pb	2.32	2.6	2.3	2.8	2.5	2.5
208Pb	2.32	2.6	2.3	2.6	2.5	2.5
209Bi		0.6	0.6	0.6	0.6	0.6
220Bkg		--	--	--	--	--
232Th	0.748	0.6	0.7	0.6	0.6	0.7
238U	0.823	0.8	0.7	0.7	0.8	0.7
254U O		--	--	--	--	--

Si Internal Isotope	NIST 614 Pub. Conc.	Count	Min	Max	Average	Sigma
7Li		10	1.5	2.1	1.8	0.5404859
9Be		5	0.6	1.3	1.0	0.5136588
11B	1.3	11	1.3	32.5	18.2	9.2352891
23Na	103860	11	93468.8	108265.8	103277.0	28858.589
25Mg		8	25.7	36.2	31.1	14.257947
27Al	10585	11	10134.8	11172.5	10512.7	2918.8551
29Si	336553.2	11	336553.2	336553.2	336553.2	93018.391
31P	30	11	9.2	30.0	12.9	6.3518569
33S		8	13.1	21.6	17.8	8.2333168
39K		8	61.7	93.7	76.4	35.110189
43Ca	85764.1	11	69130.2	87769.1	78704.9	22559.105
44Ca	85764.1	11	67620.9	85764.1	76072.7	21496.545
45Sc	0.59	9	0.6	3.4	2.6	1.3018315
47Ti	3.1	8	2.0	6.0	3.7	1.9821224
51V		10	0.8	1.2	1.0	0.2974479
52Cr		8	1.2	38.4	6.4	10.726691
53Cr		6	1.0	1.6	1.3	0.6572339
55Mn		10	1.2	1.5	1.3	0.3778937
57Fe	13.3	7	13.3	48.5	28.4	16.038916
59Co	0.73	9	0.5	0.8	0.6	0.2847304
60Ni	0.95	7	1.0	4.0	2.8	1.6125795
62Ni	0.95	2	1.0	21.0	11.0	5.7899032
65Cu	1.37	9	1.4	5.1	3.7	1.8881068
66Zn		10	2.7	4.6	3.3	1.0620745
68Zn		10	5.8	7.9	6.8	2.0415201
69Ga		10	1.1	1.3	1.2	0.3487063
72Ge		10	0.6	1.3	1.0	0.3250744
75As		6	0.4	1.6	0.8	0.5182216
77Ar Cl		0	0.0	0.0	- -	0
82Se		6	0.6	1.8	0.9	0.5259302
83Kr		0	0.0	0.0	- -	0
85Rb	0.855	10	0.7	1.0	0.9	0.3285298
86Sr	45.8	11	38.8	45.8	40.5	11.334191
88Sr	45.8	11	39.3	45.8	41.1	11.486742
89Y		10	0.6	0.7	0.6	0.1853515
90Zr		10	0.7	1.0	0.8	0.2528491
93Nb		10	0.6	0.7	0.7	0.2012624
95Mo		10	0.5	0.9	0.7	0.2277878
103Rh	1.67	11	1.6	1.7	1.6	0.4573447
105Pd	1.98	11	2.0	2.7	2.2	0.6477904
107Ag	0.42	11	0.3	0.5	0.4	0.1332686
110Cd	0.55	11	0.6	2.7	2.1	0.7635892
111Cd	0.55	10	0.3	3.0	0.7	0.7422944
115In		10	0.6	0.8	0.7	0.20469
118Sn		10	2.5	3.2	2.8	0.8359243
120Sn		10	2.5	3.1	2.7	0.8044787
121Sb	1.06	11	0.6	1.1	0.7	0.2275556
133Cs		10	0.6	0.7	0.6	0.1774742
136Ba		10	2.4	3.1	2.9	0.8532745
137Ba		10	2.3	3.2	2.9	0.8723366

Si Internal Isotope	NIST 614 Pub. Conc.	Count	Min	Max	Average	Sigma
139La	0.83	11	0.6	0.8	0.7	0.1997304
140Ce		10	0.7	0.8	0.7	0.2140445
141Pr		10	0.6	0.7	0.7	0.2001882
146Nd		10	0.4	1.2	0.7	0.2869852
147Sm		10	0.6	0.9	0.7	0.2202395
153Eu	0.99	11	0.7	1.0	0.8	0.2228008
155Gd		7	0.4	1.0	0.7	0.3691903
156Ce O		0	0.0	0.0	- -	0
157Gd		10	0.4	1.4	0.7	0.3272277
159Tb		10	0.6	0.7	0.6	0.1828926
163Dy		10	0.5	0.8	0.6	0.2008995
165Ho		10	0.6	0.7	0.7	0.1902598
166Er		10	0.5	0.6	0.6	0.175863
169Tm		10	0.5	0.7	0.6	0.1736057
172Yb		10	0.6	0.7	0.7	0.1938806
175Lu		10	0.5	0.7	0.6	0.1748007
178Hf		10	0.5	0.7	0.6	0.1807618
181Ta		10	0.5	0.6	0.6	0.1680178
182W		10	0.7	0.9	0.8	0.2283587
185Re	0.179	11	0.2	0.5	0.3	0.1202829
195Pt	2.26	11	2.3	2.6	2.4	0.6778766
197Au	0.5	11	0.4	0.6	0.5	0.1490949
205Tl	0.269	11	0.2	0.3	0.3	0.0798981
206Pb	2.32	11	2.3	3.2	2.7	0.7795342
207Pb	2.32	11	2.3	2.9	2.6	0.7450647
208Pb	2.32	11	2.3	3.3	2.6	0.7530851
209Bi		10	0.6	0.7	0.6	0.1786277
220Bkg		0	0.0	0.0	- -	0
232Th	0.748	11	0.6	0.8	0.7	0.1956063
238U	0.823	11	0.7	0.9	0.8	0.2242382
254U O		0	0.0	0.0	- -	0

Ca Internal Isotope	NIST 614 Pub. Conc.	Ap16A05	Ap16A06	Ap16B05	Ap16B06	Ap16C05
7Li		2.1	2.1	2.3	2.1	1.9
9Be		< DL	< DL	0.7	< DL	1.4
11B	1.3	37.9	36.2	24.4	22.0	18.0
23Na	103860	118370.5	123973.6	105539.3	126891.7	112800.3
25Mg		< DL	< DL	30.3	31.2	31.7
27Al	10585	12092.9	11902.1	11838.5	12552.7	10961.2
29Si	336553.2	392548.7	385792.1	380015.4	408986.7	353400.6
31P	30	13.5	12.5	13.3	14.5	10.3
33S		< DL	< DL	23.0	21.4	17.2
39K		< DL	< DL	80.0	94.0	98.3
43Ca	85764.1	83987.2	84177.3	86805.5	86188.8	92162.7
44Ca	85764.1	85764.1	85764.1	85764.1	85764.1	85764.1
45Sc	0.59	< DL	< DL	3.2	3.5	3.5
47Ti	3.1	< DL	< DL	4.2	5.0	4.7
51V		1.1	1.1	0.9	1.4	1.0
52Cr		< DL	< DL	2.9	2.0	1.4
53Cr		< DL	< DL	1.8	< DL	1.5
55Mn		1.6	1.4	1.4	1.6	1.4
57Fe	13.3	< DL	< DL	54.8	40.0	25.6
59Co	0.73	< DL	< DL	0.7	0.7	0.7
60Ni	0.95	< DL	< DL	4.5	2.3	4.1
62Ni	0.95	< DL	< DL	< DL	25.5	< DL
65Cu	1.37	< DL	< DL	4.2	5.0	3.0
66Zn		3.2	3.6	3.4	3.9	4.8
68Zn		6.8	6.8	7.6	8.0	8.3
69Ga		1.5	1.4	1.3	1.3	1.2
72Ge		1.1	1.5	0.7	1.2	1.1
75As		< DL	< DL	0.8	1.1	< DL
77Ar Cl		--	--	--	--	--
82Se		0.8	0.9	0.7	< DL	0.7
83Kr		--	--	--	--	--
85Rb	0.855	< DL	1.2	1.1	1.0	0.9
86Sr	45.8	47.8	47.8	44.8	47.2	42.7
88Sr	45.8	47.2	48.9	45.4	47.8	44.5
89Y		0.8	0.8	0.6	0.7	0.7
90Zr		0.9	1.0	1.0	0.9	0.9
93Nb		0.7	0.8	0.8	0.8	0.8
95Mo		0.9	0.9	0.8	0.7	0.9
103Rh	1.67	1.9	1.8	1.9	2.1	1.8
105Pd	1.98	2.5	2.5	2.5	2.9	2.8
107Ag	0.42	0.6	0.5	0.4	0.6	0.5
110Cd	0.55	2.7	2.8	2.4	2.5	2.8
111Cd	0.55	< DL	0.8	0.7	0.5	0.5
115In		0.8	0.9	0.8	0.8	0.8
118Sn		3.5	3.5	3.0	3.9	2.9
120Sn		3.4	3.6	2.9	3.3	2.8
121Sb	1.06	0.8	0.8	0.8	0.8	0.8
133Cs		0.7	0.8	0.7	0.7	0.6
136Ba		3.6	3.3	3.1	3.6	3.1
137Ba		3.5	3.7	3.4	3.6	2.9

Ca Internal Isotope	NIST 614 Pub. Conc.	Ap16A05	Ap16A06	Ap16B05	Ap16B06	Ap16C05
139La	0.83	0.8	0.8	0.8	0.7	0.7
140Ce		0.8	1.0	0.8	0.9	0.8
141Pr		0.8	0.9	0.7	0.9	0.8
146Nd		0.8	0.8	0.7	0.6	1.3
147Sm		0.8	0.9	1.0	0.9	0.7
153Eu	0.99	0.8	0.9	0.8	0.8	0.8
155Gd		< DL	< DL	1.1	0.7	0.7
156Ce O		--	--	--	--	--
157Gd		0.7	1.0	0.7	0.9	1.5
159Tb		0.7	0.8	0.7	0.8	0.7
163Dy		0.8	1.0	0.7	0.7	0.6
165Ho		0.8	0.8	0.7	0.8	0.6
166Er		0.7	0.7	0.7	0.6	0.7
169Tm		0.7	0.8	0.7	0.7	0.7
172Yb		0.8	0.8	0.8	0.8	0.7
175Lu		0.7	0.8	0.7	0.8	0.6
178Hf		0.7	0.7	0.6	0.8	0.6
181Ta		0.7	0.7	0.6	0.7	0.6
182W		0.9	1.0	0.9	0.8	0.8
185Re	0.179	0.5	0.5	0.4	0.4	0.5
195Pt	2.26	3.0	3.0	2.6	2.8	2.7
197Au	0.5	0.6	0.6	0.5	0.6	0.7
205Tl	0.269	0.3	0.4	0.3	0.3	0.3
206Pb	2.32	3.3	3.6	2.8	3.4	3.1
207Pb	2.32	3.2	3.3	2.6	3.0	3.0
208Pb	2.32	3.2	3.8	2.6	3.1	2.8
209Bi		0.7	0.8	0.6	0.7	0.6
220Bkg		--	--	--	--	--
232Th	0.748	0.9	0.9	0.7	0.7	0.7
238U	0.823	1.0	1.0	0.8	0.9	0.8
254U O		--	--	--	--	--

Ca Internal Isotope	NIST 614 Pub. Conc.	Ap16C06	Ap16D05	Ap16D06	Ap16E05	Ap16E06
7Li		2.1	1.9	2.1	2.1	1.9
9Be		< DL	< DL	0.9	1.4	0.9
11B	1.3	18.4	19.2	18.5	16.9	16.6
23Na	103860	115606.8	134731.5	120299.9	111819.7	111665.5
25Mg		30.3	45.0	40.2	35.0	40.6
27Al	10585	11195.6	14170.1	12185.9	11442.1	12005.6
29Si	336553.2	371778.2	426853.1	373962.2	375144.9	384364.0
31P	30	12.9	13.6	13.4	10.3	14.6
33S		19.3	16.6	16.9	24.1	23.1
39K		73.8	78.3	92.7	78.7	99.1
43Ca	85764.1	90489.9	87678.4	92070.3	94681.8	91513.3
44Ca	85764.1	85764.1	85764.1	85764.1	85764.1	85764.1
45Sc	0.59	3.1	2.7	3.8	2.9	2.9
47Ti	3.1	1.8	7.6	3.4	3.9	2.3
51V		1.2	1.0	1.0	1.0	1.1
52Cr		2.0	1.5	2.0	42.9	2.4
53Cr		1.2	1.3	1.6	< DL	1.3
55Mn		1.6	1.6	1.4	1.3	1.4
57Fe	13.3	27.2	< DL	24.9	< DL	37.2
59Co	0.73	0.6	0.7	0.7	0.9	0.8
60Ni	0.95	3.5	4.5	< DL	< DL	2.9
62Ni	0.95	< DL	< DL	< DL	< DL	< DL
65Cu	1.37	3.6	6.1	5.5	3.9	5.8
66Zn		3.5	4.3	3.7	3.9	4.1
68Zn		7.9	8.4	8.4	8.0	7.2
69Ga		1.3	1.5	1.3	1.4	1.4
72Ge		0.9	1.2	1.3	0.9	1.0
75As		0.4	0.5	1.7	1.2	< DL
77Ar Cl		--	--	--	--	--
82Se		< DL	1.0	< DL	< DL	2.0
83Kr		--	--	--	--	--
85Rb	0.855	0.9	1.0	0.9	0.8	1.0
86Sr	45.8	43.5	51.0	44.8	43.3	44.3
88Sr	45.8	44.3	52.3	45.0	43.8	45.5
89Y		0.7	0.8	0.8	0.7	0.7
90Zr		0.9	1.1	0.9	1.1	0.9
93Nb		0.7	0.8	0.7	0.8	0.7
95Mo		0.7	0.9	0.8	0.8	1.0
103Rh	1.67	1.9	2.1	1.7	1.8	1.8
105Pd	1.98	2.5	2.7	2.3	2.8	2.3
107Ag	0.42	0.5	0.4	0.5	0.4	0.5
110Cd	0.55	2.8	2.6	2.2	2.2	2.2
111Cd	0.55	0.4	3.8	0.3	0.6	0.5
115In		0.8	0.8	0.8	0.7	0.7
118Sn		3.0	3.2	3.2	2.9	3.3
120Sn		2.8	3.2	3.2	2.9	3.0
121Sb	1.06	0.7	0.9	0.8	0.8	0.8
133Cs		0.7	0.8	0.7	0.6	0.7
136Ba		3.3	3.3	3.4	2.7	3.5
137Ba		3.5	3.7	3.3	2.6	3.4

Ca Internal Isotope	NIST 614 Pub. Conc.	Ap16C06	Ap16D05	Ap16D06	Ap16E05	Ap16E06
139La	0.83	0.6	0.9	0.7	0.7	0.7
140Ce		0.7	0.9	0.9	0.8	0.8
141Pr		0.8	0.9	0.8	0.7	0.8
146Nd		0.4	0.9	1.0	0.7	0.9
147Sm		0.7	0.9	0.8	0.7	0.8
153Eu	0.99	0.8	1.0	0.8	0.8	0.8
155Gd		1.0	0.6	0.7	< DL	0.8
156Ce O		--	--	--	--	--
157Gd		0.5	0.5	0.6	0.6	0.8
159Tb		0.7	0.8	0.7	0.7	0.8
163Dy		0.6	0.8	0.8	0.6	0.6
165Ho		0.7	0.8	0.8	0.7	0.8
166Er		0.6	0.8	0.5	0.6	0.7
169Tm		0.6	0.7	0.6	0.6	0.7
172Yb		0.7	0.8	0.8	0.6	0.7
175Lu		0.6	0.7	0.7	0.6	0.6
178Hf		0.6	0.7	0.8	0.6	0.8
181Ta		0.6	0.8	0.6	0.6	0.7
182W		0.9	1.0	0.9	0.9	0.9
185Re	0.179	0.4	0.4	0.4	0.4	0.3
195Pt	2.26	2.6	2.9	2.7	2.8	2.7
197Au	0.5	0.5	0.5	0.5	0.6	0.6
205Tl	0.269	0.3	0.3	0.3	0.3	0.3
206Pb	2.32	2.9	3.3	3.0	2.9	3.1
207Pb	2.32	2.9	2.9	3.2	2.8	2.9
208Pb	2.32	2.8	2.9	2.8	2.8	2.8
209Bi		0.7	0.8	0.7	0.7	0.6
220Bkg		--	--	--	--	--
232Th	0.748	0.7	0.9	0.7	0.7	0.7
238U	0.823	0.9	0.9	0.8	0.9	0.8
254U O		--	--	--	--	--

Ca Internal Isotope	NIST 614 Pub. Conc.	Count	Min	Max	Average	Sigma
7Li		10	1.9	2.3	2.1	0.6092097
9Be		5	0.7	1.4	1.1	0.5617573
11B	1.3	11	1.3	37.9	20.8	10.717126
23Na	103860	11	103860.0	134731.5	116869.0	33382.257
25Mg		8	30.3	45.0	35.5	16.461877
27Al	10585	11	10585.0	14170.1	11902.9	3402.2292
29Si	336553.2	11	336553.2	426853.1	380854.5	107596.02
31P	30	11	10.3	30.0	14.4	6.3108516
33S		8	16.6	24.1	20.2	9.3281695
39K		8	73.8	99.1	86.9	39.526477
43Ca	85764.1	11	83987.2	94681.8	88683.6	24735.012
44Ca	85764.1	11	85764.1	85764.1	85764.1	23703.945
45Sc	0.59	9	0.6	3.8	2.9	1.4696103
47Ti	3.1	9	1.8	7.6	4.0	2.2252093
51V		10	0.9	1.4	1.1	0.3438601
52Cr		8	1.4	42.9	7.1	11.948545
53Cr		6	1.2	1.8	1.4	0.7354272
55Mn		10	1.3	1.6	1.5	0.4363055
57Fe	13.3	7	13.3	54.8	31.9	18.333103
59Co	0.73	9	0.6	0.9	0.7	0.3161964
60Ni	0.95	7	1.0	4.5	3.2	1.8433448
62Ni	0.95	2	1.0	25.5	13.2	7.0388322
65Cu	1.37	9	1.4	6.1	4.3	2.226319
66Zn		10	3.2	4.8	3.8	1.181279
68Zn		10	6.8	8.4	7.7	2.2921235
69Ga		10	1.2	1.5	1.4	0.4023859
72Ge		10	0.7	1.5	1.1	0.3742272
75As		6	0.4	1.7	1.0	0.5837196
77Ar Cl		0	0.0	0.0	- -	0
82Se		6	0.7	2.0	1.0	0.6057136
83Kr		0	0.0	0.0	- -	0
85Rb	0.855	10	0.8	1.2	1.0	0.3725672
86Sr	45.8	11	42.7	51.0	45.7	12.841745
88Sr	45.8	11	43.8	52.3	46.4	13.031228
89Y		10	0.6	0.8	0.7	0.2123516
90Zr		10	0.9	1.1	1.0	0.2906331
93Nb		10	0.7	0.8	0.8	0.2292871
95Mo		10	0.7	1.0	0.8	0.2574477
103Rh	1.67	11	1.7	2.1	1.9	0.5252493
105Pd	1.98	11	2.0	2.9	2.5	0.7388672
107Ag	0.42	11	0.4	0.6	0.5	0.1531308
110Cd	0.55	11	0.6	2.8	2.3	0.8725303
111Cd	0.55	10	0.3	3.8	0.9	0.9500843
115In		10	0.7	0.9	0.8	0.2336582
118Sn		10	2.9	3.9	3.2	0.9733587
120Sn		10	2.8	3.6	3.1	0.9309116
121Sb	1.06	11	0.7	1.1	0.8	0.242578
133Cs		10	0.6	0.8	0.7	0.2045871
136Ba		10	2.7	3.6	3.3	0.9811883
137Ba		10	2.6	3.7	3.4	1.0160014

Ca Internal Isotope	NIST 614 Pub. Conc.	Count	Min	Max	Average	Sigma
139La	0.83	11	0.6	0.9	0.8	0.2263644
140Ce		10	0.7	1.0	0.8	0.2481851
141Pr		10	0.7	0.9	0.8	0.2321838
146Nd		10	0.4	1.3	0.8	0.3096473
147Sm		10	0.7	1.0	0.8	0.2567068
153Eu	0.99	11	0.8	1.0	0.8	0.2436259
155Gd		7	0.6	1.1	0.8	0.4136614
156Ce O		0	0.0	0.0	- -	0
157Gd		10	0.5	1.5	0.8	0.3483393
159Tb		10	0.7	0.8	0.7	0.2126514
163Dy		10	0.6	1.0	0.7	0.2349106
165Ho		10	0.6	0.8	0.7	0.2235302
166Er		10	0.5	0.8	0.7	0.2017732
169Tm		10	0.6	0.8	0.7	0.2006584
172Yb		10	0.6	0.8	0.8	0.2239294
175Lu		10	0.6	0.8	0.7	0.2041751
178Hf		10	0.6	0.8	0.7	0.2101495
181Ta		10	0.6	0.8	0.7	0.1958593
182W		10	0.8	1.0	0.9	0.2625893
185Re	0.179	11	0.2	0.5	0.4	0.1375227
195Pt	2.26	11	2.3	3.0	2.7	0.7779548
197Au	0.5	11	0.5	0.7	0.6	0.164166
205Tl	0.269	11	0.3	0.4	0.3	0.0916185
206Pb	2.32	11	2.3	3.6	3.1	0.907845
207Pb	2.32	11	2.3	3.3	2.9	0.8487095
208Pb	2.32	11	2.3	3.8	2.9	0.8671813
209Bi		10	0.6	0.8	0.7	0.2075411
220Bkg		0	0.0	0.0	- -	0
232Th	0.748	11	0.7	0.9	0.8	0.2252872
238U	0.823	11	0.8	1.0	0.9	0.254935
254U O		0	0.0	0.0	- -	0

Fe Internal Isotope	NIST 614 Pub. Conc.	Ap16A05	Ap16A06	Ap16B05	Ap16B06	Ap16C05
7Li		94.5	1.4	0.6	0.7	1.0
9Be		36.7	< DL	< DL	< DL	0.7
11B	1.3	1687.7	23.8	5.9	7.3	9.3
23Na	103860	5275602.2	81550.0	25625.2	42172.3	58584.5
25Mg		993.4	< DL	7.4	10.4	16.4
27Al	10585	538961.8	7829.2	2874.4	4171.9	5692.9
29Si	336553.2	17495329.9	253774.6	92268.5	135926.2	183543.8
31P	30	603.3	8.2	3.2	4.8	5.4
33S		959.6	< DL	< DL	< DL	9.0
39K		3131.2	< DL	19.4	31.2	51.1
43Ca	85764.1	3743188.6	55371.9	21076.6	28644.7	47866.1
44Ca	85764.1	3822382.5	56415.7	20823.7	28503.6	44542.9
45Sc	0.59	139.6	< DL	0.8	1.2	1.8
47Ti	3.1	134.9	< DL	< DL	< DL	2.5
51V		50.4	0.7	0.2	0.5	0.5
52Cr		76.1	< DL	0.7	0.7	< DL
53Cr		61.4	< DL	< DL	< DL	< DL
55Mn		69.7	0.9	0.3	0.5	0.7
57Fe	13.3	< DL	< DL	< DL	< DL	< DL
59Co	0.73	37.6	< DL	0.2	0.2	0.4
60Ni	0.95	115.1	< DL	< DL	< DL	2.1
62Ni	0.95	< DL	< DL	< DL	< DL	< DL
65Cu	1.37	130.5	< DL	< DL	< DL	< DL
66Zn		140.9	2.3	0.8	1.3	2.5
68Zn		301.9	4.5	1.9	2.7	4.3
69Ga		69.0	0.9	0.3	0.4	0.6
72Ge		50.6	1.0	< DL	0.4	0.6
75As		< DL	< DL	< DL	0.4	< DL
77Ar Cl		--	--	--	--	--
82Se		36.7	0.6	< DL	< DL	< DL
83Kr		--	--	--	--	--
85Rb	0.855	48.8	< DL	0.3	0.3	0.5
86Sr	45.8	2128.2	31.4	10.9	15.7	22.2
88Sr	45.8	2103.4	32.2	11.0	15.9	23.1
89Y		33.5	0.5	0.2	0.2	0.4
90Zr		41.2	0.7	0.2	0.3	0.5
93Nb		32.7	0.6	0.2	0.3	0.4
95Mo		38.6	0.6	0.2	0.2	0.5
103Rh	1.67	83.6	1.2	0.5	0.7	0.9
105Pd	1.98	111.5	1.6	0.6	1.0	1.5
107Ag	0.42	28.0	0.3	0.1	0.2	0.2
110Cd	0.55	120.6	1.9	0.6	0.8	1.5
111Cd	0.55	13.8	0.5	0.2	0.2	0.2
115In		37.0	0.6	0.2	0.3	0.4
118Sn		155.3	2.3	0.7	1.3	1.5
120Sn		153.6	2.4	0.7	1.1	1.4
121Sb	1.06	37.6	0.5	0.2	0.3	0.4
133Cs		29.9	< DL	0.2	0.2	0.3
136Ba		161.5	< DL	0.7	1.2	1.6
137Ba		156.4	2.4	0.8	1.2	1.5

Fe Internal Isotope	NIST 614 Pub. Conc.	Ap16A05	Ap16A06	Ap16B05	Ap16B06	Ap16C05
139La	0.83	37.2	0.5	0.2	0.2	0.4
140Ce		36.1	0.6	0.2	0.3	0.4
141Pr		34.7	0.6	0.2	0.3	0.4
146Nd		33.5	0.5	0.2	0.2	0.7
147Sm		36.4	0.6	0.2	0.3	0.4
153Eu	0.99	34.7	0.6	0.2	0.3	0.4
155Gd		26.2	< DL	0.3	< DL	0.4
156Ce O		--	--	--	--	--
157Gd		32.0	0.6	< DL	0.3	0.8
159Tb		32.4	0.5	0.2	0.3	0.3
163Dy		36.6	0.6	0.2	0.2	0.3
165Ho		33.4	0.5	0.2	0.3	0.3
166Er		30.0	0.5	0.2	0.2	0.4
169Tm		30.7	0.5	0.2	0.2	0.3
172Yb		34.2	0.6	0.2	0.3	0.3
175Lu		31.9	0.5	0.2	0.2	0.3
178Hf		29.9	0.5	0.2	0.3	0.3
181Ta		29.5	0.5	0.2	0.2	0.3
182W		41.8	0.6	0.2	0.3	0.4
185Re	0.179	22.8	0.3	0.1	0.1	0.2
195Pt	2.26	133.7	2.0	0.6	0.9	1.4
197Au	0.5	26.2	0.4	0.1	0.2	0.4
205Tl	0.269	14.0	0.3	0.1	0.1	0.2
206Pb	2.32	147.5	2.4	0.7	1.1	1.6
207Pb	2.32	143.7	2.2	0.6	1.0	1.6
208Pb	2.32	141.9	2.5	0.6	1.0	1.5
209Bi		32.4	0.5	0.2	0.2	0.3
220Bkg		--	--	--	--	--
232Th	0.748	39.4	0.6	0.2	0.2	0.3
238U	0.823	45.9	0.7	0.2	0.3	0.4
254U O		--	--	--	--	--

Fe Internal Isotope	NIST 614 Pub. Conc.	Ap16C06	Ap16D05	Ap16D06	Ap16E05	Ap16E06
7Li		1.0	1.7	1.1	< DL	0.7
9Be		< DL	< DL	< DL	< DL	< DL
11B	1.3	9.0	17.4	9.9	< DL	5.9
23Na	103860	56512.4	122271.8	64294.2	< DL	39948.0
25Mg		14.8	40.8	21.5	< DL	14.5
27Al	10585	5472.8	12859.7	6512.8	< DL	4295.0
29Si	336553.2	181737.5	387378.6	199863.8	< DL	137505.0
31P	30	6.3	12.3	7.2	< DL	5.2
33S		9.5	15.1	9.0	< DL	8.3
39K		36.1	71.0	49.5	< DL	35.5
43Ca	85764.1	44234.5	79570.1	49206.9	< DL	32738.6
44Ca	85764.1	41924.3	77832.8	45836.5	< DL	30681.8
45Sc	0.59	1.5	2.5	2.0	< DL	1.0
47Ti	3.1	< DL	6.9	1.8	< DL	< DL
51V		0.6	0.9	0.6	< DL	0.4
52Cr		1.0	1.3	1.1	< DL	0.9
53Cr		< DL	1.2	< DL	< DL	< DL
55Mn		0.8	1.4	0.8	< DL	0.5
57Fe	13.3	< DL	< DL	< DL	< DL	< DL
59Co	0.73	< DL	0.6	0.3	< DL	0.3
60Ni	0.95	1.7	4.1	< DL	< DL	< DL
62Ni	0.95	< DL	< DL	< DL	81.3	< DL
65Cu	1.37	< DL	5.5	2.9	< DL	2.1
66Zn		1.7	3.9	2.0	< DL	1.5
68Zn		3.8	7.6	4.5	< DL	2.6
69Ga		0.6	1.3	0.7	< DL	0.5
72Ge		0.5	1.1	0.7	< DL	0.3
75As		0.2	0.4	0.9	< DL	< DL
77Ar Cl		--	--	--	--	--
82Se		< DL	0.9	< DL	2.5	0.7
83Kr		--	--	--	--	--
85Rb	0.855	0.5	0.9	0.5	< DL	0.3
86Sr	45.8	21.3	46.3	23.9	< DL	15.9
88Sr	45.8	21.7	47.5	24.1	< DL	16.3
89Y		0.3	0.7	0.4	< DL	0.2
90Zr		0.4	1.0	0.5	< DL	0.3
93Nb		0.4	0.8	0.4	< DL	0.3
95Mo		0.4	0.8	0.4	< DL	0.4
103Rh	1.67	0.9	1.9	0.9	< DL	0.7
105Pd	1.98	1.2	2.4	1.2	< DL	0.8
107Ag	0.42	0.3	0.4	0.3	< DL	0.2
110Cd	0.55	1.4	2.3	1.2	< DL	0.8
111Cd	0.55	0.2	3.4	< DL	< DL	0.2
115In		0.4	0.8	0.4	< DL	0.3
118Sn		1.4	2.9	1.7	< DL	1.2
120Sn		1.4	2.9	1.7	< DL	1.1
121Sb	1.06	0.4	0.8	0.4	< DL	0.3
133Cs		0.4	0.7	0.4	< DL	0.2
136Ba		1.6	3.0	1.8	< DL	1.3
137Ba		1.7	3.4	1.8	< DL	1.2

Fe Internal Isotope	NIST 614 Pub. Conc.	Ap16C06	Ap16D05	Ap16D06	Ap16E05	Ap16E06
139La	0.83	0.3	0.8	0.4	< DL	0.3
140Ce		0.4	0.9	0.5	< DL	0.3
141Pr		0.4	0.8	0.4	< DL	0.3
146Nd		0.2	0.8	0.5	< DL	0.3
147Sm		0.3	0.8	0.4	< DL	0.3
153Eu	0.99	0.4	0.9	0.4	< DL	0.3
155Gd		0.5	0.5	0.4	< DL	< DL
156Ce O		--	--	--	--	--
157Gd		0.2	0.5	0.3	< DL	0.3
159Tb		0.3	0.7	0.4	< DL	0.3
163Dy		0.3	0.7	0.4	< DL	0.2
165Ho		0.3	0.8	0.4	< DL	0.3
166Er		0.3	0.7	0.3	< DL	0.2
169Tm		0.3	0.7	0.3	< DL	0.2
172Yb		0.3	0.7	0.4	< DL	0.3
175Lu		0.3	0.7	0.4	< DL	0.2
178Hf		0.3	0.7	0.4	< DL	0.3
181Ta		0.3	0.7	0.3	< DL	0.3
182W		0.4	0.9	0.5	< DL	0.3
185Re	0.179	0.2	0.3	0.2	< DL	0.1
195Pt	2.26	1.3	2.6	1.5	< DL	1.0
197Au	0.5	0.3	0.5	0.3	< DL	0.2
205Tl	0.269	0.2	0.3	0.2	< DL	0.1
206Pb	2.32	1.4	3.0	1.6	< DL	1.1
207Pb	2.32	1.4	2.6	1.7	< DL	1.0
208Pb	2.32	1.4	2.6	1.5	< DL	1.0
209Bi		0.3	0.7	0.4	< DL	0.2
220Bkg		--	--	--	--	--
232Th	0.748	0.3	0.8	0.4	< DL	0.3
238U	0.823	0.4	0.8	0.4	< DL	0.3
254U O		--	--	--	--	--

Fe Internal Isotope	NIST 614 Pub. Conc.	Count	Min	Max	Average	Sigma
7Li		9	0.6	94.5	11.4	26.928988
9Be		2	0.7	36.7	18.7	10.519928
11B	1.3	10	1.3	1687.7	177.8	464.25044
23Na	103860	10	25625.2	5275602.2	587042.1	1443587.5
25Mg		8	7.4	993.4	139.9	282.18615
27Al	10585	10	2874.4	538961.8	59925.5	147490.62
29Si	336553.2	10	92268.5	17495329.9	1940388.1	4788797.5
31P	30	10	3.2	603.3	68.6	164.82686
33S		6	8.3	959.6	168.4	274.45886
39K		8	19.4	3131.2	428.1	891.98637
43Ca	85764.1	10	21076.6	3743188.6	418766.2	1023712.3
44Ca	85764.1	10	20823.7	3822382.5	425470.8	1045892.3
45Sc	0.59	9	0.6	139.6	16.8	38.304527
47Ti	3.1	5	1.8	134.9	29.8	36.967444
51V		9	0.2	50.4	6.1	14.353477
52Cr		7	0.7	76.1	11.7	21.724153
53Cr		2	1.2	61.4	31.3	17.627949
55Mn		9	0.3	69.7	8.4	19.864121
57Fe	13.3	1	13.3	13.3	13.3	3.6759258
59Co	0.73	8	0.2	37.6	5.0	10.320805
60Ni	0.95	5	1.0	115.1	24.8	31.618319
62Ni	0.95	2	1.0	81.3	41.1	22.449471
65Cu	1.37	5	1.4	130.5	28.5	35.804838
66Zn		9	0.8	140.9	17.4	40.053391
68Zn		9	1.9	301.9	37.1	85.896719
69Ga		9	0.3	69.0	8.3	19.677451
72Ge		8	0.3	50.6	6.9	14.423027
75As		4	0.2	0.9	0.5	0.2826125
77Ar Cl		0	0.0	0.0	- -	0
82Se		5	0.6	36.7	8.3	10.453223
83Kr		0	0.0	0.0	- -	0
85Rb	0.855	9	0.3	48.8	5.9	13.398679
86Sr	45.8	10	10.9	2128.2	236.2	582.51152
88Sr	45.8	10	11.0	2103.4	234.1	575.56139
89Y		9	0.2	33.5	4.1	9.5499412
90Zr		9	0.2	41.2	5.0	11.720807
93Nb		9	0.2	32.7	4.0	9.3109719
95Mo		9	0.2	38.6	4.7	11.012554
103Rh	1.67	10	0.5	83.6	9.3	22.879581
105Pd	1.98	10	0.6	111.5	12.4	30.514485
107Ag	0.42	10	0.1	28.0	3.0	7.6846644
110Cd	0.55	10	0.6	120.6	13.2	33.056857
111Cd	0.55	9	0.2	13.8	2.1	3.7977514
115In		9	0.2	37.0	4.5	10.55323
118Sn		9	0.7	155.3	18.7	44.287434
120Sn		9	0.7	153.6	18.5	43.809104
121Sb	1.06	10	0.2	37.6	4.2	10.299682
133Cs		8	0.2	29.9	4.0	8.5196981
136Ba		8	0.7	161.5	21.6	46.127533
137Ba		9	0.8	156.4	18.9	44.577592

Fe Internal Isotope	NIST 614 Pub. Conc.	Count	Min	Max	Average	Sigma
139La	0.83	10	0.2	37.2	4.1	10.176731
140Ce		9	0.2	36.1	4.4	10.284596
141Pr		9	0.2	34.7	4.2	9.8743331
146Nd		9	0.2	33.5	4.1	9.5403296
147Sm		9	0.2	36.4	4.4	10.369136
153Eu	0.99	10	0.2	34.7	3.9	9.4962073
155Gd		6	0.3	26.2	4.7	7.4885195
156Ce O		0	0.0	0.0	- -	0
157Gd		8	0.2	32.0	4.4	9.1216374
159Tb		9	0.2	32.4	3.9	9.2243956
163Dy		9	0.2	36.6	4.4	10.446097
165Ho		9	0.2	33.4	4.1	9.5295382
166Er		9	0.2	30.0	3.6	8.5447315
169Tm		9	0.2	30.7	3.7	8.7409557
172Yb		9	0.2	34.2	4.1	9.7519688
175Lu		9	0.2	31.9	3.9	9.0966361
178Hf		9	0.2	29.9	3.6	8.5233918
181Ta		9	0.2	29.5	3.6	8.4045364
182W		9	0.2	41.8	5.1	11.92755
185Re	0.179	10	0.1	22.8	2.5	6.2573149
195Pt	2.26	10	0.6	133.7	14.7	36.63136
197Au	0.5	10	0.1	26.2	2.9	7.1633261
205Tl	0.269	10	0.1	14.0	1.6	3.8365505
206Pb	2.32	10	0.7	147.5	16.3	40.380943
207Pb	2.32	10	0.6	143.7	15.8	39.368486
208Pb	2.32	10	0.6	141.9	15.6	38.852803
209Bi		9	0.2	32.4	3.9	9.2397861
220Bkg		0	0.0	0.0	- -	0
232Th	0.748	10	0.2	39.4	4.3	10.800774
238U	0.823	10	0.2	45.9	5.0	12.584641
254U O		0	0.0	0.0	- -	0

Scaled NIST 614	NIST 614 Pub. Conc.	Ap16A05	Ap16A06	Ap16B05	Ap16B06	Ap16C05
7Li		1.9	1.8	2.1	1.8	1.8
9Be		< DL	< DL	0.6	< DL	1.3
11B	1.3	33.1	31.9	22.3	18.5	17.1
23Na	103860	103591.9	109183.8	96108.6	106610.9	107503.9
25Mg		< DL	< DL	27.6	26.2	30.2
27Al	10585	10583.1	10482.2	10780.7	10546.4	10446.5
29Si	336553.2	343538.7	339767.9	346058.3	343619.4	336807.1
31P	30	11.8	11.0	12.1	12.2	9.8
33S		< DL	< DL	20.9	18.0	16.4
39K		< DL	< DL	72.8	79.0	93.7
44Ca	85764.1	75056.4	75532.6	78100.5	72056.6	81737.2
45Sc	0.59	< DL	< DL	2.9	2.9	3.3
47Ti	3.1	< DL	< DL	3.9	4.2	4.5
51V		2.6	4.3	0.8	1.2	1.0
53Cr		< DL	< DL	1.6	< DL	1.5
55Mn		1.4	1.3	1.2	1.4	1.3
57Fe	13.3	< DL	< DL	49.9	33.6	24.4
59Co	0.73	< DL	< DL	0.7	0.6	0.7
60Ni	0.95	< DL	< DL	4.1	2.0	3.9
65Cu	1.37	< DL	< DL	3.8	4.2	2.9
68Zn		5.9	6.0	6.9	6.7	7.9
69Ga		1.4	1.3	1.2	1.1	1.2
72Ge		1.0	1.3	0.6	1.0	1.1
75As		< DL	< DL	0.7	0.9	< DL
82Se		0.7	0.8	0.7	< DL	0.6
85Rb	0.855	< DL	1.0	1.0	0.9	0.9
88Sr	45.8	41.3	43.1	41.4	40.2	42.4
89Y		0.7	0.7	0.6	0.6	0.7
90Zr		0.8	0.9	0.9	0.7	0.9
93Nb		0.6	0.7	0.8	0.6	0.7
95Mo		0.8	0.8	0.7	0.6	0.9
103Rh	1.67	1.6	1.6	1.7	1.7	1.7
105Pd	1.98	2.2	2.2	2.3	2.4	2.7
107Ag	0.42	0.6	0.4	0.4	0.5	0.4
111Cd	0.55	< DL	0.7	0.6	0.4	0.4
115In		0.7	0.8	0.7	0.7	0.7
118Sn		3.1	3.1	2.7	3.3	2.8
121Sb	1.06	0.7	0.7	0.7	0.7	0.7
133Cs		0.6	0.7	0.6	0.6	0.6
137Ba		3.1	3.2	3.1	3.0	2.8
139La	0.83	0.7	0.7	0.7	0.6	0.7
140Ce		0.7	0.8	0.7	0.7	0.7
141Pr		0.7	0.7	0.7	0.7	0.7
146Nd		0.7	0.7	0.6	0.5	1.2
147Sm		0.7	0.8	0.9	0.7	0.7
153Eu	0.99	0.7	0.8	0.8	0.7	0.8
157Gd		0.6	0.9	0.6	0.8	1.4
159Tb		0.6	0.7	0.6	0.6	0.6
163Dy		0.7	0.9	0.6	0.6	0.6
165Ho		0.7	0.7	0.6	0.7	0.6

Scaled NIST 614	NIST 614 Pub. Conc.	Ap16A05	Ap16A06	Ap16B05	Ap16B06	Ap16C05
166Er		0.6	0.6	0.7	0.5	0.6
169Tm		0.6	0.7	0.6	0.6	0.6
172Yb		0.7	0.7	0.7	0.7	0.6
175Lu		0.6	0.7	0.6	0.6	0.6
178Hf		0.6	0.7	0.6	0.7	0.6
181Ta		0.6	0.6	0.6	0.6	0.6
182W		0.8	0.9	0.8	0.7	0.8
185Re	0.179	0.4	0.4	0.4	0.4	0.5
195Pt	2.26	2.6	2.6	2.4	2.3	2.6
197Au	0.5	0.5	0.5	0.4	0.5	0.6
205Tl	0.269	0.3	0.3	0.3	0.3	0.3
208Pb	2.32	2.8	3.3	2.3	2.6	2.7
209Bi		0.6	0.7	0.6	0.6	0.6
232Th	0.748	0.8	0.8	0.7	0.6	0.6
238U	0.823	0.9	0.9	0.7	0.8	0.8

Scaled NIST 614	NIST 614 Pub. Conc.	Ap16C06	Ap16D05	Ap16D06	Ap16E05	Ap16E06
7Li		1.9	1.5	1.9	1.9	1.7
9Be		< DL	< DL	0.8	1.3	0.8
11B	1.3	17.0	15.4	16.7	15.4	14.8
23Na	103860	103917.9	108422.5	108800.6	102088.8	100059.2
25Mg		< DL	36.0	36.4	31.9	36.4
27Al	10585	10215.5	11384.8	11021.1	10446.4	10757.8
29Si	336553.2	339513.8	342562.4	338215.6	342498.4	344414.1
31P	30	11.7	11.0	12.1	9.4	13.1
33S		< DL	< DL	15.3	22.0	20.7
39K		< DL	< DL	83.8	71.8	88.8
44Ca	85764.1	81392.1	70822.5	77566.0	78300.6	76850.0
45Sc	0.59	< DL	< DL	3.4	2.7	2.6
47Ti	3.1	< DL	< DL	3.1	3.5	2.0
51V		1.1	0.8	0.9	0.9	1.0
53Cr		< DL	< DL	1.4	< DL	1.1
55Mn		1.5	1.3	1.3	1.2	1.2
57Fe	13.3	< DL	< DL	22.5	< DL	33.3
59Co	0.73	< DL	< DL	0.6	0.8	0.7
60Ni	0.95	< DL	< DL	< DL	< DL	2.6
65Cu	1.37	< DL	< DL	5.0	3.6	5.2
68Zn		7.1	6.7	7.6	7.3	6.5
69Ga		1.2	1.2	1.2	1.3	1.2
72Ge		< DL	< DL	1.1	0.9	0.9
75As		< DL	< DL	1.6	1.1	< DL
82Se		0.5	0.8	< DL	< DL	1.8
85Rb	0.855	< DL	< DL	0.8	0.7	0.9
88Sr	45.8	41.3	42.2	40.7	39.9	40.8
89Y		0.6	0.6	0.7	0.6	0.6
90Zr		0.8	0.9	0.8	1.0	0.8
93Nb		0.7	0.7	0.7	0.8	0.7
95Mo		0.7	0.8	0.7	0.7	0.9
103Rh	1.67	1.7	1.7	1.6	1.6	1.6
105Pd	1.98	2.3	2.1	2.1	2.6	2.1
107Ag	0.42	0.5	0.3	0.4	0.4	0.5
111Cd	0.55	< DL	3.0	0.3	0.6	0.4
115In		0.7	0.7	0.7	0.7	0.7
118Sn		2.8	2.6	2.9	2.6	2.9
121Sb	1.06	0.7	0.7	0.7	0.7	0.7
133Cs		0.7	0.6	0.6	0.6	0.6
137Ba		3.2	3.0	3.0	2.4	3.0
139La	0.83	0.6	0.7	0.7	0.6	0.6
140Ce		0.7	0.8	0.8	0.7	0.7
141Pr		0.7	0.7	0.7	0.6	0.7
146Nd		< DL	0.7	0.9	0.6	0.8
147Sm		0.6	0.7	0.8	0.6	0.7
153Eu	0.99	0.7	0.8	0.7	0.7	0.8
157Gd		< DL	< DL	0.5	0.5	0.7
159Tb		0.6	0.6	0.7	0.6	0.7
163Dy		0.5	0.7	0.7	0.5	0.6
165Ho		0.6	0.7	0.7	0.6	0.7

Scaled NIST 614	NIST 614 Pub. Conc.	Ap16C06	Ap16D05	Ap16D06	Ap16E05	Ap16E06
166Er		0.6	0.6	0.5	0.6	0.6
169Tm		0.6	0.6	0.5	0.5	0.6
172Yb		0.6	0.6	0.7	0.6	0.7
175Lu		0.6	0.6	0.6	0.5	0.6
178Hf		0.6	0.6	0.7	0.5	0.7
181Ta		0.6	0.6	0.5	0.6	0.6
182W		0.8	0.8	0.8	0.8	0.8
185Re	0.179	0.3	0.3	0.3	0.4	0.3
195Pt	2.26	2.3	2.3	2.5	2.6	2.4
197Au	0.5	0.5	0.4	0.5	0.6	0.5
205Tl	0.269	0.3	0.3	0.3	0.3	0.3
208Pb	2.32	2.6	2.4	2.6	2.5	2.5
209Bi		0.6	0.6	0.6	0.6	0.6
232Th	0.748	0.6	0.7	0.7	0.6	0.7
238U	0.823	0.8	0.7	0.8	0.8	0.7

Scaled NIST 614	NIST 614 Pub. Conc.	Count	Min	Max	Average	Sigma
7Li		10	1.5	2.1	1.8	0.5501381
9Be		5	0.6	1.3	1.0	0.5192185
11B	1.3	11	1.3	33.1	18.5	9.3910172
23Na	103860	11	96108.6	109183.8	104558.9	29138.036
25Mg		7	26.2	36.4	32.1	15.76497
27Al	10585	11	10215.5	11384.8	10659.0	2960.4607
29Si	336553.2	11	336553.2	346058.3	341231.7	94357.173
31P	30	11	9.4	30.0	13.1	6.3436278
33S		6	15.3	22.0	18.9	9.5817437
39K		6	71.8	93.7	81.7	41.0888
44Ca	85764.1	11	70822.5	85764.1	77561.7	21797.06
45Sc	0.59	7	0.6	3.4	2.6	1.4580306
47Ti	3.1	7	2.0	4.5	3.5	1.811128
51V		10	0.8	4.3	1.5	1.1070693
53Cr		4	1.1	1.6	1.4	0.6859827
55Mn		10	1.2	1.5	1.3	0.3853462
57Fe	13.3	6	13.3	49.9	29.5	16.822378
59Co	0.73	7	0.6	0.8	0.7	0.3368069
60Ni	0.95	5	1.0	4.1	2.7	1.5355047
65Cu	1.37	7	1.4	5.2	3.7	2.0575859
68Zn		10	5.9	7.9	6.9	2.061452
69Ga		10	1.1	1.4	1.2	0.3552088
72Ge		8	0.6	1.3	1.0	0.469913
75As		4	0.7	1.6	1.1	0.5542818
82Se		7	0.5	1.8	0.8	0.5156136
85Rb	0.855	8	0.7	1.0	0.9	0.4205192
88Sr	45.8	11	39.9	45.8	41.7	11.632637
89Y		10	0.6	0.7	0.6	0.1876779
90Zr		10	0.7	1.0	0.9	0.2571951
93Nb		10	0.6	0.8	0.7	0.2045449
95Mo		10	0.6	0.9	0.7	0.231216
103Rh	1.67	11	1.6	1.7	1.7	0.4638171
105Pd	1.98	11	2.0	2.7	2.3	0.6557692
107Ag	0.42	11	0.3	0.6	0.4	0.1345546
111Cd	0.55	9	0.3	3.0	0.8	0.7761621
115In		10	0.7	0.8	0.7	0.2075651
118Sn		10	2.6	3.3	2.9	0.8495721
121Sb	1.06	11	0.7	1.1	0.7	0.2288458
133Cs		10	0.6	0.7	0.6	0.1801488
137Ba		10	2.4	3.2	3.0	0.8858714
139La	0.83	11	0.6	0.8	0.7	0.2014956
140Ce		10	0.7	0.8	0.7	0.2169404
141Pr		10	0.6	0.7	0.7	0.2028662
146Nd		9	0.5	1.2	0.7	0.3364905
147Sm		10	0.6	0.9	0.7	0.2242742
153Eu	0.99	11	0.7	1.0	0.8	0.2243379
157Gd		8	0.5	1.4	0.8	0.4075807
159Tb		10	0.6	0.7	0.6	0.1856719
163Dy		10	0.5	0.9	0.6	0.203188
165Ho		10	0.6	0.7	0.7	0.1931033

Scaled NIST 614	NIST 614 Pub. Conc.	Count	Min	Max	Average	Sigma
166Er		10	0.5	0.7	0.6	0.1787203
169Tm		10	0.5	0.7	0.6	0.1761057
172Yb		10	0.6	0.7	0.7	0.1969299
175Lu		10	0.5	0.7	0.6	0.1772584
178Hf		10	0.5	0.7	0.6	0.1832833
181Ta		10	0.5	0.6	0.6	0.1704225
182W		10	0.7	0.9	0.8	0.2327911
185Re	0.179	11	0.2	0.5	0.4	0.1222051
195Pt	2.26	11	2.3	2.6	2.4	0.6856523
197Au	0.5	11	0.4	0.6	0.5	0.150167
205Tl	0.269	11	0.3	0.3	0.3	0.0808448
208Pb	2.32	11	2.3	3.3	2.6	0.7608966
209Bi		10	0.6	0.7	0.6	0.1808252
232Th	0.748	11	0.6	0.8	0.7	0.1978828
238U	0.823	11	0.7	0.9	0.8	0.2272351

Si Internal Isotope	BCR-2G Pub. Conc.	Ap16A09	Ap16A10	Ap16B09	Ap16B10	Ap16C09
7Li	9	9.8	9.5	8.7	9.0	9.9
9Be		< DL	< DL	1.7	2.1	2.5
11B		18.7	16.8	14.7	16.6	14.2
23Na	23400	19195.8	20207.5	17208.8	17785.1	16410.8
25Mg	21600	20814.5	21065.6	20110.1	18970.1	20170.1
27Al	71400	80763.5	78597.1	75548.9	73027.7	74564.4
29Si	253000	253000.0	253000.0	253000.0	253000.0	253000.0
31P	1500	1147.7	1107.1	1169.8	1204.9	1187.0
33S		< DL	< DL	< DL	< DL	13.6
39K	14900	14838.5	14926.5	14975.0	14409.2	16713.9
43Ca	50900	48896.1	42859.7	45490.6	42459.7	47686.0
44Ca	50900	46512.5	42278.4	43896.8	41998.1	42928.6
45Sc	33	31.2	28.7	28.9	28.4	30.2
47Ti	13500	13050.8	12225.3	12147.3	11963.2	11758.1
51V	416	385.3	376.7	371.9	358.9	350.7
52Cr	18	14.1	13.6	13.0	12.8	14.0
53Cr	18	13.9	13.5	14.1	13.8	12.9
55Mn	1520	1467.1	1474.0	1550.0	1462.5	1431.1
57Fe	96600	99872.5	98390.3	99449.9	96223.9	91074.3
59Co	37	34.6	34.6	35.5	34.8	34.1
60Ni		< DL	< DL	11.8	11.3	11.6
62Ni		< DL	< DL	23.9	< DL	< DL
65Cu	19	< DL	< DL	17.6	15.6	16.4
66Zn	127	133.4	135.9	149.8	143.7	147.6
68Zn	127	148.4	145.9	157.6	152.4	152.3
69Ga	23	32.1	30.2	31.4	30.7	29.1
72Ge		2.6	2.4	2.7	2.6	3.1
75As		< DL	< DL	1.8	1.8	2.2
77Ar Cl		--	--	--	--	--
82Se		< DL	-0.8	< DL	< DL	< DL
83Kr		--	--	--	--	--
85Rb	48	41.8	41.1	42.4	40.8	39.3
86Sr	346	317.8	305.1	294.6	289.9	285.6
88Sr	346	320.2	305.4	293.5	285.7	279.0
89Y	37	30.6	28.1	28.0	27.4	26.8
90Zr	188	171.3	157.7	156.0	154.7	150.2
93Nb		11.1	10.0	10.6	10.3	10.1
95Mo	248	221.4	218.4	217.5	218.8	209.1
103Rh		< DL	< DL	< DL	< DL	< DL
105Pd		< DL	< DL	< DL	< DL	< DL
107Ag		0.5	< DL	0.6	0.5	0.5
110Cd		< DL	< DL	0.2	0.2	0.3
111Cd		< DL	< DL	< DL	< DL	0.4
115In		< DL	< DL	0.1	0.1	0.3
118Sn		2.0	2.5	2.3	2.3	2.5
120Sn		2.4	2.4	2.3	2.3	2.4
121Sb		< DL	< DL	0.2	0.2	0.4
133Cs	1.1	< DL	< DL	1.0	0.9	1.1
136Ba	683	653.5	609.8	582.7	559.1	572.0
137Ba	683	661.6	622.3	590.8	564.3	580.9

Si Internal Isotope	BCR-2G Pub. Conc.	Ap16A09	Ap16A10	Ap16B09	Ap16B10	Ap16C09
139La	25.4	25.6	23.6	22.8	21.9	22.7
140Ce	53	49.3	46.1	44.4	43.0	44.0
141Pr	6.5	6.3	5.5	5.6	5.4	5.6
146Nd	29	28.0	25.8	24.9	24.4	24.9
147Sm	6.6	6.2	5.5	6.0	5.6	5.9
153Eu	2	2.0	1.5	1.9	1.8	1.9
155Gd	7	6.5	5.4	5.7	5.8	5.8
156Ce O		--	--	--	--	--
157Gd	7	6.2	5.4	5.2	5.5	5.3
159Tb	1.1	0.9	< DL	0.9	0.8	1.1
163Dy	6.4	6.1	4.9	5.1	5.3	5.6
165Ho	1.25	1.1	< DL	1.0	1.0	1.3
166Er	3.6	3.0	2.7	2.8	2.8	2.9
169Tm	0.57	< DL	< DL	0.4	0.4	0.6
172Yb	3.4	3.2	2.7	2.9	2.9	2.9
175Lu	0.51	< DL	< DL	0.4	0.4	0.7
178Hf	4.8	4.4	3.6	4.0	3.9	4.6
181Ta		0.5	< DL	0.6	0.5	0.8
182W		< DL	< DL	0.5	0.5	0.7
185Re		< DL	< DL	< DL	< DL	0.1
195Pt		0.5	0.3	0.3	0.3	0.2
197Au		< DL	< DL	0.0	0.0	< DL
205Tl		0.2	< DL	0.2	0.2	0.2
206Pb	11	10.2	9.5	9.6	10.1	9.7
207Pb	11	9.2	8.5	8.9	9.1	9.1
208Pb	11	9.5	10.2	9.2	9.0	9.0
209Bi		< DL	< DL	0.0	0.0	0.2
220Bkg		--	--	--	--	--
232Th	6.2	5.8	4.9	5.1	5.1	5.1
238U	1.69	1.6	1.1	1.4	1.4	1.5
254U O		--	--	--	--	--

Si Internal Isotope	BCR-2G Pub. Conc.	Ap16C10	Ap16D09	Ap16D10	Ap16E09	Ap16E10
7Li	9	9.9	8.7	9.0	7.8	11.4
9Be		2.0	1.8	1.5	< DL	2.6
11B		15.6	12.7	13.5	14.4	17.0
23Na	23400	16184.2	18491.9	17337.6	16580.7	18131.0
25Mg	21600	19978.7	19295.6	19365.4	18412.2	19409.6
27Al	71400	72927.8	72014.7	70957.7	66674.5	68348.3
29Si	253000	253000.0	253000.0	253000.0	253000.0	253000.0
31P	1500	1152.3	1147.4	1151.3	1276.5	1272.2
33S		< DL	6.8	7.1	9.2	11.5
39K	14900	16757.6	14191.6	16331.5	17117.5	15966.5
43Ca	50900	46647.6	37969.1	44536.5	43678.9	42313.5
44Ca	50900	42078.0	35749.1	39800.2	38307.3	37209.1
45Sc	33	28.5	26.5	27.5	25.6	26.7
47Ti	13500	11704.8	11216.0	11577.9	11026.7	10919.5
51V	416	353.7	323.2	342.2	328.4	339.0
52Cr	18	12.8	13.1	13.6	11.8	12.6
53Cr	18	13.5	12.9	12.2	11.3	13.7
55Mn	1520	1488.2	1410.8	1436.5	1335.8	1332.6
57Fe	96600	94361.8	87732.3	90264.8	85437.5	88712.7
59Co	37	34.1	32.6	33.3	32.6	33.3
60Ni		11.7	11.7	10.6	12.3	12.0
62Ni		< DL	26.8	24.6	< DL	< DL
65Cu	19	14.3	14.7	17.5	19.2	17.6
66Zn	127	143.3	139.6	146.5	153.3	150.6
68Zn	127	147.9	144.3	152.7	159.2	158.0
69Ga	23	29.3	29.1	29.5	28.1	30.1
72Ge		3.1	2.7	2.8	2.1	4.0
75As		1.4	1.6	1.3	1.8	2.3
77Ar Cl		--	--	--	--	--
82Se		< DL	< DL	< DL	< DL	< DL
83Kr		--	--	--	--	--
85Rb	48	39.6	38.0	39.3	37.4	39.7
86Sr	346	278.1	280.7	265.2	254.7	261.0
88Sr	346	272.9	279.8	268.8	247.1	256.2
89Y	37	26.0	26.2	25.1	22.3	24.2
90Zr	188	144.9	148.8	142.9	130.6	133.5
93Nb		9.8	10.0	9.7	8.8	10.4
95Mo	248	200.9	204.9	205.9	200.8	210.5
103Rh		< DL	< DL	< DL	< DL	< DL
105Pd		< DL	< DL	< DL	< DL	< DL
107Ag		0.5	0.4	0.4	0.2	1.1
110Cd		< DL	0.2	0.2	< DL	0.9
111Cd		< DL	< DL	< DL	< DL	0.9
115In		0.2	0.1	0.1	< DL	0.9
118Sn		2.3	2.0	2.7	1.7	3.5
120Sn		2.4	2.2	2.9	1.7	3.4
121Sb		0.5	0.2	0.3	< DL	1.1
133Cs	1.1	1.0	0.9	0.8	0.5	1.6
136Ba	683	557.2	552.3	522.0	501.3	526.3
137Ba	683	566.7	565.4	538.3	509.0	539.4

Si Internal Isotope	BCR-2G Pub. Conc.	Ap16C10	Ap16D09	Ap16D10	Ap16E09	Ap16E10
139La	25.4	21.6	22.4	20.8	19.0	21.7
140Ce	53	43.1	42.3	40.3	38.6	42.0
141Pr	6.5	5.5	5.4	5.1	4.3	5.9
146Nd	29	24.3	23.8	23.0	20.7	23.5
147Sm	6.6	5.8	5.7	5.5	4.4	6.5
153Eu	2	2.1	1.8	1.6	1.2	2.5
155Gd	7	5.5	5.5	5.1	4.5	5.8
156Ce O		--	--	--	--	--
157Gd	7	5.3	4.9	4.8	4.0	5.3
159Tb	1.1	1.1	0.8	0.8	< DL	1.8
163Dy	6.4	5.3	5.1	4.6	3.9	5.3
165Ho	1.25	1.1	1.1	1.0	0.4	2.1
166Er	3.6	3.0	2.8	2.6	2.3	2.9
169Tm	0.57	0.4	0.4	0.4	< DL	1.2
172Yb	3.4	2.9	2.8	2.6	2.1	3.7
175Lu	0.51	0.5	0.4	0.4	< DL	1.3
178Hf	4.8	4.1	4.0	3.6	3.1	4.1
181Ta		0.7	0.6	0.6	< DL	1.3
182W		0.8	0.5	0.5	< DL	1.6
185Re		< DL	< DL	< DL	< DL	0.3
195Pt		0.3	0.3	0.3	0.3	0.3
197Au		< DL	< DL	0.0	< DL	0.1
205Tl		0.2	0.2	0.2	0.1	0.4
206Pb	11	9.9	9.6	9.8	10.5	11.7
207Pb	11	8.7	9.0	9.0	9.5	10.8
208Pb	11	9.3	8.9	9.3	9.5	11.0
209Bi		0.2	0.0	0.0	< DL	0.9
220Bkg		--	--	--	--	--
232Th	6.2	5.2	5.0	4.9	4.0	5.7
238U	1.69	1.6	1.3	1.4	0.7	2.5
254U O		--	--	--	--	--

Si Internal Isotope	BCR-2G Pub. Conc.	Count	Min	Max	Average	Sigma
7Li	9	11	7.8	11.4	9.3	2.7134413
9Be		7	1.5	2.6	2.0	1.0224713
11B		10	12.7	18.7	15.4	4.739657
23Na	23400	11	16184.2	23400.0	18266.7	5398.7135
25Mg	21600	11	18412.2	21600.0	19926.5	5576.3533
27Al	71400	11	66674.5	80763.5	73165.9	20568.461
29Si	253000	11	253000.0	253000.0	253000.0	69925.506
31P	1500	11	1107.1	1500.0	1210.6	349.17346
33S		5	6.8	13.6	9.6	5.1115582
39K	14900	11	14191.6	17117.5	15557.1	4403.6226
43Ca	50900	11	37969.1	50900.0	44858.0	12826.188
44Ca	50900	11	35749.1	50900.0	41968.9	12244.779
45Sc	33	11	25.6	33.0	28.7	8.1647818
47Ti	13500	11	10919.5	13500.0	11917.2	3373.8124
51V	416	11	323.2	416.0	358.7	102.21577
52Cr	18	11	11.8	18.0	13.6	4.02836
53Cr	18	11	11.3	18.0	13.6	4.0588347
55Mn	1520	11	1332.6	1550.0	1446.2	404.49918
57Fe	96600	11	85437.5	99872.5	93465.5	26240.925
59Co	37	11	32.6	37.0	34.2	9.5332519
60Ni		8	10.6	12.3	11.6	5.1938538
62Ni		3	23.9	26.8	25.1	11.208543
65Cu	19	9	14.3	19.2	16.9	7.4473075
66Zn	127	11	127.0	153.3	142.8	40.146596
68Zn	127	11	127.0	159.2	149.6	42.160743
69Ga	23	11	23.0	32.1	29.3	8.3959299
72Ge		10	2.1	4.0	2.8	0.936881
75As		8	1.3	2.3	1.8	0.8455177
77Ar Cl		0	0.0	0.0	- -	0
82Se		1	-0.8	-0.8	-0.8	0.2205233
83Kr		0	0.0	0.0	- -	0
85Rb	48	11	37.4	48.0	40.7	11.544078
86Sr	346	11	254.7	346.0	289.0	83.486095
88Sr	346	11	247.1	346.0	286.8	83.439135
89Y	37	11	22.3	37.0	27.4	8.3538443
90Zr	188	11	130.6	188.0	152.6	44.734068
93Nb		10	8.8	11.1	10.1	2.9456464
95Mo	248	11	200.8	248.0	214.2	60.453413
103Rh		0	0.0	0.0	- -	0
105Pd		0	0.0	0.0	- -	0
107Ag		9	0.2	1.1	0.5	0.2916706
110Cd		6	0.2	0.9	0.3	0.2457597
111Cd		2	0.4	0.9	0.7	0.2814914
115In		7	0.1	0.9	0.2	0.2464025
118Sn		10	1.7	3.5	2.4	0.8236163
120Sn		10	1.7	3.4	2.4	0.8112072
121Sb		7	0.2	1.1	0.4	0.3024023
133Cs	1.1	9	0.5	1.6	1.0	0.4912692
136Ba	683	11	501.3	683.0	574.5	166.66155
137Ba	683	11	509.0	683.0	583.8	168.45183

Si Internal Isotope	BCR-2G Pub. Conc.	Count	Min	Max	Average	Sigma
139La	25.4	11	19.0	25.6	22.5	6.4588166
140Ce	53	11	38.6	53.0	44.2	12.767816
141Pr	6.5	11	4.3	6.5	5.6	1.623992
146Nd	29	11	20.7	29.0	24.7	7.1507286
147Sm	6.6	11	4.4	6.6	5.8	1.6865208
153Eu	2	11	1.2	2.5	1.8	0.5988934
155Gd	7	11	4.5	7.0	5.7	1.6815412
156Ce O		0	0.0	0.0	- -	0
157Gd	7	11	4.0	7.0	5.4	1.6319555
159Tb	1.1	9	0.8	1.8	1.0	0.5168276
163Dy	6.4	11	3.9	6.4	5.2	1.5744441
165Ho	1.25	10	0.4	2.1	1.1	0.5497837
166Er	3.6	11	2.3	3.6	2.8	0.8427585
169Tm	0.57	8	0.4	1.2	0.5	0.3382905
172Yb	3.4	11	2.1	3.7	2.9	0.8947293
175Lu	0.51	8	0.4	1.3	0.6	0.3540309
178Hf	4.8	11	3.1	4.8	4.0	1.1914085
181Ta		8	0.5	1.3	0.7	0.3826888
182W		7	0.5	1.6	0.7	0.4669828
185Re		2	0.1	0.3	0.2	0.0880159
195Pt		10	0.2	0.5	0.3	0.107424
197Au		4	0.0	0.1	0.0	0.0210478
205Tl		9	0.1	0.4	0.2	0.1074696
206Pb	11	11	9.5	11.7	10.1	2.87172
207Pb	11	11	8.5	11.0	9.4	2.6880162
208Pb	11	11	8.9	11.0	9.6	2.7546439
209Bi		7	0.0	0.9	0.2	0.2577455
220Bkg		0	0.0	0.0	- -	0
232Th	6.2	11	4.0	6.2	5.2	1.52388
238U	1.69	11	0.7	2.5	1.5	0.577612
254U O		0	0.0	0.0	- -	0

Ca Internal Isotope	BCR-2G Pub. Conc.	Ap16A09	Ap16A10	Ap16B09	Ap16B10	Ap16C09
7Li	9	10.7	11.4	10.0	10.9	11.7
9Be		< DL	< DL	2.0	2.6	2.9
11B		20.5	20.2	17.1	20.1	16.9
23Na	23400	21006.5	24328.3	19954.3	21554.8	19458.2
25Mg	21600	22777.9	25361.4	23318.5	22991.0	23915.5
27Al	71400	88381.8	94624.9	87601.7	88506.7	88410.3
29Si	253000	276865.2	304592.6	293362.9	306626.0	299979.7
31P	1500	1256.0	1332.9	1356.4	1460.4	1407.4
33S		< DL	< DL	< DL	< DL	16.1
39K	14900	16238.2	17970.4	17364.1	17463.4	19817.5
43Ca	50900	53508.4	51599.8	52748.0	51459.5	56540.8
44Ca	50900	50900.0	50900.0	50900.0	50900.0	50900.0
45Sc	33	34.1	34.6	33.5	34.4	35.8
47Ti	13500	14281.9	14718.3	14085.2	14498.9	13941.5
51V	416	421.6	453.5	431.3	435.0	415.8
52Cr	18	15.4	16.4	15.0	15.6	16.6
53Cr	18	15.2	16.3	16.3	16.7	15.3
55Mn	1520	1605.5	1774.6	1797.3	1772.5	1696.8
57Fe	96600	109293.4	118454.3	115315.9	116619.5	107985.9
59Co	37	37.9	41.7	41.1	42.1	40.5
60Ni		13.1	< DL	13.7	13.7	13.8
62Ni		< DL	< DL	27.8	< DL	< DL
65Cu	19	< DL	< DL	20.4	19.0	19.4
66Zn	127	146.0	163.6	173.7	174.2	175.0
68Zn	127	162.4	175.7	182.8	184.7	180.6
69Ga	23	35.1	36.3	36.5	37.2	34.5
72Ge		2.8	2.8	3.1	3.1	3.7
75As		< DL	< DL	2.1	2.2	2.6
77Ar Cl		--	--	--	--	--
82Se		< DL	-0.9	< DL	< DL	< DL
83Kr		--	--	--	--	--
85Rb	48	45.7	49.5	49.2	49.5	46.6
86Sr	346	347.8	367.3	341.5	351.3	338.6
88Sr	346	350.5	367.6	340.3	346.2	330.8
89Y	37	33.5	33.8	32.4	33.2	31.8
90Zr	188	187.5	189.8	180.9	187.5	178.0
93Nb		12.1	12.0	12.3	12.5	12.0
95Mo	248	242.3	263.0	252.2	265.1	248.0
103Rh		< DL	< DL	< DL	< DL	< DL
105Pd		< DL	< DL	< DL	< DL	< DL
107Ag		0.6	< DL	0.6	0.6	0.6
110Cd		< DL	< DL	0.3	0.2	0.3
111Cd		< DL	< DL	< DL	0.2	0.4
115In		< DL	< DL	0.1	0.1	0.4
118Sn		2.2	3.1	2.7	2.8	2.9
120Sn		2.6	2.9	2.7	2.8	2.8
121Sb		< DL	< DL	0.3	0.3	0.5
133Cs	1.1	1.0	< DL	1.1	1.0	1.3
136Ba	683	715.1	734.2	675.7	677.6	678.2
137Ba	683	724.1	749.3	685.0	683.9	688.8

Ca Internal Isotope	BCR-2G Pub. Conc.	Ap16A09	Ap16A10	Ap16B09	Ap16B10	Ap16C09
139La	25.4	28.0	28.4	26.5	26.6	26.9
140Ce	53	54.0	55.6	51.5	52.1	52.2
141Pr	6.5	6.9	6.6	6.5	6.6	6.7
146Nd	29	30.6	31.0	28.9	29.5	29.6
147Sm	6.6	6.7	6.6	6.9	6.8	7.0
153Eu	2	2.1	1.8	2.2	2.1	2.3
155Gd	7	7.1	6.5	6.6	7.0	6.9
156Ce O		--	--	--	--	--
157Gd	7	6.8	6.5	6.1	6.6	6.3
159Tb	1.1	0.9	< DL	1.0	1.0	1.3
163Dy	6.4	6.7	5.9	5.9	6.5	6.6
165Ho	1.25	1.2	0.9	1.2	1.2	1.5
166Er	3.6	3.3	3.2	3.2	3.4	3.5
169Tm	0.57	< DL	< DL	0.4	0.5	0.7
172Yb	3.4	3.5	3.2	3.4	3.5	3.5
175Lu	0.51	< DL	< DL	0.5	0.5	0.8
178Hf	4.8	4.9	4.3	4.6	4.7	5.4
181Ta		0.6	< DL	0.7	0.6	0.9
182W		< DL	< DL	0.6	0.6	0.8
185Re		< DL	< DL	< DL	< DL	0.1
195Pt		0.5	0.4	0.4	0.3	0.3
197Au		< DL	< DL	0.0	0.0	< DL
205Tl		0.3	< DL	0.3	0.3	0.3
206Pb	11	11.1	11.4	11.1	12.2	11.6
207Pb	11	10.1	10.2	10.4	11.0	10.8
208Pb	11	10.4	12.3	10.7	10.9	10.7
209Bi		< DL	< DL	0.0	0.1	0.2
220Bkg		--	--	--	--	--
232Th	6.2	6.4	5.8	5.9	6.2	6.0
238U	1.69	1.7	1.3	1.6	1.7	1.8
254U O		--	--	--	--	--

Ca Internal Isotope	BCR-2G Pub. Conc.	Ap16C10	Ap16D09	Ap16D10	Ap16E09	Ap16E10
7Li	9	12.0	12.4	11.6	10.4	15.6
9Be		2.4	2.6	2.0	< DL	3.6
11B		18.8	18.0	17.3	19.1	23.3
23Na	23400	19577.4	26329.0	22172.9	22031.2	24802.2
25Mg	21600	24167.4	27473.4	24766.1	24464.8	26551.3
27Al	71400	88217.8	102535.3	90746.8	88592.3	93496.7
29Si	253000	306043.8	360224.4	323558.3	336168.5	346089.9
31P	1500	1393.9	1633.7	1472.4	1696.2	1740.2
33S		< DL	9.7	9.0	12.2	15.8
39K	14900	20271.0	20206.2	20886.1	22744.5	21841.3
43Ca	50900	56427.7	54060.8	56957.1	58037.5	57882.6
44Ca	50900	50900.0	50900.0	50900.0	50900.0	50900.0
45Sc	33	34.5	37.7	35.2	34.0	36.6
47Ti	13500	14158.8	15969.5	14806.9	14651.4	14937.3
51V	416	427.8	460.2	437.7	436.4	463.7
52Cr	18	15.5	18.7	17.4	15.7	17.2
53Cr	18	16.3	18.3	15.6	15.1	18.7
55Mn	1520	1800.2	2008.7	1837.2	1774.9	1822.9
57Fe	96600	114145.7	124914.3	115438.5	113523.4	121354.1
59Co	37	41.2	46.4	42.6	43.3	45.5
60Ni		14.1	16.6	13.6	16.3	16.4
62Ni		19.9	38.2	31.5	17.0	< DL
65Cu	19	17.3	20.9	22.4	25.4	24.1
66Zn	127	173.3	198.7	187.3	203.7	206.0
68Zn	127	178.9	205.4	195.3	211.6	216.1
69Ga	23	35.5	41.5	37.7	37.3	41.2
72Ge		3.7	3.8	3.6	2.8	5.5
75As		1.7	2.2	1.7	2.4	3.2
77Ar Cl		--	--	--	--	--
82Se		< DL	< DL	< DL	< DL	< DL
83Kr		--	--	--	--	--
85Rb	48	47.9	54.2	50.3	49.7	54.3
86Sr	346	336.4	399.7	339.2	338.4	357.1
88Sr	346	330.2	398.4	343.7	328.3	350.4
89Y	37	31.4	37.3	32.1	29.6	33.2
90Zr	188	175.2	211.9	182.7	173.6	182.6
93Nb		11.8	14.2	12.5	11.8	14.2
95Mo	248	243.1	291.8	263.3	266.8	288.0
103Rh		0.0	< DL	< DL	< DL	0.0
105Pd		< DL	< DL	< DL	< DL	< DL
107Ag		0.6	0.5	0.6	0.3	1.5
110Cd		< DL	0.3	0.3	< DL	1.2
111Cd		< DL	< DL	< DL	< DL	1.3
115In		0.2	0.1	0.1	< DL	1.2
118Sn		2.8	2.9	3.5	2.2	4.8
120Sn		2.9	3.1	3.7	2.2	4.7
121Sb		0.6	0.3	0.4	< DL	1.5
133Cs	1.1	1.2	1.2	1.1	0.7	2.2
136Ba	683	674.0	786.3	667.5	666.1	720.0
137Ba	683	685.6	805.0	688.4	676.3	737.9

Ca Internal Isotope	BCR-2G Pub. Conc.	Ap16C10	Ap16D09	Ap16D10	Ap16E09	Ap16E10
139La	25.4	26.2	31.9	26.6	25.2	29.7
140Ce	53	52.1	60.2	51.5	51.3	57.5
141Pr	6.5	6.7	7.7	6.5	5.7	8.1
146Nd	29	29.4	33.8	29.4	27.4	32.2
147Sm	6.6	7.0	8.1	7.0	5.9	8.9
153Eu	2	2.6	2.5	2.1	1.6	3.4
155Gd	7	6.6	7.9	6.5	6.0	7.9
156Ce O		--	--	--	--	--
157Gd	7	6.4	7.0	6.1	5.3	7.2
159Tb	1.1	1.3	1.2	1.0	0.4	2.5
163Dy	6.4	6.4	7.2	5.9	5.1	7.2
165Ho	1.25	1.3	1.5	1.2	0.5	2.8
166Er	3.6	3.6	3.9	3.3	3.0	4.0
169Tm	0.57	0.5	0.6	0.5	< DL	1.7
172Yb	3.4	3.5	4.0	3.3	2.8	5.1
175Lu	0.51	0.6	0.6	0.5	< DL	1.7
178Hf	4.8	4.9	5.7	4.7	4.2	5.6
181Ta		0.9	0.8	0.7	< DL	1.8
182W		0.9	0.6	0.6	< DL	2.3
185Re		< DL	< DL	0.0	< DL	0.4
195Pt		0.4	0.4	0.4	0.4	0.5
197Au		0.0	< DL	0.0	< DL	0.1
205Tl		0.3	0.3	0.3	0.2	0.5
206Pb	11	12.0	13.6	12.5	14.0	16.0
207Pb	11	10.6	12.8	11.5	12.6	14.8
208Pb	11	11.2	12.7	11.9	12.7	15.0
209Bi		0.2	0.1	0.0	< DL	1.3
220Bkg		--	--	--	--	--
232Th	6.2	6.3	7.1	6.3	5.4	7.7
238U	1.69	1.9	1.8	1.7	0.9	3.5
254U O		--	--	--	--	--

Ca Internal Isotope	BCR-2G Pub. Conc.	Count	Min	Max	Average	Sigma
7Li	9	11	9.0	15.6	11.4	3.5103459
9Be		7	2.0	3.6	2.6	1.305878
11B		10	16.9	23.3	19.1	5.7813523
23Na	23400	11	19458.2	26329.0	22237.7	6483.2404
25Mg	21600	11	21600.0	27473.4	24307.9	6895.6112
27Al	71400	11	71400.0	102535.3	89319.5	25598.832
29Si	253000	11	253000.0	360224.4	309682.9	90085.323
31P	1500	11	1256.0	1740.2	1477.2	431.9473
33S		5	9.0	16.1	12.6	6.5695635
39K	14900	11	14900.0	22744.5	19063.9	5722.9564
43Ca	50900	11	50900.0	58037.5	54556.6	15278.207
44Ca	50900	11	50900.0	50900.0	50900.0	14068.017
45Sc	33	11	33.0	37.7	34.9	9.7163611
47Ti	13500	11	13500.0	15969.5	14504.5	4051.8781
51V	416	11	415.8	463.7	436.3	121.52972
52Cr	18	11	15.0	18.7	16.5	4.6843322
53Cr	18	11	15.1	18.7	16.5	4.7183447
55Mn	1520	11	1520.0	2008.7	1764.6	501.24045
57Fe	96600	11	96600.0	124914.3	113967.7	32237.764
59Co	37	11	37.0	46.4	41.8	11.823024
60Ni		9	13.1	16.6	14.6	5.7599043
62Ni		5	17.0	38.2	26.9	14.351221
65Cu	19	9	17.3	25.4	20.9	9.2993637
66Zn	127	11	127.0	206.0	175.3	53.19222
68Zn	127	11	127.0	216.1	183.7	55.624862
69Ga	23	11	23.0	41.5	36.0	10.891395
72Ge		10	2.8	5.5	3.5	1.2497721
75As		8	1.7	3.2	2.3	1.0847889
77Ar Cl		0	0.0	0.0	- -	0
82Se		1	-0.9	-0.9	-0.9	0.2654931
83Kr		0	0.0	0.0	- -	0
85Rb	48	11	45.7	54.3	49.5	13.911563
86Sr	346	11	336.4	399.7	351.2	98.545265
88Sr	346	11	328.3	398.4	348.4	98.018741
89Y	37	11	29.6	37.3	33.2	9.4105623
90Zr	188	11	173.6	211.9	185.3	52.066584
93Nb		10	11.8	14.2	12.5	3.6969947
95Mo	248	11	242.3	291.8	261.0	73.76329
103Rh		2	0.0	0.0	0.0	0.009514
105Pd		0	0.0	0.0	- -	0
107Ag		9	0.3	1.5	0.7	0.3867988
110Cd		6	0.2	1.2	0.4	0.3346058
111Cd		3	0.2	1.3	0.6	0.3768879
115In		7	0.1	1.2	0.3	0.3339325
118Sn		10	2.2	4.8	3.0	1.092628
120Sn		10	2.2	4.7	3.0	1.0718595
121Sb		7	0.3	1.5	0.5	0.4071751
133Cs	1.1	10	0.7	2.2	1.2	0.5647605
136Ba	683	11	666.1	786.3	698.0	195.8985
137Ba	683	11	676.3	805.0	709.8	199.58337

Ca Internal Isotope	BCR-2G Pub. Conc.	Count	Min	Max	Average	Sigma
139La	25.4	11	25.2	31.9	27.4	7.7888985
140Ce	53	11	51.3	60.2	53.7	15.082063
141Pr	6.5	11	5.7	8.1	6.8	1.9553761
146Nd	29	11	27.4	33.8	30.1	8.4654477
147Sm	6.6	11	5.9	8.9	7.1	2.0854102
153Eu	2	11	1.6	3.4	2.2	0.7647965
155Gd	7	11	6.0	7.9	6.9	1.9802928
156Ce O		0	0.0	0.0	- -	0
157Gd	7	11	5.3	7.2	6.5	1.8593127
159Tb	1.1	10	0.4	2.5	1.2	0.6333076
163Dy	6.4	11	5.1	7.2	6.4	1.8434501
165Ho	1.25	11	0.5	2.8	1.3	0.6387372
166Er	3.6	11	3.0	4.0	3.5	0.9955755
169Tm	0.57	8	0.4	1.7	0.7	0.4495869
172Yb	3.4	11	2.8	5.1	3.5	1.1157865
175Lu	0.51	8	0.5	1.7	0.7	0.4703945
178Hf	4.8	11	4.2	5.7	4.9	1.4240477
181Ta		8	0.6	1.8	0.9	0.5077142
182W		7	0.6	2.3	0.9	0.6268277
185Re		3	0.0	0.4	0.2	0.1190479
195Pt		10	0.3	0.5	0.4	0.1281692
197Au		5	0.0	0.1	0.0	0.0277156
205Tl		9	0.2	0.5	0.3	0.1397749
206Pb	11	11	11.0	16.0	12.4	3.7100457
207Pb	11	11	10.1	14.8	11.4	3.4210952
208Pb	11	11	10.4	15.0	11.8	3.487824
209Bi		7	0.0	1.3	0.3	0.3515966
220Bkg		0	0.0	0.0	- -	0
232Th	6.2	11	5.4	7.7	6.3	1.8394622
238U	1.69	11	0.9	3.5	1.8	0.7565421
254U O		0	0.0	0.0	- -	0

Fe Internal Isotope	BCR-2G Pub. Conc.	Ap16A09	Ap16A10	Ap16B09	Ap16B10	Ap16C09
7Li	9	9.5	9.3	8.4	9.0	10.4
9Be		< DL	< DL	1.7	2.1	2.6
11B		18.1	16.5	14.3	16.6	15.1
23Na	23400	18566.8	19839.9	16715.7	17854.6	17406.5
25Mg	21600	20132.5	20682.3	19533.8	19044.2	21393.9
27Al	71400	78117.1	77167.0	73383.8	73313.2	79088.4
29Si	253000	244709.9	248396.5	245749.8	253989.0	268350.2
31P	1500	1110.1	1087.0	1136.3	1209.7	1259.0
33S		< DL	< DL	< DL	< DL	14.4
39K	14900	14352.3	14654.9	14545.9	14465.5	17728.0
43Ca	50900	47293.9	42079.8	44186.9	42625.7	50579.2
44Ca	50900	44988.4	41509.2	42638.9	42162.2	45533.2
45Sc	33	30.2	28.2	28.1	28.5	32.0
47Ti	13500	12623.2	12002.8	11799.1	12010.0	12471.5
51V	416	372.7	369.8	361.3	360.3	371.9
52Cr	18	13.6	13.3	12.6	12.9	14.9
53Cr	18	13.4	13.3	13.7	13.9	13.7
55Mn	1520	1419.1	1447.2	1505.6	1468.2	1517.9
57Fe	96600	96600.0	96600.0	96600.0	96600.0	96600.0
59Co	37	33.5	34.0	34.4	34.9	36.2
60Ni		< DL	< DL	11.5	11.4	12.3
62Ni		< DL	< DL	23.3	< DL	< DL
65Cu	19	< DL	< DL	17.1	15.7	17.4
66Zn	127	129.0	133.4	145.5	144.3	156.5
68Zn	127	143.5	143.3	153.1	153.0	161.6
69Ga	23	31.0	29.6	30.5	30.8	30.9
72Ge		2.5	2.3	2.6	2.6	3.3
75As		< DL	< DL	1.8	1.9	2.3
77Ar Cl		--	--	--	--	--
82Se		< DL	-0.8	< DL	< DL	< DL
83Kr		--	--	--	--	--
85Rb	48	40.4	40.4	41.2	41.0	41.7
86Sr	346	307.4	299.6	286.1	291.0	302.9
88Sr	346	309.8	299.8	285.1	286.8	296.0
89Y	37	29.6	27.6	27.2	27.5	28.4
90Zr	188	165.7	154.8	151.5	155.3	159.3
93Nb		10.7	9.8	10.3	10.3	10.7
95Mo	248	214.1	214.5	211.3	219.6	221.8
103Rh		< DL	< DL	< DL	< DL	< DL
105Pd		< DL	< DL	< DL	< DL	< DL
107Ag		0.5	< DL	0.5	0.5	0.5
110Cd		< DL	< DL	0.2	0.2	0.3
111Cd		< DL	< DL	< DL	< DL	0.4
115In		< DL	< DL	0.1	0.1	0.4
118Sn		2.0	2.5	2.2	2.3	2.6
120Sn		2.3	2.3	2.3	2.3	2.5
121Sb		< DL	< DL	0.2	0.2	0.5
133Cs	1.1	< DL	< DL	0.9	0.9	1.2
136Ba	683	632.1	598.7	566.0	561.3	606.7
137Ba	683	640.0	611.0	573.8	566.5	616.1

Fe Internal Isotope	BCR-2G Pub. Conc.	Ap16A09	Ap16A10	Ap16B09	Ap16B10	Ap16C09
139La	25.4	24.7	23.1	22.2	22.0	24.1
140Ce	53	47.7	45.3	43.2	43.2	46.7
141Pr	6.5	6.1	5.4	5.4	5.4	6.0
146Nd	29	27.1	25.3	24.2	24.5	26.5
147Sm	6.6	6.0	5.4	5.8	5.7	6.3
153Eu	2	1.9	1.4	1.8	1.8	2.1
155Gd	7	6.3	5.3	5.5	5.8	6.1
156Ce O		--	--	--	--	--
157Gd	7	6.0	5.3	5.1	5.5	5.6
159Tb	1.1	0.8	< DL	0.8	0.8	1.2
163Dy	6.4	5.9	4.8	5.0	5.4	5.9
165Ho	1.25	1.1	< DL	1.0	1.0	1.3
166Er	3.6	2.9	2.6	2.7	2.8	3.1
169Tm	0.57	< DL	< DL	0.4	0.4	0.6
172Yb	3.4	3.1	2.6	2.8	2.9	3.1
175Lu	0.51	< DL	< DL	0.4	0.4	0.7
178Hf	4.8	4.3	3.5	3.9	3.9	4.8
181Ta		< DL	< DL	0.6	0.5	0.8
182W		< DL	< DL	0.5	0.5	0.7
185Re		< DL	< DL	< DL	< DL	0.1
195Pt		0.4	0.3	0.3	0.3	0.2
197Au		< DL	< DL	0.0	0.0	< DL
205Tl		0.2	< DL	0.2	0.2	0.3
206Pb	11	9.8	9.3	9.3	10.1	10.3
207Pb	11	8.9	8.3	8.7	9.1	9.6
208Pb	11	9.2	10.0	9.0	9.1	9.5
209Bi		< DL	< DL	0.0	0.0	0.2
220Bkg		--	--	--	--	--
232Th	6.2	5.6	4.8	4.9	5.1	5.4
238U	1.69	1.5	1.1	1.3	1.4	1.6
254U O		--	--	--	--	--

Fe Internal Isotope	BCR-2G Pub. Conc.	Ap16C10	Ap16D09	Ap16D10	Ap16E09	Ap16E10
7Li	9	10.2	9.6	9.7	8.8	12.4
9Be		2.0	2.0	1.7	< DL	2.9
11B		15.9	13.9	14.5	16.2	18.5
23Na	23400	16568.1	20361.0	18554.5	18747.0	19743.0
25Mg	21600	20452.5	21246.0	20724.5	20817.7	21135.3
27Al	71400	74657.6	79293.7	75937.8	75385.5	74425.1
29Si	253000	259000.9	278572.4	270756.6	286054.6	275493.8
31P	1500	1179.6	1263.4	1232.1	1443.3	1385.3
33S		< DL	7.5	7.6	10.4	12.6
39K	14900	17155.1	15626.1	17477.7	19353.9	17386.1
43Ca	50900	47754.1	41806.8	47662.2	49385.6	46075.6
44Ca	50900	43076.0	39362.5	42593.6	43312.1	40517.3
45Sc	33	29.2	29.2	29.5	28.9	29.1
47Ti	13500	11982.4	12349.7	12390.5	12467.3	11890.3
51V	416	362.1	355.9	366.3	371.3	369.1
52Cr	18	13.1	14.4	14.5	13.4	13.7
53Cr	18	13.8	14.2	13.1	12.8	14.9
55Mn	1520	1523.5	1553.4	1537.4	1510.3	1451.1
57Fe	96600	96600.0	96600.0	96600.0	96600.0	96600.0
59Co	37	34.9	35.9	35.6	36.8	36.3
60Ni		11.9	12.9	11.4	13.9	13.1
62Ni		< DL	29.5	26.3	< DL	< DL
65Cu	19	14.7	16.2	18.8	21.7	19.2
66Zn	127	146.7	153.7	156.7	173.4	164.0
68Zn	127	151.4	158.9	163.4	180.0	172.0
69Ga	23	30.0	32.1	31.6	31.7	32.8
72Ge		3.1	2.9	3.0	2.4	4.4
75As		1.4	1.7	1.4	2.0	2.6
77Ar Cl		--	--	--	--	--
82Se		< DL	< DL	< DL	< DL	< DL
83Kr		--	--	--	--	--
85Rb	48	40.5	41.9	42.1	42.3	43.2
86Sr	346	284.7	309.1	283.9	287.9	284.3
88Sr	346	279.4	308.1	287.6	279.3	278.9
89Y	37	26.6	28.9	26.9	25.2	26.4
90Zr	188	148.3	163.9	152.9	147.7	145.4
93Nb		10.0	11.0	10.4	10.0	11.3
95Mo	248	205.7	225.6	220.3	227.0	229.3
103Rh		0.0	< DL	< DL	< DL	< DL
105Pd		< DL	< DL	< DL	< DL	< DL
107Ag		0.5	0.4	0.5	0.2	1.2
110Cd		< DL	0.3	0.3	< DL	1.0
111Cd		< DL	< DL	< DL	< DL	1.0
115In		0.2	0.1	0.1	< DL	1.0
118Sn		2.4	2.2	2.9	1.9	3.8
120Sn		2.4	2.4	3.1	1.9	3.7
121Sb		0.5	0.2	0.3	< DL	1.2
133Cs	1.1	1.0	1.0	0.9	0.6	1.8
136Ba	683	570.4	608.1	558.6	566.8	573.1
137Ba	683	580.2	622.5	576.1	575.5	587.4

Fe Internal Isotope	BCR-2G Pub. Conc.	Ap16C10	Ap16D09	Ap16D10	Ap16E09	Ap16E10
139La	25.4	22.1	24.7	22.3	21.4	23.7
140Ce	53	44.1	46.6	43.1	43.7	45.8
141Pr	6.5	5.7	6.0	5.4	4.9	6.4
146Nd	29	24.9	26.2	24.6	23.4	25.6
147Sm	6.6	5.9	6.3	5.9	5.0	7.1
153Eu	2	2.2	1.9	1.7	1.4	2.7
155Gd	7	5.6	6.1	5.5	5.1	6.3
156Ce O		--	--	--	--	--
157Gd	7	5.4	5.4	5.1	4.5	5.8
159Tb	1.1	1.1	0.9	0.8	0.3	2.0
163Dy	6.4	5.4	5.6	5.0	4.4	5.8
165Ho	1.25	1.1	1.2	1.0	0.4	2.3
166Er	3.6	3.1	3.0	2.8	2.6	3.2
169Tm	0.57	0.4	0.5	0.4	< DL	1.3
172Yb	3.4	2.9	3.1	2.8	2.3	4.0
175Lu	0.51	0.5	0.4	0.4	< DL	1.4
178Hf	4.8	4.2	4.4	3.9	3.5	4.5
181Ta		0.8	0.6	0.6	< DL	1.5
182W		0.8	0.5	0.5	< DL	1.8
185Re		< DL	< DL	< DL	< DL	0.3
195Pt		0.3	0.3	0.4	0.3	0.4
197Au		< DL	< DL	0.0	< DL	0.1
205Tl		0.3	0.2	0.2	0.2	0.4
206Pb	11	10.2	10.5	10.5	11.9	12.7
207Pb	11	9.0	9.9	9.7	10.8	11.8
208Pb	11	9.5	9.8	10.0	10.8	12.0
209Bi		0.2	0.0	0.0	< DL	1.0
220Bkg		--	--	--	--	--
232Th	6.2	5.4	5.5	5.2	4.6	6.2
238U	1.69	1.6	1.4	1.4	0.8	2.8
254U O		--	--	--	--	--

Fe Internal Isotope	BCR-2G Pub. Conc.	Count	Min	Max	Average	Sigma
7Li	9	11	8.4	12.4	9.7	2.8465209
9Be		7	1.7	2.9	2.1	1.0799532
11B		10	13.9	18.5	16.0	4.8038437
23Na	23400	11	16568.1	23400.0	18887.0	5513.2786
25Mg	21600	11	19044.2	21600.0	20614.8	5742.7829
27Al	71400	11	71400.0	79293.7	75651.7	21037.74
29Si	253000	11	244709.9	286054.6	262188.5	73636.752
31P	1500	11	1087.0	1500.0	1255.1	368.33491
33S		5	7.5	14.4	10.5	5.5363272
39K	14900	11	14352.3	19353.9	16149.6	4733.2668
43Ca	50900	11	41806.8	50900.0	46395.4	13175.176
44Ca	50900	11	39362.5	50900.0	43326.7	12298.688
45Sc	33	11	28.1	33.0	29.6	8.3093634
47Ti	13500	11	11799.1	13500.0	12317.0	3432.2889
51V	416	11	355.9	416.0	370.6	103.47072
52Cr	18	11	12.6	18.0	14.0	4.1121873
53Cr	18	11	12.8	18.0	14.1	4.09621
55Mn	1520	11	1419.1	1553.4	1495.8	415.24234
57Fe	96600	11	96600.0	96600.0	96600.0	26698.83
59Co	37	11	33.5	37.0	35.4	9.8432017
60Ni		8	11.4	13.9	12.3	5.5222048
62Ni		3	23.3	29.5	26.4	11.822912
65Cu	19	9	14.7	21.7	17.7	7.8761075
66Zn	127	11	127.0	173.4	148.2	43.05721
68Zn	127	11	127.0	180.0	155.2	44.908452
69Ga	23	11	23.0	32.8	30.4	8.7279932
72Ge		10	2.3	4.4	2.9	1.0092876
75As		8	1.4	2.6	1.9	0.900639
77Ar Cl		0	0.0	0.0	- -	0
82Se		1	-0.8	-0.8	-0.8	0.2165108
83Kr		0	0.0	0.0	- -	0
85Rb	48	11	40.4	48.0	42.1	11.792846
86Sr	346	11	283.9	346.0	298.4	84.18179
88Sr	346	11	278.9	346.0	296.1	83.826088
89Y	37	11	25.2	37.0	28.3	8.3253841
90Zr	188	11	145.4	188.0	157.5	44.893405
93Nb		10	9.8	11.3	10.5	3.0372437
95Mo	248	11	205.7	248.0	221.6	62.098993
103Rh		1	0.0	0.0	0.0	0.0063764
105Pd		0	0.0	0.0	- -	0
107Ag		9	0.2	1.2	0.5	0.3110167
110Cd		6	0.2	1.0	0.4	0.2671579
111Cd		2	0.4	1.0	0.7	0.3056967
115In		7	0.1	1.0	0.3	0.2680079
118Sn		10	1.9	3.8	2.5	0.8786805
120Sn		10	1.9	3.7	2.5	0.8633459
121Sb		7	0.2	1.2	0.4	0.3275196
133Cs	1.1	9	0.6	1.8	1.0	0.5189362
136Ba	683	11	558.6	683.0	593.2	167.60667
137Ba	683	11	566.5	683.0	602.9	169.81357

Fe Internal Isotope	BCR-2G Pub. Conc.	Count	Min	Max	Average	Sigma
139La	25.4	11	21.4	25.4	23.3	6.5415056
140Ce	53	11	43.1	53.0	45.7	12.898451
141Pr	6.5	11	4.9	6.5	5.7	1.648809
146Nd	29	11	23.4	29.0	25.6	7.2066295
147Sm	6.6	11	5.0	7.1	6.0	1.7337777
153Eu	2	11	1.4	2.7	1.9	0.6257516
155Gd	7	11	5.1	7.0	5.9	1.6995674
156Ce O		0	0.0	0.0	- -	0
157Gd	7	11	4.5	7.0	5.5	1.6276125
159Tb	1.1	10	0.3	2.0	1.0	0.5190714
163Dy	6.4	11	4.4	6.4	5.4	1.5869183
165Ho	1.25	10	0.4	2.3	1.2	0.585139
166Er	3.6	11	2.6	3.6	2.9	0.8583046
169Tm	0.57	8	0.4	1.3	0.6	0.3646086
172Yb	3.4	11	2.3	4.0	3.0	0.9241389
175Lu	0.51	8	0.4	1.4	0.6	0.3816151
178Hf	4.8	11	3.5	4.8	4.2	1.2201672
181Ta		7	0.5	1.5	0.8	0.439437
182W		7	0.5	1.8	0.8	0.5042673
185Re		2	0.1	0.3	0.2	0.0957533
195Pt		10	0.2	0.4	0.3	0.1071391
197Au		4	0.0	0.1	0.0	0.022567
205Tl		9	0.2	0.4	0.3	0.1133864
206Pb	11	11	9.3	12.7	10.5	3.057217
207Pb	11	11	8.3	11.8	9.7	2.8552713
208Pb	11	11	9.0	12.0	10.0	2.8888706
209Bi		7	0.0	1.0	0.2	0.2804809
220Bkg		0	0.0	0.0	- -	0
232Th	6.2	11	4.6	6.2	5.4	1.5543877
238U	1.69	11	0.8	2.8	1.5	0.6140986
254U O		0	0.0	0.0	- -	0

Scaled Isotope	BCR-2G Pub. Conc.	Ap16A09	Ap16A10	Ap16B09	Ap16B10	Ap16C09
7Li	9	9.6	9.5	8.9	9.4	10.2
9Be		< DL	< DL	1.8	2.2	2.6
11B		18.4	16.7	15.1	17.2	14.8
23Na	23400	18862.2	20115.7	17635.9	18487.4	17057.9
25Mg	21600	20452.8	20969.8	20609.3	19719.3	20965.4
27Al	71400	79360.0	78239.7	77424.1	75911.8	77504.4
29Si	253000	248603.5	251849.7	259279.8	262991.7	262975.6
31P	1500	1127.7	1102.1	1198.8	1252.5	1233.8
33S		< DL	< DL	< DL	< DL	14.1
39K	14900	14580.6	14858.6	15346.7	14978.3	17372.9
44Ca	50900	45704.3	42086.2	44986.4	43656.7	44621.2
45Sc	33	30.7	28.6	29.6	29.5	31.4
47Ti	13500	12824.0	12169.7	12448.8	12435.7	12221.7
51V	416	387.2	383.0	381.2	373.1	364.5
53Cr	18	13.6	13.5	14.4	14.4	13.4
55Mn	1520	1441.6	1467.3	1588.5	1520.2	1487.5
57Fe	96600	98137.0	97942.9	101918.4	100024.0	94665.2
59Co	37	34.0	34.5	36.3	36.1	35.5
60Ni		< DL	< DL	12.1	11.8	12.1
65Cu	19	< DL	< DL	18.0	16.3	17.0
68Zn	127	145.8	145.3	161.6	158.4	158.4
69Ga	23	31.5	30.0	32.2	31.9	30.3
72Ge		2.5	2.3	2.7	2.7	3.2
75As		< DL	< DL	1.8	1.9	2.3
82Se		0.0	0.0	< DL	< DL	< DL
85Rb	48	41.1	41.0	43.5	42.4	40.9
88Sr	346	314.7	304.0	300.8	297.0	290.0
89Y	37	30.0	27.9	28.7	28.5	27.8
90Zr	188	168.3	157.0	159.9	160.8	156.1
93Nb		10.9	10.0	10.8	10.7	10.5
95Mo	248	217.5	217.5	222.9	227.4	217.4
103Rh		< DL	< DL	< DL	< DL	< DL
105Pd		< DL	< DL	< DL	< DL	< DL
107Ag		0.5	< DL	0.6	0.5	0.5
111Cd		< DL	< DL	< DL	< DL	0.4
115In		< DL	< DL	0.1	0.1	0.4
118Sn		2.0	2.5	2.4	2.4	2.6
121Sb		< DL	< DL	0.2	0.3	0.4
133Cs	1.1	< DL	< DL	1.0	0.9	1.1
137Ba	683	650.1	619.5	605.4	586.6	603.8
139La	25.4	25.1	23.5	23.4	22.8	23.6
140Ce	53	48.5	45.9	45.5	44.7	45.7
141Pr	6.5	6.2	5.4	5.7	5.6	5.8
146Nd	29	27.5	25.7	25.5	25.3	25.9
147Sm	6.6	6.1	5.5	6.1	5.9	6.1
153Eu	2	1.9	1.5	1.9	1.8	2.0
157Gd	7	6.1	5.4	5.4	5.7	5.5
159Tb	1.1	0.8	< DL	0.9	0.9	1.2
163Dy	6.4	6.0	4.9	5.2	5.5	5.8
165Ho	1.25	1.1	< DL	1.0	1.0	1.3

Scaled Isotope	BCR-2G Pub. Conc.	Ap16A09	Ap16A10	Ap16B09	Ap16B10	Ap16C09
166Er	3.6	3.0	2.7	2.8	2.9	3.1
169Tm	0.57	< DL	< DL	0.4	0.4	0.6
172Yb	3.4	3.1	2.6	3.0	3.0	3.0
175Lu	0.51	< DL	< DL	0.4	0.4	0.7
178Hf	4.8	4.4	3.6	4.1	4.0	4.7
181Ta		0.5	< DL	0.6	0.6	0.8
182W		< DL	< DL	0.5	0.5	0.7
185Re		< DL	< DL	< DL	< DL	0.1
195Pt		0.5	0.3	0.3	0.3	0.2
197Au		< DL	< DL	0.0	0.0	< DL
205Tl		0.2	< DL	0.2	0.2	0.3
208Pb	11	9.4	10.2	9.4	9.4	9.3
209Bi		< DL	< DL	0.0	0.0	0.2
232Th	6.2	5.7	4.8	5.2	5.3	5.3
238U	1.69	1.5	1.1	1.4	1.5	1.6

Scaled Isotope	BCR-2G Pub. Conc.	Ap16C10	Ap16D09	Ap16D10	Ap16E09	Ap16E10
7Li	9	10.3	9.2	9.5	8.4	12.1
9Be		2.0	1.9	1.6	< DL	2.8
11B		16.2	13.5	14.2	15.4	18.1
23Na	23400	16836.0	19670.7	18273.6	17831.7	19329.0
25Mg	21600	20783.3	20525.7	20410.8	19801.3	20692.2
27Al	71400	75864.9	76605.4	74788.2	71705.0	72864.7
29Si	253000	263189.1	269127.9	266657.9	272088.8	269717.9
31P	1500	1198.7	1220.5	1213.4	1372.9	1356.2
33S		< DL	7.3	7.4	9.9	12.3
39K	14900	17432.5	15096.3	17213.1	18409.0	17021.6
44Ca	50900	43772.6	38028.0	41948.8	41197.5	39667.8
45Sc	33	29.6	28.2	29.0	27.5	28.5
47Ti	13500	12176.2	11931.0	12203.0	11858.6	11641.1
51V	416	367.9	343.8	360.7	353.2	361.4
53Cr	18	14.0	13.7	12.9	12.2	14.6
55Mn	1520	1548.2	1500.7	1514.1	1436.6	1420.6
57Fe	96600	98162.1	93324.9	95137.7	91883.8	94574.7
59Co	37	35.4	34.7	35.1	35.0	35.5
60Ni		12.1	12.4	11.2	13.2	12.8
65Cu	19	14.9	15.6	18.5	20.6	18.8
68Zn	127	153.8	153.5	161.0	171.3	168.4
69Ga	23	30.5	31.0	31.1	30.2	32.1
72Ge		3.2	2.8	3.0	2.2	4.3
75As		1.5	1.7	1.4	1.9	2.5
82Se		< DL	< DL	< DL	< DL	< DL
85Rb	48	41.2	40.5	41.4	40.2	42.3
88Sr	346	283.9	297.7	283.3	265.7	273.1
89Y	37	27.0	27.9	26.5	24.0	25.8
90Zr	188	150.7	158.3	150.6	140.5	142.3
93Nb		10.1	10.6	10.3	9.5	11.0
95Mo	248	209.0	218.0	217.0	216.0	224.5
103Rh		0.0	< DL	< DL	< DL	< DL
105Pd		< DL	< DL	< DL	< DL	< DL
107Ag		0.5	0.4	0.5	0.2	1.2
111Cd		< DL	< DL	< DL	< DL	1.0
115In		0.2	0.1	0.1	< DL	0.9
118Sn		2.4	2.1	2.9	1.8	3.8
121Sb		0.5	0.2	0.3	< DL	1.1
133Cs	1.1	1.0	0.9	0.9	0.5	1.7
137Ba	683	589.6	601.4	567.4	547.4	575.1
139La	25.4	22.5	23.8	21.9	20.4	23.2
140Ce	53	44.8	45.0	42.5	41.5	44.8
141Pr	6.5	5.8	5.8	5.4	4.6	6.3
146Nd	29	25.3	25.3	24.3	22.2	25.1
147Sm	6.6	6.0	6.1	5.8	4.8	6.9
153Eu	2	2.2	1.9	1.7	1.3	2.7
157Gd	7	5.5	5.3	5.1	4.3	5.6
159Tb	1.1	1.1	0.9	0.8	0.3	1.9
163Dy	6.4	5.5	5.4	4.9	4.2	5.6
165Ho	1.25	1.1	1.1	1.0	0.4	2.2

Scaled Isotope	BCR-2G Pub. Conc.	Ap16C10	Ap16D09	Ap16D10	Ap16E09	Ap16E10
166Er	3.6	3.1	2.9	2.7	2.4	3.1
169Tm	0.57	0.5	0.4	0.4	< DL	1.3
172Yb	3.4	3.0	3.0	2.7	2.2	4.0
175Lu	0.51	0.6	0.4	0.4	< DL	1.4
178Hf	4.8	4.3	4.3	3.8	3.4	4.4
181Ta		0.8	0.6	0.6	< DL	1.4
182W		0.8	0.5	0.5	< DL	1.8
185Re		< DL	< DL	< DL	< DL	0.3
195Pt		0.3	0.3	0.4	0.3	0.4
197Au		< DL	< DL	0.0	< DL	0.1
205Tl		0.3	0.2	0.2	0.2	0.4
208Pb	11	9.7	9.5	9.8	10.3	11.7
209Bi		0.2	0.0	0.0	< DL	1.0
232Th	6.2	5.5	5.3	5.2	4.3	6.0
238U	1.69	1.6	1.4	1.4	0.7	2.7

Scaled Isotope	BCR-2G Pub. Conc.	Count	Min	Max	Average	Sigma
7Li	9	11	8.4	12.1	9.7	2.8177484
9Be		7	1.6	2.8	2.1	1.0729674
11B		10	13.5	18.4	16.0	4.828105
23Na	23400	11	16836.0	23400.0	18863.7	5474.4268
25Mg	21600	11	19719.3	21600.0	20593.6	5712.1546
27Al	71400	11	71400.0	79360.0	75606.2	21035.94
29Si	253000	11	248603.5	272088.8	261771.1	72698.731
31P	1500	11	1102.1	1500.0	1252.4	361.84997
33S		5	7.3	14.1	10.2	5.3937461
39K	14900	11	14580.6	18409.0	16110.0	4626.3815
44Ca	50900	11	38028.0	50900.0	43324.5	12375.293
45Sc	33	11	27.5	33.0	29.6	8.3072616
47Ti	13500	11	11641.1	13500.0	12310.0	3433.5904
51V	416	11	343.8	416.0	372.0	104.35775
53Cr	18	11	12.2	18.0	14.1	4.1147786
55Mn	1520	11	1420.6	1588.5	1495.0	415.80117
57Fe	96600	11	91883.8	101918.4	96579.2	26832.51
59Co	37	11	34.0	37.0	35.4	9.8107063
60Ni		8	11.2	13.2	12.2	5.4628592
65Cu	19	9	14.9	20.6	17.6	7.7799085
68Zn	127	11	127.0	171.3	154.9	44.270805
69Ga	23	11	23.0	32.2	30.4	8.7096526
72Ge		10	2.2	4.3	2.9	0.9920225
75As		8	1.4	2.5	1.9	0.8894551
82Se		2	0.0	0.0	0.0	0
85Rb	48	11	40.2	48.0	42.0	11.791355
88Sr	346	11	265.7	346.0	296.0	84.183462
89Y	37	11	24.0	37.0	28.3	8.3802149
90Zr	188	11	140.5	188.0	157.5	45.112176
93Nb		10	9.5	11.0	10.5	3.0354895
95Mo	248	11	209.0	248.0	221.4	61.871645
103Rh		1	0.0	0.0	0.0	0.0064795
105Pd		0	0.0	0.0	- -	0
107Ag		9	0.2	1.2	0.5	0.3076957
111Cd		2	0.4	1.0	0.7	0.299316
115In		7	0.1	0.9	0.3	0.2622145
118Sn		10	1.8	3.8	2.5	0.8673018
121Sb		7	0.2	1.1	0.4	0.3213149
133Cs	1.1	9	0.5	1.7	1.0	0.5143102
137Ba	683	11	547.4	683.0	602.7	170.15601
139La	25.4	11	20.4	25.4	23.2	6.5481054
140Ce	53	11	41.5	53.0	45.6	12.913308
141Pr	6.5	11	4.6	6.5	5.7	1.6513303
146Nd	29	11	22.2	29.0	25.5	7.230257
147Sm	6.6	11	4.8	6.9	6.0	1.7312472
153Eu	2	11	1.3	2.7	1.9	0.6234201
157Gd	7	11	4.3	7.0	5.5	1.6398571
159Tb	1.1	10	0.3	1.9	1.0	0.5123451
163Dy	6.4	11	4.2	6.4	5.4	1.5930149
165Ho	1.25	10	0.4	2.2	1.2	0.5769847

Scaled Isotope	BCR-2G Pub. Conc.	Count	Min	Max	Average	Sigma
166Er	3.6	11	2.4	3.6	2.9	0.8576779
169Tm	0.57	8	0.4	1.3	0.6	0.3578158
172Yb	3.4	11	2.2	4.0	3.0	0.9209146
175Lu	0.51	8	0.4	1.4	0.6	0.37469
178Hf	4.8	11	3.4	4.8	4.2	1.215926
181Ta		8	0.5	1.4	0.7	0.4049331
182W		7	0.5	1.8	0.7	0.4956502
185Re		2	0.1	0.3	0.2	0.0937488
195Pt		10	0.2	0.5	0.3	0.1078974
197Au		4	0.0	0.1	0.0	0.0222946
205Tl		9	0.2	0.4	0.2	0.1126132
208Pb	11	11	9.3	11.7	10.0	2.8459212
209Bi		7	0.0	1.0	0.2	0.274622
232Th	6.2	11	4.3	6.2	5.4	1.55359
238U	1.69	11	0.7	2.7	1.5	0.6063705

Si Internal Isotope	BHVO-2 Pub. Conc.	Ap16A11	Ap16A12	Ap16B11	Ap16B12	Ap16C11
7Li	5	4.2	4.6	4.0	4.1	4.1
9Be		< DL	1.4	< DL	1.4	< DL
11B		17.5	16.9	15.2	14.7	12.4
23Na	16400	12849.3	13163.4	10905.5	11581.7	11900.3
25Mg	43600	50079.4	49470.2	45900.0	44437.0	51407.3
27Al	71600	80570.9	77620.4	72352.7	73920.8	79331.4
29Si	233000	233000.0	233000.0	233000.0	233000.0	233000.0
31P	1200	818.8	789.0	907.6	921.0	793.2
33S		< DL	< DL	12.8	< DL	< DL
39K	4300	4293.4	4130.7	4577.4	4713.4	4611.3
43Ca	81700	78769.2	76104.7	78189.9	80975.8	78194.1
44Ca	81700	75215.5	73699.1	73688.8	76876.0	76986.2
45Sc	32	29.3	27.9	27.9	27.8	29.0
47Ti	16300	15175.4	15050.1	14176.0	14318.3	14434.0
51V	317	278.4	271.5	258.9	260.7	260.1
52Cr	280	255.7	255.9	242.3	239.4	244.1
53Cr	280	269.6	260.8	242.9	247.4	236.9
55Mn	1290	1360.3	1360.3	1295.5	1309.1	1370.1
57Fe	86300	90457.1	92760.6	86262.2	87056.6	87662.7
59Co	45	42.2	41.3	41.1	41.3	39.9
60Ni	119	111.3	106.4	111.3	111.4	102.6
62Ni	119	< DL	< DL	109.0	109.0	109.5
65Cu	127	106.8	97.0	114.6	118.1	100.6
66Zn	103	92.2	86.0	113.7	108.5	92.5
68Zn	103	92.9	85.1	115.6	112.0	94.0
69Ga	21.7	20.0	19.7	20.9	22.2	18.6
72Ge		2.2	2.0	2.4	2.6	2.1
75As		< DL	< DL	0.6	1.0	0.7
77Ar Cl		--	--	--	--	--
82Se		-0.5	-1.2	< DL	< DL	< DL
83Kr		--	--	--	--	--
85Rb	9.8	7.4	7.8	7.8	8.0	7.5
86Sr	389	372.7	380.8	320.1	334.0	347.3
88Sr	389	369.3	382.6	319.7	335.7	342.3
89Y	26	21.1	20.3	18.2	19.1	19.4
90Zr	172	146.4	140.6	129.3	135.1	137.4
93Nb	18	15.1	15.0	14.1	14.0	14.2
95Mo		3.1	3.6	3.0	3.2	3.2
103Rh		< DL	< DL	< DL	< DL	< DL
105Pd		< DL	< DL	< DL	< DL	< DL
107Ag		< DL	0.3	0.5	0.4	0.4
110Cd		< DL	< DL	< DL	< DL	< DL
111Cd		< DL	< DL	0.2	< DL	< DL
115In		< DL	< DL	0.1	0.1	< DL
118Sn	1.9	2.0	2.1	1.8	2.0	1.6
120Sn	1.9	2.0	2.1	1.9	2.1	1.7
121Sb		< DL	< DL	0.1	0.1	< DL
133Cs		< DL	< DL	< DL	0.1	< DL
136Ba	130	120.1	126.3	104.8	110.2	117.6
137Ba	130	125.1	130.0	109.4	114.6	121.0

Si Internal Isotope	BHVO-2 Pub. Conc.	Ap16A11	Ap16A12	Ap16B11	Ap16B12	Ap16C11
139La	15.5	14.6	15.0	12.8	13.0	14.1
140Ce	37.4	34.5	36.0	30.5	31.8	32.7
141Pr	5	4.6	4.8	4.2	4.3	4.6
146Nd	25	22.4	22.8	20.1	21.2	21.8
147Sm	6.1	5.9	5.7	4.8	5.6	5.4
153Eu	2.1	1.8	2.1	1.8	1.9	1.9
155Gd	6.5	5.2	5.1	4.6	5.0	5.3
156Ce O		--	--	--	--	--
157Gd	6.5	4.9	4.9	4.8	4.4	5.0
159Tb	0.96	0.7	0.7	0.6	0.7	0.8
163Dy	5.2	4.5	4.5	3.6	4.1	4.2
165Ho	0.93	0.8	0.8	0.7	0.8	0.8
166Er	2.5	1.9	1.9	1.8	2.0	1.9
169Tm	0.36	< DL	0.3	0.2	0.3	0.2
172Yb	2	1.6	1.7	1.6	1.6	1.6
175Lu	0.28	< DL	0.3	0.2	0.2	0.2
178Hf	4.1	3.6	3.5	3.3	3.5	3.8
181Ta	1.4	0.8	0.8	0.8	0.8	0.8
182W		0.3	0.2	0.2	0.2	0.2
185Re		< DL	< DL	< DL	< DL	< DL
195Pt		0.1	< DL	0.1	0.1	0.1
197Au		0.3	0.3	0.3	0.4	0.2
205Tl		< DL	< DL	0.0	0.0	< DL
206Pb		1.4	1.5	1.7	1.7	1.5
207Pb		1.4	1.4	1.6	1.7	1.4
208Pb		1.4	1.5	1.6	1.7	1.4
209Bi		< DL	< DL	0.0	0.0	< DL
220Bkg		--	--	--	--	--
232Th	1.2	1.1	1.1	1.0	1.1	1.0
238U		0.4	0.4	0.3	0.3	0.3
254U O		--	--	--	--	--

Si Internal Isotope	BHVO-2 Pub. Conc.	Ap16C12	Ap16D11	Ap16D12	Ap16E11	Ap16E12
7Li	5	4.7	4.6	4.6	2.9	4.0
9Be		0.8	1.4	0.9	< DL	1.1
11B		12.8	14.1	13.1	10.0	13.3
23Na	16400	11785.9	12175.0	12210.9	12638.6	11957.7
25Mg	43600	52880.3	51033.1	50586.6	46930.1	49498.6
27Al	71600	79123.0	78368.4	76853.6	68116.1	71746.0
29Si	233000	233000.0	233000.0	233000.0	233000.0	233000.0
31P	1200	805.3	813.2	761.6	964.8	928.1
33S		< DL	< DL	7.4	< DL	13.8
39K	4300	4411.3	4492.7	4385.9	4829.7	4555.4
43Ca	81700	78948.4	79336.5	78361.0	70193.0	71143.7
44Ca	81700	76946.0	75337.1	75891.6	65878.7	69838.6
45Sc	32	29.0	29.6	27.6	24.5	25.5
47Ti	16300	14828.4	14829.4	14514.7	13372.5	14148.3
51V	317	269.4	265.8	261.0	267.2	280.0
52Cr	280	248.5	252.0	249.0	249.8	255.6
53Cr	280	255.4	258.5	251.8	256.3	261.9
55Mn	1290	1473.5	1349.0	1378.8	1338.9	1452.6
57Fe	86300	97095.7	85889.0	87591.0	90391.1	96270.4
59Co	45	42.5	40.6	40.5	40.5	42.2
60Ni	119	107.8	107.0	100.6	111.3	111.0
62Ni	119	115.5	99.8	106.8	93.5	123.6
65Cu	127	97.0	109.8	98.2	110.4	104.7
66Zn	103	90.6	100.9	89.2	93.7	91.4
68Zn	103	89.4	99.7	89.3	98.9	89.9
69Ga	21.7	19.6	20.4	19.0	19.7	18.5
72Ge		2.2	2.2	2.2	1.8	1.9
75As		1.6	2.0	0.7	0.8	1.7
77Ar Cl		--	--	--	--	--
82Se		< DL	< DL	< DL	< DL	< DL
83Kr		--	--	--	--	--
85Rb	9.8	8.0	7.7	7.8	7.3	7.5
86Sr	389	376.9	353.2	360.5	303.4	337.8
88Sr	389	377.4	352.8	361.7	298.7	327.5
89Y	26	21.6	21.0	20.0	15.6	17.5
90Zr	172	147.8	148.2	141.0	115.9	124.6
93Nb	18	15.5	14.8	14.7	12.3	13.6
95Mo		3.3	3.4	3.4	2.6	3.4
103Rh		< DL	< DL	< DL	< DL	< DL
105Pd		< DL	< DL	< DL	< DL	< DL
107Ag		0.4	0.3	0.3	< DL	< DL
110Cd		0.2	< DL	< DL	< DL	< DL
111Cd		< DL	< DL	< DL	< DL	< DL
115In		0.0	0.1	0.1	< DL	< DL
118Sn	1.9	1.8	1.8	1.8	0.8	1.8
120Sn	1.9	1.8	1.9	1.9	0.9	1.6
121Sb		0.1	0.1	0.1	< DL	< DL
133Cs		0.1	< DL	0.1	< DL	< DL
136Ba	130	129.5	116.6	117.5	100.6	105.4
137Ba	130	132.1	117.2	121.1	100.4	108.8

Si Internal Isotope	BHVO-2 Pub. Conc.	Ap16C12	Ap16D11	Ap16D12	Ap16E11	Ap16E12
139La	15.5	15.5	14.1	14.3	10.6	11.9
140Ce	37.4	36.6	32.1	33.6	27.6	30.6
141Pr	5	4.9	4.3	4.6	3.2	3.9
146Nd	25	24.2	21.8	22.4	17.1	19.6
147Sm	6.1	6.2	5.0	5.4	3.8	4.5
153Eu	2.1	2.1	1.9	2.0	0.7	1.6
155Gd	6.5	5.8	5.6	4.8	3.4	4.0
156Ce O		--	--	--	--	--
157Gd	6.5	5.6	4.9	5.1	3.3	4.1
159Tb	0.96	0.8	0.8	0.8	< DL	0.6
163Dy	5.2	4.6	4.5	4.1	2.7	3.6
165Ho	0.93	0.9	0.8	0.8	< DL	0.5
166Er	2.5	2.0	2.0	1.9	0.6	1.6
169Tm	0.36	0.3	0.3	0.3	< DL	0.2
172Yb	2	1.8	1.9	1.7	< DL	1.4
175Lu	0.28	0.2	0.2	0.2	< DL	0.1
178Hf	4.1	4.0	3.9	3.5	2.1	3.0
181Ta	1.4	0.9	0.9	0.8	< DL	0.6
182W		0.2	0.2	0.2	< DL	< DL
185Re		< DL	< DL	< DL	< DL	< DL
195Pt		0.1	< DL	< DL	0.1	0.1
197Au		0.2	0.2	0.3	0.3	0.3
205Tl		< DL	< DL	< DL	< DL	< DL
206Pb		1.6	1.6	1.4	0.8	1.2
207Pb		1.4	1.5	1.2	0.7	1.1
208Pb		1.4	1.6	1.3	0.7	1.1
209Bi		< DL	0.0	0.0	< DL	< DL
220Bkg		--	--	--	--	--
232Th	1.2	1.1	1.1	1.1	0.3	0.8
238U		0.4	0.3	0.4	< DL	0.2
254U O		--	--	--	--	--

Si Internal Isotope	BHVO-2 Pub. Conc.	Count	Min	Max	Average	Sigma
7Li	5	11	2.9	5.0	4.2	1.2820507
9Be		6	0.8	1.4	1.2	0.6172662
11B		10	10.0	17.5	14.0	4.4885562
23Na	16400	11	10905.5	16400.0	12506.2	3695.7313
25Mg	43600	11	43600.0	52880.3	48711.1	13745.115
27Al	71600	11	68116.1	80570.9	75418.5	21170.298
29Si	233000	11	233000.0	233000.0	233000.0	64397.798
31P	1200	11	761.6	1200.0	882.1	269.42684
33S		3	7.4	13.8	11.3	5.2594846
39K	4300	11	4130.7	4829.7	4481.9	1252.5276
43Ca	81700	11	70193.0	81700.0	77446.9	21664.879
44Ca	81700	11	65878.7	81700.0	74732.5	20994.233
45Sc	32	11	24.5	32.0	28.2	8.0048092
47Ti	16300	11	13372.5	16300.0	14649.7	4105.2406
51V	317	11	258.9	317.0	271.8	76.6414
52Cr	280	11	239.4	280.0	252.0	70.348248
53Cr	280	11	236.9	280.0	256.5	71.741594
55Mn	1290	11	1290.0	1473.5	1361.7	380.09721
57Fe	86300	11	85889.0	97095.7	89794.2	25087.781
59Co	45	11	39.9	45.0	41.6	11.556229
60Ni	119	11	100.6	119.0	109.1	30.489642
62Ni	119	9	93.5	123.6	109.5	48.014479
65Cu	127	11	97.0	127.0	107.7	31.016072
66Zn	103	11	86.0	113.7	96.5	27.845214
68Zn	103	11	85.1	115.6	97.2	28.314963
69Ga	21.7	11	18.5	22.2	20.0	5.6436294
72Ge		10	1.8	2.6	2.2	0.6538526
75As		8	0.6	2.0	1.1	0.6586759
77Ar Cl		0	0.0	0.0	- -	0
82Se		2	-1.2	-0.5	-0.8	0.3501857
83Kr		0	0.0	0.0	- -	0
85Rb	9.8	11	7.3	9.8	7.9	2.2637977
86Sr	389	11	303.4	389.0	352.3	100.43176
88Sr	389	11	298.7	389.0	350.6	100.35841
89Y	26	11	15.6	26.0	20.0	6.0335855
90Zr	172	11	115.9	172.0	139.8	40.911544
93Nb	18	11	12.3	18.0	14.7	4.2514607
95Mo		10	2.6	3.6	3.2	0.9535669
103Rh		0	0.0	0.0	- -	0
105Pd		0	0.0	0.0	- -	0
107Ag		7	0.3	0.5	0.4	0.1786451
110Cd		1	0.2	0.2	0.2	0.049264
111Cd		1	0.2	0.2	0.2	0.0485486
115In		5	0.0	0.1	0.1	0.0365249
118Sn	1.9	11	0.8	2.1	1.8	0.5758979
120Sn	1.9	11	0.9	2.1	1.8	0.5863716
121Sb		5	0.1	0.1	0.1	0.0506236
133Cs		3	0.1	0.1	0.1	0.0410681
136Ba	130	11	100.6	130.0	116.2	33.419588
137Ba	130	11	100.4	132.1	119.1	34.182246

Si Internal Isotope	BHVO-2 Pub. Conc.	Count	Min	Max	Average	Sigma
139La	15.5	11	10.6	15.5	13.8	4.0559555
140Ce	37.4	11	27.6	37.4	33.0	9.5231245
141Pr	5	11	3.2	5.0	4.4	1.3051769
146Nd	25	11	17.1	25.0	21.7	6.307214
147Sm	6.1	11	3.8	6.2	5.3	1.6057905
153Eu	2.1	11	0.7	2.1	1.8	0.6234268
155Gd	6.5	11	3.4	6.5	5.0	1.5859985
156Ce O		0	0.0	0.0	- -	0
157Gd	6.5	11	3.3	6.5	4.9	1.5335264
159Tb	0.96	10	0.6	1.0	0.8	0.2955601
163Dy	5.2	11	2.7	5.2	4.2	1.2970186
165Ho	0.93	10	0.5	0.9	0.8	0.307727
166Er	2.5	11	0.6	2.5	1.8	0.6626366
169Tm	0.36	9	0.2	0.4	0.3	0.1192492
172Yb	2	10	1.4	2.0	1.7	0.6436268
175Lu	0.28	9	0.1	0.3	0.2	0.1008661
178Hf	4.1	11	2.1	4.1	3.5	1.0884487
181Ta	1.4	10	0.6	1.4	0.9	0.3640644
182W		8	0.2	0.3	0.2	0.0972604
185Re		0	0.0	0.0	- -	0
195Pt		7	0.1	0.1	0.1	0.0455041
197Au		10	0.2	0.4	0.3	0.0847861
205Tl		2	0.0	0.0	0.0	0.0093579
206Pb		10	0.8	1.7	1.4	0.4776912
207Pb		10	0.7	1.7	1.3	0.4564449
208Pb		10	0.7	1.7	1.4	0.4689274
209Bi		4	0.0	0.0	0.0	0.0090777
220Bkg		0	0.0	0.0	- -	0
232Th	1.2	11	0.3	1.2	1.0	0.3546176
238U		9	0.2	0.4	0.3	0.1327917
254U O		0	0.0	0.0	- -	0

Ca Internal Isotope	BHVO-2 Pub. Conc.	Ap16A11 BHVO-2	Ap16A12 BHVO-2	Ap16B11 BHVO-2	Ap16B12 BHVO-2	Ap16C11 BHVO-2
7Li	5	4.5	5.1	4.4	4.4	4.3
9Be		< DL	1.6	< DL	1.5	< DL
11B		19.0	18.7	16.9	15.6	13.2
23Na	16400	13957.1	14592.5	12091.2	12308.4	12629.0
25Mg	43600	54396.8	54840.7	50890.1	47225.5	54554.9
27Al	71600	87517.1	86047.0	80218.7	78559.3	84188.8
29Si	233000	253087.4	258294.8	258330.9	247620.9	247266.4
31P	1200	889.4	874.6	1006.3	978.8	841.8
33S		< DL	< DL	14.2	< DL	< DL
39K	4300	4663.5	4579.2	5075.1	5009.2	4893.7
43Ca	81700	85560.0	84366.7	86690.4	86057.0	82981.9
44Ca	81700	81700.0	81700.0	81700.0	81700.0	81700.0
45Sc	32	31.8	30.9	31.0	29.6	30.7
47Ti	16300	16483.7	16684.0	15717.2	15216.8	15317.7
51V	317	302.4	300.9	287.0	277.0	276.0
52Cr	280	277.7	283.7	268.7	254.4	259.1
53Cr	280	292.8	289.1	269.4	263.0	251.4
55Mn	1290	1477.6	1508.0	1436.3	1391.3	1454.0
57Fe	86300	98255.6	102830.8	95640.3	92519.4	93030.2
59Co	45	45.9	45.8	45.5	43.8	42.4
60Ni	119	120.9	118.0	123.4	118.4	108.8
62Ni	119	< DL	< DL	120.8	115.8	116.2
65Cu	127	116.0	107.6	127.1	125.6	106.8
66Zn	103	100.2	95.4	126.0	115.3	98.1
68Zn	103	100.9	94.3	128.2	119.0	99.8
69Ga	21.7	21.7	21.8	23.2	23.6	19.8
72Ge		2.4	2.2	2.7	2.7	2.2
75As		< DL	< DL	0.7	1.1	0.7
77Ar Cl		--	--	--	--	--
82Se		-0.5	-1.3	< DL	< DL	< DL
83Kr		--	--	--	--	--
85Rb	9.8	8.1	8.7	8.7	8.5	8.0
86Sr	389	404.9	422.1	354.9	354.9	368.6
88Sr	389	401.2	424.2	354.4	356.7	363.3
89Y	26	22.9	22.5	20.2	20.3	20.5
90Zr	172	159.0	155.8	143.4	143.5	145.8
93Nb	18	16.4	16.7	15.7	14.9	15.1
95Mo		3.4	4.0	3.3	3.4	3.3
103Rh		< DL	< DL	< DL	< DL	< DL
105Pd		< DL	< DL	0.1	< DL	< DL
107Ag		< DL	0.4	0.5	0.4	0.4
110Cd		< DL	< DL	< DL	< DL	< DL
111Cd		< DL	< DL	0.2	< DL	< DL
115In		< DL	< DL	0.1	0.1	< DL
118Sn	1.9	2.1	2.3	2.0	2.1	1.7
120Sn	1.9	2.2	2.3	2.1	2.2	1.8
121Sb		< DL	< DL	0.1	0.1	< DL
133Cs		< DL	< DL	< DL	0.1	< DL
136Ba	130	130.5	140.1	116.2	117.1	124.8
137Ba	130	135.9	144.1	121.3	121.8	128.4

Ca Internal Isotope	BHVO-2 Pub. Conc.	Ap16A11 BHVO-2	Ap16A12 BHVO-2	Ap16B11 BHVO-2	Ap16B12 BHVO-2	Ap16C11 BHVO-2
139La	15.5	15.8	16.6	14.2	13.9	15.0
140Ce	37.4	37.5	39.9	33.8	33.8	34.7
141Pr	5	5.0	5.3	4.6	4.6	4.8
146Nd	25	24.4	25.3	22.2	22.5	23.1
147Sm	6.1	6.4	6.3	5.4	5.9	5.8
153Eu	2.1	2.0	2.4	2.0	2.0	2.1
155Gd	6.5	5.7	5.6	5.1	5.3	5.6
156Ce O		--	--	--	--	--
157Gd	6.5	5.3	5.4	5.3	4.6	5.3
159Tb	0.96	0.8	0.8	0.7	0.8	0.8
163Dy	5.2	4.9	4.9	4.0	4.4	4.4
165Ho	0.93	0.9	0.9	0.8	0.8	0.8
166Er	2.5	2.1	2.1	2.0	2.1	2.0
169Tm	0.36	0.2	0.3	0.3	0.3	0.2
172Yb	2	1.8	1.9	1.7	1.7	1.7
175Lu	0.28	< DL	0.3	0.2	0.2	0.2
178Hf	4.1	3.9	3.9	3.7	3.7	4.0
181Ta	1.4	0.9	0.9	0.9	0.9	0.8
182W		0.3	0.3	0.2	0.2	0.2
185Re		< DL	< DL	< DL	< DL	< DL
195Pt		0.1	< DL	0.1	0.1	0.1
197Au		0.3	0.3	0.3	0.4	0.3
205Tl		< DL	< DL	0.0	0.0	< DL
206Pb		1.5	1.6	1.9	1.8	1.6
207Pb		1.5	1.6	1.7	1.8	1.5
208Pb		1.6	1.6	1.8	1.8	1.4
209Bi		< DL	< DL	0.0	0.0	< DL
220Bkg		--	--	--	--	--
232Th	1.2	1.2	1.2	1.1	1.1	1.1
238U		0.4	0.4	0.3	0.4	0.3
254U O		--	--	--	--	--

Ca Internal Isotope	BHVO-2 Pub. Conc.	Ap16C12 BHVO-2	Ap16D11 BHVO-2	Ap16D12 BHVO-2	Ap16E11 BHVO-2	Ap16E12 BHVO-2
7Li	5	5.0	5.0	4.9	3.5	4.7
9Be		0.8	1.5	1.0	< DL	1.3
11B		13.6	15.3	14.1	12.3	15.6
23Na	16400	12514.1	13203.3	13145.5	15673.9	13988.6
25Mg	43600	56147.4	55343.3	54458.3	58200.8	57905.4
27Al	71600	84011.5	84987.3	82735.7	84474.8	83931.3
29Si	233000	247395.7	252679.1	250832.9	288957.0	272572.6
31P	1200	855.1	881.9	819.9	1196.5	1085.7
33S		9.5	< DL	8.0	< DL	16.2
39K	4300	4683.9	4872.2	4721.6	5989.6	5329.1
43Ca	81700	83826.2	86037.2	84358.4	87050.4	83226.7
44Ca	81700	81700.0	81700.0	81700.0	81700.0	81700.0
45Sc	32	30.8	32.1	29.7	30.4	29.9
47Ti	16300	15744.5	16081.9	15625.6	16584.0	16551.2
51V	317	286.1	288.2	281.0	331.4	327.6
52Cr	280	263.8	273.3	268.0	309.8	299.0
53Cr	280	271.2	280.4	271.1	317.9	306.4
55Mn	1290	1564.5	1463.0	1484.3	1660.4	1699.4
57Fe	86300	103094.7	93143.1	94294.9	112099.3	112620.9
59Co	45	45.1	44.0	43.6	50.2	49.3
60Ni	119	114.4	116.1	108.3	138.1	129.9
62Ni	119	122.6	108.3	115.0	116.0	144.6
65Cu	127	103.0	119.0	105.7	136.9	122.5
66Zn	103	96.2	109.4	96.0	116.2	107.0
68Zn	103	94.9	108.1	96.1	122.7	105.1
69Ga	21.7	20.8	22.1	20.4	24.4	21.6
72Ge		2.3	2.4	2.4	2.2	2.2
75As		1.7	2.1	0.8	1.0	2.0
77Ar Cl		--	--	--	--	--
82Se		< DL	< DL	< DL	< DL	< DL
83Kr		--	--	--	--	--
85Rb	9.8	8.4	8.4	8.4	9.1	8.8
86Sr	389	400.1	383.1	388.0	376.3	395.2
88Sr	389	400.7	382.6	389.4	370.5	383.1
89Y	26	23.0	22.8	21.5	19.4	20.4
90Zr	172	156.9	160.7	151.8	143.7	145.7
93Nb	18	16.4	16.0	15.9	15.3	15.9
95Mo		3.5	3.6	3.6	3.3	3.9
103Rh		< DL	< DL	< DL	< DL	< DL
105Pd		< DL	< DL	< DL	< DL	< DL
107Ag		0.4	0.3	0.3	< DL	0.1
110Cd		0.2	< DL	< DL	< DL	< DL
111Cd		< DL	< DL	< DL	< DL	< DL
115In		0.0	0.1	0.1	< DL	< DL
118Sn	1.9	1.9	2.0	2.0	1.0	2.1
120Sn	1.9	1.9	2.1	2.0	1.1	1.9
121Sb		0.1	0.1	0.1	< DL	< DL
133Cs		0.1	0.1	0.1	< DL	< DL
136Ba	130	137.5	126.5	126.5	124.7	123.3
137Ba	130	140.3	127.1	130.4	124.5	127.2

Ca Internal Isotope	BHVO-2 Pub. Conc.	Ap16C12 BHVO-2	Ap16D11 BHVO-2	Ap16D12 BHVO-2	Ap16E11 BHVO-2	Ap16E12 BHVO-2
139La	15.5	16.5	15.3	15.4	13.2	13.9
140Ce	37.4	38.9	34.8	36.2	34.2	35.8
141Pr	5	5.2	4.7	4.9	3.9	4.6
146Nd	25	25.6	23.7	24.1	21.3	22.9
147Sm	6.1	6.6	5.4	5.8	4.8	5.3
153Eu	2.1	2.3	2.1	2.1	0.9	1.8
155Gd	6.5	6.1	6.1	5.2	4.2	4.6
156Ce O		- -	- -	- -	- -	- -
157Gd	6.5	5.9	5.3	5.5	4.1	4.8
159Tb	0.96	0.9	0.9	0.8	< DL	0.7
163Dy	5.2	4.9	4.9	4.4	3.3	4.2
165Ho	0.93	0.9	0.9	0.8	< DL	0.6
166Er	2.5	2.2	2.2	2.1	0.7	1.8
169Tm	0.36	0.3	0.3	0.3	< DL	0.2
172Yb	2	1.9	2.0	1.8	0.5	1.6
175Lu	0.28	0.2	0.2	0.2	< DL	0.1
178Hf	4.1	4.2	4.2	3.7	2.6	3.5
181Ta	1.4	0.9	0.9	0.9	< DL	0.7
182W		0.2	0.2	0.2	< DL	0.2
185Re		< DL	< DL	< DL	< DL	< DL
195Pt		0.1	< DL	< DL	0.1	0.1
197Au		0.3	0.3	0.3	0.3	0.3
205Tl		< DL	< DL	< DL	< DL	< DL
206Pb		1.7	1.7	1.5	1.0	1.4
207Pb		1.5	1.6	1.3	0.9	1.3
208Pb		1.5	1.7	1.4	0.9	1.3
209Bi		< DL	0.0	0.0	< DL	< DL
220Bkg		- -	- -	- -	- -	- -
232Th	1.2	1.2	1.2	1.1	0.3	0.9
238U		0.4	0.4	0.4	< DL	0.2
254U O		- -	- -	- -	- -	- -

Ca Internal Isotope	BHVO-2 Pub. Conc.	Count	Min	Max	Average	Sigma
7Li	5	11	3.5	5.1	4.6	1.3432253
9Be		6	0.8	1.6	1.3	0.6771256
11B		10	12.3	19.0	15.4	4.8722818
23Na	16400	11	12091.2	16400.0	13682.1	3993.3452
25Mg	43600	11	43600.0	58200.8	53414.8	15318.939
27Al	71600	11	71600.0	87517.1	82570.1	23173.701
29Si	233000	11	233000.0	288957.0	255458.0	71870.571
31P	1200	11	819.9	1200.0	966.4	295.85748
33S		4	8.0	16.2	12.0	6.0936742
39K	4300	11	4300.0	5989.6	4919.7	1419.9352
43Ca	81700	11	81700.0	87050.4	84714.1	23465.23
44Ca	81700	11	81700.0	81700.0	81700.0	22580.687
45Sc	32	11	29.6	32.1	30.8	8.5538759
47Ti	16300	11	15216.8	16684.0	16027.9	4456.1215
51V	317	11	276.0	331.4	297.7	84.253384
52Cr	280	11	254.4	309.8	276.1	77.816188
53Cr	280	11	251.4	317.9	281.1	79.684463
55Mn	1290	11	1290.0	1699.4	1493.5	426.04665
57Fe	86300	11	86300.0	112620.9	98529.9	28273.184
59Co	45	11	42.4	50.2	45.5	12.762999
60Ni	119	11	108.3	138.1	119.6	33.981831
62Ni	119	9	108.3	144.6	119.8	52.530354
65Cu	127	11	103.0	136.9	117.9	34.10522
66Zn	103	11	95.4	126.0	105.7	30.629015
68Zn	103	11	94.3	128.2	106.5	31.328461
69Ga	21.7	11	19.8	24.4	21.9	6.1917395
72Ge		10	2.2	2.7	2.4	0.7030417
75As		8	0.7	2.1	1.3	0.7291732
77Ar Cl		0	0.0	0.0	- -	0
82Se		2	-1.3	-0.5	-0.9	0.387319
83Kr		0	0.0	0.0	- -	0
85Rb	9.8	11	8.0	9.8	8.6	2.4273011
86Sr	389	11	354.9	422.1	385.2	108.12692
88Sr	389	11	354.4	424.2	383.2	107.65232
89Y	26	11	19.4	26.0	21.8	6.2626817
90Zr	172	11	143.4	172.0	152.6	43.007914
93Nb	18	11	14.9	18.0	16.0	4.4983895
95Mo		10	3.3	4.0	3.5	1.0435887
103Rh		0	0.0	0.0	- -	0
105Pd		1	0.1	0.1	0.1	0.0394164
107Ag		8	0.1	0.5	0.4	0.1820507
110Cd		1	0.2	0.2	0.2	0.0523077
111Cd		1	0.2	0.2	0.2	0.0538266
115In		5	0.0	0.1	0.1	0.0395627
118Sn	1.9	11	1.0	2.3	1.9	0.612821
120Sn	1.9	11	1.1	2.3	1.9	0.6192473
121Sb		5	0.1	0.1	0.1	0.0543403
133Cs		4	0.1	0.1	0.1	0.044609
136Ba	130	11	116.2	140.1	127.0	35.741701
137Ba	130	11	121.3	144.1	130.1	36.565697

Ca Internal Isotope	BHVO-2 Pub. Conc.	Count	Min	Max	Average	Sigma
139La	15.5	11	13.2	16.6	15.0	4.2742773
140Ce	37.4	11	33.8	39.9	36.1	10.154084
141Pr	5	11	3.9	5.3	4.8	1.3699801
146Nd	25	11	21.3	25.6	23.6	6.6519332
147Sm	6.1	11	4.8	6.6	5.8	1.6760234
153Eu	2.1	11	0.9	2.4	2.0	0.6510143
155Gd	6.5	11	4.2	6.5	5.5	1.6254718
156Ce O		0	0.0	0.0	- -	0
157Gd	6.5	11	4.1	6.5	5.3	1.5726519
159Tb	0.96	10	0.7	1.0	0.8	0.3114606
163Dy	5.2	11	3.3	5.2	4.5	1.3405755
165Ho	0.93	10	0.6	0.9	0.8	0.3263407
166Er	2.5	11	0.7	2.5	2.0	0.6822985
169Tm	0.36	10	0.2	0.4	0.3	0.1091324
172Yb	2	11	0.5	2.0	1.7	0.6103434
175Lu	0.28	9	0.1	0.3	0.2	0.1071931
178Hf	4.1	11	2.6	4.2	3.8	1.126135
181Ta	1.4	10	0.7	1.4	0.9	0.3757137
182W		9	0.2	0.3	0.2	0.0926728
185Re		0	0.0	0.0	- -	0
195Pt		7	0.1	0.1	0.1	0.0500957
197Au		10	0.3	0.4	0.3	0.0939439
205Tl		2	0.0	0.0	0.0	0.0101093
206Pb		10	1.0	1.9	1.6	0.5043098
207Pb		10	0.9	1.8	1.5	0.4830754
208Pb		10	0.9	1.8	1.5	0.4960815
209Bi		4	0.0	0.0	0.0	0.009826
220Bkg		0	0.0	0.0	- -	0
232Th	1.2	11	0.3	1.2	1.1	0.369894
238U		9	0.2	0.4	0.4	0.1431206
254U O		0	0.0	0.0	- -	0

Fe Internal Isotope	BHVO-2 Pub. Conc.	Ap16A11 BHVO-2	Ap16A12 BHVO-2	Ap16B11 BHVO-2	Ap16B12 BHVO-2	Ap16C11 BHVO-2
7Li	5	4.0	4.2	4.0	4.1	4.0
9Be		< DL	< DL	< DL	1.4	< DL
11B		16.7	15.7	15.2	14.6	12.2
23Na	16400	12258.8	12246.6	10910.3	11481.0	11715.3
25Mg	43600	47777.9	46024.6	45920.1	44050.9	50608.2
27Al	71600	76868.2	72214.3	72384.5	73278.4	78098.2
29Si	233000	222292.1	216771.9	233102.2	230975.1	229378.2
31P	1200	781.2	734.0	908.0	913.0	780.9
33S		< DL	< DL	12.8	< DL	< DL
39K	4300	4096.1	3843.0	4579.4	4672.4	4539.7
43Ca	81700	75149.2	70804.1	78224.2	80272.1	76978.7
44Ca	81700	71758.9	68566.1	73721.1	76207.9	75789.5
45Sc	32	27.9	25.9	27.9	27.6	28.5
47Ti	16300	14477.9	14001.9	14182.2	14193.9	14209.6
51V	317	265.6	252.6	259.0	258.4	256.1
52Cr	280	243.9	238.1	242.4	237.3	240.3
53Cr	280	257.2	242.6	243.1	245.3	233.2
55Mn	1290	1297.8	1265.6	1296.0	1297.7	1348.8
57Fe	86300	86300.0	86300.0	86300.0	86300.0	86300.0
59Co	45	40.3	38.4	41.1	40.9	39.3
60Ni	119	106.2	99.0	111.4	110.4	101.0
62Ni	119	< DL	< DL	109.0	108.1	107.8
65Cu	127	101.9	90.3	114.7	117.1	99.1
66Zn	103	88.0	80.0	113.7	107.5	91.0
68Zn	103	88.6	79.1	115.6	111.0	92.6
69Ga	21.7	19.1	18.3	20.9	22.0	18.3
72Ge		2.1	1.9	2.4	2.5	2.1
75As		< DL	< DL	0.6	1.0	0.7
77Ar Cl		--	--	--	--	--
82Se		-0.5	-1.1	< DL	< DL	< DL
83Kr		--	--	--	--	--
85Rb	9.8	7.1	7.3	7.8	7.9	7.4
86Sr	389	355.6	354.3	320.3	331.1	341.9
88Sr	389	352.4	356.0	319.8	332.8	337.0
89Y	26	20.1	18.9	18.2	18.9	19.1
90Zr	172	139.7	130.8	129.4	133.9	135.3
93Nb	18	14.4	14.0	14.1	13.9	14.0
95Mo		3.0	3.3	3.0	3.2	3.1
103Rh		< DL	< DL	< DL	< DL	< DL
105Pd		< DL	< DL	< DL	< DL	< DL
107Ag		< DL	0.3	0.5	0.4	0.4
110Cd		< DL	< DL	< DL	< DL	< DL
111Cd		< DL	< DL	0.2	< DL	< DL
115In		< DL	< DL	0.1	0.1	< DL
118Sn	1.9	1.9	1.9	1.8	2.0	1.6
120Sn	1.9	1.9	1.9	1.9	2.1	1.7
121Sb		< DL	< DL	0.1	0.1	< DL
133Cs		< DL	< DL	< DL	0.1	< DL
136Ba	130	114.6	117.5	104.8	109.2	115.8
137Ba	130	119.4	120.9	109.4	113.6	119.2

Fe Internal Isotope	BHVO-2 Pub. Conc.	Ap16A11 BHVO-2	Ap16A12 BHVO-2	Ap16B11 BHVO-2	Ap16B12 BHVO-2	Ap16C11 BHVO-2
139La	15.5	13.9	14.0	12.8	12.9	13.9
140Ce	37.4	32.9	33.5	30.5	31.5	32.2
141Pr	5	4.4	4.4	4.2	4.3	4.5
146Nd	25	21.4	21.2	20.1	21.0	21.4
147Sm	6.1	5.6	5.3	4.9	5.5	5.4
153Eu	2.1	1.7	2.0	1.8	1.9	1.9
155Gd	6.5	5.0	4.7	4.6	4.9	5.2
156Ce O		--	--	--	--	--
157Gd	6.5	4.7	4.6	4.8	4.3	4.9
159Tb	0.96	0.7	0.7	0.6	0.7	0.8
163Dy	5.2	4.3	4.1	3.6	4.1	4.1
165Ho	0.93	0.8	0.8	0.7	0.8	0.8
166Er	2.5	1.8	1.8	1.8	2.0	1.9
169Tm	0.36	< DL	0.3	0.2	0.3	0.2
172Yb	2	1.6	1.6	1.6	1.5	1.5
175Lu	0.28	< DL	0.3	0.2	0.2	0.2
178Hf	4.1	3.4	3.3	3.3	3.4	3.7
181Ta	1.4	0.8	0.7	0.8	0.8	0.7
182W		0.3	< DL	0.2	0.2	< DL
185Re		< DL	< DL	< DL	< DL	< DL
195Pt		0.1	< DL	0.1	0.1	0.1
197Au		0.3	0.2	0.3	0.4	0.2
205Tl		< DL	< DL	0.0	0.0	< DL
206Pb		1.3	1.4	1.7	1.7	1.5
207Pb		1.3	1.3	1.6	1.7	1.4
208Pb		1.4	1.4	1.6	1.7	1.3
209Bi		< DL	< DL	0.0	0.0	< DL
220Bkg		--	--	--	--	--
232Th	1.2	1.0	1.0	1.0	1.0	1.0
238U		0.4	0.3	0.3	0.3	0.3
254U O		--	--	--	--	--

Fe Internal Isotope	BHVO-2 Pub. Conc.	Ap16C12 BHVO-2	Ap16D11 BHVO-2	Ap16D12 BHVO-2	Ap16E11 BHVO-2	Ap16E12 BHVO-2
7Li	5	4.2	4.6	4.5	2.7	3.6
9Be		< DL	1.4	0.9	< DL	1.0
11B		11.4	14.2	12.9	9.5	11.9
23Na	16400	10475.5	12233.2	12031.0	12066.6	10719.3
25Mg	43600	47000.7	51277.3	49841.0	44806.1	44372.2
27Al	71600	70325.6	78743.4	75720.8	65033.2	64315.5
29Si	233000	207093.5	234115.0	229565.7	222454.5	208869.0
31P	1200	715.8	817.1	750.4	921.1	831.9
33S		< DL	< DL	7.3	< DL	12.4
39K	4300	3920.8	4514.2	4321.2	4611.1	4083.6
43Ca	81700	70170.4	79716.2	77206.0	67016.1	63775.6
44Ca	81700	68390.6	75697.6	74773.0	62897.0	62605.7
45Sc	32	25.8	29.8	27.2	23.4	22.9
47Ti	16300	13179.6	14900.4	14300.8	12767.3	12683.0
51V	317	239.5	267.1	257.2	255.1	251.0
52Cr	280	220.8	253.2	245.3	238.5	229.1
53Cr	280	227.0	259.8	248.1	244.7	234.8
55Mn	1290	1309.6	1355.5	1358.4	1278.3	1302.2
57Fe	86300	86300.0	86300.0	86300.0	86300.0	86300.0
59Co	45	37.8	40.8	39.9	38.6	37.8
60Ni	119	95.8	107.5	99.1	106.3	99.5
62Ni	119	102.6	100.3	105.2	89.3	110.8
65Cu	127	86.2	110.3	96.7	105.4	93.9
66Zn	103	80.5	101.4	87.9	89.4	82.0
68Zn	103	79.4	100.1	88.0	94.4	80.6
69Ga	21.7	17.4	20.5	18.7	18.8	16.5
72Ge		1.9	2.2	2.2	1.7	1.7
75As		1.4	2.0	0.7	0.8	1.5
77Ar Cl		--	--	--	--	--
82Se		< DL	< DL	< DL	< DL	< DL
83Kr		--	--	--	--	--
85Rb	9.8	7.1	7.8	7.7	7.0	6.8
86Sr	389	335.0	354.9	355.1	289.7	302.8
88Sr	389	335.5	354.5	356.4	285.2	293.6
89Y	26	19.2	21.1	19.7	14.9	15.7
90Zr	172	131.4	148.9	138.9	110.6	111.7
93Nb	18	13.7	14.8	14.5	11.8	12.2
95Mo		3.0	3.4	3.3	2.5	3.0
103Rh		< DL	< DL	< DL	< DL	< DL
105Pd		< DL	< DL	< DL	< DL	< DL
107Ag		0.3	0.3	0.3	< DL	< DL
110Cd		< DL	< DL	< DL	< DL	< DL
111Cd		< DL	< DL	< DL	< DL	< DL
115In		0.0	0.1	0.1	< DL	< DL
118Sn	1.9	1.6	1.9	1.8	0.8	1.6
120Sn	1.9	1.6	1.9	1.9	0.8	1.4
121Sb		0.1	0.1	0.1	< DL	< DL
133Cs		0.1	< DL	0.1	< DL	< DL
136Ba	130	115.1	117.2	115.8	96.0	94.5
137Ba	130	117.4	117.8	119.3	95.8	97.5

Fe Internal Isotope	BHVO-2 Pub. Conc.	Ap16C12 BHVO-2	Ap16D11 BHVO-2	Ap16D12 BHVO-2	Ap16E11 BHVO-2	Ap16E12 BHVO-2
139La	15.5	13.8	14.2	14.1	10.1	10.6
140Ce	37.4	32.5	32.3	33.1	26.3	27.4
141Pr	5	4.4	4.4	4.5	3.0	3.5
146Nd	25	21.5	21.9	22.0	16.4	17.5
147Sm	6.1	5.5	5.0	5.3	3.7	4.1
153Eu	2.1	1.9	1.9	2.0	0.7	1.4
155Gd	6.5	5.1	5.6	4.7	3.3	3.6
156Ce O		- -	- -	- -	- -	- -
157Gd	6.5	5.0	4.9	5.0	3.1	3.7
159Tb	0.96	0.7	0.8	0.8	< DL	0.5
163Dy	5.2	4.1	4.6	4.1	2.6	3.2
165Ho	0.93	0.8	0.8	0.7	< DL	0.5
166Er	2.5	1.8	2.1	1.9	0.6	1.4
169Tm	0.36	0.2	0.3	0.3	< DL	0.1
172Yb	2	1.6	1.9	1.6	< DL	1.2
175Lu	0.28	0.2	0.2	0.2	< DL	0.1
178Hf	4.1	3.5	3.9	3.4	2.0	2.6
181Ta	1.4	0.8	0.9	0.8	< DL	0.5
182W		0.2	0.2	0.2	< DL	< DL
185Re		< DL	< DL	< DL	< DL	< DL
195Pt		0.1	< DL	< DL	0.1	0.1
197Au		0.2	0.2	0.3	0.3	0.2
205Tl		< DL	< DL	< DL	< DL	< DL
206Pb		1.4	1.6	1.4	0.8	1.1
207Pb		1.2	1.5	1.2	0.7	1.0
208Pb		1.3	1.6	1.3	0.7	1.0
209Bi		< DL	0.0	0.0	< DL	< DL
220Bkg		- -	- -	- -	- -	- -
232Th	1.2	1.0	1.1	1.0	0.3	0.7
238U		0.3	0.3	0.3	< DL	0.2
254U O		- -	- -	- -	- -	- -

Fe Internal Isotope	BHVO-2 Pub. Conc.	Count	Min	Max	Average	Sigma
7Li	5	11	2.7	5.0	4.1	1.2502984
9Be		4	0.9	1.4	1.2	0.5864102
11B		10	9.5	16.7	13.4	4.3484658
23Na	16400	11	10475.5	16400.0	12048.9	3629.7499
25Mg	43600	11	43600.0	51277.3	46843.5	13182.29
27Al	71600	11	64315.5	78743.4	72598.4	20534.439
29Si	233000	11	207093.5	234115.0	224328.8	62633.634
31P	1200	11	715.8	1200.0	850.3	266.14064
33S		3	7.3	12.8	10.8	4.9964622
39K	4300	11	3843.0	4672.4	4316.5	1222.5314
43Ca	81700	11	63775.6	81700.0	74637.5	21310.927
44Ca	81700	11	62605.7	81700.0	72009.8	20615.048
45Sc	32	11	22.9	32.0	27.2	7.8851447
47Ti	16300	11	12683.0	16300.0	14108.8	4008.3325
51V	317	11	239.5	317.0	261.7	74.540418
52Cr	280	11	220.8	280.0	242.6	68.442135
53Cr	280	11	227.0	280.0	246.9	69.529373
55Mn	1290	11	1265.6	1358.4	1309.1	362.94715
57Fe	86300	11	86300.0	86300.0	86300.0	23852.06
59Co	45	11	37.8	45.0	40.0	11.213527
60Ni	119	11	95.8	119.0	105.0	29.70293
62Ni	119	9	89.3	119.0	105.8	46.286163
65Cu	127	11	86.2	127.0	103.9	30.867413
66Zn	103	11	80.0	113.7	93.1	27.80113
68Zn	103	11	79.1	115.6	93.9	28.334067
69Ga	21.7	11	16.5	22.0	19.3	5.5725161
72Ge		10	1.7	2.5	2.1	0.6478631
75As		8	0.6	2.0	1.1	0.6227786
77Ar Cl		0	0.0	0.0	- -	0
82Se		2	-1.1	-0.5	-0.8	0.3267584
83Kr		0	0.0	0.0	- -	0
85Rb	9.8	11	6.8	9.8	7.6	2.2309638
86Sr	389	11	289.7	389.0	339.1	97.076069
88Sr	389	11	285.2	389.0	337.5	97.148793
89Y	26	11	14.9	26.0	19.3	5.9359336
90Zr	172	11	110.6	172.0	134.8	40.2616
93Nb	18	11	11.8	18.0	14.1	4.1662254
95Mo		10	2.5	3.4	3.1	0.914114
103Rh		0	0.0	0.0	- -	0
105Pd		0	0.0	0.0	- -	0
107Ag		7	0.3	0.5	0.3	0.1736984
110Cd		0	0.0	0.0	- -	0
111Cd		1	0.2	0.2	0.2	0.0485698
115In		5	0.0	0.1	0.1	0.0361813
118Sn	1.9	11	0.8	2.0	1.7	0.5592383
120Sn	1.9	11	0.8	2.1	1.7	0.5764739
121Sb		5	0.1	0.1	0.1	0.049381
133Cs		3	0.1	0.1	0.1	0.038214
136Ba	130	11	94.5	130.0	111.9	32.298647
137Ba	130	11	95.8	130.0	114.6	32.999516

Fe Internal Isotope	BHVO-2 Pub. Conc.	Count	Min	Max	Average	Sigma
139La	15.5	11	10.1	15.5	13.3	3.9384059
140Ce	37.4	11	26.3	37.4	31.8	9.1986141
141Pr	5	11	3.0	5.0	4.2	1.2670439
146Nd	25	11	16.4	25.0	20.9	6.1328551
147Sm	6.1	11	3.7	6.1	5.1	1.5522972
153Eu	2.1	11	0.7	2.1	1.7	0.6053646
155Gd	6.5	11	3.3	6.5	4.8	1.5621557
156Ce O		0	0.0	0.0	- -	0
157Gd	6.5	11	3.1	6.5	4.7	1.507137
159Tb	0.96	10	0.5	1.0	0.7	0.2898549
163Dy	5.2	11	2.6	5.2	4.0	1.2696343
165Ho	0.93	10	0.5	0.9	0.8	0.3005622
166Er	2.5	11	0.6	2.5	1.8	0.6545941
169Tm	0.36	9	0.1	0.4	0.2	0.116898
172Yb	2	10	1.2	2.0	1.6	0.6287603
175Lu	0.28	9	0.1	0.3	0.2	0.0983649
178Hf	4.1	11	2.0	4.1	3.3	1.0674204
181Ta	1.4	10	0.5	1.4	0.8	0.3608192
182W		6	0.2	0.3	0.2	0.1037329
185Re		0	0.0	0.0	- -	0
195Pt		7	0.1	0.1	0.1	0.0435863
197Au		10	0.2	0.4	0.3	0.0834663
205Tl		2	0.0	0.0	0.0	0.0093087
206Pb		10	0.8	1.7	1.4	0.4716851
207Pb		10	0.7	1.7	1.3	0.4518726
208Pb		10	0.7	1.7	1.3	0.4648752
209Bi		4	0.0	0.0	0.0	0.0090559
220Bkg		0	0.0	0.0	- -	0
232Th	1.2	11	0.3	1.2	0.9	0.3476689
238U		9	0.2	0.4	0.3	0.1283303
254U O		0	0.0	0.0	- -	0

Scaled Isotope	BHVO-2 Pub. Conc.	Ap16A11	Ap16A12	Ap16B11	Ap16B12	Ap16C11
7Li	5	4.0	4.4	4.1	4.2	4.0
9Be		< DL	< DL	< DL	1.4	< DL
11B		16.8	16.4	15.6	14.9	12.3
23Na	16400	12404.7	12782.5	11182.0	11785.5	11833.6
25Mg	43600	48346.2	48038.6	47063.4	45219.1	51119.0
27Al	71600	77782.5	75374.2	74186.6	75221.7	78886.4
29Si	233000	224936.3	226257.4	238905.7	237100.6	231693.1
31P	1200	790.4	766.1	930.6	937.2	788.7
33S		< DL	< DL	13.1	< DL	< DL
39K	4300	4144.8	4011.2	4693.4	4796.3	4585.5
44Ca	81700	72612.4	71566.4	75556.5	78228.9	76554.4
45Sc	32	28.2	27.1	28.6	28.3	28.8
47Ti	16300	14650.2	14614.6	14535.3	14570.3	14353.0
51V	317	275.8	270.5	265.4	265.2	258.6
53Cr	280	260.3	253.3	249.1	251.8	235.6
55Mn	1290	1313.3	1320.9	1328.3	1332.2	1362.4
57Fe	86300	87326.6	90076.3	88448.6	88588.7	87170.9
59Co	45	40.8	40.1	42.1	42.0	39.7
60Ni	119	107.5	103.4	114.1	113.3	102.0
65Cu	127	103.1	94.2	117.5	120.2	100.1
68Zn	103	89.7	82.6	118.5	114.0	93.5
69Ga	21.7	19.3	19.1	21.5	22.6	18.5
72Ge		2.2	2.0	2.5	2.6	2.1
75As		< DL	< DL	0.6	1.0	0.7
82Se		0.0	0.0	< DL	< DL	< DL
85Rb	9.8	7.2	7.6	8.0	8.1	7.5
88Sr	389	356.6	371.5	327.8	341.6	340.4
89Y	26	20.4	19.8	18.7	19.4	19.2
90Zr	172	141.3	136.5	132.6	137.4	136.7
93Nb	18	14.6	14.6	14.5	14.2	14.1
95Mo		3.0	3.5	3.1	3.3	3.1
103Rh		< DL	< DL	< DL	< DL	< DL
105Pd		< DL	< DL	< DL	< DL	< DL
107Ag		< DL	0.3	0.5	0.4	0.4
111Cd		< DL	< DL	0.2	< DL	< DL
115In		< DL	< DL	0.1	0.1	< DL
118Sn	1.9	1.9	2.0	1.9	2.0	1.6
121Sb		< DL	< DL	0.1	0.1	< DL
133Cs		< DL	< DL	< DL	0.1	< DL
137Ba	130	120.8	126.2	112.1	116.6	120.4
139La	15.5	14.1	14.6	13.1	13.3	14.0
140Ce	37.4	33.3	35.0	31.2	32.3	32.6
141Pr	5	4.5	4.6	4.3	4.4	4.5
146Nd	25	21.6	22.1	20.6	21.6	21.6
147Sm	6.1	5.7	5.5	5.0	5.7	5.4
153Eu	2.1	1.7	2.1	1.8	1.9	1.9
157Gd	6.5	4.7	4.8	4.9	4.4	4.9
159Tb	0.96	0.7	0.7	0.7	0.8	0.8
163Dy	5.2	4.4	4.3	3.7	4.2	4.2
165Ho	0.93	0.8	0.8	0.8	0.8	0.8

Scaled Isotope	BHVO-2 Pub. Conc.	Ap16A11	Ap16A12	Ap16B11	Ap16B12	Ap16C11
166Er	2.5	1.8	1.8	1.8	2.0	1.9
169Tm	0.36	< DL	0.3	0.3	0.3	0.2
172Yb	2	1.6	1.7	1.6	1.6	1.6
175Lu	0.28	< DL	0.3	0.2	0.2	0.2
178Hf	4.1	3.5	3.4	3.4	3.5	3.8
181Ta	1.4	0.8	0.8	0.8	0.8	0.8
182W		0.3	0.2	0.2	0.2	0.2
185Re		< DL	< DL	< DL	< DL	< DL
195Pt		0.1	< DL	0.1	0.1	0.1
197Au		0.3	0.2	0.3	0.4	0.2
205Tl		< DL	< DL	0.0	0.0	< DL
208Pb		1.4	1.4	1.6	1.7	1.3
209Bi		< DL	< DL	0.0	0.0	< DL
232Th	1.2	1.0	1.1	1.0	1.1	1.0
238U		0.4	0.4	0.3	0.3	0.3

Scaled Isotope	BHVO-2 Pub. Conc.	Ap16C12	Ap16D11	Ap16D12	Ap16E11	Ap16E12
7Li	5	4.6	4.6	4.6	3.0	4.0
9Be		0.8	1.4	0.9	< DL	1.2
11B		12.5	14.1	13.2	10.3	13.4
23Na	16400	11551.1	12179.6	12232.5	13100.5	12088.3
25Mg	43600	51826.7	51052.5	50675.7	48645.4	50039.4
27Al	71600	77546.5	78398.2	76989.0	70605.8	72529.9
29Si	233000	228357.6	233088.6	233410.5	241516.3	235545.7
31P	1200	789.3	813.5	763.0	1000.1	938.2
33S		< DL	< DL	7.4	< DL	14.0
39K	4300	4323.4	4494.5	4393.6	5006.3	4605.2
44Ca	81700	75412.9	75365.7	76025.3	68286.6	70601.7
45Sc	32	28.4	29.7	27.6	25.4	25.8
47Ti	16300	14532.9	14835.0	14540.3	13861.3	14302.9
51V	317	264.1	265.9	261.5	277.0	283.1
53Cr	280	250.3	258.6	252.2	265.7	264.8
55Mn	1290	1444.1	1349.6	1381.2	1387.8	1468.5
57Fe	86300	95161.2	85921.7	87745.4	93694.9	97322.2
59Co	45	41.7	40.6	40.6	41.9	42.6
60Ni	119	105.6	107.1	100.8	115.4	112.3
65Cu	127	95.1	109.8	98.3	114.4	105.8
68Zn	103	87.6	99.7	89.4	102.5	90.9
69Ga	21.7	19.2	20.4	19.0	20.4	18.7
72Ge		2.1	2.2	2.2	1.8	1.9
75As		1.6	2.0	0.7	0.9	1.7
82Se		< DL	< DL	< DL	< DL	< DL
85Rb	9.8	7.8	7.7	7.8	7.6	7.6
88Sr	389	369.9	353.0	362.3	309.6	331.0
89Y	26	21.2	21.0	20.0	16.2	17.7
90Zr	172	144.9	148.3	141.2	120.1	125.9
93Nb	18	15.1	14.8	14.8	12.8	13.8
95Mo		3.3	3.4	3.4	2.7	3.4
103Rh		< DL	< DL	< DL	< DL	< DL
105Pd		< DL	< DL	< DL	< DL	< DL
107Ag		0.4	0.3	0.3	< DL	< DL
111Cd		< DL	< DL	< DL	< DL	< DL
115In		0.0	0.1	0.1	< DL	< DL
118Sn	1.9	1.8	1.8	1.8	0.9	1.8
121Sb		0.1	0.1	0.1	< DL	< DL
133Cs		0.1	< DL	0.1	< DL	< DL
137Ba	130	129.5	117.3	121.3	104.0	110.0
139La	15.5	15.2	14.1	14.3	11.0	12.0
140Ce	37.4	35.9	32.1	33.7	28.6	30.9
141Pr	5	4.8	4.3	4.6	3.3	4.0
146Nd	25	23.7	21.8	22.4	17.8	19.8
147Sm	6.1	6.1	5.0	5.4	4.0	4.6
153Eu	2.1	2.1	1.9	2.0	0.7	1.6
157Gd	6.5	5.5	4.9	5.1	3.4	4.1
159Tb	0.96	0.8	0.8	0.8	< DL	0.6
163Dy	5.2	4.5	4.5	4.1	2.8	3.6
165Ho	0.93	0.8	0.8	0.8	< DL	0.5

Scaled Isotope	BHVO-2 Pub. Conc.	Ap16C12	Ap16D11	Ap16D12	Ap16E11	Ap16E12
166Er	2.5	2.0	2.0	1.9	0.6	1.6
169Tm	0.36	0.3	0.3	0.3	< DL	0.2
172Yb	2	1.7	1.9	1.7	0.4	1.4
175Lu	0.28	0.2	0.2	0.2	< DL	0.1
178Hf	4.1	3.9	3.9	3.5	2.2	3.0
181Ta	1.4	0.8	0.9	0.8	< DL	0.6
182W		0.2	0.2	0.2	< DL	< DL
185Re		< DL	< DL	< DL	< DL	< DL
195Pt		0.1	< DL	< DL	0.1	0.1
197Au		0.2	0.2	0.3	0.3	0.3
205Tl		< DL	< DL	< DL	< DL	< DL
208Pb		1.4	1.6	1.3	0.8	1.1
209Bi		< DL	0.0	0.0	< DL	< DL
232Th	1.2	1.1	1.1	1.1	0.3	0.8
238U		0.4	0.3	0.4	< DL	0.2

Scaled Isotope	BHVO-2 Pub. Conc.	Count	Min	Max	Average	Sigma
7Li	5	11	3.0	5.0	4.2	1.2664267
9Be		5	0.8	1.4	1.1	0.5940729
11B		10	10.3	16.8	14.0	4.411027
23Na	16400	11	11182.0	16400.0	12503.7	3684.5213
25Mg	43600	11	43600.0	51826.7	48693.3	13667.716
27Al	71600	11	70605.8	78886.4	75374.6	20994.05
29Si	233000	11	224936.3	241516.3	233073.8	64589.09
31P	1200	11	763.0	1200.0	883.4	273.38771
33S		3	7.4	14.0	11.5	5.3429869
39K	4300	11	4011.2	5006.3	4486.7	1268.1637
44Ca	81700	11	68286.6	81700.0	74719.2	20932.715
45Sc	32	11	25.4	32.0	28.2	7.9597852
47Ti	16300	11	13861.3	16300.0	14645.1	4084.9179
51V	317	11	258.6	317.0	273.1	76.933717
53Cr	280	11	235.6	280.0	256.5	71.658175
55Mn	1290	11	1290.0	1468.5	1361.7	379.71086
57Fe	86300	11	85921.7	97322.2	89796.0	25066.234
59Co	45	11	39.7	45.0	41.6	11.564371
60Ni	119	11	100.8	119.0	109.1	30.658818
65Cu	127	11	94.2	127.0	107.8	31.405455
68Zn	103	11	82.6	118.5	97.4	28.83137
69Ga	21.7	11	18.5	22.6	20.0	5.6801291
72Ge		10	1.8	2.6	2.2	0.6559619
75As		8	0.6	2.0	1.1	0.6577591
82Se		2	0.0	0.0	0.0	0
85Rb	9.8	11	7.2	9.8	7.9	2.2680199
88Sr	389	11	309.6	389.0	350.3	99.03018
89Y	26	11	16.2	26.0	20.0	5.9602891
90Zr	172	11	120.1	172.0	139.7	40.509302
93Nb	18	11	12.8	18.0	14.7	4.2156733
95Mo		10	2.7	3.5	3.2	0.9449926
103Rh		0	0.0	0.0	- -	0
105Pd		0	0.0	0.0	- -	0
107Ag		7	0.3	0.5	0.4	0.1794054
111Cd		1	0.2	0.2	0.2	0.0497791
115In		5	0.0	0.1	0.1	0.0368974
118Sn	1.9	11	0.9	2.0	1.8	0.5686234
121Sb		5	0.1	0.1	0.1	0.0508498
133Cs		3	0.1	0.1	0.1	0.0407422
137Ba	130	11	104.0	130.0	118.9	33.688856
139La	15.5	11	11.0	15.5	13.7	3.9881091
140Ce	37.4	11	28.6	37.4	33.0	9.3915098
141Pr	5	11	3.3	5.0	4.4	1.2843709
146Nd	25	11	17.8	25.0	21.6	6.224694
147Sm	6.1	11	4.0	6.1	5.3	1.5774796
153Eu	2.1	11	0.7	2.1	1.8	0.6141633
157Gd	6.5	11	3.4	6.5	4.8	1.5146112
159Tb	0.96	10	0.6	1.0	0.8	0.2941107
163Dy	5.2	11	2.8	5.2	4.1	1.2745186
165Ho	0.93	10	0.5	0.9	0.8	0.3052997

Scaled Isotope	BHVO-2 Pub. Conc.	Count	Min	Max	Average	Sigma
166Er	2.5	11	0.6	2.5	1.8	0.6568281
169Tm	0.36	9	0.2	0.4	0.3	0.1189208
172Yb	2	11	0.4	2.0	1.5	0.5767636
175Lu	0.28	9	0.1	0.3	0.2	0.1002601
178Hf	4.1	11	2.2	4.1	3.5	1.0728219
181Ta	1.4	10	0.6	1.4	0.8	0.3629202
182W		8	0.2	0.3	0.2	0.0957749
185Re		0	0.0	0.0	- -	0
195Pt		7	0.1	0.1	0.1	0.0453975
197Au		10	0.2	0.4	0.3	0.0860746
205Tl		2	0.0	0.0	0.0	0.0095499
208Pb		10	0.8	1.7	1.4	0.4671568
209Bi		4	0.0	0.0	0.0	0.0091825
232Th	1.2	11	0.3	1.2	1.0	0.3503381
238U		9	0.2	0.4	0.3	0.1313187

Si Internal Description	BIR-1 Pub. Conc.	Ap16A13	Ap16A14	Ap16B13	Ap16B14	Ap16C13
7Li	3.6	2.8	2.3	2.5	2.6	2.7
9Be	0.58	< DL	< DL	< DL	< DL	< DL
11B	0.33	15.7	15.3	14.0	14.0	12.4
23Na	13500	10729.9	9443.2	9164.2	9758.3	9830.8
25Mg	58000	61589.5	65077.0	57713.8	54162.5	57099.5
27Al	82000	86969.0	86822.2	81245.5	78168.2	76612.1
29Si	224200	224200.0	224200.0	224200.0	224200.0	224200.0
31P	92	71.8	72.0	82.5	81.7	83.4
33S		< DL	< DL	11.6	< DL	10.6
39K	250	< DL	< DL	145.0	163.5	148.3
43Ca	95100	76958.2	86346.5	87646.1	77376.3	70856.7
44Ca	95100	75552.8	81831.2	81170.6	74002.8	67048.8
45Sc	44	35.8	36.9	35.4	33.4	31.8
47Ti	5800	4892.6	4923.0	4792.6	4473.9	4341.6
51V	310	261.0	258.7	249.3	234.7	242.0
52Cr	370	326.3	311.1	302.2	291.7	312.6
53Cr	370	323.8	328.5	315.5	299.1	319.6
55Mn	1360	1343.7	1355.2	1297.7	1216.3	1292.5
57Fe	79000	79325.8	82524.5	77741.9	71786.5	75718.2
59Co	52	48.6	49.2	49.7	48.6	47.3
60Ni	170	154.6	162.2	165.0	154.3	154.5
62Ni	170	< DL	< DL	147.7	161.0	176.2
65Cu	125	102.6	96.9	107.8	109.8	102.1
66Zn	70	83.9	91.9	103.3	102.4	96.2
68Zn	70	80.3	89.6	102.2	103.0	95.5
69Ga	16	14.5	15.1	17.1	16.7	15.3
72Ge		2.1	2.2	2.5	2.6	2.3
75As	0.44	< DL	< DL	1.6	1.1	0.5
77Ar Cl		- -	- -	- -	- -	- -
82Se		-0.2	-1.2	< DL	< DL	< DL
83Kr		- -	- -	- -	- -	- -
85Rb		< DL	< DL	0.2	0.2	0.1
86Sr	110	96.0	94.8	91.8	85.8	87.4
88Sr	110	97.2	95.0	90.4	85.7	84.7
89Y	16	11.7	11.8	10.7	10.5	9.9
90Zr	18	12.0	12.2	11.1	10.7	11.2
93Nb	0.6	0.3	0.4	0.4	0.4	0.4
95Mo		< DL	< DL	0.2	0.2	< DL
103Rh		< DL	0.0	< DL	< DL	< DL
105Pd		< DL	< DL	< DL	< DL	0.2
107Ag		0.3	0.3	0.4	0.5	0.4
110Cd		< DL	< DL	< DL	0.2	< DL
111Cd		< DL	< DL	0.3	0.4	0.3
115In		< DL	< DL	0.1	0.1	< DL
118Sn		1.5	1.1	1.4	1.2	1.2
120Sn		1.4	1.3	1.1	1.2	1.2
121Sb	0.58	0.6	0.5	0.5	0.5	0.4
133Cs		< DL	< DL	< DL	< DL	0.1
136Ba	7	7.1	5.4	6.1	4.8	5.6
137Ba	7	6.2	5.7	5.0	5.5	5.9

Si Internal Description	BIR-1 Pub. Conc.	Ap16A13	Ap16A14	Ap16B13	Ap16B14	Ap16C13
139La	0.71	0.6	0.4	0.6	0.5	0.5
140Ce	2.1	1.7	1.7	1.5	1.5	1.5
141Pr	0.42	0.3	0.3	0.3	0.3	0.4
146Nd	2.5	2.4	2.1	1.9	2.1	1.9
147Sm	1.1	1.1	1.0	0.9	0.8	1.0
153Eu	0.58	0.5	0.5	0.4	0.4	0.4
155Gd	2	1.8	1.3	1.1	1.4	1.0
156Ce O		--	--	--	--	--
157Gd	2	1.3	1.5	1.4	1.4	1.4
159Tb	0.43	0.3	0.3	0.3	0.3	0.2
163Dy	2.7	2.2	2.1	2.0	1.9	1.8
165Ho	0.59	0.4	0.4	0.5	0.4	0.4
166Er	1.7	1.4	1.3	1.2	1.1	1.2
169Tm	0.33	0.2	0.2	0.2	0.2	0.1
172Yb	1.7	1.5	1.4	1.3	1.4	1.4
175Lu	0.26	0.2	0.1	0.2	0.2	0.1
178Hf	0.6	0.5	0.4	0.4	0.4	0.5
181Ta		< DL	< DL	0.0	0.0	0.1
182W		< DL	< DL	< DL	< DL	< DL
185Re		< DL	< DL	0.1	< DL	0.1
195Pt		0.6	0.5	0.5	0.5	1.2
197Au		0.1	0.1	0.1	0.1	0.1
205Tl		< DL	< DL	< DL	< DL	< DL
206Pb	3	3.7	4.0	4.6	5.1	4.9
207Pb	3	3.5	3.7	4.4	4.7	4.7
208Pb	3	3.7	3.8	4.5	4.7	4.6
209Bi		< DL	< DL	0.0	0.0	0.0
220Bkg		--	--	--	--	--
232Th		< DL	< DL	0.0	< DL	0.1
238U		< DL	< DL	< DL	< DL	0.0
254U O		--	--	--	--	--

Si Internal Description	BIR-1 Pub. Conc.	Ap16C14	Ap16D13	Ap16D14	Ap16E13	Ap16E14
7Li	3.6	2.4	2.7	2.5	2.2	2.5
9Be	0.58	< DL	< DL	< DL	< DL	< DL
11B	0.33	12.1	10.9	10.2	10.8	10.7
23Na	13500	9132.0	9989.5	9962.2	9411.3	9366.5
25Mg	58000	53964.6	55637.8	57457.8	54429.8	58181.6
27Al	82000	74492.9	72827.6	73760.2	71864.4	72766.8
29Si	224200	224200.0	224200.0	224200.0	224200.0	224200.0
31P	92	77.3	79.4	78.3	83.9	87.0
33S		9.8	14.6	16.0	12.9	13.0
39K	250	166.2	141.3	142.8	137.5	161.1
43Ca	95100	71863.9	66484.7	66446.0	64817.5	74117.4
44Ca	95100	66939.8	62920.3	61745.4	60506.5	64663.6
45Sc	44	31.6	29.3	29.3	28.1	29.7
47Ti	5800	4325.6	4192.7	4165.9	4134.1	4123.4
51V	310	244.8	223.6	226.1	234.3	234.2
52Cr	370	313.5	292.6	292.1	298.0	283.5
53Cr	370	317.0	304.0	291.5	292.4	292.8
55Mn	1360	1285.9	1182.1	1206.3	1171.1	1207.0
57Fe	79000	77900.9	70513.8	70375.1	69404.5	72130.7
59Co	52	48.5	46.4	45.8	46.5	45.0
60Ni	170	166.7	146.0	142.9	145.6	149.9
62Ni	170	148.1	169.5	125.3	145.3	139.8
65Cu	125	106.1	96.7	88.2	94.3	93.2
66Zn	70	100.8	85.6	76.3	88.1	87.7
68Zn	70	104.3	89.1	79.2	88.6	88.9
69Ga	16	16.6	15.3	14.0	14.9	14.9
72Ge		2.8	2.5	2.2	2.3	2.5
75As	0.44	1.4	1.5	0.4	< DL	0.9
77Ar Cl		--	--	--	--	--
82Se		< DL	< DL	< DL	< DL	< DL
83Kr		--	--	--	--	--
85Rb		< DL	0.3	< DL	< DL	< DL
86Sr	110	84.5	81.4	78.1	80.1	77.9
88Sr	110	83.5	80.4	80.7	77.8	76.6
89Y	16	10.1	9.6	9.6	9.7	9.2
90Zr	18	10.8	10.0	10.3	10.3	9.6
93Nb	0.6	0.4	0.4	0.4	0.3	0.4
95Mo		< DL	< DL	0.3	< DL	< DL
103Rh		< DL	< DL	< DL	< DL	< DL
105Pd		< DL	0.2	< DL	< DL	0.2
107Ag		0.5	0.3	0.3	0.2	0.4
110Cd		< DL	< DL	< DL	< DL	< DL
111Cd		< DL	< DL	0.2	0.2	< DL
115In		0.1	0.0	0.1	< DL	0.1
118Sn		1.3	1.1	1.0	1.1	1.0
120Sn		1.2	1.1	0.9	1.0	1.2
121Sb	0.58	0.5	0.5	0.4	0.4	0.5
133Cs		< DL	< DL	< DL	0.1	< DL
136Ba	7	4.5	5.4	4.9	5.4	5.3
137Ba	7	5.5	5.0	5.6	6.9	4.8

Si Internal Description	BIR-1 Pub. Conc.	Ap16C14	Ap16D13	Ap16D14	Ap16E13	Ap16E14
139La	0.71	0.5	0.5	0.4	0.4	0.4
140Ce	2.1	1.6	1.5	1.3	1.4	1.4
141Pr	0.42	0.3	0.3	0.3	0.1	0.3
146Nd	2.5	1.7	1.9	1.8	1.8	1.6
147Sm	1.1	0.6	1.0	0.6	1.0	0.6
153Eu	0.58	0.5	0.5	0.4	0.4	0.3
155Gd	2	1.0	1.5	1.2	1.0	1.1
156Ce O		--	--	--	--	--
157Gd	2	1.2	1.4	1.2	0.9	1.4
159Tb	0.43	0.2	0.3	0.2	0.1	0.2
163Dy	2.7	1.7	1.7	1.6	1.5	1.7
165Ho	0.59	0.4	0.4	0.4	0.2	0.3
166Er	1.7	1.1	1.1	1.0	1.1	1.0
169Tm	0.33	0.2	0.2	0.2	< DL	< DL
172Yb	1.7	1.2	1.4	1.1	1.2	0.9
175Lu	0.26	0.1	0.2	0.2	< DL	0.2
178Hf	0.6	0.4	0.4	0.4	0.3	0.4
181Ta		0.0	0.1	< DL	< DL	< DL
182W		< DL	0.1	< DL	< DL	< DL
185Re		< DL	< DL	< DL	< DL	< DL
195Pt		1.3	0.7	0.5	0.7	0.7
197Au		0.1	0.1	< DL	0.1	0.1
205Tl		< DL	< DL	< DL	< DL	< DL
206Pb	3	5.5	4.3	3.8	4.6	4.6
207Pb	3	4.9	4.0	3.4	4.1	4.2
208Pb	3	5.0	3.8	3.5	4.1	4.2
209Bi		< DL	0.0	< DL	< DL	< DL
220Bkg		--	--	--	--	--
232Th		< DL	0.0	< DL	< DL	< DL
238U		< DL	< DL	< DL	< DL	< DL
254U O		--	--	--	--	--

Si Internal Description	BIR-1 Pub. Conc.	Count	Min	Max	Average	Sigma
7Li	3.6	11	2.2	3.6	2.6	0.7960687
9Be	0.58	1	0.6	0.6	0.6	0.1603035
11B	0.33	11	0.3	15.7	11.5	4.9490172
23Na	13500	11	9132.0	13500.0	10026.2	2993.3402
25Mg	58000	11	53964.6	65077.0	57574.0	16202.012
27Al	82000	11	71864.4	86969.0	77957.2	22135.343
29Si	224200	11	224200.0	224200.0	224200.0	61965.606
31P	92	11	71.8	92.0	80.9	23.015053
33S		7	9.8	16.0	12.6	6.286609
39K	250	9	137.5	250.0	161.7	75.551223
43Ca	95100	11	64817.5	95100.0	76183.0	22883.963
44Ca	95100	11	60506.5	95100.0	71952.9	22174.303
45Sc	44	11	28.1	44.0	33.2	10.1116
47Ti	5800	11	4123.4	5800.0	4560.5	1343.8534
51V	310	11	223.6	310.0	247.2	71.76042
52Cr	370	11	283.5	370.0	308.5	88.021908
53Cr	370	11	291.5	370.0	314.0	89.264298
55Mn	1360	11	1171.1	1360.0	1265.3	355.66298
57Fe	79000	11	69404.5	82524.5	75129.3	21160.145
59Co	52	11	45.0	52.0	48.0	13.38442
60Ni	170	11	142.9	170.0	155.6	43.827603
62Ni	170	9	125.3	176.2	153.7	67.902621
65Cu	125	11	88.2	125.0	102.1	29.67926
66Zn	70	11	70.0	103.3	89.6	26.626848
68Zn	70	11	70.0	104.3	90.1	26.771172
69Ga	16	11	14.0	17.1	15.5	4.3750013
72Ge		10	2.1	2.8	2.4	0.7255294
75As	0.44	8	0.4	1.6	1.0	0.6090669
77Ar Cl		0	0.0	0.0	- -	0
82Se		2	-1.2	-0.2	-0.7	0.3358287
83Kr		0	0.0	0.0	- -	0
85Rb		4	0.1	0.3	0.2	0.1088973
86Sr	110	11	77.9	110.0	88.0	25.86436
88Sr	110	11	76.6	110.0	87.5	25.842207
89Y	16	11	9.2	16.0	10.8	3.4619234
90Zr	18	11	9.6	18.0	11.5	3.8060145
93Nb	0.6	11	0.3	0.6	0.4	0.1294931
95Mo		3	0.2	0.3	0.2	0.1088182
103Rh		1	0.0	0.0	0.0	0.0101509
105Pd		3	0.2	0.2	0.2	0.0779864
107Ag		10	0.2	0.5	0.4	0.134006
110Cd		1	0.2	0.2	0.2	0.071458
111Cd		5	0.2	0.4	0.3	0.1373289
115In		6	0.0	0.1	0.1	0.0290189
118Sn		10	1.0	1.5	1.2	0.3737123
120Sn		10	0.9	1.4	1.2	0.3538845
121Sb	0.58	11	0.4	0.6	0.5	0.1452546
133Cs		2	0.1	0.1	0.1	0.026677
136Ba	7	11	4.5	7.1	5.6	1.7182642
137Ba	7	11	4.8	7.0	5.7	1.717711

Si Internal Description	BIR-1 Pub. Conc.	Count	Min	Max	Average	Sigma
139La	0.71	11	0.4	0.7	0.5	0.1703243
140Ce	2.1	11	1.3	2.1	1.6	0.4721728
141Pr	0.42	11	0.1	0.4	0.3	0.1103296
146Nd	2.5	11	1.6	2.5	2.0	0.5991151
147Sm	1.1	11	0.6	1.1	0.9	0.2923391
153Eu	0.58	11	0.3	0.6	0.4	0.1376058
155Gd	2	11	1.0	2.0	1.3	0.4749683
156Ce O		0	0.0	0.0	- -	0
157Gd	2	11	0.9	2.0	1.4	0.4469452
159Tb	0.43	11	0.1	0.4	0.3	0.1044387
163Dy	2.7	11	1.5	2.7	1.9	0.6068205
165Ho	0.59	11	0.2	0.6	0.4	0.1428107
166Er	1.7	11	1.0	1.7	1.2	0.3805105
169Tm	0.33	9	0.1	0.3	0.2	0.0955176
172Yb	1.7	11	0.9	1.7	1.3	0.4089171
175Lu	0.26	10	0.1	0.3	0.2	0.0773226
178Hf	0.6	11	0.3	0.6	0.4	0.1360126
181Ta		5	0.0	0.1	0.0	0.0228845
182W		1	0.1	0.1	0.1	0.0145348
185Re		2	0.1	0.1	0.1	0.0202592
195Pt		10	0.5	1.3	0.7	0.327826
197Au		9	0.1	0.1	0.1	0.0401471
205Tl		0	0.0	0.0	- -	0
206Pb	3	11	3.0	5.5	4.4	1.3732224
207Pb	3	11	3.0	4.9	4.1	1.2515173
208Pb	3	11	3.0	5.0	4.1	1.2522499
209Bi		4	0.0	0.0	0.0	0.0116918
220Bkg		0	0.0	0.0	- -	0
232Th		3	0.0	0.1	0.0	0.0181918
238U		1	0.0	0.0	0.0	0.011683
254U O		0	0.0	0.0	- -	0

Ca Internal Description	BIR-1 Pub. Conc.	Ap16A13	Ap16A14	Ap16B13	Ap16B14	Ap16C13
7Li	3.6	3.5	2.7	2.9	3.3	3.8
9Be	0.58	< DL	< DL	< DL	< DL	< DL
11B	0.33	19.7	17.8	16.3	18.0	17.6
23Na	13500	13506.0	10974.4	10736.8	12540.2	13943.8
25Mg	58000	77524.0	75629.1	67617.9	69603.5	80988.2
27Al	82000	109469.8	100900.3	95187.7	100452.9	108664.4
29Si	224200	282205.5	260553.7	262674.2	288116.5	317998.7
31P	92	90.4	83.6	96.6	105.0	118.3
33S		< DL	< DL	13.6	< DL	15.1
39K	250	208.2	186.5	169.8	210.2	210.4
43Ca	95100	96869.0	100347.5	102686.8	99435.3	100501.0
44Ca	95100	95100.0	95100.0	95100.0	95100.0	95100.0
45Sc	44	45.1	42.9	41.4	42.9	45.2
47Ti	5800	6158.4	5721.3	5615.0	5749.3	6158.0
51V	310	328.5	300.7	292.1	301.6	343.3
52Cr	370	410.7	361.5	354.1	374.8	443.4
53Cr	370	407.5	381.8	369.6	384.3	453.3
55Mn	1360	1691.4	1574.9	1520.4	1563.0	1833.2
57Fe	79000	99849.2	95905.7	91082.9	92251.9	107396.5
59Co	52	61.2	57.2	58.3	62.5	67.1
60Ni	170	194.6	188.5	193.3	198.3	219.2
62Ni	170	< DL	< DL	173.1	206.9	249.8
65Cu	125	129.2	112.6	126.3	141.1	144.8
66Zn	70	105.5	106.8	121.0	131.5	136.4
68Zn	70	101.1	104.2	119.7	132.4	135.4
69Ga	16	18.2	17.6	20.0	21.5	21.7
72Ge		2.6	2.6	2.9	3.4	3.3
75As	0.44	< DL	< DL	1.9	1.4	0.7
77Ar Cl		- -	- -	- -	- -	- -
82Se		-0.3	-1.4	< DL	< DL	< DL
83Kr		- -	- -	- -	- -	- -
85Rb		< DL	< DL	0.3	0.3	0.2
86Sr	110	120.8	110.2	107.6	110.3	124.0
88Sr	110	122.4	110.4	106.0	110.1	120.2
89Y	16	14.7	13.7	12.5	13.5	14.0
90Zr	18	15.1	14.1	13.0	13.8	15.9
93Nb	0.6	0.4	0.4	0.5	0.5	0.6
95Mo		< DL	< DL	0.2	0.3	0.2
103Rh		< DL	0.0	< DL	0.0	< DL
105Pd		< DL	< DL	< DL	< DL	0.2
107Ag		0.4	0.4	0.5	0.6	0.6
110Cd		< DL	< DL	< DL	0.3	< DL
111Cd		< DL	< DL	0.3	0.5	0.4
115In		< DL	< DL	0.1	0.1	0.0
118Sn		1.9	1.3	1.6	1.6	1.7
120Sn		1.7	1.5	1.3	1.5	1.7
121Sb	0.58	0.7	0.5	0.6	0.7	0.6
133Cs		< DL	< DL	< DL	< DL	0.1
136Ba	7	8.9	6.3	7.1	6.2	8.0
137Ba	7	7.8	6.6	5.8	7.1	8.4

Ca Internal Description	BIR-1 Pub. Conc.	Ap16A13	Ap16A14	Ap16B13	Ap16B14	Ap16C13
139La	0.71	0.7	0.5	0.7	0.7	0.7
140Ce	2.1	2.2	1.9	1.8	1.9	2.2
141Pr	0.42	0.4	0.4	0.4	0.3	0.5
146Nd	2.5	3.0	2.5	2.2	2.7	2.7
147Sm	1.1	1.3	1.1	1.1	1.0	1.4
153Eu	0.58	0.6	0.5	0.5	0.6	0.6
155Gd	2	2.3	1.5	1.3	1.8	1.5
156Ce O		--	--	--	--	--
157Gd	2	1.7	1.7	1.6	1.8	1.9
159Tb	0.43	0.4	0.4	0.4	0.3	0.3
163Dy	2.7	2.8	2.4	2.3	2.4	2.5
165Ho	0.59	0.5	0.5	0.5	0.5	0.6
166Er	1.7	1.8	1.5	1.4	1.4	1.7
169Tm	0.33	0.3	0.2	0.2	0.3	0.2
172Yb	1.7	1.9	1.6	1.5	1.8	2.0
175Lu	0.26	0.3	0.2	0.2	0.3	0.2
178Hf	0.6	0.6	0.5	0.4	0.6	0.7
181Ta		< DL	< DL	0.0	0.0	0.1
182W		< DL	< DL	< DL	0.1	< DL
185Re		< DL	< DL	0.1	< DL	0.1
195Pt		0.7	0.6	0.6	0.7	1.7
197Au		0.1	0.1	0.1	0.1	0.2
205Tl		< DL	< DL	< DL	< DL	< DL
206Pb	3	4.7	4.6	5.4	6.5	6.9
207Pb	3	4.4	4.3	5.2	6.0	6.6
208Pb	3	4.6	4.4	5.3	6.0	6.5
209Bi		< DL	< DL	0.0	0.0	0.0
220Bkg		--	--	--	--	--
232Th		< DL	< DL	0.0	< DL	0.1
238U		< DL	< DL	< DL	< DL	0.1
254U O		--	--	--	--	--

Ca Internal Description	BIR-1 Pub. Conc.	Ap16C14	Ap16D13	Ap16D14	Ap16E13	Ap16E14
7Li	3.6	3.4	4.1	3.8	3.5	3.7
9Be	0.58	< DL	0.8	< DL	< DL	< DL
11B	0.33	17.2	16.5	15.7	17.0	15.7
23Na	13500	12973.6	15098.6	15343.8	14792.1	13775.2
25Mg	58000	76666.3	84093.0	88496.3	85549.2	85566.9
27Al	82000	105830.4	110074.2	113605.2	112951.7	107017.2
29Si	224200	318516.1	338864.0	345311.9	352382.5	329728.1
31P	92	109.8	120.1	120.6	131.9	128.0
33S		13.9	22.1	24.6	20.2	19.1
39K	250	236.1	213.6	219.9	216.1	236.9
43Ca	95100	102095.5	100487.3	102339.8	101875.9	109003.5
44Ca	95100	95100.0	95100.0	95100.0	95100.0	95100.0
45Sc	44	44.9	44.3	45.1	44.1	43.7
47Ti	5800	6145.3	6337.1	6416.4	6497.7	6064.2
51V	310	347.7	337.9	348.3	368.3	344.4
52Cr	370	445.4	442.2	450.0	468.4	416.9
53Cr	370	450.4	459.5	448.9	459.6	430.6
55Mn	1360	1826.9	1786.7	1857.9	1840.7	1775.1
57Fe	79000	110672.2	106577.1	108391.5	109085.4	106081.7
59Co	52	68.8	70.2	70.5	73.1	66.2
60Ni	170	236.8	220.7	220.0	228.9	220.5
62Ni	170	210.4	256.1	193.0	228.4	205.6
65Cu	125	150.7	146.1	135.9	148.2	137.1
66Zn	70	143.3	129.4	117.5	138.4	129.0
68Zn	70	148.1	134.6	122.0	139.2	130.8
69Ga	16	23.6	23.1	21.6	23.4	22.0
72Ge		4.0	3.8	3.4	3.7	3.7
75As	0.44	2.0	2.3	0.6	< DL	1.3
77Ar Cl		--	--	--	--	--
82Se		< DL	< DL	< DL	< DL	< DL
83Kr		--	--	--	--	--
85Rb		< DL	0.4	< DL	0.2	< DL
86Sr	110	120.1	123.0	120.2	125.9	114.6
88Sr	110	118.6	121.4	124.3	122.3	112.6
89Y	16	14.4	14.5	14.9	15.3	13.5
90Zr	18	15.4	15.1	15.8	16.3	14.0
93Nb	0.6	0.6	0.6	0.6	0.5	0.5
95Mo		< DL	0.2	0.5	< DL	< DL
103Rh		< DL	< DL	< DL	< DL	< DL
105Pd		< DL	0.3	< DL	< DL	0.2
107Ag		0.7	0.5	0.4	0.4	0.6
110Cd		0.2	0.2	< DL	< DL	< DL
111Cd		0.3	0.2	0.4	0.3	< DL
115In		0.1	0.1	0.1	< DL	0.1
118Sn		1.9	1.7	1.5	1.7	1.5
120Sn		1.8	1.7	1.4	1.6	1.7
121Sb	0.58	0.7	0.7	0.7	0.6	0.7
133Cs		< DL	< DL	< DL	0.1	< DL
136Ba	7	6.5	8.2	7.6	8.4	7.8
137Ba	7	7.8	7.6	8.7	10.8	7.0

Ca Internal Description	BIR-1 Pub. Conc.	Ap16C14	Ap16D13	Ap16D14	Ap16E13	Ap16E14
139La	0.71	0.8	0.7	0.7	0.6	0.6
140Ce	2.1	2.2	2.2	2.1	2.2	2.0
141Pr	0.42	0.4	0.4	0.4	0.1	0.4
146Nd	2.5	2.4	2.9	2.7	2.8	2.4
147Sm	1.1	0.9	1.5	0.9	1.5	0.9
153Eu	0.58	0.7	0.7	0.7	0.6	0.5
155Gd	2	1.4	2.2	1.9	1.5	1.7
156Ce O		--	--	--	--	--
157Gd	2	1.8	2.0	1.8	1.4	2.1
159Tb	0.43	0.3	0.4	0.3	0.2	0.2
163Dy	2.7	2.5	2.5	2.4	2.4	2.4
165Ho	0.59	0.5	0.6	0.6	0.3	0.4
166Er	1.7	1.6	1.6	1.6	1.8	1.4
169Tm	0.33	0.3	0.2	0.2	0.1	< DL
172Yb	1.7	1.8	2.1	1.7	1.9	1.4
175Lu	0.26	0.2	0.3	0.2	< DL	0.2
178Hf	0.6	0.5	0.6	0.6	0.5	0.6
181Ta		0.0	0.1	< DL	< DL	< DL
182W		< DL	0.1	< DL	< DL	< DL
185Re		< DL	< DL	< DL	< DL	< DL
195Pt		1.8	1.1	0.8	1.1	1.0
197Au		0.2	0.1	0.0	0.1	0.1
205Tl		< DL	< DL	< DL	< DL	< DL
206Pb	3	7.8	6.4	5.8	7.3	6.8
207Pb	3	7.0	6.1	5.3	6.4	6.2
208Pb	3	7.2	5.8	5.4	6.4	6.2
209Bi		< DL	0.0	0.0	< DL	< DL
220Bkg		--	--	--	--	--
232Th		< DL	0.1	< DL	< DL	< DL
238U		< DL	< DL	0.0	< DL	< DL
254U O		--	--	--	--	--

Ca Internal Description	BIR-1 Pub. Conc.	Count	Min	Max	Average	Sigma
7Li	3.6	11	2.7	4.1	3.5	1.0291798
9Be	0.58	2	0.6	0.8	0.7	0.2539919
11B	0.33	11	0.3	19.7	15.6	6.4151348
23Na	13500	11	10736.8	15343.8	13380.4	3948.2884
25Mg	58000	11	58000.0	88496.3	77248.6	22949.667
27Al	82000	11	82000.0	113605.2	104195.8	30012.328
29Si	224200	11	224200.0	352382.5	301868.3	91516.461
31P	92	11	83.6	131.9	108.8	33.566694
33S		7	13.6	24.6	18.4	9.38274
39K	250	11	169.8	250.0	214.3	62.729807
43Ca	95100	11	95100.0	109003.5	100976.5	28095.796
44Ca	95100	11	95100.0	95100.0	95100.0	26284.251
45Sc	44	11	41.4	45.2	44.0	12.198732
47Ti	5800	11	5615.0	6497.7	6060.2	1697.17
51V	310	11	292.1	368.3	329.3	93.758065
52Cr	370	11	354.1	468.4	412.5	119.95861
53Cr	370	11	369.6	459.6	419.6	120.91117
55Mn	1360	11	1360.0	1857.9	1693.7	491.85413
57Fe	79000	11	79000.0	110672.2	100572.2	29250.938
59Co	52	11	52.0	73.1	64.3	18.756515
60Ni	170	11	170.0	236.8	208.3	60.501241
62Ni	170	9	170.0	256.1	210.4	94.389287
65Cu	125	11	112.6	150.7	136.1	39.113373
66Zn	70	11	70.0	143.3	120.8	38.418306
68Zn	70	11	70.0	148.1	121.6	39.282891
69Ga	16	11	16.0	23.6	20.8	6.1876865
72Ge		10	2.6	4.0	3.3	1.0627226
75As	0.44	8	0.4	2.3	1.3	0.8329552
77Ar Cl		0	0.0	0.0	- -	0
82Se		2	-1.4	-0.3	-0.8	0.3908581
83Kr		0	0.0	0.0	- -	0
85Rb		5	0.2	0.4	0.3	0.1454729
86Sr	110	11	107.6	125.9	117.0	32.882938
88Sr	110	11	106.0	124.3	116.2	32.656623
89Y	16	11	12.5	16.0	14.3	4.041102
90Zr	18	11	13.0	18.0	15.1	4.3697632
93Nb	0.6	11	0.4	0.6	0.5	0.1586934
95Mo		5	0.2	0.5	0.3	0.1502101
103Rh		2	0.0	0.0	0.0	0.0129243
105Pd		3	0.2	0.3	0.3	0.1154627
107Ag		10	0.4	0.7	0.5	0.1836244
110Cd		3	0.2	0.3	0.3	0.115002
111Cd		7	0.2	0.5	0.3	0.1696234
115In		7	0.0	0.1	0.1	0.0386399
118Sn		10	1.3	1.9	1.6	0.4971774
120Sn		10	1.3	1.8	1.6	0.4781118
121Sb	0.58	11	0.5	0.7	0.7	0.1896023
133Cs		2	0.1	0.1	0.1	0.0397879
136Ba	7	11	6.2	8.9	7.4	2.2180454
137Ba	7	11	5.8	10.8	7.7	2.4393186

Ca Internal Description	BIR-1 Pub. Conc.	Count	Min	Max	Average	Sigma
139La	0.71	11	0.5	0.8	0.7	0.2023633
140Ce	2.1	11	1.8	2.2	2.1	0.5862717
141Pr	0.42	11	0.1	0.5	0.4	0.1350165
146Nd	2.5	11	2.2	3.0	2.6	0.7530999
147Sm	1.1	11	0.9	1.5	1.2	0.3834978
153Eu	0.58	11	0.5	0.7	0.6	0.1775197
155Gd	2	11	1.3	2.3	1.7	0.5657888
156Ce O		0	0.0	0.0	- -	0
157Gd	2	11	1.4	2.1	1.8	0.531511
159Tb	0.43	11	0.2	0.4	0.3	0.1121991
163Dy	2.7	11	2.3	2.8	2.5	0.6981959
165Ho	0.59	11	0.3	0.6	0.5	0.1673854
166Er	1.7	11	1.4	1.8	1.6	0.4557399
169Tm	0.33	10	0.1	0.3	0.2	0.0987929
172Yb	1.7	11	1.4	2.1	1.7	0.5167466
175Lu	0.26	10	0.2	0.3	0.2	0.0957706
178Hf	0.6	11	0.4	0.7	0.6	0.1698738
181Ta		5	0.0	0.1	0.1	0.0329107
182W		2	0.1	0.1	0.1	0.0251356
185Re		2	0.1	0.1	0.1	0.0264859
195Pt		10	0.6	1.8	1.0	0.4877767
197Au		10	0.0	0.2	0.1	0.0514916
205Tl		0	0.0	0.0	- -	0
206Pb	3	11	3.0	7.8	5.9	2.0872613
207Pb	3	11	3.0	7.0	5.5	1.8782523
208Pb	3	11	3.0	7.2	5.5	1.8640608
209Bi		5	0.0	0.0	0.0	0.0153696
220Bkg		0	0.0	0.0	- -	0
232Th		3	0.0	0.1	0.1	0.0257028
238U		2	0.0	0.1	0.0	0.0166951
254U O		0	0.0	0.0	- -	0

Fe Internal Description	BIR-1 Pub. Conc.	Ap16A13	Ap16A14	Ap16B13	Ap16B14	Ap16C13
7Li	3.6	2.8	2.2	2.5	2.8	2.8
9Be	0.58	< DL	< DL	< DL	< DL	< DL
11B	0.33	15.6	14.6	14.2	15.4	12.9
23Na	13500	10685.8	9039.9	9312.5	10738.8	10256.9
25Mg	58000	61336.5	62297.7	58647.8	59605.0	59574.3
27Al	82000	86611.8	83114.2	82560.3	86022.9	79932.7
29Si	224200	223279.1	214624.8	227828.2	246728.7	233917.3
31P	92	71.5	68.9	83.8	90.0	87.0
33S		< DL	< DL	11.8	< DL	11.1
39K	250	< DL	< DL	147.3	180.0	154.7
43Ca	95100	76642.1	82658.8	89064.5	85151.5	73927.8
44Ca	95100	75242.5	78336.3	82484.2	81438.9	69954.8
45Sc	44	35.7	35.4	36.0	36.7	33.2
47Ti	5800	4872.5	4712.8	4870.2	4923.5	4529.7
51V	310	259.9	247.7	253.3	258.3	252.5
52Cr	370	325.0	297.8	307.1	321.0	326.2
53Cr	370	322.4	314.5	320.6	329.1	333.4
55Mn	1360	1338.2	1297.3	1318.7	1338.5	1348.5
57Fe	79000	79000.0	79000.0	79000.0	79000.0	79000.0
59Co	52	48.4	47.1	50.6	53.5	49.4
60Ni	170	153.9	155.3	167.7	169.8	161.2
62Ni	170	< DL	< DL	150.1	177.2	183.8
65Cu	125	102.2	92.8	109.5	120.9	106.5
66Zn	70	83.5	88.0	105.0	112.7	100.3
68Zn	70	80.0	85.8	103.8	113.4	99.6
69Ga	16	14.4	14.5	17.3	18.4	16.0
72Ge		2.1	2.1	2.5	2.9	2.4
75As	0.44	< DL	< DL	1.7	1.2	0.5
77Ar Cl		--	--	--	--	--
82Se		-0.2	-1.1	< DL	< DL	< DL
83Kr		--	--	--	--	--
85Rb		< DL	< DL	0.3	0.2	0.1
86Sr	110	95.6	90.7	93.3	94.4	91.2
88Sr	110	96.8	90.9	91.9	94.3	88.4
89Y	16	11.7	11.3	10.9	11.5	10.3
90Zr	18	12.0	11.6	11.3	11.8	11.7
93Nb	0.6	0.3	0.4	0.4	0.4	0.4
95Mo		< DL	< DL	0.2	0.2	< DL
103Rh		< DL	0.0	< DL	0.0	< DL
105Pd		< DL	< DL	< DL	< DL	0.2
107Ag		0.3	0.3	0.4	0.5	0.5
110Cd		< DL	< DL	< DL	0.3	< DL
111Cd		< DL	< DL	0.3	0.4	0.3
115In		< DL	< DL	0.1	0.1	< DL
118Sn		1.5	1.0	1.4	1.4	1.2
120Sn		1.4	1.2	1.2	1.3	1.2
121Sb	0.58	0.6	0.4	0.5	0.6	0.5
133Cs		< DL	< DL	< DL	< DL	0.1
136Ba	7	7.0	5.2	6.2	5.3	5.9
137Ba	7	6.1	5.4	5.0	6.1	6.2

Fe Internal Description	BIR-1 Pub. Conc.	Ap16A13	Ap16A14	Ap16B13	Ap16B14	Ap16C13
139La	0.71	0.6	0.4	0.6	0.6	0.6
140Ce	2.1	1.7	1.6	1.5	1.7	1.6
141Pr	0.42	0.3	0.3	0.3	0.3	0.4
146Nd	2.5	2.4	2.0	1.9	2.3	2.0
147Sm	1.1	1.1	0.9	0.9	0.9	1.0
153Eu	0.58	0.5	0.4	0.5	0.5	0.4
155Gd	2	1.8	< DL	1.1	1.5	1.1
156Ce O		- -	- -	- -	- -	- -
157Gd	2	1.3	1.4	1.4	1.5	1.4
159Tb	0.43	0.3	0.3	0.3	0.3	0.2
163Dy	2.7	2.2	2.0	2.0	2.0	1.9
165Ho	0.59	0.4	0.4	0.5	0.4	0.5
166Er	1.7	1.4	1.2	1.2	1.2	1.2
169Tm	0.33	0.2	0.2	0.2	0.2	0.2
172Yb	1.7	1.5	1.3	1.3	1.5	1.4
175Lu	0.26	0.2	0.1	0.2	0.2	0.1
178Hf	0.6	0.5	0.4	0.4	0.5	0.5
181Ta		< DL	< DL	0.0	0.0	0.1
182W		< DL	< DL	< DL	0.0	< DL
185Re		< DL	< DL	0.1	< DL	0.1
195Pt		0.6	0.5	0.5	0.6	1.2
197Au		0.1	0.1	0.1	0.1	0.1
205Tl		< DL	< DL	< DL	< DL	< DL
206Pb	3	3.7	3.8	4.7	5.6	5.1
207Pb	3	3.5	3.5	4.5	5.2	4.9
208Pb	3	3.7	3.6	4.6	5.2	4.8
209Bi		< DL	< DL	0.0	0.0	0.0
220Bkg		- -	- -	- -	- -	- -
232Th		< DL	< DL	0.0	< DL	0.1
238U		< DL	< DL	< DL	< DL	0.0
254U O		- -	- -	- -	- -	- -

Fe Internal Description	BIR-1 Pub. Conc.	Ap16C14	Ap16D13	Ap16D14	Ap16E13	Ap16E14
7Li	3.6	2.5	3.0	2.8	2.5	2.7
9Be	0.58	< DL	< DL	< DL	< DL	< DL
11B	0.33	12.3	12.2	11.5	12.3	11.7
23Na	13500	9260.8	11191.8	11183.2	10712.5	10258.5
25Mg	58000	54725.9	62333.8	64499.6	61955.0	63722.5
27Al	82000	75543.8	81592.3	82800.0	81800.0	79696.7
29Si	224200	227363.1	251182.1	251676.9	255196.6	245551.6
31P	92	78.4	89.0	87.9	95.5	95.3
33S		10.0	16.4	17.9	14.6	14.3
39K	250	168.5	158.3	160.2	156.5	176.4
43Ca	95100	72877.8	74486.0	74589.3	73778.8	81175.9
44Ca	95100	67884.3	70492.6	69312.6	68871.7	70821.8
45Sc	44	32.1	32.8	32.8	31.9	32.6
47Ti	5800	4386.6	4697.3	4676.5	4705.6	4516.0
51V	310	248.2	250.5	253.8	266.7	256.5
52Cr	370	317.9	327.8	328.0	339.2	310.5
53Cr	370	321.5	340.6	327.2	332.9	320.7
55Mn	1360	1304.1	1324.4	1354.1	1333.0	1321.9
57Fe	79000	79000.0	79000.0	79000.0	79000.0	79000.0
59Co	52	49.1	52.0	51.4	52.9	49.3
60Ni	170	169.1	163.6	160.4	165.7	164.2
62Ni	170	150.2	189.9	140.7	165.4	153.1
65Cu	125	107.6	108.3	99.0	107.3	102.1
66Zn	70	102.3	95.9	85.6	100.2	96.1
68Zn	70	105.7	99.8	88.9	100.8	97.4
69Ga	16	16.8	17.1	15.7	16.9	16.4
72Ge		2.9	2.8	2.4	2.7	2.8
75As	0.44	1.4	1.7	0.4	< DL	1.0
77Ar Cl		--	--	--	--	--
82Se		< DL	< DL	< DL	< DL	< DL
83Kr		--	--	--	--	--
85Rb		< DL	0.3	< DL	< DL	< DL
86Sr	110	85.7	91.2	87.6	91.2	85.3
88Sr	110	84.7	90.0	90.6	88.6	83.9
89Y	16	10.3	10.7	10.8	11.1	10.1
90Zr	18	11.0	11.2	11.5	11.8	10.5
93Nb	0.6	0.4	0.4	0.4	0.4	0.4
95Mo		< DL	< DL	0.3	< DL	< DL
103Rh		< DL	< DL	< DL	< DL	< DL
105Pd		< DL	0.2	< DL	< DL	0.2
107Ag		0.5	0.4	0.3	0.3	0.4
110Cd		< DL	< DL	< DL	< DL	< DL
111Cd		< DL	0.2	0.3	0.2	< DL
115In		0.1	0.1	0.1	< DL	0.1
118Sn		1.3	1.2	1.1	1.2	1.1
120Sn		1.3	1.3	1.0	1.1	1.3
121Sb	0.58	0.5	0.6	0.5	0.5	0.5
133Cs		< DL	< DL	< DL	0.1	< DL
136Ba	7	4.6	6.1	5.5	6.1	5.8
137Ba	7	5.6	5.6	6.3	7.8	5.2

Fe Internal Description	BIR-1 Pub. Conc.	Ap16C14	Ap16D13	Ap16D14	Ap16E13	Ap16E14
139La	0.71	0.5	0.5	0.5	0.4	0.4
140Ce	2.1	1.6	1.7	1.5	1.6	1.5
141Pr	0.42	0.3	0.3	0.3	0.1	0.3
146Nd	2.5	1.7	2.1	2.0	2.0	1.8
147Sm	1.1	0.6	1.1	0.7	1.1	0.7
153Eu	0.58	0.5	0.5	0.5	0.4	0.3
155Gd	2	1.0	1.6	1.4	1.1	1.3
156Ce O		--	--	--	--	--
157Gd	2	1.3	1.5	1.3	1.0	1.5
159Tb	0.43	0.2	0.3	0.2	0.1	0.2
163Dy	2.7	1.8	1.9	1.8	1.7	1.8
165Ho	0.59	0.4	0.5	0.4	0.2	0.3
166Er	1.7	1.2	1.2	1.1	1.3	1.0
169Tm	0.33	0.2	0.2	0.2	< DL	< DL
172Yb	1.7	1.3	1.5	1.2	1.3	1.0
175Lu	0.26	0.1	0.2	0.2	< DL	0.2
178Hf	0.6	0.4	0.5	0.5	0.4	0.4
181Ta		0.0	0.1	< DL	< DL	< DL
182W		< DL	0.1	< DL	< DL	< DL
185Re		< DL	< DL	< DL	< DL	< DL
195Pt		1.3	0.8	0.6	0.8	0.7
197Au		0.1	0.1	< DL	0.1	0.1
205Tl		< DL	< DL	< DL	< DL	< DL
206Pb	3	5.6	4.8	4.2	5.3	5.1
207Pb	3	5.0	4.5	3.9	4.6	4.6
208Pb	3	5.1	4.3	3.9	4.7	4.6
209Bi		< DL	0.0	0.0	< DL	< DL
220Bkg		--	--	--	--	--
232Th		< DL	0.0	< DL	< DL	< DL
238U		< DL	< DL	0.0	< DL	< DL
254U O		--	--	--	--	--

Fe Internal Description	BIR-1 Pub. Conc.	Count	Min	Max	Average	Sigma
7Li	3.6	11	2.2	3.6	2.8	0.8269302
9Be	0.58	1	0.6	0.6	0.6	0.1603035
11B	0.33	11	0.3	15.6	12.1	5.0653389
23Na	13500	11	9039.9	13500.0	10558.2	3128.1877
25Mg	58000	11	54725.9	64499.6	60608.9	16950.073
27Al	82000	11	75543.8	86611.8	81970.4	22822.366
29Si	224200	11	214624.8	255196.6	236504.4	66598.999
31P	92	11	68.9	95.5	85.4	24.98097
33S		7	10.0	17.9	13.7	6.9350987
39K	250	9	147.3	250.0	172.4	78.824326
43Ca	95100	11	72877.8	95100.0	79950.2	23097.19
44Ca	95100	11	67884.3	95100.0	75449.1	22196.847
45Sc	44	11	31.9	44.0	34.8	10.140422
47Ti	5800	11	4386.6	5800.0	4790.1	1366.9885
51V	310	11	247.7	310.0	259.8	73.562152
52Cr	370	11	297.8	370.0	324.6	91.356219
53Cr	370	11	314.5	370.0	330.3	92.317751
55Mn	1360	11	1297.3	1360.0	1330.8	368.25723
57Fe	79000	11	79000.0	79000.0	79000.0	21834.447
59Co	52	11	47.1	53.5	50.5	14.083962
60Ni	170	11	153.9	170.0	163.7	45.533381
62Ni	170	9	140.7	189.9	164.5	72.564875
65Cu	125	11	92.8	125.0	107.4	30.830068
66Zn	70	11	70.0	112.7	94.5	28.283021
68Zn	70	11	70.0	113.4	95.0	28.6701
69Ga	16	11	14.4	18.4	16.3	4.6419249
72Ge		10	2.1	2.9	2.6	0.7856754
75As	0.44	8	0.4	1.7	1.0	0.6457626
77Ar Cl		0	0.0	0.0	- -	0
82Se		2	-1.1	-0.2	-0.7	0.3217064
83Kr		0	0.0	0.0	- -	0
85Rb		4	0.1	0.3	0.2	0.1174774
86Sr	110	11	85.3	110.0	92.4	26.258276
88Sr	110	11	83.9	110.0	91.8	26.193309
89Y	16	11	10.1	16.0	11.3	3.4678599
90Zr	18	11	10.5	18.0	12.0	3.8051585
93Nb	0.6	11	0.3	0.6	0.4	0.1321152
95Mo		3	0.2	0.3	0.3	0.1192996
103Rh		2	0.0	0.0	0.0	0.0107379
105Pd		3	0.2	0.2	0.2	0.0855484
107Ag		10	0.3	0.5	0.4	0.1399846
110Cd		1	0.3	0.3	0.3	0.0786384
111Cd		6	0.2	0.4	0.3	0.142379
115In		6	0.1	0.1	0.1	0.0308465
118Sn		10	1.0	1.5	1.3	0.3838188
120Sn		10	1.0	1.4	1.2	0.3637972
121Sb	0.58	11	0.4	0.6	0.5	0.1503296
133Cs		2	0.1	0.1	0.1	0.029034
136Ba	7	11	4.6	7.0	5.9	1.7566862
137Ba	7	11	5.0	7.8	6.0	1.8284878

Fe Internal Description	BIR-1 Pub. Conc.	Count	Min	Max	Average	Sigma
139La	0.71	11	0.4	0.7	0.5	0.171294
140Ce	2.1	11	1.5	2.1	1.6	0.4769273
141Pr	0.42	11	0.1	0.4	0.3	0.1104617
146Nd	2.5	11	1.7	2.5	2.1	0.6114099
147Sm	1.1	11	0.6	1.1	0.9	0.3016528
153Eu	0.58	11	0.3	0.6	0.5	0.1402477
155Gd	2	10	1.0	2.0	1.4	0.5963303
156Ce O		0	0.0	0.0	--	0
157Gd	2	11	1.0	2.0	1.4	0.4518879
159Tb	0.43	11	0.1	0.4	0.3	0.1027207
163Dy	2.7	11	1.7	2.7	2.0	0.601627
165Ho	0.59	11	0.2	0.6	0.4	0.1429368
166Er	1.7	11	1.0	1.7	1.3	0.3806489
169Tm	0.33	9	0.2	0.3	0.2	0.0968222
172Yb	1.7	11	1.0	1.7	1.4	0.4166228
175Lu	0.26	10	0.1	0.3	0.2	0.080296
178Hf	0.6	11	0.4	0.6	0.4	0.1395883
181Ta		5	0.0	0.1	0.0	0.0247327
182W		2	0.0	0.1	0.1	0.0195167
185Re		2	0.1	0.1	0.1	0.0208761
195Pt		10	0.5	1.3	0.8	0.3399559
197Au		9	0.1	0.1	0.1	0.042118
205Tl		0	0.0	0.0	--	0
206Pb	3	11	3.0	5.6	4.6	1.4897616
207Pb	3	11	3.0	5.2	4.3	1.3512655
208Pb	3	11	3.0	5.2	4.3	1.342868
209Bi		5	0.0	0.0	0.0	0.0120983
220Bkg		0	0.0	0.0	--	0
232Th		3	0.0	0.1	0.0	0.01933
238U		2	0.0	0.0	0.0	0.0122762
254U O		0	0.0	0.0	--	0

Scaled Isotope	BIR-1 Pub Data	Ap16A13	Ap16A14	Ap16B13	Ap16B14	Ap16C13
7Li	3.6	2.8	2.3	2.6	2.7	2.9
9Be	0.58	< DL	< DL	< DL	< DL	< DL
11B	0.33	15.8	15.2	14.4	14.9	13.2
23Na	13500	10853.5	9392.3	9480.9	10411.1	10519.5
25Mg	58000	62299.0	64726.4	59708.7	57786.0	61099.1
27Al	82000	87970.9	86354.5	84053.8	83397.7	81978.6
29Si	224200	226782.8	222992.2	231949.6	239199.2	239904.6
31P	92	72.6	71.6	85.3	87.2	89.3
33S		< DL	< DL	12.0	< DL	11.4
39K	250	< DL	< DL	150.0	174.5	158.7
44Ca	95100	76423.2	81390.4	83976.3	78953.6	71745.4
45Sc	44	36.2	36.7	36.6	35.6	34.1
47Ti	5800	4948.9	4896.5	4958.3	4773.2	4645.7
51V	310	266.2	259.5	257.9	250.4	259.0
53Cr	370	327.5	326.7	326.4	319.1	342.0
55Mn	1360	1359.2	1347.9	1342.6	1297.6	1383.0
57Fe	79000	80239.7	82079.9	80429.1	76589.1	81022.1
59Co	52	49.1	48.9	51.5	51.9	50.7
60Ni	170	156.4	161.3	170.7	164.6	165.4
65Cu	125	103.8	96.4	111.5	117.2	109.2
68Zn	70	81.2	89.1	105.7	109.9	102.2
69Ga	16	14.6	15.1	17.7	17.8	16.4
72Ge		2.1	2.2	2.6	2.8	2.5
75As	0.44	< DL	< DL	1.7	1.2	0.5
82Se		0.0	0.0	< DL	< DL	< DL
85Rb		< DL	< DL	0.3	0.2	0.1
88Sr	110	98.4	94.5	93.6	91.4	90.7
89Y	16	11.8	11.7	11.1	11.2	10.6
90Zr	18	12.1	12.1	11.5	11.5	12.0
93Nb	0.6	0.4	0.4	0.4	0.4	0.4
95Mo		< DL	< DL	0.2	0.2	< DL
103Rh		< DL	0.0	< DL	< DL	< DL
105Pd		< DL	< DL	< DL	< DL	0.2
107Ag		0.3	0.3	0.4	0.5	0.5
111Cd		< DL	< DL	0.3	0.4	0.3
115In		< DL	< DL	0.1	0.1	< DL
118Sn		1.5	1.1	1.4	1.3	1.3
121Sb	0.58	0.6	0.5	0.5	0.6	0.5
133Cs		< DL	< DL	< DL	< DL	0.1
137Ba	7	6.2	5.7	5.1	5.9	6.3
139La	0.71	0.6	0.4	0.6	0.6	0.6
140Ce	2.1	1.7	1.6	1.6	1.6	1.6
141Pr	0.42	0.3	0.3	0.3	0.3	0.4
146Nd	2.5	2.4	2.1	2.0	2.2	2.0
147Sm	1.1	1.1	1.0	0.9	0.8	1.0
153Eu	0.58	0.5	0.5	0.5	0.5	0.5
157Gd	2	1.3	1.5	1.4	1.5	1.5
159Tb	0.43	0.3	0.3	0.3	0.3	0.2
163Dy	2.7	2.2	2.1	2.0	2.0	1.9
165Ho	0.59	0.4	0.4	0.5	0.4	0.5

Scaled Isotope	BIR-1 Pub Data	Ap16A13	Ap16A14	Ap16B13	Ap16B14	Ap16C13
166Er	1.7	1.4	1.3	1.2	1.2	1.3
169Tm	0.33	0.2	0.2	0.2	0.2	0.2
172Yb	1.7	1.5	1.4	1.3	1.5	1.5
175Lu	0.26	0.2	0.1	0.2	0.2	0.1
178Hf	0.6	0.5	0.4	0.4	0.5	0.5
181Ta		< DL	< DL	0.0	0.0	0.1
182W		< DL	< DL	< DL	< DL	< DL
185Re		< DL	< DL	0.1	< DL	0.1
195Pt		0.6	0.5	0.5	0.6	1.2
197Au		0.1	0.1	0.1	0.1	0.2
205Tl		< DL	< DL	< DL	< DL	< DL
208Pb	3	3.7	3.7	4.7	5.0	4.9
209Bi		< DL	< DL	0.0	0.0	0.0
232Th		< DL	< DL	0.0	< DL	0.1
238U		< DL	< DL	< DL	< DL	0.0

Scaled Isotope	BIR-1 Pub Data	Ap16C14	Ap16D13	Ap16D14	Ap16E13	Ap16E14
7Li	3.6	2.6	3.0	2.7	2.5	2.7
9Be	0.58	< DL	< DL	< DL	< DL	< DL
11B	0.33	13.0	12.0	11.2	12.0	11.6
23Na	13500	9850.5	10951.0	10886.9	10426.1	10181.8
25Mg	58000	58210.9	60992.8	62791.1	60298.3	63245.6
27Al	82000	80354.4	79836.9	80606.8	79612.6	79100.2
29Si	224200	241841.5	245778.3	245010.5	248372.6	243713.8
31P	92	83.4	87.1	85.6	92.9	94.6
33S		10.6	16.0	17.4	14.2	14.2
39K	250	179.2	154.9	156.0	152.3	175.1
44Ca	95100	72207.1	68976.1	67476.7	67030.1	70291.8
45Sc	44	34.1	32.1	32.0	31.1	32.3
47Ti	5800	4666.0	4596.3	4552.6	4579.8	4482.2
51V	310	264.0	245.1	247.1	259.6	254.5
53Cr	370	342.0	333.3	318.5	324.0	318.3
55Mn	1360	1387.1	1295.9	1318.3	1297.4	1312.0
57Fe	79000	84030.7	77300.4	76907.5	76887.5	78408.7
59Co	52	52.3	50.9	50.1	51.5	48.9
60Ni	170	179.8	160.1	156.1	161.3	163.0
65Cu	125	114.5	106.0	96.4	104.5	101.3
68Zn	70	112.5	97.6	86.6	98.1	96.7
69Ga	16	17.9	16.7	15.3	16.5	16.2
72Ge		3.1	2.8	2.4	2.6	2.8
75As	0.44	1.5	1.7	0.4	< DL	0.9
82Se		< DL	< DL	< DL	< DL	< DL
85Rb		< DL	0.3	< DL	< DL	< DL
88Sr	110	90.0	88.1	88.2	86.2	83.2
89Y	16	10.9	10.5	10.5	10.8	10.0
90Zr	18	11.7	10.9	11.2	11.5	10.4
93Nb	0.6	0.5	0.4	0.4	0.4	0.4
95Mo		< DL	< DL	0.3	< DL	< DL
103Rh		< DL	< DL	< DL	< DL	< DL
105Pd		< DL	0.2	< DL	< DL	0.2
107Ag		0.6	0.3	0.3	0.3	0.4
111Cd		0.2	0.2	0.2	0.2	< DL
115In		0.1	0.1	0.1	< DL	0.1
118Sn		1.4	1.2	1.1	1.2	1.1
121Sb	0.58	0.5	0.5	0.5	0.4	0.5
133Cs		< DL	< DL	< DL	0.1	< DL
137Ba	7	5.9	5.5	6.1	7.6	5.2
139La	0.71	0.6	0.5	0.5	0.4	0.4
140Ce	2.1	1.7	1.6	1.5	1.5	1.5
141Pr	0.42	0.3	0.3	0.3	0.1	0.3
146Nd	2.5	1.9	2.1	1.9	2.0	1.8
147Sm	1.1	0.7	1.1	0.7	1.1	0.7
153Eu	0.58	0.5	0.5	0.5	0.4	0.3
157Gd	2	1.3	1.5	1.3	1.0	1.5
159Tb	0.43	0.3	0.3	0.2	0.1	0.2
163Dy	2.7	1.9	1.8	1.7	1.7	1.8
165Ho	0.59	0.4	0.5	0.4	0.2	0.3

Scaled Isotope	BIR-1 Pub Data	Ap16C14	Ap16D13	Ap16D14	Ap16E13	Ap16E14
166Er	1.7	1.2	1.2	1.1	1.2	1.0
169Tm	0.33	0.2	0.2	0.2	< DL	< DL
172Yb	1.7	1.3	1.5	1.2	1.3	1.0
175Lu	0.26	0.1	0.2	0.2	< DL	0.2
178Hf	0.6	0.4	0.4	0.5	0.4	0.4
181Ta		0.0	0.1	< DL	< DL	< DL
182W		< DL	0.1	< DL	< DL	< DL
185Re		< DL	< DL	< DL	< DL	< DL
195Pt		1.4	0.8	0.6	0.8	0.7
197Au		0.1	0.1	< DL	0.1	0.1
205Tl		< DL	< DL	< DL	< DL	< DL
208Pb	3	5.4	4.2	3.8	4.5	4.6
209Bi		< DL	0.0	0.0	< DL	< DL
232Th		< DL	0.0	< DL	< DL	< DL
238U		< DL	< DL	0.0	< DL	< DL

Scaled Isotope	BIR-1 Pub Data	Count	Min	Max	Average	Sigma
7Li	3.6	11	2.3	3.6	2.8	0.8212393
9Be	0.58	1	0.6	0.6	0.6	0.1603035
11B	0.33	11	0.3	15.8	12.2	5.1200186
23Na	13500	11	9392.3	13500.0	10586.7	3094.8335
25Mg	58000	11	57786.0	64726.4	60832.5	16943.554
27Al	82000	11	79100.2	87970.9	82296.9	22897.672
29Si	224200	11	222992.2	248372.6	237249.6	66104.943
31P	92	11	71.6	94.6	85.6	24.632912
33S		7	10.6	17.4	13.7	6.8386521
39K	250	9	150.0	250.0	172.3	78.817456
44Ca	95100	11	67030.1	95100.0	75779.1	22355.659
45Sc	44	11	31.1	44.0	35.0	10.215436
47Ti	5800	11	4482.2	5800.0	4809.0	1370.8267
51V	310	11	245.1	310.0	261.2	73.938465
53Cr	370	11	318.3	370.0	331.6	92.702346
55Mn	1360	11	1295.9	1387.1	1336.5	370.67995
57Fe	79000	11	76589.1	84030.7	79354.1	22044.059
59Co	52	11	48.9	52.3	50.7	14.060237
60Ni	170	11	156.1	179.8	164.4	45.885747
65Cu	125	11	96.4	125.0	107.8	30.857872
68Zn	70	11	70.0	112.5	95.4	28.834511
69Ga	16	11	14.6	17.9	16.4	4.6417266
72Ge		10	2.1	3.1	2.6	0.7860096
75As	0.44	8	0.4	1.7	1.1	0.6512015
82Se		2	0.0	0.0	0.0	0
85Rb		4	0.1	0.3	0.2	0.116375
88Sr	110	11	83.2	110.0	92.2	26.317916
89Y	16	11	10.0	16.0	11.4	3.4770353
90Zr	18	11	10.4	18.0	12.1	3.8189521
93Nb	0.6	11	0.4	0.6	0.4	0.1327411
95Mo		3	0.2	0.3	0.3	0.1169425
103Rh		1	0.0	0.0	0.0	0.0100962
105Pd		3	0.2	0.2	0.2	0.0848486
107Ag		10	0.3	0.6	0.4	0.1435279
111Cd		7	0.2	0.4	0.3	0.1346434
115In		6	0.1	0.1	0.1	0.0312262
118Sn		10	1.1	1.5	1.3	0.3892358
121Sb	0.58	11	0.4	0.6	0.5	0.149962
133Cs		2	0.1	0.1	0.1	0.0290155
137Ba	7	11	5.1	7.6	6.1	1.8080389
139La	0.71	11	0.4	0.7	0.5	0.1731395
140Ce	2.1	11	1.5	2.1	1.6	0.4800173
141Pr	0.42	11	0.1	0.4	0.3	0.1124153
146Nd	2.5	11	1.8	2.5	2.1	0.6089948
147Sm	1.1	11	0.7	1.1	0.9	0.3007267
153Eu	0.58	11	0.3	0.6	0.5	0.1416187
157Gd	2	11	1.0	2.0	1.4	0.4529231
159Tb	0.43	11	0.1	0.4	0.3	0.1037819
163Dy	2.7	11	1.7	2.7	2.0	0.6067566
165Ho	0.59	11	0.2	0.6	0.4	0.1443612

Scaled Isotope	BIR-1 Pub Data	Count	Min	Max	Average	Sigma
166Er	1.7	11	1.0	1.7	1.3	0.3831763
169Tm	0.33	9	0.2	0.3	0.2	0.0974011
172Yb	1.7	11	1.0	1.7	1.4	0.4176252
175Lu	0.26	10	0.1	0.3	0.2	0.0796389
178Hf	0.6	11	0.4	0.6	0.4	0.1388053
181Ta		5	0.0	0.1	0.0	0.0247184
182W		1	0.1	0.1	0.1	0.0159337
185Re		2	0.1	0.1	0.1	0.0213378
195Pt		10	0.5	1.4	0.8	0.3567771
197Au		9	0.1	0.2	0.1	0.0430237
205Tl		0	0.0	0.0	- -	0
208Pb	3	11	3.0	5.4	4.3	1.3573836
209Bi		5	0.0	0.0	0.0	0.0121367
232Th		3	0.0	0.1	0.0	0.0195081
238U		2	0.0	0.0	0.0	0.0125663

Electron Microprobe Analyses - Arfvedsonite & Aegirine
Element Weight Percent

Pt#	Si	Ti	Al	Cr	Fe	Mn	Mg	Ca	Na	K	Cl	F
1	23.84	0.3981	0.1834	0.013	24.67	0.4709	0.13	0.1056	6.84	1.378	0.0207	1.7409
2	23.5	0.7971	0.308	0	24.8	0.5236	0.3326	0.3127	6.88	1.1348	0	1.6751
1	23.5	0.7971	0.308	0	24.8	0.5236	0.3326	0.3127	6.88	1.1348	0	1.6751
2	23.6	0.7825	0.3017	0	24.61	0.5733	0.1517	0.3098	6.57	1.14	0.0205	1.5489
3	23.58	0.6378	0.1989	0.0355	25.06	0.3793	0.1252	0.1582	6.79	1.3142	0.0103	2.0341
4	23.49	0.5903	0.1263	0.0097	24.3	0.7206	0.0899	0.1173	6.37	1.9564	0.0068	1.3342
5	23.82	0.7071	0.1332	0.0162	24.48	0.7236	0.066	0.0843	6.34	1.8784	0	1.275
6	23.62	0.7185	0.2221	0	24.53	0.5022	0.1181	0.2428	6.63	1.2244	0.0205	1.7525
7	23.62	0.7277	0.1722	0	24.83	0.6411	0.0236	0.0374	6.6	1.6147	0	2.2013
8	23.65	0.9256	0.1488	0	24.6	0.5644	0.0241	0.0602	6.79	1.515	0.0218	2.0394
9	24.24	0.7038	0.1144	0	22.65	0.2615	0.0005	0.1226	10.36	0	0	0
10	24.44	0.6455	0.1384	0	23.03	0.1933	0.0228	0.1486	10.06	0	0.0186	0
11	24.35	0.3832	0.1225	0	22.46	0.3549	0.0015	0.0312	10.12	0.0055	0.0126	0
12	24.47	0.4111	0.3604	0.0162	22.42	0.3236	0	0.0665	10.08	0	0	0
13	24.3	0.6991	0.1201	0	22.23	0.3454	0.0077	0.0702	10.23	0.0014	0	0
14	24.44	0.1711	0.1267	0.0065	20.91	2.4789	0.3474	0.0208	6.42	2.2567	0.008	2.3349
15	24.26	0.1814	0.1075	0	21.7	1.7044	0.2037	0.0092	6.46	2.3103	0.0182	2.4624
16	24.14	0.3051	0.1638	0.0065	22.65	1.0275	0.0964	0.0256	6.22	2.4747	0	2.2269
17	24.18	0.1643	0.1261	0	21.84	1.8184	0.1251	0.0055	6.26	2.1603	0.0136	2.426

Electron Microprobe Analyses - Arfvedsonite & Aegirine
Element Weight Percent

O	Total	X(mm)	Y(mm)	Date	Time	Label
37.6	97.4	12.2747	18.5575	4/21/2005	52:26 PM	56a-1a #1
37.81	98.07	12.2865	20.6	4/21/2005	18:27 PM	56a-1a #2
37.81	98.07	12.2865	20.6	4/21/2005	23:50 PM	56a-1a #2
37.64	97.25	12.428	14.0687	4/21/2005	38:42 PM	56a-1a #3
37.55	97.88	9.5112	30.6752	4/21/2005	56:09 PM	TTR 26 #1
37.17	96.28	13.1445	31.2805	4/21/2005	6:57 PM	TTR 26 #2
37.62	97.14	13.3377	30.3465	4/21/2005	16:51 PM	TTR 26 #3
37.49	97.07	14.8685	29.6172	4/21/2005	26:55 PM	TTR 26 #4
37.51	97.99	8.8045	77.7657	4/21/2005	43:40 PM	SL Cb #1
37.63	97.98	9.1385	78.2802	4/21/2005	53:04 PM	SL Cb #2
38.41	96.86	7.907	77.5827	4/21/2005	3:41 PM	SL Cb #3
38.63	97.32	19.6927	69.9652	4/21/2005	20:03 PM	SL Cb #4
38.18	96.02	69.307	70.2857	4/21/2005	31:11 PM	SL1-12a #1
38.53	96.68	71.5597	68.1717	4/21/2005	43:50 PM	SL1-12a #2
38.32	96.32	72.1542	69.6177	4/21/2005	57:45 PM	SL1-12a #3
37.72	97.25	52.5167	16.762	4/21/2005	10:26 PM	46S-3a #1
37.43	96.84	52.555	16.7505	4/21/2005	20:03 PM	46S-3a #2
37.39	96.72	52.575	16.7112	4/21/2005	29:26 PM	46S-3a #3
37.26	96.38	52.7135	16.6382	4/21/2005	40:09 PM	46S-3a #4

Electron Microprobe Analyses - Arfvedsonite & Aegirine

Element Weight Percent

Si	Ti	Al	Cr	Fe	Mn	Mg	Ca	Na	K	Pt#	Cl	F
24.48	0.4088	0.1883	0.0133	25.33	0.4835	0.1335	0.1084	7.03	1.4148	1	0.0212	1.7874
23.96	0.8127	0.3141	0	25.29	0.5339	0.3392	0.3188	7.02	1.1571	2	0	1.708
23.96	0.8127	0.3141	0	25.29	0.5339	0.3392	0.3188	7.02	1.1571	1	0	1.708
24.27	0.8046	0.3103	0	25.31	0.5895	0.156	0.3186	6.75	1.1723	2	0.0211	1.5927
24.1	0.6516	0.2032	0.0363	25.6	0.3875	0.1279	0.1616	6.94	1.3427	3	0.0105	2.0782
24.4	0.6131	0.1312	0.0101	25.24	0.7484	0.0933	0.1218	6.61	2.032	4	0.0071	1.3857
24.52	0.7279	0.1371	0.0167	25.2	0.7449	0.0679	0.0867	6.52	1.9337	5	0	1.3126
24.33	0.7402	0.2288	0	25.27	0.5174	0.1216	0.2501	6.83	1.2614	6	0.0211	1.8053
24.11	0.7426	0.1758	0	25.34	0.6542	0.0241	0.0382	6.74	1.6479	7	0	2.2465
24.14	0.9447	0.1519	0	25.11	0.5761	0.0246	0.0614	6.93	1.5462	8	0.0222	2.0815
25.03	0.7267	0.1182	0	23.38	0.27	0.0005	0.1265	10.69	0	9	0	0
25.11	0.6632	0.1422	0	23.67	0.1986	0.0234	0.1527	10.33	0	10	0.0191	0
25.36	0.399	0.1276	0	23.39	0.3696	0.0016	0.0324	10.54	0.0058	11	0.0132	0
25.31	0.4252	0.3728	0.0168	23.19	0.3347	0	0.0688	10.43	0	12	0	0
25.22	0.7258	0.1247	0	23.08	0.3586	0.008	0.0728	10.62	0.0014	13	0	0
25.13	0.176	0.1303	0.0067	21.5	2.5491	0.3572	0.0214	6.61	2.3206	14	0.0082	2.4011
25.05	0.1873	0.111	0	22.4	1.7601	0.2103	0.0095	6.67	2.3857	15	0.0188	2.5428
24.96	0.3154	0.1694	0.0067	23.41	1.0624	0.0997	0.0265	6.43	2.5586	16	0	2.3024
25.09	0.1705	0.1308	0	22.66	1.8868	0.1298	0.0057	6.49	2.2415	17	0.0141	2.5172

Electron Microprobe Analyses - Arfvedsonite & Aegirine
Element Weight Percent

O	Total	X(mm)	Y(mm)	Date	Time	Label
38.6	100	12.2747	18.5575	4/21/2005	52:26 PM	56a-1a #1
38.55	100	12.2865	20.6	4/21/2005	18:27 PM	56a-1a #2
38.55	100	12.2865	20.6	4/21/2005	23:50 PM	56a-1a #2
38.71	100	12.428	14.0687	4/21/2005	38:42 PM	56a-1a #3
38.37	100	9.5112	30.6752	4/21/2005	56:09 PM	TTR 26 #1
38.6	100	13.1445	31.2805	4/21/2005	6:57 PM	TTR 26 #2
38.73	100	13.3377	30.3465	4/21/2005	16:51 PM	TTR 26 #3
38.62	100	14.8685	29.6172	4/21/2005	26:55 PM	TTR 26 #4
38.28	100	8.8045	77.7657	4/21/2005	43:40 PM	SL Cb #1
38.4	100	9.1385	78.2802	4/21/2005	53:04 PM	SL Cb #2
39.66	100	7.907	77.5827	4/21/2005	3:41 PM	SL Cb #3
39.69	100	19.6927	69.9652	4/21/2005	20:03 PM	SL Cb #4
39.76	100	69.307	70.2857	4/21/2005	31:11 PM	SL1-12a #1
39.85	100	71.5597	68.1717	4/21/2005	43:50 PM	SL1-12a #2
39.78	100	72.1542	69.6177	4/21/2005	57:45 PM	SL1-12a #3
38.79	100	52.5167	16.762	4/21/2005	10:26 PM	46S-3a #1
38.65	100	52.555	16.7505	4/21/2005	20:03 PM	46S-3a #2
38.66	100	52.575	16.7112	4/21/2005	29:26 PM	46S-3a #3
38.66	100	52.7135	16.6382	4/21/2005	40:09 PM	46S-3a #4

Appendix E

Appendix to Chapter 6 – "Extreme hydrothermal HFSE mobility and enrichment in the Strange Lake peralkaline complex, northeastern Canada"

46-5-3a	De29A03	De29A04	De29A05	De29A06	De29A07	De29A08	De29A09	De29A10
Element	Arfv	Arfv	Arfv	Arfv	Arfv	Aeg	Aeg	Aeg
Unit	ppm	ppm	ppm	ppm	ppm	ppm	ppm	ppm
Li	361.2	645.1	517.6	604.4	595.5	21.8	22.8	27.5
Be	7.2	14.1	28.2	11.1	12.9	26.3	13.5	19.6
B	166.9	131.2	98.4	138.7	105.6	178.0	143.0	161.4
Na	86275.0	70767.8	66493.6	59636.0	62460.7	101978.5	94145.8	93143.1
Mg	19950.3	6232.1	4892.4	3609.8	4004.9	638.8	621.9	927.3
Al	5618.6	1799.6	1553.4	1485.2	1210.9	1763.6	1530.8	1679.9
Si	324325.7	262361.0	283991.1	273267.4	269398.5	252634.4	277130.6	272306.2
P	26.8	0.0	8.2	0.0	0.0	35.6	23.4	13.2
K	10792.5	22622.8	19517.4	20142.5	20417.8	561.5	684.8	828.6
Ca	31518.2	3051.1	2697.6	3500.0	178.3	1170.8	290.8	1315.5
Sc	6.0	8.0	7.6	7.7	8.2	10.7	6.1	8.6
Ti	646.4	1808.2	1740.1	1747.8	1492.5	9395.4	6406.4	7649.2
V	0.7	1.0	1.5	0.0	0.7	3.6	3.7	0.9
Cr	2.3	0.3	0.1	0.2	0.9	3.3	1.4	0.1
Mn	6023.2	22512.7	19443.2	19826.9	23548.8	1831.7	1214.6	1880.7
Fe	57500.6	195657.1	173236.5	199052.4	199509.5	226072.8	200616.1	204771.9
Co	0.5	1.1	1.0	1.4	1.0	1.3	0.6	1.1
Ni	0.2	0.0	0.0	0.0	0.0	0.0	1.3	0.5
Cu	1.8	0.8	1.9	0.0	1.7	5.3	2.8	3.0
Zn	2278.9	9215.8	9045.2	8010.3	11120.9	1698.1	1192.3	1747.9
As	1084.5	269.3	167.1	57.2	15.9	36.5	36.2	16.3
Rb	29.3	39.8	33.6	34.9	33.3	3.3	64.4	2.0
Sr	25.5	3.2	2.7	2.1	0.9	0.7	1.3	0.9
Y	5.0	7.5	8.8	10.1	10.4	21.7	21.1	15.1
Zr	145.8	178.2	181.3	198.5	179.1	1971.8	1159.7	1491.4
Nb	9.8	26.9	28.8	30.5	26.1	168.3	58.0	153.9
Mo	0.1	0.9	1.0	0.9	0.8	0.0	0.3	0.1
Ag	0.0	0.0	0.1	0.1	0.1	0.1	0.2	0.1
Cd	0.0	0.2	0.0	0.1	0.0	0.2	0.3	0.4
In	0.3	0.9	0.7	1.0	0.9	1.1	1.1	2.2
Sn	33.9	110.6	104.7	98.0	99.2	129.2	153.2	251.7
Sb	0.4	0.1	0.2	0.1	0.0	1.0	0.4	0.7
Cs	0.3	0.0	0.2	0.0	0.0	0.4	14.6	0.0
Ba	155.2	17.2	14.2	5.9	2.0	5.7	229.9	2.2
La	1.8	0.7	1.2	1.5	1.3	2.9	3.6	1.7
Ce	3.9	1.6	3.1	2.9	4.4	13.1	8.1	9.5
Pr	0.5	0.1	0.3	0.3	0.4	1.2	0.7	0.6
Nd	1.9	1.1	2.0	1.4	2.0	5.8	3.9	3.8
Sm	0.5	0.6	0.9	0.8	1.0	3.3	2.1	1.5
Eu	0.2	0.1	0.1	0.1	0.1	0.2	0.1	0.4
Gd	0.7	0.2	1.2	1.2	1.8	4.8	3.0	1.7
Tb	0.1	0.1	0.4	0.2	0.3	0.8	0.6	0.5
Dy	1.2	1.2	1.7	2.0	2.6	6.5	3.6	3.7
Ho	0.2	0.4	0.6	0.6	0.5	1.7	1.0	1.1
Er	1.4	4.4	4.4	4.2	4.7	5.0	4.2	5.8
Tm	0.8	2.5	2.4	2.5	2.7	1.2	1.7	2.1
Yb	14.1	48.7	41.2	52.9	45.6	24.7	36.7	50.9
Lu	3.2	10.0	8.1	12.0	10.3	8.4	12.9	15.4
Hf	4.9	7.2	6.9	7.2	5.6	103.1	66.0	52.9

46-5-3a	De29A03	De29A04	De29A05	De29A06	De29A07	De29A08	De29A09	De29A10
Element	Arfv	Arfv	Arfv	Arfv	Arfv	Aeg	Aeg	Aeg
Ta	0.3	0.4	0.6	0.7	0.4	6.2	2.1	3.8
W	0.1	0.0	0.5	0.4	0.1	18.7	1.4	7.4
Au	0.0	0.0	0.0	0.0	0.0	0.0	0.0	0.0
Tl	0.1	0.1	0.1	0.1	0.2	0.3	12.2	0.1
Pb	13.7	9.7	16.5	17.8	40.8	127.5	145.3	81.3
Bi	0.0	0.0	0.0	0.0	0.0	0.0	0.0	0.0
Th	2.4	2.0	5.6	5.9	6.9	42.0	16.5	20.7
U	1.0	0.7	1.5	3.0	2.8	10.5	5.2	6.4

46-5-3a Element	De29A11 Aeg	46-5-3a Element	Average Arfv (n=4)	Average Aeg (n=4)
Unit	ppm	Unit	ppm	ppm
Li	14.0	Li	590.62	21.52
Be	33.5	Be	16.56	23.21
B	125.5	B	118.48	151.96
Na	92409.1	Na	64839.51	95419.14
Mg	1204.5	Mg	4684.81	848.10
Al	1731.7	Al	1512.26	1676.51
Si	281818.5	Si	272254.51	270972.41
P	42.3	P	2.04	28.62
K	399.1	K	20675.14	618.52
Ca	2378.3	Ca	2356.77	1288.84
Sc	8.4	Sc	7.88	8.46
Ti	7612.5	Ti	1697.15	7765.89
V	1.0	V	0.80	2.29
Cr	0.0	Cr	0.37	1.21
Mn	1553.1	Mn	21332.88	1620.02
Fe	189458.5	Fe	191863.87	205229.84
Co	1.0	Co	1.13	0.97
Ni	2.7	Ni	0.00	1.12
Cu	2.6	Cu	1.10	3.41
Zn	1631.6	Zn	9348.05	1567.49
As	34.1	As	127.36	30.77
Rb	1.5	Rb	35.42	17.79
Sr	1.7	Sr	2.21	1.13
Y	30.7	Y	9.19	22.13
Zr	1120.6	Zr	184.26	1435.86
Nb	142.0	Nb	28.07	130.57
Mo	0.2	Mo	0.91	0.13
Ag	0.1	Ag	0.06	0.12
Cd	0.5	Cd	0.08	0.32
In	1.2	In	0.88	1.38
Sn	151.0	Sn	103.11	171.26
Sb	1.8	Sb	0.08	0.99
Cs	0.0	Cs	0.04	3.76
Ba	5.4	Ba	9.81	60.79
La	3.1	La	1.15	2.84
Ce	20.2	Ce	3.01	12.74
Pr	1.0	Pr	0.27	0.87
Nd	4.4	Nd	1.62	4.47
Sm	2.7	Sm	0.82	2.43
Eu	0.3	Eu	0.09	0.25
Gd	4.5	Gd	1.10	3.47
Tb	1.1	Tb	0.27	0.76
Dy	8.4	Dy	1.88	5.55
Ho	2.5	Ho	0.52	1.57
Er	9.7	Er	4.42	6.17
Tm	2.9	Tm	2.55	2.00
Yb	41.4	Yb	47.10	38.45
Lu	11.5	Lu	10.11	12.08
Hf	41.3	Hf	6.71	65.85

46-5-3a Element	De29A11 Aeg
Ta	3.6
W	17.3
Au	0.0
Tl	0.1
Pb	115.1
Bi	0.0
Th	26.3
U	8.9

46-5-3a Element	Average Arfv (n=4)	Average Aeg (n=4)
Ta	0.52	3.93
W	0.25	11.19
Au	0.00	0.01
Tl	0.14	3.14
Pb	21.21	117.30
Bi	0.01	0.03
Th	5.10	26.35
U	1.98	7.77

56A-1a	De31A03	De31A04	De31A05	De31A06	De31A09a	De31A10	De31A11	De31A07
Element	Arfv	Arfv	Arfv	Arfv	Arfv	Arfv	Arfv	Aeg
Unit	ppm	ppm	ppm	ppm	ppm	ppm	ppm	ppm
Li	319.1	329.4	255.4	250.7	294.1	300.6	297.2	33.0
Be	7.0	23.4	13.1	7.6	34.5	47.0	45.5	12.7
B	100.0	96.2	88.7	75.2	118.5	91.6	85.4	161.2
Na	63222.7	71314.7	58891.1	68623.6	66560.6	59040.1	68992.9	93115.6
Mg	1303.0	1441.8	1769.6	2122.1	2172.7	1630.4	1481.0	360.0
Al	2449.4	2581.6	2592.5	2670.6	3312.6	3371.2	2849.4	4180.0
Si	270994.6	269345.9	271678.3	264044.5	260546.9	268909.3	263018.8	268118.5
P	0.0	0.0	18.0	37.8	12.4	0.0	0.0	26.8
K	9403.6	11378.8	10354.8	10318.1	10225.4	10012.7	11840.1	441.2
Ca	1524.7	2426.8	2192.0	3262.5	4857.5	2990.2	4347.9	2660.1
Sc	4.3	5.8	14.0	13.7	15.5	12.3	17.4	20.8
Ti	5454.1	4672.0	6182.4	5700.6	6679.3	7580.7	7296.7	7480.8
V	0.0	0.4	3.6	7.1	8.3	3.9	9.0	7.6
Cr	0.9	2.6	3.3	1.2	4.5	3.6	2.3	1.4
Mn	5861.6	5066.3	5025.4	4897.4	6438.6	7541.0	6954.2	2000.8
Fe	225776.6	217515.4	227594.4	228942.5	229330.5	223116.0	219257.1	206689.3
Co	2.6	3.0	2.0	3.0	3.3	2.7	2.6	0.9
Ni	1.6	0.0	0.0	6.7	0.0	0.0	16.1	0.0
Cu	0.0	9.7	5.6	1.6	13.2	5.3	0.0	29.0
Zn	3578.4	3501.1	2639.2	2879.0	4120.1	5792.2	6175.7	1340.9
As	0.0	2.4	5.6	3.0	0.0	8.0	0.0	6.9
Rb	37.4	43.0	37.0	37.0	35.3	27.3	31.9	2.7
Sr	1.7	1.6	1.8	2.3	4.9	3.6	6.6	1.1
Y	26.4	64.1	18.8	32.0	147.2	73.2	605.2	162.9
Zr	1281.6	2121.0	1294.4	1249.2	1450.8	1088.3	1286.3	2362.2
Nb	56.7	79.5	66.4	67.2	100.6	82.5	128.2	381.6
Mo	0.1	0.3	0.0	0.2	0.4	0.4	0.3	0.1
Ag	0.3	0.1	0.1	0.1	0.0	0.2	0.1	0.1
Cd	1.1	2.1	3.0	3.8	1.8	0.9	0.9	0.1
In	1.4	1.8	2.2	2.3	2.5	1.3	1.9	2.4
Sn	77.4	106.0	78.4	62.5	57.9	68.7	86.5	111.0
Sb	0.0	0.0	0.0	0.0	0.1	0.0	0.1	0.3
Cs	0.0	0.1	0.0	0.0	1.3	0.0	0.1	0.1
Ba	1.1	2.7	0.8	0.7	6.2	1.3	2.2	5.0
La	5.8	15.9	4.4	8.2	60.6	13.8	508.7	52.6
Ce	9.7	26.2	10.2	20.5	97.9	28.2	99.9	57.9
Pr	1.6	5.1	1.4	3.2	22.6	5.0	16.7	13.5
Nd	7.1	20.2	6.0	11.9	81.3	18.2	76.8	92.1
Sm	2.2	5.5	1.6	2.2	26.6	5.2	25.5	14.5
Eu	0.0	0.3	0.0	0.2	1.3	0.1	1.5	1.0
Gd	1.1	6.0	0.3	4.2	19.0	5.2	84.4	15.9
Tb	0.4	1.2	0.2	0.5	3.6	1.1	5.0	4.7
Dy	4.0	11.9	2.3	4.4	23.7	8.7	38.0	28.8
Ho	1.1	3.1	1.2	1.8	5.9	2.0	14.8	8.4
Er	11.2	14.3	9.8	11.3	24.5	17.0	32.4	32.1
Tm	3.2	3.5	3.1	3.6	5.7	4.2	6.5	6.6
Yb	39.2	40.3	41.8	47.7	70.4	53.2	71.3	76.7
Lu	8.4	8.0	9.7	10.7	16.2	12.5	13.9	14.1
Hf	56.4	115.7	61.0	54.4	51.5	42.4	48.2	71.9

56A-1a	De31A03	De31A04	De31A05	De31A06	De31A09a	De31A10	De31A11	De31A07
Element	Arfv	Arfv	Arfv	Arfv	Arfv	Arfv	Arfv	Aeg
Ta	0.7	3.3	0.9	0.7	3.7	0.8	2.5	16.7
W	0.0	0.1	0.3	0.1	0.4	0.0	0.2	0.7
Au	0.0	0.0	0.0	0.0	0.0	0.0	0.0	0.1
Tl	0.1	0.1	0.1	0.0	4.9	0.0	0.2	1.0
Pb	5.3	57.6	6.7	10.4	46.1	7.8	54.6	50.9
Bi	0.0	0.8	0.0	0.1	1.1	0.0	0.0	2.6
Th	1.4	14.0	0.2	1.5	22.5	7.8	8.1	40.9
U	0.1	3.1	0.0	0.2	3.8	0.5	1.4	5.2

56A-1a Element	De31A08 Aeg	De31A09b Aeg	De31A12 Aeg	De31A13 Aeg	Element 56A-1a	Average Arfv (n=7)	Average Aeg (n=5)
Unit	ppm	ppm	ppm	ppm	Unit	ppm	ppm
Li	20.5	46.9	26.5	30.2	Li	292.36	31.43
Be	0.6	4.4	5.1	5.6	Be	25.44	5.69
B	140.1	115.4	99.9	119.5	B	93.66	127.20
Na	93730.4	102131.8	98272.1	103994.6	Na	65235.09	98248.91
Mg	203.3	462.0	293.7	342.2	Mg	1702.92	332.23
Al	3623.7	2586.3	1703.3	2874.8	Al	2832.48	2993.62
Si	263048.2	268519.0	260220.3	262592.6	Si	266934.06	264499.70
P	31.0	19.5	0.0	18.7	P	9.73	19.20
K	241.6	1061.4	862.4	1022.0	K	10504.79	725.71
Ca	705.0	1517.2	1523.5	1788.8	Ca	3085.94	1638.89
Sc	11.0	10.8	11.3	12.1	Sc	11.86	13.21
Ti	4699.1	7053.0	6229.1	7044.7	Ti	6223.70	6501.35
V	5.3	2.5	1.7	2.7	V	4.61	3.96
Cr	0.5	1.5	1.0	1.2	Cr	2.63	1.11
Mn	945.2	1816.2	1764.4	1850.6	Mn	5969.22	1675.45
Fe	224939.1	201971.4	220611.8	207168.4	Fe	224504.64	212275.99
Co	0.2	0.6	0.6	0.6	Co	2.73	0.59
Ni	0.0	0.0	0.0	3.7	Ni	3.49	0.73
Cu	0.0	6.6	10.6	15.6	Cu	5.07	12.35
Zn	704.9	1559.8	1910.8	1742.1	Zn	4097.94	1451.68
As	3.2	0.9	4.4	0.0	As	2.72	3.08
Rb	0.6	3.6	3.2	3.7	Rb	35.56	2.74
Sr	0.5	0.7	0.6	0.4	Sr	3.21	0.64
Y	109.1	87.1	37.6	64.6	Y	138.14	92.26
Zr	1301.4	1160.5	2968.3	2760.5	Zr	1395.93	2110.56
Nb	47.5	99.4	36.4	280.0	Nb	83.02	168.97
Mo	0.0	0.4	0.0	0.1	Mo	0.23	0.12
Ag	0.0	0.0	0.1	0.2	Ag	0.12	0.08
Cd	0.4	0.9	1.6	2.1	Cd	1.94	1.03
In	1.2	1.9	2.1	2.1	In	1.90	1.94
Sn	71.0	81.3	174.9	212.5	Sn	76.77	130.13
Sb	0.1	0.2	0.1	0.1	Sb	0.02	0.15
Cs	0.0	0.1	0.0	0.3	Cs	0.22	0.10
Ba	2.1	3.9	0.9	2.9	Ba	2.16	2.96
La	42.8	39.0	4.6	17.0	La	88.22	31.19
Ce	47.7	58.4	9.9	23.3	Ce	41.79	39.44
Pr	10.8	14.1	1.7	4.7	Pr	7.96	8.98
Nd	48.1	41.6	8.3	17.5	Nd	31.62	41.52
Sm	13.5	11.0	2.8	6.6	Sm	9.85	9.69
Eu	1.0	0.8	0.1	0.4	Eu	0.50	0.68
Gd	14.0	12.1	3.2	5.9	Gd	17.18	10.21
Tb	5.2	2.2	0.8	1.2	Tb	1.72	2.81
Dy	19.7	21.1	5.0	11.1	Dy	13.29	17.16
Ho	4.3	7.6	1.8	3.4	Ho	4.28	5.12
Er	19.0	14.4	13.8	19.4	Er	17.22	19.74
Tm	3.2	3.0	6.2	7.0	Tm	4.26	5.21
Yb	38.0	35.1	114.0	102.8	Yb	51.98	73.32
Lu	8.3	8.8	26.1	21.8	Lu	11.36	15.83
Hf	37.7	42.6	78.5	100.1	Hf	61.38	66.18

56A-1a Element	De31A08 Aeg	De31A09b Aeg	De31A12 Aeg	De31A13 Aeg
Ta	1.7	2.4	2.6	5.5
W	0.0	1.1	0.1	0.2
Au	0.0	0.0	0.0	0.0
Tl	0.0	0.2	0.0	0.6
Pb	49.1	54.1	11.9	51.0
Bi	3.4	1.1	0.0	0.0
Th	44.2	25.7	6.9	32.7
U	7.5	5.6	2.3	6.0

Element 56A-1a	Average Arfv (n=7)	Average Aeg (n=5)
Ta	1.80	5.76
W	0.16	0.42
Au	0.01	0.01
Tl	0.77	0.35
Pb	26.91	43.43
Bi	0.30	1.42
Th	7.93	30.08
U	1.30	5.30

Element	Mr20A03	Mr20A04	Mr20A05	Mr20A06	Mr20A07	Mr20A08	Mr20A09	Mr20A10
TTR 26	Arfv	Arfv	Arfv	Arfv	Arfv	Arfv	Arfv	Arfv
Unit	ppm	ppm	ppm	ppm	ppm	ppm	ppm	ppm
Li	2063.0	2161.3	2468.7	2444.7	2411.2	2053.0	2422.9	2542.7
Be	17.7	16.7	15.7	15.4	14.2	58.3	12.4	14.0
B	62.1	58.2	64.9	63.1	46.7	51.4	57.8	58.3
Na	69398.6	77145.4	71736.1	86174.6	65640.3	60144.5	64933.7	76681.5
Mg	3027.0	1473.9	795.7	1085.3	1594.6	20689.9	1118.2	1287.0
Al	4453.5	4141.8	3263.6	3680.6	3506.0	10968.9	2457.8	3174.8
Si	287227.6	305555.6	304552.7	291405.1	317405.4	300700.4	312435.8	311855.4
P	11.2	8.6	5.0	5.1	3.0	11.6	9.8	8.3
K	5857.2	5717.3	7186.5	9126.4	6652.1	6939.3	7733.4	10519.4
Ca	5873.8	4034.2	2038.1	2644.4	2408.0	9457.6	2230.5	2331.7
Sc	13.4	10.7	3.8	8.0	4.7	3.9	6.4	5.8
Ti	6132.5	6001.3	6441.5	7143.8	4940.1	10144.9	6020.9	6169.1
V	0.0	0.2	0.0	0.9	1.1	0.0	0.0	0.0
Cr	0.0	0.2	0.0	0.2	0.0	0.9	0.0	0.3
Mn	4255.8	3681.3	3669.6	3699.0	4388.7	4120.2	4101.8	4251.5
Fe	184572.5	150635.6	160853.9	162413.2	143662.1	125608.8	154871.7	137972.5
Co	2.2	1.9	1.3	2.1	0.7	0.5	0.4	0.5
Ni	0.0	0.5	0.0	1.2	0.0	0.2	0.0	1.1
Cu	5.8	5.7	3.2	2.1	4.1	74.8	1.3	2.9
Zn	2388.0	2996.9	2126.3	2624.4	4565.5	3753.7	2756.9	3715.2
As	0.0	0.0	1.9	0.0	0.0	0.0	0.0	1.9
Rb	19.2	23.6	28.6	39.1	34.0	55.1	49.8	65.2
Sr	4.9	3.4	1.1	1.6	2.3	20.5	0.9	0.9
Y	58.1	49.7	23.5	30.2	42.6	459.3	19.5	21.8
Zr	1326.5	1306.8	1282.3	1532.3	1124.9	1308.0	922.4	957.7
Nb	73.3	71.5	57.0	66.5	84.9	919.5	61.0	70.1
Mo	0.1	0.0	0.2	0.3	0.2	0.5	0.3	0.9
Ag	0.0	0.1	0.1	0.1	0.0	0.1	0.1	0.1
Cd	2.4	2.8	1.5	2.5	1.4	0.8	1.2	1.5
In	2.1	2.0	0.9	1.4	1.3	1.5	0.9	1.1
Sn	46.8	41.8	56.3	62.9	75.6	237.1	84.2	111.2
Sb	0.0	0.0	0.0	0.0	0.0	0.2	0.1	0.0
Cs	0.0	0.0	0.0	0.0	0.0	0.1	0.0	0.0
Ba	1.1	1.0	0.6	1.0	1.5	17.8	0.8	0.6
La	16.6	13.8	2.2	3.8	8.1	303.6	1.9	1.5
Ce	32.3	28.6	5.2	9.3	9.0	124.0	3.7	3.3
Pr	6.1	5.6	1.0	1.6	2.7	80.6	0.8	0.7
Nd	27.7	25.7	4.0	6.7	12.2	349.7	3.2	2.8
Sm	10.2	5.0	0.9	1.6	2.6	81.0	1.0	0.8
Eu	0.4	0.2	0.1	0.1	0.1	2.4	0.0	0.1
Gd	7.5	4.4	0.8	1.1	3.3	68.9	0.7	0.6
Tb	0.9	0.8	0.3	0.3	0.6	11.0	0.2	0.3
Dy	7.7	7.0	2.7	3.9	5.6	64.9	2.4	2.8
Ho	3.2	2.6	1.4	1.7	2.0	14.1	1.1	1.3
Er	15.8	15.1	9.7	11.9	10.5	41.6	8.3	9.0
Tm	5.3	5.1	3.4	4.3	3.3	7.1	3.0	3.2
Yb	69.4	64.3	46.3	54.4	42.1	66.6	40.0	41.8
Lu	16.7	15.4	11.4	13.0	9.9	13.1	9.5	10.0
Hf	50.6	51.7	49.9	62.1	48.6	53.8	36.8	38.9

Element	Mr20A03	Mr20A04	Mr20A05	Mr20A06	Mr20A07	Mr20A08	Mr20A09	Mr20A10
TTR 26	Arfv	Arfv	Arfv	Arfv	Arfv	Arfv	Arfv	Arfv
Ta	1.1	1.0	0.6	0.8	1.8	50.2	0.7	0.6
W	0.0	0.3	0.1	0.1	0.2	1.1	0.0	0.1
Au	0.0	0.0	0.0	0.0	0.0	0.0	0.0	0.0
Tl	0.1	0.0	0.1	0.1	0.1	0.1	0.1	0.1
Pb	10.9	12.1	7.9	11.7	13.9	120.9	12.0	11.1
Bi	0.0	0.0	0.0	0.0	0.1	0.9	0.1	0.0
Th	0.0	0.0	0.0	0.0	1.3	19.9	0.0	0.0
U	0.1	0.1	0.0	0.0	0.5	16.0	0.1	0.1

Element	Mr20A11	Mr20A12	Mr20A13	Mr20A14	Mr20A15	Mr20A16	Mr20A17	Mr20A18
TTR 26	Arfv	Arfv	Arfv	Arfv	Arfv	Arfv	Arfv	Arfv
Unit	ppm	ppm	ppm	ppm	ppm	ppm	ppm	ppm
Li	2201.4	2264.6	2386.1	2396.1	2580.2	2551.2	2147.9	2270.9
Be	12.5	12.4	12.5	10.3	9.1	16.1	20.3	22.7
B	68.1	66.1	57.9	53.6	69.0	60.8	53.5	63.6
Na	69562.0	76131.2	72620.1	83551.8	73570.9	74378.9	64011.0	65258.0
Mg	633.7	470.9	904.0	757.5	2004.9	2784.5	1506.0	1635.6
Al	1629.3	3204.2	3366.3	3373.3	3952.7	3544.1	3597.6	3520.2
Si	308255.8	309213.9	310581.1	300905.3	305502.5	305033.7	314210.1	325365.4
P	2.8	11.4	8.7	6.7	10.2	4.0	3.8	6.1
K	11120.5	12865.4	6951.6	7808.8	7093.8	8701.3	6527.0	7115.8
Ca	3050.2	1799.9	2014.6	1783.4	2869.8	3898.7	3853.9	3149.3
Sc	2.9	5.0	4.5	5.8	6.6	7.7	11.7	13.4
Ti	4276.3	4841.9	4415.6	4746.6	5537.1	6232.8	6154.4	5745.1
V	0.0	0.3	0.0	1.0	0.5	0.6	1.2	2.7
Cr	0.0	0.2	0.7	1.3	0.0	0.1	0.0	0.2
Mn	5143.1	5296.0	3541.7	3382.9	3708.5	3765.3	3830.2	4507.5
Fe	152659.2	140883.8	152585.3	156089.3	153881.1	149797.5	150640.9	128650.1
Co	0.6	1.0	0.6	1.0	1.8	1.8	2.0	1.6
Ni	1.9	0.6	0.0	0.9	0.0	7.1	0.0	2.2
Cu	0.8	1.5	0.0	0.7	8.1	14.6	1.4	1.8
Zn	5894.0	6020.5	2159.1	2514.9	2266.3	2906.0	2256.7	4109.4
As	0.0	0.0	0.0	0.4	1.9	0.8	0.0	1.0
Rb	56.4	76.1	32.1	44.4	33.3	42.1	26.0	30.2
Sr	4.2	1.5	2.1	1.3	1.5	1.9	4.1	7.7
Y	36.9	32.6	34.1	31.4	92.3	34.5	43.9	124.2
Zr	1304.5	1111.1	1395.6	1505.5	1934.8	1521.7	1303.6	1284.2
Nb	153.0	130.0	62.6	65.5	60.8	60.6	69.4	81.7
Mo	0.3	1.2	0.0	0.0	0.2	0.2	0.2	0.3
Ag	0.1	0.1	0.1	0.1	0.1	0.0	0.1	0.1
Cd	1.2	1.9	1.7	1.9	2.0	2.2	2.0	1.2
In	1.6	1.8	1.2	1.5	1.5	1.5	1.7	1.7
Sn	157.3	185.1	53.3	69.3	68.2	74.0	43.7	65.4
Sb	0.0	0.1	0.0	0.1	0.1	0.2	0.0	0.0
Cs	0.0	0.0	0.0	0.0	0.0	0.0	0.0	0.0
Ba	1.3	0.8	1.0	0.9	1.1	2.0	1.3	1.6
La	4.1	1.5	9.6	4.1	9.2	4.3	11.1	12.6
Ce	11.9	3.2	8.0	7.8	10.7	6.8	24.7	18.3
Pr	2.3	0.6	2.4	1.6	2.9	2.9	5.2	4.6
Nd	8.9	2.9	10.5	7.1	14.9	6.6	21.0	17.8
Sm	2.7	0.8	1.8	1.9	5.7	1.7	4.3	3.9
Eu	0.2	0.0	0.0	0.1	0.1	0.1	0.2	0.1
Gd	1.2	0.3	2.3	1.8	4.1	1.5	2.5	5.0
Tb	0.5	0.2	0.4	0.5	1.4	0.6	0.6	1.8
Dy	4.8	3.6	4.1	3.7	14.3	4.3	6.4	18.8
Ho	1.7	1.7	1.6	1.6	4.1	1.7	2.5	2.6
Er	8.6	11.7	10.9	10.0	13.0	10.0	13.7	13.7
Tm	2.5	3.8	3.4	3.2	3.9	3.4	4.5	4.4
Yb	32.3	48.7	42.7	41.0	47.1	45.2	60.8	62.1
Lu	7.0	9.9	9.3	9.3	10.9	10.8	14.5	12.1
Hf	78.0	61.1	55.0	62.1	97.5	60.5	47.3	53.3

Element	Mr20A11	Mr20A12	Mr20A13	Mr20A14	Mr20A15	Mr20A16	Mr20A17	Mr20A18
TTR 26	Arfv	Arfv	Arfv	Arfv	Arfv	Arfv	Arfv	Arfv
Ta	1.2	0.7	0.8	1.0	1.4	0.9	0.8	0.8
W	0.0	0.1	0.0	0.0	0.1	0.1	0.0	0.0
Au	0.0	0.0	0.0	0.0	0.0	0.0	0.0	0.0
Tl	0.1	0.2	0.1	0.1	0.1	0.1	0.1	0.1
Pb	12.7	12.6	7.6	12.3	21.4	36.5	8.9	7.0
Bi	0.0	0.0	0.0	0.1	0.3	0.3	0.0	0.0
Th	0.1	0.6	0.0	0.0	0.2	0.4	0.1	0.5
U	1.2	0.2	0.1	2.9	3.6	0.9	0.3	0.3

Element	Average
TTR 26	Arfv (n=15)
Unit	ppm
Li	2354.19
Be	14.80
B	60.24
Na	72719.60
Mg	1405.25
Al	3391.05
Si	307300.38
P	6.98
K	8065.10
Ca	2932.03
Sc	7.35
Ti	5653.28
V	0.57
Cr	0.20
Mn	4081.53
Fe	152011.25
Co	1.31
Ni	1.03
Cu	3.60
Zn	3286.67
As	0.54
Rb	40.02
Sr	2.63
Y	45.01
Zr	1320.93
Nb	77.86
Mo	0.28
Ag	0.06
Cd	1.82
In	1.47
Sn	79.67
Sb	0.04
Cs	0.01
Ba	1.11
La	6.96
Ce	12.19
Pr	2.74
Nd	11.45
Sm	2.99
Eu	0.12
Gd	2.48
Tb	0.62
Dy	6.15
Ho	2.05
Er	11.46
Tm	3.78
Yb	49.21
Lu	11.32
Hf	56.89

Element TTR 26	Average Arfv (n=15)
Ta	0.94
W	0.08
Au	0.01
Tl	0.08
Pb	13.24
Bi	0.07
Th	0.21
U	0.69

SL-Cb	Mr20B03	Mr20B04	Mr20B05	Mr20B06	Mr20B07	Mr20B08	Mr20B15	Mr20B16
Element	Arfv	Arfv	Arfv	Arfv	Arfv	Arfv	Arfv	Arfv
Unit	ppm	ppm	ppm	ppm	ppm	ppm	ppm	ppm
Li	2652.2	2478.0	2361.7	2715.7	2126.6	2405.9	2939.2	3083.4
Be	8.7	9.9	8.8	10.5	15.4	15.8	13.2	14.1
B	49.4	41.6	47.7	45.9	47.1	47.3	48.1	44.4
Na	72013.2	70927.0	68123.1	75427.5	61879.1	71494.9	71970.3	70843.6
Mg	459.4	561.6	305.7	441.3	1440.5	935.4	465.2	856.6
Al	2320.5	2390.6	1946.7	2418.8	2005.6	2123.8	2315.5	2404.4
Si	310253.5	315880.8	321940.2	299033.8	317982.2	310885.8	306982.7	307795.0
P	9.5	9.3	11.5	5.3	11.1	7.1	0.3	8.0
K	7538.0	7358.5	6737.6	9826.3	6702.6	7439.6	7765.8	8018.4
Ca	889.2	2123.5	1086.5	2185.7	5015.5	4726.5	1216.1	4308.5
Sc	3.9	5.6	4.4	5.6	5.7	3.3	2.2	3.0
Ti	4864.4	4731.5	5539.7	6026.8	4906.5	5675.8	6198.3	5375.7
V	1.2	1.3	0.2	0.6	0.3	0.0	0.0	0.0
Cr	0.0	0.6	1.1	1.1	0.6	0.0	0.2	0.0
Mn	3476.9	3486.9	3336.5	4312.4	4129.2	4344.6	3873.2	4524.9
Fe	155636.9	145810.1	140830.1	162867.7	147810.0	146254.4	156876.7	151681.9
Co	0.8	1.0	0.2	0.3	0.1	0.3	0.2	0.3
Ni	0.0	0.5	0.3	1.3	1.7	0.0	0.0	0.0
Cu	0.2	1.1	1.0	1.2	12.9	7.0	0.9	4.5
Zn	2763.6	3379.2	3151.2	4105.0	3734.9	4757.8	3021.3	4519.2
As	0.0	1.9	0.0	2.0	0.0	0.0	0.0	0.3
Rb	44.6	41.0	41.0	53.8	34.9	46.9	46.8	56.7
Sr	0.4	1.2	0.6	0.7	1.7	4.1	0.7	1.6
Y	12.8	19.6	19.9	22.0	39.5	36.8	21.2	35.0
Zr	881.9	902.5	914.7	1168.4	1061.2	1606.8	1558.1	1065.0
Nb	53.4	73.5	65.1	69.9	73.2	127.0	63.9	89.9
Mo	0.2	0.2	0.1	0.2	0.2	0.3	0.3	0.1
Ag	0.0	0.1	0.0	0.1	0.0	0.1	0.1	0.0
Cd	1.1	2.1	1.5	2.0	2.3	2.4	2.0	2.5
In	1.2	1.3	1.1	1.3	0.9	1.3	1.2	1.2
Sn	86.8	86.9	114.3	138.3	92.1	138.6	128.1	104.6
Sb	0.0	0.0	0.0	0.0	0.1	0.1	0.0	0.0
Cs	0.0	0.0	0.0	0.0	0.0	0.3	0.0	0.0
Ba	0.3	1.1	0.7	0.6	1.2	2.6	0.5	1.7
La	0.5	1.4	0.8	0.6	2.3	5.0	0.8	1.9
Ce	1.3	3.0	1.8	2.0	2.3	6.2	1.7	3.0
Pr	0.2	0.5	0.4	0.3	0.7	1.0	0.3	0.7
Nd	0.8	1.9	1.1	1.4	2.8	4.2	1.2	2.6
Sm	0.3	0.6	0.4	0.3	1.0	1.1	0.4	0.6
Eu	0.1	0.0	0.1	0.1	0.1	0.1	0.0	0.0
Gd	0.2	0.4	0.3	0.4	1.6	1.3	0.4	0.9
Tb	0.1	0.2	0.1	0.1	0.4	0.4	0.1	0.3
Dy	1.5	1.8	2.0	2.2	4.4	4.2	2.2	3.8
Ho	0.7	0.9	1.2	1.2	1.7	1.6	1.1	1.5
Er	5.4	7.2	8.9	9.0	9.9	9.5	7.5	10.4
Tm	2.0	2.5	3.1	3.2	3.1	3.0	2.9	3.7
Yb	26.7	34.1	40.8	42.4	38.5	38.6	38.8	47.2
Lu	6.9	7.8	9.3	9.6	8.3	9.0	9.1	9.8
Hf	35.4	38.7	42.3	60.7	56.9	93.3	82.5	45.4

SL-Cb	Mr20B03	Mr20B04	Mr20B05	Mr20B06	Mr20B07	Mr20B08	Mr20B15	Mr20B16
Element	Arfv	Arfv	Arfv	Arfv	Arfv	Arfv	Arfv	Arfv
Ta	0.6	0.9	0.8	0.8	1.1	2.6	0.9	1.4
W	0.0	0.0	0.0	0.0	0.1	0.1	0.0	0.0
Au	0.0	0.0	0.0	0.0	0.0	0.0	0.0	0.0
Tl	0.1	0.1	0.1	0.1	0.1	2.3	0.1	0.1
Pb	4.7	7.0	8.9	8.7	9.5	16.4	7.0	12.2
Bi	0.0	0.1	0.0	0.0	0.6	1.0	0.0	0.0
Th	0.0	0.0	0.0	0.0	0.1	0.2	0.0	0.1
U	0.0	0.3	0.5	0.2	4.5	4.2	0.1	1.2

SL-Cb	Mr20B09	Mr20B10	Mr20B11	Mr20B12	Mr20B13	Mr20B14
Element	Aeg	Aeg	Aeg	Aeg	Aeg	Aeg
Unit	ppm	ppm	ppm	ppm	ppm	ppm
Li	34.1	146.3	31.6	46.7	70.1	52.4
Be	7.8	21.0	12.0	9.5	24.1	17.3
B	69.3	67.0	66.9	62.0	67.8	62.2
Na	100531.6	105663.6	98366.3	96128.8	93872.1	91998.3
Mg	505.3	7482.3	630.9	1802.0	2651.0	1931.0
Al	4650.1	4475.5	4669.8	3023.0	2804.6	17137.9
Si	303207.6	293769.9	303653.1	309933.0	307260.4	310601.5
P	0.0	5.7	11.1	3.1	4.3	9.4
K	210.7	182.1	31.7	34.1	65.5	5891.6
Ca	1964.3	5320.6	2275.8	2669.3	3214.7	2529.3
Sc	2.3	3.9	1.0	5.1	1.6	3.0
Ti	4625.6	7580.8	4842.1	5502.3	4222.1	3087.8
V	0.0	0.0	0.0	0.0	0.3	0.0
Cr	0.0	1.4	0.0	1.0	0.5	0.8
Mn	1557.0	2225.6	2497.3	2635.3	2184.5	1725.9
Fe	147589.6	137362.5	146271.5	136608.5	144446.2	118290.2
Co	0.1	0.0	0.0	0.0	0.0	0.0
Ni	1.7	9.2	1.6	1.1	0.8	0.0
Cu	3.7	9.9	4.6	7.3	7.2	3.1
Zn	1314.7	2281.9	1805.7	2284.4	1973.1	1877.5
As	0.0	18.2	1.1	0.0	0.0	0.0
Rb	11.2	4.8	0.4	1.4	0.8	236.2
Sr	1.5	10.6	3.1	2.7	5.9	4.5
Y	16.7	54.1	65.5	51.8	95.8	56.4
Zr	829.1	1272.3	904.9	1184.2	1030.1	764.9
Nb	98.4	348.7	157.7	221.3	228.5	181.0
Mo	0.0	0.0	0.0	0.3	0.0	0.0
Ag	0.0	0.1	0.0	0.0	0.1	0.0
Cd	1.2	0.7	1.4	1.3	0.9	1.0
In	1.3	11.0	3.7	5.3	4.6	5.1
Sn	162.4	2059.4	817.9	1088.5	1048.9	1089.4
Sb	0.1	0.2	0.1	0.1	0.0	0.1
Cs	0.7	0.3	0.0	0.1	0.0	0.1
Ba	4.0	8.4	3.1	2.8	5.4	13.9
La	7.8	16.8	14.6	11.1	23.6	12.3
Ce	15.5	23.5	15.7	17.1	27.8	16.4
Pr	2.3	4.4	3.6	2.9	4.6	2.4
Nd	8.0	16.3	14.6	11.1	16.9	8.5
Sm	1.5	4.4	4.2	2.9	3.9	2.1
Eu	0.0	0.1	0.1	0.1	0.2	0.1
Gd	1.0	3.5	4.9	2.6	5.7	3.2
Tb	0.3	0.8	1.1	0.8	1.6	0.8
Dy	2.1	6.4	8.9	6.2	12.7	6.9
Ho	0.7	1.8	2.4	1.8	3.3	1.8
Er	4.1	7.5	8.1	7.0	12.4	6.8
Tm	1.7	1.6	1.6	1.6	2.3	1.4
Yb	27.0	22.1	16.4	20.0	23.3	15.0
Lu	6.5	4.8	3.6	4.9	5.0	3.5
Hf	41.3	49.1	26.7	34.6	45.3	32.1

SL-Cb	Mr20B09	Mr20B10	Mr20B11	Mr20B12	Mr20B13	Mr20B14
Element	Aeg	Aeg	Aeg	Aeg	Aeg	Aeg
Ta	3.2	9.7	12.0	16.1	7.5	4.8
W	0.1	0.2	0.1	0.2	0.1	0.1
Au	0.0	0.0	0.0	0.0	0.0	0.0
Tl	3.2	0.3	0.0	0.2	0.1	0.7
Pb	8.2	13.9	4.6	4.2	5.1	4.0
Bi	0.2	0.6	0.3	0.0	0.2	0.1
Th	0.4	2.6	0.3	0.3	0.5	0.3
U	2.1	4.6	2.2	2.7	1.4	0.9

SL-Cb Element	Average Arfv (n=8)	Average Aeg (n=6)
Unit	ppm	ppm
Li	2595.33	63.53
Be	12.06	15.28
B	46.44	65.85
Na	70334.85	97760.12
Mg	683.23	2500.41
Al	2240.74	6126.83
Si	311344.25	304737.58
P	7.77	5.61
K	7673.36	1069.28
Ca	2693.95	2995.67
Sc	4.22	2.82
Ti	5414.82	4976.80
V	0.45	0.04
Cr	0.44	0.61
Mn	3935.58	2137.59
Fe	150970.98	138428.10
Co	0.41	0.03
Ni	0.47	2.39
Cu	3.61	5.96
Zn	3679.03	1922.89
As	0.53	3.22
Rb	45.71	42.47
Sr	1.40	4.74
Y	25.84	56.71
Zr	1144.82	997.58
Nb	76.98	205.95
Mo	0.19	0.05
Ag	0.05	0.05
Cd	2.00	1.08
In	1.20	5.17
Sn	111.21	1044.42
Sb	0.03	0.10
Cs	0.05	0.22
Ba	1.10	6.28
La	1.66	14.38
Ce	2.66	19.34
Pr	0.51	3.37
Nd	2.00	12.59
Sm	0.59	3.17
Eu	0.06	0.11
Gd	0.68	3.49
Tb	0.23	0.90
Dy	2.77	7.20
Ho	1.25	1.97
Er	8.48	7.64
Tm	2.94	1.71
Yb	38.39	20.61
Lu	8.73	4.73
Hf	56.89	38.18

SL-Cb Element	Mr20B17 Aeg (alt)	Mr20B18 Aeg (alt)
Unit	ppm	ppm
Li	111.7	62.1
Be	33.2	23.7
B	81.8	75.4
Na	88751.2	95709.9
Mg	4199.5	1935.6
Al	3587.8	3261.4
Si	308071.9	310164.2
P	11.6	13.4
K	92.4	33.2
Ca	5304.2	3721.4
Sc	2.4	1.6
Ti	4661.5	5114.4
V	0.1	0.0
Cr	1.6	1.1
Mn	2746.1	2793.9
Fe	139987.4	134173.0
Co	0.1	0.0
Ni	2.5	1.2
Cu	24.5	10.1
Zn	2246.5	2563.5
As	15.6	9.3
Rb	1.7	1.0
Sr	10.9	8.2
Y	627.5	409.7
Zr	1592.4	1443.1
Nb	725.0	571.6
Mo	0.4	0.1
Ag	0.1	0.1
Cd	1.3	1.7
In	2.7	2.8
Sn	555.6	603.8
Sb	0.4	0.4
Cs	0.2	0.1
Ba	15.7	8.6
La	50.5	39.7
Ce	42.8	34.3
Pr	11.2	10.2
Nd	46.5	41.0
Sm	14.1	12.0
Eu	0.7	0.5
Gd	26.0	18.6
Tb	6.0	4.8
Dy	56.8	39.6
Ho	16.0	11.5
Er	52.3	36.7
Tm	7.8	5.4
Yb	50.6	40.9
Lu	10.0	8.4
Hf	49.1	41.2

SL-Cb	Average Arfv (n=8)	Average Aeg (n=6)
Ta	1.13	8.90
W	0.03	0.11
Au	0.01	0.01
Tl	0.38	0.75
Pb	9.30	6.68
Bi	0.22	0.24
Th	0.06	0.74
U	1.37	2.32

SL-Cb Element	Mr20B17 Aeg (alt)	Mr20B18 Aeg (alt)
Ta	43.2	37.0
W	1.2	0.8
Au	0.0	0.0
Tl	0.0	0.0
Pb	18.7	16.1
Bi	0.2	0.3
Th	3.3	3.1
U	7.2	5.8

SL-Ab Element Unit	Ja02A03 Fib Rep ppm	Ja02A04 Fib Rep ppm	Ja02A05 Fib Rep ppm	Ja02A06 Fib Rep ppm	SL-Ab Element Unit	Average Fib Rep ppm
Li	2.5	4.6	1.3	1.4	Li	2.4
Be	5.3	25.6	14.2	9.8	Be	13.7
B	33.8	51.4	64.2	67.9	B	54.3
Na	11302.6	21155.5	23056.6	26418.9	Na	20483.4
Mg	2464.8	4000.6	6204.3	7412.5	Mg	5020.5
Al	1286.6	2301.9	2927.3	2820.8	Al	2334.2
Si	240010.5	259179.2	238697.9	247703.5	Si	246397.8
P	64.3	186.7	170.3	120.7	P	135.5
K	1110.3	1520.6	1322.1	1665.9	K	1404.7
Ca	100119.6	92953.4	135291.9	194774.9	Ca	130784.9
Sc	26.8	27.5	25.3	15.5	Sc	23.8
Ti	349.7	446.2	248.7	165.7	Ti	302.6
V	2.5	8.6	8.5	5.3	V	6.2
Cr	5.1	10.0	11.8	8.6	Cr	8.9
Mn	2380.2	2766.5	1574.3	1369.3	Mn	2022.6
Fe	2498.5	3571.2	3028.6	2020.4	Fe	2779.7
Co	3.5	1.0	0.6	0.4	Co	1.4
Ni	19.9	63.8	61.1	37.4	Ni	45.5
Cu	3.0	7.9	8.4	8.2	Cu	6.9
Zn	235.7	253.9	222.5	142.2	Zn	213.6
As	155.2	275.5	338.6	433.2	As	300.6
Rb	19.8	27.5	9.1	9.2	Rb	16.4
Sr	79.3	93.6	111.5	173.2	Sr	114.4
Y	2495.3	2036.4	1942.2	1087.8	Y	1890.4
Zr	222247.0	185303.0	171282.5	95346.2	Zr	168544.7
Nb	240.4	389.0	181.0	115.7	Nb	231.5
Mo	0.4	0.4	0.2	0.1	Mo	0.3
Ag	18.9	16.0	14.2	7.1	Ag	14.0
Cd	5.1	3.7	5.0	2.7	Cd	4.1
In	2.4	2.5	2.5	1.6	In	2.2
Sn	603.3	625.6	565.7	420.4	Sn	553.8
Sb	1.6	1.3	0.8	0.5	Sb	1.0
Cs	0.5	1.2	0.5	0.3	Cs	0.6
Ba	156.1	211.6	163.5	140.6	Ba	168.0
La	31.7	35.8	55.1	72.5	La	48.8
Ce	74.4	70.5	59.6	48.5	Ce	63.2
Pr	8.2	9.7	10.1	10.6	Pr	9.6
Nd	29.1	31.5	41.5	36.4	Nd	34.6
Sm	10.0	10.5	10.9	8.7	Sm	10.1
Eu	1.1	1.3	1.1	0.6	Eu	1.0
Gd	28.8	27.6	22.0	14.3	Gd	23.2
Tb	18.9	15.3	13.1	7.0	Tb	13.6
Dy	271.0	228.8	213.6	110.0	Dy	205.9
Ho	109.6	87.9	88.2	49.1	Ho	83.7
Er	551.7	447.0	474.3	260.9	Er	433.5
Tm	132.1	111.3	126.7	68.4	Tm	109.6
Yb	1296.1	1163.7	1282.0	709.8	Yb	1112.9
Lu	168.0	145.5	172.1	99.5	Lu	146.3
Hf	6096.8	4996.9	4522.1	2697.1	Hf	4578.2

SL-Ab Element	Ja02A03 Fib Rep	Ja02A04 Fib Rep	Ja02A05 Fib Rep	Ja02A06 Fib Rep
Ta	78.4	65.9	57.5	38.7
W	0.3	0.3	0.2	0.2
Au	0.3	0.2	0.2	0.1
Tl	0.1	0.4	0.1	0.1
Pb	347.1	351.1	175.1	94.4
Bi	0.0	0.0	0.0	0.0
Th	16.3	14.0	13.3	6.6
U	126.3	103.8	79.4	49.1

SL-Ab Element	Average Fib Rep
Ta	60.1
W	0.3
Au	0.2
Tl	0.2
Pb	241.9
Bi	0.0
Th	12.5
U	89.7

	SL1-12a (pegmatite)		
	Ja09B03 Boat Xtal	**Ja09B04 Boat Xtal**	**Average Boat Xtal**
	ppm	ppm	ppm
Li	3.05	4.55	3.80
Be	30.66	68.66	49.66
B	92.92	110.66	101.79
Na	42207.62	25523.15	33865.39
Mg	7691.70	5067.71	6379.70
Al	4414.22	5366.75	4890.48
Si	262688.87	253094.31	257891.59
P	371.92	152.83	262.37
K	2229.77	7149.84	4689.80
Ca	77524.74	83418.89	80471.82
Sc	24.61	17.75	21.18
Ti	114.39	147.43	130.91
V	14.62	7.36	10.99
Cr	16.65	10.03	13.34
Mn	10224.40	11915.41	11069.90
Fe	6904.20	4801.49	5852.85
Co	0.92	0.68	0.80
Ni	181.01	72.36	126.69
Cu	25.92	14.57	20.24
Zn	496.77	376.46	436.62
As	573.89	322.92	448.40
Rb	28.26	272.14	150.20
Sr	352.84	385.44	369.14
Y	7857.55	9691.71	8774.63
Zr	141035.38	163215.61	152125.50
Nb	520.91	581.91	551.41
Mo	< DL	< DL	< DL
Ag	14.91	13.04	13.97
Cd	5.24	5.93	5.58
In	9.23	8.78	9.00
Sn	2330.93	2082.43	2206.68
Sb	3.90	3.34	3.62
Cs	1.41	2.24	1.83
Ba	563.32	318.57	440.95
La	178.23	244.29	211.26
Ce	390.42	469.78	430.10
Pr	32.94	44.94	38.94
Nd	127.51	169.92	148.71
Sm	115.91	133.19	124.55
Eu	15.22	18.27	16.74
Gd	203.41	238.00	220.71
Tb	121.54	139.18	130.36
Dy	1415.10	1582.02	1498.56
Ho	409.79	444.82	427.30
Er	1831.70	1876.13	1853.92
Tm	496.65	494.02	495.33
Yb	4937.98	4464.68	4701.33

	SL1-12a (pegmatite)		
	Ja09B03 Boat Xtal	**Ja09B04 Boat Xtal**	**Average Boat Xtal**
	ppm	ppm	ppm
Lu	528.97	440.79	484.88
Hf	2777.95	2963.43	2870.69
Ta	84.63	87.24	85.93
W	0.50	0.60	0.55
Au	0.20	0.07	0.14
Tl	0.98	1.85	1.42
Pb	2134.16	2461.36	2297.76
Bi	< DL	< DL	< DL
Th	218.21	288.56	253.38
U	382.91	502.16	442.53

	SL-Ab (pegmatite)				
	Ja02A03 Fib Rep	Ja02A04 Fib Rep	Ja02A05 Fib Rep	Ja02A06 Fib Rep	Average Fib Rep
	ppm	ppm	ppm	ppm	ppm
Li	2.5	4.6	1.3	1.4	2.4
Be	5.3	25.6	14.2	9.8	13.7
B	33.8	51.4	64.2	67.9	54.3
Na	11302.6	21155.5	23056.6	26418.9	20483.4
Mg	2464.8	4000.6	6204.3	7412.5	5020.5
Al	1286.6	2301.9	2927.3	2820.8	2334.2
Si	240010.5	259179.2	238697.9	247703.5	246397.8
P	64.3	186.7	170.3	120.7	135.5
K	1110.3	1520.6	1322.1	1665.9	1404.7
Ca	100119.6	92953.4	135291.9	194774.9	130784.9
Sc	26.8	27.5	25.3	15.5	23.8
Ti	349.7	446.2	248.7	165.7	302.6
V	2.5	8.6	8.5	5.3	6.2
Cr	5.1	10.0	11.8	8.6	8.9
Mn	2380.2	2766.5	1574.3	1369.3	2022.6
Fe	2498.5	3571.2	3028.6	2020.4	2779.7
Co	3.5	1.0	0.6	0.4	1.4
Ni	19.9	63.8	61.1	37.4	45.5
Cu	3.0	7.9	8.4	8.2	6.9
Zn	235.7	253.9	222.5	142.2	213.6
As	155.2	275.5	338.6	433.2	300.6
Rb	19.8	27.5	9.1	9.2	16.4
Sr	79.3	93.6	111.5	173.2	114.4
Y	2495.3	2036.4	1942.2	1087.8	1890.4
Zr	222247.0	185303.0	171282.5	95346.2	168544.7
Nb	240.4	389.0	181.0	115.7	231.5
Mo	0.4	0.4	0.2	0.1	0.3
Ag	18.9	16.0	14.2	7.1	14.0
Cd	5.1	3.7	5.0	2.7	4.1
In	2.4	2.5	2.5	1.6	2.2
Sn	603.3	625.6	565.7	420.4	553.8
Sb	1.6	1.3	0.8	0.5	1.0
Cs	0.5	1.2	0.5	0.3	0.6
Ba	156.1	211.6	163.5	140.6	168.0
La	31.7	35.8	55.1	72.5	48.8
Ce	74.4	70.5	59.6	48.5	63.2
Pr	8.2	9.7	10.1	10.6	9.6
Nd	29.1	31.5	41.5	36.4	34.6
Sm	10.0	10.5	10.9	8.7	10.1
Eu	1.1	1.3	1.1	0.6	1.0
Gd	28.8	27.6	22.0	14.3	23.2
Tb	18.9	15.3	13.1	7.0	13.6
Dy	271.0	228.8	213.6	110.0	205.9
Ho	109.6	87.9	88.2	49.1	83.7
Er	551.7	447.0	474.3	260.9	433.5
Tm	132.1	111.3	126.7	68.4	109.6
Yb	1296.1	1163.7	1282.0	709.8	1112.9

	SL-Ab (pegmatite)				
	Ja02A03 Fib Rep	Ja02A04 Fib Rep	Ja02A05 Fib Rep	Ja02A06 Fib Rep	Average Fib Rep
	ppm	ppm	ppm	ppm	ppm
Lu	168.0	145.5	172.1	99.5	146.3
Hf	6096.8	4996.9	4522.1	2697.1	4578.2
Ta	78.4	65.9	57.5	38.7	60.1
W	0.3	0.3	0.2	0.2	0.3
Au	0.3	0.2	0.2	0.1	0.2
Tl	0.1	0.4	0.1	0.1	0.2
Pb	347.1	351.1	175.1	94.4	241.9
Bi	0.0	0.0	0.0	0.0	0.0
Th	16.3	14.0	13.3	6.6	12.5
U	126.3	103.8	79.4	49.1	89.7

	SL1-12a (pegmatite)						
	Ja09B09b	Ja09B09c	Ja09B09d	Ja09B10b	Ja09B10c	Ja09B10d	Average
	Alt Aeg 1	Alt Aeg 2	Alt Aeg 3	Alt Aeg 1	Alt Aeg 2	Alt Aeg 3	Alt Aeg
	ppm	ppm	ppm	ppm	ppm	ppm	ppm
Li	26.94	22.86	6.69	20.32	35.44	35.82	24.68
Be	2828.91	1498.90	387.14	9634.92	1717.97	1946.36	3002.37
B	1240.48	768.76	195.44	3078.28	985.45	816.49	1180.82
Na	15632.69	37520.73	23479.89	29472.80	36718.06	56585.91	33235.01
Mg	17728.96	32363.94	8870.92	10214.54	23675.92	20905.29	18959.93
Al	5266.32	8672.46	2542.40	3446.56	5933.62	6804.73	5444.35
Si	194749.72	244752.12	212201.65	197808.83	224770.42	243139.48	219570.37
P	54.50	76.51	< DL	< DL	89.31	< DL	73.44
K	545.08	1961.42	863.50	349.86	648.52	426.08	799.08
Ca	90305.60	71213.51	98370.54	70430.61	66598.21	43998.97	73486.24
Sc	8.14	12.66	8.86	9.50	2.64	8.71	8.42
Ti	1436.04	983.64	604.83	2019.16	2467.21	3120.07	1771.82
V	< DL	< DL	< DL	< DL	2.17	1.95	2.06
Cr	< DL	4.52	< DL	5.41	5.09	< DL	5.01
Mn	6833.59	4795.16	3435.77	6213.98	5010.12	4419.70	5118.05
Fe	27536.35	20533.09	24297.60	55648.89	58366.15	102634.84	48169.49
Co	< DL	0.43	< DL	1.35	< DL	< DL	0.89
Ni	< DL	< DL	< DL	< DL	< DL	< DL	< DL
Cu	51.00	79.51	9.87	72.32	70.25	42.79	54.29
Zn	2791.97	2650.82	901.40	3012.89	3447.12	3973.27	2796.24
As	200.13	646.15	383.70	113.89	194.42	153.17	281.91
Rb	14.83	23.54	14.36	9.42	16.21	10.43	14.80
Sr	269.19	211.84	235.87	331.94	210.42	122.90	230.36
Y	55547.15	25332.61	106279.59	57546.66	43530.68	18171.89	51068.10
Zr	143694.89	103873.39	69123.68	87354.05	87649.33	58907.11	91767.08
Nb	6565.81	3320.74	4889.39	4540.14	4718.49	2541.05	4429.27
Mo	0.65	0.24	< DL	1.11	< DL	0.73	0.68
Ag	14.60	8.24	6.91	7.56	10.42	7.54	9.21
Cd	5.28	1.40	3.49	4.27	8.40	2.24	4.18
In	9.18	5.67	5.18	8.87	12.05	5.69	7.77
Sn	2338.84	1441.22	1208.43	2300.03	2867.70	1483.31	1939.92
Sb	7.07	4.37	5.03	13.50	4.85	5.38	6.70
Cs	0.86	0.86	1.03	0.82	2.43	0.90	1.15
Ba	439.18	353.34	392.00	298.70	340.25	232.65	342.69
La	1763.52	827.35	1047.50	4157.58	1297.95	884.79	1663.12
Ce	2233.93	1099.77	1843.35	9560.04	1715.70	1648.77	3016.93
Pr	611.23	282.03	360.77	1806.36	430.97	409.47	650.14
Nd	2969.95	1577.37	1808.54	9757.72	2372.38	2045.44	3421.90
Sm	2379.05	1136.24	1931.54	6581.65	1801.43	1299.12	2521.51
Eu	204.62	92.72	213.91	395.81	121.11	92.30	186.75
Gd	4123.42	1868.69	4662.42	8881.99	3159.53	2456.70	4192.12
Tb	1483.49	671.97	2004.11	2417.52	1085.58	807.14	1411.63
Dy	11304.50	5433.74	18657.78	15699.50	8869.95	5266.34	10871.97
Ho	2453.33	1193.28	4578.91	2712.16	1847.29	1078.94	2310.65
Er	6698.67	3411.10	13002.03	6592.89	5153.02	2968.54	6304.38
Tm	1034.75	554.55	2060.00	848.50	779.55	454.47	955.30
Yb	7173.17	4274.02	13346.16	4744.79	5281.75	3024.50	6307.40

	SL1-12a (pegmatite)						
	Ja09B09b	**Ja09B09c**	**Ja09B09d**	**Ja09B10b**	**Ja09B10c**	**Ja09B10d**	**Average**
	Alt Aeg 1	**Alt Aeg 2**	**Alt Aeg 3**	**Alt Aeg 1**	**Alt Aeg 2**	**Alt Aeg 3**	**Alt Aeg**
	ppm	ppm	ppm	ppm	ppm	ppm	ppm
Lu	680.47	391.30	1218.36	426.53	557.59	321.31	599.26
Hf	2753.72	1778.47	1272.69	1543.50	1779.41	1601.70	1788.25
Ta	184.54	99.46	115.48	104.75	125.30	98.07	121.27
W	4.76	1.20	3.69	7.12	4.19	2.89	3.98
Au	0.35	0.10	< DL	0.12	< DL	< DL	0.19
Tl	0.42	0.29	0.27	0.16	< DL	0.11	0.25
Pb	1263.65	685.61	939.85	1724.96	843.13	1090.25	1091.24
Bi	< DL	< DL	< DL	0.04	< DL	< DL	0.04
Th	9.03	7.42	5.53	44.68	7.46	10.10	14.03
U	244.94	160.74	196.32	615.35	247.27	248.40	285.50

	SL1-12a (pegmatite)		
	Ja09B09a Unalt' Aeg	**Ja09B10a Unalt' Aeg**	**Average Unalt' Aeg**
	ppm	ppm	ppm
Li	16.48	19.08	17.78
Be	< DL	85.98	85.98
B	66.14	123.39	94.76
Na	106995.69	103949.79	105472.74
Mg	< DL	1455.21	1455.21
Al	2285.41	2081.12	2183.26
Si	247802.10	275922.94	261862.52
P	< DL	< DL	< DL
K	14.84	177.39	96.11
Ca	1306.62	3145.54	2226.08
Sc	7.13	3.17	5.15
Ti	3238.31	3874.72	3556.52
V	11.13	5.50	8.31
Cr	< DL	< DL	< DL
Mn	1892.58	2211.53	2052.05
Fe	231814.53	181164.77	206489.65
Co	< DL	< DL	< DL
Ni	< DL	< DL	< DL
Cu	28.82	7.12	17.97
Zn	3701.74	4037.29	3869.51
As	21.99	10.43	16.21
Rb	< DL	4.95	4.95
Sr	0.88	5.38	3.13
Y	1212.80	1329.88	1271.34
Zr	1223.09	3247.63	2235.36
Nb	80.06	166.34	123.20
Mo	1.00	< DL	1.00
Ag	< DL	0.28	0.28
Cd	< DL	< DL	< DL
In	5.68	8.92	7.30
Sn	1587.60	2332.05	1959.83
Sb	< DL	0.21	0.21
Cs	0.48	0.27	0.38
Ba	< DL	13.21	13.21
La	16.53	38.20	27.36
Ce	17.83	44.53	31.18
Pr	10.40	12.69	11.54
Nd	44.93	61.88	53.40
Sm	54.26	36.89	45.57
Eu	4.60	3.71	4.16
Gd	104.61	75.90	90.25
Tb	41.26	29.80	35.53
Dy	402.79	306.84	354.81
Ho	98.52	64.72	81.62
Er	241.46	212.97	227.21
Tm	50.18	27.65	38.92
Yb	1751.52	230.67	991.10

	SL1-12a (pegmatite)		
	Ja09B09a Unalt' Aeg	Ja09B10a Unalt' Aeg	Average Unalt' Aeg
	ppm	ppm	ppm
Lu	23.49	19.29	21.39
Hf	37.73	82.75	60.24
Ta	21.30	12.98	17.14
W	0.60	0.42	0.51
Au	< DL	< DL	< DL
Tl	< DL	< DL	< DL
Pb	2.59	59.56	31.08
Bi	< DL	< DL	< DL
Th	0.00	0.16	0.08
U	0.91	11.16	6.04

	SL-Cb (pegmatite)						
	Mr20B03	**Mr20B04**	**Mr20B05**	**Mr20B06**	**Mr20B07**	**Mr20B08**	**Mr20B15**
	Arfv	**Arfv**	**Arfv**	**Arfv**	**Arfv**	**Arfv**	**Arfv**
	ppm	ppm	ppm	ppm	ppm	ppm	ppm
Li	2652.2	2478.0	2361.7	2715.7	2126.6	2405.9	2939.2
Be	8.7	9.9	8.8	10.5	15.4	15.8	13.2
B	49.4	41.6	47.7	45.9	47.1	47.3	48.1
Na	72013.2	70927.0	68123.1	75427.5	61879.1	71494.9	71970.3
Mg	459.4	561.6	305.7	441.3	1440.5	935.4	465.2
Al	2320.5	2390.6	1946.7	2418.8	2005.6	2123.8	2315.5
Si	310253.5	315880.8	321940.2	299033.8	317982.2	310885.8	306982.7
P	9.5	9.3	11.5	5.3	11.1	7.1	0.3
K	7538.0	7358.5	6737.6	9826.3	6702.6	7439.6	7765.8
Ca	889.2	2123.5	1086.5	2185.7	5015.5	4726.5	1216.1
Sc	3.9	5.6	4.4	5.6	5.7	3.3	2.2
Ti	4864.4	4731.5	5539.7	6026.8	4906.5	5675.8	6198.3
V	1.2	1.3	0.2	0.6	0.3	0.0	0.0
Cr	0.0	0.6	1.1	1.1	0.6	0.0	0.2
Mn	3476.9	3486.9	3336.5	4312.4	4129.2	4344.6	3873.2
Fe	155636.9	145810.1	140830.1	162867.7	147810.0	146254.4	156876.7
Co	0.8	1.0	0.2	0.3	0.1	0.3	0.2
Ni	0.0	0.5	0.3	1.3	1.7	0.0	0.0
Cu	0.2	1.1	1.0	1.2	12.9	7.0	0.9
Zn	2763.6	3379.2	3151.2	4105.0	3734.9	4757.8	3021.3
As	0.0	1.9	0.0	2.0	0.0	0.0	0.0
Rb	44.6	41.0	41.0	53.8	34.9	46.9	46.8
Sr	0.4	1.2	0.6	0.7	1.7	4.1	0.7
Y	12.8	19.6	19.9	22.0	39.5	36.8	21.2
Zr	881.9	902.5	914.7	1168.4	1061.2	1606.8	1558.1
Nb	53.4	73.5	65.1	69.9	73.2	127.0	63.9
Mo	0.2	0.2	0.1	0.2	0.2	0.3	0.3
Ag	0.0	0.1	0.0	0.1	0.0	0.1	0.1
Cd	1.1	2.1	1.5	2.0	2.3	2.4	2.0
In	1.2	1.3	1.1	1.3	0.9	1.3	1.2
Sn	86.8	86.9	114.3	138.3	92.1	138.6	128.1
Sb	0.0	0.0	0.0	0.0	0.1	0.1	0.0
Cs	0.0	0.0	0.0	0.0	0.0	0.3	0.0
Ba	0.3	1.1	0.7	0.6	1.2	2.6	0.5
La	0.5	1.4	0.8	0.6	2.3	5.0	0.8
Ce	1.3	3.0	1.8	2.0	2.3	6.2	1.7
Pr	0.2	0.5	0.4	0.3	0.7	1.0	0.3
Nd	0.8	1.9	1.1	1.4	2.8	4.2	1.2
Sm	0.3	0.6	0.4	0.3	1.0	1.1	0.4
Eu	0.1	0.0	0.1	0.1	0.1	0.1	0.0
Gd	0.2	0.4	0.3	0.4	1.6	1.3	0.4
Tb	0.1	0.2	0.1	0.1	0.4	0.4	0.1
Dy	1.5	1.8	2.0	2.2	4.4	4.2	2.2
Ho	0.7	0.9	1.2	1.2	1.7	1.6	1.1
Er	5.4	7.2	8.9	9.0	9.9	9.5	7.5
Tm	2.0	2.5	3.1	3.2	3.1	3.0	2.9
Yb	26.7	34.1	40.8	42.4	38.5	38.6	38.8

	SL-Cb (pegmatite)						
	Mr20B03	Mr20B04	Mr20B05	Mr20B06	Mr20B07	Mr20B08	Mr20B15
	Arfv	Arfv	Arfv	Arfv	Arfv	Arfv	Arfv
	ppm	ppm	ppm	ppm	ppm	ppm	ppm
Lu	6.9	7.8	9.3	9.6	8.3	9.0	9.1
Hf	35.4	38.7	42.3	60.7	56.9	93.3	82.5
Ta	0.6	0.9	0.8	0.8	1.1	2.6	0.9
W	0.0	0.0	0.0	0.0	0.1	0.1	0.0
Au	0.0	0.0	0.0	0.0	0.0	0.0	0.0
Tl	0.1	0.1	0.1	0.1	0.1	2.3	0.1
Pb	4.7	7.0	8.9	8.7	9.5	16.4	7.0
Bi	0.0	0.1	0.0	0.0	0.6	1.0	0.0
Th	0.0	0.0	0.0	0.0	0.1	0.2	0.0
U	0.0	0.3	0.5	0.2	4.5	4.2	0.1

	SL-Cb (pegmatite)						
	Mr20B16	Average	Mr20B09	Mr20B10	Mr20B11	Mr20B12	Mr20B13
	Arfv	Arfv	Aeg	Aeg	Aeg	Aeg	Aeg
	ppm		ppm	ppm	ppm	ppm	ppm
Li	3083.4	2595.3	34.1	146.3	31.6	46.7	70.1
Be	14.1	12.1	7.8	21.0	12.0	9.5	24.1
B	44.4	46.4	69.3	67.0	66.9	62.0	67.8
Na	70843.6	70334.8	100531.6	105663.6	98366.3	96128.8	93872.1
Mg	856.6	683.2	505.3	7482.3	630.9	1802.0	2651.0
Al	2404.4	2240.7	4650.1	4475.5	4669.8	3023.0	2804.6
Si	307795.0	311344.3	303207.6	293769.9	303653.1	309933.0	307260.4
P	8.0	7.8	0.0	5.7	11.1	3.1	4.3
K	8018.4	7673.4	210.7	182.1	31.7	34.1	65.5
Ca	4308.5	2693.9	1964.3	5320.6	2275.8	2669.3	3214.7
Sc	3.0	4.2	2.3	3.9	1.0	5.1	1.6
Ti	5375.7	5414.8	4625.6	7580.8	4842.1	5502.3	4222.1
V	0.0	0.5	0.0	0.0	0.0	0.0	0.3
Cr	0.0	0.4	0.0	1.4	0.0	1.0	0.5
Mn	4524.9	3935.6	1557.0	2225.6	2497.3	2635.3	2184.5
Fe	151681.9	150971.0	147589.6	137362.5	146271.5	136608.5	144446.2
Co	0.3	0.4	0.1	0.0	0.0	0.0	0.0
Ni	0.0	0.5	1.7	9.2	1.6	1.1	0.8
Cu	4.5	3.6	3.7	9.9	4.6	7.3	7.2
Zn	4519.2	3679.0	1314.7	2281.9	1805.7	2284.4	1973.1
As	0.3	0.5	0.0	18.2	1.1	0.0	0.0
Rb	56.7	45.7	11.2	4.8	0.4	1.4	0.8
Sr	1.6	1.4	1.5	10.6	3.1	2.7	5.9
Y	35.0	25.8	16.7	54.1	65.5	51.8	95.8
Zr	1065.0	1144.8	829.1	1272.3	904.9	1184.2	1030.1
Nb	89.9	77.0	98.4	348.7	157.7	221.3	228.5
Mo	0.1	0.2	0.0	0.0	0.0	0.3	0.0
Ag	0.0	0.0	0.0	0.1	0.0	0.0	0.1
Cd	2.5	2.0	1.2	0.7	1.4	1.3	0.9
In	1.2	1.2	1.3	11.0	3.7	5.3	4.6
Sn	104.6	111.2	162.4	2059.4	817.9	1088.5	1048.9
Sb	0.0	0.0	0.1	0.2	0.1	0.1	0.0
Cs	0.0	0.1	0.7	0.3	0.0	0.1	0.0
Ba	1.7	1.1	4.0	8.4	3.1	2.8	5.4
La	1.9	1.7	7.8	16.8	14.6	11.1	23.6
Ce	3.0	2.7	15.5	23.5	15.7	17.1	27.8
Pr	0.7	0.5	2.3	4.4	3.6	2.9	4.6
Nd	2.6	2.0	8.0	16.3	14.6	11.1	16.9
Sm	0.6	0.6	1.5	4.4	4.2	2.9	3.9
Eu	0.0	0.1	0.0	0.1	0.1	0.1	0.2
Gd	0.9	0.7	1.0	3.5	4.9	2.6	5.7
Tb	0.3	0.2	0.3	0.8	1.1	0.8	1.6
Dy	3.8	2.8	2.1	6.4	8.9	6.2	12.7
Ho	1.5	1.2	0.7	1.8	2.4	1.8	3.3
Er	10.4	8.5	4.1	7.5	8.1	7.0	12.4
Tm	3.7	2.9	1.7	1.6	1.6	1.6	2.3
Yb	47.2	38.4	27.0	22.1	16.4	20.0	23.3

	SL-Cb (pegmatite)						
	Mr20B16	Average	Mr20B09	Mr20B10	Mr20B11	Mr20B12	Mr20B13
	Arfv	Arfv	Aeg	Aeg	Aeg	Aeg	Aeg
	ppm		ppm	ppm	ppm	ppm	ppm
Lu	9.8	8.7	6.5	4.8	3.6	4.9	5.0
Hf	45.4	56.9	41.3	49.1	26.7	34.6	45.3
Ta	1.4	1.1	3.2	9.7	12.0	16.1	7.5
W	0.0	0.0	0.1	0.2	0.1	0.2	0.1
Au	0.0	0.0	0.0	0.0	0.0	0.0	0.0
Tl	0.1	0.4	3.2	0.3	0.0	0.2	0.1
Pb	12.2	9.3	8.2	13.9	4.6	4.2	5.1
Bi	0.0	0.2	0.2	0.6	0.3	0.0	0.2
Th	0.1	0.1	0.4	2.6	0.3	0.3	0.5
U	1.2	1.4	2.1	4.6	2.2	2.7	1.4

	SL-Cb (pegmatite)	
	Mr20B14	Average
	Aeg	Aeg
	ppm	
Li	52.4	63.5
Be	17.3	15.3
B	62.2	65.8
Na	91998.3	97760.1
Mg	1931.0	2500.4
Al	17137.9	6126.8
Si	310601.5	304737.6
P	9.4	5.6
K	5891.6	1069.3
Ca	2529.3	2995.7
Sc	3.0	2.8
Ti	3087.8	4976.8
V	0.0	0.0
Cr	0.8	0.6
Mn	1725.9	2137.6
Fe	118290.2	138428.1
Co	0.0	0.0
Ni	0.0	2.4
Cu	3.1	6.0
Zn	1877.5	1922.9
As	0.0	3.2
Rb	236.2	42.5
Sr	4.5	4.7
Y	56.4	56.7
Zr	764.9	997.6
Nb	181.0	205.9
Mo	0.0	0.1
Ag	0.0	0.1
Cd	1.0	1.1
In	5.1	5.2
Sn	1089.4	1044.4
Sb	0.1	0.1
Cs	0.1	0.2
Ba	13.9	6.3
La	12.3	14.4
Ce	16.4	19.3
Pr	2.4	3.4
Nd	8.5	12.6
Sm	2.1	3.2
Eu	0.1	0.1
Gd	3.2	3.5
Tb	0.8	0.9
Dy	6.9	7.2
Ho	1.8	2.0
Er	6.8	7.6
Tm	1.4	1.7
Yb	15.0	20.6

	SL-Cb (pegmatite)	
	Mr20B14	Average
	Aeg	Aeg
	ppm	
Lu	3.5	4.7
Hf	32.1	38.2
Ta	4.8	8.9
W	0.1	0.1
Au	0.0	0.0
Tl	0.7	0.7
Pb	4.0	6.7
Bi	0.1	0.2
Th	0.3	0.7
U	0.9	2.3

	SL1-12a (pegmatite)		
	Ja09B03 Boat Xtal	**Ja09B04 Boat Xtal**	**Average Boat Xtal**
	ppm	ppm	ppm
Li	3.05	4.55	3.80
Be	30.66	68.66	49.66
B	92.92	110.66	101.79
Na	42207.62	25523.15	33865.39
Mg	7691.70	5067.71	6379.70
Al	4414.22	5366.75	4890.48
Si	262688.87	253094.31	257891.59
P	371.92	152.83	262.37
K	2229.77	7149.84	4689.80
Ca	77524.74	83418.89	80471.82
Sc	24.61	17.75	21.18
Ti	114.39	147.43	130.91
V	14.62	7.36	10.99
Cr	16.65	10.03	13.34
Mn	10224.40	11915.41	11069.90
Fe	6904.20	4801.49	5852.85
Co	0.92	0.68	0.80
Ni	181.01	72.36	126.69
Cu	25.92	14.57	20.24
Zn	496.77	376.46	436.62
As	573.89	322.92	448.40
Rb	28.26	272.14	150.20
Sr	352.84	385.44	369.14
Y	7857.55	9691.71	8774.63
Zr	141035.38	163215.61	152125.50
Nb	520.91	581.91	551.41
Mo	< DL	< DL	< DL
Ag	14.91	13.04	13.97
Cd	5.24	5.93	5.58
In	9.23	8.78	9.00
Sn	2330.93	2082.43	2206.68
Sb	3.90	3.34	3.62
Cs	1.41	2.24	1.83
Ba	563.32	318.57	440.95
La	178.23	244.29	211.26
Ce	390.42	469.78	430.10
Pr	32.94	44.94	38.94
Nd	127.51	169.92	148.71
Sm	115.91	133.19	124.55
Eu	15.22	18.27	16.74
Gd	203.41	238.00	220.71
Tb	121.54	139.18	130.36
Dy	1415.10	1582.02	1498.56
Ho	409.79	444.82	427.30
Er	1831.70	1876.13	1853.92
Tm	496.65	494.02	495.33
Yb	4937.98	4464.68	4701.33
Lu	528.97	440.79	484.88

	SL1-12a (pegmatite)		
	Ja09B03 Boat Xtal	**Ja09B04 Boat Xtal**	**Average Boat Xtal**
	ppm	ppm	ppm
Hf	2777.95	2963.43	2870.69
Ta	84.63	87.24	85.93
W	0.50	0.60	0.55
Au	0.20	0.07	0.14
Tl	0.98	1.85	1.42
Pb	2134.16	2461.36	2297.76
Bi	< DL	< DL	< DL
Th	218.21	288.56	253.38
U	382.91	502.16	442.53

	SL1-12a (pegmatite)		
	Ja09B05 Cubic Xtal	**Ja09B06 Cubic Xtal**	**Average Cubic Xtal**
	ppm	ppm	ppm
Li	16.15	8.71	12.43
Be	712.08	794.59	753.34
B	298.03	327.31	312.67
Na	18063.61	19135.71	18599.66
Mg	16118.59	13770.93	14944.76
Al	12245.68	7936.13	10090.91
Si	198098.15	193300.97	195699.56
P	242.44	236.01	239.22
K	8064.51	4274.87	6169.69
Ca	17019.02	50287.25	33653.14
Sc	< DL	< DL	< DL
Ti	769.22	1332.85	1051.03
V	< DL	< DL	< DL
Cr	< DL	< DL	< DL
Mn	7128.48	7730.56	7429.52
Fe	40925.69	53385.75	47155.72
Co	< DL	161.16	161.16
Ni	< DL	< DL	< DL
Cu	1308.87	823.23	1066.05
Zn	1517.81	1251.64	1384.73
As	526.99	634.21	580.60
Rb	207.02	106.31	156.66
Sr	252.55	902.30	577.43
Y	41061.33	50161.40	45611.36
Zr	1801.58	4682.94	3242.26
Nb	3250.80	9894.20	6572.50
Mo	< DL	0.25	0.25
Ag	2.94	3.53	3.24
Cd	1.18	1.19	1.18
In	0.87	1.44	1.15
Sn	297.31	360.52	328.92
Sb	24.24	25.22	24.73
Cs	3.60	3.21	3.41
Ba	802.97	1127.53	965.25
La	1747.53	2090.76	1919.15
Ce	13433.28	15034.54	14233.91
Pr	404.89	509.99	457.44
Nd	1807.59	2267.12	2037.35
Sm	1445.89	1754.36	1600.12
Eu	85.87	85.79	85.83
Gd	2906.44	3342.43	3124.43
Tb	1216.14	1378.40	1297.27
Dy	11264.22	12882.48	12073.35
Ho	2660.65	3006.48	2833.57
Er	7630.94	8612.78	8121.86
Tm	1149.87	1218.26	1184.07
Yb	6560.07	7123.88	6841.97
Lu	558.93	591.96	575.44

	SL1-12a (pegmatite)		
	Ja09B05 Cubic Xtal	**Ja09B06 Cubic Xtal**	**Average Cubic Xtal**
	ppm	ppm	ppm
Hf	60.28	119.68	89.98
Ta	78.13	215.47	146.80
W	26.28	19.99	23.14
Au	< DL	0.03	0.03
Tl	0.76	0.55	0.65
Pb	4145.98	3923.38	4034.68
Bi	< DL	< DL	< DL
Th	235772.61	174144.06	204958.33
U	2763.37	1477.09	2120.23

	SL1-12a (pegmatite)				
	Ja09B07	**Ja09B08a**	**Ja09B08b**	**Ja09B08c**	**Average**
	Spinel-form	**Spinel-form 3**	**Spinel-form 1**	**Spinel-form 2**	**Spinel-form**
	ppm	ppm	ppm	ppm	ppm
Li	12.03	2.28	6.72	4.25	6.32
Be	< DL	< DL	< DL	7.06	7.06
B	64.51	42.88	36.88	49.61	48.47
Na	69008.50	21742.34	37346.27	32289.17	40096.57
Mg	< DL	216.44	993.35	782.06	663.95
Al	131.52	434.41	554.16	229.67	337.44
Si	15865.97	32121.68	35872.46	23632.01	26873.03
P	155.00	32.64	44.10	63.36	73.78
K	179.03	310.81	414.36	227.38	282.90
Ca	19385.40	23533.75	21839.46	23731.61	22122.55
Sc	< DL	< DL	< DL	< DL	< DL
Ti	14036.52	15994.54	18370.38	19315.33	16929.19
V	< DL	< DL	< DL	< DL	< DL
Cr	2.99	< DL	< DL	< DL	2.99
Mn	289.81	560.79	319.55	282.54	363.17
Fe	6475.09	18043.63	9188.95	8759.88	10616.88
Co	< DL	< DL	1.07	< DL	1.07
Ni	< DL	< DL	< DL	< DL	< DL
Cu	4.41	10.48	6.24	8.97	7.53
Zn	165.05	617.26	171.34	226.93	295.15
As	< DL	39.94	58.91	9.20	36.01
Rb	< DL	5.51	2.39	1.43	3.11
Sr	373.80	589.05	413.48	393.51	442.46
Y	111.50	478.41	395.04	575.65	390.15
Zr	1162.05	1491.18	1683.25	1577.14	1478.41
Nb	482103.52	473877.16	456649.83	465157.64	469447.04
Mo	4.95	5.34	5.50	4.51	5.08
Ag	0.43	6.96	2.42	4.75	3.64
Cd	2.61	3.84	3.55	2.42	3.11
In	4.04	3.48	3.06	4.01	3.65
Sn	1204.68	1072.03	957.98	945.42	1045.03
Sb	2.57	3.14	1.08	3.18	2.49
Cs	0.98	1.54	0.39	0.42	0.83
Ba	305.63	974.87	402.26	422.71	526.37
La	37202.60	38070.93	36669.40	39340.04	37820.74
Ce	84962.08	86896.62	90267.87	102073.65	91050.06
Pr	7882.94	8702.42	8840.73	9745.59	8792.92
Nd	19878.95	23738.28	24822.70	26259.16	23674.77
Sm	1747.11	2111.31	2397.62	2435.84	2172.97
Eu	44.35	65.92	72.97	88.10	67.84
Gd	439.28	559.54	662.06	748.47	602.34
Tb	28.29	53.52	53.69	64.44	49.99
Dy	72.15	192.21	186.62	282.27	183.31
Ho	4.31	33.34	23.42	38.58	24.91
Er	11.64	76.83	53.60	97.50	59.89
Tm	0.50	9.12	6.42	11.20	6.81
Yb	0.47	61.29	39.19	65.19	41.54
Lu	< DL	6.26	3.30	5.90	5.16

	SL1-12a (pegmatite)				
	Ja09B07 Spinel-form	**Ja09B08a Spinel-form 3**	**Ja09B08b Spinel-form 1**	**Ja09B08c Spinel-form 2**	**Average Spinel-form**
	ppm	ppm	ppm	ppm	ppm
Hf	22.17	31.83	31.06	33.07	29.53
Ta	15802.70	16512.26	16943.20	15956.59	16303.69
W	95.73	90.05	110.89	154.52	112.80
Au	6.31	8.50	5.43	8.21	7.11
Tl	0.78	0.07	0.21	0.25	0.33
Pb	631.20	1929.16	951.72	1575.82	1271.98
Bi	0.13	< DL	< DL	< DL	0.13
Th	26.96	34.15	38.78	33.62	33.38
U	3133.29	3051.79	2017.02	2088.68	2572.69

	SL1-12a (pegmatite)		
	Ja09B09a Unalt' Aeg	Ja09B10a Unalt' Aeg	Average Unalt' Aeg
	ppm	ppm	ppm
Li	16.48	19.08	17.78
Be	< DL	85.98	85.98
B	66.14	123.39	94.76
Na	106995.69	103949.79	105472.74
Mg	< DL	1455.21	1455.21
Al	2285.41	2081.12	2183.26
Si	247802.10	275922.94	261862.52
P	< DL	< DL	< DL
K	14.84	177.39	96.11
Ca	1306.62	3145.54	2226.08
Sc	7.13	3.17	5.15
Ti	3238.31	3874.72	3556.52
V	11.13	5.50	8.31
Cr	< DL	< DL	< DL
Mn	1892.58	2211.53	2052.05
Fe	231814.53	181164.77	206489.65
Co	< DL	< DL	< DL
Ni	< DL	< DL	< DL
Cu	28.82	7.12	17.97
Zn	3701.74	4037.29	3869.51
As	21.99	10.43	16.21
Rb	< DL	4.95	4.95
Sr	0.88	5.38	3.13
Y	1212.80	1329.88	1271.34
Zr	1223.09	3247.63	2235.36
Nb	80.06	166.34	123.20
Mo	1.00	< DL	1.00
Ag	< DL	0.28	0.28
Cd	< DL	< DL	< DL
In	5.68	8.92	7.30
Sn	1587.60	2332.05	1959.83
Sb	< DL	0.21	0.21
Cs	0.48	0.27	0.38
Ba	< DL	13.21	13.21
La	16.53	38.20	27.36
Ce	17.83	44.53	31.18
Pr	10.40	12.69	11.54
Nd	44.93	61.88	53.40
Sm	54.26	36.89	45.57
Eu	4.60	3.71	4.16
Gd	104.61	75.90	90.25
Tb	41.26	29.80	35.53
Dy	402.79	306.84	354.81
Ho	98.52	64.72	81.62
Er	241.46	212.97	227.21
Tm	50.18	27.65	38.92
Yb	1751.52	230.67	991.10
Lu	23.49	19.29	21.39

	SL1-12a (pegmatite)		
	Ja09B09a Unalt' Aeg	**Ja09B10a Unalt' Aeg**	**Average Unalt' Aeg**
	ppm	ppm	ppm
Hf	37.73	82.75	60.24
Ta	21.30	12.98	17.14
W	0.60	0.42	0.51
Au	< DL	< DL	< DL
Tl	< DL	< DL	< DL
Pb	2.59	59.56	31.08
Bi	< DL	< DL	< DL
Th	0.00	0.16	0.08
U	0.91	11.16	6.04

	SL1-12a (pegmatite)						
	Ja09B09b Alt Aeg 1	Ja09B09c Alt Aeg 2	Ja09B09d Alt Aeg 3	Ja09B10b Alt Aeg 1	Ja09B10c Alt Aeg 2	Ja09B10d Alt Aeg 3	Average Alt Aeg
	ppm	ppm	ppm	ppm	ppm	ppm	ppm
Li	26.94	22.86	6.69	20.32	35.44	35.82	24.68
Be	2828.91	1498.90	387.14	9634.92	1717.97	1946.36	3002.37
B	1240.48	768.76	195.44	3078.28	985.45	816.49	1180.82
Na	15632.69	37520.73	23479.89	29472.80	36718.06	56585.91	33235.01
Mg	17728.96	32363.94	8870.92	10214.54	23675.92	20905.29	18959.93
Al	5266.32	8672.46	2542.40	3446.56	5933.62	6804.73	5444.35
Si	194749.72	244752.12	212201.65	197808.83	224770.42	243139.48	219570.37
P	54.50	76.51	< DL	< DL	89.31	< DL	73.44
K	545.08	1961.42	863.50	349.86	648.52	426.08	799.08
Ca	90305.60	71213.51	98370.54	70430.61	66598.21	43998.97	73486.24
Sc	8.14	12.66	8.86	9.50	2.64	8.71	8.42
Ti	1436.04	983.64	604.83	2019.16	2467.21	3120.07	1771.82
V	< DL	< DL	< DL	< DL	2.17	1.95	2.06
Cr	< DL	4.52	< DL	5.41	5.09	< DL	5.01
Mn	6833.59	4795.16	3435.77	6213.98	5010.12	4419.70	5118.05
Fe	27536.35	20533.09	24297.60	55648.89	58366.15	102634.84	48169.49
Co	< DL	0.43	< DL	1.35	< DL	< DL	0.89
Ni	< DL	< DL	< DL	< DL	< DL	< DL	< DL
Cu	51.00	79.51	9.87	72.32	70.25	42.79	54.29
Zn	2791.97	2650.82	901.40	3012.89	3447.12	3973.27	2796.24
As	200.13	646.15	383.70	113.89	194.42	153.17	281.91
Rb	14.83	23.54	14.36	9.42	16.21	10.43	14.80
Sr	269.19	211.84	235.87	331.94	210.42	122.90	230.36
Y	55547.15	25332.61	106279.59	57546.66	43530.68	18171.89	51068.10
Zr	143694.89	103873.39	69123.68	87354.05	87649.33	58907.11	91767.08
Nb	6565.81	3320.74	4889.39	4540.14	4718.49	2541.05	4429.27
Mo	0.65	0.24	< DL	1.11	< DL	0.73	0.68
Ag	14.60	8.24	6.91	7.56	10.42	7.54	9.21
Cd	5.28	1.40	3.49	4.27	8.40	2.24	4.18
In	9.18	5.67	5.18	8.87	12.05	5.69	7.77
Sn	2338.84	1441.22	1208.43	2300.03	2867.70	1483.31	1939.92
Sb	7.07	4.37	5.03	13.50	4.85	5.38	6.70
Cs	0.86	0.86	1.03	0.82	2.43	0.90	1.15
Ba	439.18	353.34	392.00	298.70	340.25	232.65	342.69
La	1763.52	827.35	1047.50	4157.58	1297.95	884.79	1663.12
Ce	2233.93	1099.77	1843.35	9560.04	1715.70	1648.77	3016.93
Pr	611.23	282.03	360.77	1806.36	430.97	409.47	650.14
Nd	2969.95	1577.37	1808.54	9757.72	2372.38	2045.44	3421.90
Sm	2379.05	1136.24	1931.54	6581.65	1801.43	1299.12	2521.51
Eu	204.62	92.72	213.91	395.81	121.11	92.30	186.75
Gd	4123.42	1868.69	4662.42	8881.99	3159.53	2456.70	4192.12
Tb	1483.49	671.97	2004.11	2417.52	1085.58	807.14	1411.63
Dy	11304.50	5433.74	18657.78	15699.50	8869.95	5266.34	10871.97
Ho	2453.33	1193.28	4578.91	2712.16	1847.29	1078.94	2310.65
Er	6698.67	3411.10	13002.03	6592.89	5153.02	2968.54	6304.38
Tm	1034.75	554.55	2060.00	848.50	779.55	454.47	955.30
Yb	7173.17	4274.02	13346.16	4744.79	5281.75	3024.50	6307.40
Lu	680.47	391.30	1218.36	426.53	557.59	321.31	599.26

	SL1-12a (pegmatite)						
	Ja09B09b Alt Aeg 1	**Ja09B09c Alt Aeg 2**	**Ja09B09d Alt Aeg 3**	**Ja09B10b Alt Aeg 1**	**Ja09B10c Alt Aeg 2**	**Ja09B10d Alt Aeg 3**	**Average Alt Aeg**
	ppm	ppm	ppm	ppm	ppm	ppm	ppm
Hf	2753.72	1778.47	1272.69	1543.50	1779.41	1601.70	1788.25
Ta	184.54	99.46	115.48	104.75	125.30	98.07	121.27
W	4.76	1.20	3.69	7.12	4.19	2.89	3.98
Au	0.35	0.10	< DL	0.12	< DL	< DL	0.19
Tl	0.42	0.29	0.27	0.16	< DL	0.11	0.25
Pb	1263.65	685.61	939.85	1724.96	843.13	1090.25	1091.24
Bi	< DL	< DL	< DL	0.04	< DL	< DL	0.04
Th	9.03	7.42	5.53	44.68	7.46	10.10	14.03
U	244.94	160.74	196.32	615.35	247.27	248.40	285.50